

Environmental Science and Engineering

Keiji Ujikawa
Mikio Ishiwatari
Eric van Hullebusch *Editors*

Environment and Sustainable Development

Proceedings of the 2021 6th Asia
Conference on Environment and
Sustainable Development



Environmental Science and Engineering

Series Editors

Ulrich Förstner, Buchholz, Germany

Wim H. Rulkens, Department of Environmental Technology, Wageningen,
The Netherlands

Wim Salomons, Institute for Environmental Studies, University of Amsterdam,
Haren, The Netherlands

The ultimate goal of this series is to contribute to the protection of our environment, which calls for both profound research and the ongoing development of solutions and measurements by experts in the field. Accordingly, the series promotes not only a deeper understanding of environmental processes and the evaluation of management strategies, but also design and technology aimed at improving environmental quality. Books focusing on the former are published in the subseries Environmental Science, those focusing on the latter in the subseries Environmental Engineering.

More information about this series at <https://link.springer.com/bookseries/7487>

Keiji Ujikawa · Mikio Ishiwatari ·
Eric van Hullebusch
Editors

Environment and Sustainable Development

Proceedings of the 2021 6th Asia Conference
on Environment and Sustainable Development



Springer

Editors

Keiji Ujikawa
Yokohama National University
Yokohama, Kanagawa, Japan

Mikio Ishiwatari
Japan International Cooperation Agency
Tokyo, Tokyo, Japan

Eric van Hullebusch
Institut de Physique du Globe de Paris
University of Paris
Paris, Paris, France

ISSN 1863-5520

ISSN 1863-5539 (electronic)

Environmental Science and Engineering

ISBN 978-981-19-1703-5

ISBN 978-981-19-1704-2 (eBook)

<https://doi.org/10.1007/978-981-19-1704-2>

© The Editor(s) (if applicable) and The Author(s), under exclusive license to Springer Nature Singapore Pte Ltd. 2022

This work is subject to copyright. All rights are solely and exclusively licensed by the Publisher, whether the whole or part of the material is concerned, specifically the rights of translation, reprinting, reuse of illustrations, recitation, broadcasting, reproduction on microfilms or in any other physical way, and transmission or information storage and retrieval, electronic adaptation, computer software, or by similar or dissimilar methodology now known or hereafter developed.

The use of general descriptive names, registered names, trademarks, service marks, etc. in this publication does not imply, even in the absence of a specific statement, that such names are exempt from the relevant protective laws and regulations and therefore free for general use.

The publisher, the authors and the editors are safe to assume that the advice and information in this book are believed to be true and accurate at the date of publication. Neither the publisher nor the authors or the editors give a warranty, expressed or implied, with respect to the material contained herein or for any errors or omissions that may have been made. The publisher remains neutral with regard to jurisdictional claims in published maps and institutional affiliations.

This Springer imprint is published by the registered company Springer Nature Singapore Pte Ltd. The registered company address is: 152 Beach Road, #21-01/04 Gateway East, Singapore 189721, Singapore

Preface

It is our great pleasure to invite you to join 2021 6th Asia Conference on Environment and Sustainable Development (ACESD 2021), which will be held in November as a fully virtual conference. ACESD 2021 aims to provide a forum for researchers, practitioners, and professionals from the industry, academia, and government to discourse on research and development, professional practice in environmental issues, and sustainable development. The conference serves to foster communication among researchers and practitioners working in a wide variety of scientific areas with a common interest in improving the environment and sustainable development.

Through our efforts, we tried to spread the news about ACESD2021 to as many relevant researchers of the world as possible. Toward that, we were blessed with an energetic team, the members of which worked side by side which resulted in optimization of coordination among all.

This volume of proceedings contains 36 selected papers which were presented at ACESD 2021. In the proceedings, readers can find the most cutting-edge knowledge about environment and sustainable development not only from Asia but all around the world. Topics include environmental pollution and management, environmental chemical engineering and wastewater treatment, hydrology and water resources management, etc.

On behalf of the organizing committee, we are very delighted to say that this conference has been successfully held, and the participants have presented high-quality papers and engaged in lively discussions during the conference. We will continue to organize this conference in the future to provide a much effective platform for further exchange of new knowledge and perhaps potential collaboration in research areas of environmental issues and sustainable development.

We would like to express our grateful thanks to the conference program chairs and committee members and all the reviewers for their great professionalism and efforts in reviewing these submitted papers and thank all the participants and sponsors for their valuable contributions and support to ACESD2021.

Mitsuo Yoshida
General Chair

Conference Committees

International Advisory Chair

Vincenzo Belgiorno University of Salerno, Italy

Honorary Chair

Richard Haynes University of Queensland, Australia

General Chair

Mitsuo Yoshida International Network for Environmental
and Humanitarian Cooperation,
Nonprofit Inc., Japan

Conference Co-chairs

Chettiyappan Visvanathan Asian Institute of Technology, Thailand
Shane Snyder Nanyang Technological University, Singapore

Local Organizing Chairs

Shabbir Gheewala King Mongkut's University of Technology
Rajendra P. Shrestha Thonburi, Thailand
Asian Institute of Technology, Thailand

Program Chairs

Eric van Hullebusch University of Paris, France
Mikio Ishiwatari Japan International Cooperation Agency (JICA),
Japan
P. W. T. Pong New Jersey Institute of Technology, USA

Publicity Chair

Keiji Ujikawa

Yokohama National University, Japan

International Program Committees

Violeta Mugica Alvarez

Universidad Autonoma Metropolitana
Azcapotzalco, Mexico

Muslum Arici

Kocaeli University, Turkey

Chodchanok Attaphong

King Mongkut's Institute of Technology
Ladkrabang, Thailand

H. A. Aziz

Universiti Sains Malaysia, Malaysia

Isabel Paula Lopes Bras

Polytechnic Institute of Viseu, Portugal

Joe Dong

UNSW Sydney, Australia

Fatine Ezbakhe

University of Geneva, Switzerland

Izaskun Garrido

University of the Basque Country, Spain

Luca Giupponi

University of Milan, Italy

Radu Godina

Universidade Nova de Lisboa, Portugal

Yuk Feng Huang

Universiti Tunku Abdul Rahman, Malaysia

Sakul Hovanotayan

King Mongkut's Institute of Technology

Ladkrabang, Thailand

Shiu-Wan Hung

National Central University, Taiwan

Dimitrios Karamanis

University of Patras, Greece

Kosuke Kawai

National Institute for Environmental Studies,
Japan

Manoj Khandelwal

Federation University Australia, Australia

Alban Kurraqi

University of Lisbon, Portugal

Kevin Liu

Ming Chi University of Technology, Taiwan

Dina Matthew

Instituto Politecnico de Tomar, Portugal

Paulo Mendonca

University of Minho, Portugal

Gassan Hodaifa Meri

Pablo de Olavide University, Spain

Maegala Nallapan Maniyam

University Selangor, Malaysia

Vinod Phogat

South Australian Research and Development

Institute, Australia

Cheerawit Rattanapan

Mahidol University, Thailand

Borja Gonzalez Reguero

University of California, USA

Shehzar Shahzad Sheikh

National University of Science and Technology
(NUST), Pakistan

Yahya Sheikhnejad

University of Aveiro, Portugal

Pierluigi Siano

University of Salerno, Italy

Małgorzata Szczepanek

UTP University of Science and Technology,
Poland

Caloiero Tommaso

National Research Council of Italy
(CNR-ISAFOM), Italy

Angel Torriero

Deakin University, Australia

Contents

Environmental Pollution and Management

Evaluating the Potential of Vegetation to Capture Pollutants in Urban Environment	3
Miguel Martins, Lujain Hadba, Paulo Mendonça, and Lígia T. Silva	
Reference Levels for Heavy Metals in Soil in the City of Cerro de Pasco - Peru - 2020	14
Heiner Saldaña, Cesar Muñoz, Doris Esenarro, Ciro Rodriguez, and Pedro Amaya	
Urban Environmental Risk Spatial Pattern Assessment Supported by Remote Sensing and GIS—Shanghai, China	29
Qianqian Yang and Yishao Shi	
A Review on RES Energy Transition-Climate Change Interaction Effects	44
Dimitris Karamanis	
Socially Engaged Buddhism of Kalmykia: Land Degradation and the Ecological Initiatives of the Central Khurul	51
Bato Dondukov, Galina Dondukova, and Oyuna Dorzhigushaeva	
Preliminary Concentration-Response Functions on the Relationship Between Long-Term PM_{2.5} Exposure and Incidence and Prevalence of Depression Based on Systematic Review and a Meta-Analysis	63
Ying Li and Mengmeng Zhang	
Global INDCs Gap, Dilemma and Innovative Path of Carbon Sink Increase	78
He Hu, Weigu Fang, Tingyu Luo, and Guoliang Jin	
Effect of Hedgerows on CO Diffusion from Vehicle Exhaust Emissions in Street Canyons	91
Xin Jiang, Changzhao Qian, and Changping Chen	

Environmental Chemical Engineering and Wastewater Treatment

- Synthesis of Green Nano Composite Using Sugar Cane Waste for the Treatment of Cr Ions from Waste Water** 103
M. Amin Mir

- Heavy Metal Water Pollution: Transport and Transformation, Impacts and Treatment Technologies** 110
Guoye Ma and Lingyun Jia

- The Removal Effect of Organic Pollutants by Different Fillers in Constructed Rapid Infiltration System** 125
J. B. Zhang, M. L. Zhu, P. L. Xu, H. Jiang, and Y. L. Han

- Comparative Study on Nitrogen Removal Efficiency of Surface Water by Three New Combined Processes of Autotrophic Denitrification** 133
H. Jiang, M. L. Zhu, Y. L. Han, J. B. Zhang, and P. L. Xu

- Development of a Composite Solid Desiccant Dehumidifier for Ventilation Air** 143
Srimuk Jintana, Chirarattananon Surapong, Chaiiwatworakul Pipat, Nathakaranakule Adisak, Rakkwamsuk Pattana, and Chiarakorn Siriluk

Hydrology and Water Resources Management

- Applicability Analysis of Hydrological Models in the Middle and Upper Reaches of Yangtze River** 155
Xin Yang, Jianzhong Zhou, Wei Fang, and Yurong Wang

- Analysis on the Response of Lake Level Changes: A Hybrid Stepwise-Cluster Factorial Approach** 163
X. B. Zhai and Y. P. Li

- Seepage Experiment on a Permeable Dam Formed by Debris Flow from River Tributaries** 173
Fu-Ming Chang

- Assessment of Climate Change Impacts on Streamflow - A Case Study of Naryn River Basin, Central Asia** 186
Jiansen Wu, Guohe Huang, Jing Liu, Li Sun, and Jie Sun

- Joint-Risk Evaluation of Extreme Precipitation Using Copulas** 193
L. Sun, J. Sun, and Y. P. Li

- Optimal Allocation of Flood Control Capacity of Multiple Reservoir System** 200
Hongya Qiu, Jianzhong Zhou, Lu Chen, and Yuxin Zhu

- Experimental Study for Optimizing of Low Impact Development Facilities in Taiwan** 210
Fu-Ming Chang

Green Building Technology and Urban Planning	
Design of Green Infrastructure for the Revaluation of the Ventanilla-Peru Wetlands and the Protection of the Environment	225
Doris Esenarro, Josseline Quijano, Ciro Rodriguez, Jennifer Arteaga, and Karina Hinojosa	
Effect of the Window Design Features on Natural Ventilation	239
Inoka Manthilake, Anusha Wijewardane, and Rumesh Rangana	
How to Make Green Building Certification & Rating Systems More Pandemic-Sustainable?	248
A. Tleukan, G. Tokazhanov, M. Guney, A. Turkyilmaz, and F. Karaca	
Assessing Risk Factors in the Implementation of Green Building Projects: Empirical Research from Vietnam	261
Hung D. Nguyen, Quang N. H. Do, and Laura Macchion	
Environmental Affordances: A Practical Approach for Designing Child-Friendly Streets in High-Density Community	272
Qianxi Zhang, Wu Deng, Yat Ming Loo, Siyu Ma, Yuanli Ma, and Weixuan Chen	
Study on the Ecological Regeneration Strategy of Urban Industrial Sites—Taking Diamond Bay in Dalian as an Example	283
Jun Wang, XiaoYu Qiu, and Su Xu	
Resource Management, Green Behavior and Sustainable Development	
Scenario Analysis of Annual Heating Energy Demand in North China from 2020 to 2050	295
Haizhu Zhou, Xionglei Cheng, Yitong Li, Lining Zhou, and Xiaoping Li	
An Integrated Bi-level Optimization Model for Planning Water-Food-Energy Nexus System Under Uncertainty	304
Y. Ma, Y. P. Li, and G. H. Huang	
Recovery of Eco-friendly Spaces for Ecotourism and the Integration of Visitors in Morro de Calzada – Peru	315
Doris Esenarro, Judith Ocmín, Elizabeth Segovia, Carla Tassara, and Violeta Vega	
Planning Water-Food-Energy Nexus System Towards Sustainable Development Under Uncertainty	328
Y. F. Zhang, Y. P. Li, and G. H. Huang	
Assessing Consumers' Intentions Towards Green Alternatives of Disposable Packaging: A Case Study in Beijing and Shanghai	339
Kaiyan Yang and Sujitra Vassanadumrongdee	

Environmental Biology and Biodiversity Conservation	
Comparative Evaluation of APTI of Plant Species at Two Different Sites Near CCI-Rajban Cement Factory, Sirmaur	355
M. Amin Mir, Kim Andrews, and Bilal Ahmad Mir	
Elemental Status of European Mole (<i>T. Europaea</i>) in the Conditions of the Plast Region of the Chelyabinsk Oblast in Russian	367
Margarita Samburova, Vladimir Safonov, Tatyana Bratashova, and Emil Salimzade	
Effects of Crude Oil and Chemically Dispersed Crude Oil on the Antioxidant Response and Apoptosis in the Respiratory Tree of Sea Cucumber (<i>Apostichopus japonicus</i>)	375
Xishan Li, Deqi Xiong, Nan Li, Yuhang Zou, Wei Yang, Zhonglei Ju, and Guoxiang Liao	
Environmental Impact of Fluorine Pollution in Tursunzade Manufactured Biogeochemical Province (Tajikistan)	384
Vladimir Safonov, Vadim Ermakov, and Margarita Samburova	
Analysis on Bird Communities Response to Different Urban Land-Cover and Land-Use Types in Greater Manchester	393
Yihao Liu	
Author Index	403

Environmental Pollution and Management



Evaluating the Potential of Vegetation to Capture Pollutants in Urban Environment

Miguel Martins¹, Lujain Hadba² , Paulo Mendonça² , and Lígia T. Silva¹

¹ School of Engineering, Civil Engineering Department, CTAC, University of Minho,
4800-058 Guimarães, Portugal
lsilva@civil.uminho.pt

² School of Architecture, Art and Design, Lab2PT, University of Minho,
4800-058 Guimarães, Portugal

Abstract. Urban environments are subject to a concentration of air pollutants that may cause several health problems and discomfort to their inhabitants. Pollutant emissions are related with several anthropogenic sources, such as biomass heating systems in buildings, the vicinity of industries and especially the intense road traffic. Improvements in air quality and consequent mitigation of climate changes are essential to achieve a more sustainable urban environment. The presence of vegetation sprawled in urban areas is important to achieve this goal. This paper analysis the capacity of several plant species to capture atmospheric pollutants, and specifically Particulate Matter (PM) in urban environment. The adopted methodology focuses on measuring and calculating the ability to absorb PM by three plant species - *Parthenocissus quinquefolia*, *Hedera Helix* and *Quercus palustris* Muenchh - in periods of exposure to pollutants from 3 to 14 days. The specific removal of air pollutants by plants is a parameter influenced by several factors, such as the type of associated green infrastructure, leaf area, leaf density, plant species, location, exposure time and the type of the polluting source. From this research it can be concluded that the type of plant and its morphological characteristics are more influential than the size of its leaves.

Keywords: Green areas · Urban pollution · PM capture

1 Introduction

In 2018, 55% of the world's population was living in urban areas and forecasts suggest that this percentage will increase to 68% by 2050 [1]. The growth of the urban population has created impacts on the environment, whether directly or indirectly. If we compare the growth of human population and the CO₂ emissions in the world since 1900, we verify that these two indicators are correlated, as it can be seen on Figs. 1 and 2. It means that it is not possible to keep increasing world population without increasing pollutant emissions till reaching unsustainable levels. The increase of temperature in cities; the higher concentration of air pollutants; and the increase in noise, mainly from road traffic, are the most significant impacts [2]. The presence of vegetation is fundamental for reducing the levels of pollutants in urban areas [3, 4].

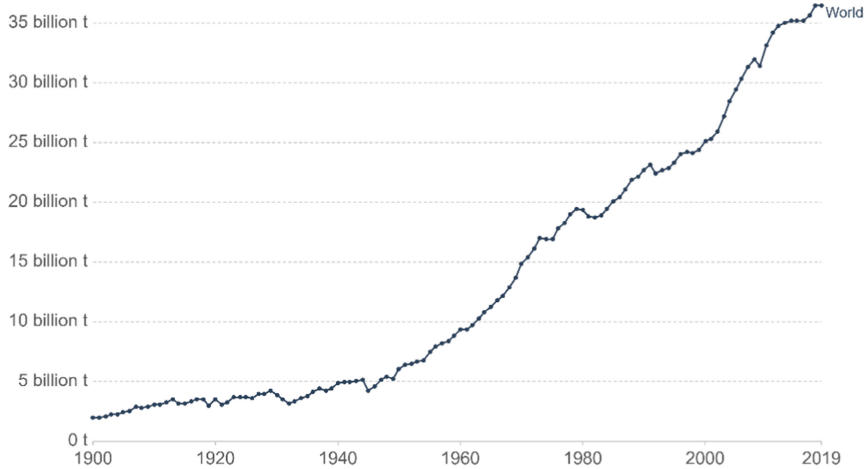


Fig. 1. World CO₂ emissions growth since 1900 (adapted from [5]).

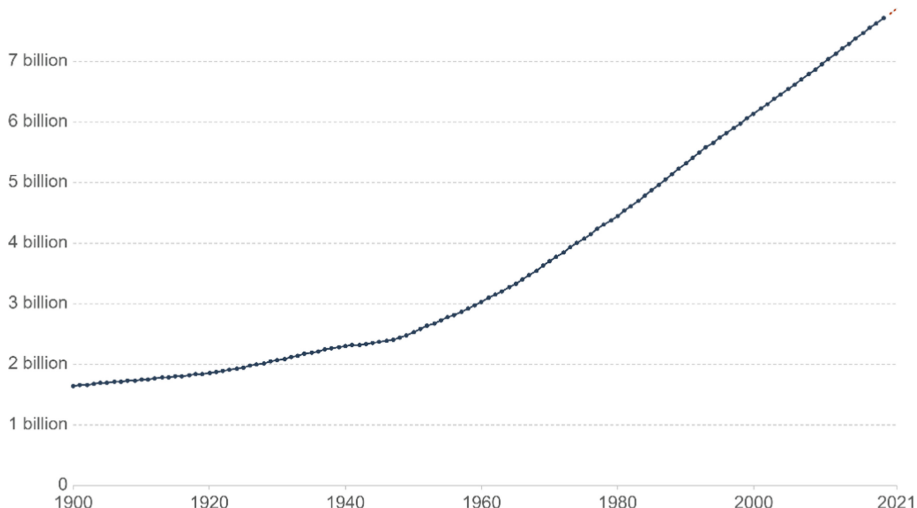


Fig. 2. World population growth since 1900 (adapted from [6]).

Vegetation acts as porous bodies that influence the dispersion patterns of air pollutants, creating a barrier between polluting sources and receptors, as well as helping to reduce toxins in the air [7]. Apart from enhancing air quality, vegetation may provide protection against solar radiation, reduce the heat island effect felt in centers and increase thermal comfort in cities [8].

Urban planning should be able to combine social, economic and environmental values [9]. It needs to contemplate the increase of green areas in urban environments to gain recognition. Despite the commonly accepted benefits of vegetation, the impact generated using different species in urban areas needs to be quantified and qualified. This

research aims to study the deposition and capture process of atmospheric pollutants of two plant species in urban areas, namely in the vicinity of roads with traffic concentration.

2 Urban Air Pollution and Green Infrastructure

Polluting emissions are mostly related with activities of anthropogenic origin, such as the burning of fossil fuels used in electricity generation, transport, industry and household equipment.

According to Silva et al. [10, 11], the main atmospheric pollutants in urban areas are nitrogen oxides (NO_x), carbon monoxide (CO), ozone (O_3), PM10 and PM2.5.

PM is the term used for particles present in the air, including ash, dust, smoke and small liquid droplets. PM can be classified according to their size, considering the average aerodynamic diameter of the particles. The coarse inhalable particles (PM10) have diameters that vary between $2.5 \mu\text{m}$ and $10 \mu\text{m}$, and the fine particles (PM2.5) have diameters below $2.5 \mu\text{m}$. PM can remain in the air for long periods of time, others, however, due to their weight, fall because of gravity and only stay in the air for a few seconds. Some particles are emitted directly into the atmosphere, and are thus considered to be of primary origin. Kumar et al. [12] state that transport is the main source of air pollution in urban environments. Transport is now subject of environmental pressure in the European Union due to its contribution to climate change.

2.1 Atmospheric Deposition

Atmospheric deposition allows to remove air pollutants by gravity sedimentation. There are two types of atmospheric deposition:

Dry deposition - settling of gases and particles from the atmosphere to different surfaces that occurs in the absence of precipitation. It is characterized as a sequence of three main processes: first, there is the turbulent transport of gases and particles from the atmosphere to the thin layer of static air immediately above the surface, on which there will be deposition; second, there is transport by diffusion to the organic surface in that thin layer of air; third, the pollutants are captured through the organic surface by adsorption, absorption or intercepting [13].

Wet deposition - gases and particles are intercepted and removed from the atmosphere by drops of water such as clouds, rain, snow or fog. The amount of pollutants removed by wet deposition depends on the amount of precipitation [13]. It is estimated that around 70% of the particles present in the external photosynthetic surface of the plants are completely removed after continuous precipitation with an average duration of 5 days [14]. The fall of precipitation is more effective in eliminating the coarse fraction from the atmosphere than the fine fraction [10].

According to Chen et al. [14], humidity and low temperatures have the greatest impact on the removal of PM10, which indicates the importance of relative humidity in local analyses to capture pollutants. Litschke et al. [15] reports that the fundamental effect of moisture on atmospheric deposition is related to the hygroscopicity of the particles, and that their size varies due to their absorption and discharge of water. Therefore, the local relative humidity generates a change in the deposition characteristics of the particles as it

increases the size and weight of the particles, which influences the speed of deposition. In addition to the physical characteristics of the particles, i.e., size and shape, atmospheric deposition is subject to the influence of other factors, such as wind speed and direction, pressure and temperature, atmospheric conditions, relative humidity, and the chemical characteristics of particles and gases, in addition to the characteristics of the surfaces on which they will be deposited. The morphological characteristics of the plants, i.e., species and leaf type, are also relevant issues [15].

2.2 Selection of Plant Species

Kumar et al. [7] suggest some measures when selecting plant species for PM capture. When choosing the species is fundamental to know its tolerance to air pollution in Urban environment, remaining healthy and efficient in their mitigation. It is also important to know their characteristics, such as leaf area index, total leaf area and height are considered fundamental for determining the total capacity for removing air pollutants [16]. Persistent leaf plants are preferable as their filtering action is more continuous over the time. Invasive species should not be used, as well as species that are poisonous or that may cause allergic reactions. The introduction of non-indigenous species into the ecosystem can lead to predation, competition with native species, and the transmission of pathogens or parasites, seriously affecting biological diversity, economic activities and public health. It is also essential to pay attention to road safety, as dense vegetation can cause loss of visibility or create obstacles to the circulation of drivers, cyclists and pedestrians.

In facades and green roofs, herbaceous species, shrubs and small trees should be selected depending on the conditions to which the plants will be subjected to. Plants may receive solar radiation in different amounts depending on their position regarding shading obstacles and orientation. Concerning coverage, height is an important factor, as well as the variation in temperatures throughout the day.

2.3 Green Infrastructures

Green Infrastructures (GI) can be defined as a strategically planned network of natural and semi-natural structures. GI should be considered as a priority to integrate in the urban design and planning processes [17]. They serve different needs in the urban areas in which they are integrated, such as water purification, air quality and climate change mitigation by reducing the annual temperature increase and the heat island effect. It can also provide protection against solar radiation [8]. GI allows to soften the artificial finishing of buildings and pavements, introduces color, reduces reflections and reduces noise by increasing acoustic absorption.

GI can minimize exposure to atmospheric pollution [18] by creating natural barriers such as vertical green systems, green roofs, trees, green barriers and urban forests, protecting human health [4, 7, 18]. They can also help in urban stormwater management [19]. Dover [8] refers that by increasing the permeable soil area the capacity of precipitation absorption is also increased, and so the probability of floods is reduced.

Being surrounded by a more natural environment, people are motivated to perform outdoor exercise and leisure activities and to socialize, reducing stress. The proximity

of green areas together with the creation of ecologic routes, such as pedestrian and cycle eco-paths, encourage the use of environmentally friendly transport to the detriment of vehicles powered by fossil fuels. Contact with nature helps to foster environmental awareness, especially for younger generations. Urban gardens are an increasing trend in large cities. They allow to produce organic and healthy food associated with reducing industrial production and less waste. Local food production also help to reduce pollutant emissions resulting from the transport of goods.

Investment in GI can contribute to local economic growth. Gore et al. [20] state that GI enhance the attractiveness of neighborhoods. According to Leskinen et al. [21] (2020), sustainability is a significant success factor for real estate, for example certifying green buildings and neighborhoods had a positive impact on property value.

3 Case Studies

In this section, a brief description of the sampling sites, monitoring program and procedures are presented. The adopted methodology was focused on measuring and forecasting the ability to capture air pollutants through photosynthetic surfaces. The procedures were based on Singh et al. [22] and Yanmei et al. [23].

3.1 Sampling Site Location

The experimental work was carried in Guimarães, North of Portugal. Guimarães' climate is characterized by cool winters and moderate to hot summers. The average minimum temperature of the coldest month varies between 2 and 5 °C, the average maximum temperature of the hottest month varies between 23 and 32 °C. Guimarães presents high levels of precipitation due to the passage of frontal surfaces, combined with the effect of the mountains, presenting annual precipitation totals above 1500 mm. It has intense economic and tourist activities, and therefore is an urban center subject to increasing levels of pollution. Collection sites were selected based on exposure to polluting sources such as road traffic. More details are available in Martins [24].

Sampling took place in the parishes of Urgeses and São Paio. The first sampling area, shown in Fig. 3 a), was Dr. Ricardo Marques Street in the city center. The species at the M1 site was *Parthenocissus Quinquefólia* deciduous. In this location, there were no barriers or obstacles between the receiver and the source. The main source of air pollution was road traffic in the city center.

The second sampling zone (Fig. 3 b)), is located in an industrial zone in Guimarães, next to the national two-way road EN105. The species in this zone is the persistent leaf *Hedera Helix*. The harvests were carried out at 1.5 m from the ground, and the main polluting source was road traffic. No barriers or obstacles exist between the receiver and the source.

For each selected site, three harvest points spaced 10 m and with a height of 1.5 m were defined, based on the methodology preconized by Singh et al. [22]. The selection of several collection points prevents the destruction of the samples due to abnormal events such as pruning or cutting during maintenance actions.



Fig. 3. a) Dr. Ricardo Marques Street, Guimarães – 41°26'28.1"N 8°17'20.6"W, source CM-Guimarães; b) Road N105 6-8, Guimarães - 41°25'30.6"N 8°18'15.8"W, source first author.

The harvests were carried out at intervals of 3 to 4 days. The first harvest was performed after 3 days of exposure, the 2nd after 7 days, the 3rd after 10 days and the 4th after 14 days. Laboratory tests were performed on the same day as the collection, avoiding sample degradation. The leaves used for PM capture measuring were cleaned with water and dried with tissue paper, what established the temporal beginning of the campaign. The average temperature registered during the campaign was 26.5 °C, with an average relative humidity of 45%, with no precipitation registered.

During the test, the collected pollutant particles with dimensions greater than 8 µm were weighed. In order to perform that, paper filters with 8 µm porosity were used, submitted to drying and weighing procedures before use. Filters were placed in an oven at 60 °C between 8 to 16 h to dry. The cooling time of the filters was respected, and they were weighed quickly so that the filter remains were free of humidity.

After collecting the leaves “in situ”, the samples were taken to the laboratory and placed in glass beakers with a previously measured amount of distilled water (depending on the leaf sizes, different amounts of solution were used) and magnetic stirring was used to start the washing process. The leaves were then drained between two glass rods to minimize the loss of pollutants that were still attached to the leaf surface.

After finishing the filtration, the filters were not removed immediately because they were damp and still very fragile. They were allowed to dry a little inside the funnel and were then removed using metal tweezers. Metallic tweezers were used to handle the filters in order to avoid transmission of particles and any grease on the skin or gloves.

When the filters were ready, they had to be put back in the oven to dry between 8 am and 10 am. After filtering, the used filters are dried. After drying, the filters are weighed and the test ends.

Leaf Area (LA) was also calculated. LA is the surface of the plant with photosynthetic capacity. According to Favarin J. et al. [25], the LA is a parameter indicative of the productivity of a plant, considering that its photosynthetic yield is directly linked to the number of leaves per unit area. The leafs were scanned and the images obtained were transformed into JPEG, monochrome files (Fig. 4 a)) The determination of the area of leafs was made using ImageJ® image analysis software (Fig. 4 b)).

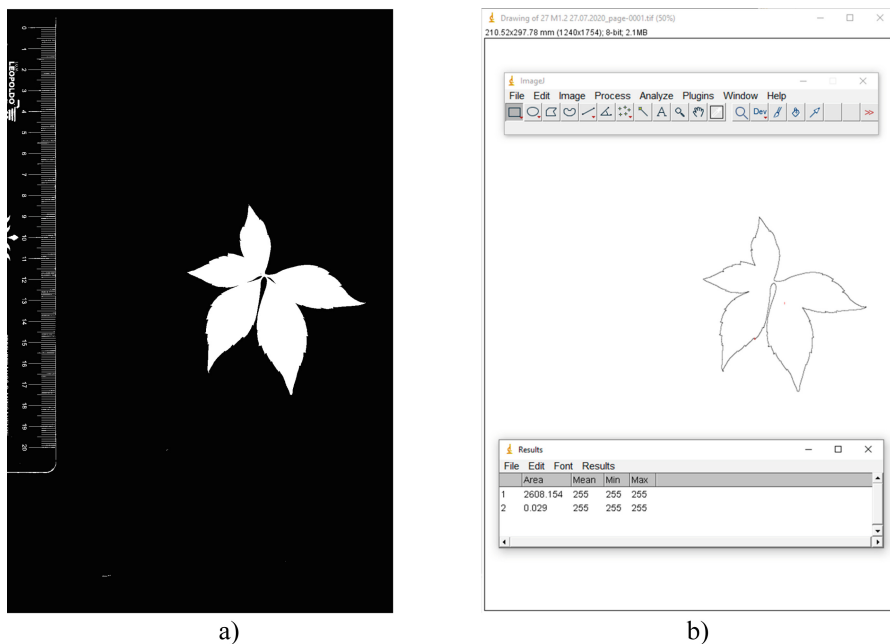


Fig. 4. Determination of the area of *Hedera Helix* leaf using: a) scanner and monochromatic image manipulation; b) image analysis software ImageJ® [23].

4 Results and Discussion

The obtained results were compiled and analyzed in order to assess the relation between atmospheric deposition overtime of the different species of vegetation.

The Leaf Area calculated of the species tested is presented in Table 1.

Table 1. Leaf Area (LA) of species tested.

Species	Sample	LA (m^2)	Accumulated LA (m^2)	Average LA (m^2)
<i>P. Quinquefólia</i>	M1.1	0,0042	0.023	0.0054
	M1.2	0,0052		
	M1.3	0,0072		
	M1.4A	0,0057		
	M1.4B	0,0048		
<i>Hedera Helix</i> (L2 Site)	M2.1	0,0061	0.014	0.0034
	M2.2	0,0027		
	M2.3	0,0025		
	M2.4A	0,0029		
	M2.4B	0,0030		

In the tests carried out, the process of capturing air pollutants with an equivalent diameter approximately greater than 8 μm (PM) is presented in Table 2 and Fig. 5.

Table 2. Results of PM8 captured by tested species.

Species	Sample	Exp. days	PM8 capt. (mg)	Total PM8 cap (mg)
<i>P. Quinquefólia</i>	M1.1 ^a	3	-0,50	14,30
	M1.2	7	0,60	
	M1.3	10	2,40	
	M1.4A	14	5,80	
	M1.4B	14	5,50	
<i>Hedera Helix</i>	M2.1	3	0,20	10,80
	M2.2	7	1,10	
	M2.3	10	5,10	
	M2.4A ^a	14	10,30	
	M2.4B	14	4,40	

^a samples rejected

The relationship between the capacity to capture PM and the various characteristics of the plants was observed, such as the leaf area, type of plant, location, emission of the polluting source.

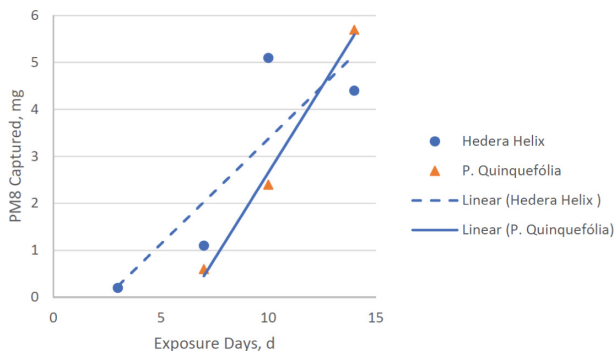


Fig. 5. Results of PM8 captured by tested species.

When analyzing the specific removal values (mg/m^2) of each analyzed species, it was observed that the exposure time influences the amount of pollutant captured, this relationship is shown in the following trend line equations:

$$\text{Parthenocissus Quinquefólia: } SR = 175.81d \quad (R^2 = 0.643)$$

$$\text{Hedera Helix M: } SR = 425.57d \quad (R^2 = 0.625)$$

Where,

SR – Specific Removal mg/m².

d – Days of exposure.

By analyzing Fig. 5, the exposure time influences the amount of pollutant captured. The Hedera Helix has the best line fit for the data analysed.

5 Conclusions

This research aimed to observe the ability of vegetation to capture pollutants in an urban context. This ability is influenced by several factors, such as the type of green infrastructure, total leaf area, plant species, location, time of exposure and the polluting source type.

In this study, two sampling sites were selected and the capacity for capturing PMs by plant leaf surfaces was calculated. Two species of plants were tested, Parthenocissus Quinquefólia and Hedera Helix. Plants are able to retain Particulate Matter (PM) through the process of atmospheric deposition of PM on the leaf surfaces as a result of gravity sedimentation.

In the tests performed, the samples of Parthenocissus Quinquefolia located at M1, captured a total of 14.3 mg of PM8 with an accumulated leaf area of 0.023 m². The Hedera Helix species, located in M2, captured a total of 10.8 mg of pollutants with an accumulated leaf area of 0.014 m². The Parthenocissus Quinquefolia species has the higher value of PM8 captured. It was also noticed that, although the species Hedera Helix registered the lowest values of tested leaf area, this species recorded high values of captured PM8. According to the observed results, the time of the exposure of vegetation to the polluting sources influences the amount of pollutant captured by leaf surfaces.

Analyzing the daily removal of pollutants, the following values were collected: the Parthenocissus Quinquefólia species (M1) had an average leaf area of 0.0054 m² and the average specific daily removal was 40.83 mg/m².24 h; the Hedera Helix species (M2) had an average leaf area of 0.0034 m² and the average specific daily removal was 94.47 mg/m².24 h. Therefore, Hedera Helix proved to be the most efficient in daily retention of polluting particles.

Acknowledgments. This work was partially supported by the Project FCT/C-TAC Research Centre for Territory, Environment and Construction of University of Minho and Project Lab2PT - Landscapes, Heritage and Territory laboratory - UIDB/04509/2020 through FCT - Fundação para a Ciência e a Tecnologia.

References

1. United Nations, Department of Economic and Social Affairs, Population Division. World Urbanization Prospects: The 2018 Revision (ST/ESA/SER.A/420). United Nations, New York (2019)
2. IPCC: Climate Change Synthesis Report. Contribution of Working Groups I, II and III to the Fifth Assessment Report of the Intergovernmental Panel on Climate Change, Geneva, Switzerland (2014)
3. Air Quality Expert Group: Impacts of Vegetation on Urban Air Pollution (2018). <https://uk-air.defra.gov.uk/>
4. Abhijith, KV., et al.: Air pollution abatement performances of green infrastructure in open road and built-up street canyon environments – a review. *Atmos. Environ.* **162**, 71–86 (2017)
5. Ritchie, H., Roser, M.: CO₂ and Greenhouse Gas Emissions. Published online at OurWorldInData.org (2020). <https://ourworldindata.org/co2-and-other-greenhouse-gas-emissions>. Accessed 19 July 2021
6. Roser, M, Ritchie, H., Ortiz-Ospina, E.: World Population Growth. Published online at OurWorldInData.org (2013). <https://ourworldindata.org/world-population-growth>. Accessed 19 July 2021
7. Kumar, P., et al.: Implementing green infrastructure for air pollution abatement: general recommendations for management and plant species selection. Global Centre for Clean Air Research, University of Surrey (2019)
8. Dover, J.: Green infrastructure: incorporating plants and enhancing biodiversity in buildings and urban environments. United States of America (2015)
9. Madureira, H.: Infra-estrutura verde na paisagem urbana contemporânea: o desafio da conectividade e a oportunidade da multifuncionalidade. *Geografia : Revista da Faculdade de Letras da Universidade do Porto*. **1**, 33–43 (2012)
10. Silva, L.T., Fonseca, F., Pires, M., Mendes B.: SAUS: A tool for preserving urban green areas from air pollution. *Urban Forest. Urban Greening* **46**(126440), 1–12 (2019). <https://doi.org/10.1016/j.ufug.2019.126440>
11. Silva, L.T., Pinho, J.L., Nurusman, H.: Traffic air pollution monitoring based on an air–water pollutants deposition device. *Int. J. Environ. Sci. Technol.* **11**(8), 2307–2318 (2014). <https://doi.org/10.1007/s13762-014-0625-9>
12. Kumar, P., Rivas, I., Singh, A., Ganesh, V., Ananya, M., Frey, H.: Dynamics of coarse and fine particle exposure in transport microenvironments. *npj Clim. Atmos. Sci.* (2018, in Press). <https://doi.org/10.1038/s41612-018-0023-y>
13. Erisman, J., et al.: Atmospheric deposition - in relation to acidification and eutrophication. *Stud. Environ. Sci.* **63**, 1–405 (1995)
14. He, C. et al.: Particulate matter capturing capacity of roadside evergreen vegetation during winter season. *Urban For. Urban Green.* (2019)
15. Litschke, T., et al.: Review on the reduction of urban particle concentration by vegetation. *Meteorologische Zeitschrift* **17**(3) (2008)
16. Mori, J., et al.: Air pollution mitigation by urban greening, review n.34. *Italus Hortus* **25**(1), 13–22 (2018)
17. Walmsley, A.: Greenways: multiplying and diversifying in the 21st century. *Landsc. Urban Plan.* **76**(1–4), pp. 252–290 (2006). ISSN 0169-2046. <https://doi.org/10.1016/j.landurbplan.2004.09.036>
18. Kumar, P., et al.: Quantifying particulate matter reduction and their deposition on the leaves of green infrastructure. *Environ. Pollut.* **265**, 114884 (2020)
19. Shaneyfelt, K., et al.: Air quality considerations for stormwater green street design. *Environ. Pollut.* **231**, 768–778, Part 1 (2017)

20. Gore, T., et al.: Green Infrastructure's contribution to economic growth: a review. Project Report. London, EFTEC (2013)
21. Leskinen, N., Vimpari, J., Junnila, S.: A review of the impact of green building certification on the cash flows and values of commercial propertie. *Sustainability* **12**, 2729 (2020). <https://doi.org/10.3390/su12072729>
22. Singh, P., et al.: Response of dust accumulation on roadside plant species due to open cast mining at Jhansi-Allahabad NH-76, Uttar Pradesh, India. *Spatiotemporal Var. Surf. Temp. Res. Artic. Landsc. Ecol.*, **25**, 17–33 (2017)
23. Yanmei, L., et al.: Potential of thirteen Urban Greening Plants to capture particule matter on leaf surfaces across three levels of ambient atmospheric pollution. *Int. J. Environ. Res. Public Health* **16**, 402 (2019)
24. Martins, M.: Infraestruturas Verdes – Impacto em Meio Urbano, Escola de Engenharia da Universidade do Minho, Portugal (2021)
25. Favarin, J., et al.: Equações para a estimativa do índice de área foliar do cafeiro, Brasília, 2002. Ong B., - Green plot ratio: an ecological measure for architecture and urban planning. *Landsc. Urban Plan.* **63**, 197–211 (2003)



Reference Levels for Heavy Metals in Soil in the City of Cerro de Pasco - Peru - 2020

Heiner Saldaña¹(✉), Cesar Muñoz¹, Doris Esenarro^{1,2,3}, Ciro Rodriguez^{1,2}, and Pedro Amaya^{1,2}

¹ National University Federico Villarreal, Lima, Peru

{2009237448, cmunoz, crodriguez, pamaya}@unfv.edu.pe,
doris.esenarro@urp.edu.pe

² Instituto Especializado de Investigación de Ecosistemas y Recursos Naturales, Lima, Peru

³ Ricardo Palma University URP, Lima, Peru

Abstract. This research focuses on determining the reference levels for aluminum, barium, chromium, copper, manganese, lead and zinc were determined in the soils surrounding the city of Cerro de Pasco, considering the background levels of these metals and the physicochemical properties of the soil. The study area had an extension of 3201 ha of land, performing a simple random statistical sampling, obtaining 21 composite samples from 63 simple and superficial samples (0–30 cm deep), where the total concentrations of heavy metals are correlated with the physicochemical parameters of the soil. From the results, there is a correlation coefficient greater than 0.7 with respect to the cation exchange capacity (C.E.C.), organic matter (OM) and pH, for almost all the metals evaluated, except for chromium, manganese and lead. As a result of this correlation, linear equations were generated from CIC, OM and pH, to define the reference levels of aluminum (24439 mg/kg), barium (161 mg/kg), copper (29 mg/kg) and zinc (552mg/kg). kg), considering UCL95 as the background level since it presented a better statistical fit with respect to the descriptive statistics. However, the expression $NR = \bar{X} + nDE$ was used to establish the reference levels of chromium (26 mg/kg), manganese (966 mg/kg) and lead (62 mg/kg), because they did not show a correlation with the physicochemical properties of the soil.

Keywords: Background levels · Reference levels · Heavy metals · UCL95

1 Introduction

Contamination by heavy metals in the soil is one of several countries' significant problems in the world [1]. Also, due to their toxic, mobile, and cumulative nature, they interact with the soil's edaphic properties, which in some cases facilitate their entry into the trophic chain, water bodies, crops, and even affect people's health [2]. The contribution of heavy metals in the soil is due to natural sources, such as volcanic eruptions, geysers, thermal waters, and adaptogenic processes and weathering of the parent material; as well as anthropic sources linked to industrial activities (mining, chemical industry, hydrocarbons, etc.) [3]. Given this, some developed countries such as Germany,

the United States, Switzerland, among others, have established reference levels for heavy metals in soil with normative rank to obtain better management in this resource's planning and environmental management.

Likewise, it is necessary to define the total concentrations of heavy metals in a given place with little or no anthropic intervention (background levels) for each edaphological region; and, based on this, to establish reference levels for each geographic zone [4]. These values were determined based on the soil's physicochemical properties, such as clay and organic matter content in the Netherlands' case. The USA elaborated the Soil Screening Guidance, including a methodology to assess the risk and screening levels for contaminants in soils. In Spain, criteria for declaring a soil contaminated were established through the Spanish Royal Decree 9/2005 as well as reference values; which are determined from the sum of the average concentration plus twice the standard deviation of the existing concentrations in soils of nearby non-contaminated areas, with similar geological substrates [5].

Peru has currently established Environmental Quality Standards (EQS) for Soil for the three (03) land uses Agricultural, Residential/Parks, and Commercial/Industrial/Extractive [5]; however, it does not have a properly-established methodology to determine reference levels for heavy metals in soil. That is why the present research aims to reference these reference levels by applying statistical methods that involve the background levels of heavy metals and the physicochemical parameters of the soil that influence the behavior of these heavy metals in each geographic space. These reference levels would complement the current environmental regulations (ECA Soils) for heavy metals, considering the national territory's prevailing natural conditions.

2 Materials and Method

2.1 Study Area

The study area is located in the district of Simón Bolívar, province and department of Pasco, comprising the upper part of the San Juan River sub-basin, as part of the Mantaro river basin. Specifically, it is located west of the Cerro de Pasco U.E.A. at an altitude of 4200 m and covering 3201.6 ha. It has UTM Datum WGS-84 coordinates E:354925 m and N: 8819917 m, as well as geographic coordinates Long: $-76^{\circ} 19' 35.1''$ and Lat: $-10^{\circ} 40' 5.76''$ (Fig. 1).

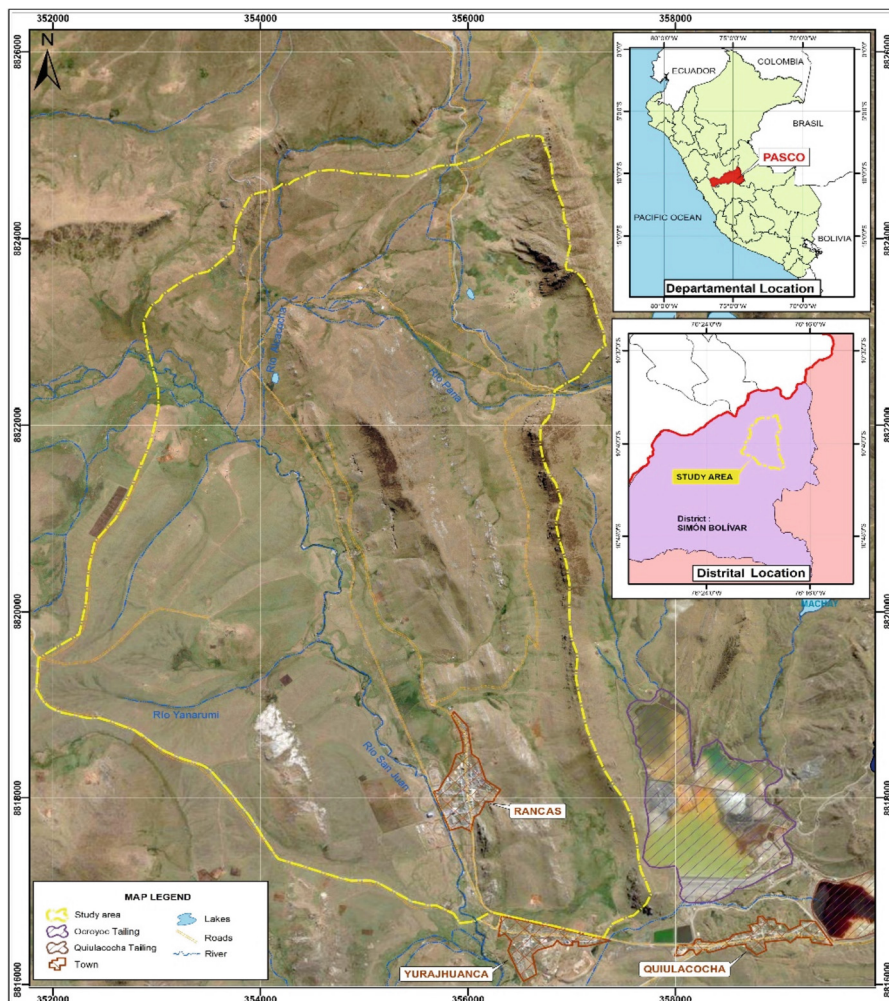


Fig. 1. Location of the study area.

2.2 Geology

Cerro de Pasco's city is located on the northern limit of the Inter-Andean Highlands, which separates the Western Cordillera from the Eastern Cordillera, characterized by the predominant polymetallic mining activity, such as the Cerro de Pasco, Colquijirca, and Quicay mines [6]. The Inter-Andean Valleys and the Plains are characterized by fine clastic materials resulting from the Eastern and Western Cordilleras' fluvioglacial erosion processes. The study area is characterized by these plains and part of the Eastern Cordillera's western edge due to the notorious elevations and lithic outcrops representing them.

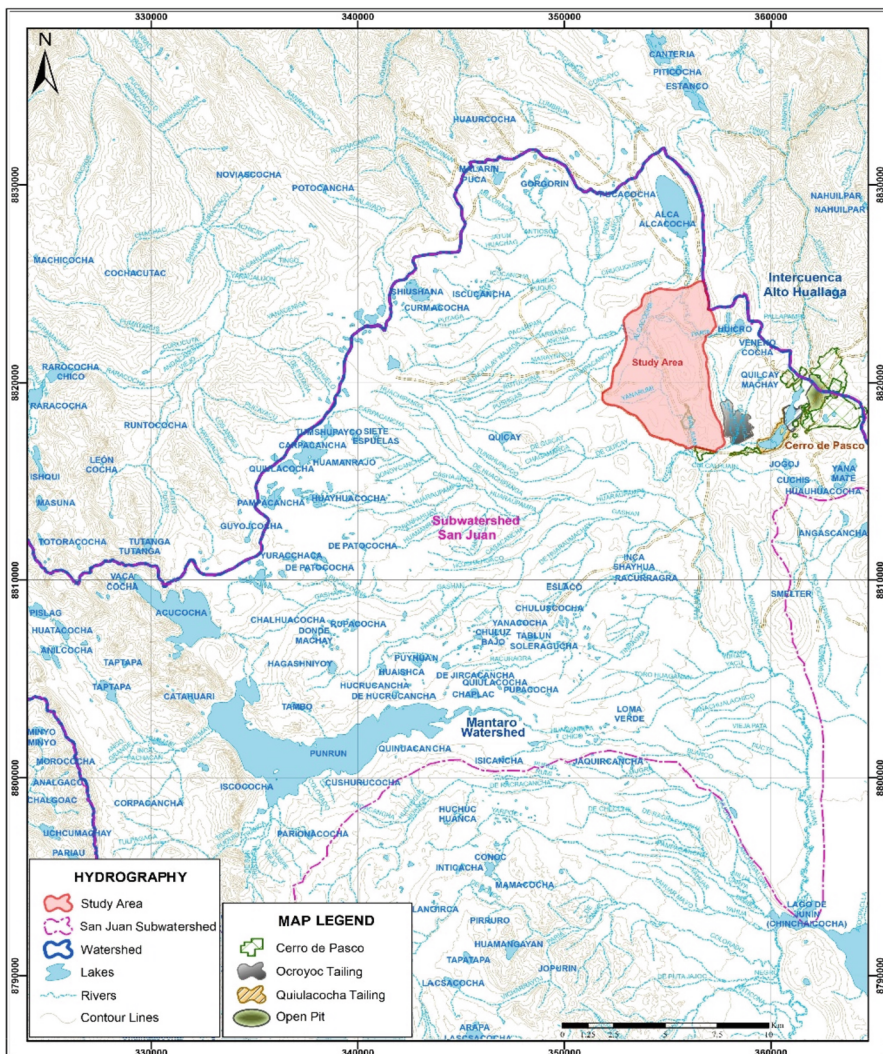


Fig. 2. Location of the study area.

As shown in Fig. 2, the San Juan River sub-basin has an area of $1,171 \text{ km}^2$ and an altitude of 4,190 m, where the river of the same name flows with an average flow of $10 \text{ m}^3/\text{s}$ and a length of 36 km in a southeasterly direction to the Junín (or Chinchaycocha) lagoon, which is the source of the Mantaro River. It also borders the Perene river basin to the east, the Upper Huallaga River basin to the north, the Huaura river basin to the west, and the south's Mantaro river.

2.3 Materials

For the survey of the location of the area, ARGIS 10.4 and Google Earth Pro software was used; statistical software was used for the analysis; Garmin 64s GPS, a plastic container for the laboratory sample, shovel, pickaxe, dense polyethylene bags, technical sheets, and a camera were used to collect soil samples.

2.4 Methodology

Field sampling work was carried out on October 19, 20, and 21, 2019, considering the location and soil sampling pattern established in the cabinet. For this purpose, 21 composite samples were taken from a total of 63 surface-level and straightforward samples, being this representative within the study area and at a depth between 0–30 cm. For the soil sampling procedure, the first stage began with identifying the proposed points with GPS help, which were defined in the field, considering the terrain conditions (vegetation cover, lithic outcrops, wetlands, steep slopes, among others). However, in areas where conditions were not favorable, the sampling points were relocated.



Fig. 3. Field identification of soil sampling points and vegetation cover clearing.

As shown in Fig. 3, once the point was identified on the ground, the vegetation cover was cleared (in most of the sampling points) using shovels and pickaxes without affecting these species for subsequent insertion; then, a survey of dimensions 0.30 m (length) \times 0.30 m (width) \times 0.30 m (depth) was carried out. At the end of the study with the planned dimensions, the data sheets were filled out with the data from the sampling point (date, time, point code, and UTM WGS-84 coordinates). Subsequently, the soil characteristics were described. The sampling sheet was filled out with the features of the environment, as shown in Fig. 4 [7].

A shovel was used to take the soil sample, the samples from three (03) sampling points were placed in a plastic container to carry out the process of quartering the sample, obtaining one (01) composite soil sample of approximately 1 kg for the analysis of heavy metals, as well as one (01) duplicate sample for the study of the physico-chemical parameters of the soil. The composite samples and their respective duplicates were packed and duly labeled with the field data (date, time, code, and UTM WGS-84 coordinates). Subsequently, the chain of custody of the samples taken was filled out.



Fig. 4. Description of the sampling point, Packing, and labeling of the soil sample.

3 Results

3.1 Concentrations of Heavy Metals in Soil

A total of twenty-one (21) composite soil samples representative of the study area were considered, from which the total concentrations of aluminum, barium, chromium, copper, manganese, lead, and zinc was obtained, as detailed in Table 3, where we can see that the concentrations of heavy metals are given from highest to lowest by aluminum, followed by manganese, barium, zinc, lead, chromium, and copper, according to the averages of each one.

Aluminum presented higher concentrations at sampling points M-07, M-17, M-18, M-19, and M-21, which are located in the western part of the study area, and the soils are characterized by a sandy-clay loam texture and, to a lesser extent, sandy loam soils, with a conglomerate matrix composed of gravels with subrounded limestone clasts [8].

Manganese presented high concentrations in sampling points M-01, M-02, M-03, M-13, M-23, and M-24; associated with soils with a clay loam-sandy loam texture in their totality and given the conditions of these plots could present a more significant mobilization in the grounds. Likewise, the predominant geological contribution can be attributed to the Pucará Group (western zone) formed by massive dolomites or stratified chert.

Concerning barium, high concentrations were recorded at sampling points M-07, M-17, M-18, M-19, M-21, and M-22; associated with soils with a sandy clay loam texture and, to a lesser extent, with clay loam soils, in addition to presenting a conglomerate matrix composed of gravels with subrounded clasts typical of the Jeroc formation. These concentrations are directly proportional to the attention of aluminum recorded in the same plots.

According to laboratory results, zinc recorded high concentrations in sampling points M-17, M-18, M-19, M-21, and M-22, associated with soils with a clay loam-sandy texture. These concentrations are also directly proportional to barium and aluminum's attention since they present the same matrix [9].

Lead presented the highest concentrations at sampling points M-02, M-04, M-06, M-15, M-16, M-19, M-21, and M-24; associated with loamy-clay-sandy texture and,

to a lesser extent, with loam soils. According to their location, they are related to low slope areas and are characterized by a matrix resulting from the combination of alluvial and fluvioglacial processes that characterize this sector of the study area. Chromium registered high concentrations at sampling points M-15, M-22, and M-23, associated with soils with a sandy-clay loam texture and, to a lesser extent, sandy loam soils. Due to their location, they do not present a uniform distribution, given the geological predominance of the Pucará Group (western zone) formed by massive dolomites and limestones of gray and brown colors in thick strata alluvial and fluvioglacial deposits.

The results obtained indicate that not all heavy metals are highly correlated with each other with a high significance ($P < 0.01$) as in the case of the pairs of elements Zn-Al ($r = 0.686$), Zn-Ba ($r = 0.710$), Zn-Cu ($r = 0.726$), Ba-Al ($r = 0.810$), Cu-Al ($r = 0.652$) and Cu-Ba ($r = 0.760$), which could indicate that the increase in the content of one metal would be related to the rise in the other metals and thus present an expected behavior or come from similar sources. Furthermore, the soils present are under development, as in plot M-23, which reported high concentrations of manganese and chromium [10].

3.2 Normality Test – Shapiro Wilkinson Test

To determine whether the contents of the physicochemical parameters present a normal distribution, the Shapiro-Wilkinson Test ($n < 50$) was applied, the results of which are detailed in Table 1.

Table 1. Shapiro-Wilkinson test for the physicochemical properties of the soil

Variables	Asymmetry	Kurtosis	Statistical	Nº samples	P*	Distribution
Sand	-0,144	-0,570	0,955	21	0,424	Normal
Silt	0,272	-0,595	0,944	21	0,259	Normal
Clay	0,144	-0,748	0,962	21	0,565	Normal
pH	-0,012	-1,536	0,909	21	0,052	Normal
C.E	1,193	0,713	0,838	21	0,003	Not normal
C.I.C	0,442	-1,268	0,899	21	0,033	Not normal
M.O	0,863	-0,558	0,872	21	0,011	Not normal
Phosphorus	1,733	3,881	0,812	21	0,001	Not normal
Potassium	3,437	13,621	0,595	21	0,000	Not normal

From Table 1, it can be observed that the high values of asymmetry and kurtosis belong to potassium, phosphorus, electrical conductivity, organic matter, and cation exchange capacity (from highest to lowest), which denotes a non-normal distribution due to the heterogeneity of the values, as well as the presence of discordant values. The factor analysis can also be used to explain the relationships between the physicochemical properties of the soil, where the principal components that define the percentage of the variance of each of them are identified.

Table 2. Factor analysis for the physicochemical properties of the soil

Variables	Principal components		
	Component 1	Component 2	Component 3
C.E	0,905	-0,012	0,088
pH	0,898	0,024	-0,271
C.I.C	0,877	0,228	0,304
M.O	0,853	0,148	0,342
Phosphorus	-0,670	0,028	0,236
Clay	0,074	0,938	0,303
Sand	-0,078	-0,915	0,384
Silt	0,013	0,044	-0,950
Potassium	-0,017	-0,009	-0,309
Eigenvalue	3,717	1,696	1,550
Explained variance	41,3%	18,8%	17,2%

Table 2 shows that 77.3% of the variance can be explained by three principal components (Component 1, Component 2, and Component 3) since the eigenvalues greater than one is taken. Although this leads to a loss of explanatory power, it is not significant [11].

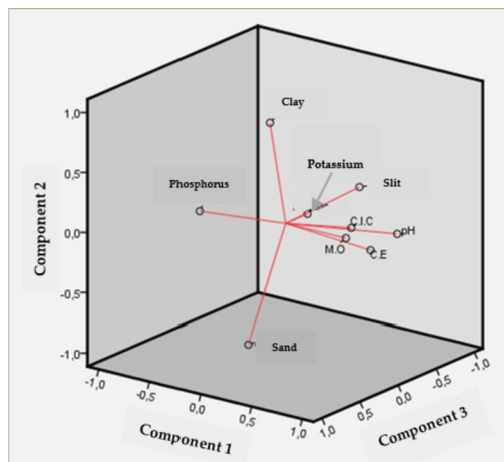
**Fig. 5.** Principal components in rotated space.

Figure 5 shows the graphic representation of the different components identified, where we can observe that Component 1 explains 41.3% of the variance, which is made up of the E.C., pH, C.I.C., and M.O.; Component 2 explains 18.8% of the conflict, which includes the clay content, which has a positive influence, M.O.; Component 2 explains 18.8% of the competition, which consists of the clay content that has a positive impact and the sand content that has a negative influence. Component 3 explains 17.2% of the

variance, which is negatively influenced by the silt content and, to a lesser extent, by potassium.

The pH presented a highly significant correlation ($P < 0.01$) with aluminum, barium, copper, and zinc; however, manganese showed a significant negative correlation ($P < 0.05$). The high correlation coefficients ($r > 0.500$) indicate the remarkable variability of pH in the soils of the study area that leads to the passage of heavy metals in soluble forms to insoluble forms with increasing pH [12]. Also, the pH ranges obtained in the study area (4.26–6.7) are acidic due to the high precipitation that originates intense chemical alteration processes and the washing of bases in the mountainous regions, and the mineralogical characteristics of the predominant material [13].

The E.C. presents a highly significant correlation ($P < 0.01$) with aluminum, barium, copper, and zinc, where their correlation coefficients demonstrate high values, followed by manganese which presented a significant correlation ($P < 0.05$). This means that soil salinity could influence these metals' dynamics, where their transfer to other environmental compartments would not be favored, and their total contents in the soil would not decrease [14]. The C.I.C. is related to the M.O. contents and presents a highly significant correlation ($P < 0.01$) with aluminum, barium, copper, and zinc, where their correlation coefficients offer high values. However, manganese and copper did not present correlations with this element, indicating that cation exchange processes would not entirely regulate their concentrations in the soil.

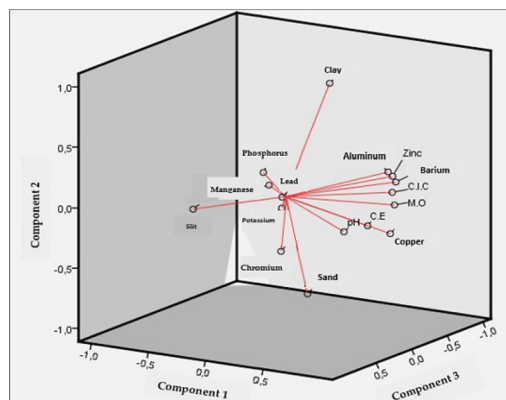


Fig. 6. Principal components in rotated space.

Figure 6, the graphical representation of the principal components for total heavy metal contents and soil physicochemical parameters.

3.3 Linear Regression Lines

To determine which soil physicochemical properties influence the total heavy metal contents in the grounds surrounding the city of Cerro de Pasco, linear regression lines are applied considering the regression coefficients (R) and coefficients of determination (R^2). To determine if these independent variables (physicochemical properties of the soil) explain the behavior of heavy metals due to their degree of correlation.

For this purpose, all variables are considered in the analysis, and those that did not reach a normal distribution have been considered in their logarithmic transformation until reaching normality; such is the case of aluminum (Log-Al), copper (Log-Cu), E.C. (Log-C.E.), C.I.C. (Log-CIC), M.O. (Log-M.O.) and phosphorus (Log-P). In addition, those variables that had a normal distribution with the elimination of discordant values, such as chromium and potassium, were included in the analysis.

Manganese presents a significant negative correlation ($P < 0.05$) with the contents of M.O. and pH, without prejudice, that their correlation coefficients are low; nevertheless, their relationship indicates that these variables would not contribute or explain directly on their total contents in the soil, but in the decrease due to their negative relationship, as well as their variability in the soil that would be influenced and/or explained by other variables.

This expression was applied for the total chromium, manganese, and lead contents for this research since they did not present a statistically significant correlation with the physicochemical properties. Likewise, Table 3 shows the linear equations for each of the heavy metals estimated in the study area and the reference levels calculated from these, for which a standard soil has been defined with mean values for M.O. of 5%, pH of 5, and C.I.C. of 24 meq/100g according to the sampling carried out [15].

At the same time, a second equation was generated in which the values obtained from the UCL95 calculation were considered as a background level since it is a statistically robust value according to the distribution of heavy metals. From the results obtained, the values obtained from the UCL95 calculation are proposed as reference levels as the background level, since they present a better adjustment according to the statistical distribution of heavy metal concentrations in the soil of the study area, as well as the contribution and/or influence of the physicochemical properties of the soil.

It should be noted that the methodology used assumes a standard soil that represents the entire population of the study area or is representative [17], which also leads to a difficulty in making an approximation that involves all the relevant physicochemical properties of the soil, given their relationship with heavy metals and the variety of factors that may intervene in the soil. However, it represents an advantage to determine specific reference levels, where similar conditions and/or similarities in the predominance of soil physicochemical properties are present.

Table 3. Proposed reference levels for heavy metals

Total metals	Level of background		Linear equations	Reference level (mg/kg)
	Method	Value (mg/kg)		
Aluminum	Descriptive Statistics	19982	$19\ 982 + 0,23\ CIC + 0,15\ MO + 0,1\ pH$	19989
	UCL95	24432	$24\ 432 + 0,23\ CIC + 0,15\ MO + 0,1\ pH$	24439
Barium	Descriptive Statistics	69	$69 + 0,5\ CIC + 0,39\ MO + 0,23\ pH$	84
	UCL95	146	$146 + 0,5\ CIC + 0,39\ MO + 0,23\ pH$	161
Chromium ^a	Descriptive Statistics	17	$17 + 2\ DE$	24
	UCL95	19 ^b	$19 + 2\ DE$	26
Copper	Descriptive Statistics	13	$13 + 0,31\ CIC + 0,29\ MO + 0,19\ pH$	23
	UCL95	19 ^b	$19 + 0,31\ CIC + 0,29\ MO + 0,19\ pH$	29
Manganese ^a	Descriptive Statistics	405	$405 + 2\ DE$	877
	UCL95	494	$494 + 2\ DE$	966
Lead ^a	Descriptive Statistics	36	$36 + 2\ DE$	58
	UCL95	40	$40 + 2\ DE$	62
Zinc	Descriptive Statistics	81	$81 + 15,97\ CIC + 9,97\ MO + 5,6\ pH$	542
	UCL95	91	$91 + 15,97\ CIC + 9,97\ MO + 5,6\ pH$	552

Note. The proposed linear equations to determine the Reference Levels of heavy metals in the study area adjacent to the city of Cerro de Pasco.

For this element, the expression $NR = \bar{X} + nDE$ at 95% of the data population was considered, where DE: Standard deviation and \bar{X} : Background Level.

^bUCL95 calculated without discordant values.

There is lithological variety in the study area. Therefore, the method could be applied by structuring the data according to geology. The results are explicitly expressed for each lithological unit present. Annex 5 shows the spatial distribution of the total contents of the heavy metals evaluated in the study area in contrast to the reference levels obtained for each of them [16] (Fig. 7).

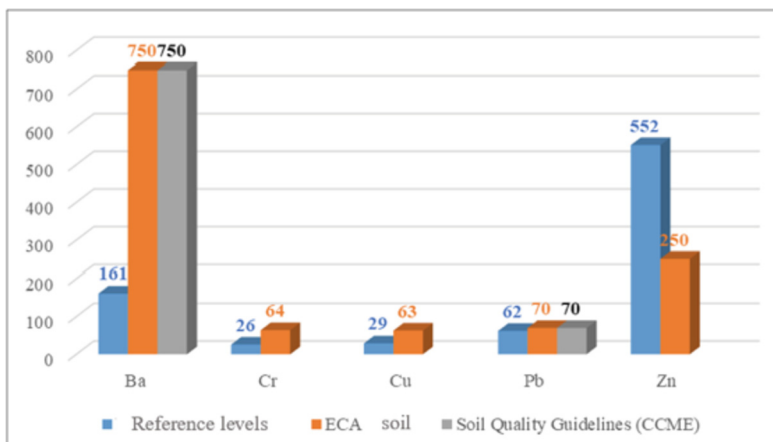


Fig. 7. Reference levels and environmental quality standards.

Comparison of the Reference Levels obtained in this research and their comparison with the Soil ECA (national) and the Soil Quality Guidelines of Canada (international); both in the Agricultural Use category.

4 Discussion

The total aluminum, barium, chromium, copper, manganese, lead, and zinc concentrations were subjected to statistical treatment. The entire contents of chromium and copper presented discordant values, indicating a more significant variability in their spatial distribution in the soil.

Conflicting values were determined for the total contents of copper, chromium, and lead in the soil, which Copper presented background levels of 13 and 19 mg/kg calculated through descriptive statistical parameters and the UCL95, respectively, which are lower than those proposed by OEFA, where a value of 33.21 mg/kg was obtained for soils of the Regosol dístrico - Cambisol dístrico type, based on the calculation of the UCL95.

Background levels for this metal are postulated between 22.97 and 20.25 mg/kg for topsoil and subsoil [17], respectively, in the soils of the Ju region (China), which have been associated with traditional agricultural activities and have undergone a rapid transition to the development of industrial activities and are close to the results of Mirzaei [18], who determined background levels for copper of 23.9 mg/kg for the soils of Golestan province (Iran). Likewise, Micó Llopis obtained a value of 21 mg/kg [19], and Dos Santos & Alleoni received weights of 39.4 and 47.9 mg/kg from aqua regia and EPA 3051 analytical methods. However, Quiroz Ramírez reported a background level for copper of 1.48 mg/kg, which is the lowest of the other authors. The study area corresponds to the Picuroyacu micro-watershed located in the Selva Alta region of Peru, where mineralization differs from the soils of the Andean region.

In the case of the Netherlands, a standard soil with 10% OM and 25% Micó Llopis clay was defined, where the linear equation method was applied, and reference levels

were obtained for chromium (100 mg/kg), zinc (140 mg/kg), copper (36 mg/kg) and lead (85 mg/kg) [19]. Likewise, the Basque Country also defined a standard soil with 5% OM and 30% clay (IHOBE, 1998), which through the method of the linear equation, determined the reference levels for zinc (106 mg/kg), chromium (53 mg/kg), copper (24 mg/kg) and lead (44 mg/kg). In both countries, the reference levels for copper and lead were close to the reference levels obtained in the present investigation, notwithstanding the predominance of the physicochemical properties of the soils evaluated in Holland and the Basque Country, which differ significantly concerning the grounds near the city of Cerro de Pasco.

On the other hand, Dos Santos & Alleoni proposed reference levels from the 75th percentile for cobalt (21.3 and 15 mg/kg), chromium (44.8 and 55.5 mg/kg), copper (20.6 and 24.7 mg/kg), nickel (2.1 and 10.3 mg/kg), lead (9 and 18.1 mg/kg) and zinc (3 to 20, 1 mg/kg) concerning the analytical methods EPA 3051 and by Agua Regia for the soils of Mato Grosso and Rondônia (Brazil) [20], having values close to the reference levels for chromium (24–26 mg/kg) and copper (23–29 mg/kg) determined in the present investigation. It is essential to consider that the geographical area of Mato Grosso and Rondônia corresponds to a tropical zone with acid soils of low fertility and low phosphorus availability. Quiroz Ramírez determined the reference levels for copper (3.28 mg/kg), lead (20.1 mg/kg), cadmium (20.1 mg/kg), and zinc (20.1 mg/kg) from descriptive statistical parameters; considering the expression $NR = \bar{X} + 2DE$ (95% of the data population) where \bar{X} the background level and SD the standard deviation; since he did not obtain a significant correlation between clay and M.O. contents about his study area [22].

5 Conclusions

The background levels were determined from the descriptive statistical parameters; considering the arithmetic mean for the total contents of chromium (17 mg/kg), manganese (405 mg/kg), lead (36 mg/kg), and zinc (81 mg/kg) because of their Normal distribution; the geometric mean for the total aluminum (19,982 mg/kg) and copper (13 mg/kg) contents due to their Log-Normal distribution; and, finally, the median only for barium (17 mg/kg) due to its high variability in the soil of the study area and its Non-Normal distribution. The UCL95 was calculated for each heavy metal according to its spatial distribution, where the values for chromium (19 mg/kg), copper (19 mg/kg), lead (40 mg/kg), and zinc (91 mg/kg) are slightly higher than the values calculated through the statistical parameters; while aluminum (24 432 mg/kg), barium (146 mg/kg) and manganese (494 mg/kg) registered significantly higher background level values.

The E.C. and C.I.C. presented a highly significant and positive correlation with the total contents of aluminum, barium, copper, and zinc; where the first would be conditioning the dynamics and transfer of heavy metals in the soil, and the second would regulate the cation exchange processes for these heavy metals. These results were corroborated by the Principal Component Analysis (PCA), which determined five components that explain 83.3% of the variance, where Component 1 explains 42.6% of this variance and is comprised of the contents of barium, copper, aluminum, zinc, pH, E.C., C.I.C., M.O., and phosphorus (the latter presented an inverse sense) where manganese is not included in this principal component.

The statistical correlations between the soil's physicochemical parameters and the total contents of heavy metals made it possible to define which edaphic properties have a significant contribution, influence, and condition the entire contents of aluminum, barium, chromium, copper, manganese, lead, and zinc. The individual contributions of C.I.C., M.O., and pH were obtained through the linear regression lines for each heavy metal evaluated in the soil, which presented a significant correlation that varies for each of their chromium, manganese, and lead. The M.O. showed a highly significant correlation ($P < 0.01$) with the contents of aluminum, barium, copper, and zinc; and to a lesser extent, a negative correlation with the contents of manganese; the same behavior occurs with the C.I.C., except that there is no significant correlation (null) with the contents of chromium, manganese, and lead. Finally, pH presented the same case as M.O. by offering a highly significant correlation ($P < 0.01$) with the contents of aluminum, barium, copper, and zinc.

The reference levels for heavy metals indicate the concentration allowed in the soil to consider it uncontaminated [21]. The linear equations generated from the mean values of C.I.C., M.O., and pH in the study area and the background levels coming from the descriptive statistics allowed calculating the reference levels for aluminum (19 989 mg/kg), barium (84 mg/kg), copper (23 mg/kg) and zinc (542 mg/kg); however, these concentrations were lower concerning the reference levels calculated for aluminum (24 439 mg/kg), barium (161 mg/kg), copper (29 mg/kg) and zinc (552 mg/kg) where UCL95 was considered as background level. In both cases, the equations generated think a standard soil that represents the entire population of the study area and presents the average contents of the physicochemical properties of the soil used for its formulation (C.I.C.M.O. and pH); these approximations being more realistic.

However, for chromium, manganese, and lead, reference levels were not established from the C.I.C., M.O., and pH since the linear regression lines did not show a statistically significant correlation; given this, the expression $NR = \bar{X} + nDE$ was considered to establish the reference levels for chromium (24 mg/kg), manganese (877 mg/kg) and lead (58 mg/kg), considering as background level (\bar{X}) the descriptive statistics, whose values were lower concerning the reference levels for chromium (26 mg/kg), manganese (966 mg/kg) and lead (62 mg/kg), where UCL95 was considered as background level (\bar{X}). The variation therefore, in these concentrations is due to the calculation of background levels, whose values will depend on the statistical distribution presented by the attention of heavy metals. Finally, the reference levels calculated in the present investigation represent soils adjacent to the city of Cerro de Pasco, which allow defining contaminated soils resulting from mining activities dating back to 1902 and representing risks to health or the environment.

References

1. Wei, J., et al.: The levels, sources, and spatial distribution of heavy metals in soils from the drinking water sources of Beijing, China. *Sustainability* **13**(7), 3719 (2021)
2. He, L., Gao, B., Luo, X., Jiao, J., Qin, H., Zhang, C., et al.: Health risk assessment of heavy metals in surface water near a uranium tailing pond in Jiangxi Province, South China. *Sustainability* **10**(4), 1113 (2018)

3. Xu, Y., Shi, H., Fei, Y., Wang, C., Mo, L., Shu, M.: Identification of soil heavy metal sources in a large-scale area affected by industry. *Sustainability* **13**(2), 511 (2021)
4. Tang, J., Chai, L., Li, H., Yang, Z., Yang, W.: A 10-year statistical analysis of heavy metals in river and sediment in hengyang segment, Xiangjiang river Basin, China. *Sustainability* **10**(4), 1057 (2018)
5. Quero Jiménez, P.C., Velazco, M.Z., Fernández, S.M.: Determinación de la contaminación por metales pesados en suelos aledaños a la empresa electroquímica de agua. *Cent Azucar* **44**(3), 53–62 (2017)
6. Yu, G., Wang, X., Liu, J., Jiang, P., You, S., Ding, N., et al.: Applications of nanomaterials for heavy metal removal from water and soil: a review. *Sustainability* **13**(2), 713 (2021)
7. MINAM. Estándares de Calidad Ambiental (ECA) para Suelo. SINIA, Peru (2017)
8. Luján Soto, R., Cuéllar Padilla, M., de Vente, J.: Participatory selection of soil quality indicators for monitoring the impacts of regenerative agriculture on ecosystem services. *Ecosyst. Serv.* **45**, 101157 (2020)
9. Muñoz-Rojas, M.: Soil quality indicators: critical tools in ecosystem restoration. *Curr. Opin. Environ. Sci. Health* **5**, 47–52 (2018)
10. Guo, Y., Abdalla, M., Espenberg, M., Hastings, A., Hallett, P., Smith, P.: A systematic analysis and review of the impacts of afforestation on soil quality indicators as modified by climate zone, forest type, and age. *Sci. Total Environ.* **757**, 143824 (2021)
11. Lan, T., Guo, S.-W., Han, J.-W., Yang, Y.-L., Zhang, K., Zhang, Q., et al.: Evaluation of physical properties of typical urban green space soils in Binhai area, Tianjin, China. *Urban Urban Green.* **44**, 126430 (2019)
12. Robin, P., Morel, C., Vial, F., Landrain, B., Toudic, A., Li, Y., et al.: Effect of three types of exogenous organic carbon on soil organic matter and physical properties of a sandy technosol. *Sustainability* **10**(4), 1146 (2018)
13. Calderón Medina, C.L., Bautista Mantilla, G.P., Rojas, G.S.: Propiedades químicas, físicas y biológicas del suelo, indicadores del estado de diferentes ecosistemas en una terraza alta del departamento del Meta. *Orinoquia* **22**(2), 141–157 (2018)
14. Xiang, H., Guo, L., Zhang, J., Zhao, B., Wei, H.: In situ earthworm breeding to improve soil aggregation, chemical properties, and enzyme activity in papayas. *Sustainability* **10**(4), 1193 (2018)
15. Poccard-Chapuis, R., et al.: Mapping land suitability to guide landscape restoration in the Amazon. *Land* **10**(4), 368 (2021)
16. Xiang, M., Li, Y., Yang, J., Lei, K., Li, Y., Li, F., et al.: Heavy metal contamination risk assessment and correlation analysis of heavy metal contents in soil and crops. *Environ. Pollut.* **278**, 116911 (2021)
17. Guzman Morales, A., Cruz La Paz, O., Valdes Carmenate, R.: Effects of the pollution by heavy metals in a soil with agricultural use. *Cienc. Téc. Agropecu.* **28**(1), 1–9 (2019)
18. Pacheco, F.A.L.: Sustainable Use of Soils and Water: The Role of Environmental Land Use Conflicts. *Sustainability* **12**(3), 1163 (2020)
19. Niemiec, M., Chowaniak, M., Sikora, J., Szeląg-Sikora, A., Gródek-Szostak, Z., Komorowska, M.: Selected properties of soils for long-term use in organic farming. *Sustainability* **12**(6), 2509 (2020)
20. Oliveira, E., Tobias, S., Hersperger, A.M.: Can strategic spatial planning contribute to land degradation reduction in urban regions? State of the art and future research. *Sustainability* **10**(4), 949 (2018)
21. Martínez, S.: Niveles de fondo y de referencia de metales pesados en suelos desarrollados de material parental volcánico, metamórfico y sedimentario en la Región de Murcia. [Tesis doctoral, Universidad Politécnica de Cartagena], no. 1, pp. 12–13 (2009)
22. Saldaña, H.: Niveles de referencia para metales pesados en el suelo - Cerro de Pasco. Universidad Nacional Federico Villarreal (2020)



Urban Environmental Risk Spatial Pattern Assessment Supported by Remote Sensing and GIS—Shanghai, China

Qianqian Yang^(✉) and Yishao Shi

College of Surveying and Geo-Informatics, Tongji University, Shanghai 200092, China
yangqianqian@tongji.edu.cn

Abstract. With the economic development, the environmental problem has become a global problem affecting the sustainable development of human beings. Starting from the urban scale, this paper comprehensively selects the spatial factors that can represent urban economic development, human production and life, industrial distribution, natural habitat, land cover and other factors that affect environmental change. These spatial impact factors are distance to the Shanghai city center, distance to the district centers, distance to national level development zones, distance to municipal development zone, distance to forests, land surface temperature, refers to ambient air particles with a diameter of 2.5μ or less and average building floor area ratio. The environmental risk in Shanghai is evaluated by criteria importance though intermarriage correlation method, and the range of environmental risk assessment score is [0, 1], the higher the score is, the higher the environmental risk is. In order to further intuitively identify the areas requiring management and restoration of urban environmental risks, we divided the environmental risk score into the 4 levels (I, II, III and IV) of environmental risk. Shanghai environmental risk assessment results show that: the spatial pattern of environmental risk in Shanghai presents from downtown to suburban area. The regions with environmental risk management level I and II are mainly concentrated in Chongming, so it only needs to continue to maintain and does not need to invest large manpower and financial resources for restoration and protection. Generally speaking, the areas with environmental risk management level IV are mainly concentrated in the downtown, Baoshan, Jiading and Minhang, the environmental risk supervision of these areas should be strengthened.

Keywords: Environmental risk assessment · Criteria importance though intermarriage correlation · Spatial patterns analysis

1 Introduction

Environmental risk refers to the potential threats to the environments, human health and socioeconomic development caused by risk factors that can be transmitted through various media [1]. ER can also be expressed as the uncertainties in the consequences of environmental events, and the damage degree of environmental accidents [2]. With the

acceleration of industrialization and urbanization, land-use change has led to degradation in ecosystems and natural environments [3]. The industrial and domestic waste also produces potential environmental risks that may threaten the sustainable urban development [4].

The environmental risks have been studied during the past 20 years, and the topics can be grouped into three categories. 1) the assessment environmental risks caused by hazardous materials and chemicals, 2) the assessment environmental risks caused by pollution accidents, and 3) the spatial assessment of regional/urban environmental risks. The fist category studies several aspects such as the uncertainties in caused by chemicals [5], ant the environmental risks on water and aquatic life, the environmental risks caused by waste waters [6]. The assessment of toxicological risk [7] and the human health risk [8] has also been performed in recent years. The second category identifies the environmental risks caused by human activities and pollution accidents such as Chernobyl and Fukushima [9]. The third category evaluates regional environmental risks associated with risk sources, risk receptors, and risk retardation for macro perspective [10], offering possible counter-measures that could eliminate the regional environmental risks accompanied by the rapid industrialization and urbanization.

Despite of the progress in regional environmental risk studies, efforts should be made to improve the assessment considering physical and socioeconomic driving forces. Also, the environments ear substantially affected by global change. Problem concerning environmental risks can be raised as: how to objectively parameterize the models in assessing the spatial patterns of regional environmental risks.

While analytical hierarchy process [11] and the expert evaluation method [12] substantially can well address environmental risk without the prior knowledge of environmental risk levels, they could lead to the subjective model parameterized that influences the credibility of the evaluation results. In contrast, criteria importance though inter-criteria correlation (CRITIC) is an objective assessment method [13] to derive the information from original datasets. Meanwhile, the use of GIS facilitates the spatial visualization of environmental risk assessment and geospatially quantitative analysis of environment risk patterns [14], providing intuitive and quantitative understanding of the regional environmental risks.

To address the key issues, we assessed the regional environmental risk patterns in Shanghai city of eastern coast in China. Specifically we proposed a CRITIC-based method to assess the Shanghai's environmental risk, and we divided the environmental risk scores into 8 levels to recognize the state of the environmental risk in the 30 m * 30 m grid. The assessment model was constructed based the distance to Shanghai's city center (*DSCC*) and district centers (*DDC*), the distance to national level development zones (*DNLDZ*), municipal development zones (*DMDZ*), and forests (*DF*), the land surface temperature (*LST*), the *PM2.5* levels in the air (*PM2.5*) and the average building floor area ratio (*ABFAR*). These influencing factors reflect the the human activities, the socioeconomic development, the state of environment and the land coverage. Subsequent paragraphs, however, are indented.

2 Materials and Methodology

2.1 Procedure

We synthetically utilized raw datasets (including administrative maps, development zones planning map, vector data of land use, Landsat images PM2.5 map and vector data of building), criteria importance through intermarriage correlation (CRITIC) method and spatial overlay to assess the environmental risk of Shanghai in 2020 (see Fig. 1). spatial factors (including *DSCC*, *DDC*, *DNLDZ*, *DMDZ*, *DF*, *LST*, *PM2.5* and *ABFAR*) that impact the environmental risk of Shanghai were abstracted by administrative maps, development zones planning map and *PM2.5* map (2020), while used Landsat image to compute the land surface temperature. And the vector data of land use and building were used to extract the spatial factors of *DF* and *ABFAR*, respectively. The results of the eight spatial factors for CRITIC were used as input data to capture the ER spatial patterns of Shanghai in 2020.

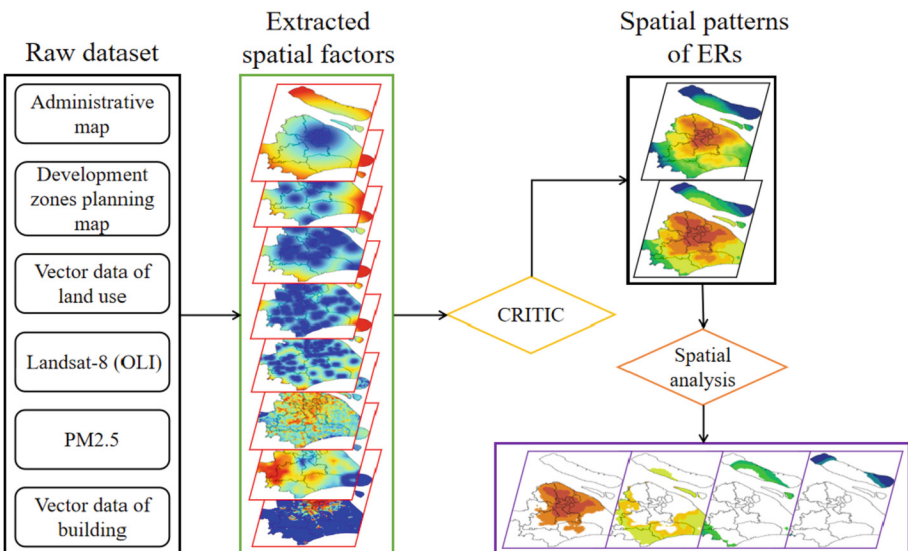


Fig. 1. Workflow of this study.

2.2 Study Area

Shanghai is located in the West Bank of Pacific, the central point on north and south coasts of China, the estuary of the Yangtze River. The city is bounded by $120^{\circ}52'$ to $122^{\circ}12'$ east longitude and $30^{\circ}41'$ to $31^{\circ}53'$ north latitude (see Fig. 2a). And the city covers $6,340.5 \text{ km}^2$, and consists of 7 central districts (A.Yangpu, B.Hongkou, C.Jin'an, D.Putuo, E.Changning, F.Xuhui, G.Huangpu) and 9 non-central districts (Chongming, Baoshan, Jiading, Qingpu, Songjiang, Minhang, Pudong, Jinshan, Fengxian) (see Fig. 2b). The central districts and non-central districts area is 290 km^2 and

6050.5 km², accounting for 4.57%, 95.43%, respectively [15]. It is reported that in 2020, Shanghai's GDP reached 3.87058 trillion yuan, ranking sixth among cities in the world, and third in the global financial center index (Government 2021), and the per capita disposable income of the city's residents reached 72,000 yuan [15]. In 2020, the population of permanent residents in Shanghai reached 24.8709 million. Compared with 16.09 million in 2000, the growth rate of permanent residents in Shanghai was 54.57% in 20 years [15]. In addition, the average permanent population density in the central urban area has reached 23,070/km² [15]. With the increase of economic activities and permanent population in Shanghai, the land use pattern changes rapidly, and the continuous expansion of urban development intensity poses a severe challenge to the ecological environment system. We chosen Shanghai as the study area for environmental risk pattern assessment to reduce a general evaluation method for evaluation environmental risk in developed cities in the world.

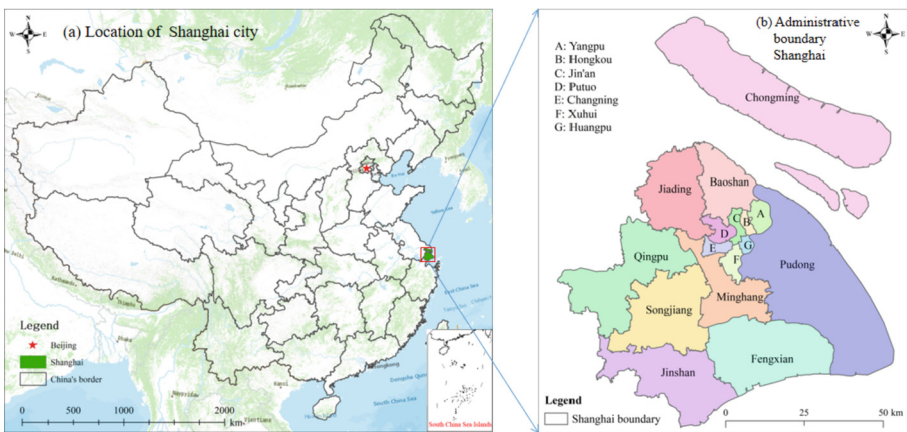


Fig. 2. Location and administrative boundary of Shanghai City, China

2.3 Original Datasets and Processing Method

In this study, we obtained the Shanghai administrative map to extract the administrative boundaries of Shanghai and the positions of the Shanghai municipal government and 16 district governments. The location of municipal government and district government represents the location of downtown Shanghai and each district center, respectively. The development zones planning map was used to extract the central location of development zone of different levels (national level development zone, municipal development zone). Shanghai land use vector map was utilized to extract forest land and calculate the center of each forest area. Remote sensing image was used to retrieve land surface temperature. $PM_{2.5}$ image were directly downloaded from the website (Table 1). After clipping and extracting analysis, the $PM_{2.5}$ image of this research area are obtained. The building vector data includes base area of construction and the height of the construction. We use the height of the construction to calculate the number of construction floors, and

multiply base area of construction by the number of building floors to calculate the total area of each construction. We divided the city into different blocks by urban roads, and calculated the total area of construction on the each block. The average floor area ratio on each block is equal to the total area of construction divided by the area of the block (Table 1).

Table 1. Spatial graphics and satellite images vector datasets used in this research

Raw data	Type	Date	Description	Provider
Administrative map	Graphic	2020	The map of administrative boundary and location of municipal and districts governments	National Catalogue Service for Geographic Information (www.webmap.cn)
Development zones planning map	Graphic	2020	A vector map for the boundary and location of the national level development zones and municipal development zones	Shanghai Municipal Development & Reform Commission (fgw.sh.gov.cn)
Vector map of land use	Graphic	2020	A map production of the boundary of the forests	Shanghai Institute of land Resource survey (www.sigs.cn)
Landsat-8 (OLI)	Image	2020.7	A remote sensing image for inversion of land surface temperature	Open Spatial Data Sharing Project (ids.ceode.ac.cn)
PM2.5	Image	2020	PM2.5 data of Shanghai were extracted by using PM2.5 grid data products	Atmospheric Composition Analysis Group (fizz.phys.dal.ca/~atmos)
Vector data of building	Graphic	2020.1	A vector map of Shanghai's building floor area and number of building floors	Baidu map open platform (lbsyun.baidu.com)

We mainly selected the spatial factors that can represent the intensity of land use development, land cover state, human production and living concentration, urban development, natural ecological landscape and air condition to comprehensively evaluate

the environmental risk pattern in Shanghai. Distance to Shanghai city center and distance to district centers can represent the distribution of human production and life. Distance to national level development zones and distance to municipal development zones represent the concentrated distribution of urban industries. Distance to forest centers and PM2.5 spatial impact factor represent natural ecological landscape and urban air condition respectively. Land surface temperature and average floor area ratio represent urban spatial development intensity and land construction coverage respectively (Table 2). We selected the above eight spatial risk factors to comprehensively evaluate the environmental risk in Shanghai.

Table 2. Selected spatial factors of the environmental risk assessment in Shanghai

Acronym	Meaning	Purpose
<i>DSCC</i>	Distance to the Shanghai city center	Produce the distance to the Shanghai City center and evaluate its impact on the environments
<i>DDC</i>	Distance to the district centers	Produce the distances to the district centers and evaluate their impact on the environments
<i>DNLDZ</i>	Distance to national level development zones	Produce the distance to the national level development zones to assess its impact on the environments
<i>DMDZ</i>	Distance to municipal development zones	Open Spatial Data Sharing Project (ids.ceode.ac.cn)
<i>DF</i>	Distance to forests	Produce the distance to the forests and evaluate its impact on the environments
<i>LST</i>	Land surface temperature	Evaluate the land surface temperature's impact on the environments
<i>PM2.5</i>	Refers to ambient air particles with a diameter of 2.5 microns or less	Evaluate the <i>PM2.5</i> 's impact on the environments
<i>ABFAR</i>	Average building floor area ratio	Evaluate average building floor area ratio's impact on the environments

2.4 Spatial Factors for Environmental Risk Assessment

The spatial factors we selected were *DSCC*, *DDC*, *DNLDZ*, *DMDZ*, *DF*, *ABFAR*, *LST* and *PM2.5* (see Fig. 3) concentration to evaluate environmental risks in Shanghai. The spatial factor of *DSCC* and *DDC* represents the changes of the intensity of human economic activities and the intensity of land development. The closer the distance is to the city center and the district center, the more intense the intensity of human economic activities is, and the greater the intensity of land development is, the greater the impact on the urban environment and the higher the risk of urban environment. The furthest

distance from the center of Shanghai is 72.45 km (see Fig. 3a), and the furthest distance from the center of district is 46.67 km (see Fig. 3b).

The development zone is the area specially engaged in economic production activities set up by the government to promote the rapid development of regional economy, which is the urban industrial gathering area. Development zones are divided into national level development zones, provincial level development zones and municipal level development zones in China (The state council the people's republic of China, China Development Zone Review Bulletin Directory [16]). Because Shanghai is a municipality directly under the central government, the municipal development zone mentioned in the article is actually equivalent to the provincial level development zone. In this paper, *DNLDZ* and *DMDZ* were selected to measure the intensity of urban economic production activities to evaluate the impact of economic production activities on urban environment. The closer the distance to the national and municipal development zones, the higher the degree of industrial aggregation, the greater the intensity of economic production activities, and the greater the impact on the urban environment. There are 20 national development zones (China 2018) in Shanghai, and the furthest distance from national development zones is 51.04 km (see Fig. 3c). There are 39 municipal development zones (China 2018), the furthest distance from municipal development zones is 39.88 km (see Fig. 3d).

As the original natural ecological landscape of the city, forest is less affected by human activities and is an area with a very good ecological environment in the city [17]. We select the distance between space factor and forest center to evaluate its impact on urban environment. The closer it is to the center of the forest, the less the human activities change the natural environment, the less the impact on the natural environment, and the better the natural ecological environment.

By the end of 2020, the forest coverage rate of Shanghai is 18.2% [18], and the farthest distance from the forest center is 26.80 km (see Fig. 3e). Surface buildings are the most direct embodiment of human activities changing the land cover and affecting the pattern of natural ecological environment. The higher the floor area ratio of buildings, the greater the intensity of land cover changes and the greater the impact on the natural ecological environment. The average maximum floor area ratio of buildings in Shanghai is 4.83 (see Fig. 3f).

$PM_{2.5}$ refers to particulate matter with an aerodynamic equivalent diameter of 2.5 microns or less in ambient air. It can be suspended in the air for a long time, and the higher its concentration in the air, the more serious the air pollution. $PM_{2.5}$ has small particle size, large area and strong activity, with toxic and harmful substances (such as heavy metals and microorganisms) attached, and it stays in the atmosphere for a long time and is transported for a long distance, so it has a greater impact on human health and atmospheric environmental quality. $PM_{2.5}$ concentration was selected as an impact factor to evaluate the state of the urban environment, and the impact of human activities on the spatial environment was considered comprehensively, which is another representation of the urban environment. The higher the $PM_{2.5}$ concentration in the air, the higher the environmental risk, and the lower the $PM_{2.5}$ concentration, the lower the environmental risk. $PM_{2.5}$ concentration range in Shanghai in 2020 is 44.50–67.50 $\mu g/m^3$ (see Fig. 3g).

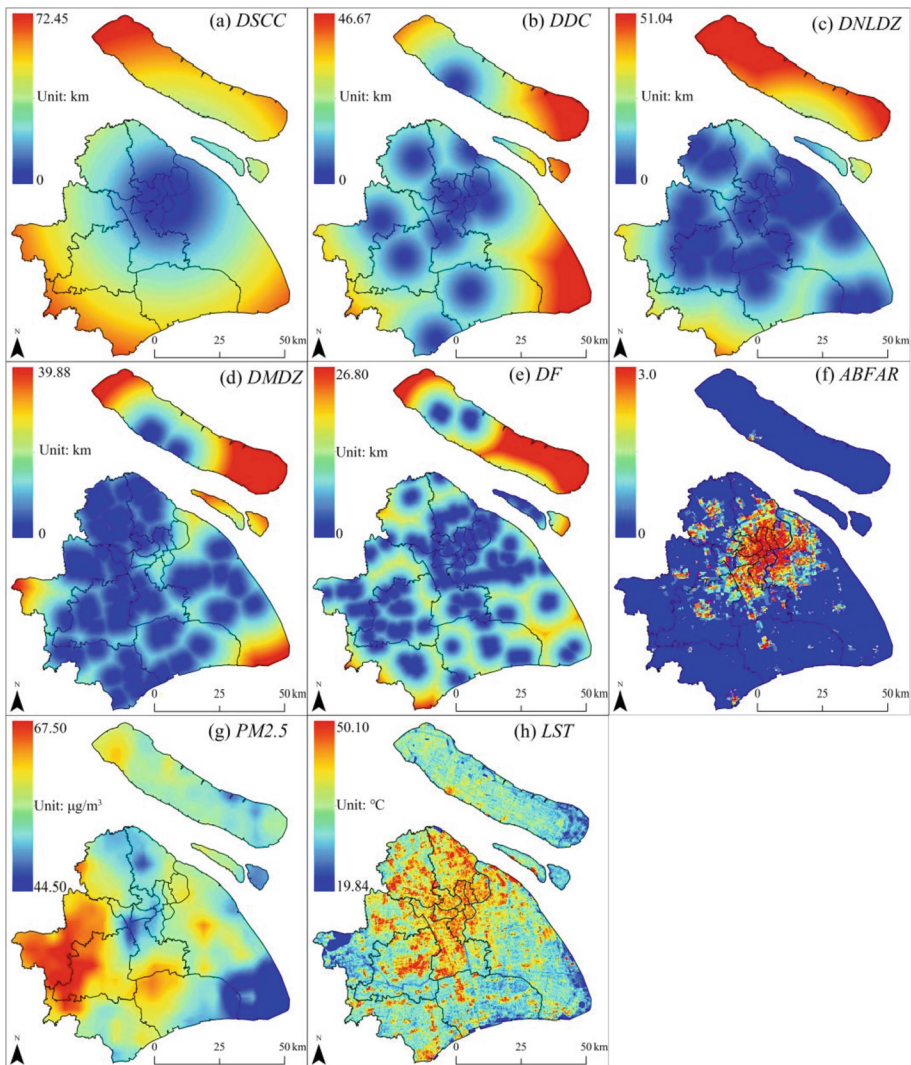


Fig. 3. Spatial factors of environmental risk pattern assessment

Land surface temperature is the temperature of the earth's surface after the sun's heat energy reaches the ground and part of it is absorbed by the ground. There are many factors that affect surface temperature, such as surface humidity, temperature, light intensity and surface material. For a small area with relatively flat terrain, the difference of LST in this area mainly depends on population density and industrial development degree. We choose surface temperature as a spatial factor to represent the spatial impact of urban population density and urban industrial development on the urban environment. Studies show that the higher the surface temperature is, the greater the population density is, the greater the intensity of urban industrial development is, and the greater the impact on the

urban environment is. The range of surface temperature retrieved from remote sensing images of Shanghai in June 2020 was 19.84–50.10 °C (see Fig. 3h).

2.5 Method for Environmental Risk Assessment

In the evaluation of the spatial pattern of environmental risk in Shanghai, in order to avoid the deviation of evaluation results caused by subjective cognition, we start from the data itself, using objective evaluation method, CRITIC method to evaluate the spatial pattern of environmental risk in Shanghai.

CRITIC method is an indicator importance method based on indicator correlation. In this method, in the process of determining the weight, the value of each scheme is determined by the standard deviation. The larger the standard deviation is, the larger the difference between the schemes is, which can reflect the difference between each scheme and serve as the basis of weight assignment. The conflict of evaluation indexes is expressed by correlation, and the degree of conflict can be determined by calculating correlation coefficient or correlation coefficient matrix between indexes.

If the absolute value of correlation coefficient is greater than or equal to 0.8, it indicates that there is a high correlation between the two, that is, the conflict between the two is low. If the absolute value of the correlation coefficient is less than 0.3, it indicates that there is a low correlation between the two, that is, the conflict between the two is high. The CRITIC method comprehensively considers the influence of the difference within the index and the conflict between the index on the weight, which is an improvement of the entropy weight method and can objectively determine the weight. The determination of the objective weight of each index is measured by the conflict between the evaluation indexes and the variability within the indexes.

The weight determination process of CRITIC method is as follows:

$$\rho_{XY} = \frac{\sum_{i=1}^N (X_i - \bar{X})(Y_i - \bar{Y})}{\sqrt{\sum_{i=1}^N (X_i - \bar{X})^2} \sqrt{\sum_{i=1}^N (Y_i - \bar{Y})^2}} \quad (1)$$

The standard deviation of the index is:

$$\sigma = \sqrt{\frac{1}{n} \sum_{i=1}^n (X_i - \bar{X})^2} \quad (2)$$

Where, n is the evaluation quantity of the same index; X_i and Y_i are the value of the two indexes respectively; \bar{X} and \bar{Y} are the average values of the two indexes respectively; N is the number of indicator values.

The amount of information contained in the j indicator E_j is:

$$E_j = \sigma_j / \sum_{i=1}^n (1 - \rho_{ij}) \quad (3)$$

Where, $\sum_{i=1}^n (1 - \rho_{ij})$ is the quantization result of conflict between the j index and other n indexes.

The larger E_j is, the greater the entropy is, indicating the greater the amount of information contained in this evaluation index, the greater the relative importance of this index, and the greater the proportion of this index in environmental risk assessment.

The objective weight w_j of the j index is

$$w_j = E_j / \sum_{j=1}^m E_j \quad (4)$$

In the formula, m is the number of evaluation indicators.

3 Results

The weight of CRITIC method is calculated based on the variability of evaluation indicators and the conflict between evaluation indicators. Index variability measure to use standard deviation, the greater the standard deviation, the greater the weight; Conflictive use of indicators to measure the correlation coefficient between, between indicators. Amount of calculation for variability and the conflict between the product of the indicators. The final weight is normalized by the amount of information to calculate. Based on CRITIC method using spatial factors of 6741 samples to evaluate environmental risk in Shanghai shows: the weight of each factors from big to small, respectively are $PM2.5(19.00\%)$, $DDC(16.91\%)$, $DNLDZ(16.10\%)$, $DSCC(15.65\%)$, $DMDZ(13.10\%)$, $DF(11.82\%)$, $LST(6.88\%)$ (Table 3). $PM2.5$ concentration is the most important factors influencing the environmental risk of Shanghai, while the surface temperature of LST in Shanghai has little effect on environmental risks.

Table 3. Selected spatial factors of the environmental risk assessment in Shanghai

Spatial factors	Mean	Standard deviation	Weight (%)	Index conflict
<i>DSCC</i>	0.490	0.207	15.65	5.753
<i>DDC</i>	0.316	0.214	16.91	6.022
<i>DNLDZ</i>	0.239	0.226	16.10	5.436
<i>DMDZ</i>	0.166	0.185	13.10	5.404
<i>DF</i>	0.190	0.166	11.82	5.426
<i>LST</i>	0.451	0.063	6.88	8.295
<i>PM2.5</i>	0.563	0.182	19.00	7.93
<i>ABFAR</i>	0.002	0.005	0.530	8.128

Based on the CRITIC method of the weight of each spatial factor in the evaluation of environmental risk in Shanghai, using the spatial analysis method to show environmental risk pattern of Shanghai (see Fig. 4). Figure 4a shows spatial patterns of environmental risk in Shanghai with environmental risk score range of [0, 1], the higher the score, the higher the risk environment. Environmental risk score close to 1, namely the area with very high environmental risk mainly distribute in the center districts (A.Yangpu, B.Hongkou, C.Jin'an, D.Putuo, E.Changning, F.Xuhui, G.Huangpu) of Shanghai. While environmental risk score is less than 0.5, namely low environmental risk areas are mainly concentrated in the suburbs of Shanghai (Chongming, Qingpu,

Songjiang, Jinshan, Fengxian and Pudong), and environmental risk score is less than 0.2, namely the area of environmental risk is very low concentrated on chongming.

We divided environmental risk score into eight grades: environmental risk score for [0, 0.125) range, environmental risk grade is the lowest; environmental risk score for [0.125, 0.250) range, environmental risk grade is the low; the score range is [0.250, 0.375), environmental risk grade is the medium low; the score range is [0.375, 0.500), environmental risk grade is the medium; the score range is [0.500, 0.625), environmental risk grade is the neutral high; the score range is [0.625, 0.750), environmental risk grade is the medium high; the score range is [0.750, 0.875), environmental risk grade is the high; the score range is [0.875, 1], environmental risk grade is the highest. Shanghai environmental risk classification visualization (see Fig. 4b) is shown: the environmental risk grade of all downtown areas of Shanghai is the highest, except Yangpu, and Yangpu, Baoshan and Minhang only have the highest and high environmental risk grade. Jinshan and Fengxian and Qingpu do not have the highest grade of environmental risk, and most of the environmental risk in Jinshan is below the medium high grade. Chongming is the region with the lowest environmental risk grade, and all regions have the lowest environmental risk grade. Only a small number of regions located in the center of Chongming have the neutral high environmental risk grade, and Chongming has the largest proportion of the lowest environmental risk grade. On the whole, the environmental risk level of Shanghai presents a trend of gradually decreasing from downtown to suburban areas.

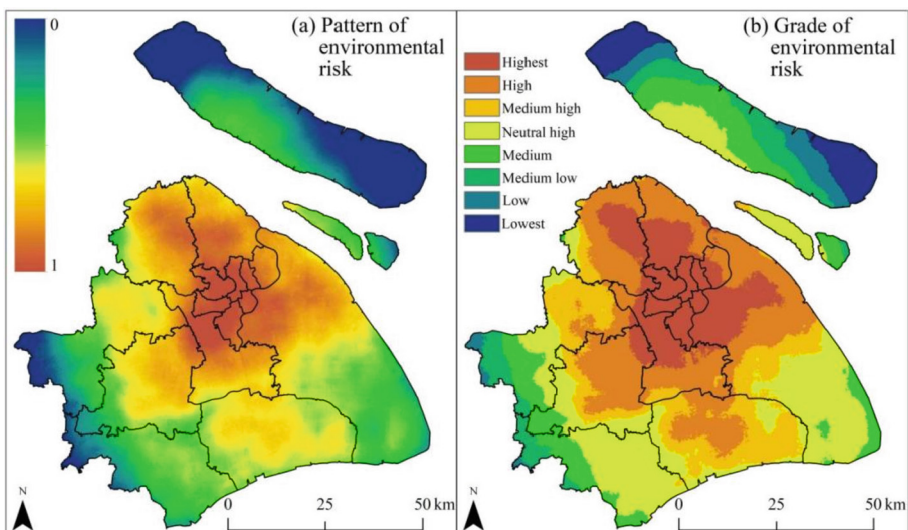


Fig. 4. Spatial pattern of environmental risk in Shanghai

In order to facilitate the identification of which areas of the environment need human intervention management, we divided environmental risks into I, II, III and IV environmental risk management levels. Level I means that the environmental risk is very low, and there is no need to carry out artificial ecological environment restoration, as long as the status quo of the ecological environment in the region is maintained. Level II indicates

that the environmental risk is low and the environmental protection work can be carried out to a certain extent. Level III indicates high environmental risk, and ecological and environmental restoration work should be carried out in time to manage the ecological and environmental risk status of the region. Level IV indicates that the environmental risk in this region is very high (see Fig. 5), and it is necessary to strengthen the management of environmental risk in this region and limit the human economic activities, production activities and land development intensity in this region.

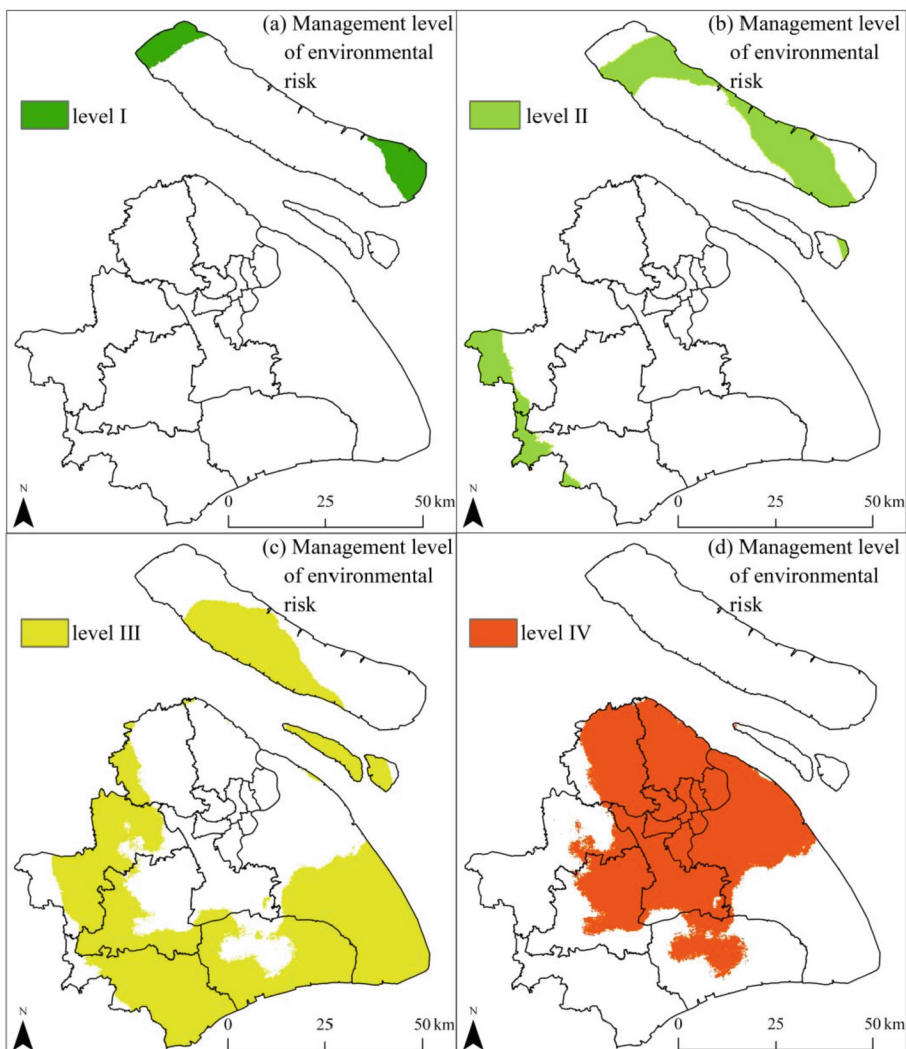


Fig. 5. Spatial distribution of different management levels of environmental risk in Shanghai

In general, the environmental risk level of most areas in Shanghai is III and IV, with an area of 2557.43 km² and 2503.04 km² respectively, accounting for 37.89% and 37.09%. However, the area of I and II with lower environmental risk is relatively small, especially the area of I with lower environmental risk, accounting for only 7.94% (Table 4).

Table 4. The area and percentage of each environmental risk grade and management level of environmental risk

Grade of environmental risk	Area (km ²)	Percentage (%)	Management level of environmental risk	Area (km ²)	Percentage (%)
Lowest	275.30	4.55	I	480.4	7.94
Low	205.11	3.39			
Medium low	398.73	6.59	II	1033.43	17.08
Medium	634.70	10.49			
Neutral high	1442.44	23.84	III	2292.53	37.89
Medium high	850.10	14.05			
High	1363.18	22.53	IV	2244.13	37.09
Highest	880.95	14.56			
Total	6050.5	100	Total	6050.5	100

4 Conclusion

In this paper, the CRITIC method is adopted to evaluate the environmental risk, and combining the spatial pattern of visual spatial analysis method in the Shanghai environmental risk, environmental risk score respectively according to different standards will be divided into environmental risk grade and environmental risk management of different level, different for different regional environment risk level identification and environmental risk management. Our evaluation results show that the highest environmental risks are mainly concentrated in the downtown area of Shanghai (B.Hongkou, C.Jin'an, D.Putuo, E.Changning, F.Xuhui, G.Huangpu), while the lowest environmental risks are mainly concentrated in Chongming. The environmental risk in Jinshan and Fengxian is generally low. Generally speaking, the environmental risk pattern of Shanghai is from downtown to suburban area, and the grade is from high to low. At present, 74.98% of the areas (environmental risk grade III and IV) in Shanghai need environmental risk management, and 37.09% of the areas (environmental risk grade IV) need to strengthen the restoration of ecological environment and environmental risk management.

In recent years, China has been practicing the concept of green development and participating deeply in global environmental governance. As the financial center of China, Shanghai is making great efforts to build a green and ecological urban area of

Shanghai with the rapid development of urban economy. This paper evaluates the spatial pattern of environmental risk in Shanghai, which is conducive to the green development of the city, and also provides a method to evaluate the pattern of environmental risk in other Cities in China.

5 Discussion

In this paper, an objective evaluation method, CRITIC method, is adopted to evaluate the environmental risk pattern of Shanghai. Compared with subjective evaluation methods such as expert evaluation method and analytic hierarchy process, this method removes the deviation of evaluation results caused by human factors from the data itself, so that the evaluation results are carried out at a unified scale.

In terms of the selected environmental impact factors, this paper only discusses the impact of different levels and scales of development zones on the urban environment, but in fact, the types of development zones may also have an impact on the urban environment. For example, The Chemical industrial zone in Shanghai is a professional development zone focusing on petroleum and fine chemicals, which may cause great damage to the surrounding natural environment. Emphasis on Shanghai international tourist resort, tourism, cultural creative industry, exhibition industry, trade services, sports leisure, sports medical services, business services, this type of development zone, pay attention to the protection of natural ecological environment, the natural ecological environment and the regional industry development combined type, less damage to environment.

Due to data acquisition reasons, this paper only evaluated the environmental risk of Shanghai in 2020. It is necessary to improve the environmental risk assessment of Shanghai at a time scale and analyze the change rule of environmental risk pattern in Shanghai over time, so as to provide a solid foundation for more accurate understanding of the characteristics and causes of environmental risk pattern change in Shanghai. This paper needs to further quantify the response relationship between urban environmental risk and relevant spatial factors, so as to provide countermeasures and suggestions for reducing urban environmental risk, improving urban ecological environment and building a livable city with high quality development.

This paper is supported by the International Exchange Program for Graduate Students, Tongji University.

References

1. Alharbi, O.M.L., Khattab, R.A., Ali, I.: Health and environmental effects of persistent organic pollutants. *J. Mol. Liq.* **263**, 442–453 (2018)
2. Lankarani, K.B., Heydari, S.T., Aghabeigi, M.R., et al.: The impact of environmental factors on traffic accidents in Iran. *J. Inj. Violence Res.* **6**(2), 64 (2014)
3. Cecchini, M., Zambon, I., Pontrandolfi, A., et al.: Urban sprawl and the ‘olive’ landscape: Sustainable land management for ‘crisis’ cities. *GeoJournal* **84**(1), 237–255 (2019)
4. Liddle, B., Lung, S.: Age-structure, urbanization, and climate change in developed countries: revisiting STIRPAT for disaggregated population and consumption-related environmental impacts. *Popul. Environ.* **31**(5), 317–343 (2010)

5. Verdonck, F.A.M., Van Sprang, P.A., Vanrolleghem, P.A.: Uncertainty and precaution in European environmental risk assessment of chemicals. *Water Sci. Technol.* **52**(6), 227–234 (2005)
6. Rivera-Jaimes, J.A., Postigo, C., Melgoza-Alemán, R.M.: Study of pharmaceuticals in surface and wastewater from Cuernavaca, Morelos, Mexico: occurrence and environmental risk assessment. *Sci. Total Environ.* **613**, 1263–1274 (2018)
7. Milan, M., Pauletto, M., Bozzo, L.: Transcriptomic resources for environmental risk assessment: a case study in the Venice lagoon. *Environ. Pollut.* **197**, 90–98 (2015)
8. Topuz, E., Talinli, I., Aydin, E.: Integration of environmental and human health risk assessment for industries using hazardous materials: a quantitative multi criteria approach for environmental decision makers. *Environ. Int.* **37**(2), 393–403 (2011)
9. Kryshev, I.I., Ryazantsev, E.P.: Environmental risk of the radiological accidents at Chernobyl and Fukushima (Japan) NPP. *At. Energy* **122**(1), 58–68 (2017)
10. Zhang, C., Li, Y., Xiong, S., et al.: Regional environmental risk assessment and management guide for rapid urbanization process of a city cluster in China. *Hum. Ecol. Risk Assess. Int. J.* **22**(2), 283–301 (2016)
11. Narimisa, M.R., Narimisa, M.R.: The research of environmental impact assessment for oil refineries in Iran based on AHP and GIS. *Int. J. Humanit. Cult. Stud.* **1**(1), 1396–1416 (2016)
12. Feng, Y., Yang, Q., Tong, X.: Evaluating land ecological security and examining its relationships with driving factors using GIS and generalized additive model. *Sci. Total Environ.* **633**, 1469–1479 (2018)
13. Miao, C., Teng, J., Wang, J., et al.: Population vulnerability assessment of geological disasters in China using CRITIC–GRA methods. *Arab. J. Geosci.* **11**(11), 1–12 (2018)
14. Ali-Akbarpour, M., Mohammadbeigi, A., Tabatabaei, S.H.R.: Spatial analysis of eco-environmental risk factors of cutaneous leishmaniasis in southern Iran. *J. Cutan. Aesthet. Surg.* **5**(1), 30 (2012)
15. Shanghai Statistics Bureau: Shanghai Statistical Yearbook 2020. China Statistics Press, Shanghai (2021)
16. National Development and Reform Commission: China Development Zone Review Bulletin Directory, 2018 edition
17. Steiner, F.: Landscape ecological urbanism: Origins and trajectories. *Landsc. Urban Plan.* **100**(4), 333–337 (2011)
18. Shanghai Municipal Government: Report on the work of the Shanghai Municipal Government in 2020, Shanghai (2020)



A Review on RES Energy Transition-Climate Change Interaction Effects

Dimitris Karamanis^(✉)

Department of Environmental Engineering, University of Patras, 30100 Agrinio, Greece
dkaraman@upatras.gr

Abstract. The role of CO₂ emissions in climate change from fossil fuel burning is well documented and the need of renewable energy sources (RES) development well accepted. An impetus in the research aiming in proposing mitigation measures and energy transition is currently under way towards a zero-carbon society after the mid of the century. However, an unprecedented growth of RES installations with an unconditional economic development could potentially raise new environmental and societal concerns. Since energy transition will be based on anthropogenic conversion of solar and wind energy sources in useful energy for developing purposes, RES interaction with regional climate should be thoroughly investigated. Moreover, the magnitude and potential impact of this interaction should be assessed in detail in order to avoid potential environmental problems like those caused by the vast exploitation of conventional energy resources in past century. In this frame, the aim of this work is to review the current scientific knowledge on the RES-climate change interaction and the potential effect of photovoltaics (PV) and wind turbines (WTs) electricity generation to regional climate change. Greece is selected as a European case study due to abundant RES availability for energy transition. Contradictory results of global and regional climate models reveal that more research and experimental work is needed for a sustainable development based on renewable energy sources.

Keywords: Climate change · Solar energy · Wind energy

1 Introduction

The continuous exploitation of fossil and mineral fuels the last two hundred years has substantially improved the quality and duration of human life but has disturbed the earth energy balance with higher mean annual temperature and negative health and environmental impact. As a result of increased concern, the Paris agreement was signed by 175 parties with a goal to keep temperature increase even below 1.5 °C. In this context, International Energy Agency has called for urgent actions in the most recent net zero scenario by 2050 towards the replacement of conventional energy resources in the energy mix with renewable energy sources [1]. Is this energy transition feasible? In a simple model of PV and wind turbines development with the same rate as the last year in Greece up to 2030 (14.37% for PV grid installations and 13.83% for WT grid connected

systems), 10% and 8% respectively up to 2040 and 5% for both up to 2050, 37.3 GW of PV systems and 39.1 GW of WTs will be required for a 100% energy transition in order all the non-industrial final energy use of Fig. 1 to be covered by PV and WTs. Even in the model of Jacobson et al. with a 45.6% reduction in the final energy use of Greece [2], a 19.2 GW of water/wind/solar (WWS) power needs to be implemented with a land area requirement of 0.74% while even higher load will be required in the models of [3] or [4] (Table 1). These power requirements are high but not unreachable since 1864 applications were submitted at the last call of the National Regulatory Authority for Energy (RAE) in December 2020 for RES applications of 45.55 GW (36.339 GW of PVs, 8.704 GW of WTs and less than 200 MW other RES). Therefore, the land and space requirements for such a transition is not negligible. It will account for at least a digit percentage of space area (Table 1). However, there are 419 regions in Greece protected by the NATURA 2000 network that account for the 27.29% of mainland and 6.12% of territorial waters of Greece. In order to be in line with the 14 and 15 UN goals of sustainable development, the protected areas should be left undisturbed without the presence of RES energy conversion systems [5]. This principle conservation is feasible

Table 1. RES energy transition in Greece up to 100% of final non-industrial energy use.

Scenario	PV (GW)	WIND (GW)	HYDRO (GW)	Electricity (TWh) or Total Installed (GW) at 2050 and space requirement	Ref
1	39.1	37.3	3.0	144 TWh (76.483 GW) (100%); 0.7% of land for PV of 40 W/m ² ; 7% of space (onshore and offshore) for WTs of 1.1 W/m ²	100% of RES for non-industrial energy use with a Business As Usual scenario
2	7.8	9.1	1.67	WWS: 19.2 GW (100%); 0.74% of land for WWS; 45.78% reduction from present needs	[2]
3	12 (23%)	12 (35%)	3.56 + 2.7 HPS	74 TWh (WWS: 30.26 GW + 7.1 NG + 0.125CHP + 0.6BM)	[3]
4	14	11.5	5.5 + 3 HPS + other RES	40 GW RES for maximum 70% CO ₂ reduction in 2050 compared to 2005 (70% RES in total final energy consumption)	[4]

in Greece even for an extended windfarm-free zone [6] where wind farms can be applied at moderate wind speed sources [7]. Although, public acceptance of many WTs and PV needs policy attention (e.g. participatory framework of local communities) due to a raising negative attitude against new WTs installations in many places in Greece, new scientific needs are also emerging due to the massive RES utilization. Among these, material availability is important and has received substantial interest with many recent publications and reports. However, the effect on RES-climate change interactions have received much less attention. Increasing RES systems deployment will result in an increasing use of solar, wind and water atmospheric energy resources for technoeconomic purposes with a direct disturbing effect on the atmospheric energy balance and regional climate at different scale. Although, specific RES-climate change interaction studies are being emerged as individual cases, an integrated compilation of significant findings for both directions (RES to climate change effect and vice versa) is missing from scientific literature. In this context, the aim of this work is to review the research on the RES-climate change loop interaction: the potential impact of climate change to future regional electricity generation from PV and wind turbines and vice versa, the potential impact of PV and wind turbines electricity generation to regional climate change. Due to the abundant RES availability and recent intense efforts for energy transition, the investigation is focused on Greece as a European case study.

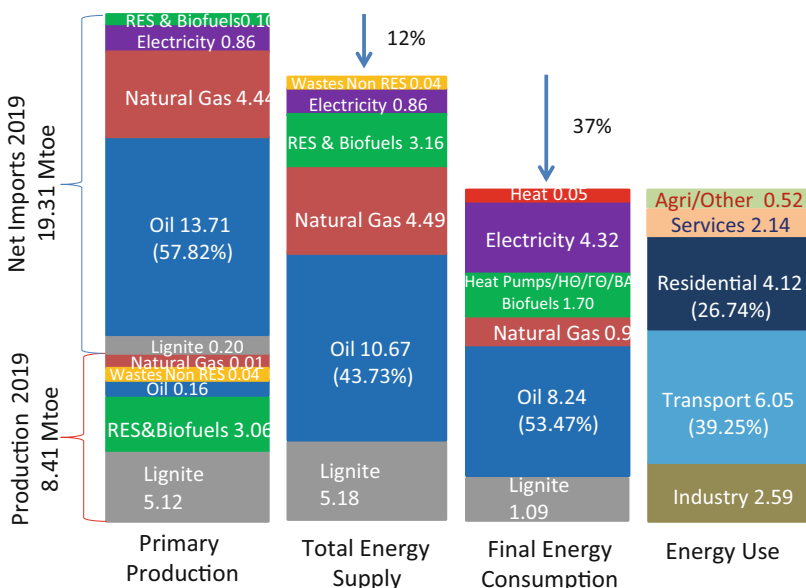


Fig. 1. Energy production, imports and final energy consumption in Greece for 2019 (based on Eurostat data).

2 Methodology

Since all the scenarios of the future energy transition of Table 1 rely mainly on the renewable energy sources of wind and solar, the literature review was not extended to other potential RES in Greece. Articles from the Scopus database that refer to the effect of climate change on these sources and vice versa (specifically for the country or as part of European studies) were analysed in order to provide valuable insights for research gaps and needs as well as to reveal potential discrepancies between the different scales of general circulation model simulation and dynamic downscaling with regional climate models. Although, articles on hydropower and buildings-climate interaction were also evident (with more pronounced climate impact to energy production or needs), their analysis will be reported in future work.

3 Results and Discussion

3.1 The Effect of Climate Change on Solar Energy and PV Electricity Production

Solar radiation has been found globally to be increased by projected climate change till the end of the century, but PV electricity production is also influenced by temperature and wind speed variation. In Greece, Panagea et al. [8] studied the projections of global horizontal irradiation from five RCMs for historical and future periods and found minor increases ($2.0\text{--}3.0 \text{ W/m}^2$ by 2011–2050 and 5.0 W/m^2 by 2061–2100) in power output to the outweighed of projected temperature increase ($+3.5^\circ\text{C}$) by the expected increase of total radiation. These results were further confirmed by Katopodis et al. [9] and on average, mean annual global horizontal irradiance (GHI) variations showed values of similar magnitude and pattern between two future scenarios (RCPs 4.5 and 8.5). An enhancement in PV electricity production has been also projected by recent European studies of the three atmospheric variables [10] and for other countries like Germany and Spain although rather as exceptions in Europe [11]. However, under a fixed scenario of high-PV penetration, a general and progressive decline of the generated PV power is found in all regions along the entire period. Finally, in a recent European study, projected solar PV generation on three levels of global warming above preindustrial levels, i.e. 1.5°C , 2°C and 3°C warming that occur at different times among simulations) showed very small changes for the countries of Greece, Portugal, Spain and Cyprus in South Europe [12]. However, the studies have been mainly focused on regional effects on the country scale with the absence of studies at the urban scale where effects of microclimate change or extreme weather events are enhanced [13].

3.2 The Effect of Climate Change on Wind Energy and WT Electricity Production

Climate change impact on wind energy sources in Greece was studied recently by Katopodis et al. [14] by projecting the wind potential of Greece up to 2045 with the EURO-CORDEX RCA4 model data, a horizontal resolution of $\sim 12 \text{ km}$ and the RCP scenarios of radiative forcing of 2.6 , 4.5 and 8.5 W/m^2 . According to their analysis, the

changes in the mean wind speed in Greece were within $\pm 5\%$ and did not vary significantly for the different RCP scenarios. Wind gusts exceeding 52 m/s appeared more frequently in RCP 8.5 by about 2–4 times per decade, affecting mostly the South Ionian Sea while a tendency for calming of the “Etesians” winds over the Aegean Sea in future summers was determined [14]. Latter was not observed in European studies where the wind energy potential is projected to increase in northern and central Europe while it may experience a decrease in all seasons over onshore southern Europe except for the Aegean Sea due to stronger relative influence of local wind systems [15]. A tendency toward a decrease of the wind power potential over Mediterranean areas (but within ± 15 and $\pm 20\%$ by mid and late century respectively) was found by Tobin et al. [16]. More recently, the same research collaboration projected wind energy changes positive for Greece while overall reductions in wind power potential were projected (ensemble mean results) for all European countries [12]. These results combined with the stochastic nature of wind point to the need of more regional studies to investigate the impact of climate change on wind energy production.

3.3 The Effect of PV Electricity Production on Regional Climate

The installation of ground-mounted PV arrays has the potential to affect surface albedo, cause shading and intercept precipitation and atmospheric deposition, as well as influencing wind speed and turbulence at the land surface. However, the research studies are limited and mainly focused on the urban microclimate impact.

3.4 The Effect of WTs Electricity Production on Regional Climate

The operation of wind turbines can affect surface meteorology by changing atmospheric boundary layer condition of wind speed, turbulence and mixing, and thus the vertical distribution of energy and exchange between the land surface and atmosphere. Wakes from single wind turbines and large wind farms reduce the rate of radiative surface cooling and enhance night-time surface temperature. According to observations reported by Rajewski et al. [17], changes in the early evening transition due to the generation of turbulence from single wind turbines may influence transport of heat, water, and carbon dioxide from a non-vegetative surface. The only work on the impact of WT electricity production in Greece is reported by Vautard et al. [18] in the frame of climatic impact of wind farms in Europe. Under a power development scenario of 7 GW from 2014 to 2020, authors present mean summer temperature increase up to 0.3 K which depends on WT siting. Moreover, it has been also reported that keeping the global mean temperature below 2 °C can result in higher warming of Europe than the global average with a general increase in heavy precipitation and summer extreme temperatures [19]. According to Miller and Keith [20], the warming effect of wind energy is small when compared with projections of 21st century warming with Business As Usual policies, approximately equivalent to the reduced warming achieved by decarbonizing global electricity generation, and large compared with the reduced warming achieved by decarbonizing US electricity with wind. For the same generation rate, the climatic impacts from solar photovoltaic systems are about ten times smaller than wind systems. In this corresponding scale of regional wind installations combined with PV, it is envisaged that more

detailed RES-climate interaction studies should be performed with additional wind farm observations to improve predictive skill of wind energy-atmosphere interactions.

4 Conclusions

It is evident from this review that there have been limited studies on regional RES-climate change interaction and further research attention is needed. In the larger scale of European or global studies, concerns have been raised on the warming effect of wind energy analogous to urban heat islands which can be non-negligible and comparable to temperature reduction upon decarbonization with large scale installation of wind farms. Therefore, it is of paramount importance to improve the accuracy of regional climate change models and reduce the major sources of uncertainty and bias corrections thorough their validation by accurate earth and satellite monitoring systems. Additionally, the effects of variability in future power systems and their demand/supply flexibility should be considered in their interaction with climate change and prioritizing actions should be proposed for a 100% renewable energy transition. PV building integration for zero energy buildings, EV transition with increased share of public transportation and unnecessary travel avoidance could be prioritized with the growth of annual installation rate of WTs and PVs. Mature storage technologies based on batteries for transport and pumping storage for electricity can be complementary used to cover all energy needs with RES. In this context, the barriers to 100% energy transition are not scientific and technical-economic but mainly social, structural and political and with decisive policies and new approaches to implementing technological and behavioural change, the challenges can be addressed.

References

1. Net zero by 2050, A roadmap for the global energy sector, International Energy Agency, May 2021. www.iea.org
2. Jacobson et al. (2017). <https://thesolutionsproject.org/why-clean-energy/>. Accessed on 24 Apr 2021
3. Dianellou, A., Christakopoulos, T., Caralis, G., Kotroni, V., Lagouvardos, K., Zervos, A.: Is the large-scale development of wind-PV with hydro-pumped storage economically feasible in Greece? *Appl. Sci.* **11**, 2368 (2021)
4. Tigas, K., et al.: Wide scale penetration of renewable electricity in the Greek energy system in view of the European decarbonization targets for 2050. *Renew. Sustain. Energy Rev.* **42**, 158–169 (2015)
5. Rehbein, J.A., et al.: Renewable energy development threatens many globally important biodiversity areas. *Glob. Change Biol.* **26**, 3040–3051 (2020)
6. Kati, V., Kassara, C., Vrontisi, Z., Moustakas, A.: The biodiversity-wind energy-land use nexus in a global biodiversity hotspot. *Sci. Total Environ.* **768**, 144471 (2021)
7. Karamanis, D.: Management of moderate wind energy coastal resources. *Energy Conv. Manage.* **52**, 2623–2628 (2011)
8. Panagea, I.S., Tsanis, I.K., Koutroulis, A.G., Grillakis. M.G.: Climate change impact on photovoltaic energy output: the case of Greece. *Adv. Meteorol.* 264506 (2014)

9. Katopodis, T., Markantonis, I., Politi, N., Vlachogiannis, D., Sfetsos, A.: High-resolution solar climate atlas for Greece under climate change using the weather research and forecasting (WRF) model. *Atmosphere* **11**, 761 (2020)
10. Jerez, S., Tobin, I., Vautard, R., Montávez, J.P., et al.: The impact of climate change on photovoltaic power generation in Europe. *Nat. Commun.* **6**, 10014 (2015)
11. Wild, M., Folini, D., Henschel, F., Fischer, N., Müller, B.: Projections of long-term changes in solar radiation based on CMIP5 climate models and their influence on energy yields of photovoltaic systems. *Sol. Energy* **116**, 12–24 (2015)
12. Tobin, I., et al.: Vulnerabilities and resilience of European power generation to 1.5 °C, 2°C and 3°C warming. *Environ. Res. Lett.* **13**(4), 044024 (2018)
13. Van der Schrieck, T., Varotsos, K.V., Giannakopoulos, C., Founda, D.: Projected future temporal trends of two different urban heat islands in Athens (Greece) under three climate change scenarios: a statistical approach. *Atmosphere* **11**(6), 637 (2020)
14. Katopodis, T., Vlachogiannis, D., Politi, N., Gounaris, N., Karozis, S., Sfetsos, A.: Assessment of climate change impacts on wind resource characteristics and wind energy potential in Greece. *J. Renew. Sustain. Energy* **11**, 066502 (2019)
15. Hueging, H., Haas, R., Born, K., Jacob, D.J., Pinto, J.G.: Regional changes in wind energy potential over Europe using regional climate model ensemble projections. *J. Appl. Meteorol. Clim.* **52**(4), 903–915 (2013)
16. Tobin, I., et al.: Assessing climate change impacts on European wind energy from ENSEMBLES high-resolution climate projections. *Clim. Change* **128**(1–2), 99–112 (2014). <https://doi.org/10.1007/s10584-014-1291-0>
17. Rajewski, D.A., Takle, E.S., et al.: Observations show that wind farms substantially modify the atmospheric boundary layer thermal stratification transition in the early evening. *Geophys. Res. Lett.* **47** (2020)
18. Vautard, R., Thais, F., Tobin, I., Bréon, F.-M., et al.: Regional climate model simulations indicate limited climatic impacts by operational and planned European wind farms. *Nat. Commun.* **5**, 3196 (2014)
19. Vautard, R., Gobiet, A., Sobolowski, S., Kjellström, E., Stegehuis, A., et al.: The European climate under a 2 °C global warming. *Environ. Res. Lett.* **9**, 034006 (2014)
20. Miller, L.M., Keith, D.W.: Climatic impacts of wind power. *Joule* **2**, 2618–2632 (2018)



Socially Engaged Buddhism of Kalmykia: Land Degradation and the Ecological Initiatives of the Central Khurul

Bato Dondukov¹ Galina Dondukova² , and Oyuna Dorzhigushaeva¹

¹ East-Siberia State University of Technology and Management,
Ulan-Ude, Klyuchevskaya Str. 40v 670013, Russia
dondukovb@gmail.com

² Institute for Mongolian, Buddhist and Tibetan Studies of the Siberian Branch of the Russian Academy of Sciences, Ulan-Ude, Sakhyanovoy Str. 6 670047, Russia

Abstract. In recent years desertification turned into the main ecological problem of the republic of Kalmykia, Russia. With 80% of its territory desertified Kalmykia is defined as an ecological disaster zone. The article is the result of an expedition of scholars from the East Siberia State University of Technology and Management, Ulan-Ude, Russia, to the Republic of Kalmykia, Russia, in spring 2021. The field work was devoted to the collection of materials about ecological projects of the Central Khurul of the republic of Kalmykia, one of the traditional Buddhist regions of Russia, which were connected to the problem of land degradation. We argue that the ecological initiatives of the Buddhist clergy can be divided into religious, ideological and collaborative. Religious initiatives include activities aimed at improvement of ecological conditions on sacral level, achieved through Buddhist theory and related religious practices. Ideological activities imply cultivation of ecological values in the society by the Buddhist sangha, including both secular ideas of ecological thinking, and purely religious concepts based on Buddhist doctrine. Collaborative activities introduce such environmental initiatives, where Buddhist sangha as a traditional and highly reputable institution engages other social and state organizations into environmental projects, ensuring their interaction.

Keywords: Land degradation · Desertification · Socially Engaged Buddhism · Republic of Kalmykia · Central Khurul

1 Introduction

Nowadays religious institutions start to engage into activities that go beyond religious field [1, 2]. Being influential in the society, religious institutions can offer answers to different challenges of our time in social, economic, and even environmental spheres. The ecological situation throughout the world is getting worse year after year. Buddhism, as one of the oldest world religions, does not stand aside from modern environmental problems, offering various ways to improve the situation. The article is devoted to the

ecological initiatives of the Central Khurul of the republic of Kalmykia, one of the traditional Buddhist regions of Russia. The research is the result of an expedition of scholars from the East Siberia State University of Technology and Management, Ulan-Ude, Russia, to the Republic of Kalmykia in spring 2021.

We argue that when speaking about traditional Buddhist regions, the ecological initiatives of Buddhist clergy can be divided into religious, ideological and collaborative. *Religious* initiatives include activities aimed at improvement of ecological conditions on sacral level, which can be achieved through Buddhist theory and related religious practices. *Ideological* activities imply cultivation of ecological values in the society by the Buddhist sangha, including both secular ideas of ecological thinking, and purely religious concepts based on Buddhist doctrine. *Collaborative* activities introduce such environmental initiatives, where Buddhist sangha as a traditional and highly reputable institution engages other social and state organizations into environmental projects, ensuring their interaction.

2 Materials and Methods

2.1 Buddhism in Kalmykia

Tibetan Buddhism has become a traditional religion of *Oirats*, the ancestors of the Kalmyks, since the second half of the 16th century. In the 17th century, part of the Oirats migrated to the territory of modern Kalmykia and thus brought Buddhism to the new lands [3]. Nowadays Kalmykia represents the only area in Europe where Tibetan Buddhism is the national religion.

Nowadays the Buddhism of Kalmykia is headed by Telo Tulku Rinpoche (Ombadykow Erdne), who was born in Philadelphia, USA, in a Kalmyk family of immigrants. From early childhood, the boy expressed a desire to become a Buddhist monk. Later, when he was six years old, His Holiness the 14th Dalai Lama recommended to send him to Tibetan monastery Drepung Gomang in India where he was trained for 12 years and where he was recognized as the current reincarnation (Tulku) of Tilopa, a revered Buddhist saint. In 1991 Telo Tulku Rinpoche first visited Kalmykia with the delegation of Dalai Lama and received an invitation to become Shajin Lama (Supreme lama, the head of Buddhism of Kalmykia) [4]. In 1992, Telo Tulku Rinpoche became the 19th Shajin lama of Kalmykia, and the head of the “Association of Buddhists of Kalmykia”, which consists of 27 Buddhist organizations. As an honorary representative of the 14th Dalai Lama in Russia, CIS countries, and Mongolia, one of the directions of his activity is to strengthen ties between Kalmykia and the Tibetan community, thanks to which, today, not only Kalmyk, but Tibetan monks operate in Kalmykia.

The center of Buddhism in Kalmykia is the Central Khurul (Buddhist temple) “The Golden Abode of Buddha Shakyamuni” built in 2005. In 2004, during his second visit to Kalmykia, the 14th Dalai Lama advised to build in Elista the main Buddhist temple, which would become the administration of all the affairs of Buddhism in Kalmykia. Through the efforts of Telo Tulku Rinpoche and the 1st President of the Republic of Kalmykia, Ilyumzhinov K.N., as well as with the support from the people, the Central Khurul was built in the shortest possible time (Fig. 1).



Fig. 1. Central Khurul “The Golden Abode of Buddha Shakyamuni”, April 2021. Source: Courtesy of the authors.

Khurul consists of 7 levels. There is a library, a museum and a conference room on the first level; a prayer hall (dugan) with a 9-m statue of Buddha Shakyamuni on the second level. On the third level, there are rooms, where monks, doctors of Tibetan medicine and astrologers accept believers. The administration is also located on this level. The fourth level is the residence of the leader of the Buddhists of Kalmykia – Telo Tulku Rinpoche and a small conference hall. On the fifth level, there is the residence of His Holiness the 14th Dalai Lama Tenzin Gyatso. On the sixth level, there are utility rooms. On the seventh level, there is a meditation room, which can be visited exclusively by clergy. In addition to wide educational work (museum, library, study of native language, foundations of Buddhist philosophy, lectures), the Central Khurul holds a deep symbolic meaning for the Kalmyks, as a center for the revival of traditional culture and Buddhism. The temple integrates around itself both believers and those who feel involved in Buddhism as a cultural tradition. Khurul is not only a place for faith, but also a large-scale cultural project, a way to position regional trends [5]. Thus, important issues, which determine the vector of development of Buddhism in Kalmykia, are discussed and accepted by the Central Khurul.

2.2 Ecological Situation in Kalmykia

The current ecological situation in Kalmykia is of significant concern. Located in the semi-desert and desert area in the southeast of the European part of Russia, Kalmykia

is the driest (average annual precipitation ranges from 170 to 350 mm/year, while evaporation exceeds precipitation 3–4 times) and the most treeless region of Russia (forest cover is 16.8 thousand hectares, which is only 0.2% of its territory) [6]. Desertification, thus, is the main ecological problem of Kalmykia: with 80% of its territory desertified Kalmykia is defined as an ecological disaster zone.

The causes of land degradation and desertification are both natural and anthropogenic. Natural factors include wind and water erosion, soil salinization, and climate change, which increases aridization. Anthropogenic factors are the most destructive and are mainly connected to irrational agricultural land use in crop farming and cattle breeding. Plowing of land for cultivation of cereals is accompanied by artificial irrigation of fields. However, low level of construction of the irrigation systems causes resalinization which further causes irrigative desertification on the irrigated lands, irrigation, caused by secondary soil salinization, begins to spread [7]. As for the cattle-breeding, it is the most developed kind of agricultural activity in Kalmykia which has the greatest negative impact on desertification of the Republic. Despite the fact that for centuries these territories traditionally have been used for pastoralism by various groups of peoples, cattle breeding turned into destructive activity only in the last century mainly due to the economic policy of the USSR. There are several factors that lead to the current state of affairs. First of all, it is the loss of the traditional Kalmyk diversity of livestock in times of collectivization of 1917 (horses, camels, cattle and sheep which were adapted to the local ecosystem). The main emphasis was placed on sheep following the replacement of Kalmyk fat-tailed breeds on fine-wooled ones, which had sharp hooves, different style of walking and plants consumption, thereby disrupting the soil structure [8]. The traditional system of nomadic pastoralism was lost and substituted by the year-round use of territories for grazing livestock. The number of livestock was increased, and while the territory of the Republic could provide forage for about 1.8 million heads of sheep, from 1960–1970 the number of livestock has grown to 2.2 million, and by 1990 reached 5 million [6]. All these factors led to a significant increase in load of pastures, as a result of which, sheep breeding today turned into one of the main reasons of soil degradation on the territory of Kalmykia. Thus, both natural and anthropogenic factors within decades accumulated and led to the current situation of an ecological disaster, when most of the territory of the Republic is exposed to desertification.

3 Results

3.1 Religious Rituals of Ecological Significance

In spring 2021, during an academic expedition to Kalmykia, we had an opportunity to interview Yonten Gelyung (Sergey Vladimirovich Kirishov), the head of the Administration of the Central Khurul, who told us that the sangha does not stand aside of environmental problems of the Republic, actively promoting initiatives in both religious, and secular sphere.

Religious sphere is mainly associated with ritual practices performed by the Central Khurul. Along with regular ceremonies, *tentu yultu* ritual is of particular interest to our research. *Tentu yultu* is carried out for several days consequently in various regions of the republic. Its main purpose is purification of energy vibes of an area (Yonten Gelyung, personal interview to Dondukov B., April 13, 2021). But what is more, the ceremony facilitates precipitation. With a request to perform this ritual a lot of people from ordinary rural men, agricultural workers to authorities of the Ministry of Agriculture of Kalmykia come to sangha [9].

To be more specific, the ritual is an appeal to the god Vajravidāraṇa (Tibetan *rdo rje rnam 'joms*), a semi-wrathful form of Vajrapāni, whose mantra is known for its healing and purifying effect. In the text of Vajravidāraṇa Dhāraṇī it is said that the guardians of the four sides of the world turned to Buddha and spoke that evil overcomes good in the world, and then the Enlightened asked Vajrapāni to find the solution to protect the pure spirits. Vajrapāni took the form of Vajravidāraṇa and acquired exceptional abilities to purify negative energy [10]. At this point, it is also worth noting, that Vajrapāni is a deity-guardian of the Mongolian peoples, therefore, it is of particular veneration among the Kalmyks and the Buryats. In addition, Vajrapāni is considered to be the patron of serpentine water spirits – *nagas* who occupy an important place in Buddhism. Such characteristics of the deity Vajravidāraṇa explain why rituals aimed at eliminating problems with drought occur by referring specifically to the cleansing form of Vajrapāni.

Yonten Gelyung emphasizes that the ritual is aimed not so much to deliver rains, as to purify both the area energy and karma of the local people, which, in turn, results in precipitation. That is why sangha asks the people to participate in the ritual by recitation of Vajravidāraṇa mantra: “Nama Chanda Vajra Krodhaya Hulu Hulu Tishtha Tishtha Bhandha Bhandha Hana Hana Amrite Hum Phat.

Vajravidāraṇa purification ceremony is widely practiced in the Himalayas and Tibet. It is performed to increase the vital forces of a person and traditionally includes a symbolic ritual bath with purified water (a few drops on the head and other parts of body). As for Kalmykia, or Buryatia, people often hold the ritual of *zhaptuy* (or *zhaptu*, *zhabtuy*, *zhabty*, *dzhaptuy*, *dzhaptu*, *dzhabtuy*, *dzhabty*), by which the energy and negative karma of a man is cleared, frustration is decreased, vitality is restored. The ritual includes the water purified by Vajravidāraṇa as well as *lud*, a dough figurine designed to substitute a person. During the ritual, a person is washed with water, and all the negative is transferred to the *lud*. After washing, water flowing from a man and his figurine are thrown away. In such a way a person gets purification and is cleaned from negativity of ill-wishers and evil spirits [11].

The ritual *tentu yultu*, is very similar to *zhaptuy*, but the object of purification is not a person, but a large area, with all its inhabitants. During *tentu yultu* ritual the purified water and *lud* figurine are also used (Fig. 2).



Fig. 2. *Tentu yultu* ritual, Day 3, July 29, 2020. Source: Official website of Central Khurul of Kalmykia [12].

Tentu yultu ritual demonstrates the Buddhist sangha's view on the problem of drought and desertification, where the causes of environmental problems are not only external factors, but also the internal state of the land's energy, as well as karma of the local population. In other words, the environment corresponds the karmic state of the people inhabiting it. Consequently, the improvement of the internal conditions of the energy of the territories and the karma of the people can have a good effect on the external environmental conditions.

This thesis is also confirmed by the fact that, according to Yonten Gelyung sangha, in addition to *tentu yultu* ritual regularly performs the ritual *amin dolig* (life redemption). The idea of the ceremony is to save lives of animals to create positive karmic conditions. Most often, Buddhists buy fish from fishermen with the aim of releasing them back into the water. With the help of sangha campaigns of buying out a large number of fish (usually from companies that breed small fry for sale as bait for fishing) are organized. In 2020, under the leadership of sangha, about 10 thousand fish were released, which resulted in stocking with fish several reservoirs (Yonten Gelyung, personal interview to Dondukov B., April 13, 2021). According to Yonten Gelyung, redemption of life can improve significantly the karma of a participant; as a result, it would be possible to avoid disease and other negative phenomena. This ritual has become particularly important in times of COVID-19 pandemic, when the Buddhists "redeemed" lives in order to weaken the growth of the pandemic in the country.

Thus, the ritual part of environmental initiatives of sangha is aimed both at external benefits, by calling for rains, and at the internal ones, by purifying the energy of the territories and improving the karma of the people. The interrelation of external and internal conditions transmits to the population the foundations of the Buddhist worldview, which, in prospect may develop the ecological consciousness of the society.

3.2 Joint Project of KalmSU and Central Khurul

In addition to purely religious ways of solving environmental problems, sangha also participates in secular projects, collaborating with academia. Scientists see phytomelioration as one of the ways to improve the ecological situation with desertification of the territories of Kalmykia. Various researches suggest transition to the technology of integrated development of open sands, which would recover deserted and degraded pastures by planting adapted plants [6].

In autumn 2020, a joint phytomelioration project of Central Khurul and the Kalmyk State University (KalmSU) was initiated through the efforts of Eviev Valery Andreevich, Doctor of Technical Sciences, the dean of Engineering and Technology faculty, and Salaev Badma Katinovich, the rector of the Kalmyk State University. The project presupposes procurement of seeds of phytomeliorative plants, such as willow shrub, eurotia, and camphor-fume, aimed at restoration of pastures after the catastrophic drought of 2020. In an interview with V. A. Eviev we learned that due to severe drought of recent years, especially in the eastern part of Kalmykia, the natural seed base of the above mentioned plants has practically disappeared. Scientists of KalmSU began artificial cultivation of plants, first on private plots, later on plots belonging to the university. In 2020, the scientists of KalmSU, headed by the rector, turned to the Central Khurul with a request to allocate part of the territory of the Geden Sheddup Choi Korling monastery in order to form a seed base of willow shrub, eurotia, and camphor-fume on it. The Central Khurul responded to the proposal and provided 10 hectares of Geden Sheddup Choi Korling, which were fenced from livestock penetration. The territory is under constant supervision of the monks of the Buddhist monastery.

Geden Sheddup Choikorling Monastery was opened in 1996, six kilometers from Elista, near the village of Arshan (the monastery is also called Arshansky Khurul). The first building of the Khurul monastery “Syakyusn Syume” is actually the first Buddhist temple to open after the collapse of the Soviet Union and thus is of great importance for the Kalmyks, symbolizing the revival of Buddhism in Kalmykia (Fig. 3).



Fig. 3. Student practice at the field of willow shrub near Arshansky Khurul, May 23, 2021. Source: Official website of Kalmyk State University [13].

In an interview, V. A. Eviev told us that it is also important that the project received a blessing from the Buddhist clergy. The plant nursery is located on the territory of monastery, which has a beneficial energy. Further on, Yonten Gelyung told us that during the planting process, the monks of the Arshansky Khurul performed prayers which would encourage successful implementation of the project. In critical environmental conditions, when the slightest negative factor can lead to the failure of projects on improving fragile arid systems, the appeal to sacred forces through the Buddhist sangha is not so surprising. In turn, the Buddhist sangha shows interest and is ready to provide comprehensive support in the implementation of environmental projects (Eviev V.A., personal interview to Dondukov B., July 4, 2021).

The next stage of the project after procurement of seeds is its distribution to problem areas, where phytomelioration will be carried out, among others, by the efforts of local farmers. According to V.A. Eviev, in this case, sangha, using its authority among the local people, can potentially assume the role of popularizers of this movement, enlightening and engaging a significant part of the population into the implementation of the project. Since the project is associated with a Buddhist center, and the seeds are grown in a holy place, religious values are also interwoven into the project and can cause additional motivation for cooperation among the population. Thus, the participation of the Buddhist sangha is not limited to land issues, but includes sacred forces and its high collaboration potential.

3.3 “Green Belt” Around Arshansky Khurul” Project

Another interesting environmental project of Central Khurul is the creation of a “green belt” of trees around the Geden Sheddup Choi Korling monastery (Arshansky Khurul). The monks of the monastery have been familiar with plant growing for a long time. First, in 2011, at the initiative of the monk Ngawang Lodoi one hundred fruit trees, mainly apple, pear, sweet cherry, apricot and others, were planted near the house for monks on the territory of the monastery. Ninety-nine of those trees survived. In subsequent years, about twenty walnut trees and about thirty juniper bushes were planted. For watering the trees the monks built a drip irrigation system. Today, the harvest from the orchard is used for the needs of sangha. Surplus fruits are sold and sale proceeds are used to purchase the necessary goods for the garden [14] (Fig. 4).

Based on this experience, the administration of the Central Khurul came up with an idea of creating a green belt of trees around Arshansky Khurul. The implementation of the project started after the visit of a famous Tibetan Buddhist teacher Kundeling Tatsak Jedrung Rinpoche in 2019. During his visit to the monastery, Kundeling Rinpoche drew attention to the fact that the monastery is located in an open area unprotected from steppe dunes and drought, that is why he supported and blessed the idea of creating a “green belt” around Arshansky Khurul. The same year, the Central Khurul, together with the Government of the Republic of Kalmykia, the Ministry of Natural Resources, the Ministry of Youth and Sports and other organizations, carried out tree planting within the framework of the All-Russian Environmental Action. The initiative gained a wide public response, as a result, about 3,000 people came to participate in tree planting, and 6,000 trees were planted in one day. The trees were mainly elms and acacias, which are



Fig. 4. “Green belt” around Arshansky Khurul, April 2021. Source: Courtesy of the authors.

best adapted to the climatic conditions of the region. During the planting process, ritual ceremonies were carried out, which should contributed to survival of the seedlings.

Almost all the republican authorities, including the head of the republic, Batu Sergeevich Khasikov, took part in that action. Thus, the tree planting project, initiated by the Buddhist sangha, became a truly unifying campaign in which society, government and religion, on equal terms, united to implement an environmental project (Fig. 5).



Fig. 5. The Head of the republic of Kalmykia, Batu Khasikov, is planting a tree near Arshansky Khurul, October 19, 2019. Source: RIA Novosti, Kalmykia News website [15].

The experience of tree planting shows that the social authority of the Buddhist sangha in Kalmykia is very high and can unite various social institutions as well as ordinary people around environmental initiatives in the shortest time possible. Such widespread involvement of people and institutions is achieved thanks to behavior patterns of traditional Buddhist regions, where participation in sangha initiatives brings karmic benefits, and in the case of political participants can positively affect their reputation.

Thus, Arshansky Khurul, which is located not far from the capital of the republic, with its vast territories and deep symbolic meaning for the Kalmyks, today has encompassed the major environmental and practical projects of the republic. What is more, the projects can be characterized by immediate implementation and high interest of society and the authorities. Today it is too early to talk about the success of the discussed environmental initiatives, since the projects were launched relatively recently. However, if the “green belt” initiative and creation of seed base is successful, the territory of the Buddhist monastery will turn into a micromodel of favorable environmental conditions that are potentially achievable throughout the republic. Yonten Gelyung explained in the interview that along with ecological education of the population, the role of the sangha is also to exemplify on a practical level how to pay attention to environmental problems. On the example of Arshansky Khurul sangha aims to show what kind of ecological conditions can be created in Kalmykia.

4 Conclusion

Traditional Buddhist regions usually observe social engagement of sangha. Ecological issues today come to the forefront, since every year they start to occupy a more significant position among other challenges of our time. This article shows that in case of Buddhism in Kalmykia, the clergy today are making efforts to improve the local ecology at different levels. The rituals aimed at improving the ecological situation demonstrate the view of the Buddhist clergy on the environmental problems: external improvement is not possible without improvement of internal characteristics of the population and the territories. In addition to religious initiatives, we observed a practical project of creating a micromodel of favorable environmental conditions around the Arshansky Khurul, which can serve as an example for the entire region. It is peculiar, that the initiatives of the Central Khurul manage to ensure interaction of various social institutions in order to achieve the common good. The initiatives described in the article show the versatile potential of a religious institution, which can influence the ecological state of the region, both at the religious and secular levels. Despite the fact that today it is too early to talk about the effectiveness of the proposed projects, we can conclude that religious component plays an important role in the improvement of ecological situation in a traditional Buddhist region.

Acknowledgement. The article is part of the research funded by RSF, project №19–18-00412.

References

1. King, S.B. (ed.): Socially Engaged Buddhism. University of Hawaii Press, Hawaii (2009)
2. Queen, C.S.: Socially engaged Buddhism: emerging patterns of theory and practice. In: Emmanuel, S.M. (ed.) A Companion to Buddhist Philosophy, pp. 524–535. Wiley, New York (2013)
3. Bakaeva, E.P.: Buddizm v Kalmykii. Istoriko-etnograficheskiye ocherki [Buddhism in Kalmykia. Historical and ethnographic essays]. Kalmytskoye knizhnoye izdatel'stvo, Elista (1994)
4. Bakaeva, E.P.: Ob osobennostyakh sovremennoy religioznoy situatsii v Kalmykii (Buddizm i "posvyashchennyye") [On the Features of the Modern Religious Situation in Kalmykia (Buddhism and "Initiates")]. Etnograficheskoye obozreniye [Ethnographic Review] **3**, 23–39 (2004)
5. Tarbastaeva, I.S.: Sotsial'nyy institut buddizma v sovremennoy Rossii: Buryatiya, Kalmykiya, Tuva [Social Institute of Buddhism in Modern Russia: Buryatia, Kalmykia, Tuva]. Sibirskiy filosofskiy zhurnal [Siberian Philosophical Journal] **17**(4), 144–156 (2019)
6. Kishtanov, B.V., Kostin, M.V.: O problemakh zashchitnogo lesorazvedeniya v Respublike Kalmykiya [On the problems of protective afforestation in the Republic of Kalmykia]. Ekologicheskiye i biologicheskiye osnovy povysheniya produktivnosti i ustoychivosti prirodnykh i iskusstvenno vozobnovlennykh lesnykh ekosistem [Ecological and biological foundations for increasing the productivity and sustainability of natural and artificially renewed forest ecosystems], 407–414 (2018)
7. Dedova, E.B., Goldvarg, B.A., Tsagan-Mandzhiev, N.L.: Degradatsiya zemel' Respublikи Kalmykiya: problemy i puti ikh vosstanovleniya [Land degradation in the Republic of Kalmykia: problems and ways of their restoration]. Aridnyye ekosistemy [Arid Ecosystems] **26**(2), 63–71 (2020)
8. Ochir-Goryaeva, M.V., Ekmaer, A., Waizenegger, V.: Dinamika protsessov opustynivaniya v Respublike Kalmykiya s serediny 1980-kh godov do nastoyashchego vremeni [Dynamics of desertification processes in the Republic of Kalmykia from the mid-1980s to the present]. Oriental Stud. **13**(6), 1613–1622 (2020)
9. V Kalmykii projdet 4-h dnevnyj ritual na ustranenie zasuhi [Kalmykia will host a 4-day ritual to eliminate drought] (26 July 2020) Official website of Central Khurul of Kalmykia. <http://www.khurul.ru/2020/07/26/v-kalmykii-projdet-4-h-dnevnyj-ritual-na-ustranenie-zasuhi/>. Accessed 20 Jul 2021
10. Barkova, A.L.: Buddiyskaya mifologiya: urovni simvoliki [Buddhist mythology: levels of symbolism]. Trudy Ob'yedinennogo nauchnogo tsentra problem kosmicheskogo myshleniya [Proceedings of the Joint Scientific Center for Problems of Space Thinking] 1, 498–533 (2007)
11. Ritual ZHaptuj - pri upadke sil, boleznyah, neudachah [Ritual Zhatpuj – with a breakdown, illness, failure] (20 April 2016) Asia-Russia Daily. <https://asiarussia.ru/buddhism/12018/>. Accessed 20 Jul 2021
12. V Kalmykii prodolzhayutsya chetyrekhnevnye ritualy [Four-day rituals continue in Kalmykia] (29 July 2021) Official website of Central Khurul of Kalmykia. <https://www.khurul.ru/2020/07/29/v-kalmykii-prodolzhayutsya-chetyrekhnevnye-ritualy/>. Accessed 20 Sep 2021
13. Uchebnye praktiki na novom oborudovanii [Training practices on new equipment] (23 May 2021) Official website of Kalmyk State University. <https://www.kalmgu.ru/news/uchebnye-praktiki-na-novom-oborudovanii/>. Accessed 20 Sep 2021
14. Cvetushchij sad gen Ngavang Lodoja [Ngawang Lodoys blooming garden] (4 November 2020) News of Elista and Kalmykia. http://www.elista.org/culture/cvetuwij_sad_gen_ngavang_lodoya/. Accessed 20 Jul 2021

15. V Kalmykii vokrug Arshanskogo hurula vysadili 6 tysyach sazhencev [6 thousand trees were planted in Kalmykia around Arshansky Khurul] (19 October 2019) RIA Novosti Kalmykia. <https://riakalm.ru/index.php/news/128-dobrye-novosti/20609-v-kalmykii-aktsiya-sokhranim-les-privlekla-3-tysyachi-chelovek-fotoreportazh-3>. Accessed 20 Sep 2021



Preliminary Concentration-Response Functions on the Relationship Between Long-Term PM_{2.5} Exposure and Incidence and Prevalence of Depression Based on Systematic Review and a Meta-Analysis

Ying Li^{1(✉)} and Mengmeng Zhang²

¹ Nanjing Foreign Language School, Nanjing, Jiangsu, China

liying_louisechina@163.com

² University of California-Santa Cruz, Santa Cruz, USA

mzhan117@ucsc.edu

Abstract. Previous epidemiological studies have investigated the relationship of ambient air pollution and depression, but the results haven't led to a concentration-response function. In this study, we conduct an updated systematic review and meta-analysis of the evidence, and apply a simulation-based approach to develop a concentration-response function between long-term PM_{2.5} exposure and depression. We search the PubMed database for studies that report quantitatively estimated effects between incidence and prevalence of depression and long-term PM_{2.5} exposure. Of the 234 records identified, 14 studies meet our inclusion criteria. We extracted data from these studies to develop preliminary concentration-response functions for incidence and prevalence of depression respectively. We fit both log-linear and nonlinear functional forms, and use a Monte Carlo simulation approach to quantify the uncertainty. We then examine several sensitivity cases to investigate the robustness of the models. We provide suggestions regarding model selection, and show that the nonlinear model could be a better function to estimate the incidence of depression, while the loglinear model is more robust when estimating the prevalence of depression attributable to PM_{2.5} exposure. Overall, results from epidemiological studies suggest increased risks in both incidence and prevalence of depression with long-term exposure to PM_{2.5}. We discuss the caveats of our work, and suggest future epidemiological studies to investigate more on this linkage in both relatively low and relatively high exposure regions. Such efforts will be very useful in reducing the uncertainty of these concentration-response functions.

Keywords: Long-term PM_{2.5} exposure · Meta-analysis · Concentration-response function · Incidence of depression · Prevalence of depression

1 Introduction

Major depressive disorder, also referred as depression, is a prevalent mental illness that negatively affects one's overall wellbeing [1]. Indeed, about one in five people experience at least one mental health concern at some point during their lifetime, making mental disorder a major public health concern [2, 3]. Symptoms of depression contain exhaustion, persistent poor mood and low productivity, which severely affect not only the patient themselves, but also their entire social network [4].

Given the significant personal and social cost, it is critical to understand and modify the risk factors that may cause depression. In particular, long-term exposure to ambient particulate matter (PM) with an aerodynamic diameter $<2.5 \mu\text{m}$ ($\text{PM}_{2.5}$) is associated with a variety of health impairments, and some are still not fully understood. Based on the Global Burden of Diseases (GBD) in 2019, air pollution is responsible for almost 7 billion deaths due to its association with respiratory diseases, cardiovascular diseases, cancers, and diabetes [4, 5]. Meanwhile, increasing evidence from some previous studies indicates that $\text{PM}_{2.5}$ is related with necroinflammation and brain oxidative stress, routes that are linked to mental illness, leading to behavior deficits and central nervous system diseases in human [6–12].

Despite multiple researchers have been investigating the link between air pollution and depression since the last decades, the findings are conflicting. Some evidence shows positive correlation [13–16] while some shows no association [17, 18]. This can be related with the heterogeneity of the studies. For example, the research subjects vary from teenagers [19, 20] to middle aged and older [17]. Location of the studies ranged from developed countries [14, 21] to developing countries [22, 23]. Further, some studies focus on exposures across multiple countries [22] whereas others focus primarily on a regional district [20].

Systematic reviews from previous studies have shown mostly consistent results regarding increased risk of depression-related outcomes associated with long-term exposure to air pollution. Epidemiologic evidence from Braithwaite et al. [24], Calderón-Garcidueñas et al. [25] and Gu et al. [26] has all pointed out that $\text{PM}_{2.5}$ has a strong association with depression, making it a potential risk factor of the global burden of mental health diseases. Yet, the studies also have some limitations. Due to the insufficient number of existing studies specifically investigating the linkage between long-term fine particulate matter exposure and depression, evidence of comparable exposure–outcome combinations included in the meta-analysis may be limited, and large heterogeneities present in the reported result [24, 25]. Furthermore, the results may not be applicable to all population subgroups due to the lack of individual characteristic data. The insufficiency in the coverage and consistency of the epidemiological evidence limits development of a concentration-response function (CRF) between long-term $\text{PM}_{2.5}$ exposures and depression. Consequently, it is by far difficult to estimate the global impacts of $\text{PM}_{2.5}$ on depression.

As such, here we conduct an updated systematic review of the evidence, and adopt a simulation-based approach developed by Ru et al. [27] to statistically simulate the CRF based on the results of previous research on this connection in a quantitative manner. Specifically, we use a randomized bootstrap approach to resample the observed effects within the uncertainty ranges reported in epidemiological studies in our review. Then,

using Monte Carlo simulation, we created a prototype CRF for the linkage between PM_{2.5} levels and incidence and prevalence of depression respectively. We also ran a series of sensitivity tests to further assess the robustness of the uncertainty association of the functions with findings from the simulations.

The goal of this study is to conduct a systematic review of studies on incidence and prevalence of depression related to long-term exposure to PM_{2.5}, and use the data reported from the studies to derive a preliminary concentration-response function (CRF). We also evaluate the uncertainty and sensitivity of this function, to provide an updated understanding of the strength of evidence on the link between PM_{2.5} and depression.

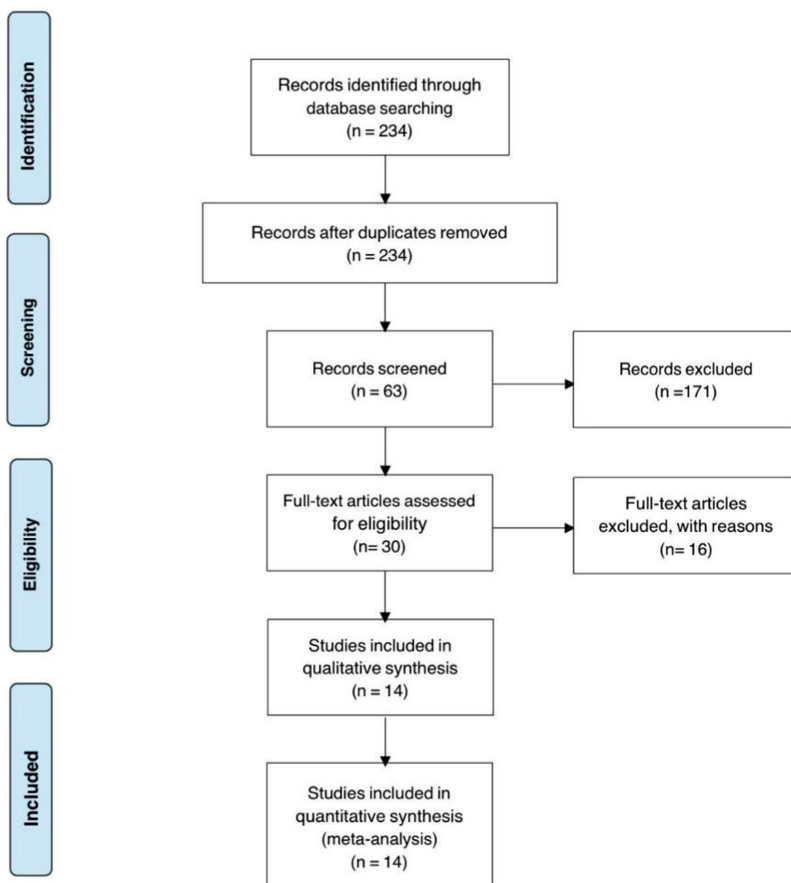


Fig. 1. Flow-chart of the systematic review following the PRISMA suggestion.

2 Methodology

2.1 Search Strategy

We searched for epidemiologic studies which reported quantitative measures of risk of depression associated with long term exposure to particulate matter with diameter smaller than $2.5\text{ }\mu\text{m}$ ($\text{PM}_{2.5}$) in a major database (PubMed, <https://pubmed.ncbi.nlm.nih.gov/>), based on the search keywords: ((((((mental health[Title/Abstract]) OR (psychosis[Title/Abstract])) OR (neurosis[Title/Abstract])) OR (depression[Title/Abstract]))) OR (Self-harm[Title/Abstract]))) OR (Suicide[Title/Abstract])) OR (Bipolar[Title/Abstract])))) AND ((Air pollutant[Title/Abstract]) OR (Particulate matter[Title/Abstract])). As shown above, we limit our search to keywords in title and abstract. We then followed the PRISMA protocol to screen for all the search results, accessing the full text of the selected literature, and followed our inclusion/exclusion criteria to accomplish data collection (Fig. 1). In addition, we searched for newly published results every two weeks to update our review, so that our study included all the latest studies on this topic, until August 2021. We also compared our final research results with previous systematic review and meta-analysis papers to make sure our research is comprehensive enough.

2.2 Inclusion/Exclusion Criteria

Our inclusion/exclusion criteria are as follows: 1) we included cohort, cross-sectional, and case-control studies. 2) We only included studies focused on long-term exposure to $\text{PM}_{2.5}$, and the difference between long-term and short-term exposure type was distinguished according to the studies themselves. 3) Studies with subjects of all ages, genders, races, and regions were all included in our search. 4) Studies with different approaches to define depression, such as antidepressant use, depression diagnosis, or self-reported depressive symptoms, were all included. 5) Studies on both the prevalence or incidence of depression were included.

However, some studies are excluded as they are not sufficiently comparable to the others. For example, we didn't include a study using internet searches for depression-related terms on Baidu, as it could not be directly linked to the morbidity of depression [28]. In addition, we didn't include studies focusing on populations with a specific condition. For example, we excluded a study that linked maternal depression symptoms to air quality [22].

2.3 Data Extraction and Transformation

For each study included in our meta-analysis, we extracted information on the study period, population in the cohort, the age group of participants, exposure types, evaluation metrics of depression, and the observed effect. The observed effect was usually reported in three ways: relative risk (*RR*), hazard ratio (*HR*), or odd ratio (*OR*) of depression incidence or prevalence associated with a unit range of $\text{PM}_{2.5}$ concentration; coefficients in the regression models; and percentage changes relative to a control group. We considered *RR* equivalent to *HR* and *OR* and used *RR* to represent the estimated effect in the study.

We also extracted concentration ranges in each study, and transformed them to comparable metrics of the 5th and 95th percentiles of PM_{2.5} concentrations in the cohort. When a study did not directly report the 5th and 95th percentiles, we implemented the following transformation: when mean and standard deviation of concentrations were reported, we calculated the 5th and 95th percentiles based on a normal distribution.

The calculated values were compared to the minimum and maximum concentrations reported, to make sure our estimated ranges were consistent with the limits of observations.

In addition, studies often present different models with different covariates adjusted. We extracted effects from the models with adjustments of age, sex, race/ethnicity, body mass index, physical activity, smoking status, alcohol consumption, years, region, family income, educational level, marital status and population density. We, however, did not include uncommon variables for adjustment, such as neighborhood social capital [23].

RR or *HR* on the originally reported range of PM_{2.5} were then transformed into those under the unit range of 10 µg/m³, following:

$$RR_{standardized} = \exp(\ln(RR_{original}) \times \frac{10}{unit_{original}}) \quad (1)$$

Also, we calculated the effect size (beta) per 1 µg/m³ using the *RR* based on Eq. 3.

2.4 Statistical Analysis-Fit the Model-Function

We conducted model-fitting based on Ru et al. [27]. Specifically, we established the counterfactual PM_{2.5} concentration level x_{cf} , under which we assumed that there was no risk of depression. We used the minimum level of the 5th percentiles reported by all the studies to represent x_{cf} and calculated PM_{2.5} concentration level x as shown in Eq. 2. This was to reduce the influence of outliers in the PM_{2.5} ranges in each study.

$$x = PM\ 2.5 - x_{cf} \quad (2)$$

We fit the CRF for incidence and prevalence of depression respectively. We used the log-linear functional form to establish the relationship:

$$RR = \exp(\beta x) \quad (3)$$

where *RR* is the relative risk of depression, β is the coefficient of the effect size, and x is the transformed PM_{2.5} exposure according to Eq. 2.

Additionally, we applied a nonlinear function to test which model fits better. Originally developed by Nasari et al. [29] for subject-level modeling and adapted by Burnett et al. [30] for cohort-level modeling, this approach used three parameters (α, μ, τ) to allow for more flexibility in the fitting, expressed as:

$$RR = \exp(\theta T(x)) \quad (4)$$

$$T(x) = \log(1 + x/\alpha)\omega(x) \quad (5)$$

$$\omega(x) = 1/\{1 + \exp[-(x - \mu)/(\tau r)]\} \quad (6)$$

where x is calculated as in Eq. 2; θ is the regression coefficient, which represents the effect size for a unit change in concentrations. Parameter α adjusts for the different levels of concentrations; $\omega(x)$ is a weighting function, where μ and τ respectively determines the shape and curvature of ω , and r represents the PM_{2.5} exposure range, calculated as the difference between the lowest 5th percentile and the highest 95th percentile in exposure ranges of all studies.

For both functional forms, we used log-likelihood to compare the relative goodness of fit [29]. In particular, the larger the value of log-likelihood is, the better the function fits.

2.5 Sensitivity Analysis

We conducted sensitivity analyses to test the robustness of our methods. In order to examine if the fitted CRFs are sensitive to the input data, we implemented the same statistical analysis described in Sect. 2.4 in each sensitivity case. Sensitivity cases were either identified when a study reported effects outside of 2 times of standard deviation in the distribution of all the collected effect sizes, or when a different age group was reported.

3 Results and Discussion

Table 1. CRF for both incidence and prevalence of depression in both log linear and nonlinear forms

Endpoint	Age group	Sampling	model	ZCF	β	β_{SE}	a	mu	tau	Range	Loglik
Depression incidence	Adult	Normal	Log linear	6.8	0.03	0.01	/	/	/	/	0.7
Depression incidence	Adult	Normal	Nonlinear	6.8	0.13	0.05	1.14	3.2	0.1	20.0	1.9
Depression prevalence	Adult	Normal	Log linear	0	0.03	0	/	/	/	/	-23.1
Depression prevalence	Adult	Normal	Nonlinear	0	1.43	0.55	4.45	53	0.17	144.4	-5.5

3.1 Results from the Systematic Review

From the 234 results, we retained 30 articles from 63 full texts retrieved for the systemic review after careful examination. Finally, we retained 14 papers investigating the results

of 15 studies. Table 2 summaries the baseline characteristics of the 15 studies we analyzed. We each included 2 studies performed in China, USA, Netherlands, and Korea. Another 3 of the studies were performed in England and 1 study each was performed in Finland, Germany and Barcelona. We also included a transnational investigation among China, Ghana, India, Mexico, Russia and South Africa. Among the evidence, 5 studies are classified to be the incidence of depression and 9 studies to the prevalence of depression.

Figure 2 and 3 presents the *RR* per $10 \mu\text{g}/\text{m}^3 \text{PM}_{2.5}$ associated with the incidence and prevalence of depression from our systematic review. Among the studies on incidence of depression, no outliers were identified. Two studies are focused on children [19, 20], while others are focused on adults. As the two studies on children reported relatively higher RRs (1.35; 1.21583612146216, respectively) compared to the other studies, we excluded these two as they were not sufficient for us to determine if there is a systematic upward bias for the risk for children. Future research should try to better understand the effects on depression related to air pollution among children.

All of the results included for prevalence are based on data for adults, yet Pun et al. [14], specifically focused on age 57–85, so we excluded it in the main model. As its reported result was not systematically different from the others, itself did not indicate a systematic bias. We thus included it as a sensitivity analysis of the main model. Furthermore, two studies [31, 32] reported significantly large values of RR (6.42 and 4.38, respectively), which could be identified as outliers based on our rule of 2 times of standard deviation. We removed these two cases as another sensitivity analysis. Notably, among the results, two studies [23, 33] are conducted in where $\text{PM}_{2.5}$ concentrations were significantly higher (mean concentrations $70.35 \mu\text{g}/\text{m}^3$ and $57.5 \mu\text{g}/\text{m}^3$, respectively, both located in China). These two studies significantly extended the range of CRF, and were thus important for our functions to be applied in high concentration regions. However, these are still not yet sufficient. Future studies for both incidence and prevalence of depression should consider to focus on regions with high levels of $\text{PM}_{2.5}$ pollution.

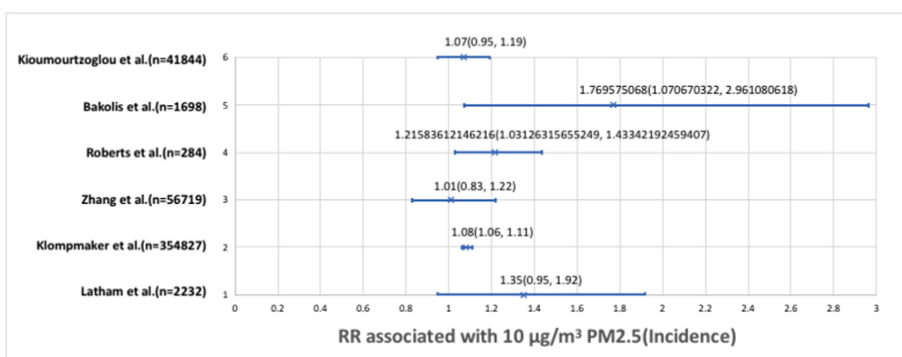


Fig. 2. *RR* associated with $10 \mu\text{g}/\text{m}^3 \text{PM}_{2.5}$ for incidence of depression

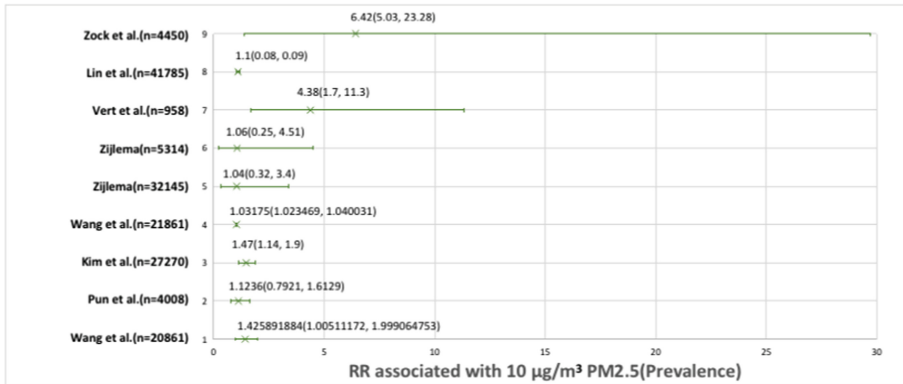


Fig. 3. RR associated with $10 \mu\text{g}/\text{m}^3 \text{PM}_{2.5}$ for prevalence of depression

3.2 Results of Sensitivity Analysis

Figure 4 presents the CRF produced for incidence of depression, where the left panel shows the fit to the original data in β , and the right panel shows the actual CRF. The log-linear function (red) showed a fixed effect size over the entire range of $\text{PM}_{2.5}$, whereas the non-linear function predicted decreasing effect size as $\text{PM}_{2.5}$ concentrations increase. Thus, when the exposure of $\text{PM}_{2.5}$ is high, the log-linear CRF performs as almost a linear extrapolation, which may lead to unrealistically high risks. The nonlinear CRF (blue), on the other hand, flattens as $\text{PM}_{2.5}$ levels are above $25 \mu\text{g}/\text{m}^3$. Plus, the log-linear function has a larger range of uncertainty. Therefore, in the case of incidence, nonlinear CRF can be a more realistic option when applied to regions with high levels of $\text{PM}_{2.5}$ concentration.

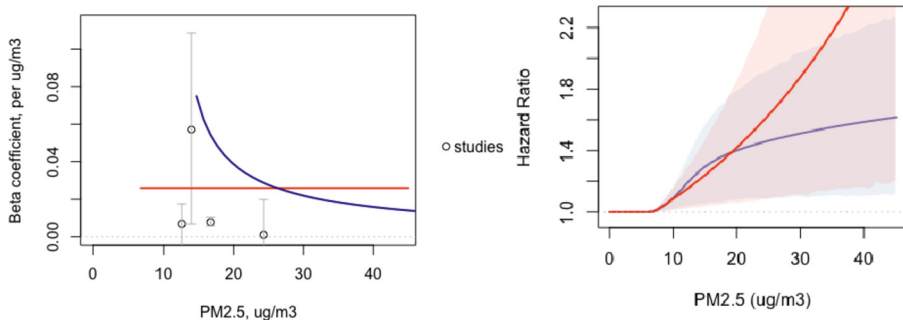


Fig. 4. CRF for incidence of depression, where the left panel shows the estimated effects in both log-linear and nonlinear functional forms and the range of reported effects for beta from studies in our review, and the right panel shows the CRF in the loglinear (red) and nonlinear (blue) forms.

For prevalence (Fig. 5), log-linear (red) and nonlinear functional (blue) forms result in very similar CRFs in the main model. The uncertainty range predicted is much smaller for the log-linear function. The nonlinear function fits better than the log-linear function,

since the log-likelihood of fitting the nonlinear function (-5.5) is much larger than that of fitting the log-linear function (-23.1). Overall, the log-linear CRF can be a better option for the prevalence of depression.

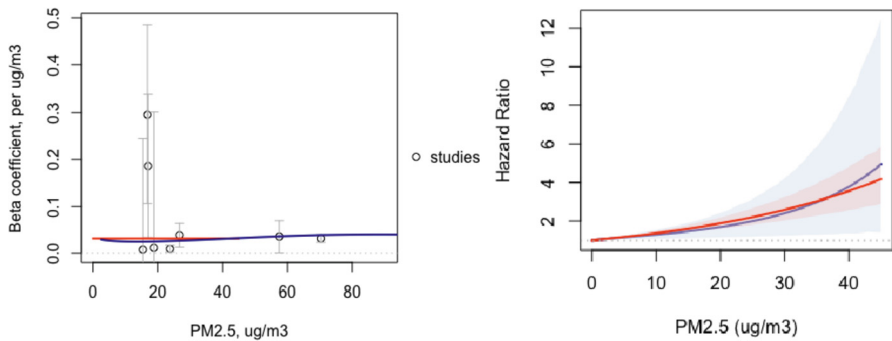


Fig. 5. CRF for prevalence of depression, where the left panel shows the estimated effects in both log-linear and nonlinear functional forms and the range of reported effects for beta from studies in our review, and the right panel shows the CRF in both functional forms.

3.3 Results of Sensitivity Analysis

We compared each sensitivity case described above (Table 3, Fig. 6, 7) to the main results (Table 1, Fig. 3), for prevalence associated with PM_{2.5}. Estimates for β log-linear functions are 0.03 in both sensitivity cases, same with the estimate in the main model (Table 1). For the nonlinear model, the coefficients are 1.55 and 1.50 in the two sensitivity cases (Table 3), slightly higher than 1.43 in the main model. As such, both functional forms are generally robust, especially the log-linear functions. This further demonstrates the log-linear CRF can be a better option to estimate prevalence associated with PM_{2.5}.

3.4 Strengths and Limitations

The study provides a comprehensive examination of the relationship between long-term PM_{2.5} exposure and depression, including the search based on a broad range of outcomes. The method and results in these studies are generally consistent with each other.

Yet there are also limitations to our meta-analysis. To begin with, the evaluation of depression may include heterogeneities. Among the studies included, the evaluation standard of depression varies, consisting of antidepressant use, depression diagnosis, or self-reported depressive symptoms. The different evaluation standards of depression in studies may disrupt the accuracy of the results. In addition, the studied population in the present studies mainly came from households in middle-high income countries with only a few focused on middle-to-low income countries. However, we are not able to present a more detailed subgroup analysis due to the limited studies involved. Moreover, we lack results of the evidence for incidence of depression of both high and low PM_{2.5} concentration areas in our systematic review, causing the z_{cf} result to be very high. Future study should further complete the fundamental epidemiological evidence.

Consequently, more studies should investigate relations of long-term PM_{2.5} exposures and depression. Although our results suggested increased risk with PM_{2.5} exposures over the range examined, this association still requires further investigation on the mechanism and variations of effects in different populations and regions. For future studies, authors should develop their focus more on the locations with low and high PM_{2.5} levels. Following mechanistic studies are encouraged to further modify advanced approaches, as well as precise definitions and diagnostic criteria of depression to prevent numerical estimates and bias concerns.

4 Conclusion

This study conducts an updated systematic review examining the relations between long-term PM_{2.5} exposures and major depressive disorder, whereas our results support the hypothesis of a positive association between the two in terms of incidence and prevalence. The sensitivity analyses we conducted shows the CRFs developed here are likely robust. The limitations and challenges in this field, including evaluations of depression, heterogeneous outcome definitions, and limited evidence presented, suggest that further high-quality studies are necessary to investigate the possibly causative links between long term PM_{2.5} exposure and major depressive disorder.

Appendices

This study conducts an updated systematic review examining the relations between long-term PM_{2.5} exposures and major depressive disorder, whereas our results support the hypothesis of a positive association between the two in terms of incidence and prevalence. The sensitivity analyses we conducted shows the CRFs developed here are likely robust. The limitations and challenges in this field, including evaluations of depression, heterogeneous outcome definitions, and limited evidence presented, suggest that further high-quality studies are necessary to investigate the possibly causative links between long term PM_{2.5} exposure and major depressive disorder.

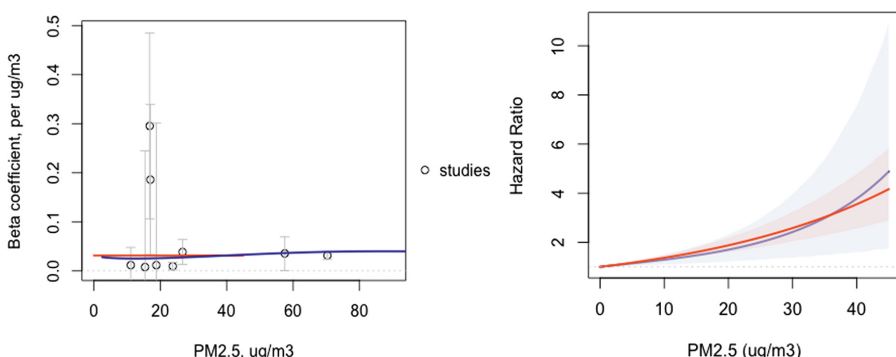


Fig. 6. CRF of the sensitivity case where all studies focused on prevalence of depression are included, where the left panel shows the estimated effects in both log-linear and nonlinear functional forms and the range of reported effects for beta from studies in our review, and the right panel shows the CRF in the loglinear (red) and nonlinear (blue) forms.

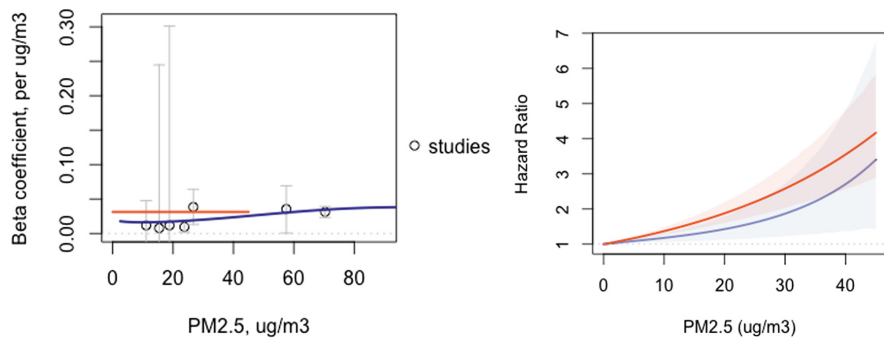


Fig. 7. CRF of the sensitivity case where two studies [31, 32] are excluded from the studies focused on prevalence of depression, where the left panel shows the estimated effects in both log-linear and nonlinear functional forms and the range of reported effects for beta from studies in our review, and the right panel shows the CRF in the loglinear (red) and nonlinear (blue) forms.

Table 2. Summaries the baseline characteristics of the 15 studies we analyzed.

Study	Outcome	Number of study subjects	PM _{2.5} type	Cohort	Time of study	Mean annual average PM _{2.5} (mg/m^3)	5th/95th percentile of annual average PM _{2.5} (mg/m^3)	Relative risk between 5 and 95th percentile of exposures (95% CI) [1]
1. Wang et al. [23]	Prevalence of depressive symptoms by CES-D scale	20,861	AAP	China	2015	57.5	20/95	1.14 (1.00–1.29)
2. Kioumourtzoglou et al. [17]	Incidence of depression (depression diagnosis)	41,844	AAP	the USA	1996–2008	12.58	6.84/18	1.07 (0.95–1.19)
3. Pun et al. [14]	Prevalence of depression (CESD-11 ≥ 9)	4,008 (middle aged and older women 62–87)	AAP	the USA	Wave 1: 2005.07–2006.03 Wave 2: 2010.08–2011.05	11.1	4.76/15.14	1.12 (0.792–1.61)
4. Kim et al. [13]	Prevalence of Major Depressive Disorder (MDD)	27,270	AAP	Seoul, Republic of Korea	2002–2010	26.7	24.9/29.8	1.47 (1.14–1.9)
5. Bakolis et al. [34]	Survey common mental health disorder	1,698	AAP	South East London, England	2008–2013	13.95	9.74/18.16	1.77 (1.07–2.96)

(continued)

Table 2. (*continued*)

Study	Outcome	Number of study subjects	PM _{2.5} type	Cohort	Time of study	Mean annual average PM _{2.5} (mg/m ³)	5th/95th percentile of annual average PM _{2.5} (mg/m ³)	Relative risk between 5 and 95th percentile of exposures (95% CI) [1]
6. Latham et al. [19]	Incidence of the risk of major depressive disorder (MDD)	2,232	AAP	(UK) England	2004	12.07	7.80/16.34	1.35 (0.95–1.92)
7. Wang et al. [33]	Prevalence of depression based on CES-D scale	21,861	AAP	China	2016	70.35	-3.72/144.42	1.03 (1.02–1.04)
8. Zhang et al. [11]	Incidence of depression with CES-D score and reported diagnoses	56,719	AAP	Seoul and Suwon, South Korea	2011–2015	24.3	21.752/26.85	1.01 (0.83–1.22)
9. Zijlema et al. [21]	Prevalence of depressive moods with MINI diagnostic interview Prevalence of depressive moods with PHQ-9 interview version	32,145	AAP	Netherlands, Germany	2007–2013	15.4 18.8	15.28/15.52 15.24/22.36	1.04 (0.32–3.4) 1.06 (0.25–4.51)
10. Vert et al. [32]	Prevalence of depression and anxiety symptoms	958	AAP	Barcelona	2009–2014	16.8	14.84/18.76	4.38 (1.7–11.3)
11. Lin et al. [22]	Prevalence of depressive symptoms	41,785	AAP	China, Ghana, India, Mexico, Russia, South Africa	2007–2010	23.75	23.45/ 24.05	1.1 (1.02–1.19)
12. Zock et al. [31]	Prevalence and determinants of disease groupings	4,450	AAP	Netherlands	2013	17	16.06/17.94	6.42 (1.39–29.7)
13. Roberts et al. [20]	Psychiatric diagnoses symptoms	284	AAP	England	2007–2013	14.09	12.74/15.44	1.22 (1.03–1.43)
14. Klompmaker et al. [35]	Incidence of psychological distress	354,827	AAP	Netherlands	2012	16.7	15.07/18.33	1.08 (1.06–1.11)

Table 3. CRF of both sensitivity cases for prevalence of depression in both log linear and nonlinear forms, where the first two rows correspond to the sensitivity case (Fig. 6) including all studies focused on prevalence of depression, and the last two rows correspond to the sensitivity case (Fig. 7) excluding two studies [31, 32] based on the first sensitivity case.

Endpoint	Age group	Sampling	Model	ZCF	β	β _SE	a	mu	tau	Range	Log likelihood
Depression prevalence	Adult	Normal	Log linear	0	0.03	0	/	/	/	/	-25.4
Depression prevalence	Adult	Normal	Nonlinear	0	1.55	0.49	5.77	51.3	0.17	144.42	-6.71
Depression prevalence	Adult	Normal	Log linear	0	0.03	0	/	/	/	/	-20.33
Depression prevalence	Adult	Normal	Nonlinear	0	1.37	0.55	3.87	56.46	0.18	144.42	-4.22

References

1. Lim, G.Y., et al.: Prevalence of depression in the community from 30 countries between 1994 and 2014. *Sci. Rep.* **8**(1), 1–10 (2018)
2. World Health Organization: The global burden of disease: 2004 update. World Health Organization (2008)
3. Trautmann, S., Rehm, J., Wittchen, H.U.: The economic costs of mental disorders: Do our societies react appropriately to the burden of mental disorders? *EMBO Rep.* **17**(9), 1245–1249 (2016)
4. Murray, C.J., et al.: Global burden of 87 risk factors in 204 countries and territories, 1990–2019: a systematic analysis for the Global Burden of Disease Study 2019. *Lancet* **396**(10258), 1223–1249 (2020)
5. World Health Organization: Ambient air pollution: a global assessment of exposure and burden of disease (2016)
6. Cascio, W.E., Long, T.C.: Ambient air quality and cardiovascular health: translation of environmental research for public health and clinical care. *N. C. Med. J.* **79**(5), 306–312 (2018)
7. Kim, H., Kim, W.H., Kim, Y.Y., Park, H.Y.: Air pollution and central nervous system disease: a review of the impact of fine particulate matter on neurological disorders. *Front. Public Health* **8** (2020)
8. Hurley, L.L., Tizabi, Y.: Neuroinflammation, neurodegeneration, and depression. *Neurotox. Res.* **23**(2), 131–144 (2013)
9. Block, M.L., Calderón-Garcidueñas, L.: Air pollution: mechanisms of neuroinflammation and CNS disease. *Trends Neurosci.* **32**(9), 506–516 (2009)
10. Craig, L., et al.: Air pollution and public health: a guidance document for risk managers. *J. Toxicol. Environ. Health A* **71**(9–10), 588–698 (2008)
11. Zhang, Z., et al.: Long-term particulate matter exposure and onset of depression in middle-aged men and women. *Environ. Health Perspect.* **127**(7), 077001 (2019)
12. Thomson, E.M., et al.: Self-rated stress, distress, mental health, and health as modifiers of the association between long-term exposure to ambient pollutants and mortality. *Environ. Res.* **191**, 109973 (2020)
13. Kim, K.N., Lim, Y.H., Bae, H.J., Kim, M., Jung, K., Hong, Y.C.: Long-term fine particulate matter exposure and major depressive disorder in a community-based urban cohort. *Environ. Health Perspect.* **124**(10), 1547–1553 (2016)

14. Pun, V.C., Manjourides, J., Suh, H.: Association of ambient air pollution with depressive and anxiety symptoms in older adults: results from the NSHAP study. *Environ. Health Perspect.* **125**(3), 342–348 (2017)
15. Petkus, A.J., et al.: Outdoor air pollution exposure and inter-relation of global cognitive performance and emotional distress in older women. *Environ. Pollut.* **271**, 116282 (2021)
16. Liu, Q., et al.: Association between particulate matter air pollution and risk of depression and suicide: a systematic review and meta-analysis. *Environ. Sci. Pollut. Res.*, 1–21 (2021)
17. Kioumourtzoglou, M.A., et al.: The association between air pollution and onset of depression among middle-aged and older women. *Am. J. Epidemiol.* **185**(9), 801–809 (2017)
18. Wang, Y., et al.: Ambient air pollution and depressive symptoms in older adults: results from the MOBILIZE Boston study. *Environ. Health Perspect.* **122**(6), 553–558 (2014)
19. Latham, R.M., et al.: Childhood exposure to ambient air pollution and predicting individual risk T of depression onset in UK adolescents. *J. Psychiatr. Res.* **138**, 60–67 (2021)
20. Roberts, S., et al.: Exploration of NO₂ and PM2.5 air pollution and mental health problems using high-resolution data in London-based children from a UK longitudinal cohort study. *Psychiatr. Res.* **272**, 8–17 (2019)
21. Zijlema, W.L., et al.: The association of air pollution and depressed mood in 70,928 individuals from four European cohorts. *Int. J. Hyg. Environ. Health* **219**(2), 212–219 (2016)
22. Lin, Y., et al.: The impacts of air pollution on maternal stress during pregnancy. *Sci. Rep.* **7**(1), 1–11 (2017)
23. Wang, R., Xue, D., Liu, Y., Liu, P., Chen, H.: The relationship between air pollution and depression in China: is neighbourhood social capital protective? *Int. J. Environ. Res. Public Health* **15**(6), 1160 (2018)
24. Braithwaite, I., Zhang, S., Kirkbride, J.B., Osborn, D.P., Hayes, J.F.: Air pollution (particulate matter) exposure and associations with depression, anxiety, bipolar, psychosis and suicide risk: a systematic review and meta-analysis. *Environ. Health Perspect.* **127**(12), 126002 (2019)
25. Calderón-Garcidueñas, L., et al.: Air pollution and your brain: what do you need to know right now. *Prim. Health Care Res. Dev.* **16**(4), 329–345 (2015)
26. Gu, X., et al.: Association between particulate matter air pollution and risk of depression and suicide: systematic review and meta-analysis—RETRACTED. *Br. J. Psychiatr.* **215**(2), 456–467 (2019)
27. Ru, M., Brauer, M., Lamarque, J.F., Shindell, D.: Exploration of the global burden of dementia attributable to PM2.5: what do we know based on current evidence? *Geo-Health*, e2020GH000356 (2021)
28. He, G., et al.: The association between PM2.5 and depression in China. *Dose-Response* **18**(3), 1559325820942699 (2020)
29. Nasari, M.M., et al.: A class of non-linear exposure-response models suitable for health impact assessment applicable to large cohort studies of ambient air pollution. *Air Qual. Atmos. Health* **9**(8), 961–972 (2016)
30. Burnett, R., et al.: Global estimates of mortality associated with long-term exposure to outdoor fine particulate matter. *Proc. Natl. Acad. Sci.* **115**(38), 9592–9597 (2018)
31. Zock, J.P., et al.: The impact of social capital, land use, air pollution and noise on individual morbidity in Dutch neighbourhoods. *Environ. Int.* **121**, 453–460 (2018)
32. Vert, C., et al.: Effect of long-term exposure to air pollution on anxiety and depression in adults: a cross-sectional study. *Int. J. Hyg. Environ. Health* **220**(6), 1074–1080 (2017)
33. Wang, R., et al.: Cross-sectional associations between long-term exposure to particulate matter and depression in China: the mediating effects of sunlight, physical activity, and neighborly reciprocity. *J. Affect. Disord.* **249**, 8–14 (2019)
34. Bakolis, I., et al.: Mental health consequences of urban air pollution: prospective population-based longitudinal survey. *Soc. Psychiat. Psychiatr. Epidemiol.* **56**(9), 1587–1599 (2021)

35. Klompmaker, J.O., et al.: Associations of combined exposures to surrounding green, air pollution and traffic noise on mental health. *Environ. Int.* **129**, 525–537 (2019)
36. Edition, F.: Diagnostic and statistical manual of mental disorders. Am. Psychiat. Assoc. **21**, 591–643 (2013)
37. Lin, H., et al.: Exposure to air pollution and tobacco smoking and their combined effects on depression in six low-and middle-income countries. *Br. J. Psychiat.* **211**(3), 157–162 (2017))
38. Peters, R., et al.: Air pollution and dementia: a systematic review. *J. Alzheimer's Dis.* **70**(s1), S145–S163 (2019)
39. Stanaway, J.D., et al.: Global, regional, and national comparative risk assessment of 84 behavioural, environmental and occupational, and metabolic risks or clusters of risks for 195 countries and territories, 1990–2017: a systematic analysis for the Global Burden of Disease Study 2017. *Lancet* **392**(10159), 1923–1994 (2018)



Global INDCs Gap, Dilemma and Innovative Path of Carbon Sink Increase

He Hu, Weigu Fang, Tingyu Luo, and Guoliang Jin^(✉)

School of Economics and Management, Beihang University, Beijing 100083, China
pkuemba@hotmail.com

Abstract. Mitigating global warming is an urgent task facing all countries in the world, which requires the joint efforts of all countries. In the context of INDCs and the framework of the Paris Agreement, this paper estimates the gaps in CO₂ concentration, atmospheric temperature, and emission quantity with respect to global INDCs targets. Based on global carbon budget, the dilemma of global carbon emission is analysed and quantified in this paper. Furthermore, this paper reveals the huge potential of blue carbon system in the ocean to mitigate climate change, and proposes developing an innovative path to increase blue carbon sinks from China's point of view.

Keywords: Climate change · Carbon emission · INDCs · Blue carbon · Global warming

1 Introduction

Coping with climate warming is an urgent issue that all countries in the world must face together [1–5]. The Intended Nationally Determined Contributions (INDCs) are action targets in response to global climate change of each individual signatory country under “United Nations Framework Convention on Climate Change” in light of their own circumstances. Regarding the actual situation of individual signatory countries, scholars have carried out some studies on how to achieve the targets of INDCs [6–11]. China is currently the world’s largest carbon emitter, and its policies, technologies and measures to deal with climate change have attracted extensive attention [12–14]. Many international researches by various scenario models of climate emission reduction have shown that, in terms of the INDCs emission reduction targets and the strength of climate governance policies of individual signatory countries, there is still a huge gap to meet the target of the Paris Agreement on climate change by 2030 and 2050. It is not enough to achieve the goal of keeping global temperature rises at 2 °C. In this paper, we make a systematical estimation on the actual difference in concentration, temperature and quantity of global INDCs targets, and discuss carbon emission dilemma with respect to global carbon budget. Furthermore, we reveal the potential of blue carbon sinks stored in the ocean to mitigate climate change, and propose an innovative path to increase blue carbon sinks.

2 Analysis of Global INDCs Gap

2.1 Concentration Gap of Global INDCs

The open data from Global Carbon Project (GCP) and Global Carbon Data from the Madrid Climate Conference in December 2019 have shown that, since the Industrial Revolution, the annual emissions of artificial CO₂ are approximately 2.37×10^{10} tCO₂e, and the cumulative CO₂ emissions of developed countries account for 70% of global CO₂ emissions in the same period. The data also indicated that global CO₂ concentration from 2016 to 2019 has reached the highest level in the past 80 million years, and the climate change risk is imminent, as shown in Fig. 1.

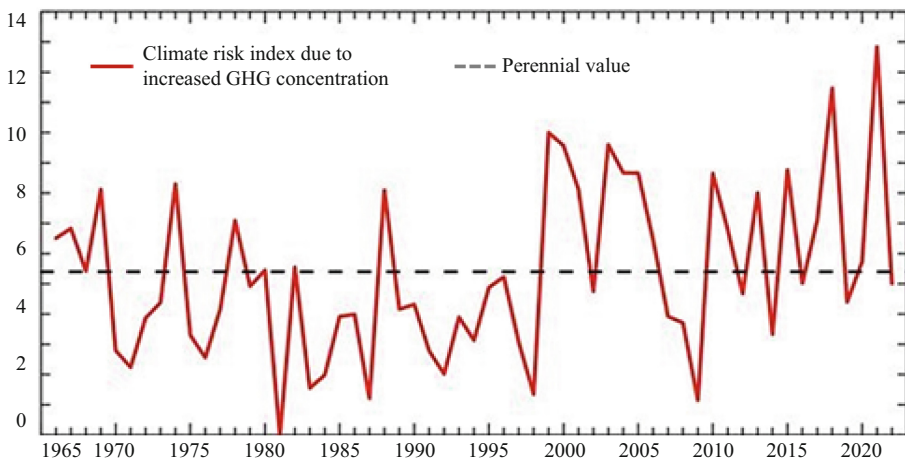


Fig. 1. Climate risk index of global GHG stock concentration. (Source: China Blue Paper on Climate Change 2019)

According to historical emission data, the CO₂ concentration rose from 277 ppm to 403 ppm between 1750 and 2019, with a 45% increase. In this period, the CO₂ concentration exceeded 400 ppm in 2016 at the first time in history, and reached 420 ppm in 2017 with an annual growth of 2.5 ppm. It is expected to reach 450 ppm in about 10 years and continue rising to 550 ppm, leading to a 50% probability of rising temperature over 3 °C. According to existing developing scenario, it is estimated that the annual growth of CO₂ concentration is 3–4 ppm. In the end of this century, CO₂ concentration will increase by 57% to 550–850 ppm, causing over 50% probability of 3.5–5 °C temperature rises, while the Paris Agreement aims to control CO₂ concentration within the stock interval of 450–550 ppm. International Environmental Protection Organization forecast the probability of global temperature rises within 1.5 °C, corresponding to CO₂ concentration of 430 ppm, would be less than 50%.

2.2 Temperature Gap of Global INDCs

Global meteorological observation records show that the warming trend continues. The global average temperature in 2019 was about 1.1 °C higher than in pre-industrial period,

making it the second warmest year on record. 2015 to 2019 were the five warmest years since full temperature records began, and every consecutive decade since the 1980s has been warmer than the previous decade. Correspondingly, after the first 3 years of emission stable period, the world has been witnessed a strong growing trend again in 2017, reaching 4.1×10^{10} tCO₂e. Eliminating the influencing factors of Covid-19 in 2020, a new emission growth period will be entered in the future. The whole world set an updated climate target after the Paris Agreement, i.e., control the global temperature rises within 1.5 °C. To realize this target, global net zero emissions must be achieved by 2050.

Gap in Temperature Rises of 2 °C. Climate Action Tracker Project of WMO assessed INDCs of individual signatory countries and concluded that global warming would be projected to 2.9–3.1 °C by 2050, even if the recently updated emission reduction targets are strictly adhered to. So emissions would have to be cut down by more than 85% by 2050 compared with 2000, so as to meet the target probabilistically. Obviously, the target of keeping global temperature rises within 2 °C compared with 1750 in the pre-industrial era cannot be achieved.

In the scenario of controlling temperature rises within 2 °C (Table 1), IPCC required the balance of global INDCs' emission level in 4.2×10^{10} tCO₂ before 2050, and in order to control temperature rises within 2 °C, global INDCs must be reduced by 2.3×10^{10} tCO₂e. Current INDCs scenario stipulates that annual emission reduction will be 5.0×10^9 tCO₂e, and by 2030 the emissions will be reduced to $4.0\text{--}6.0 \times 10^9$ tCO₂e. If the above INDCs scenario can be fully performed, it is expected to reduce emissions up to 1.1×10^{10} tCO₂e by 2030. To reduce to 5.4×10^{10} tCO₂e level, the emissions must be further reduced by 1.2×10^{10} tCO₂e, while global temperature will still rise by 3 °C. It will cause a 57% increase in global emissions at the end of this century, reaching the level of 5.4×10^{10} tCO₂e, and causing atmosphere CO₂ concentration up to 550 ppm and global temperature rises to 3.5 °C track [15]. UNDP forecast global CO₂ concentration and temperature rises in 2100 under different emission reduction scenarios, and showed a yellow card for current global efforts for mitigating climate change. Current INDCs of individual signatory countries are estimated to reach only one-third of the stipulated emission reduction in 2030. Even if the targets are updated and fully implemented, global warming is likely to rise by more than 3 °C by 2100, which has a great difference from the climate target of 2 °C (see Fig. 2). Considering the US has withdrawn from the Paris Agreement on November 4, 2020, things may get worse in the future.

Table 1. INDCs scenario for global temperature rises of 2 °C. Unit: 10^8 tCO₂e

National INDCs	Cumulative emission reduction by policies	Expected emission reduction by 2030	Emission target in 2050	Gap
Without INDCs	0	650	420	230
With INDCs	110	540	420	120

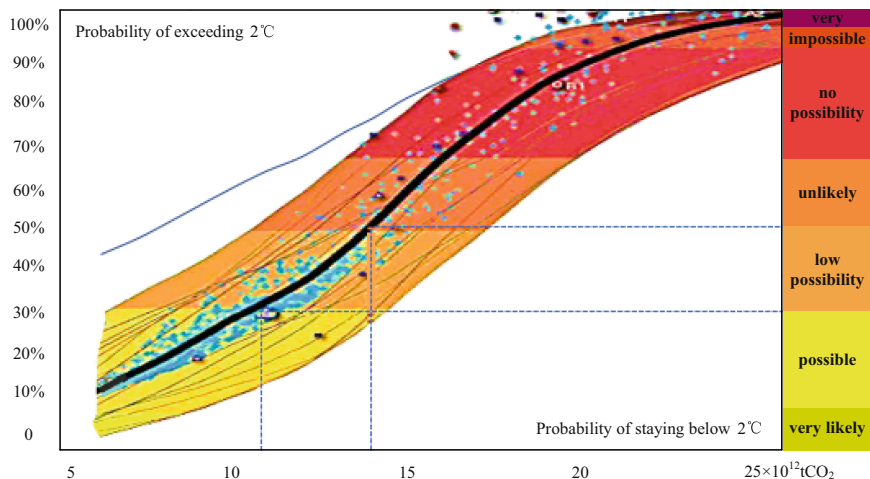


Fig. 2. Possibility of global temperature rises within 2 °C (Source: CDIAC/GCP Data 2019)

Gap in Temperature Rises of 1.5 °C. World Wide Fund for Nature reported that emissions must plummet after a peak in 2030 if global warming was to be controlled within 2 °C or a lower target of 1.5 °C. Total affirmatory emission reduction of current global INDCs was only to reach the half of target, thus having a gap of 1.2×10^{10} tCO₂– 1.6×10^{10} tCO₂e. Under the current INDCs target scenario, global temperatures will rise between 2.6 °C and 3 °C by 2100 and 3.5 °C by 2200. Therefore, most climate researchers believe that current climate target of 1.5 °C is not scientifically justified. There is a high probability of prediction that emissions will reach 5.5×10^{10} tCO₂e level in 2030. The global INDCs target falls short of the 2 °C target by 2030. Only when reducing the emissions to 4.2×10^{10} tCO₂e level, which is far greater than the existing level of emission reduction of INDCs target, it is possible to control the temperature rises within 1.5 °C.

According to the gear mechanism of the Paris Agreement, the US Department of Energy made an overall estimation of global INDCs target, and believed that to keep the temperature rises within 2 °C, it was necessary to achieve global net zero emissions in 2080–2090, while the temperature rises within 1.5 °C would require net zero emissions in 2050–2080. It is not sufficient for existing global INDCs to achieve temperature rises of 2 °C, let alone the target of 1.5 °C. Even if the US returns to the Paris Agreement and implements the protocol with EU, China, and other parties in the future, it is necessary to reduce the emissions to 50% of current level by 2050. In this situation, CO₂ concentration will not exceed 450 ppm, while global temperature can only decrease by 0.07 °C. In addition, annual cost will reach up to \$1.0– 4.0×10^{11} , which will be disproportionate to benefits. Now Alliance of Small Island States and the least developed countries demand that temperature rises should not be more than 1.5 °C and CO₂ concentration should not be over 350 ppm, then global CO₂ emissions must be reduced by more than 90% in 2050. However, this scenario is basically impossible to achieve.

2.3 Quantity Gap of Global INDCs

Climate Change Impact Assessment 2010–2030 of IPCC Report (AR5, 2013) [16] indicates that the artificial CO₂ increases 2.37×10^{10} tCO₂e per year, causing the level of global CO₂ 39% higher than that in the past 650,000 years. It is estimated that the world will increase 100 million new poverty-stricken population, with total emissions of 6.5×10^{10} tCO₂e.

Emissions Gap Report 2019, released by UNDP, argued that despite some achievements in climate policies made by many signatory countries, global emissions continued to grow without any sign of reaching a peak. In the past decade, global emissions increased at an annual growth rate of 1.5%, and reached 5.53×10^{10} tCO₂e only from 2018 to 2019, which hit a record high. Even if all the current unconditional commitments of INDCs are fulfilled, global temperature rises are still likely to reach 3.2 °C. The report estimated that global annual emissions must be decreased by another 1.50×10^{10} tCO₂e on the basis of the updated INDCs schemes of individual signatory countries in 2030 if the temperature rises were controlled within 2 °C, while the global annual emissions must be decreased by 3.20×10^{10} tCO₂e in order to achieve the target of temperature rises within 1.5 °C. Estimating the annual average emission reduction rate for 2020–2030, we have to reduce emissions by 2.7% per year to achieve the target of 2 °C, while reduce emissions by 7.6% per year to reach the target of 1.5 °C.

WRI research data showed that global cumulative CO₂ emissions were about 1.1×10^{12} tCO₂e during 1850–2000. If the probability of global temperature rises of 2 °C was not more than 50%, then the global cumulative emissions cannot exceed 1.44×10^{12} tCO₂e and the annual average emissions cannot exceed 2.88×10^{10} tCO₂e. If the probability of global temperature rises of 2 °C was no more than 1/3, then the global cumulative emissions cannot exceed 1.16×10^{12} tCO₂e and the annual average emissions cannot exceed 2.32×10^{10} tCO₂e. We can conclude that it is necessary to reduce emissions by 50% in 2050 than in 1990, and the cumulative emissions must arrive at the level of 1.2×10^{12} tCO₂e from 2000 to 2050. However, current global INDCs is expected to reduce emissions up to 1.10×10^{10} tCO₂e, which is not enough to cut down the emissions of 6.5×10^{10} tCO₂e in 2030 so as to balance at the level of 4.2×10^{10} tCO₂e, thus existing a huge gap. For this purpose, Greenpeace Organization expressed that it was necessary to suspect the actual effectiveness of the Paris Agreement on curbing emissions. IPCC also clearly indicated that when updating the global target in 2020, individual signatory countries would have to improve their visions for reducing emissions and update their climate targets.

As shown in Fig. 3, under the scenario of 2 °C target, it is highly possible to experience a positive emission growth of 3% or above, in spite of China temporarily, which accounts for 28% of global total carbon emissions and has annual GDP growth rate of 6%–8%. And even if all countries follow INDCs pledge, they will only be able to achieve 30% of the Paris Agreement target by 2050.

If lacking efficient emission reduction policies and incentives, only the four large economic entities, including China, US, EU and India, will exhaust the emission reduction quota in 2030 due to the inertial factors of world economic development and human life, leaving no spare quota or emission space available to other countries. Thus, the

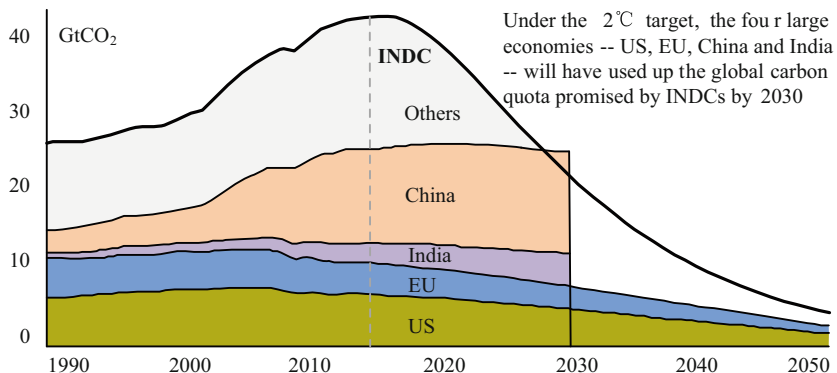


Fig. 3. Global INDCs and space for emission reduction after 2030 (Source: CDIAC/GCP data 2019)

world needs innovative solutions to reduce emission and develop new paths to increase carbon sinks.

3 Carbon Budget and Emission Reduction Dilemma

The Future Earth project have updated its data of Global Carbon Atlas and released Global Carbon Budget. Since the era of industrialization, artificial emissions were about 2×10^{12} tCO₂e, accounting for 70% contribution to global temperature rises. According to IPCC, total emissions need to be controlled within 3.2×10^{12} tCO₂e to keep temperature rises of 2 °C, leaving only 1.2×10^{12} tCO₂e quota. By January 2020, The top 5 economies in terms of carbon emissions are China (27.2%), US (14.6%), the 28 EU countries (9.6%), India (6.8%), and Russia (5.0%). Japan also has higher emissions (2.56%), just behind Russia. Germany and UK in the EU account for 2.2% and 1.1% of emissions respectively. Table 2 shows the global shares of carbon emissions in developed and developing countries.

Table 2. Emission shares of developed and developing countries

Duration	Shares of emissions from top 10 developed countries	Shares of emissions from developing countries
1750–1949	95%	5%
1950–1999	77%	23%
2000–2011	75%	23%
2012–2014	70%	30%
2015 and beyond	50%–60%	40%–50% (China accounts for a quarter of global emissions)

The International Energy Agency (IEA) released 2019 annual report of global carbon emissions, pointing out that global carbon emissions have increased by 1.6% in 2017 and 2.7% in 2018, and the emissions resulted from economic growth have been roughly offset by emission reduction actions in 2019. Global carbon emissions were 3.3×10^{10} tCO₂e, in which EU, US, Japan and other developed countries still accounted for 1/3 of global emissions. Along with the rapid development of world's emerging economic entities, the proportional pattern of global emissions has emerged a new trend. The emissions from developed countries have actually been replaced by outsource processing emissions with annual growth rate of 11%, affecting global emission peaking in 2030 and the balance of net zero emissions in 2050. In general, developed countries ought to reduce 80% emissions in 2050 than 1990, and cumulative emissions per capita must be maintained at the level of 560tCO₂e, thus achieving the target of net zero emissions.

China National Center for Climate Strategy Research analyzed the dynamic growth index under low-carbon scenario, and found that the cumulative emission ratios of US, EU and China during 1750–2030 were 1.4:1.2:1, and China's emissions in 2030 would be still lower than the historical cumulative emission level of US and Europe during 1750–2015. If China's carbon intensity reduces by 60%, China will hit an emission peak at approximately 1.28×10^{10} tCO₂e in 2030. And if the carbon intensity reduces by 65%, the emission peak of China will be about 1.12×10^{10} tCO₂e in 2030 (see Fig. 4).

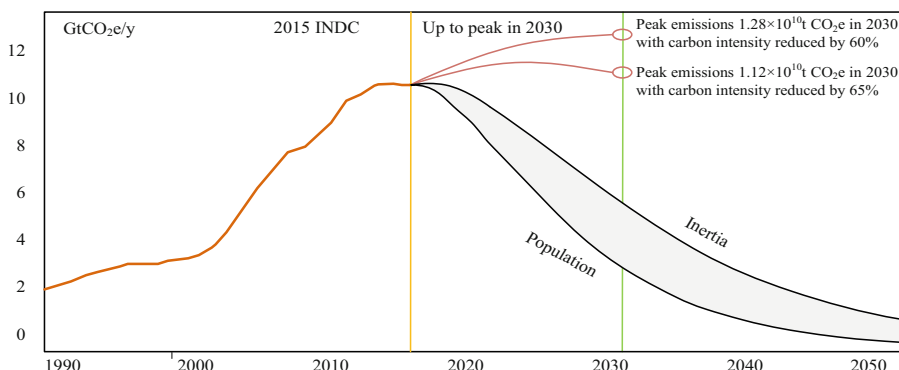


Fig. 4. Emission peaking of China in 2030 with carbon intensity reduced by 60% and 65% (Source: GCP data 2019)

International Environment Organization predicted global population would be 9 billion in 2050, with 1.5 billion and 7.5 billion living in developed and developing countries, respectively [17]. CAT organization analyzed global medium- and long-term carbon emission trends, and concluded that carbon emissions would increase to 1.39×10^{11} tCO₂e in 2100 under normal development scenarios of the Paris Agreement from global emissions of 5.7×10^{10} tCO₂e in 2015. In this case, compared with pre-industrial, global temperature will increase 2.7–5.9 °C, and the concentration stock of CO₂ will reach the historical extreme value of 889–922 ppm, causing the climate to become extremely dangerous [18].

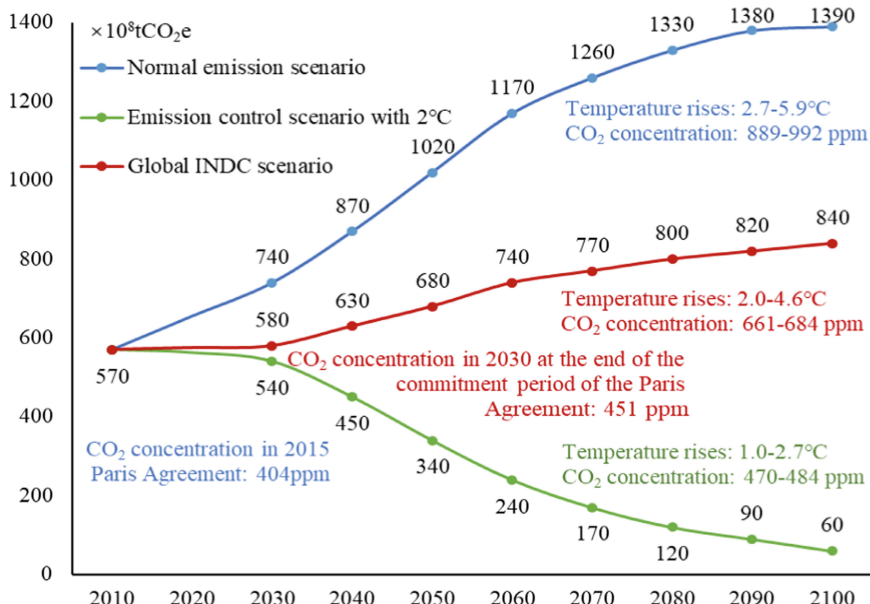


Fig. 5. Global emission scenarios for CO₂ concentration and temperature rise control in 2030, 2050 and 2100 (Source: GCP Data 2019)

In Fig. 5, the three colored curves represent different trends of temperature rises under different emission scenarios, where the intersection point represents global carbon emission level before the 2015 Paris Agreement. If we can follow the 2 °C temperature control scenario (green line) and the global INDCs commitment scenario (red line), then the temperature rise will peak steadily over the next decade or so, and then decline or continue gentle evolution. Under these two scenarios, in theory it is possible to achieve the INDCs commitments to control CO₂ concentration in 450 ppm in 2030 and temperature rises within 2 °C. However, if current normal emission scenario continues, 2100 will witness temperature rises of 2.7–5.9 °C as shown in the blue line, which would be completely unsustainable for the natural ecology.

According to the Global Carbon Project (GCP), the artificial carbon emissions arrived at a new high point during 2017–2018 at $3.68 \pm 1.8 \times 10^{10} \text{tCO}_2\text{e}$. Based on current growth rate, artificial emissions will increase to $4.1 \times 10^{10} \text{tCO}_2\text{e}$. The world will run out of carbon budget quota in next 20–30 years. Even if we improve current temperature control target of 2 °C to a more practical level of 3 °C, namely increasing the carbon budget to $2–2.5 \times 10^{12} \text{tCO}_2\text{e}$, the carbon budget will still be used up in about 30 years, see Fig. 6. Based on current emission trend and INDCs target committed by individual signatory countries, global warming will be at least 3 °C by the end of this century (UNEP, 2019), which is twice the temperature control target of 1.5 °C set by the Paris Agreement. The catastrophic effects will increase exponentially with each 1 °C increase in atmospheric temperature. Therefore, there are 114 countries around the world having announced plans to update their targets with enhanced INDCs, and 121 countries having pledged to realize carbon neutrality by around 2050.

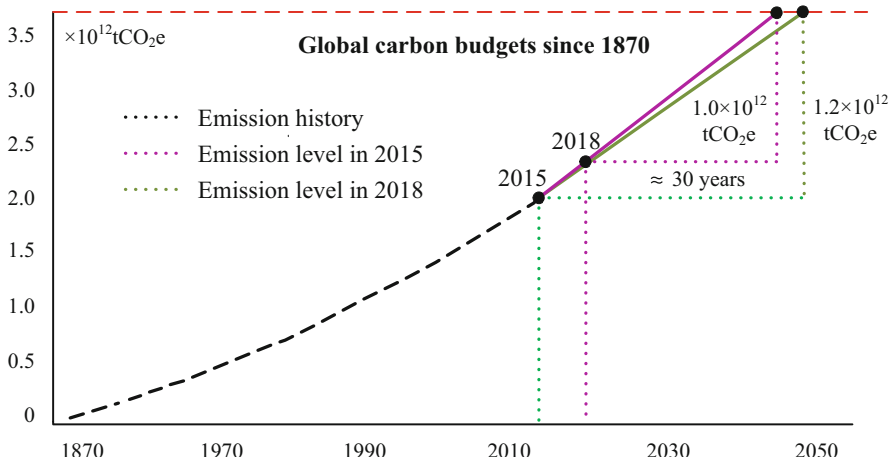


Fig. 6. Global carbon budgets compliant with concentration control (Source: GCP Data 2019)

4 New Path to Increase Carbon Sinks

It is necessary to keep global long-term temperature rises within 1.5 °C to avoid serious consequences caused by climate change. Considering the existing global carbon estimates, the emission reduction capacity of INDCs, and IPCC's targets including emission peak in 2030, carbon balance by 2050 and net carbon emissions by 2100, the solution to climate change cannot continue to arbitrarily maintain existing carbon quota. So far, US maintains 18% of global carbon emissions, which is unfair because other countries will lose out development opportunity due to limited carbon emission space.

What is more equitable is the scheme featured with per capita cumulative emissions based on absolute equality of annual cumulative emissions of global population, because countries at different development stages need different development drivers and less developed countries need more space for their carbon budgets. The third scheme is the compromise between the first two schemes. Nature Climate Change argues for a moderate scheme that both respects history and limits global carbon budget, taking into account the mixed factors of national development status and population balance. Figure 7 shows different arrangement plans for global residual carbon budgets with respect to different emission reduction control schemes. Obviously, a more effective strategy to respond to climate change is to allocate climate resources globally by using a market-based pattern and to give full play to the potential of new pathway to carbon sink increase, based on their optimal emission reduction targets put forward by individual signatory countries.

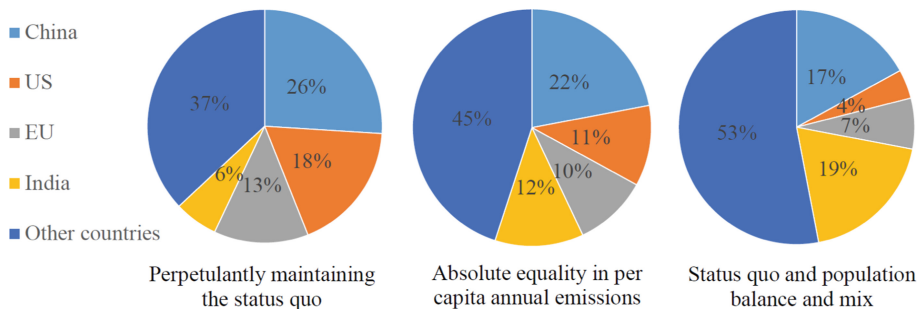


Fig. 7. Residual carbon budgets under different emission reduction schemes (Source: GCP data 2019)

The blue carbon system in the ocean, accounting for more than half of global climate resources, provides a new way to reduce emission for the market-oriented solution to global climate change, which will play a vital role in mitigating climate change. At present, the global understanding of ocean blue carbon mechanism is still very poor, especially the research on the process of ocean workings and its ecological effect is still at the stage of conceptual exploration or laboratory simulation.

The blue ocean is honored as the earth's climate regulator. Ocean absorbs CO₂ in atmosphere and forms carbon capacity or sequestered carbon sinks in a long period, with inorganic, organic, particles, dissolved carbon, and other physical and chemical forms. There are quite a number of brown carbon, black carbon, and green carbon enter into the ocean through micro aerosols and river sediment. Data from Blue Carbon Report (2009) [19] showed that, the ocean covered 70.8% of the earth's surface area, and 93% of the earth's CO₂ is stored in the ocean and participates in carbon cycle through the ocean. Of the carbon captured by photosynthesis alone, 55% forms blue carbon sinks, whose composition containing carbon sequestration by microorganisms which account for more than 90% of marine biomass, and blue carbon ecosystems in important coastal zones such as mangroves, seagrass meadows and salt marshes. Studies have shown that large algae, shellfish, and even micro creatures and phytoplankton in the ocean dissolve CO₂ and then turn them into organic carbon and carbon particles, which gradually move from the ocean surface to the deep layer and realize efficient carbon sequestration and storage capacity through the direct effect of marine organisms and the indirect effect of the ecological food chain, thus forming the biggest aggregation system of carbon sink in the earth's ecosystem. The storage of blue carbon sinks is about 50 times and 20 times that of atmospheric and terrestrial carbon sinks, respectively, thus affecting global phenological pattern, ecological resource form and distribution of food chain elements. It absorbs 30% of GHG generated by human activities since the industrial revolution, and plays an extremely important role in mitigating climate change and stabilizing global ecological balance.

With the development of science and technology and the deepening awareness of climate change, people gradually understand that the ocean ecology affects major global climate patterns. Report of IPCC (AR5, 2013) [16] and related studies [20, 21] pointed out that the necessity and importance of studying ocean ecology along with its role in

balancing the natural carbon cycle. The report of IPCC positioned the ocean ecosystem as the largest active carbon pool on earth, and blue carbon may have become the most major carbon sink in the post-industrial era, emphasizing to pay attention to the role of ocean system in reducing CO₂ and enhancing carbon sink capacity. The report considered that developing blue carbon sinks would not only make full use of ocean energy, develop climate resources, and expand human living space, but also provide the most practical and feasible way to reduce CO₂ emission and mitigate climate warming. The report emphasized to expand the application mode of global blue carbon sinks by drawing on existing international emission reduction mechanism and framework, build a blue carbon sink framework within the full carbon spectrum system, and develop oceanic carbon sink standards and measurement methodologies. Blue carbon provides a new direction for shaping the international product of carbon sink as a public resource and improving the ecological compensation mechanism. It also provides a new and effective path to increase carbon sinks in market-oriented response to global climate change.

China is the second largest economy and a major maritime power in the world. China's continental coastline is 1.84×10^4 km long and spans 22 latitudes, which is rich in coastal resources with seagrass beds, mangroves, salt marsh wetlands and a wide continental shelf sea. China possesses a rich and unique diversity of ocean biological resources, the largest fisheries carbon sinks in the world, and the most potential for blue carbon development. At present, the industrial structure and functions in China's coastal development zones are perfect, and the coastal zone economy occupies an important position in the total economic volume of China. Hence, China has had the capability to establish the ocean blue economy development mode based on its ecosystem.

5 Conclusions

This paper quantifies systematically the gap between global carbon emissions and INDCs targets in terms of CO₂ concentration, climate temperature, CO₂ emission quantity and other key indicators, investigates global carbon budget and carbon emission reduction dilemma. Consequently, this paper puts forward to develop the blue carbon as an innovative path to increase carbon sinks in future global climate governance. Due to the diversity of acting parties and the multi-polarization of competition, climate change is not only reflected in technology and economy, but also reflected in the political pattern game among countries. It is clear that developed countries have absolute advantages and have the ability to lead the layout of rules, thus becoming the leaders of new technologies, the drivers of new standards or even the monopolists of patents in future global climate governance. It is predictable that developed countries are about to win the initiative in a new round of protracted competition and once again gap with developing countries in national development potential in the future.

China is playing a leading role in global climate governance. As the second largest economy and the largest developing country in the world, at present China has the highest carbon emission level in history due to its development stage. It is imperative for China to explore the blue carbon sink system in climate resources and strengthen policy innovation in climate response mechanism. Therefore, China must take advantage of its unique conditions to develop blue carbon sinks, establish technical indicators of blue

carbon sinks, develop an evaluation system for blue carbon accounting standards, and formulate carbon emission lists for ocean basins and coastal zones. Equally important, China needs to build the market framework, transaction procedure and service support system based on the scheme of blue carbon sink increase, thus striving to incorporate blue carbon into the index system of INDCs under the Paris Agreement.

References

1. Liu, J.-Y., Fujimori, S., Masui, T.: Temporal and spatial distribution of global mitigation cost: INDCs and equity. In: Fujimori, S., Kainuma, M., Masui, T. (eds.) Post-2020 Climate Action, pp. 45–63. Springer, Singapore (2017). https://doi.org/10.1007/978-981-10-3869-3_4
2. Wang, H., Wang, Y., Qi, L.: Evaluation of emission reduction targets contributed by BASIC countries from the perspective of global temperature control targets. Environ. Sci. Pollut. Res. **28**(6), 6843–6865 (2020). <https://doi.org/10.1007/s11356-020-10860-7>
3. Dong, C., Dong, X.C., Jiang, Q.Z., et al.: What is the probability of achieving the carbon dioxide emission targets of the Paris agreement? Evidence from the top ten emitters. Sci. Total Environ. **622**, 1294–1303 (2018)
4. Frakos, P., Tasios, N., Paroussos, L., et al.: Energy system impacts and policy implications of the European intended nationally determined contribution and low-carbon pathway to 2050. Energy Policy **100**, 216–226 (2017)
5. Iyer, G.C., Edmonds, J.A., Fawcett, A.A., et al.: The contribution of Paris to limit global warming to 2 degrees C. Environ. Res. Lett. **10**(12), 125002 (2015)
6. Sarkar, M.S.K., Al-Amin, A.Q., Filho, W.L.: Revisiting the social cost of carbon after INDC implementation in Malaysia: 2050. Environ. Sci. Pollut. Res. **26**(6), 6000–6013 (2019). <https://doi.org/10.1007/s11356-018-3947-1>
7. Hasegawa, T., Fujimori, S., Boer, R., et al.: Land-based mitigation strategies under the mid-term carbon reduction targets in Indonesia. Sustainability **8**(12), 1283 (2016)
8. Dioha, M.O., Kumar, A.: Exploring the energy system impacts of Nigeria's nationally determined contributions and low-carbon transition to mid-century. Energy Pol. **144**, 111703 (2020)
9. Zeshan, M.: Carbon footprint accounts of Pakistan: an input-output life cycle assessment model. Environ. Sci. Pollut. Res. **26**(29), 30313–30323 (2019). <https://doi.org/10.1007/s11356-019-06196-6>
10. Nguyen, H.T., Aviso, K.B., Le, D.Q., et al.: A linear programming input-output model for mapping low-carbon scenarios for Vietnam in 2030. Sustain. Prod. Cons. **16**, 134–140 (2018)
11. Oshiro, K., Kainuma, M., Masui, T.: Implications of Japan's 2030 target for long-term low emission pathways. Energy Policy **110**, 581–587 (2017)
12. Xing, R., Hanaoka, T., Kanamori, Y., Masui, T.: Achieving China's intended nationally determined contribution and its co-benefits: effects of the residential sector. J. Clean. Prod. **172**, 2964–2977 (2018)
13. Yang, X., Teng, F.: Air quality benefit of China's mitigation target to peak its emission by 2030. Climate Policy **18**(1), 99–110 (2018)
14. Pan, X.Z., Chen, W.Y., Clarke, L.E.: China's energy system transformation towards the 2 degrees C goal: Implications of different effort-sharing principles. Energy Policy **103**, 116–126 (2017)
15. Lin, J., Qi, Y., Cai, W.J., Wang, C.: A review on the studies of equitable sharing in national mitigation contributions to achieve the Paris agreement ambitions. Clim. Change Res. **14**(5), 529–539 (2018)

16. IPCC: Climate change 2013. The physical science basis. Contribution of working group I to the fifth assessment report of the intergovernmental panel on climate change. In: Stocker, T.F., et al., eds. New York, Cambridge University Press, Cambridge (2013)
17. IPCC: Climate change 2007. The Physical science basis. Contribution of working groups I, II and III to the fourth assessment report of the intergovernmental panel on climate change. In: Solomon S., et al., (eds.) New York, Cambridge University Press, Cambridge (2007)
18. Pearce, F.: With Speed and Violence: Why Scientists Fear Tipping Points in Climate Change. Beacon Press, Boston (2007)
19. UNEP, FAO, UNESCO, IOC: Blue Carbon: The Role of Healthy Oceans in Binding Carbon—A Rapid Response Assessment (UNEP, Earthprint, 2009) (2009)
20. Wen, X., Bouri, E., Roubaud, D.: Can energy commodity futures add to the value of carbon assets? *Econ. Model.* **62**, 194–206 (2017)
21. Yu, J., Mallory, M.L.: Exchange rate effect on carbon credit price via energy markets. *J. Int. Money Financ.* **47**, 145–161 (2014)



Effect of Hedgerows on CO Diffusion from Vehicle Exhaust Emissions in Street Canyons

Xin Jiang¹, Changzhao Qian², and Changping Chen^{1,2,3(✉)}

¹ College of Civil Engineering, Xiamen University, Xiamen, China
cpchen@hnu.edu.cn

² Fujian Provincial Key Laboratory of Wind Disaster and Wind Engineering, Xiamen University of Technology, Xiamen, China

³ Xiamen Ocean Vocational College, Xiamen, China

Abstract. This paper studies the influence of hedgerow green belt on the flow field of street canyon and the CO diffusion of vehicle emission in street canyon. The commercial CFD package and post-processing software were used for numerical simulation and analysis. The green belt was established as a porous medium model. The steady-state standard k-turbulence model combined with the component transport equation was used to simulate the CO diffusion process of vehicle exhaust in the street canyon with hedgerows on both sides of the road. The simulation results were compared with the wind tunnel test to verify the accuracy of the results. It is found that the flow field in the street canyon changes after the slope transformation of the hedgerow green belt on both sides of the street. Compared with several working conditions, it is found that the overall CO concentration in the street canyon after transformation is lower and the CO diffusion situation is better than that before transformation, no matter in the case of low or high wind speed.

Keywords: Street canyon · Hedgerow · Pollutant dispersion · Numerical simulation

1 Introduction

With the rapid development of cities, the number of motor vehicles becomes more and more, and the pollution problem caused by motor vehicle exhaust is more serious. Especially in urban streets, due to the special structure of the street canyon itself, the diffusion of motor vehicle exhaust is hindered, and the exhaust pollution in the street valley is aggravated [1], which seriously endangers the health of surrounding residents and pedestrians. The layout of green belts in street valleys can not only play an aesthetic role, but also dust removal and purify the air. However, relevant studies show that the layout of green belts in street valleys can affect the flow field and pollutant diffusion, reduce the ventilation efficiency in the street valleys, and make the overall concentration of pollutants in the street valleys higher [2]. Therefore, how to arrange green belts to

improve ventilation efficiency and pollutant diffusion in the street valley has practical and important research significance. This paper focuses on the impact of the green belts (hedgerows) on the side of the street canyon road with the aspect ratio of 1:1 on the CO diffusion of automobile emissions.

2 Method

2.1 Numerical Model

The establishment of the street valley model is shown in Fig. 1. Hedgerows are arranged on both sides of the driveway. The green isolation bandwidth is 0.8 m, the height is 1 m, the sidewalk width is 3 m, the overall street width is 15 m, the building height on both sides is 15 m, and the height-width ratio of the street canyon is 1:1. The pollution source is set as the CO entrance of the line source, and the exit is located in the center of the driveway to simulate automobile exhaust emissions.

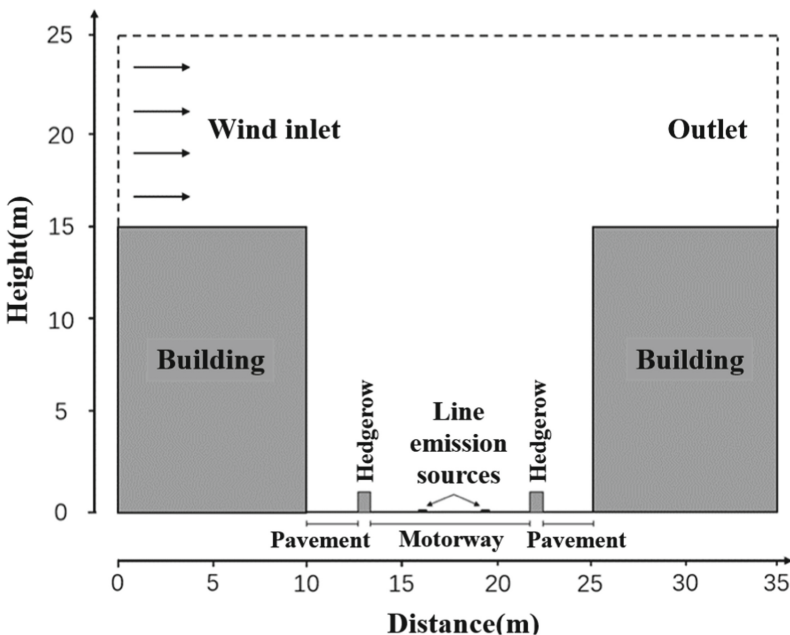


Fig. 1. Street canyon model

Tong's research shows that at low wind speeds, solid vegetation barriers (solid barriers covered by vegetation) have a similar effect on the diffusion of traffic emissions [3]. Gromke, C. and Gallagher, J.'s study also showed that dense leafy vegetation barriers can be simulated as solid barriers [4, 5]. Considering that urban street shrubs are mostly dense leafy vegetation, hedgerows are modeled as solid barriers in this study.

This study explores hedgerow appearance effect on the spread of CO, so on shrub shape, as shown in the hedgerow appearance is conducted on the basis of original form a slope cutting, the cutting and chose not to extend upwards, because extended upward and structural slope changed the original hedgerow size and impact of the results will not be of research significance, And cutting processing is more practical, to the future of urban road reconstruction to provide practical convenience. In this study, hedgerows were given three slope angles, 15° , 30° and 45° . Hedgerow model is shown in Fig. 2.

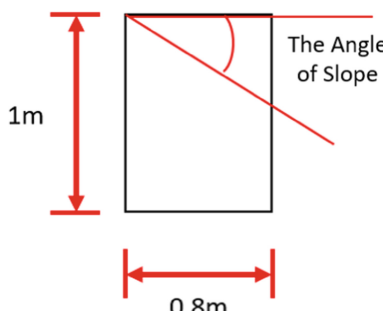


Fig. 2. Schematic diagram of hedgerow

2.2 Boundary Conditions

The wind inlet is set to 2 m/s. Pollution source emissions refer to the estimation of road vehicle exhaust and non-exhaust emissions by Nagpure [6], and the order of magnitude $1e^{-5}$ m/s of CO emission rate is taken as the inlet speed of CO line source in accordance with the actual situation. Some parameters of numerical simulation are shown in Table 1.

Table 1. Summary of key parameters in numerical simulation

Type	Name		Value	Unit
Street canyon	Configuration	Aspect ratio	1	
Meteorology	Wind	Velocity	2	m/s
		Direction	90	°
	Temperature		27	°
Vegetation	Hedgerows	Slope	0,15,30,45	°
		Height	1	m
		Width	0.8	m
Pollutant (CO)	Emission source	Velocity	$1e^{-5}$	m/s
		Mass	12.5	mg/s

3 Results and Discussion

When the valley of the wind direction is perpendicular to the street, because of the impact of buildings on both sides, valley street within a large clockwise vortex, flow diagram as shown in Fig. 3, valley street, is similar to a square cavity, because of the effect of flow field, the upstream building lee windward surface contaminant concentration is higher than the downstream building the concentration of the pollutants, and contaminants gathered in the leeward side corner, cannot efficiently, This is how pollutants spread in street Canyons, and hedgerows on both sides of the road can effectively reduce the concentration of pollutants at sidewalk breathing level.

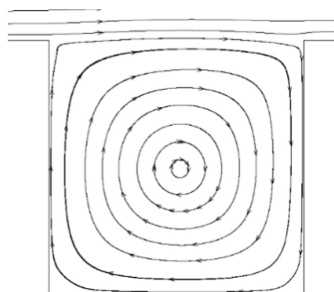
**Fig. 3.** Flow field in street Valley

Figure 4 (a), (b), (c) and (d) were isographs of CO mass fraction in street-valleys when the wind speed was 2 m/s for hedgerows with slopes of 0° , 15° , 30° and 45° , respectively, showing CO diffusion in street-valleys. As can be seen from Fig. 4, CO diffusion was better in the other three street-valleys with sloping hedgerows than in the original ones. The overall concentration of CO in street-valleys was lower, especially the 30° sloping hedgerows, which had the best effect on CO diffusion.

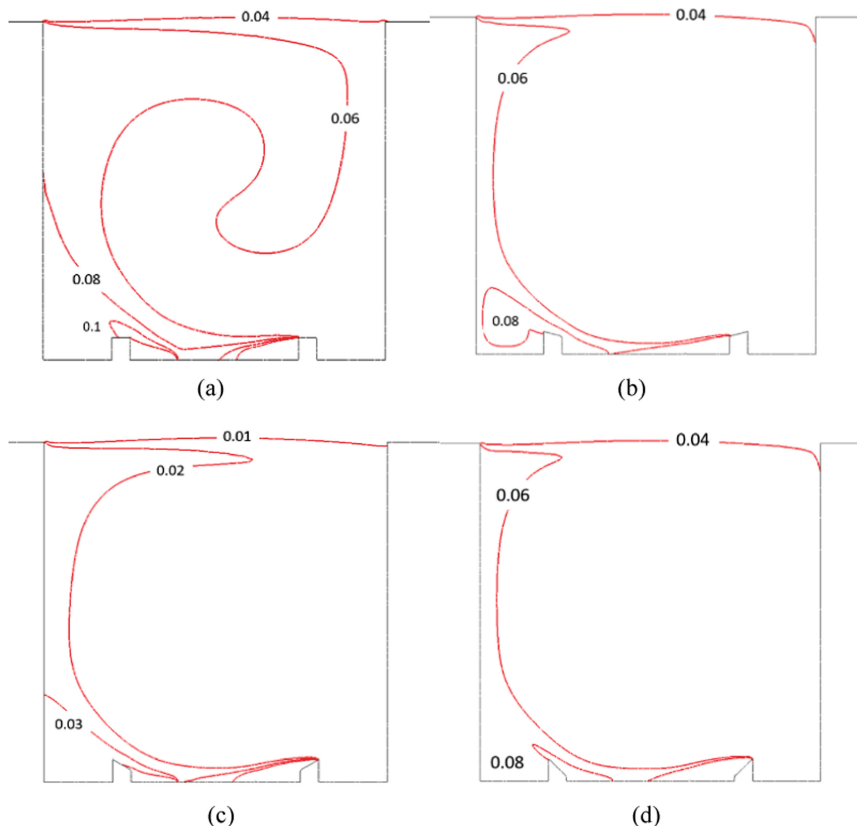


Fig. 4. Isogram of pollutant mass fraction at 2 m/s wind speed

As can be seen from the wind speed vector diagram in Fig. 5, after slope modification of hedgerows on the leeward side, the blocking effect of the central vortex on the street valley is weakened. The slope of hedgerows is close to the edge of the central vortex, so the wind speed of the central vortex there will not be weakened due to the blocking of hedgerows. As can be seen from the wind speed cloud in Fig. 6, in the leeward side of buildings where pollutants gather, the maximum wind speed here is 0.7 m/s in the street valley with common hedgerows, while it can reach 0.9 m/s in the street valley with sloping shrubs.

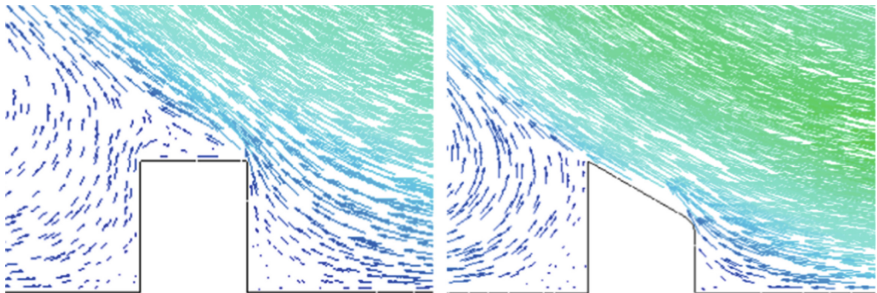


Fig. 5. Velocity vector diagram of leeward pavement at 2 m/s wind speed

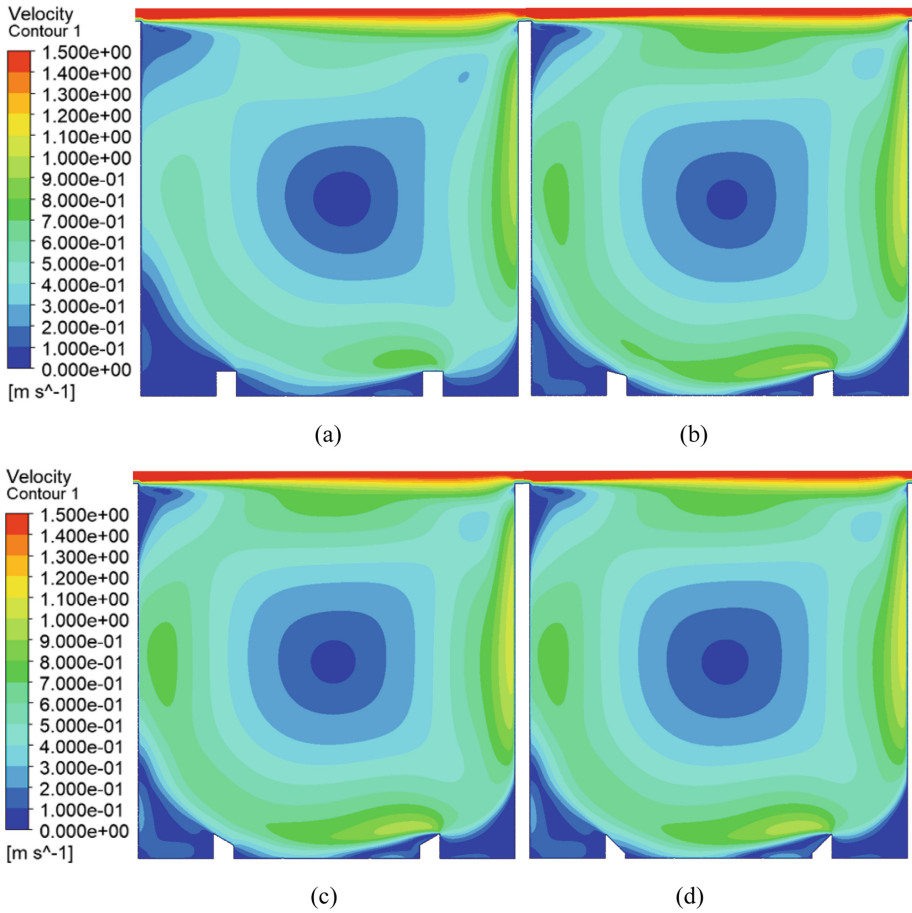


Fig. 6. Cloud chart of wind speed in street Valley at 2 m/s wind speed

In the leeward side near the ground, because of the influence of the valley center of vortex street, will form a low-speed counterclockwise vortex, here in Fig. 7, you can see, because the hedgerow with slope surface better fit the center of the edge of large vortex street and the make the center edge vortex wind speed increase, thus speeding up

the leeside sidewalk anticlockwise vortex edge at low speed wind speed. As a result, the overall wind speed of the low-speed vortex increases. The wind speed on the left side of the vortex is 0.15 m/s in the no-slope shrub street canyons, but it can increase to 0.2 m/s in the 15° and 45° shrub street canyons, and to 0.25 m/s in the 30° shrub street canyons. Below the vortex, the wind speed increased from 0.1 m/s to 0.2 m/s after increasing the shrub slope.

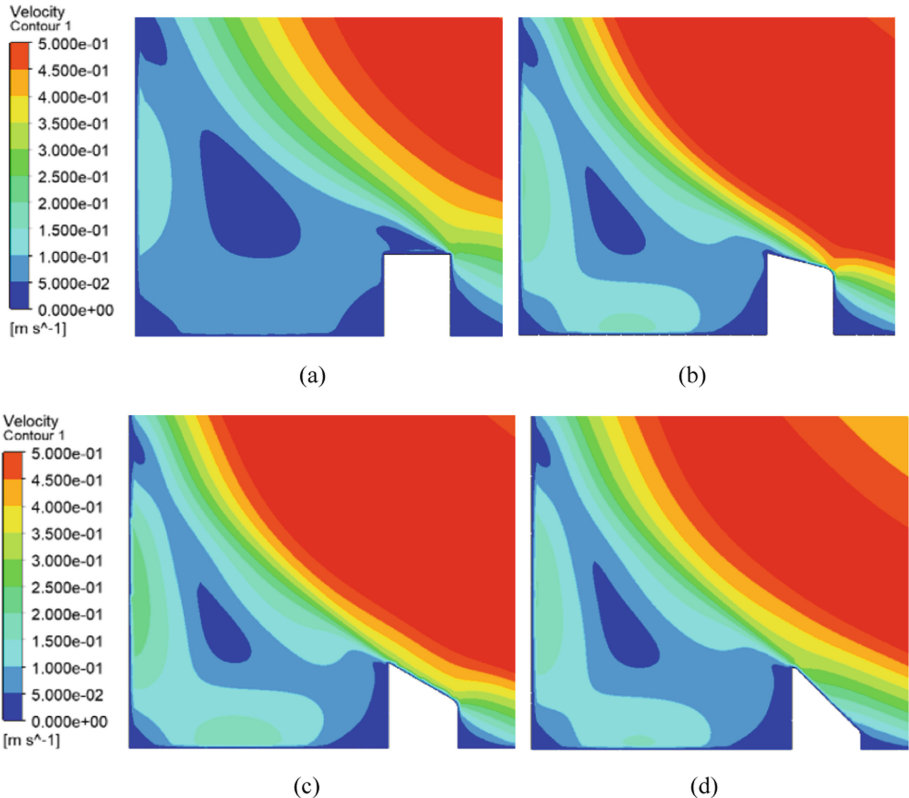


Fig. 7. Velocity cloud chart of leeward pavement at 2 m/s wind speed

As can be seen in the flow diagram in Fig. 8, the vortex center moved down 35 cm in the 15° hedgerow street valley, 40 cm in the 30° hedgerow street valley, and 38 cm in the 45° hedgerow street valley. The area of low-speed vortex decreases as the wind speed at the vortex edge increases. Therefore, CO gathered in the leeward corner can better diffuse out of the street-valley with the rise of eddy wind speed. Therefore, after the slope modification of the original hedgerows, the wind speed of the flow field in the whole street-valley is increased to a certain extent, thus speeding up the air circulation inside and outside the street-valley, and thus facilitating the better discharge of CO.

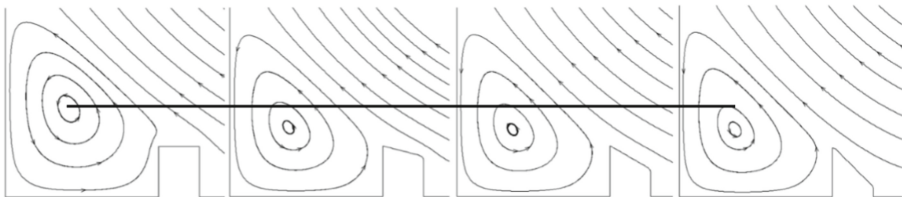


Fig. 8. Streamline diagram of leeward pavement at 2 m/s wind speed

Measuring points were arranged along the vertical height at 5 cm on the wall of the building on the leeward side of the street valley and 5 cm above the ground, with a spacing of 0.25 m. In Fig. 9, the CO mass fraction at the vertical height of the leeward building wall decreases slowly with the rise of the height. In street canyons with sloping hedgerows, the mass fraction of CO at building walls was lower. Under the influence of 15° hedgerows and 45° hedgerows, the CO concentration at the wall was lower, by 14% and 21%, respectively, and in the street valley of 30° hedgerows, the CO concentration at the wall decreased by 70%. Effectively improve the window ventilation environment of the residents in the lee. Measuring points were arranged horizontally at the pedestrian height (1.7 m), with a spacing of 0.25 m. In Fig. 10, the CO mass fraction at the pedestrian level of street valley (1.7 m) from the leeward side to the windward side. Due to the flow field, CO emissions from street vehicles concentrated near the leeward hedgerows, so there was a rising stage and then a decline. It can also be seen that in the 15° and 45° hedgerows, the CO concentration at the pedestrian level was lower than in the normal hedgerows, by 14% and 21%, respectively. In the 30° hedgerows, the CO concentration at the pedestrian level decreased by 70%.

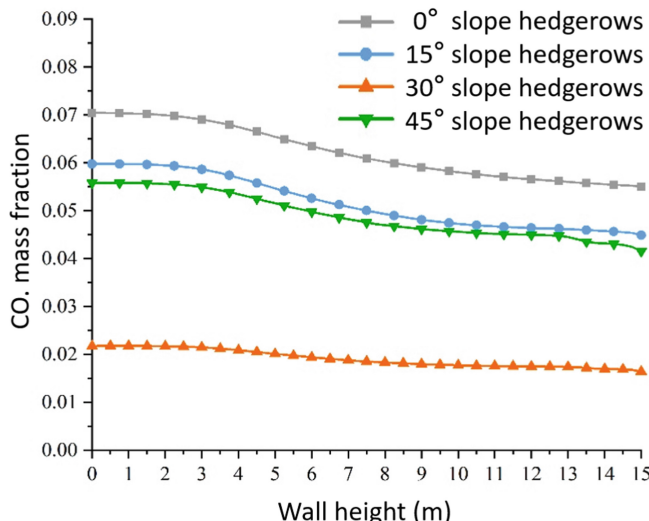


Fig. 9. Line chart of CO mass fraction at vertical height of leeward wall

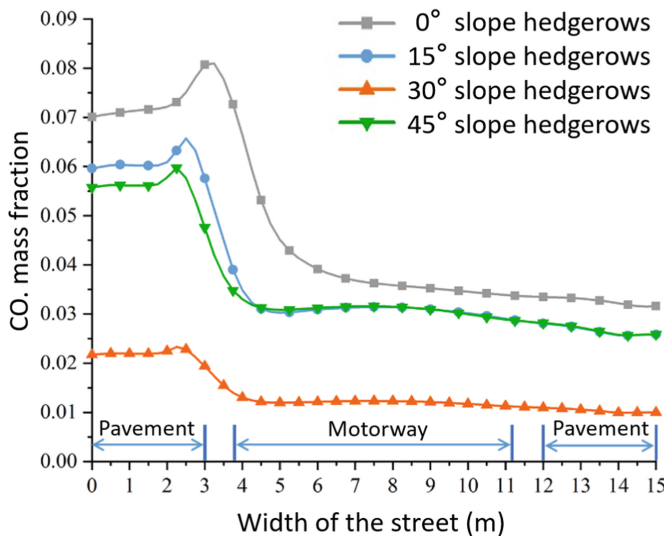


Fig. 10. Line chart of CO mass fraction at the level of 1.7 m pedestrian walk

4 Conclusion

- (1) In the street-valleys with sloping hedgerows, the wind speed of the whole vortex is higher than that of the original hedgerows. Under the influence of the flow field, pollutants in the street-valleys can be effectively removed and the overall concentration in the street-valleys is lower.
- (2) because of the influence of the hedgerow, in the leeward side near the ground will be a low vortex, lead to CO gathered here, hedgerow with slope surface of street in the valley, lee side near the ground vortex wind speed is greater at low speed, smaller, closer to the ground and vorticity center, that had gathered near the sidewalk CO to better spread.
- (3) Among the hedgerows with slopes of 15°, 30° and 45°, the hedgerows with slopes of 30° had the best diffusion of pollutants in street-canyons. Compared with the street-canyons with original hedgerows, the CO concentration near the wall and at pedestrian height decreased by 70%.

References

1. N'Riaim, C.M., Fisher, B., Martin, C.J., Littler, J.: Flow field and pollution dispersion in a central London street. Environ. Monit. Assess. **52**(1–2) (1998)
2. Gromke, C., Jamarkattel, N., Ruck, B.: Influence of roadside hedgerows on air quality in urban street canyons Atmos. Environ. **139**, 75–86 (2016)
3. Tong, Z., Baldauf, R.W., Isakov, V., Deshmukh, P., Zhang, K.M.: Roadside vegetation barrier designs to mitigate near-road air pollution impacts Sci. Tot. Environ. **541**, 920–927 (2016)

4. Gromke, C., Buccolieri, R., Di Sabatino, S., Ruck, B.: Dispersion study in a street canyon with tree planting by means of wind tunnel and numerical investigations—evaluation of CFD data with experimental data *Atmos. Environ.* **42**(37), 8640–8650 (2008)
5. Gallagher, J., Baldauf, R., Fuller, C.H., Kumar, P., Gill, L.W., McNabola, A.: Passive methods for improving air quality in the built environment: a review of porous and solid barriers *Atmos. Environ.* **120**, 61–70 (2015)
6. Nagpure, A.S., Gurjar, B.R., Kumar, V., Kumar, P.: Estimation of exhaust and non-exhaust gaseous: particulate matter and air toxics emissions from on-road vehicles in Delhi *Atmos. Environ.* **127**, 118–124 (2016)

Environmental Chemical Engineering and Wastewater Treatment



Synthesis of Green Nano Composite Using Sugar Cane Waste for the Treatment of Cr Ions from Waste Water

M. Amin Mir^(✉)

Department of Mathematics and Natural Sciences, Prince Mohammad Bin Fahd University,
Al Khobar, Saudi Arabia
mmir@pmu.edu.sa

Abstract. A lot of agricultural waste is generated in India and the farmers mostly burnt that waste and create environmental problems. Efforts are being made to convert that waste into some useful products and Nano-technology stays no behind in making that agricultural waste into a useful product. Nano-technology helps by making Nano-composites using agri-residues like bagasse and some industrial wastes like fly ash and thereby reduce the environmental pollution. Carbon and its compounds and have an ionic attraction for metals compounds and property helps in the removable of heavy metals present in water. Graphite based Nano composite prepared were applied to various waste water bodies of pulp and paper industry and it had been found that the colour of the water gets reduced by 60–80%, decline in BOD by 40–70% and COD by 70–80%.

Keywords: Nano-composite · Sugarcane waste · Graphite · Water purification · SEM

1 Introduction

Nanotechnology in science refers to a field where materials ranging from the size 1 to 100 nm are dealt with. It will have significant effect in the areas of food industries, development of new functional materials, products, as nanotech research will definitely aid agro-waste in next sage. Implementation of agro-waste would be undoubtedly a strong step towards sustainable development through nanotechnology.

Although nanotechnology based methods are generally believed to be more expensive, we found early where they offer cheaper and more effective alternatives to conventional techniques. In addition, Nano-based techniques may become extremely important in meeting increasingly stringent water quality standards, especially for removal of emerging pollutant and low levels of contaminants. The current study reveals the importance of water purification application using carbon and its allotropes and the measurement of water purification efficiency with conventional techniques.

Firstly nanoparticles are the small size particles which on undergo mixing give rise to Nanocomposite with nanometre range (1 nm to 100 nm). Nanocomposite embodied have established a new range to overcome success of micro composites and monolithic. The

preparations of nanocomposite are of different types with or without agro waste. Some methods by which nanocomposite being prepared are solution blending method, melt intercalation method, in-situ polymerization method, sol gel method, hummers method etc.

Sugarcane agro waste is the popular relevant source of conduct towards of waste water. Sugarcane is called as bagasse which is an abundant industrial waste and a fibrous produces waste after the sugar extraction. About in approximately 5×10^8 tons of sugarcane in dry form catalyse 280 kg of dried sugarcane from 1 ton of sugarcane yearly. And from this 280 kg 50% sugarcane has nearly used in generating heat, energy to sprint mills, and left has being added to the environment causing problems. Therefore, it is significant to use this left behind bagasse in many value added examples like fuels, water treatment etc. sugarcane is major component of cellulose as (40–50%), lignin as (15–35%), and hemicellulose as (25–35%) and other non- useful particles within.

The property of graphite helps in the removal of impurities from waste water. Hence it is popular for antimicrobial properties and in other way disinfected properties in many other techniques. Carbon allotropes and its composites are the necessary pollutant and heavy metal absorbent found in surface. Water purification is also done by applied surface modification technique. Juan Carlos et al. [1] studied about the sugarcane bagasse and its potential as effluent treatment. These results into the removal of 86.4% various parameters and achieve maximum adsorption of 95.0%. William Neil Gilfillan [2] reported the using of sugarcane bagasse a dry fibre of 1500 kg/m^3 density to enhance the physic-chemical properties of starch based composite film. Seyed Ali Hosseini [3] studied the Nano composite using Graphene Oxide and MgFe_2O_4 for reduction of Cr (VI) ions from waste water to deplete environmental pollutant. M Jannatin [4] studied the preparation of graphene oxide and magnetite composite. They prepared the composite stepwise reaction with bagasse as a raw material at 400°C also graphene oxide from graphite powder by hummer's method which is widely used in process. Shafeeq Rahman [5] have the main focus on the preparation of Nano composite of graphene and sugarcane sand for water purification. Leila shahriary and Anjali A. Athawale [6] developed a method used by them was prepared graphene oxide from graphite oxide exfoliating in distilled water with ultrasonic waves. Ayse Alemdar and Mohini Sain [7] studied the characterization and isolation of agriculture residues. The main agro-waste which was used by them are wheat straw and soy hulls. N. Tensingh Baliah [8] studied the green synthesis of nanocomposite. They take part in green synthesis towards the nanotechnology science.

2 Materials and Methods

2.1 Chemicals Required

The materials used were Effluent, sugarcane as agro-waste material, graphite (thin films with agro-waste) HCl, H_2O_2 , Acetone, H_2SO_4 etc. Then the prepared Nano-materials were analysed by ultra-visible spectroscopy (UV-spectroscopy), scanning electron microscope (SEM), Fourier transform infrared spectroscopy (FTIR), X-ray powder diffraction, transmission electron microscope (TEM), laser diffraction and other methods etc.

2.2 Agro Waste in Nano Form

The Sugarcane waste material after the extraction of juice from the juice was collected form the local juice market of Dehradun. The sugarcane material was then dried and the fibre so obtained was taken. The sugarcane dry fibre was washed using water and then HCl. Then the fibre was dried in the hot oven at 150 °C for 2 and a half hour. The drying process was repeated. The dried form of the material was then made into powder and the powder was milled and sieved to Nano range.

2.3 Preparation of Graphene Oxide

By modified hummer's method, graphene oxide was first prepared from graphite powder. 2 g of graphite powder and 1 g of NaNO₃ were gradually added in presence of conc. H₂SO₄ in a beaker surrounded by ice in an ice bath to keep the temperature below 10 °C with continuous stirring for about 30 min followed by slow addition of KMnO₄ (6 g). The whole mixture was then continuously stirred for about 2 h followed by the addition of 50 ml of distilled water, and then hydrogen peroxide solution, due to which the colour of the solution changes form brown to yellow. The mixture was centrifuged and washed, to get a solid material. The resulting solid precipitate was then dried at 70 °C for about 24 h to obtain graphene oxide. Then a thin layer of layer of GSC was prepared known as graphene sugarcane composite. The GSC was done by taking 15 g of Starch and 5.6 ml of glycerol in a beaker with addition of 450 ml of distilled water. All the components were mixed well and then heated for 30 min with further addition of bagasse 3 g. The whole mixture was then made to cool followed by allowing the mixture to dry at not more than 80 °C using oven. Finally the film preparation of GSC was done with obtaining a thin film of bagasse graphene Nano composite.

3 Results and Discussion

3.1 Nano Particle Size of Bagasse

Nano particles of sugarcane bagasse was prepared by converted into mesh particle size of Nano range. For the preparation of bagasse nanoparticles following steps are carried out. Before it, take 30 g of sugarcane bagasse pulpy white substance from outer cover of it then- First, bagasse was washed with distilled water to remove the impurities and tray dries it for 2 days 5 h each day. Next the dried sugarcane bagasse was grinded into mixer so that the small particle size of bagasse was obtained (not to fine). Then the grinded small particles were sieved from the BSS-6 to obtain the Nano particle size. Sieving process was continued and finally the nanoparticles of bagasse sugarcane were obtained.

3.2 UV Characterisation

For UV spectroscopy first we prepared the stock solution of chromium and diluted it into 3 parts as 1%, 2% and 3% ml solution of chromium with addition of Nano composite into it. Then kept the solution for 1 h and after 1 h UV has been done with different chromium solution (Table 1).

Table 1. Spectroscopic analysis of the nano-composites

Sample	Wavelength/parameters	Absorbance	Parameter	Wavelength-absorbance
Sample A	Original	240 nm–2.091	Sample (after 1 h)	350 nm–2.85
Sample B	Original	230 nm–2.72	Sample (after 1 h)	320 nm–2.51
Sample C	Original	250 nm–1.21	Sample (after 1 h)	250 nm–2.65

Graph Interpretation

See Fig. 1.

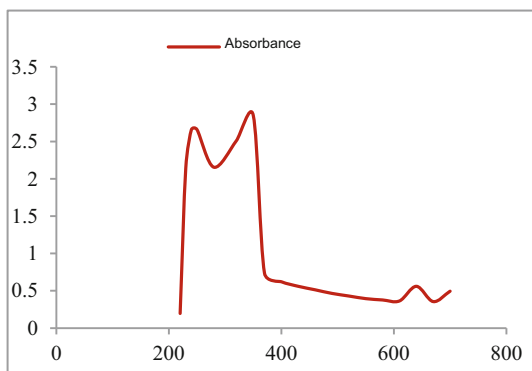


Fig. 1. Original parameters of wavelength-Absorbance graph for chromium solution.

3.3 SEM Analysis

The working of scanning electron microscope (SEM) generates signals using a focused pointed beam which has a high energy density for the matter state. The signals that derive from electron microscopy reveal information about the sample including external morphology (texture), chemical composition, and crystalline structure and orientation of materials making up the sample. Scanning electron microscopy (SEM) is an important and unique analysis method through which images of matters produces on the screen.

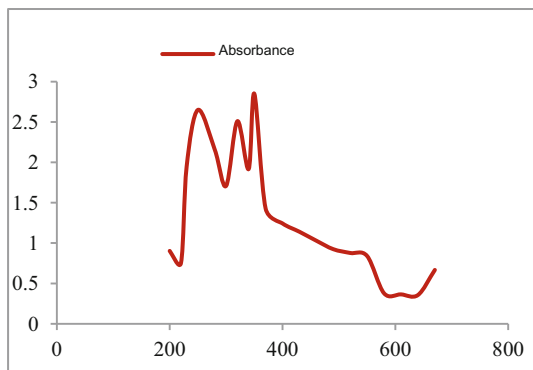


Fig. 2. Sample parameters of wavelength-Absorbance graph after 1 h.

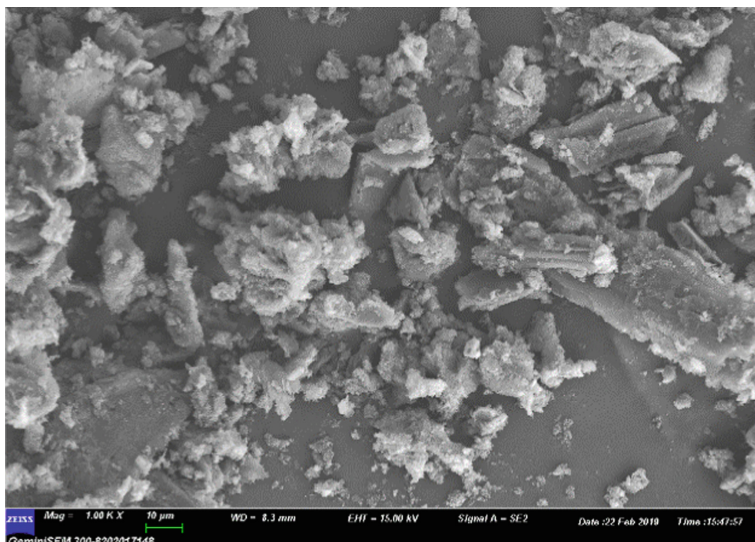


Fig. 3. Shows the prepared Nano composite of GSC.

In order to find out the particle size and morphology of an element, SEM analysis was the process which is carried. The SEM images clearly reveal the sheet-like structure of Graphene oxide between the Nano composite. The morphology of the synthesised GO resembles flake-like structures as shown in Figs. 2 and 3. It clearly shows that the particles of sugarcane and graphene oxide are strongly bounded together with Nano size of 10 nm. The particle size of composite nearly falls into the Nano range as between the 1–100 nm (Fig. 4).

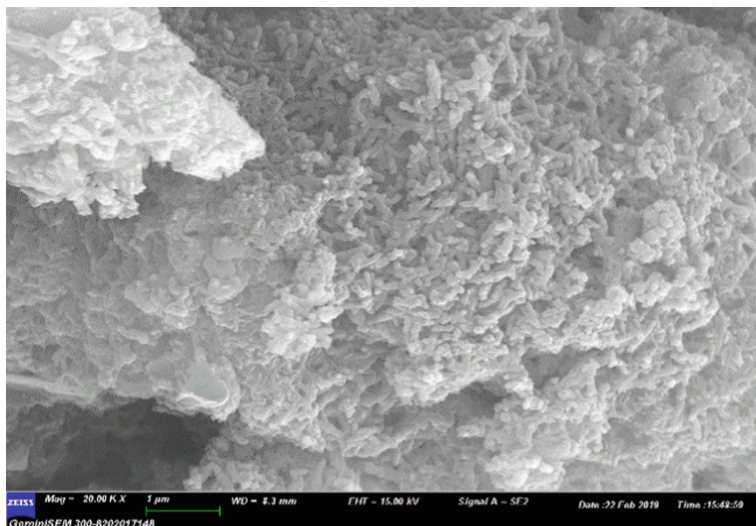


Fig. 4. Shows the image of normalised Nano composite between the sugarcane particles and the graphene oxide particles.

4 Conclusion

The study in reference carried out synthesizes of Nano composite of GSC with a great attraction power towards the removal of heavy metals especially chromium metal. The synthesis of Nano-composites was characterised by spectroscopic techniques like, UV visible and SEM analysis. By using GSC it had been found that wastes from the water bodies can be cleared effectively. The further study may be applied for the removal of other metals. In conclusion it could be mentioned that synthesis of GSC from agriculture waste can help in the removal of chromium from the waste water.

References

1. Cueva-Orjuela, J.C., Del Socorro Hormaza-Anaguano, A., Merino-Restrepo, A.: Sugarcane bagasse and its potential use for the textile effluent treatment. DYNA **84**(203), 291–297 (2017)
2. Neil Gilfillan, W., Moghaddam, L., Doherty, W.O.S.: Preparation and characterization of composites from starch with sugarcane bagasse nanofibres. Cellulose **21**(4), 2695–2712 (2014)
3. Ali Hosseini, S., Tabebipour, S., Neyestani, M.R.: Graphene oxide MgFe₂O₄ nano composite for Cr (VI) remediation: a comparative modelling study. Nanotechnol. Environ. Eng. **3**(10) (2018)
4. Jannatin, M., Supriyanto, G., Abdulloh, Ibrahim, W.A.W., Rukman, N.K.: Graphene oxide from bagasse/magnetite composite: preparation and characterization. IOP Conf. Ser. Earth Environ. Sci. **217**, 012007 (2019)
5. Rahman, S., Praseetha, P.K.: Analysis of water purification efficiency of graphene sand nanocomposite. Int. J. Eng. Res. Afr. **24**, 17–25 (2016)
6. Shahriary, L., Athawale, A.A.: Graphene oxide synthesized by using modified hummers approach. Int. J. Renew. Energy Environ. Eng. **2**, 58–63 (2014)

7. Alemdar, A., Sain, M.: Biocomposites from wheat straw nanofibers: morphology, thermal and mechanical properties. *Compos Sci. Technology* **68**(2), 557–565 (2016)
8. Tensingh Baliah, N., Muthulakshmi, P., Lega Priyatharsini, S.: Synthesis and characterization of onion mediated silver doped zinc oxide nanoparticles. *Int. J. S. Res. Sci. Eng. Technol.* **4**(11), 111–120 (2018)



Heavy Metal Water Pollution: Transport and Transformation, Impacts and Treatment Technologies

Guoye Ma and Lingyun Jia^(✉)

School of Life Sciences, Northwest Normal University, Lanzhou, China
2316148152@qq.com

Abstract. With the rapid development of industrialization and urbanization, the content of toxic heavy metals in the environment has increased significantly. This article explores how heavy metals can migrate from the land to the atmosphere, as well as from the land to rivers and future to the ocean and even to the deep sea. Heavy metals undergo changes in external morphology and internal structure during migration, and it also changes form with the energy flow of the food chain. Heavy metal pollution in the water environment is a very serious problem, because heavy metals can cause serious harm to plants and animals and even to the entire ecosystem and human health. We provide an overview of current heavy metal treatment measures in water and compare their advantages and disadvantages. This review can help researchers to understand the migration and transformation mechanisms of heavy metals in the aqueous environment and to choose appropriate measures for the treatment of heavy metal pollution according to the difference of pollution types. Further, it provides valuable advice for the management of heavy metal water pollution.

Keywords: Water pollution · Heavy metals · Migration and transformation

1 Introduction

Water pollution is defined as the unfavorable alteration of the environment through the direct or indirect action of man. From the United Kingdom, where the industrial revolution was first realized, to China, where industrial technology is booming today, it is impossible to avoid water pollution. Water is a primary resource on earth and access to clean water is critical for human development and life and health. However, in recent years, pollution of the water environment has occurred frequently, and heavy metals are one of the main types of pollution. With no doubt, heavy metal pollution of water is a global problem, common to both developed and developing countries. Statistically, articles about heavy metal water pollution treatment in the Scopus database rose 1700% between 2000 and 2019 [1].

Since heavy metals are not degradable, they have been present for centuries and continue to accumulate [2]. Harmful heavy metals in water mainly include mercury, arsenic, lead and cadmium, which are enriched in living organisms with the water cycle

and food chain and have a series of hazards to nature and human health. For example, Methylmercury is highly toxic and has been classified as a probable carcinogen by the International Agency for Research on Cancer [3]. arsenic rank first on the current list of substances that poses the most significant potential threat to human health according the Agency for Toxic Substances and Disease Registry's (ATSDR) Substance Priority List [4]. Lead pollution is considered by the World Health Organization as the number one threat to human health in environmental pollution. Lead also pollutes the world's environment, and for this reason the 1991 Berne Convention has explicitly called for a ban on the use of lead in ammunition [5].

This review firstly investigated the migration pathways and transformation mechanisms of heavy metals in water pollution in nature, and then emphasized its impacts on plants and animals, ecological system and human health. Finally, we propose some solutions for heavy metal pollution control in water from three aspects: physical, chemical and biological, and compare the advantages and disadvantages of several methods. This review enriches the theoretical study of heavy metal water pollution and provides some references for the management of heavy metal water pollution. It promotes the further research of heavy metal water pollution.

2 Migration and Transformation of Heavy Metals in Water

2.1 Migration Pathways of Heavy Metals

Heavy metal pollution in water is characterized by difficulty of degradation, wide range of toxicity and sustainability, and can be transferred between different components of the ecosystem, such as terrestrial to freshwater river and atmospheric, river to ocean and deep sea. Due to the flexibility of heavy metals, the presence of heavy metals is prevalent in all corners of the world, which already a global threat.

2.1.1 Transfer from Land to Freshwater Rivers

To a large extent, land is the source of heavy metal production, metals on the road can be injected into the river in various ways. Approximately 40% of the lakes and rivers of the planet have been polluted by heavy metals [6]. The discharge of domestic sewage and industrial wastewater is the main way of heavy metal pollution in rivers. Although this effluent is treated with wastewater, it contains trace amounts of heavy metals. In particular, industrial wastewater is extremely productive and the total number of heavy metals is huge after a series of transformations, dispersions and enrichments. These treated effluents injected into rivers also transfer heavy metals to freshwater rivers. For example, when mercury is added to dyed cloth as a red dye, the residual mercury metals in the industrial wastewater that is subsequently purified and treated are then injected into the rivers. The mining resource development process also generates heavy metal pollution, which leaches into surrounding water bodies and is injected into rivers, realizing the transfer of heavy metals from land to rivers. For example, heavy metals from tailings and slag from metal mines enter water sources after acid rain or oxidation by water or air, and are eventually transferred to freshwater rivers.

2.1.2 Transfer from the Land to the Atmosphere

Heavy metals adsorbed by soils on land can be transported to the atmosphere in the form of soil particles, and some heavy metals are transported to the atmosphere by human activities. For example, chromium adsorbed on the surface of particles below 2.5 μm can be moved within the atmosphere by wind action [7]. Automobile emissions are the main anthropogenic contributor to elevated atmospheric lead levels. Due to both high urban tailpipe emissions and airborne lead falling into the soil, lead levels in soil particles were three times higher in urban areas than in suburban areas within the entire United States during 1996–2016 [8]. Batteries and used lamps in garbage also release heavy metal particles into the air during incineration. School-age children in a township waste incinerator area in Zhejiang, China, still had relatively high levels of heavy metals in their bodies when there were no significant differences in their intake of heavy metals in rice, soil, vegetables, and drinking water compared to control areas. After a year of research experiments, researchers proved that high metal levels in children in the garbage incinerator area were caused by inhaling heavy metal particles released during the garbage combustion process [9]. Some metals are extremely volatile and can evaporate into the air as vapor if not stored properly, such as mercury. Survey shows China emitted 444 tons of mercury into the atmosphere in 2017 [10].

2.1.3 Transfer from Rivers to Oceans and Deep Oceans

The heavy metals in the river and the river water together inject into the ocean, which is an important pathway for heavy metals to migrate from the river to the ocean [11]. Heavy metals dilute and spread with the movement of the ocean, thus spreading them throughout the ocean. Estuaries are capable of transporting large amounts of heavy metals from rivers to the ocean, which is the transition zone between rivers and the ocean. The study showed that heavy metal concentrations in Haizhou Bay, Lianyungang City, Jiangsu Province, China, decreased with increasing distance from the Linghong estuary [12]. Therefore, it can be proved that the heavy metals in Linhong River can migrate to the sea area of Haizhou Bay and become diluted in the sea water. The heavy metal survey of the Ganges estuary in India shows that the estuary contains high levels of Co, Ni and Cu [13]. With the movement of water, it is easy to wash heavy metals from the estuary into the Indian Ocean. Heavy metals in the ocean can also be adsorbed on solid particles to precipitate to the deep sea. For example, heavy metal particles can be adsorbed on the surface of micro-plastics in seawater. Substances or pollutants with adsorption capacity in seawater are easily adsorbed heavy metal ions in the process of charge balance after weathering and oxidation [14]. Heavy metals migrate to deep or distant seas with the movement of adsorbed particles. In addition, the heavy metals in seawater can react with salt ions that It can form a strong precipitation of compounds. In this way, heavy metals can be transferred to the deep sea. The Modaomen estuary of the Pearl River in China is invaded by seawater, and heavy metals in the water can form precipitates with salt ions [15].

2.2 Migration and Transformation Mechanism of Heavy Metals in Water

2.2.1 Mechanical Migration and Transformation

Mechanical migration and transformation of heavy metals refers to the migration of heavy metals with the movement of water, which mainly includes solid and ionic forms. In solid form, heavy metals are adsorbed on the surface of solid particles, for example, mercury is mostly adsorbed on suspended solid particles and settles on the bottom of water. The ionic form allows heavy metals in water to migrate further away. Both forms allow for the spatial and distance movement of heavy metals with the water flow. The adsorption capacity of heavy metals depends mainly on the specific surface area of rock and soil mineral particles, the larger the specific surface area, the finer the particles, the larger the scale of exchange adsorption. A current study found that the movement of tidal desertification in Daya-Dapeng Bay leads to the movement of heavy metals in intertidal soils [16].

2.2.2 Physical-Chemical Migration and Transformation

Heavy metals exist in water in a variety of forms, mainly in dissolved and particulate states. Due to the differences in temperature, pH, dissolved oxygen, biological community and other factors in different water quality, heavy metals will migrate and transform through a series of physico-chemical interactions such as adsorption and desorption, precipitation and dissolution oxidation and reduction, complexation, chelation and hydrolysis. Take lead as an example, the lead adsorbed on the suspended matter will absorb heat to resolve and sink to the bottom of the water during the summer months. In acidic water, lead ions are converted to PbSo and PbS. In the other hand, lead ions are converted to lead hydroxide sedimentation.

2.2.3 Biological Migration and Transformation

Heavy metals in water cannot be degraded by microorganisms and can only be enriched and transferred through the food chain which mainly means plants and algae in water and terrestrial plants take up heavy metals in their ionic state and fix them in their bodies, and then transferred cascade by cascade with the food chain. The energy flow is shown in Fig. 1. Shellfish have a strong enrichment effect on heavy metals in water, and can transfer heavy metals from water to human body through the food chain to endanger human health. Copper has been tested in shellfish along the Egyptian Red Sea coast at levels that exceed the ideal level for shellfish, which has adverse effects on the health of local children [17]. China is the largest country in terms of mercury production, consumption and anthropogenic emissions, and some studies have found that the mercury content of people in the coastal regions of China mainly originates from fish and inland areas mainly from rice [10]. Accordingly, it can be assumed that the mercury in the Chinese people may be caused by enrichment in the food chain.

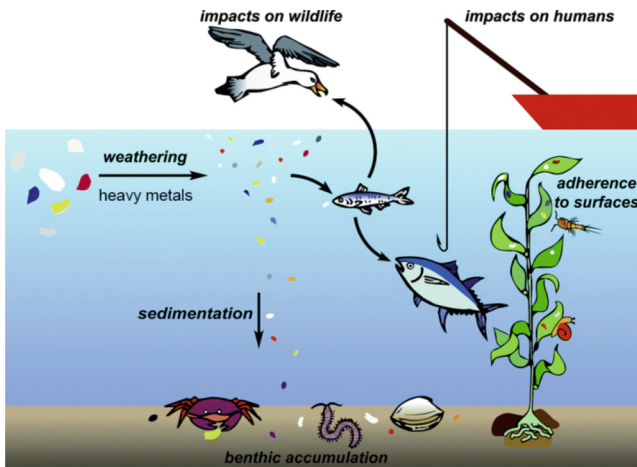


Fig. 1. Migration and transformation of heavy metals in the food chain [18].

3 The Hazard of Heavy Metals in Water

3.1 Hazards to Plants

Heavy metals in excess of discharge standards can cause soil contamination and damage the growth and development of plants. When plants absorb excessive amounts of heavy metals, some symptoms of heavy metal poisoning can occur, such as inhibition of germination, interference with photosynthesis, reduced biomass and inadequate nutrient uptake [19]. It has been shown that the higher the metal concentration, the lower the germination rate of seeds cultured in different concentration gradients of Cr solutions [20]. As the first plant organ to come into contact with heavy metals, roots suffer the most from heavy metal poisoning, which can lead to nutrient absorption deficiencies in plants.

3.2 Hazards to Aquatic Animals

Heavy metals in water mainly enter animals through their respiration, water osmosis and blood circulation, and have a series of effects on aquatic animals. Pollution of the Lake Mariout by heavy metals has led to a significant decline in fish populations, and fishing production has been steadily declining since 1980 [21]. Nickel is acutely toxic to freshwater ciliates and that high concentrations of nickel can even inhibit the development of freshwater ciliate populations [22]. These phenomena prove that when water bodies are contaminated with heavy metals, the number of aquatic animal species is affected to varying degrees and decreases. Heavy metals also can disrupt the sex ratio of biological populations by affecting the production and quality of sperm in aquatic animals. Arsenic inhalation in Japanese freshwater crabs disrupts endocrine structures and thus delays sperm production, while cadmium causes superstructural deformation in all developmental stages of sperm [23]. Some experiments have shown that certain

heavy metals in water can affect the growth of fish. Multiple salvage of fish from the west coast of the UAE revealed that manganese and cadmium affect the size of the fish [24]. The higher the content of manganese and cadmium, the smaller the fish will be.

3.3 Hazards to the Ecosystem

Ecosystem is a complete composed of organisms and environment, the continuous discharge of heavy metals into the water environment will cause irreversible harm to its ecosystem. This damage can interact across ecosystems, ultimately destroying the largest ecosystem-the biosphere. Heavy metals first affect the plants and animals at the bottom of the ecosystem food chain, and are then enriched in animals at the top of the food chain. This result will reduce the population size and density of the ecosystem and lose the ability of the ecosystem to stabilize and recover. When heavy metals exceed the carrying capacity of the ecosystem, it will cause degradation or even the disappearance of the ecosystem. For example, Mangroves are the marginal ecosystem which shares their resources with other nearby vital coastal systems such as seagrass beds and coral reefs. heavy metals (Hg, Cd, Ni, Pb, Cu, Cr, and Zn) enter into this system, The global mangrove area has been lost between 20% and 35% for the past two decades, the Asian subcontinent alone has lost more than half of its original mangrove habitats [25]. Severely, the absence of mangrove fixation of heavy metals also leads to a higher risk of heavy metal contamination of other species within this ecosystem, altering population density and biodiversity and even affecting other surrounding coastal systems and the regional atmosphere.

3.4 Hazards to Human Health

The higher the percentage of water resources contaminated with heavy metals, the less beneficial use of water will be and the harm of heavy metals in water will be exposed. The substances containing heavy metals on human health hazards and the World Health Organization (WHO) restrictions on heavy metals in drinking water are shown in Table 1. Heavy metals can cause damage to cell membranes, genetic material, the nervous system and proteins in the body. For example, heavy metals combined with proteins may lead to enzyme inactivation. The toxic pathways of heavy metals to the human body are shown in Fig. 2. Heavy metals in water can enter the human body by direct or indirect methods such as drinking water and food chain, causing continuous harm to human health. Mercury, cadmium and arsenic in drinking water are an important way to enter the human body, and the long-term accumulation in the body can induce various diseases. Areas with severe heavy metal pollution in the water can even experience collective heavy metal poisoning. The sensational Minamata disease in Japan was caused by the long-term consumption of water containing methylmercury by local residents. Villagers in some villages have shown some symptoms of chronic arsenic poisoning due to excessive arsenic in the drinking water source in Kurdistan Province in the west of Iran including pigment disorders, keratosis of palms and soles [26]. Some heavy metals can indirectly damage human health by entering the body through the respiratory tract, digestive tract or skin. The contact of skin with either with metallic Ni or soluble Ni compounds may produce skin rash and allergic dermatitis. Women working in Ni hydrometallurgy plants

are more exposed to Ni hence their babies showed enhanced structure abnormalities [27]. Heavy metals in seafood can enter the body through the digestive tract and endanger human health. By investigating the heavy metal content of scallops in ten sample sites in the Bohai sea and Yellow Seas, researchers found that the cadmium content in scallops seriously exceeded the standard [28]. Consumers who buy and eat things with excessive levels of cadmium can pose a potential health risk.

Table 1. Daily heavy metal substances and their toxicity

Heavy metal	Common household items	Toxicity	Safe limits by WHO in drinking water (mg/L)	Reference
Cr	Leather, pigments	Kidney damage, allergies, respiratory cancers, asthma	0.05	[2, 29–32]
Cu	Wires, coins	Liver damage, Wilson's disease, insomnia	2	[33, 34]
Cd	Phosphate fertilizer, e-waste	Kidney injury, kidney disease, Itai-Itai, Pulmonary edema	0.007	[2, 35–37]
Ni	Batteries, cables, textiles, bathroom accessories	Dermatitis, nausea, chronic asthma, cough	0.07	[2, 33, 38]
Hg	Thermometers, batteries, cosmetics	Neurological and behavioral disorders, insomnia	0.006	[2, 36]
Pb	Lead batteries, paint, toys	Coma, convulsions, mental retardation, anemia	0.01	[2, 33, 36]

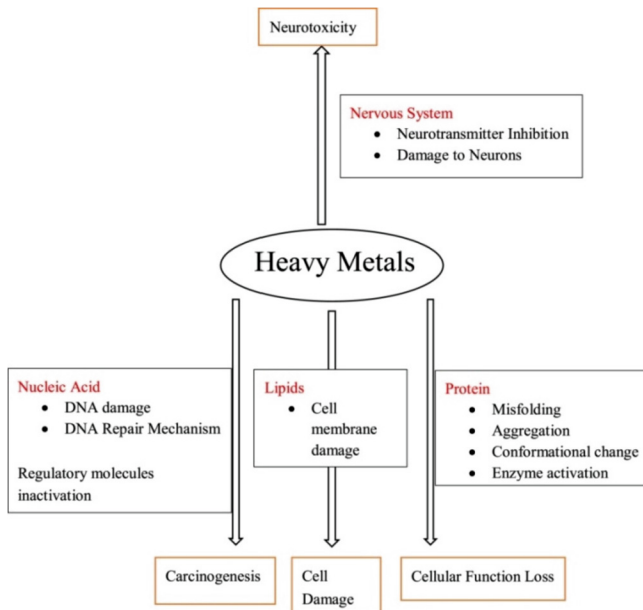


Fig. 2. Damage ways of heavy metals in the human body [39].

4 Treatment Technology of Heavy Metals

4.1 Physical Technology

The main physical methods includes adsorption, membrane separation and air floatation. Adsorption is the use of porous organic or inorganic materials to adsorb heavy metals in water through intermolecular gravitational-van der Waals forces [40]. Compared to other means of heavy metal removal, adsorption produces almost no chemical by-products and sludge [41]. It is considered to be the most promising technology for the absorption of heavy metals from industrial wastewater and groundwater. Because of its developed pore structure and specific surface area, activated carbon has a strong adsorption capacity for heavy metals in water and it is one of the common materials for adsorption. With the development of technology, the adsorption capacity of activated carbon for heavy metals in water has been further improved. Experiments have proven that cracks form when activated carbon changes rapidly between 95 °C and 2 °C. Cracks can enhance its porosity and improve the adsorption capacity of activated carbon [42]. The membrane separation method consists of three main types of mechanisms: size sieving, membrane adsorption and charge rejection. Among them, size screening is divided into low-pressure membrane size screening and high-pressure membrane size screening due to the difference of membrane density. The separation process of heavy metals is shown in Fig. 3 [43]. The air flotation method uses a solid-liquid separation mechanism to achieve the separation of heavy metals in water. The hydrophobic particles with heavy

metals are less dense than water and float upwards [44]. This is the time to get out the heavy metals on the surface of the water in time.

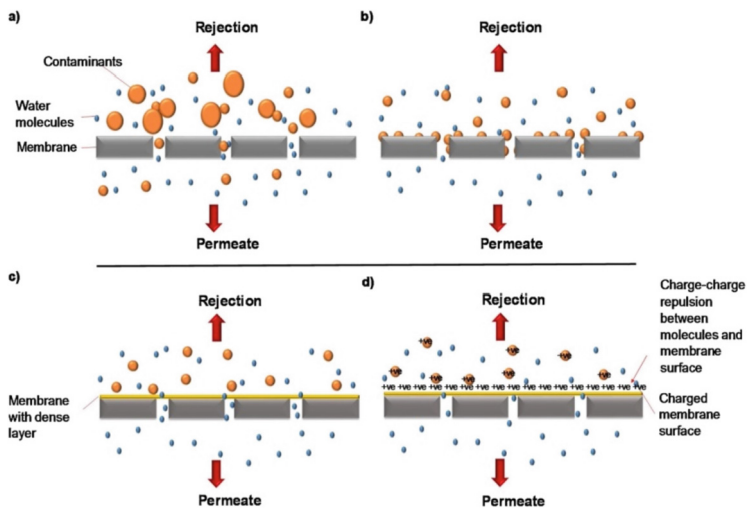


Fig. 3. Dissolution mechanism of membrane treatment technology. (a) Low pressure membrane size exclusion (b) Low pressure membrane adsorption (c) High pressure membrane size exclusion (d) Charging rejection.

4.2 Chemical Technology

Chemical methods mainly include chemical precipitation and electrolysis, both of which precipitate heavy metals from water in the form of solid precipitation. Chemical precipitation is widely used to treat wastewater discharged from paper production and electroplating industries due to its low economic cost and ease of automation [6]. The alum, lime, iron salts and some polymers in this process can combine with heavy metal ions and filter them out in the form of precipitation. The removal of heavy metals by electrolysis is a process of redox reaction, in which metal cations get electrons to produce precipitation. This method not only removes heavy metals from water, but also recycles them. Printed circuit boards contain a high percentage of heavy metals in the form of copper. In order to avoid the transfer of copper to water bodies, electrolysis can be used for recovery. Experiments have proven that 98% of copper from printed circuit boards can be recovered according to standard electrolysis methods [45]. The electrolysis process is shown in Fig. 4.

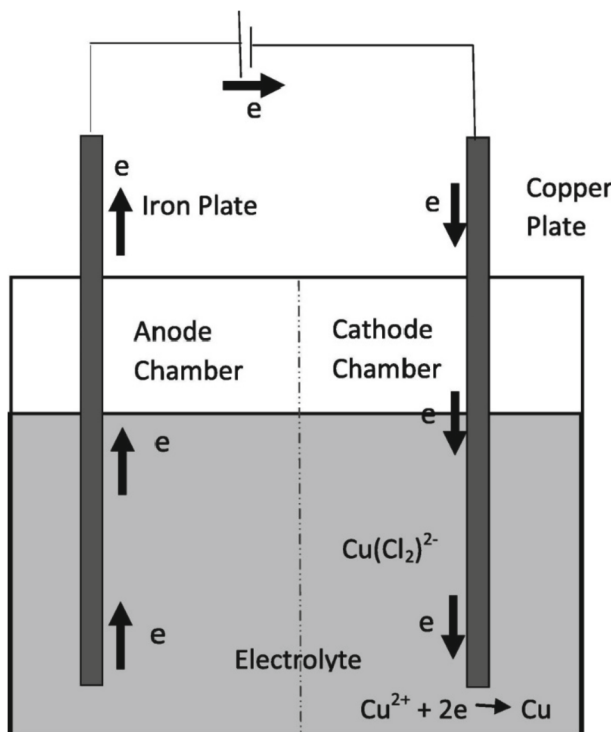


Fig. 4. Electrolysis process [45].

4.3 Biological Technology

Plants can absorb heavy metals from water and store them in their roots, stems and leaves. Therefore, this feature of plants can be used for heavy metal treatment, and phytoremediation is one of the common methods for biosorption of heavy metals. This method has low installation and maintenance costs and can be implemented on a large scale. It is worth mentioning that the characteristics of heavy metal contamination need to be identified before phytoremediation is applied. The growth rate of the plants, their adaptability to the environment and the time required to reduce the pollutant levels to a reasonable range are also considered before treatment. In addition, some heavy metal-loving microorganisms are resistant to heavy metals. Some microorganisms can absorb heavy metals and store them in their bodies. Under certain conditions, the secretions of some microorganisms are able to form precipitates with metal ions. So they can be used to break down and transform the medium heavy metals in water. For example, Acid mine drainage contains large amounts of iron, aluminum, manganese and zinc. Hydrogen sulfide produced by bacteria on the bioreactor is able to produce hydroxide precipitation with metal ions in the wastewater at a certain pH [46]. This is a method of removing heavy metals from water using biomineratization by microorganisms [47].

4.4 Comparative Analysis

A total of three measures for the treatment of heavy metal water pollution in physical, chemical and biological aspects are presented above. Each treatment measure is characterized by two aspects of advantages and shortcomings in the treatment of heavy metals, and their advantages and shortcomings are shown in Table 2. Careful discussion of the pros and cons of each measure will facilitate the selection of the best means of heavy metal water pollution control. Cost-effective adsorption is the most common treatment technology, but it also suffers from the deficiencies of difficult reuse of adsorbent and limited adsorption capacity [40, 41]. Membrane separation technology is highly efficient in removing heavy metals and can get out some organic and inorganic wastes at the same time. Its treatment process has no chemical additive chemistry and does not cause secondary pollution [6]. However, the process of membrane treatment technology is complex and costly, and there are also problems of membrane contamination and low membrane permeability that need to be solved. Air flotation is economical and simple to operate which basically does not produce secondary pollution in the process. Although this method cannot completely remove heavy metals, it needs further optimization [48].

Table 2. Methods of treating heavy metals in water and their advantages and disadvantages

	Processing method	Advantages	Disadvantages	Reference
Physical methods	Physical adsorption	Low cost, simple operation, no toxic by-products	Difficult to reuse adsorbent, limited adsorption capacity	[40, 41]
	Membrane Separation	Energy saving, high efficiency, environmental protection, multi-functional	Complex process, high cost, membrane contamination and low permeate flux	[6]
	Dissolved air float	Economical, simple, no recontamination	Cannot be completely removed	[48]
Chemical methods	Chemical precipitation	Low cost, simple operation, automation	Toxic by-products	[34]
	Electrolysis	Simple and environmental friendly, less labor	Expensive electricity, limited by metal ion concentration	
Biological methods	Plant uptake	Economical and environmentally friendly, highly applicable	Slow process	[49, 50]
	Microbiological treatment	Safe, low cost	Limited types of treatment, incomplete degradation	[51]

The chemical precipitation method is low cost and easy to automate the treatment of heavy metals in water, but it produces toxic sludge that requires further treatment [34]. Therefore its operation is complicated. The electrolysis method is simple and environmentally friendly and can reduce the number of laborers. However, the electrolysis method is costly in terms of power consumption and the treatment efficiency can be limited by the concentration of heavy metal ions in the solution. Biological methods mainly include plant absorption and microbial treatment, both of which are economical and environmentally friendly [49, 50], but inefficient [51].

5 Conclusion

Heavy metals have many adverse effects on both the natural environment and human society. It is an inevitable trend to strengthen the treatment of heavy metal water pollution. This study summarizes the three pathways of heavy metal transport in the environment. Heavy metals on land can be transferred to the atmosphere by dust particles or evaporation, or they can be discharged into rivers by acid rain or sewage. Heavy metals in rivers can be transferred to the ocean even deep sea with the movement of water. Heavy metals are also subject to a number of transformations during transport, including morphological transformations, chemical transformations and transformations of carriers in the food chain. Heavy metals in the natural environment are a serious hazard to plants, animals and the entire ecosystem. The accumulation of heavy metals in the body can also be harmful to human health and may lead to various diseases. This paper investigates different mechanisms of heavy metal wastewater treatment measures and compares the advantages and shortcomings of several means, which can help one to choose the most suitable treatment method according to the type of pollution. The purpose of this review is to promote research on heavy metal pollution in the aquatic environment and to prevent the adverse effects of heavy metals on ecosystems and human health. It has also helped to strengthen the worldwide attention and rethinking of heavy metal pollution in water.

Acknowledgments. I promise that the paper meets the academic requirements and that the data cited in the paper are true and reliable.

References

1. Nazaripour, M., Reshadi, M.A.M., Mirbagheri, S.A., Nazaripour, M., Bazargan, A.: Research trends of heavy metal removal from aqueous environments. *J. Environment. Manage.* **287**, 112322 (2021)
2. Numan, A., Gill, A.A.S., Rafique, S., Guduri, M., Zhan, Y., Maddiboyina, B., Li, L., Singh, S., Nguyen Dang, N.: Rationally engineered nanosensors: a novel strategy for the detection of heavy metal ions in the environment. *J. Hazard. Mater.* **409** 124493 (2021)
3. Gyamfi, O., Sørensen, P.B., Darko, G., Ansah, E., Vorkamp, K., Bak, J.L.: Contamination, exposure and risk assessment of mercury in the soils of an artisanal gold mining community in Ghana. *Chemosphere* **267**, 128910 (2021)

4. Yadav, M.K., Saidulu, D., Gupta, A.K., Ghosal, P.S., Mukherjee, A.: Status and management of arsenic pollution in groundwater: A comprehensive appraisal of recent global scenario, human health impacts, sustainable field-scale treatment technologies. *J. Environment. Chem. Eng.* **9**(3), 105203 (2021)
5. Monclús, L., Shore, R.F., Krone, O.: Lead contamination in raptors in Europe: a systematic review and meta-analysis. *Sci. Total Environ.* **748**, 141437 (2020)
6. Zamora-Ledezma, C., Negrete-Bolagay, D., Figueiroa, F., Zamora-Ledezma, E., Ni, M., Alexis, F., Guerrero, V.H.: Heavy metal water pollution: a fresh look about hazards, novel and conventional remediation methods. *Environ. Technol. Innov.* **22**, 101504 (2021)
7. Kim, K.-H., Kang, C.-H., Ma, C.-J., Lee, J.-H., Choi, K.-C., Youn, Y.-H.: Airborne cadmium in spring season between Asian dust and non-Asian dust periods in Korea. *Atmos. Environ.* **42**(4), 623–631 (2008)
8. Frank, J.J., Poulakos, A.G., Tornero-Velez, R., Xue, J.: Systematic review and meta-analyses of lead (Pb) concentrations in environmental media (soil, dust, water, food, and air) reported in the United States from 1996 to 2016. *Sci. Total Environ.* **694**, 133489 (2019)
9. Xu, P., Chen, Y., He, S., Chen, W., Wu, L., Xu, D., Chen, Z., Wang, X., Lou, X.: A follow-up study on the characterization and health risk assessment of heavy metals in ambient air particles emitted from a municipal waste incinerator in Zhejiang, China. *Chemosphere* **246**, 125777 (2020)
10. Wang, B., Chen, M., Ding, L., Zhao, Y., Man, Y., Feng, L., Li, P., Zhang, L., Feng, X.: Fish, rice, and human hair mercury concentrations and health risks in typical Hg-contaminated areas and fish-rich areas, China. *Environ. Int.* **154**, 106561 (2021)
11. Karaouzas, I., Kapetanaki, N., Mentzafou, A., Kanellopoulos, T.D., Skoulikidis, N.: Heavy metal contamination status in Greek surface waters: a review with application and evaluation of pollution indices. *Chemosphere* **263**, 128192 (2021)
12. Liu, B., Wang, J., Xu, M., Zhao, L., Wang, Z.: Spatial distribution, source apportionment and ecological risk assessment of heavy metals in the sediments of Haizhou Bay national ocean park, China. *Mar. Pollut. Bull.* **149**, 110651 (2019)
13. Samanta, S., Dalai, T.K.: Massive production of heavy metals in the Ganga (Hooghly) River estuary, India: global importance of solute-particle interaction and enhanced metal fluxes to the oceans. *Geochim. Cosmochim. Acta* **228**, 243–258 (2018)
14. Gao, F., et al.: Study on the capability and characteristics of heavy metals enriched on microplastics in marine environment. *Mar. Pollut. Bull.* **144**, 61–67 (2019)
15. Jia, Z., Li, S., Liu, Q., Jiang, F., Jiatang, H.: Distribution and partitioning of heavy metals in water and sediments of a typical estuary (Modaomen, South China): the effect of water density stratification associated with salinity. *Environ. Poll.* **287**, 117277 (2021)
16. Liao, J., Qian, X., Liu, F., Deng, S., Lin, H., Liu, X., Wei, C.: Multiphase distribution and migration characteristics of heavy metals in typical sandy intertidal zones: insights from solid-liquid partitioning. *Ecotoxicol. Environ. Safe.* **208**, 111674 (2021)
17. El Nemr, A., El-Said, G.F., Ragab, S., Khaled, A., El-Sikaily, A.: The distribution, contamination and risk assessment of heavy metals in sediment and shellfish from the Red Sea coast, Egypt. *Chemosphere* **165**, 369–380 (2016)
18. Lin, V.S.: Research highlights: impacts of microplastics on plankton. *Environ. Sci. Process Impacts* **18**(2), 160–163 (2016)
19. Yesil, H., Tugtas, A.E.: Removal of heavy metals from leaching effluents of sewage sludge via supported liquid membranes. *Sci. Total Environ.* **693**, 133608 (2019)
20. Diaconu, M., et al.: Characterization of heavy metal toxicity in some plants and microorganisms—a preliminary approach for environmental bioremediation. *New Biotechnol.* **56**, 130–139 (2020)

21. Abu El-Magd, S.A., Taha, T.H., Pienaar, H.H., Breil, P., Amer, R.A., Namour, P.: Assessing heavy metal pollution hazard in sediments of Lake Mariout, Egypt. *J. Afr. Earth Sci.* **176**, 104116 (2021)
22. Madoni, P.: The acute toxicity of nickel to freshwater ciliates. *Environ. Pollut.* **109**(1), 53–59 (2000)
23. Harlıoğlu, M.M., Farhadi, A., Gür, S.: Determination of sperm quality in decapod crustaceans. *Aquaculture* **490**, 185–193 (2018)
24. Al-Yousuf, M.H., El-Shahawi, M.S., Al-Ghais, S.M.: Trace metals in liver, skin and muscle of *Lethrinus lentjan* fish species in relation to body length and sex. *Sci. Total Environ.* **256**(2), 87–94 (2000)
25. Sandilyan, S., Kathiresan, K.: Decline of mangroves – a threat of heavy metal poisoning in Asia. *Ocean Coast Manage.* **102**, 161–168 (2014)
26. Barati, A.H., Maleki, A., Alasvand, M.: Multi-trace elements level in drinking water and the prevalence of multi-chronic arsenical poisoning in residents in the west area of Iran. *Sci. Total Environ.* **408**(7), 1523–1529 (2010)
27. Rehman, A.U., Nazir, S., Irfshad, R., Tahir, K., Ur Rehman, K., Islam, R.U., Wahab, Z.: Toxicity of heavy metals in plants and animals and their uptake by magnetic iron oxide nanoparticles. *J. Mol. Liq.* **321**, 114455 (2021)
28. Lin, Y., Lu, J., Wu, J.: Heavy metals pollution and health risk assessment in farmed scallops: Low level of Cd in coastal water could lead to high risk of seafood. *Ecotoxicol. Environ. Saf.* **208**, 111768 (2021)
29. Prasad, S., Yadav, K.K., Kumar, S., Gupta, N., Cabral-Pinto, M.M.S., Rezania, S., Radwan, N., Alam, J.: Chromium contamination and effect on environmental health and its remediation: a sustainable approaches. *J. Environ. Manage.* **285**, 112174 (2021)
30. DesMarias, T.L., Costa, M.: Mechanisms of chromium-induced toxicity. *Curr. Opin. Toxicol.* **14**, 1–7 (2019)
31. Sharma, N., Sodhi, K.K., Kumar, M., Singh, D.K.: Heavy metal pollution: Insights into chromium eco-toxicity and recent advancement in its remediation. *Environ. Nanotechnol. Monit. Manage.* **15**, 100388 (2021)
32. Shahid, M., et al.: Chromium speciation, bioavailability, uptake, toxicity and detoxification in soil-plant system: a review. *Chemosphere* **178**, 513–533 (2017)
33. Mao, S., Gao, M.: Functional organoclays for removal of heavy metal ions from water: A review. *J. Mol. Liq.* **334**, 116143 (2021)
34. Shrestha, R., Ban, S., Devkota, S., Sharma, S., Joshi, R., Tiwari, A.P., Kim, H.Y., Joshi, M.K.: Technological trends in heavy metals removal from industrial wastewater: a review. *J. Environ. Chem. Eng.* **9**(4), 105688 (2021)
35. Yoshinaga, M., Hiromasa Ninomiya, M.M., Hossain, A.A., Sudo, M., Akhand, A.A., Nazmul Ahsan, M., Abdul Alim, M., Khalequzzaman, M.I., Yajima, I., Ohgami, N., Kato, M.: A comprehensive study including monitoring, assessment of health effects and development of a remediation method for chromium pollution. *Chemosphere* **201**, 667–675 (2018)
36. Rahman, M.M., et al.: Selenium and zinc protections against metal-(loids)-induced toxicity and disease manifestations: a review. *Ecotoxicol. Environ. Saf.* **168**, 146–163 (2019)
37. Kurniawan, T.A., Chan, G.Y.S., Lo, W.-H., Babel, S.: Physico-chemical treatment techniques for wastewater laden with heavy metals. *Chem. Eng. J.* **118**(1), 83–98 (2006)
38. Kumar, A., Jigyasu, D.K., Kumar, A., Subrahmanyam, G., Mondal, R., Shabnam, A.A., Cabral-Pinto, M.M.S., Malyan, S.K., Chaturvedi, A.K., Gupta, D.K., Fagodiya, R.K., Khan, S.A., Bhatia, A.: Nickel in terrestrial biota: comprehensive review on contamination, toxicity, tolerance and its remediation approaches. *Chemosphere* **275**, 129996 (2021)
39. Briffa, J., Sinagra, E., Blundell, R.: Heavy metal pollution in the environment and their toxicological effects on humans. *Heliyon* **6**(9), e04691 (2020)

40. Kong, Q., Shi, X., Ma, W., Zhang, F., Yu, T., Zhao, F., Zhao, D., Wei, C.: Strategies to improve the adsorption properties of graphene-based adsorbent towards heavy metal ions and their compound pollutants: a review. *J. Hazard. Mater.* **415**, 125690 (2021)
41. Gupta, A.D., Rawat, K.P., Bhadauria, V., Singh, H.: Recent trends in the application of modified starch in the adsorption of heavy metals from water: a review. *Carbohydrate Polym.* **269**, 117763 (2021)
42. Kharrazi, S.M., Mirghaffari, N., Dastgerdi, M.M., Soleimani, M.: A novel post-modification of powdered activated carbon prepared from lignocellulosic waste through thermal tension treatment to enhance the porosity and heavy metals adsorption. *Powder Technol.* **366**, 358–368 (2020)
43. Abdullah, N., Yusof, N., Lau, W.J., Jaafar, J., Ismail, A.F.: Recent trends of heavy metal removal from water/wastewater by membrane technologies. *J. Ind. Eng. Chem.* **76**, 17–38 (2019)
44. Al-Zoubi, H., Ibrahim, K.A., Abu-Sbeih, K.A.: Removal of heavy metals from wastewater by economical polymeric collectors using dissolved air flotation process. *J. Water Process. Eng.* **8**, 19–27 (2015)
45. Choubey, S., Goswami, P., Gautam, S.: Recovery of copper from waste PCB boards using electrolysis. *Mater. Today Proc.* **42**, 2656–2659 (2021)
46. Luptakova, A., Ubaldini, S., Macingova, E., Fornari, P., Giuliano, V.: Application of physical–chemical and biological–chemical methods for heavy metals removal from acid mine drainage. *Process Biochem.* **47**(11), 1633–1639 (2012)
47. Sharma, R., Jasrotia, T., Kumar, R., Kumar, R., Alothman, A.A., Al-Anazy, M.M., Alqahtani, K.N., Umar, A.: Multi-biological combined system: a mechanistic approach for removal of multiple heavy metals. *Chemosphere* **276**, 130018 (2021)
48. Hu, T., Chen, W.-Z., Bu, H., Li, W.-X., Li, Z.-L., Liu, B.-N., Lan, L.-M., Guo, C., Wang, Q., Jiang, G.-B.: A novel technique for Cd removal from soil based on alginate-derived floatable spheres. *Chem. Eng. J.* **414**, 128777 (2021)
49. Cui, J., Xie, Y., Sun, T., Chen, L., Zhang, W.: Deciphering and engineering photosynthetic cyanobacteria for heavy metal bioremediation. *Sci. Total Environ.* **761**, 144111 (2021)
50. Zhang, H., Yuan, X., Xiong, T., Wang, H., Jiang, L.: Bioremediation of co-contaminated soil with heavy metals and pesticides: Influence factors, mechanisms and evaluation methods. *Chem. Eng. J.* **398**, 125657 (2020)
51. Verma, S., Kuila, A.: Bioremediation of heavy metals by microbial process. *Environ. Technol. Innov.* **14**, 100369 (2019)



The Removal Effect of Organic Pollutants by Different Fillers in Constructed Rapid Infiltration System

J. B. Zhang^{1,2}, M. L. Zhu^{1,2(✉)}, P. L. Xu^{1,2}, H. Jiang^{1,2}, and Y. L. Han^{1,2}

¹ School of Environmental Science and Engineering, Xiamen University of Technology, Xiamen 361024, China
292890310@qq.com

² The Key Laboratory of Water Resources Utilization and Protection of Xiamen, Xiamen University of Technology, Xiamen 361024, China

Abstract. In recent years, the concept of ecological treatment of rural domestic sewage and tail water reuse has been strongly advocated by the Ministry of Ecology and Environment. Constructed rapid infiltration (CRI) system is a low-cost and suitable ecological sewage treatment measure in rural areas. There are many kinds of filter materials in CRI system, but there are few reports on the research of filter materials based on Farmland Irrigation Standard (GB18918-2002) as the effluent discharge standard. In this study, red sandy soil, black volcanic rock, red volcanic rock, slag and biological ceramicsite were selected as the filter media of CRI system, and five CRI systems were constructed. Under the condition of hydraulic loading rate (HLR) of 1 m·d⁻¹ and test period of 30 days, the removal efficiencies for chemical oxygen demand (COD) and five-days biochemical oxygen demand (BOD₅) by each CRI system were studied, and the best filter media for organic pollutants removal was finally selected. The results show that red volcanic rock has the best removal efficiency for COD and BOD₅. The effluent concentrations of COD and BOD₅ are 43.8 mg/L and 30.2 mg/L, respectively, and the corresponding removal rates are 72.1% and 74.4%, respectively. The effluent can meet the standards of Class B and Class A vegetables in Farmland Irrigation Standard, respectively. This study provided a theoretical basis for the rational selection of filter material in practical engineering application of CRI system to improve the removal performance of organic pollutants.

Keywords: Constructed rapid infiltration system · Fillers · COD · BOD₅

1 Introduction

In China, point source and non-point source pollution has become a growing concern, especially the discharge of domestic sewage in rural areas. It is reported that the annual discharge of domestic sewage in villages and towns in China has reached 20 billion cubic meters [1]. However, most rural areas in China are not equipped with perfect drainage pipe network and sewage treatment system, so that sewage is directly discharged into the

surrounding receiving water without treatment. Rural domestic sewage contains a large amount of organic pollutants, such as chemical oxygen demand (COD), five-days biochemical oxygen demand (BOD_5), etc. If it is discharged directly without treatment, it will not only threaten the safety of ecology and water environment, but also cause potential safety hazards to rural water sources, aggravate the crisis of fresh water resources, make farmland irrigation unable to be effectively guaranteed, and affect the survival and development of farmers [2, 3]. Therefore, it is urgent to take an eco-friendly sewage treatment technical measure to treat rural domestic sewage.

In recent years, the Ministry of Ecology and Environment and the Ministry of Housing and Urban-Rural Development jointly issued the Notice on Accelerating the Formulation of Local Rural Domestic Sewage Treatment Discharge Standards, which proposed: 1) Promote the extension of sewage pipe network to villages; 2) Encourage the adoption of ecological treatment technology, and require strengthening the source reduction of domestic sewage and the recycling of tail water. In rural areas, because of the complexity of terrain and the dispersion of villagers' residences, the cost and difficulty of building sewage pipe network are increased. Thus, the method of adopting ecological treatment technology is more suitable for rural areas, and farmland irrigation is a very suitable way of sewage recycling in rural areas.

Constructed Rapid Infiltration (CRI) system is a kind of ecological wastewater treatment technology with low cost, no energy consumption and good water purification effect. It is developed from the traditional Rapid Infiltration (RI) system and uses the medium with better permeability to replace the natural soil layer. It is especially suitable for the treatment of rural domestic sewage [4, 5]. Many scholars have carried out a large number of studies on the water purification effect of CRI system. 1) Most of the studies focus on the removal of nitrogen and phosphorus by CRI system [6–8], However, the nitrogen and phosphorus substances rich in sewage can be used as nutrients of crops, which is conducive to the growth of crops and plants. Hence, treating rural domestic sewage to meet the Farmland Irrigation Standard (GB5084-2005) and reusing it in farmland not only “turns waste into wealth” but also conforms to the sewage reuse concept mentioned in the above notice; 2) A few scholars have studied the removal efficiency of organic pollutants by CRI system. Shi X et al. [9] investigated the treatment effect of various fillers on sewage, and the results showed that the COD removal rate of anthracite, round ceramic and gravel only reached 50%, indicating a phenomenon of low removal rate. 3) In existing studies, most of the sewage treatment discharge standards after CRI system treatment are Urban Sewage Treatment Plant Pollutant Discharge Standards (GB18918-2002). However, few reports have investigated the effect of CRI systems on the removal of COD and BOD_5 from wastewater using the Agricultural Irrigation Standard (GB5084-2005) as the sewage discharge standard.

In this study, five different filter media were selected as the filter media of CRI system, namely red sandy soil, black volcanic rock, red volcanic rock, slag and biological ceramsite, and five test column of CRI system were built to investigate the changes of COD and BOD_5 concentration and removal effect of the inlet and outlet water of CRI system with different kinds of filter media, aiming to select the filter media with the best performance in the removal of COD and BOD_5 , which can provide the basis for

improving the removal of organic pollutants in CRI systems, thus promoting the practical application of CRI systems in the field of rural domestic wastewater treatment.

2 Materials and Methods

2.1 Test Process and Device

The experimental procedure and installation of the CRI system are shown in Fig. 1. First, the test water was taken from the inlet of the domestic wastewater treatment station on the campus of Xiamen Institute of Technology (Fig. 1A). Secondly, a polyethylene plastic box (Fig. 1B) was used to contain the collected domestic wastewater and then transferred to the laboratory for use. Then, a peristaltic pump (Fig. 1C) was used to lift the domestic wastewater in the polyethylene plastic box to the water distribution port of the CRI system test column (Fig. 1D). Finally, the COD and BOD_5 concentrations in the inlet and outlet water of the CRI system test column were measured.

CRI system test column made of plexiglass, column height of 60 cm, inner diameter of 9 cm, outer diameter of 10 cm, filter material thickness of 30 cm. The water pipe is used to distribute water evenly to the CRI system, and the water intake can be controlled by adjusting the speed of the peristaltic pump. The water outlet is located at the bottom of the test column, and each column is equipped with one water outlet.

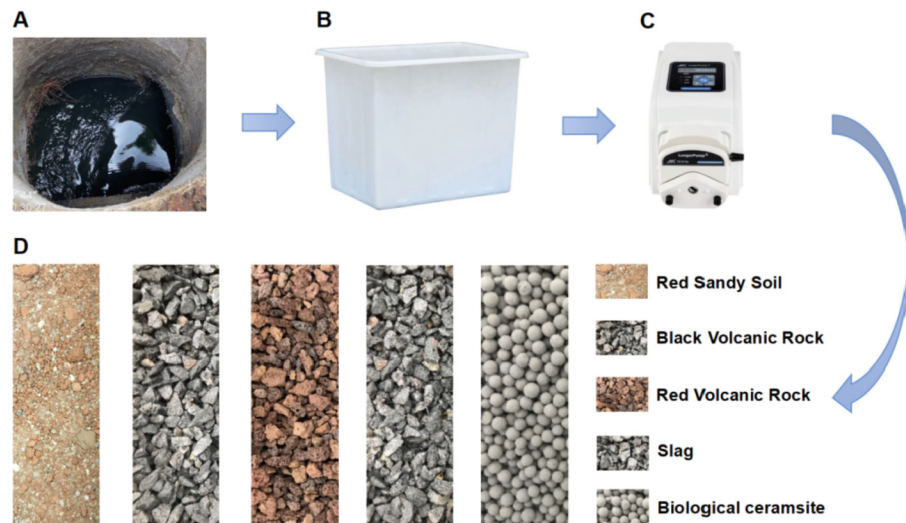


Fig. 1. Flow chart of CRI system for treatment of domestic sewage (A: inlet of domestic sewage treatment station of Xiamen University of Technology; B: Sewage storage tank for collecting domestic sewage at the inlet; C: Peristaltic pump, used to transfer sewage and distribute water to CRI system; D: CRI system test column, the thickness of the filter material is 30 cm)

2.2 Test Filter Material Type

There are five kinds of filter media in this experiment, which are: 1) red sandy soil, a kind of composite filter media which is evenly mixed by two kinds of filter media whose mass ratio is red loam: miscellaneous sand = 1: 1, and the permeability coefficient is $2.78 * 10^{-4}$; 2) Black volcanic rock, an irregular porous particle filter material with black appearance, with a particle size of 2–4 mm and a permeability coefficient of $4.88 * 10^{-3}$; 3) Red volcanic rock, an irregular porous particle filter material with red appearance, with a particle size of 2–4 mm and a permeability coefficient of $3.94 * 10^{-3}$; 4) slag, a new filter material with high removal efficiency of suspended solids, large sludge interception load and good prospect of popularization and application, with a particle size of 2–4 mm and a permeability coefficient of $4.03 * 10^{-3}$; 5) biological ceramsite, a new biofilm carrier filter material with the advantages of light weight, large specific surface area and strong adsorption capacity, with a particle size of 2–4 mm and a permeability coefficient of $3.98 * 10^{-3}$.

2.3 Inlet Water Condition and Inlet Water Quality

The test inlet water was taken from the inlet of the campus sewage treatment station, and the specific inlet water concentration range was as follows: COD = $126.8 \sim 233.3 \text{ mg/L}$, $\text{BOD}_5 = 89 \sim 104 \text{ mg/L}$. Five CRI system test columns with different filter media were used to operate under the same inflow conditions, with hydraulic loading rate of $1 \text{ m} \cdot \text{d}^{-1}$ and daily inflow of 6.4 L. The total duration of the experiment was 30 days, and every day was divided into three cycles of water distribution, each cycle was run for 2 h, respectively from 8:00 to 10:00, 12:00 to 14:00, and 18:00 to 20:00, and the wet-dry ratio was 1: 4. The inlet and outlet water quality of CRI system test column was monitored every 2 days to investigate the removal effect of different filter materials on COD and BOD_5 in domestic sewage. The daily water inflow of CRI system was calculated with Eq. (1).

$$Q = \text{HLR} * \pi R^2 * T \quad (1)$$

Where, Q is the daily water inflow of CRI system test column (m^3); HLR is Hydraulic loading rate ($\text{m} \cdot \text{d}^{-1}$). R is the radius of the test column (m); T is time (d).

2.4 Testing Items and Methods of Water Quality Indexes

Test items of inlet and outlet water quality indexes include COD and BOD_5 . The detection method of COD was rapid digestion spectrophotometry (HJ/T 399.2007), and the detection instruments were Lianhua 5B-1 (V8 version) digestion device and Lianhua 5B-3B (V8 version) multi-parameter water quality tester. BOD_5 was detected by dilution and inoculation method (HJ 505-2009) with BODTrak biochemical oxygen demand analyzer.

3 Results and Discussion

3.1 Removal Effect of COD by Different Filter Materials

During the whole test period, the removal of COD by CRI systems with different filter media is shown in Fig. 2. As can be seen from Fig. 2A, The influent COD concentration of CRI system ranged from 126.8 mg/L to 233.3 mg/L, The average concentration of effluent after the CRI system of various filter materials runs stably is as follows: red volcanic rock (43.8 mg/L), slag (60.6 mg/L), red sandy soil (79.3 mg/L), black volcanic rock (83.7 mg/L), and biological ceramsite (123.8 mg/L), that is, the order of removal efficiency of COD by five filter media is red volcanic rock > slag > red sandy soil > black volcanic rock > biological ceramsite, so red volcanic rock has the best removal efficiency of COD, and only the effluent of red volcanic rocks can meet the irrigation standard of Class B vegetables in Farmland Irrigation Standard (GB5084-2005).

Figure 2B shows the removal rates of COD by different filter materials. After stable operation, the corresponding removal rates are: red volcanic rock (72.1%) > slag (60.9%) > red sandy soil (46.3%) > black volcanic rock (43.5%) > biological ceramsite (23.6%). The COD removal rate curve of red volcanic rocks shows a gradual upward trend as a whole; From the first day to the 20th day of the experiment, the COD removal rate curve fluctuated. From the 20th to 30th days, the removal rate of COD began and finally stabilized, because the removal of COD in the early stage of the experiment depended on the adsorption of red volcanic rock, and in the later stage, due to the gradual formation and stability of biofilm, adsorption and biodegradation contributed to the decomposition of COD [10]. The COD removal rate curves of slag and red sandy soil are similar to those of red volcanic rock, with a trend of “rising first and then stabilizing”, but the COD removal rate of red sandy soil is lower than that of slag. The removal of COD by black volcanic rocks is “stable-fluctuating-stable again”, COD removal rate did not increase in the later stage of the experiment, It is related to the adsorption performance of black volcanic rock, Because the adsorption sites of black volcanic rock are few, with the experiment, the adsorption sites on the surface of filter media are gradually occupied, resulting in the decrease of adsorption performance, so that the removal of COD in the later stage of the experiment mainly depends on the degradation of microorganisms, so the removal of COD in the early and later stages of the experiment depends on the adsorption and microbial degradation of black volcanic rock respectively. The COD removal rate curve of biological ceramsite showed a downward trend as a whole, Because the surface of biological ceramsite is spherical and smooth, which is not suitable for the growth of microorganisms, it is difficult to form and stabilize biofilm, so its removal of COD only depends on adsorption, but with the experiment, the adsorption gradually weakens, resulting in a significant reduction in removal rate and poor COD removal effect.

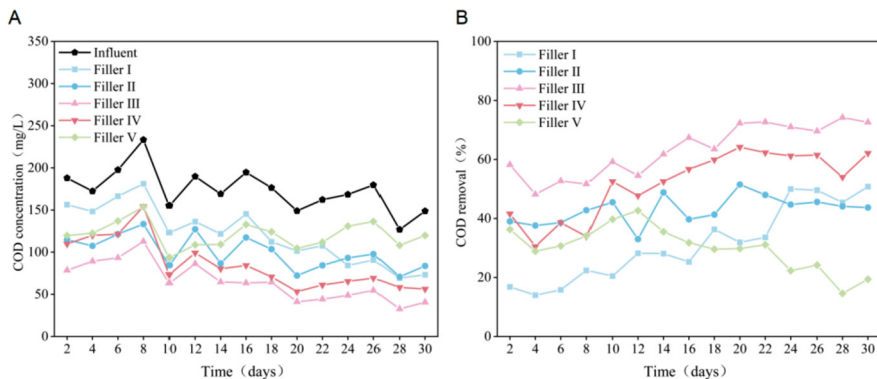


Fig. 2. The removal effect of different filter materials on COD.

3.2 Removal Effect of BOD₅ by Different Filter Materials

Figure 3 shows the removal of BOD₅ by five filter media. As shown in Fig. 3A, The influent BOD₅ concentration of each filter material in CRI system ranges from 89 mg/L to 104 mg/L (average concentration is 95.5 mg/L), The effluent concentrations are red sandy soil (44–72 mg/L), black volcanic rock (56–74 mg/L), red volcanic rock (22–48 mg/L), slag (30–60 mg/L) and biological ceramsite (67–80 mg/L), and the corresponding average concentrations after stabilization are red sandy soil (54.0 mg/L), black volcanic rock (63.8 mg/L), red volcanic rock (30.2 mg/L), slag (42.3 mg/L) and biological ceramsite (73.8 mg/L), respectively. That is to say, red volcanic rock has the best removal effect on BOD₅, and only the effluent of red volcanic rock can meet the irrigation standard of Class A vegetables in Farmland Irrigation Standard (GB5084-2005).

As shown in Fig. 3B, after the CRI system with five filter materials runs stably, the removal rates of BOD₅ are red sandy soil (49.8%), black volcanic rock (36.6%), red volcanic rock (74.4%), slag (63.6%) and biological ceramsite (23.1%). The BOD₅ removal rate curves of red sandy soil, red volcanic rock, black volcanic rock and slag all show a

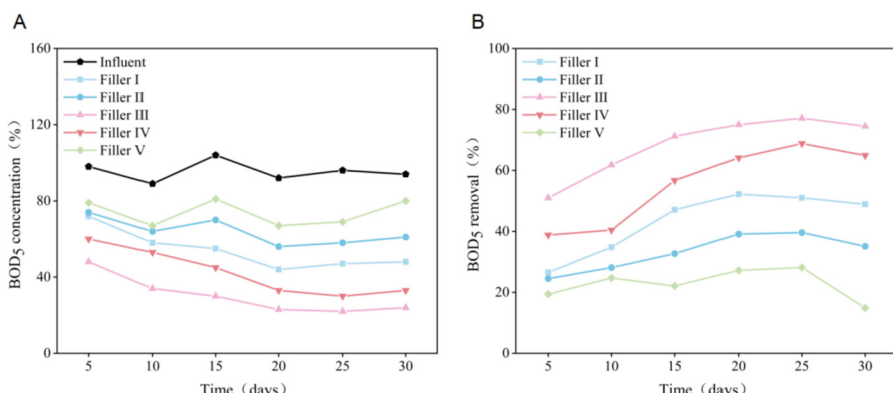


Fig. 3. The removal effect of different filter materials on BOD₅.

“slow upward” trend, which is due to the rough surface of these four filter media, which is more suitable for microbial growth. With the experiment, the biofilm gradually grows and stabilizes, which is beneficial to the degradation of organic pollutants. However, the biological ceramsite shows a trend of “fluctuating first, then declining”, and the removal effect of BOD_5 is not good, which is due to the smooth surface of biological ceramsite, which is not suitable for microbial growth, resulting in the difficulty in forming biofilm, so the removal performance of organic pollutants is poor.

4 Conclusion

Five different filter media, red sandy soil, black volcanic rock, red volcanic rock, slag and biological ceramsite, were selected as the test materials of CRI system, and then the removal effects of different filter media on COD and BOD_5 concentrations in domestic sewage were investigated. The following conclusions can be drawn:

- (1) Red volcanic rock has excellent removal efficiency of COD. The COD concentration of effluent is 43.8 mg/L, and the corresponding removal rate is 72.1%. The effluent quality can meet the irrigation standard of Class B vegetables in Farmland Irrigation Standard (GB5084–2005).
- (2) Red volcanic rock has good removal effect on BOD_5 . The concentration of BOD_5 in the effluent is 30.2 mg/L, and the corresponding removal rate is 74.4%, respectively. The effluent quality can meet the irrigation standard of Class A vegetables in Farmland Irrigation Standard (GB5084–2005).
- (3) Red volcanic rock has outstanding removal ability for COD and BOD_5 , the reasons are: 1) There are many adsorption sites on the surface of filter media, which have strong adsorption ability; 2) The surface is porous, which is suitable for microbial growth and reproduction, and is beneficial to the formation and stability of biofilm. Therefore, the adsorption of red volcanic rocks and the degradation of microorganisms jointly promote the removal of organic pollutants.

Acknowledgement. This work was financially supported by “Fujian Provincial Science and Technology Project (2019I0021)”.

References

1. Xie, Y.D., et al.: Towards the formulation of rural sewage discharge standards in China Science of the Total Environment **759**, 143533 (2021)
2. Chen, F.M., et al.: The cotreatment of old landfill leachate and domestic sewage in rural areas by deep subsurface wastewater infiltration system (SWIS): performance and bacterial community. Environ. Poll. **274**, 115800 (2021)
3. Li, X., Li, Y.Y., Lv, D.Q., Li, Y., Wu, J.S.: Nitrogen and phosphorus removal performance and bacterial communities in a multi-stage surface flow constructed wetland treating rural domestic sewage. Sci. Total Environ. **709**, 136235 (2020)

4. Xu, W.L., Yang, Y.N., Cheng, C., Pei, X.J., Luo, J.: Treat Phoenix river water by constructed rapid infiltration system. *J. Coastal Res.* **73**, 386–390 (2015)
5. Xu, W.L., Xu, S.L., Zhang, J.Q.: Removal performance and mechanism of TP in constructed rapid infiltration system. *Fresenius Environ. Bull.* **22**, 1826–1830 (2013)
6. Zhang, X.L., et al.: Phosphorus removal and mechanisms by Zn-layered double hydroxide (Zn-LDHs)-modified zeolite substrates in a constructed rapid infiltration system. *RSC Adv.* **9** 39811–39823 (2019)
7. Su, C.Y., et al.: Removal efficiency and pathways of phosphorus from wastewater in a modified constructed rapid infiltration system: removal efficiency and pathways of phosphorus in a modified. *CRIS J. Clean. Prod.* **267**, 122063 (2020)
8. Chen, J., Lu, Y.X., Cheng, J., Zhang, J.Q.: Effect of starvation on the nitrification performance of constructed rapid infiltration systems. *Environ. Technol.* **40**, 1408–1417 (2019)
9. Shi, X., Fan, J., Zhang, J., Shen, Y.: Enhanced phosphorus removal in intermittently aerated constructed wetlands filled with various construction wastes. *Environ. Sci. Pollut. Res.* **24**(28), 22524–22534 (2017)
10. Wang, M.C., Zhang, H.Z.: Chemical oxygen demand and ammonia nitrogen removal in a non-saturated layer of a strengthened constructed rapid infiltration system. *Water Air Soil Poll.* **228**, 1–8 (2017)



Comparative Study on Nitrogen Removal Efficiency of Surface Water by Three New Combined Processes of Autotrophic Denitrification

H. Jiang^{1,2}, M. L. Zhu^{1,2(✉)}, Y. L. Han^{1,2}, J. B. Zhang^{1,2}, and P. L. Xu^{1,2}

¹ School of Environmental Science and Engineering, Xiamen University of Technology,
Xiamen 361024, China
292890310@qq.com

² The Key Laboratory of Water Resources Utilization and Protection of Xiamen,
Xiamen 361024, China

Abstract. Surface water usually has high dissolved oxygen, low BOD_5 and C/N. In the process of water self-purification, denitrification reaction cannot be carried out due to insufficient carbon source and difficulty in forming anaerobic environment, so it is easy to present nitrate nitrogen pollution. In this study, three new combined processes were proposed to remove nitrogen from high dissolved oxygen micro-pollution surface water: 1) Iron autotrophic denitrification combined with moving bed biofilm reactor (MBBR); 2) Hydrogen autotrophic denitrification combined with MBBR; 3) Hydrogen autotrophic, iron autotrophic denitrification and MBBR combined process, and the nitrogen removal effects of three combined processes were compared. The results showed that NO_3^- -N and TN removal rates of iron autotrophic and MBBR combinations, hydrogen autotrophic and MBBR combinations, and iron autotrophic, hydrogen autotrophic and MBBR combinations were 60.9%, 57.1%, 62.1% and 34.3%, 20.5%, 35.2%. After laboratory deblocking, the water sample has evaporated more than half, but the removal rate of NO_3^- -N and TN increased to 67.5%, 84.3% and 47.5%, 63.9% by iron autotrophic and MBBR combination and iron autotrophic, hydrogen autotrophic and MBBR combination. The research results provide a technical reference for denitrification of high dissolved oxygen micro-polluted surface water.

Keywords: Micro-polluted surface water · Hydrogen autotrophic denitrification · Iron autotrophic denitrification · Moving bed biofilm reactor (MBBR)

1 Introduction

The traditional biological nitrogen removal process is firstly that organic nitrogen is converted into ammonia nitrogen by ammoniation. Ammonia nitrogen is converted into nitrate nitrogen by nitrifying bacteria in an aerobic environment, and then nitrate nitrogen is reduced to nitrogen by denitrifying bacteria in an anaerobic environment. Surface

water has two characteristics: high dissolved oxygen and micro-pollution (low organic pollutant content). In the process of water self-purification, high dissolved oxygen will compete with nitrate for carbon source and inhibit the synthesis of denitrification-related reductase [1], leading to the failure of denitrification due to insufficient carbon sources and difficult to form anaerobic environment, resulting in surface water nitrate pollution.

At present, in order to solve the problem of insufficient carbon source in surface water denitrification process, researchers have proposed heterotrophic denitrification method with additional carbon source and autotrophic denitrification method without adding carbon source. Zhang M et al. [2] used the biological filter with methanol as organic carbon source to treat nitrate nitrogen pollution in micro-polluted surface water, but the process can only achieve certain nitrogen removal effect when the influent carbon-nitrogen ratio of the filter is greater than 5, and the treatment cost is high, which is not suitable for engineering. Cao J S et al. [3] proposed to use the photoautotrophic biofilm system to solve the nitrate nitrogen pollution in surface water and improve water purification effect. However, the photoautotrophic biofilm has strict requirements on light, temperature and nutrient level, and has great problems in implementation and application. In addition, a small number of researchers have proposed the use of moving bed biofilm reactor (MBBR) to achieve nitrogen removal from surface water in view of the difficulty in forming an anaerobic environment for surface water with high dissolved oxygen. The biological packing balls are put into surface water, and the microorganisms are attached to the surface of the filler ball to form a biofilm. The anaerobic and aerobic environments inside and outside the membrane meet the needs of simultaneous nitrification and denitrification (SND), making the biological nitrogen removal process proceed smoothly. For example, Zhou Z X et al. [4] used the treatment process of “6-stage MBBR biological oxidation tank” to treat micro-polluted river water. The results showed that SND accounted for 7.97% of nitrogen removal, and had a general effect on nitrate nitrogen removal, and the process was relatively complex. In summary, the nitrogen removal process of high dissolved oxygen and micro-pollution surface water is not perfect, and it is rare to study both high dissolved oxygen and micro-pollution at the same time.

Therefore, in order to solve the above two problems at the same time, this study carried out the process combination based on previous research results, and proposed three new processes of autotrophic denitrification and MBBR combination: 1) Iron autotrophic denitrification and MBBR combined process; 2) Hydrogen autotrophic denitrification and MBBR combined process; 3) Hydrogen autotrophic coupled iron autotrophic denitrification and MBBR combined process. The removal effects of nitrate nitrogen and total nitrogen in micro-polluted surface water by these three combined new processes were compared and studied, so as to provide some reference for the denitrification of micro-polluted surface water with dissolved oxygen.

2 Materials and Methods

In this study, the nitrogen removal experiment of micro-polluted surface water was carried out based on the following three combined processes of autotrophic denitrification: 1) Iron autotrophic denitrification and MBBR combined process, 2) Hydrogen autotrophic denitrification and MBBR combined process; 3) Iron autotrophic coupled Hydrogen autotrophic denitrification and MBBR combined process. We used polyurethane sponge carrier as MBBR biological filler, sponge iron as microbial carrier for iron autotrophic denitrification, and high purity graphite rod and activated carbon fiber felt as electrode materials to provide electron donors for hydrogen autotrophic denitrification after electrification.

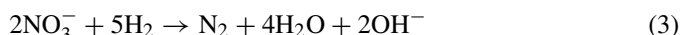
2.1 Experimental Materials

Polyurethane Sponge Biological Packing ($\Phi = 150 \text{ mm}$). Polyurethane sponge biological packing is made by injection molding with polyurethane as the main raw material. In the biochemical treatment of water, it has the characteristics of full three-dimensional structure, large specific surface area, direct placement, no need to fix, easy to form biofilms on the surface, and no blockage.

Electrode Materials. In this study, a high purity graphite rod ($\Phi = 200 \text{ mm}$, $H = 500 \text{ mm}$) was used as the anode, and a high purity graphite rod coated with activated carbon fiber felt was used as the cathode.

Graphite rod is a non-metallic product made of carbon, graphite and appropriate adhesive, then copper plated after being extruded and roasted at 2200°C . It has the characteristics of high temperature resistance, good electrical conductivity and not easy to break. Activated carbon fiber felt has a very developed microporous structure, which makes it a good adsorption material with large adsorption capacity, fast adsorption speed and easy regeneration, and high mechanical strength, large specific surface area and good electrical conductivity.

The Eqs. (1), (2) and (3) of the two electrodes are as follows:



Nitrate nitrogen can be degraded by both biological and electrochemical processes, and micro-electric currents can stimulate metabolic activities of microorganisms. The hydrogen autotrophic denitrifying bacteria attached to the cathode surface used the H_2 produced by electrolytic water as the electron donor to achieve nitrate reduction [5].

Sponge Iron (Size 1–3 mm). Sponge iron, also known as direct reduced iron, is made from iron ore reduced at lower melting temperature. Its composition is similar to that

of ordinary zero-valent iron. Its surface is porous and spongy with dense pores, which can provide sufficient space for the enrichment and growth of microorganisms. In this way, various aerobic and anaerobic microorganisms can carry out nitrification and denitrification reactions in a good environment [6], which is a better filter material for water treatment.

In the process of iron autotrophic denitrification, sponge iron acts as microbial carrier. With the operation of the reactor, denitrifying microorganisms attached to the surface of sponge iron use Fe^{2+} or $\text{Fe}^{(0)}$ as electron donors to reduce nitrate or nitrite to nitrogen [7].

2.2 Experimental System

Experimental Methods. Table 1 shows three new combined processes of autotrophic denitrification and the materials used. In addition, a blank group was set up for comparison in this study.

Table 1. Three new combined processes and materials for autotrophic denitrification

Technical number	Denitrification process	Material
1#	Iron autotrophic denitrification and MBBR combined process	Sponge iron (stuffed with filler ball); polyurethane spherical biological filler (filling rate 30%)
2#	Hydrogen autotrophic denitrification and MBBR combined process	Electrode device; polyurethane spherical biological filler (filling rate 30%)
3#	Iron autotrophic coupled Hydrogen autotrophic denitrification and MBBR combined process	Sponge iron (filled with filler ball); electrode device; polyurethane spherical biological filler (filling rate 30%)

Among them, the weight of sponge iron in 1# and 3# is 2 g, the electrode device in 2# and 3# is graphite rod in anode and graphite rod wrapped in activated carbon fiber felt in cathode, the surface area of cathode (S) = 62.832 cm^2 , current density (ρ) = 0.083 mA/cm^2 [8], current intensity (I) = 5 mA, Plate spacing (D) = 5 cm.

Experimental Device. The experimental device is located in the laboratory on the 4th floor, Building 8, Xiamen University of Technology. The experiment set up 4 buckets, each filled with 14 L water.

2.3 Source Water

This experiment is a study on nitrogen removal of micro-polluted surface water. In this experiment, sewage from the second sedimentation tank of a sewage treatment plant

in Xiamen is first used to hang membrane, and the hanging time is from 2021/9/10 to 2021/9/19, for 10 days. After the membrane hanging, the lake was taken for surface water nitrogen removal experiment, which lasted for 9 days from 2021/9/11 to 2021/10/11. During the period, due to the epidemic prevention and control notice, the laboratory was closed from 2021/9/19 to 2021/10/7, and the experiment could not be carried out. The water quality of the lake is shown in Table 2.

Table 2. The water quality of Polytechnic Lake of Xiamen University of Technology

Water quality index	DO (mg/L)	COD (mg/L)	TN (mg/L)	NH ₄ ⁺ -N (mg/L)	NO ₃ ⁻ -N (mg/L)	NO ₂ ⁻ -N (mg/L)	TP (mg/L)	pH
Data	10.8	56	5.21	0.218	4.68	0.01	0.02	8.0

2.4 Analytical Methods

All samples were filtered through a 0.45 μm membrane filter before analysis and were tested within 1 h of collecting. The specific detection methods and instruments are shown in Table 3.

Table 3. Testing methods and instruments for water quality index

Water quality index	Testing methods	Detection method
Total nitrogen	TOC total carbon and total nitrogen tester	Nondispersive Infrared Absorption Spectrometry
Nitrate nitrogen	Ultraviolet spectrophotometer	Ultraviolet spectrophotometry
DO	HACH LDO portable dissolved oxygen meter	Electrochemical probe

3 Results and Discussion

3.1 Removal Effect of Nitrate Nitrogen by Three New Combined Processes of Autotrophic Denitrification

As shown in Fig. 1, after 9 days of water purification, nitrate nitrogen concentration increased with the influent concentration, and decreased after the second day. By the 9th day, the nitrate nitrogen concentration of iron autotrophic denitrification and MBBR combined process (1#), hydrogen autotrophic denitrification and MBBR combined process (2#), hydrogen autotrophic coupled iron autotrophic denitrification and MBBR combined process (3#) and the control blank were 1.83 mg/L, 2.01 mg/L, 1.82 mg/L and

3.80 mg/L. The nitrate nitrogen removal rates of 1#, 2# and 3# were 60.9%, 57.1% and 62.1%. The nitrate nitrogen removal rates of blank group were 18.3%. Compared with the blank group, the nitrate nitrogen removal rate of the three new combined processes is 38.8%–43.8% higher.

At the beginning of the experiment, nitrate nitrogen in 1# was mainly removed by the reduction of Fe^{2+} and $\text{Fe}^{(0)}$ in sponge iron. With the increase of experimental time, denitrifying microorganisms attached to the surface of sponge iron [9], and nitrate nitrogen in water was removed by denitrifying bacteria. The electrode device was set up in 2#, and the current in the reactor may have two functions [10]: one is electrolysis of aquatic hydrogen to provide electron donors for hydrogen autotrophic denitrifying bacteria. The other is to stimulate the metabolism of microorganisms and improve the denitrification rate. 3# coupled iron autotrophic and hydrogen autotrophic denitrification, but the removal rate of nitrate nitrogen did not improve much compared with the other two combined new processes.

Nine days later, the laboratory was closed for epidemic prevention and control, and the experiment was suspended for half a month. When the experiment was started again, it was found that about half of the water sample was evaporated, but the nitrate nitrogen concentration of 1# and 3# still decreasing, and reached equilibrium after 28 days, the nitrate nitrogen concentrations of 1# and 3# were 1.41 mg/L and 0.736 mg/L, and the nitrate nitrogen removal rates of 1# and 3# were 63.5% and 84.3%. It can be seen that the degradation rate of nitrate nitrogen caused by iron autotrophic denitrification is much higher than the accumulation rate of nitrate nitrogen caused by mass evaporation of water samples. However, the nitrate nitrogen concentration of the 2# and blank groups did not decrease but increased, and the nitrate nitrogen concentration on the 28th day was 5.92 mg/L and 6.19 mg/L, which was caused by the accumulation of nitrate nitrogen due to the mass evaporation of water samples. At the same time, the 2# electrode was closed, unable to provide the electron donor required by hydrogen autotrophic denitrification, resulting in the cessation of hydrogen autotrophic denitrification reaction. After 28 days, the electrode was turned on and hydrogen autotrophic denitrification was carried out at 2#.

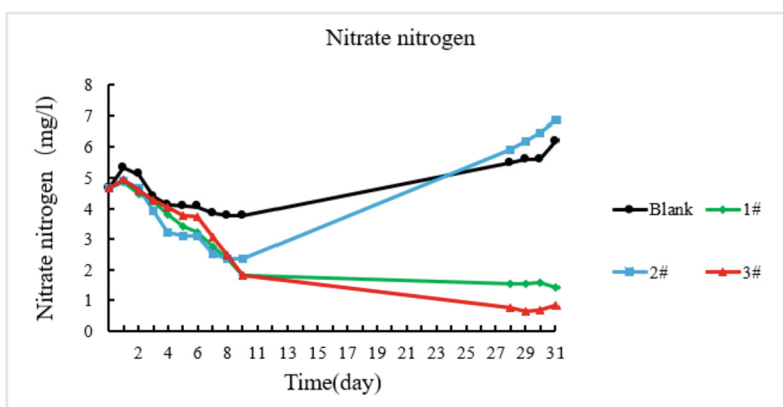


Fig. 1. Changes of nitrate nitrogen under different denitrification processes

However, the rate of nitrate nitrogen degradation by hydrogen autotrophic denitrification was less than the accumulation rate of nitrate nitrogen caused by evaporation. Therefore, the concentration of nitrate nitrogen was still rising.

It can be seen that the three new combined processes all have the effect of removing nitrate nitrogen, and the order of removal effect of the three new combined processes is 3#, 1# and 2# from good to bad.

3.2 Removal Effect of Total Nitrogen by Three New Combined Processes of Autotrophic Denitrification

As shown in Fig. 2, after 9 days of water purification, the total nitrogen concentrations of the 1#, 2#, 3# and blank groups were 3.42 mg/L, 4.14 mg/L, 3.38 mg/L and 5.38 mg/L. The total nitrogen removal rate of 1#, 2# and 3# were 34.3%, 20.5% and 35.2%, and the total nitrogen removal rate of blank group was -3.2%. Compared with the blank group, the total nitrogen removal rate of the three new combined processes is 23.7%-38.4% higher.

Total nitrogen is the sum of ammonia nitrogen, nitrate nitrogen, nitrite nitrogen and organic nitrogen. The removal effect of the three denitrification processes on total nitrogen is obviously not as good as that on nitrate nitrogen. The reason may be that in the process of hydrogen autotrophic denitrification, if the generation rate of nitrite nitrogen is higher than its reduction rate [11], the accumulation of nitrite nitrogen will occur, while in the process of nitrate nitrogen reduction, nitrogen and ammonia nitrogen will be generated by sponge iron [12].

28 days later, the total nitrogen concentration of 1# and 3# reached the equilibrium state, which was 2.73 mg/L and 1.88 mg/L, and the total nitrogen removal rate was 47.5% and 63.9%. It may be because the autotrophic denitrification of iron is still going on, and the nitrogen removal rate is higher than the nitrogen accumulation rate caused by evaporation. However, the increase of total nitrogen concentration in group 2# and blank was due to total nitrogen accumulation caused by water sample evaporation.

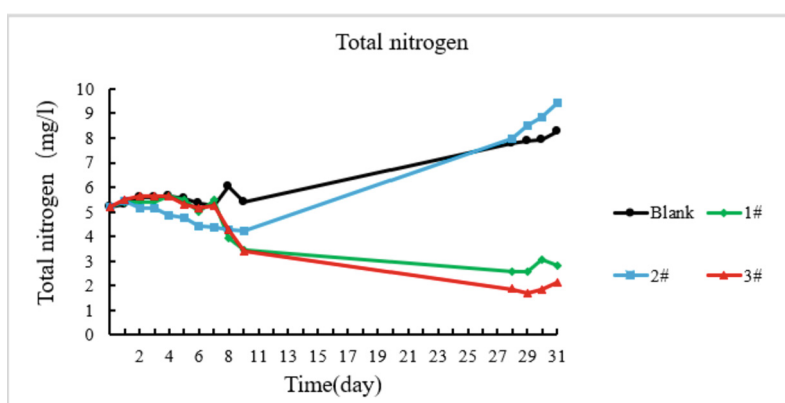


Fig. 2. Changes of total nitrogen under different denitrification processes

It can be seen that the three new combined processes have good nitrogen removal effects, and the order of removal effects of these three new combined processes from good to bad is: 3#, 1#, 2#.

3.3 Effects of Three New Combined Processes of Autotrophic Denitrification on DO

It can be seen from Fig. 3 that after water purification for the first 9 days, DO in group 1#, 2#, 3# and blank group were 2.83 mg/L, 3.82 mg/L, 2.60 mg/L and 7.83 mg/L. DO of 1#, 2#, and 3# decreased by 73.7%, 64.5%, and 75.8%, while DO of blank group decreased by 27.3%. The decrease of DO in the blank group was due to the self-purification ability of the water, while the decrease of DO in the 1 #, 2 # and 3 # water samples was more obvious. It may be because the microbial biomass in the biological denitrification process is much higher than that in the blank group, which needs to consume a large amount of oxygen [13]. After 9 days, the laboratory was closed for half a month. When the experiment began again, it was found that about half of the water sample evaporated, and the dissolved oxygen in the water increased, and reached a dynamic balance until 28 days.

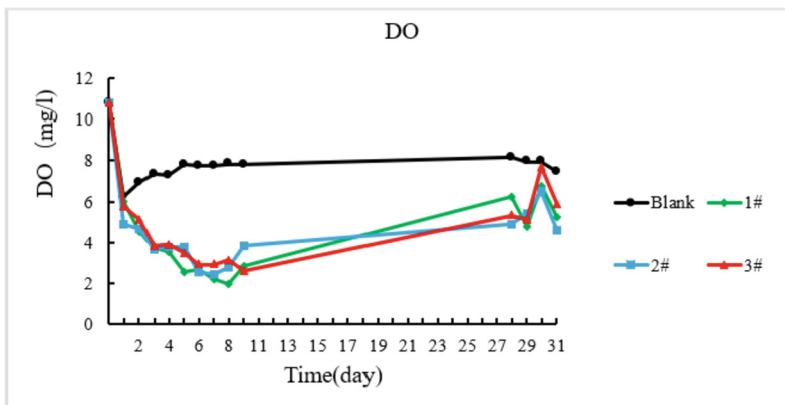


Fig. 3. DO changes under different nitrogen removal processes

4 Conclusions

In this study, the removal effects of nitrate nitrogen and total nitrogen by three new combined autotrophic denitrification processes were studied, and the following conclusions were drawn:

- (1) In the experiment of the first 9 days, the nitrate nitrogen removal rates of iron autotrophic denitrification and MBBR combined process (1# process), hydrogen autotrophic denitrification and MBBR combined process (2# process), hydrogen

autotrophic coupled iron autotrophic denitrification and MBBR combined process (3# process) were 60.9%, 57.1%, 62.1%. In the blank group, the removal rate of nitrate nitrogen by water self-purification was 18.3%, which increased by 38.8%–43.8% compared with the blank group. It can be seen that the three new combined processes can remove nitrate nitrogen well. The laboratory was closed during the pandemic and experiments resumed on day 28, but about half of the water samples had evaporated, causing nitrate nitrogen to accumulate. At this time, the nitrate nitrogen removal rates of the 1#, 2#, 3# and blank groups were 67.5%, –35.7%, 84.3% and –22.0%, indicating that the nitrate nitrogen removal effects of the three new combined processes are as follows: 3#, 1# and 2# from good to bad.

- (2) In the first 9 days of the experiment, the total nitrogen removal rates of 1#, 2# and 3# were 34.3%, 20.5% and 35.2%, and the total nitrogen removal rate of the blank group was –3.2%, which was 23.7%–38.4% higher than that of the blank group. It can be seen that the three new combined processes have good nitrogen removal effects. The laboratory was closed during the pandemic and experiments resumed on day 28, but about half of the water samples had evaporated, resulting in a buildup of total nitrogen. At this time, the total nitrogen removal rates of the 1#, 2#, 3# and blank groups were 47.5%, –62.0%, 63.9% and –51.6%, indicating that the total nitrogen removal effects of the three new combined processes were in descending order: 3#, 1# and 2#.
- (3) The best denitrification effect of the three new autotrophic denitrification combined processes is 3#, and the second best is 1#. The nitrate nitrogen removal rate of 3# is 20.8% higher than that of 1#, and the total nitrogen removal rate of 3# is 16.4% higher than that of 1#.
- (4) The DO of 1#, 2# and 3# decreased by 73.7%, 64.5% and 75.8%, and the DO of blank group decreased by 27.3%, indicating that the microbial biomass in three new autotrophic combination processes is much greater than that in water self-purification, resulting in DO content decreased more obvious.

Acknowledgments. This work was financially supported by “the research project funds of the removal technology of total nitrogen in surface water with high dissolved oxygen and micro-pollution under normal and low temperature conditions” from “Yellow River Survey, Planning and Design Institute Co., Ltd.”.

References

1. Wang, Z.: Comparison of Autotrophic and Heterotrophic Denitrification Processes for Nitrate Removal from Micro-polluted Surface Water. Shanghai Jiao Tong University (2018)
2. Zhang, M., Gao, J.W., He, S.B., et al.: Performance of biological filter in treatment nitrate micro-polluted surface water. Technol. Water Treat. **39**(002), 98–101 (2013)
3. Cao, J.S., Bai, W.J., Wang, C., Wang, H.S., Zhang, Y.X.: Study on formation mechanism of phototrophic biofilm and its denitrogenation influencing factors. Environ. Pollut. Control **33**(1), 78–82 (2011)
4. Zhou, Z.X., Sun, X.Y., Wu, D., et al.: Study on Nitrification performance of MBBR process in treatment of micro polluted water. Technol. Water Treat. **46**(8), 5

5. Yang, L., Guo, J.S., Tang, J., et al.: Review on denitrification by electrode-biofilm process. *Environ. Ecol. Three Gorges* **34**(001), 52–55 (2012)
6. Zheng, S.Z.: Study on Autotrophic-Heterotrophic Coupling Deep Denitrification System. College of Environmental Science and Engineering Guilin University of Technology, 2016 September to June 2019
7. Wang, R., Zhao, Z.G., Zheng, P., et al.: Iron-dependent denitrification—a novel technology to remove nitrogen from wastewaters. *Chem. Ind. Eng. Prog.* **38**(331), 414–421 (2019)
8. Tang, Y.M.: Study on immobilization technology of denitrifying bacteria and denitrification in drinking water. Tongji Medical College, Huazhong University of Science and Technology; Huazhong University of Science and Technology (2002)
9. Zhao, Y.P.: Study on Influencing Factors of Nitrogen Removal and Carbon Source Utilization Method in Biological Sponge Iron System. Lanzhou Jiao tong University (2020)
10. Lu, C.X.: Removal of high concentration nitrate in drinking water by hydrogen autotrophic reactor. Tianjin University (2010)
11. Till, B.A., et al.: Fe(0)-supported autotrophic denitrification. *Environ. Sci. Technol.* **32**(5), 634–639 (1998)
12. Li, T., Zhu, Y.C., Kang, X., et al.: Research on the influencial factors of nitrate nitrogen in micro-polluted source water by sponge iron reduction. *Ind. Water Treat.* **036**(011), 85–88, 89 (2016)
13. Sun, Y.P.: Application of bio-nitrogen removal new technologies in low C/N ratio wastewater. *Environ. Sci. Manage.* **32**(006), 114–115 (2007)



Development of a Composite Solid Desiccant Dehumidifier for Ventilation Air

Srimuk Jintana¹, Chirarattananon Surapong¹(✉), Chaiwiwatworakul Pipat¹, Nathakaranakule Adisak², Rakkwamsuk Pattana², and Chiarakorn Siriluk²

¹ The Joint Graduate School of Energy and Environment, King Mongkut's University of Technology Thonburi, Bangkok, Thailand
Surapong.chi@kmutt.ac.th

² School of Energy, King Mongkut's University of Technology Thonburi, Environment, and Materials, Bangkok, Thailand

Abstract. The composite solid desiccant dehumidification systems have been considered as an alternative air dehumidifying system. Their inherent energy saving capability added with their ability to act as an independent dehumidification system for ventilation air make them an attractive undertaking for research. In this study, fin tube heat exchangers (FTHX) coated with composite solid desiccant have been developed to act as a dehumidifier for supplying ventilation air. Aluminum surface of FTHX was dipped with Polyurethane (PU) glue and the desiccant was attached on the FTHX surface as the PU glue acted as a binding material. The adhesion between composite desiccant and fin surface was investigated by scanning electron method (SEM) and it showed good bonding between two materials. The objective of this paper is to study the performance of the dehumidifier i.e. the solid desiccant coated on fin and tube heat exchangers. An experimental setup was created in such a way that when the humid air passed through the FTHX it provided dehumidification in half cycle and after that in another half cycle desiccant coated FTHX was regenerated. In order to save energy, waste heat from the condensing unit was utilized for regeneration and the cool water from the cooling tower was used for dehumidification. The experimental results with the prevailing experimental conditions showed higher effectiveness in the regeneration process when compared to dehumidification process.

Keywords: Composite desiccant · Dehumidification · An independent dehumidification system

1 Introduction

Nowadays, there are several methods for removing moisture from the air before supplying it to the conditioned space. Researchers have considered different desiccant components and there is a lot of published works on silica gel coated on heat exchangers [1]. However, after an intensive literature review it is found that the efficiency of the systems in most of the research work is low. Because their systems require high temperature for the regeneration process and the capacity of the water content of desiccant is limited

by its absorption property. So, composite desiccants were used to increase the dehumidification capacity. A lot of porous substrates such as mesoporous or microporous silica gel, alumina, porous carbon, and amorphous polymer are fabricated by impregnating into inorganic salts such as LiCl, CaCl₂, MgCl₂ or LiBr. Mesoporous silica gel – Lithium chloride composite desiccant has dehumidification rate greater than pure silica gel 20–40% [2]. The composite desiccants have higher dynamic sorption quantity and a reasonable diffusion rate constant [3]. In addition to this, several researchers developed desiccant coated on heat exchanger (DCHE) for solving humidity problems.

The desiccant coated fin-tube heat exchanger (DCFTHX) has two processes. First one is the dehumidification process, which uses cool water to increase effectiveness of desiccant. And the second one is the regeneration process, in which hot water is utilized to remove moisture from the desiccant [4].

Zheng et al. [5] studied pure silica gel and composite desiccant silica gel with LiCl, with different concentration: 10, 20, 30 and 40% by weight. Their results show that when the sorption kinetic of composite desiccant increases, the concentration of LiCl also increases. The water sorption capacity of pure silica gel smoothly grew with the increase of relative pressure. The isotherm illustrated the limiting amount adsorbed by the composite sample which is higher than pure silica gel. It is because the composite desiccant has both chemical and physical bonding with the moisture.

Ge et al. [6] studied composite desiccant by impregnating potassium formate (CHKO₂), with various concentrations of CHKO₂: 15, 45, and 75% by weight, into the pore silica gel. Their results show when adsorption performance of different coating desiccant materials under the same operating conditions are compared, both adsorption mass and initial adsorption rate increase with the increment of concentrations of CHKO₂ solution. They concluded that impregnating CHKO₂ into porous silica gel is an effective method to improve adsorption capacity. They recommended to keep saturated CHKO₂ solution with 75% by weight in the composite desiccant under experimental conditions.

Hu et al. [7] studied performance of composite desiccant coated on heat exchanger (DCHE-C) and compared it with conventional silica gel coated on heat exchanger (DCHE-S). They reported that the dehumidification performance of DCHE-S reaches its saturation faster than DCHE-C since the moisture absorption ability of DCHE-S is limited by silica gel. However, the dehumidification capacity for DCHE-C is higher than DCHE-S.

Jiang et al. [8] reported their study on composite desiccant and conventional silica-gel coated fin-tube heat exchangers (CCHE and SGCHE). They performed an experiment to test the dynamic performance of SGCHE and CCHE. Regarding the regeneration process in their experiment, the moisture released from CCHE was much greater than SGCHE. However, the regeneration time of CCHE was longer than SGCHE. Regarding the dehumidification process, the dehumidification ability of CCHE was greater than other one although the dehumidification time was longer for CCHE.

T.S. Ge et al. [9] carried out a study on the temperature of hot water in regeneration process against COP of desiccant coated on heat exchanger (DHE). COP was calculated based on the ratio of the sensible and latent heat capacity of the system and the thermal energy consumed in the regeneration process. The COP of the system increased with increasing water temperature in the regeneration process.

2 Synthesis of Composite Desiccants and Their Properties

2.1 Method

A composite desiccant is a multiphase of solid material. In this study, mesoporous silica gels with a pore size of 10 and 15 nm were reinforced by Lithium Chloride. Details of chemical materials are shown in Table 1.

Table 1. Characteristics of materials.

Name	Type	Manufacture
Mesoporous silica gel with a pore size of 10 nm	Hight purity grade, pore size 100 Å , particle size 200–400 mesh	Fluka
Mesoporous silica gel with a pore size of 15 nm	Hight purity grade (Davis Grade 643), pore size 150 Å , 200–425 mesh	Sigma-Aldrich
Lithium chloride	Anhydrous 98%	Loba Chemie pvt.ltd

The details of the preparation of composite desiccant are shown in the following steps:

- 1) The mesoporous silica gel was weighed and then it was dried in an oven at the temperature of 373.15 K for at least 3 h until the weight was constant.
- 2) The ratio of mesoporous silica gel and lithium chloride aqueous solution with mass concentrations in 40 wt.% was 3:1.
- 3) Dry mesoporous silica gel was impregnated in a solution of Lithium Chloride at a room temperature for 24 h.
- 4) The composite desiccant was filtered from the solution with a vacuum filter and excess LiCl was cleaned with deionized water.
- 5) The composite desiccant was dried in an oven at 373.15 K for at least 24 h until the weight remained constant.
- 6) BET technique was used for the determination of texture properties of desiccants.

2.2 Texture Properties

Texture properties such as BET surface area, total pore volume, and average pore size of mesoporous silica gel and composite desiccant are illustrated in Table 2.

It can be seen from Table 2 that BET-specific surface area was reduced when more salt particles were immersed. The pore volume of composite desiccant decreased when impregnating mass concentration of LiCl solution.

Table 2. Texture properties of mesoporous silica gels and their composite desiccant.

Sample	Surface area (m ² /g)	Total pore volume (cm ³ /g)	Mean pore diameter (nm)
Mesoporous silica gel with a pore size of 10 nm	327.16	0.889	10.865
Mesoporous silica gel with a pore size of 15 nm	292.88	1.103	15.069
Composite desiccant base on mesoporous silica gel with a pore size of 10 nm	179.82	0.5581	12.414
Composite desiccant base on mesoporous silica gel with a pore size of 15 nm	156.15	0.6168	15.801

3 The Deposition of Desiccants on Fin-Tube Heat Exchanger

During the deposition process, suitable binders are necessary to ensure continuous contact between the FTHE surface and desiccant materials. Moreover, the geometry of the FTHE is complicated, so the Aluminum sheets for the FTHE were used for the procedure of binder selection.

3.1 Binder Options

Experiments were conducted on four types of binder, namely: Cyanoacrylate, Hydroxyethyl cellulose (HEC), Polyurethane glue (Polyurethane in solvent from Bond-Tech company) and spray glue for metal surfaces combined with Polyurethane glue. Results of adhesion of the glue and Aluminum surface are shown in Table 3.

Table 3. Binders selection and their adhesion.

Binder selection	Results
Cyanoacrylate glue	This binder had poor adhesion between desiccant and Aluminum surfaces
HEC starch glue	The HEC glue had poor adhesion on the Aluminum surface
Polyurethane glue, (Polyurethane dissolved into its solvent from Bond-Tech company)	It had good adhesion with desiccant, but the glue layer peeled off from the substrate surface
Spray glue for metal surface amalgamates with polyurethane glue	It had good adhesion with desiccant and an Aluminum surface

3.2 The Detail of Capability of Spray Glue for Metal Surface Amalgamates with Polyurethane Glue

The Spray glue for the metal surface was sprayed on the Aluminum surface as primer. Then, the Aluminum was dipped into the Polyurethane glue. After that the desiccant was deposited on the top of the glue with a shaker machine. A scanning electron microscope was used to produce an image of the composite desiccant particle and Aluminum which showed the topography and composition of these two materials. This image is used to investigate the adhesion between composite desiccant and fin surface.

An image from the scanning electron microscopic of deposition of desiccant over the metal surface is shown in the Fig. 1.

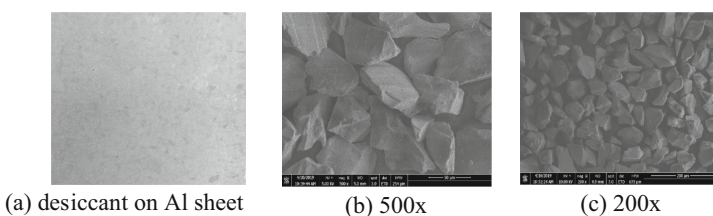


Fig. 1. Photo and SEM image of deposition of desiccant on an Aluminum surface.

The aim was to have a thin layer of Polyurethane glue over the fin surface, with desiccant over this PU layer for proper moisture absorption. But instead, when the binder adhered between desiccant and the sample of a fin-tube heat exchanger, which is cut for 2.54 cm^3 as shown in Fig. 2 (a), PU glue not only bonded desiccant and fin-tube surface but also covered the surface of desiccant. The PU glue for the flow through the gap of a fin during the dipping process covered the surface of the desiccant due to its high viscosity as shown as in Fig. 2 (b). The polyurethane glue couldn't be diluted with a solvent as it has a long chain with engagement.

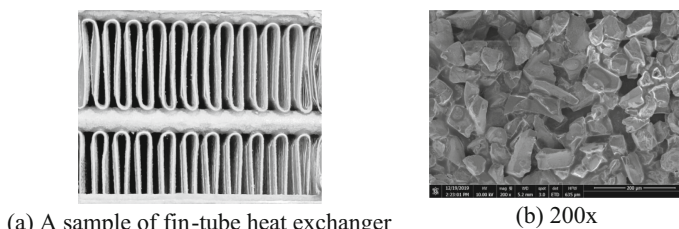
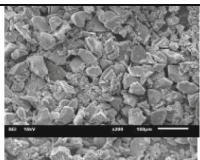
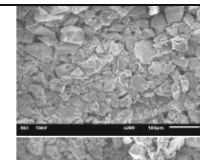
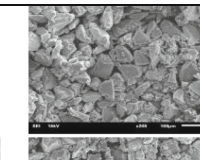
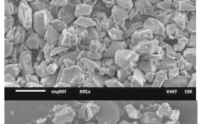
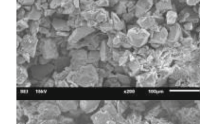
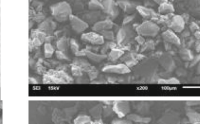
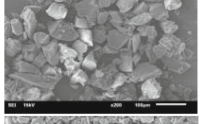
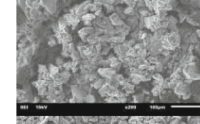
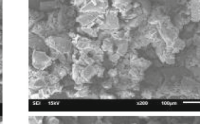
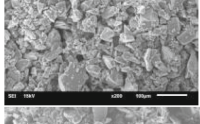
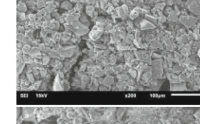
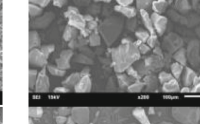
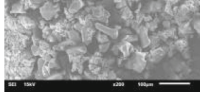
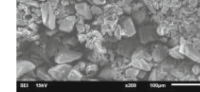
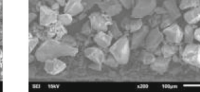


Fig. 2. Photo of a fin-tube sample (a) and SEM image of desiccant was deposited on the surface of the fin-tube sample (b).

Due to this prevailing problem, a new polyurethane glue with short chain was used which is polymerized urethane monomer and oligomer. The new binder was used for the deposition of desiccant on the surface of fin-tube samples. The adhesion of synthesized

polyurethane glue was tested 2 times; 3 samples were used each time. The sample was cut at 3 positions of the fin to investigate the adhesion and arrangement of desiccant on the fin surface by SEM technique. Some position on the fin had a single layer of desiccant while some other position had two-layer of desiccant as illustrated in SEM images as shown in Table 4. Overall, the new PU glue had a pretty good arrangement and adhesion of particles of desiccant over the Al surface as shown in Table 4.

Table 4. SEM images of desiccant deposited on the fin surface of fin-tube samples at 200x zoom.

Sample / Positions of fin	1 st position	2 nd position	3 rd position
No.1			
No.2			
No.3			
No.4			
No.5			
No.6			

4 Desiccant Dehumidification

Dehumidification performance of composite desiccant, which is based on mesoporous silica gel with pore size of 15 nm, was tested by depositing the desiccant on the fin-tube

heat exchanger. The fin tube heat exchanger after deposition and drying was set up as dehumidifier unit. The temperature of cooling water for the dehumidification process and hot water for the regeneration process were set as 303.15 ± 3 K and 323.15 ± 3 K, respectively. The temperature of cold water is close to ambient temperature and the temperature of hot water is low. This implies that, hot water can be used from low-grade energy sources like the water from the condensing unit and the cold water can be used from the cooling tower. The inlet absolute humidity and air velocity of the process air are $24 \text{ kg}_{\text{wv}}/\text{kg}_{\text{da}}$ and 0.4 m/s, respectively. The time of both the dehumidification and regeneration process is 20 min.

The dehumidification system comprises of two dehumidifier units. One of the dehumidifier units work on the dehumidification process so it was supplied with cool water to adsorb moisture in ambient air, while the other dehumidifier units work on the regeneration process, was supplied with hot water to remove water from the saturated desiccant. Two of these dehumidifiers work simultaneously; while one dehumidifies the working air, the other gets regenerated. The two switch their operations periodically to achieve dehumidification of the work in process.

The outlet absolute humidity of process air and temperature of the water from the measurements are illustrated in Fig. 3. The outlet absolute humidity of process air in the absorption process decreased slightly. However, the outlet absolute humidity of process air in desorption process increased gradually.

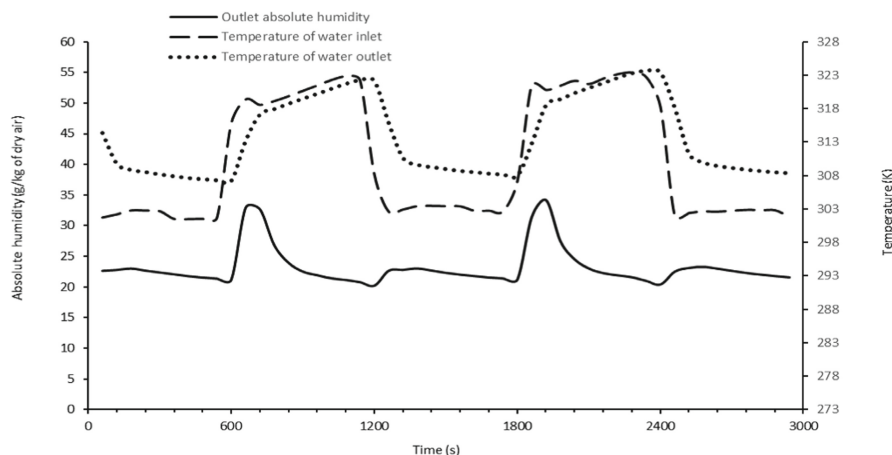


Fig. 3. The dehumidification and regeneration process utilizing the composite desiccant coated FTHX.

4.1 Performance Parameters

4.1.1 Moisture Removal Capacity in the Process (MRC)

This term represents the amount of moisture that is removed after the process air passes through the desiccant in the dehumidification process.

$$MRC = \dot{m}_{a,deh} \times (w_{inlet} - w_{outlet}) \quad (1)$$

where, $\dot{m}_{a,deh}$ is the mass flow rate of dehumidification process air (kg/s) and w_{inlet} and w_{outlet} are the absolute humidity of inlet and outlet air of the process air ($\text{kg}_{\text{wv}}/\text{kg}_{\text{da}}$), respectively.

4.1.2 Moisture Removal Regeneration (MRR)

It is the amount of moisture that is removed from the desiccant after the desiccant adsorbs moisture and reaches equilibrium.

$$MRR = \dot{m}_{a,reg} \times (w_{inlet} - w_{outlet}) \quad (2)$$

where $\dot{m}_{a,reg}$ is mass flow rate of regeneration process air (kg/s).

4.1.3 Dehumidification Effectiveness (E_{deh})

It represents the ratio of the amount of humidity reduction to inlet humidity in the adsorption process.

$$E_{deh} = \frac{W_{in} - W_{out}}{W_{in}} \quad (3)$$

4.1.4 Regeneration Effectiveness (E_{reg})

It is the ratio of the amount of humidity removal to the inlet humidity in desorption process.

$$E_{reg} = \frac{W_{in} - W_{out}}{W_{in}} \quad (4)$$

The maximum amount of moisture removal value in dehumidification and regeneration process in this experiment are 0.22 kg/s and 0.63 kg/s, respectively. In addition to this, dehumidification and regeneration effectiveness are 0.15 and 0.42 respectively.

5 Conclusion

The composite desiccant was deposited on the fin-tube heat exchanger surface and the experiment was conducted with the conditions to imitate the real-world application. The effectiveness of regeneration process is higher than the dehumidification process which means the studied dehumidifier i.e. the FTHE coated with composite desiccant can handle the moisture in the air-conditioned room. This experiment shows the potential of a composite solid desiccant dehumidifier system in hot and humid climate of Thailand. Field experiments of the desiccant dehumidifier are necessary future work to access the potential application of this system in the hot and humid climate of Thailand.

References

1. Learboonkarnkit, P., Chiraratananon, S.: Experimental investigation on a desiccant air dehumidifier constructed from a water-to-air heat exchanger. *Energy Procedia* **138**, 628–634 (2017)
2. Zheng, X., Ge, T.S., Wang, R.Z., Hu, L.M.: Performance study of composite silica gels with different pore sizes and different impregnating hygroscopic salts. *Chem. Eng. Sci.* **120**, 1–9 (2014)
3. Zheng, X., Ge, T.S., Hu, L.M., Wang, R.Z.: Development and characterization of Mesoporous Silicate–LiCl composite desiccants for solid desiccant cooling systems. *Am. Chem. Soc.* **54**(11), 2966–2973 (2015)
4. Mrinal, J., Lee, P.S.: Mathematical modeling and performance evaluation of a desiccant coated fin-tube heat exchanger. *Appl. Energy* **212**, 401–415 (2018)
5. Zheng, X., Ge, T.S., Jiang, Y., Wang, R.Z.: Experimental study on silica gel-LiCl composite desiccants for desiccant coated heat exchanger. *Int. J. Refrig.* **51**, 24–32 (2015)
6. Ge, T.S., Zhang, J.Y., Dai, Y.J., Wang, R.Z.: Experimental study on performance of silica gel and potassium formate composite desiccant coated heat exchanger heat exchanger. *Energy* **141**, 149–158 (2017)
7. Hu, L.M., Ge, T.S., Jiang, Y., Wang, R.Z.: Performance study on composite desiccant material coated fin-tube heat exchangers. *Int. J. Heat Mass Transf.* **90**, 109–120 (2015)
8. Jiang, Y., Ge, T.S., Wang, R.Z., Hu, L.M.: Experimental investigation and analysis of composite silica-gel coated fin-tube heat exchangers. *Int. J. Refrig.* **51**, 169–179 (2015)
9. Ge, T.S., Dai, Y.J., Wang, R.Z.: Performance study of desiccant coated heat exchanger air conditioning system in winter. *Energy Convers. Manage.* **123**, 559–568 (2016)

Hydrology and Water Resources Management



Applicability Analysis of Hydrological Models in the Middle and Upper Reaches of Yangtze River

Xin Yang^{1,2(✉)}, Jianzhong Zhou^{1,2}, Wei Fang^{1,2}, and Yurong Wang^{1,2}

¹ School of Civil and Hydraulic Engineering, Huazhong University of Science and Technology, Wuhan 430074, People's Republic of China
d201880948@hust.edu.cn

² Hubei Key Laboratory of Digital Valley Science and Technology, Wuhan 430074, China

Abstract. At present, there are many hydrological models in the world with different structures. The application conditions of these hydrological models are also different. How to select the appropriate hydrological model according to the characteristics of the basin and the performance of the hydrological model is the key problem to improve the accuracy of hydrological prediction in the basin. Taking the middle and upper reaches of the Yangtze River as the study area, this paper analyzed the runoff simulation result of the Xinanjiang model, the TANK model, and the TOPMODEL by using Nash coefficient (NS), mean percentage error (MPE), and root mean square error (RMSE). The results show that the runoff simulation accuracy of hydrological models is different in different regions of the middle and upper reaches of the Yangtze River. Finally, based on the simulation accuracy of the model, the hydrological models suitable for different sections of the middle and upper reaches of the Yangtze River basin are recommended.

Keywords: Hydrological models · Yangtze River

1 Introduction

The hydrological phenomenon is a complex process that is interacted by many factors. It is closely related to the atmosphere, crustosphere, and biosphere. It is a comprehensive natural phenomenon. Up to now, it has not been possible to describe hydrological phenomena with strict physical laws. The common research method is to generalize the complex hydrological phenomena, ignore the secondary and random factors, retain the main factors and parts with basic laws, establish a mathematical physical model with certain physical significance, and realize it through computer simulation. Hydrological models simulate the physical process from precipitation to runoff generation, which is the product of hydrology development to a certain stage.

According to the degree of spatial dispersion, the hydrological models can be subdivided into conceptual hydrological models and distributed hydrological models. In 1960, Linsley and Crawford proposed the first lumped conceptual hydrological model, the Stanford Model [1], which coupled the infiltration theory, the unit line theory, and the

regression theory. Then McCuen put forward the Sacramento watershed hydrological model in 1982 [2], the Sacramento model is developed based on the Stanford model. Model production flow is divided into the direct runoff, surface runoff, soil flow, fast and slow groundwater five parts, including soil grains, fast and slow groundwater using linear reservoir simulation, the river channel is calculated using the dimensionless unit line bus. At the same time, the Japanese scholar Masami Sugawara proposed the TANK model [3], whose basic idea is that the outflow and infiltration amount in the basin is assumed to be the function of the corresponding water storage depth in the basin. In the subsequent research, the model structure was developed and improved, and the snowmelt runoff module was added to improve the adaptability of the model. Zhao proposed the Xinanjiang model in 1984 [4]. The model is mainly composed of a water storage capacity curve and a free water capacity curve. The water storage capacity curve represents the change of runoff area when rainfall is evenly distributed, while the free water capacity curve is used to control the composition and distribution of runoff. The conceptual hydrological model has been widely used in basins where hydrological data are scarce because of its simple model structure, small data requirements, few parameters, and clear physical meaning. Such conceptual models simulate the watershed as a whole and describe many structural links through conceptual elements or empirical function relations, and the model parameters often lack clear physical meanings. Besides, these kinds of models do not take into account the spatial distribution of rainfall, which is inconsistent with the actual situation that runoff formation is a dispersed input and a lumped output, so it is often difficult to obtain a satisfactory simulation result.

With the application of meteorological remote sensing data, digital elevation model, vegetation cover situation, and so on in watershed modeling, distributed hydrological model comes into being. The distributed hydrological model can not only get the hydrological calculation results of the outlet section of the basin but also describe the local hydrological change process of the basin in a fine way. Beven and Kirby proposed TOPMODEL, a distributed hydrological model based on topographic index [5], which used topographic index to reflect the influence of uneven topographic distribution in the basin on the hydrological system.

Hydrologists have proposed a variety of hydrological models, but each hydrological model has different applicable conditions. Therefore, it is necessary to analyze the applicability of hydrological models according to specific basins. Based on the above research background, research work takes the middle and upper reaches of the Yangtze River as the study area. The Xianjiang model, the water tank model, and the TOPMODEL were used to simulate the runoff in the study area, and the accuracy of the simulation results were analyzed to evaluate the applicability of each model in the study area. The remaining chapters of this paper are arranged as follows: In section Data And Methods, the data and hydrological model are described. And then, the parameter calibration method and evaluation are introduced. In the section results, the results are demonstrated. In Section conclusions, relevant conclusions are drawn.

2 Data and Methods

2.1 Research Area and Dataset

The Yangtze River is the longest river in Asia. Its total length is 6,387 km, with a basin area of 1.8 million km², accounting for about 20% of the total area of the Chinese mainland. Among them, the upper reaches of the Yangtze River basin is the area from the headwaters of the Yangtze River to Yichang City, Hubei Province, located at 100°–112°E, latitude 23°–35°N, about 4,500 km, and the basin controls an area of 1 million km². The area from Xiluodu to Yichang on the mainstream of the upper basin of the Yangtze River was taken as the study area. Subsequent paragraphs, however, are indented.

There are obvious differences in natural conditions between the upper and lower reaches of the basin. Therefore, the key hydrological stations and reservoirs on the mainstream were taken as the sub-interval boundary points, and the study area was divided into five intervals. The rainfall-runoff model was established for each interval, and the applicability of the hydrological model in the upper reaches of the Yangtze River was analyzed by comparing the simulation results of the model with the observed runoff in the same period in history. The six intervals are respectively between Longjie-Xiluodu (LJ-XLD), Xiluodu-Xiangjiaba (XLD-XJB), Xiangjiaba-Zhutuo (XJB-ZT), Zhutuo-Cuntan (ZT-CT), and Cuntan-Yichang (CT-YC). The basic information of each interval is shown in Table 1.

Table 1. Basic information of sub interval.

Sub-interval	River name	Station	Area (km ²)
LJ-XLD	Jinsha River	XLD	37733
XLD-XJB	Jinsha River	XJB	18418
XJB-ZT	Jinsha River	ZT	33761
ZT-CT	Yangtze River	CT	12829
CT-YC	Yangtze River	YC	54185

Due to the limitation of data, the synchronous rainfall and runoff data from 2014 to 2017 in flood season (June to September) were selected for modeling. Among them, the data from 2014 to 2016 in flood season are used to calibrate the parameters of the hydrological model, and the data of 2017 in flood season is used to verify the simulation performance of the model.

2.2 Introduction to Hydrological Models

Xinanjiang Model

Xinanjiang Model is a typical conceptual rainfall-runoff model proposed by Professor Zhao for the forecast of inflow of Xinanjiang Reservoir [5]. The core principle of Xinanjiang model is excess storage conception. At first, the Xinanjiang model was a two-water source model, which only divided the runoff into surface runoff and underground runoff without considering the soil flow, resulting in poor runoff forecast accuracy of the model. Later, Zhao borrowed from “hillside hydrology” and developed the two-source Xinanjiang model into the three-source Xinanjiang model. Compared with the two-source Xinanjiang model, the three-source Xinanjiang model has a more perfect structure and stronger prediction performance and has been widely used abroad the world. More details about Xinanjiang model can be found in Zhao [5].

TANK Model

TANK Model is a conceptual rain-runoff Model proposed by Masahi Sugahara in Japan in 1961 [3]. Subsequently, the model has been continuously developed and improved, and now it has been widely used in humid and semi-humid areas in many countries. The basic principle of the TANK model is to convert the complicated rainfall-runoff relationship into the relationship between water storage and discharge in the basin for simulation. The process of rainfall-runoff conversion can be divided into several links, such as evaporation, runoff generation, slope confluence, and river confluence, etc. The TANK model adopts several interconnected water tanks to simulate the rainfall-runoff conversion process. In a single tank, the water storage depth was taken as the control variable, and the process of runoff generation and confluence in the basin was simulated by the height of the side hole and the outlet of the bottom hole. Although the TANK model has no definite physical quantity, it has high elasticity and is not limited to specific river basins, climate conditions, and other natural geographical factors. More details about TANK model can be found in Sugahara [3].

TOPMODEL

Topmodel model is a semi-distributed hydrological model with topographic index as the main form, which simulates the change of runoff within a certain spatial range based on the theoretical concept of variable runoff area and the principle of hydrological flow movement. Its structure is simple and clear, and the number of parameters is few. In addition, the model combines the digital terrain model and geographic information system, makes full use of the easily obtained terrain data, and visualizes the calculation results. More details about TOPMODEL can be found in Beven [6].

2.3 Parameter Calibration Method

The Multi-objective Shuffled Complex Differential Evolution (MOSCDE) algorithm was proposed by Guo [6] in 2013. In this algorithm, cultural evolution (CA) was adopted as the optimization framework and shuffled complex evolution (SCE-UA) was taken as the core operator of CA evolution to improve the reliability of evolutionary calculus. Differential evolution algorithm is chosen to replace the simplex method for global optimization, which can improve the efficiency of global search. The cauchy mutation operator is introduced to avoid falling into the local optimum. Compared with the traditional optimization algorithm, MOSCDE multi-objective optimization calibration algorithm can make full use of the effective information carried by the group, and improve the convergence speed while ensuring convergence accuracy. The detailed information about MOSCDE can be found in Guo [6].

2.4 Performance Evaluation

According to Table 1, in order to analyze the applicability of different hydrological models, Nash coefficient (NS), root mean square error (RMSE) and mean percentage error (MPE) are adopted in this paper to evaluate the accuracy of different hydrological models. The calculation formulas of the three evaluation indexes are as follows:

$$MPE = \frac{1}{T} \sum_{i=1}^T \frac{P_i - \hat{P}_i}{P_i} \times 100\% \quad (1)$$

$$RMSE = \sqrt{\frac{1}{T} \sum_{i=1}^T (Q_i - \hat{Q}_i)^2} \quad (2)$$

$$NS = 1 - \frac{\sum_{i=1}^T (Q_i - \bar{Q}_i)^2}{\sum_{i=1}^T (Q_i - \bar{Q}_i)^2} \quad (3)$$

where, Q_i is the measured value, \hat{Q}_i is the forecast value, and T is the length of the forecast sequence.

3 Results

3.1 Result Analysis of Xinanjiang Model

According to Table 2, in the calibration period, the NS of the Xinanjiang model in each interval is greater than 0.95, and the RMSE is between 300–1600. The variation of MPE was obvious, the minimum was -4.72% and the maximum was 4.18% . In the validation period, the NS of TOPMODEL in each interval is greater than 0.90, and RMSE is between 290–1400 m³/s. Except for XLD, the MPE of the model simulation results concentrates between 0.12% and 4.23%. Therefore, the accuracy of Xinanjiang model of each interval can meet the requirements of runoff forecast (Table 2).

Table 2. Evaluate index of Xinanjiang model.

Station	Period	MPE	RMSE	NS
XLD	Calibration	-4.72	411.049	0.982
	Validation	12.7	392.052	0.973
XJB	Calibration	4.18	637.868	0.963
	Validation	4.23	582.383	0.942
ZT	Calibration	0.12	1027.859	0.952
	Validation	0.89	876.649	0.943
CT	Calibration	0.44	769.288	0.985
	Validation	0.28	697.886	0.975
SX	Calibration	0.73	1563.261	0.958
	Validation	1.91	1364.017	0.919

3.2 Result Analysis of TANK Model

According to Table 3. In the calibration period, the NS of the TANK model in each interval is greater than 0.94, the RMSE is between 300–1400, and the MPE is between -10.9%–7.38%. In the validation period, the NS of TANK model in each interval is greater than 0.9, the RMSE is between 290–1300 m³/s, and the MPE is between 0.26%–14.5%. In general, the accuracy level of each section tank model is satisfying, which can meet the requirements of hydrological forecast.

Table 3. Evaluate index of TANK model.

Station	Period	MPE	RMSE	NS
XLD	Calibration	-10.9	373.215	0.985
	Validation	14.5	459.509	0.962
XJB	Calibration	7.38	643.751	0.962
	Validation	2.10	760.917	0.901
ZT	Calibration	1.33	851.629	0.946
	Validation	2.38	1303.308	0.923
CT	Calibration	0.40	821.326	0.983
	Validation	0.26	704.174	0.975
SX	Calibration	0.28	1333.953	0.969
	Validation	1.01	1215.466	0.934

3.3 Result Analysis of TOPMODEL

According to Table 4, in the calibration period, the NS of the TOPMODEL in each interval is greater than 0.94, and the RMSE is between 300–1800. The MPE range from –5.17%–5.41%. In the validation period, the NS of TOPMODEL in each interval is greater than 0.91, and RMSE is between 290–1300 m³/s. The maximum value of MPE is 15.2%, and the minimum value is 0.34%. Therefore, the accuracy level of each section tank model is satisfying, which can meet the requirements of hydrological forecast.

Table 4. Evaluate index of Xianjiang model.

Station	Period	MPE	RMSE	NS
XLD	Calibration	–5.17	433.393	0.980
	Validation	15.2	467.764	0.961
XJB	Calibration	6.22	505.203	0.977
	Validation	8.03	368.931	0.977
ZT	Calibration	1.90	993.290	0.955
	Validation	2.28	851.629	0.946
CT	Calibration	1.15	851.618	0.982
	Validation	0.34	697.886	0.975
SX	Calibration	5.41	1818.008	0.944
	Validation	2.60	1344.624	0.921

4 Conclusions

It can be seen from the above results table that the Xianjiang model, the TANK model, and the TOPMODEL have their own advantages and disadvantages. By a comprehensive comparison of the accuracy of the three models in each interval, it can be seen that the accuracy of the three models in each interval is basically similar. However, the simulation accuracy of different models is slightly different in each interval. In the LJ-XLD region, the accuracy of the TANK model and TOPMODEL is roughly the same, but the Xianjiang model is slightly better than them. In the XLD-XJB interval, the order of superiority of simulation is TOPMODEL model, Xianjiang model, and TANK model. In the interval from Xiangjiaba to Zhutuo (XJB-ZT), the simulation accuracy of TOPMODEL and Xianjiang model is roughly the same and both are better than the TANK model. In the ZT-CT interval, the NS of the three models is very close, indicating that the simulation results of the three models are roughly the same. In the region from Cuntan to Yichang (CT-YC), The simulation accuracy of the three models from high to low is TANK model, Xianjiang model, and TOPMODEL.

Because the Xianjiang model and TANK model are conceptual models, the simulation of runoff will be greatly limited when the rain stations are unevenly distributed or

the rainfall is unevenly distributed. The structure of TANK model is more flexible than that of the Xinanjiang model, and the number of water tanks of TANK model can be changed according to the need, so it has strong basin adaptability.

Compared with the conceptual model, TOPMODEL is a semi-distributed model, which adopts a topographic index to reflect topographic spatial changes. TOPMODEL takes into account the influence of topographic, landform, soil, and other factors on runoff formation, and describes the spatial-temporal distribution of hydrology in a refined manner. However, many factors are affecting the accuracy of the model, mainly terrain index and model parameters. Different calculation methods of terrain index (single flow method, multi-flow method, etc.) and the size of the grid will result in a different distribution of terrain index. Therefore, the TOPMODEL model performs well in mountainous areas with large undulating terrain, while the advantage of plain areas is not obvious. The terrain of XLD-XJB interval, XJB-ZT interval, and ZT-CT interval varies greatly, while the terrain of other intervals does not change significantly. Therefore, TOPMODEL has high simulation accuracy in XLD-XJB interval, XJB-ZT interval, and ZT-CT interval, while its advantage is not obvious in other intervals.

In general, the three models are all suitable for the study area. However, due to the different structural characteristics of each model and the limitation of data in the study area, from the perspective of comprehensive simulation results, the TANK model is recommended for CT-YC interval. Xinanjiang model is recommended for LJ-XLD interval, and TOPMODEL model is recommended for XLD-XJB interval, XJB-ZT, and ZT-CT interval.

Acknowledgments. This study is supported by the National Natural Science Foundation Key Project of China (No. 52039004) and National Natural Science Foundation of China (No. U1865202).

References

1. Linsley, K., Crawford, H.: Computation of a synthetic streamflow record on a digital computer. *Int. Assoc. Sci. Hydrol. Publ.* **51** (1960)
2. Mccuen, H.: A Guide to Hydrologic Analysis Using SCS Methods. Prentice Hall, Englewood Cliffs, New Jersey (1982)
3. Sugawara, M.: Tank Model with Snow Component. Study Report of National Research Center for Disaster Prevention, p. 293 (1984)
4. Zhao, R.: Xinanjiang model applied in China. *J. Hydrol.* **135**(1–4), 371–381 (1992)
5. Beven, J., Kirkby, J.: A physically based, variable contributing area model of basin hydrology. *Hydrol. Sci. Bull.* **24**(1), 43–69 (1979)
6. Guo, J., Zhou, J., Zou, Q., Liu, Y., Song, L.: A novel multi-objective shuffled complex differential evolution algorithm with application to hydrological model parameter optimization. *Water Resour. Manage.* **27**(8), 2923–2946 (2013)



Analysis on the Response of Lake Level Changes: A Hybrid Stepwise-Cluster Factorial Approach

X. B. Zhai¹ and Y. P. Li^{1,2}

¹ School of Environment, Beijing Normal University, Beijing 100875, China
yongping.li@iseis.org

² Institute for Energy, Environment and Sustainable Communities, University of Regina,
Regina, SK S4S 7H9, Canada

Abstract. In this study, a hybrid stepwise-cluster factorial (HSCF) method is proposed through integrating stepwise-cluster analysis (SCA) and factorial analysis (FA) into a general framework. HSCF can not only reflect the complex relationships between multiple factors and historical water level through a cluster tree, but also qualitatively analyze the contribution of key factors. The results from the study indicate that: (i) the main factors influencing the water level are FA_T (16.44%) > FA_E (10.76%) > FA_P (7.09%) > FA_A (1.73%). The main factors affecting WLL are temperature, evapotranspiration and precipitation; (ii) interactions among precipitation, evapotranspiration, temperature and agricultural water can significantly affect WLL. The contribution rates of key interaction factors are: FA_P*FA_E (7.33%) > FA_P*FA_A (5.07%) > FA_T*FA_E (4.82%) > FA_T*FA_A (4.28%) > FA_E*FA_A (3.53%); (iii) the influence of meteorological factors on WLL is dominant. The findings can help reveal the relationships among multiple impact factors of WLL and provide useful information for watershed management.

Keywords: Factorial analysis · Stepwise cluster analysis · Multiple factors

1 Introduction

Lakes are the important part of the hydrological cycle of basin. The changes of lake area and water level are closely related to water resources in the basin [1]. In recent years, with the aggravation of global climate change, the spatial distribution of regional water resources and the surface water cycle in arid and semi-arid regions have undergone significant changes under the dual influence of climate change and human activities [2], causing a series of ecological and environmental crises [3]. It is of great significance to deeply understand the characteristics and driving factors of lake level change in arid and semi-arid regions and evaluate the impact of climate change and human activities on lake change.

At present, the impact of global change on water resources of lake has become the focus of common concern of human society. According to the third report of IPCC, the

global temperature increased about 0.4–0.8 °C from 1860 to 2000. Temperature changes cause fluctuations in other climate parameters, and these changes have a major impact on the ecosystem [4]. The variation of water level of lake is affected by both climate change and human activities. The change of lake area affects the water balance of the basin where the lake is located, which is closely related to human survival and development. As a typical inland alpine lake in Central Asia, Issyk-Kul Lake is constantly affected by climate fluctuations and human activities, with its water level dropping by nearly 2 m from 1950 to 2000 [5]. The sharp decrease of water level has caused a series of ecological and environmental problems, such as soil salinization, desertification and increasing salinity [6]. Therefore, it is of great significance to analyse the relationship among human activities, climate change and lake level change and find out the main factors affecting the water level of Issyk-Kul Lake.

A lot of studies have been reported on changes in the water level of Issyk-Kul Lake [7]. A large number of statistical models have been used to analyse the factors affecting water level changes. Traditional statistical methods include: support vector regression (SVR), artificial neural network (ANN), multiple linear regression (MLR) [8]. However, the traditional method cannot capture the nonlinear relationship between variables effectively. More robust statistical methods need to be developed to identify the major factors affecting water levels. Stepwise cluster analysis, a robust statistical method, has been widely used in meteorology, hydrology and environmental pollution control [9], and factorial analysis (FA) as a multivariate inference method [10], is used for quantifying the individual and interactive effects of parameters on model response.

Therefore, in this study, a hybrid stepwise-cluster factorial (HSCF) method is developed for analyzing the main driving factors that affect the variation of water level of Issyk-Kul Lake (WLL). The results of this study are conducive to correct the evaluation of climate change and human activities on the changes in the lake. It is useful to provide necessary support for water resources management, and the sustainable development of the ecological environment.

2 Materials and Methods

2.1 Study Area and Data

The Issyk-Kul Lake ($42^{\circ}25'N$, $77^{\circ}15'N$) is an endorheic mountain lake, which is located in the northeast part of Kyrgyzstan with an altitude of 1607 m (Fig. 1). The volume of Issyk-Kul Lake is approximately 1736 km^3 , with the maximum depth of 668 m. The area of modern glaciers in the mountain area of the basin is about 650.4 km^2 . The annual precipitation is about 200–300 mm, up to 800–1000 mm in mountainous areas, and the evaporation is about 820 mm [11]. Precipitation in the northwest of Issyk-Kul Lake basin is low, especially in winter, with an average annual precipitation of only 115 mm. The main source of water in the Lake Issyk basin is surface runoff, with more than 118 rivers flowing into Issyk-Kul Lake [12]. Due to climate change and the intensification of human activities, the water level of Issyk-Kul Lake has changed significantly. During 1961–2012, the water level of the lake generally decreased, with a rate of 0.28 m/10a. The decrease of Lake water level causes changes in salinity and salinity, leading to a series of ecological and environmental problems, such as salinization, loss of biodiversity

and damage of ecosystem. To analyze the variation of WLL, nine factors are selected, including: temperature (FA_T), evapotranspiration (FA_E), runoff (FA_R), precipitation (FA_P), agricultural water consumption (FA_A), industrial water consumption (FA_I), domestic water consumption (FA_D), normalized difference vegetation index (FA_N) and vegetation coverage (FA_V). The meteorological and hydrological data are obtained from the National Centers for Environmental Prediction (NCEP) Climate Forecast System Reanalysis (CFSR) (<https://globalweather.tamu.edu/>) and Global Runoff Data Center (<https://portal.grdc.bafg.de/>). The human activity data is obtained from the website (<http://www.cawater-info.net/>) and statistical yearbooks of Kyrgyzstan. Ecological data is gained from the MODIS product (<https://modis.gsfc.nasa.gov>; <https://lpdaac.usgs.gov>).

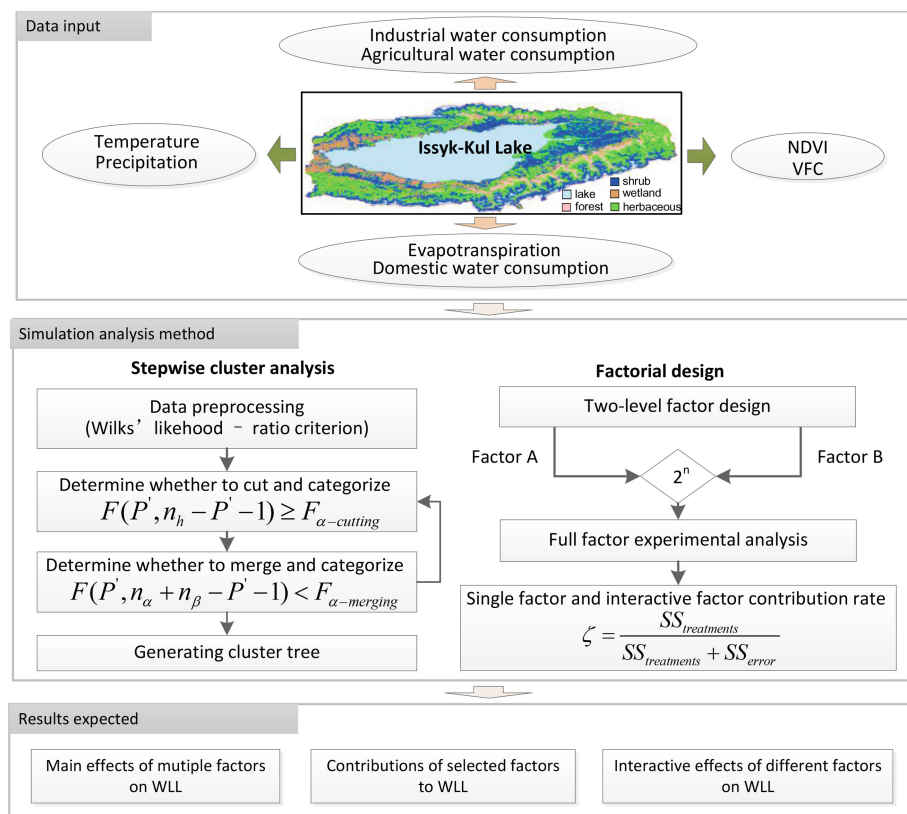


Fig. 1. The framework of this study

2.2 Stepwise-Cluster Analysis

Stepwise clustering analysis is widely used in statistical analysis, which can effectively capture the discrete and nonlinear relationships between variables. By generating cluster

trees, it is widely used in hydrology, climate and ecology research. The core of progressive clustering is to generate a cluster tree by cutting and merging a series of samples. The Wilks likelihood-ratio criterion is the basis of the stepwise cluster analysis. By using F test, let cluster u, which contains nu samples, be cut into two sub-clusters e and f ($n_u = n_e + n_f$). The cutting point is optimal when the value of Wilk's Λ ($\Lambda = |W|/|W + T|$) is minimum. T is the sums of squares and cross products (SSCP) matrix (denoted as f_i), and W is the within-groups SSCP matrix (denoted as e_i), thus the formulation can be:

$$\Lambda = \frac{\sum (e_i - \bar{e})(e_i - \bar{e})^T + \sum (f_i - \bar{f})(f_i - \bar{f})^T}{\sum (e_i - \bar{e})(e_i - \bar{e})^T + \sum (f_i - \bar{f})(f_i - \bar{f})^T + (n_e n_f / (n_e + n_f))(\bar{e} - \bar{f})(\bar{e} - \bar{f})^T} \quad (1)$$

where \bar{e} and \bar{f} are the mean values of samples e and f. when the new ei as the tip branch where the new data input and then the output $\{y_i\}$ can be:

$$y_i = \frac{1}{n_{e'}} \sum_{k=1}^{n_{e'}} y_{i,k}^{(e')} \pm \left\{ \max_{k=1}^{n_{e'}} (y_{i,k}^{(e')}) - \min_{k=1}^{n_{e'}} (y_{i,k}^{(e')}) \right\} / 2 \quad (2)$$

2.3 Factorial Analysis

Factorial analysis (FA), is a useful multivariate inference method, which can effectively reveal the response of output factors, and measure the variation between the individual factors and the responding factors. The two level factorial design is widely used in a lot of researches for reveal the effects of multiple factors. Each input factor has two levels (e.g. low (L) and high (H)). The sum of squares for selected factors can be calculated by the following formula:

$$SS_A = \frac{1}{MN} \sum_{i=1}^I \left(\sum_{m=1}^M \sum_{n=1}^N Y_{imn} \right)^2 - \frac{1}{IMN} \left(\sum_{i=1}^I \sum_{m=1}^M \sum_{n=1}^N Y_{imn} \right)^2 \quad (3)$$

$$SS_B = \frac{1}{IN} \sum_{m=1}^M \left(\sum_{i=1}^I \sum_{n=1}^N Y_{imn} \right)^2 - \frac{1}{IMN} \left(\sum_{i=1}^I \sum_{m=1}^M \sum_{n=1}^N Y_{imn} \right)^2 \quad (4)$$

$$SS_C = \frac{1}{IM} \sum_{n=1}^N \left(\sum_{i=1}^I \sum_{m=1}^M Y_{imn} \right)^2 - \frac{1}{IMN} \left(\sum_{i=1}^I \sum_{m=1}^M \sum_{n=1}^N Y_{imn} \right)^2 \quad (5)$$

where SS_A , SS_B , and SS_C are the sums of squares of factor A, B, and C respectively. Y_{imn} denotes the system response with factor A, factor B and factor C under the i th level, m th level and n th level. Identifying the appropriate p level is a key issue for the stepwise cluster analysis. For different p levels will lead to cluster trees with different classification strictness. In stepwise cluster analysis, a highly complex cluster tree can be generated under selected p levels through forcing multiple samples. Thus, Nash-Sutcliffe efficiency (NSE) [13], coefficient of determination (R^2) [14] and root mean

square error-observations standard deviation ratio (RSR) [15] are selected for choosing the p level:

$$NSE = 1 - \frac{\sum_{i=1}^n (H_{obs,i} - H_{sim,i})^2}{\sum_{i=1}^n (H_{obs,i} - \bar{H}_{obs})^2} \quad (6)$$

$$R^2 = \frac{\left(n \sum_{i=1}^n H_{obs,i} H_{sim,i} - \sum_{i=1}^n H_{obs,i} \sum_{i=1}^n H_{sim,i} \right)^2}{\left[n \sum_{i=1}^n H_{obs,i}^2 - \left(\sum_{i=1}^n H_{obs,i} \right)^2 \right] \left[n \sum_{i=1}^n H_{sim,i}^2 - \left(\sum_{i=1}^n H_{sim,i} \right)^2 \right]} \quad (7)$$

$$RSR = \frac{\sqrt{\sum_{i=1}^n (H_{obs,i} - H_{sim,i})^2}}{\sqrt{\sum_{i=1}^n (H_{obs,i} - \bar{H}_{obs})^2}} \quad (8)$$

where $H_{obs,i}$ is the observed value of sample i, $H_{sim,i}$ is the simulated value of sample i, n is the number of samples and \bar{H}_{obs} is the average measured value.

3 Results and Discussion

By building a simulation analysis model of water level of Issyk-Kul Lake based on HSCF method, the factors affecting water level of Issyk-Kul Lake are further analyzed, and the main influencing factors are identified.

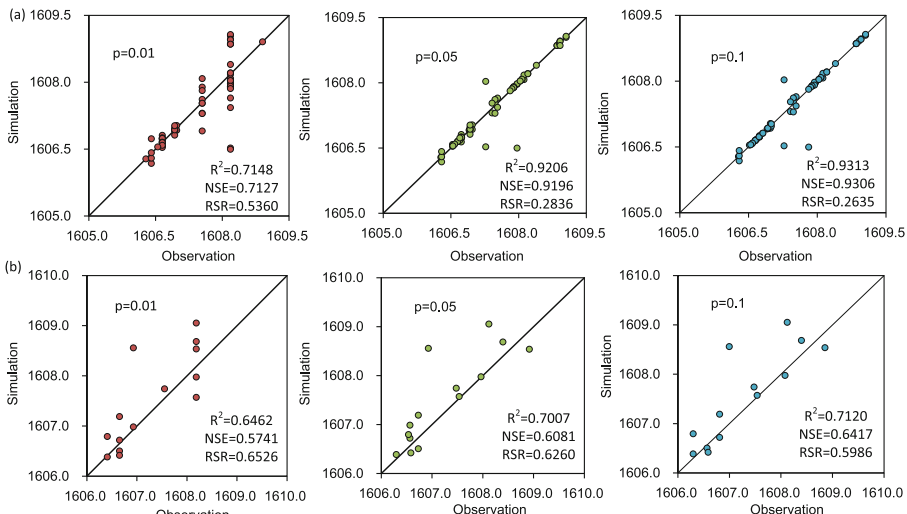


Fig. 2. Water level simulated under different p levels (a, calibration and b, validation).

Figure 2 presents NSE, R^2 and RSR of the HSCF model under different p levels. For example, when $p = 0.01$, the Nash coefficient of HSCF model is 0.7127, the determination coefficient is 0.7148, and the observation error standard deviation ratio is 0.5360 in the calibration period; the Nash coefficient of model is 0.5741, the determination coefficient is 0.6462, and the observation error standard deviation ratio is 0.6526 in the validation period. With the p level increase, the effect of model evaluation index becomes better. For instance, when the $p = 0.05$, in the calibration period the NSE, R^2 and RSR of the HSCF model is 0.9196, 0.9206 and 0.2836, respectively; in the validation period, the NSE, R^2 and RSR of the HSCF model is 0.6081, 0.7007 and 0.6260, respectively. When the $p = 0.1$, both in the calibration period and validation period, the NSE and R^2 increase and the RSR decrease. The results indicate that with the increase of p level, the simulation effect of the model becomes better with statistical significance. In general, model evaluation indexes and progressive clustering tree structure at different p levels are comprehensively compared. The $p = 0.1$ is selected to simulate the historical water level of Issyk-Kul Lake (WLL).

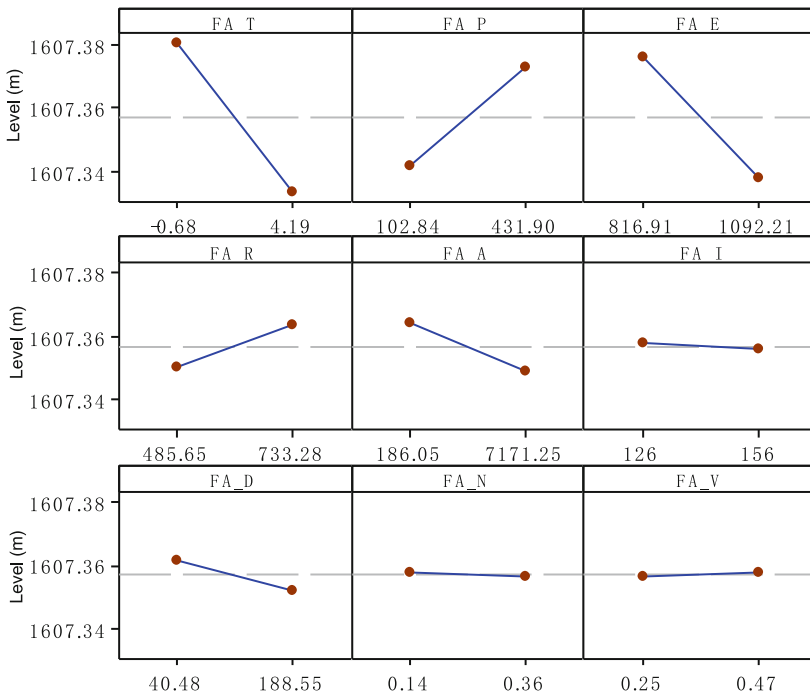


Fig. 3. The main effects of factors on WLL

Figure 3 presents main effects of driving factors on WLL. The degree of inclination of the oblique line in the figure indicates the sensitivity of the driving factor to WLL. Results indicate that temperature (FA_T) and evapotranspiration (FA_E) have significant negative impact on WLL. Take the plot of FA-T as an example, when the temperature increasing from low level to high level, WLL decreases from 1607.38 m to 1607.33 m.

The slope of line is negative, indicating that FA_T has negative effect on WLL. The reason is that Issyk-Kul Lake basin is dissipative watershed where high temperature lead to increased water loss. From the results, FA_R and FA_P have positive effects on WLL, and the slopes of human activities factors (agricultural water consumption (FA_A), domestic water consumption (FA_D) and industrial water consumption (FA_I)) are negative, indicating that human activities could exacerbate the lake drop. The reason is that agricultural irrigation is the major water use sector, accounting for more than 90% of the total water consumption. The expansion of arable land and the waste of water resources further aggravate the consumption of agricultural water resources.

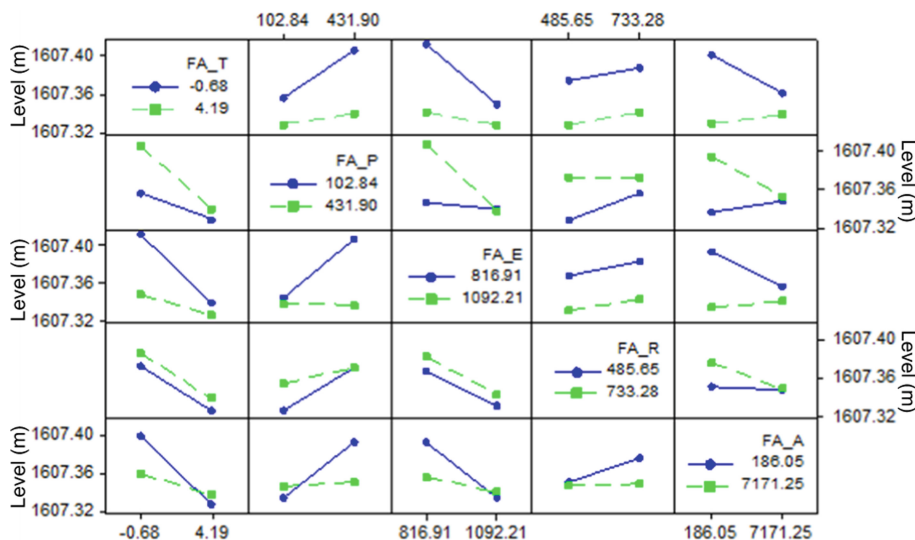


Fig. 4. The effects of interaction factors on WLL

Figure 4 shows the effects of interaction factors on WLL. Results indicate that interactions are mainly exist in FA_P * FA_E, FA_P * FA_A, and FA_T * FA_E. For instance, when temperature (FA_T) at low level, evapotranspiration (FA_E) increasing from 816.81 mm to 1092.21 mm, WLL decreases from 1607.41 m to 1607.35 m; when temperature (FA_T) at high level, evapotranspiration (FA_E) increasing from 816.81 mm to 1092.21 mm, WLL decreases from 1607.34 m to 1607.33 m. This is mainly because high temperature level increases runoff inflow. However, high temperature is conducive to the intensification of evapotranspiration. The results also indicate that agricultural water consumption (FA_A) has significant negative impact on WLL when the temperature is at low level. For example, when the temperature (FA_T) increase from low level to high, the impact causing by FA_A is 0.04 m and 0.01 m, respectively. This indicates that the interaction between temperature and agricultural water consumption can affect WLL. The complex relationship is exist between temperature (FA_T) and agricultural water consumption (FA_A).

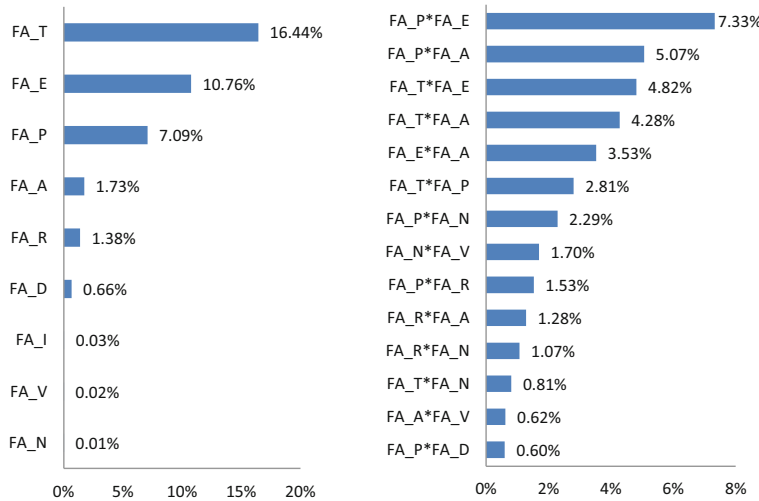


Fig. 5. Contribution rates of individual factors and interactive factors

Figure 5 presents the contributions of individual factors and interactive factors to the variation of WLL. From the results, temperature (FA_T) is the most significant factor, accounting for 16.44%, followed by evapotranspiration (FA_E) (10.76%), and precipitation (FA_P) (7.09%). This is mainly because evapotranspiration in the Issyk-Kul Lake basin is relatively large, and the meteorological factors, especially the change of temperature, has significantly impact on the evapotranspiration. FA_A (agricultural water consumption) is also an important factor with a contribution of 1.73%. The results also indicate that interactive factors (FA_P * FA_E, FA_P * FA_A, FA_T * FA_E, and FA_T * FA_A) have significant impact on WLL. Contributions of FA_P * FA_E, FA_P * FA_A, FA_T * FA_E, and FA_T * FA_A are 7.33%, 5.07%, 4.82% and 4.28%, respectively. The interaction between meteorological factors is significant. The reason is that Issyk-Kul Lake is an inland lake in where water level is mainly affected by evapotranspiration, precipitation, and runoff.

4 Conclusions

In this study, a hybrid stepwise-cluster factorial (HSCF) method is developed for quantitatively analyzing effects of multiple factors on WLL. Through integrating stepwise cluster analysis (SCA) and factorial analysis (FA) into a general framework, the HSCF method can effectively identify the complex relationship among the multiple factors (climate, hydrology, ecology and human activities), and quantitatively analyze the effects of individual factors and interaction factors on WLL. Results indicate that: (i) the main factors affecting the WLL are FA_T (16.44%) > FA_E (10.76%) > FA_P (7.09%) > FA_A (1.73%). It can be seen from the results that the main factors affecting WLL are temperature, evapotranspiration and precipitation; (ii) interactions among precipitation, evapotranspiration, temperature and agricultural water can significantly affect WLL. The contribution rate among key interaction factors are: FA_P * FA_E (7.33%) > FA_P *

FA_A (5.07%) > FA_T * FA_E (4.82%) > FA_T * FA_A (4.28%) > FA_E * FA_A (3.53%); (iii) the influence of meteorological factors on WLL is dominant, and more meteorological factors should be considered in the next study.

Acknowledgements. This research is supported by the Strategic Priority Research Program of Chinese Academy of Sciences (XDA20060302), and the National Key Research and Development Program of China (2016YFC0502803).

References

1. Yuan, H., et al.: Water-level fluctuations regulate the availability and diffusion kinetics process of phosphorus at lake water–sediment interface. *Water Res.* **200**, 117258 (2021)
2. Martin Perales, K., Hein, C.L., Lottig, N.R., Zanden, J.V.: Lake water level response to drought in a lake-rich region explained by lake and landscape characteristics. *Canadian J. Fish. Aquat. Sci.* **77**(11), 1836–1845 (2020). <https://doi.org/10.1139/cjfas-2019-0270>
3. Zhang, D., Yang, S., Wang, Z., Yang, C., Chen, Y.: Assessment of ecological environment impact in highway construction activities with improved group AHP-FCE approach in China. *Environ. Monit. Assess.* **192**, 7 (2020). <https://doi.org/10.1007/s10661-020-08400-4>
4. Robinson S.: Climate change adaptation in SIDS: a systematic review of the literature pre and post the IPCC fifth assessment report. *Wiley Interdisc. Rev. Climate Change*, **11**(3) (2020)
5. Alifujiang, Y., Abuduwaili, J., Maihemuti, B., et al.: Innovative trend analysis of precipitation in the lake Issyk-Kul basin. *Kyrgyzstan. Atmos.* **11**(4), 332 (2020)
6. Cheng, X., Ling, J., Zhou, F.: Analysis of Suzhou’s ecological environment construction measures based on Caohu’s experience and achievements. *IOP Conf. Ser. Earth Environ. Sci.* **781**(3), 032067 (2021)
7. Leroy, S., Ricketts, R.D., Rasmussen, K.A.: Climatic and limnological changes 12,750 to 3600 years ago in the Issyk-Kul catchment, Tien Shan, based on palynology and stable isotopes. *Quarter. Sci. Rev.* **259**(3), 106897 (2021)
8. Morave, J.M., Amani, P., Hosseini-Moghari, S.M.: Groundwater level simulation and forecasting using interior search algorithm-least square support vector regression (ISA-LSSVR). *Groundwater Sustain. Dev.* **11**, 100447 (2020)
9. Liu, Y.R., Li, Y.P., Sun, J.: Statistical downscaling of temperature using stepwise cluster analysis method – a case study in Nur Sultan, Kazakhstan. *IOP Conf. Ser. Earth Environ. Sci.* **435**, 012019 (2020)
10. Wang, P.P., Li, Y.P., Huang, G.H., Wang, S.G., Ma, Y.: A multi-scenario factorial analysis and multi-regional input-output model for analyzing CO₂ emission reduction path in Jing-Jin-Ji region. *J. Clean. Product.* **2**, 126782 (2021)
11. Rojas-Jimenez, K., Araya-Lobo, A., Quesada-Perez, F., Akerman-Sanchez, J., Grossart, H.P.: Variation of bacterial communities along the vertical gradient in lake Issyk-Kul Kyrgyzstan. *Environ. Microbiol. Rep.* **13**(3), 337–347 (2021)
12. Abakumov, A.I., Pak, S.Y., Morozov, M.A., Tyntybekov, A.K.: Model estimation of the phytoplankton biomass of Lake Issyk-Kul using remote sensing data. *Inland Water Biol.* **12**, 111–118 (2019)
13. Nash, J.E., Sutcliffe, J.V.: River flow forecasting through conceptual models part I-a discussion of principles. *J. Hydrol.* **10**(3), 282–290 (1970)
14. Legates, D.R., McCabe, G.J.: Evaluating the use of “goodness-of-fit” measures in hydrologic and hydroclimatic model validation. *Water Res. Res.* **35**(1), 233–241 (1999). <https://doi.org/10.1029/1998WR900018>

15. Moriasi, D.N., Arnold, J.G., Van Liew, M.W., Bingner, R.L., Harmel, R.D., Veith, T.L.: Model evaluation guidelines for systematic quantification of accuracy in watershed simulations. *Trans. ASABE* **50**(3), 885–900 (2007)



Seepage Experiment on a Permeable Dam Formed by Debris Flow from River Tributaries

Fu-Ming Chang^(✉)

Da-Yeh University, No.168, University Rd., Dacun, Changhua 515006, Taiwan
Changfm@mail.dyu.edu.tw

Abstract. Rivers in Taiwan are characterized by steep slopes, rapid currents, and unstable geology. Frequent typhoons and a long-lasting rainy season drive large amounts of soil and sand deposits into rivers. Because substantial amounts of rainfall converge into the reservoirs, dredging operations must be conducted to minimize damage. Sediment disposition is a common problem in Taiwan's river systems, particularly in the mountainous areas. River tributaries typically convey numerous rocks and sand deposits, which can form natural dams. Such dams have different permeability levels, depending on the rock composition of their structure. To understand the process of silt movement and the dynamic influence of deposits on downstream geology, an indoor small-scale physical model was designed to replicate an on-site situation. The model was used to simulate the changes of the main river when a particular natural dam is removed or collapsed. The volume of water flow was varied in this experiment to observe the formation and collapse of the permeable natural dam and its impact on the downstream geological properties.

Keywords: Permeable dam · Seepage · Physical model experiment

1 Introduction

In recent years, various numerical methods and mathematical theories have been applied to studying dam improvement. Dai [1] reported that the colonies of the Formosan landlocked salmon, or *Oncorhynchus masou formosanus*, in Taiwan have experienced many changes over time. Among these changes, increasing river discharge by typhoons has affected the species most drastically by changing riverbed silt and sediment composition, thus reducing the number of the salmon and at times threatening it with extinction. Yeh et al. [2] suggested that, to restore fish habitats in a river, partially removing a dam can increase the stability of the river and thus restore the river to its natural state. Yeh [2] investigated the riverbed and silt composition of the Chichiawan Brook in Taiwan and determined that the water of the brook washed fine sand downstream and formed a protective layer of sediment for the river way. Among various riverbed materials in the brook, Material #6 (large boulders, particle size of > 51.2 cm) accounted for the largest percentage (up to 40%). Similar to the Kao-Shan River, the Chichiawan Brook exhibited Riverbed Material #1 (smooth-surface, particle size of < 0.2 cm) composed of the finest

sand grains in the stream, indicating indicated that in this scour section, fine sand grains were transported downward to the riverbed.

Konrad [3] stated that the United States Department of Energy planned to remove two dams (30 and 60 m long, respectively) from the Elwha River. The removal would save the reservoir of the river from stream erosion and sediment deposition and thereby restore the ecosystem of the river. A one-dimensional model could be applied to simulating sediment transportation, sediment particle size distribution, and river restoration time. However, after the removal of the dams, the excessive amount of silt could also reduce the diversity of the ecosystem. In 2007, the CALFED Ecosystem Restoration Program [4] conducted several experiments in a flume that was 28 m long, 0.86 m wide, and 0.9 m deep. Sand grains were first added into the flume. Acoustic and laser-beam scanners were then used to measure the water surface profiles and waterbed topography. The following aspects were subsequently discussed: (a) the bed slope and grain size distribution; (b) the relationships of riverbed grain size distribution with sediment transportation range and fine sand infiltration; and (c) the fact that fine sediments should be transported forward along the waterbed. Gibson [5] proposed a schematic of two fine infiltration processes for static gravels. The schematic indicates that if there is a sufficiently connected interstitial space, small diameter sand grains are likely to fall through the pores of the gravel waterbed until any physical barrier impedes their progress.

Lin et al. [6] conducted a physical modeling experiment to compare hydraulic phenomena before and after dam construction, and deduced the similarity rate of a movable riverbed. Lin also employed a prototype and model by applying a method similar to the hydraulic model of a movable riverbed, which was developed by the Delft Hydraulic Research Institute, as well as the Engelund–Hansen formula to derive the sediment transport equation as follows:

$$\frac{q_s}{D_s^{3/2} \sqrt{g}} = 0.084 \left(\frac{\mu h s}{D_s} \right)^{5/2} \quad (1)$$

A semimovable riverbed experiment revealed that the course of the river flow is mainly concentrated toward the right bank. Because of the topographic influence of mountain areas, a minor error exists between the flood level at the frequency of 200 years and the level calculated using mathematical modeling; nevertheless, this error is within a reasonable range. Kleinhans [7] called this process unimpeded static percolation. Gravel particles remain static, enabling finer deposits to pass. Einstein (1968) [8] observed this process in an initial water trough test. In addition, Lunt and Bridge [9] reported this mechanism in their open-type gravel document; however, the mechanism associated with natural systems is not dominant, as indicated in Diplas and Parker [10]. According to statistical data on 467 barrages removed in the 20th century in the United States, Poff and Hart [11] discovered that the number of removed dams increased rapidly in the previous 20 years, and the total number of removed dams approximated 200. However, they determined that nearly half of the removed barrages were small (lower than 5 m), and barrages lower than 17 m constituted 70% of the total number of barrages. Moreover, they presented a flowchart illustrating the effect of barrages on a local place, or the biophysical process engendered by the geographic environment.

Most of Taiwan's rivers originate from high mountains with the characteristics of fast currents and steep slopes. The reservoirs in Taiwan are located mostly in the mountains, where there are large amounts of rainfall and unstable geology. In every typhoon or rainy season, the heavy rainfall washes down large amounts of sediment into the river, forming deposits and thus hindering the flow of the rivers. Landslides and mudslides are commonly occurred in Taiwan. (For information on the influence of hydrological geography on landslides, please refer to Hsiao et al. [12] For gravel distributions such as gravel colluvium alongside main rivers, and for the effects of the slope and water level on mudslides, please refer to Ku et al. [13].

Numerous small-scale sediment retention and dam structures are present upstream of the Shihmen Reservoir. In the current study, an experiment was conducted to investigate the collapse of a small sediment retention dam located 20 m downstream of Junghua Dam (Fig. 1) and to determine how water flows from the branch into the mainstream of Junghua Dam (Fig. 2). We examined the phenomenon associated with the formation of a permeable dam when the branch converged into the mainstream during the events of typhoons and floods in the dam area. The observation results will be discussed further in the future.

Liu [14] investigated the correlations between the rainfall and water level of the Liyutan Reservoir by running simulations and comparison and statistical analyses by using seepage discharge records and current seepage discharge factors from the monitored data of Liyutan Dam. Liu [14] executed a curvilinear regression on the seepage discharge value of the water level of the reservoir. Thus, the seepage discharge value could be determined according to both the water level in the reservoir and the amount of rainfall. Because curvilinear regression was used to determine the seepage discharge of

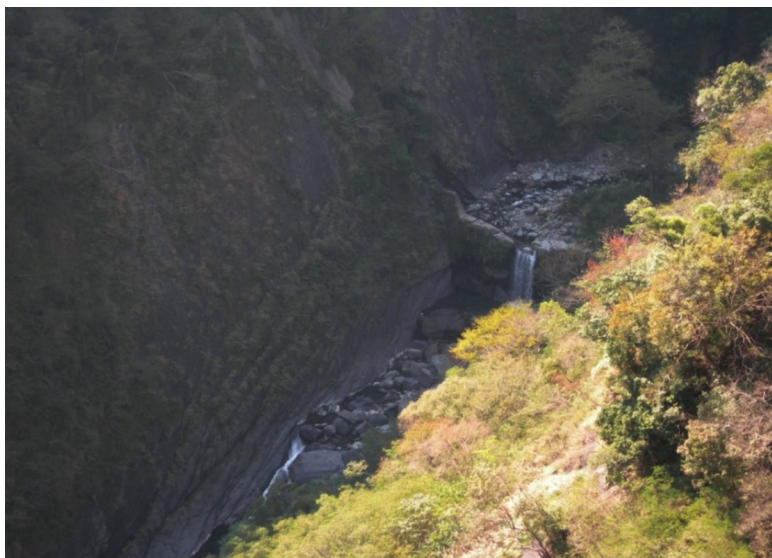


Fig. 1. Collapse of a small sediment retention dam



Fig. 2. On site picture of the branch converge into the mainstream.

the dam, information on excess seepage discharge and warning standards was estimated, and such information can serve as a reference for dam management teams.

An embankment dam is a matter of porosity [15]. Rocks, which are fairly rigid, constitute the main component of an embankment dam; the fluid travels through the rocks in a similar manner as water running down a pipeline. The K value represents the permeability coefficient of average size pores in an embankment dam [16]. Because the groundwater flowing under an embankment dam exists on an unknown free water surface, the seepage of an embankment dam can be classified as an unconfined aquifer (for a detailed description of embankment dam seepage, please refer to Schaffernak [17]. Furthermore, the surface runoff caused by rainfall can affect the embankment dam seepage condition. Katopodes and Strelkoff [18, 19], and Balloffet and Scheffler [20] have separately established two-dimensional models for simulating the water flow of both a river course and flooded land in low and flat areas after dam collapse.

When the downward water flow slows down, the partial slight slope flow concept can be used to ensure a simplified analysis (Ivanov, [21]; Yomota et al., [22]). For simulating the low and flat areas of a farmland, Kadoya and Hayase [23] proposed a reservoir model concept in a diffusion model, and Chen et al. [24] proposed an improved method for controlling the variables of the diffusion model for application in Taiwan.

2 Materials and Methods

This experiment was mainly conducted to understand the phenomenon of silt of fine particle size filling a downstream gravel-type river bed when the silt is trapped by a dam and to determine the impact of upstream silt of fine particle size on a downstream habitat environment after an upstream dam is removed or collapses. Thus, we could roughly estimate the time at which silt of fine particle size remains in the gravel-type river bed, and this estimation can be used to provide a reference for restoring the habitat in the future.

2.1 Experimental Setup

Figure 3 shows the experimental setup. The experimental channel model had a length of 90 cm and a width of 2 cm. The bottom of the channel was filled with fine sand, and a gravel inlet was installed in the middle of the channel, with a piece of clay mounted to represent the dam. A tank was established beneath the channel for collecting water during the course of the experiment. On the other side above the channel, a constant head tank was set up. A stilling basin was established at the influx with a flow meter controlling the water flow. Three flow rates served as the experimental variables: 6.48, 9.71, and 13.19 mL/s. Figure 4 shows these flow rates. The coefficient of determination is 0.9966, indicating a stable flow rate, and the rate of sand replenishment is 45 g/min.

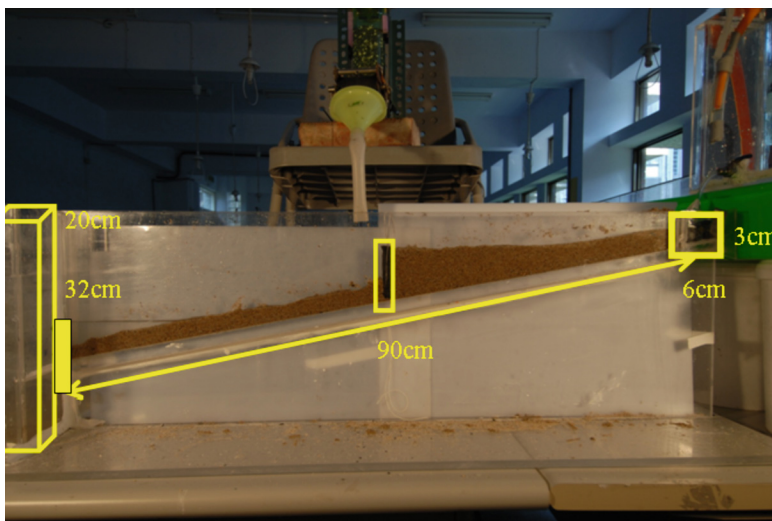


Fig. 3. Experiment setup and configuration.

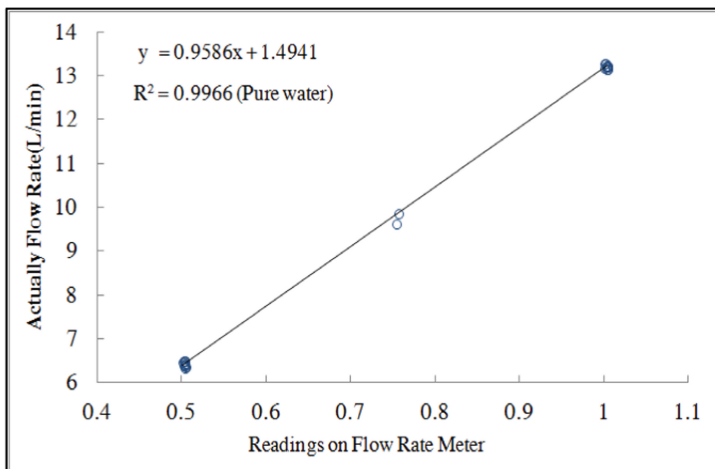


Fig. 4. Graph of the actual flow rate vs. flow meter readings.

2.2 Experimental Procedure

At the beginning of the experiment, water at a low flow rate (6.48 mL/s) was allowed into the channel. When the water reached the clay dam in the middle of the channel, the water level rose above the dam structure, leading to the formation of a trench in the sand layer beneath the dam. The dam was removed precisely 10 s into the experiment, and the sand layer above the dam was immediately washed downstream. During the removal of the dam, gravel was allowed to flow into the channel. The gravel formed a loose structure of a permeable dam in the channel. Precisely 2 min into the experiment, the flow rate was changed to 9.71 mL/s; at 2 min and 20 s, the flow rate was changed to 13.19 mL/s. The experiment was stopped and thus completed at 5 min and 30 s with all the data collected.

2.3 Experimental Theory

In the experimental process, experimental conditions were assumed by applying several theories, and theoretical values were calculated on the basis of these conditions. The theoretical and experimental values were compared to obtain appropriate results. This experiment involved presuming that the low sand layer was the lower permeation coefficient and that a permeable dike had formed above the sand layer; these presumptions formed the theoretical design of the dam body. Figures 5, 6 and 7 illustrate the experimental theory. The water level rises to the height of the dam body, and the dam breaks when the water level exceeds the height of the dam body. Figure 6 illustrates the major theoretical values.

Because the angle of the dam body shown in Fig. 6 is 45° , the low part of the dam body, $K \approx 0$, and water level are at the same height as the dam body; therefore, the theoretical resolution is calculated. Suppose that $\vec{\nabla} \bullet \vec{q} = 0$ is calculated; in this expression, q can be calculated using $\vec{q} = -k \vec{\nabla} h$, and $h = z + \frac{p}{\gamma}$ (h : experimental

height; z : horizontal distance; p : velocity; and γ : unit weight) can be used to create different resolutions for the three sides of the dam body, which are respectively expressed as follows: $h = z + \frac{\gamma(H-z)}{\gamma} = H$ (left side); $h = z$ (right side); and $\vec{q} \bullet \vec{n} = 0$ (low part), $\psi(x, z)$, $q_x = \frac{\partial \psi}{\partial z}$ and $q_z = -\frac{\partial \psi}{\partial x}$.

Finally, $K \vec{\nabla} \bullet \vec{\nabla} h = 0$ is calculated. The Laplace equation is used to calculate the theoretical resolution of $H = \frac{2q}{K}$, where H represents the dam height, q represents the discharge, and K represents the rate of permeability.

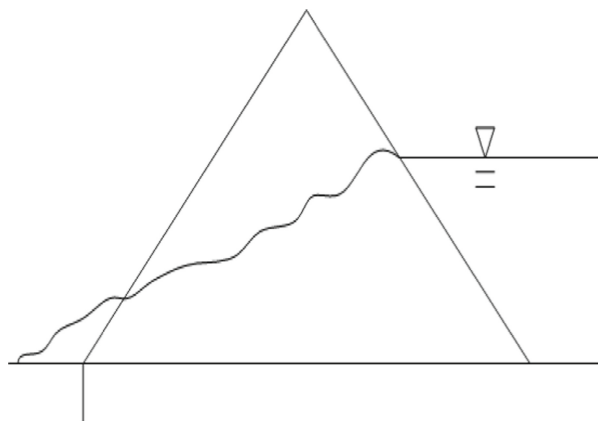


Fig. 5. Illustrator of water level at 1/2 height of the dam.

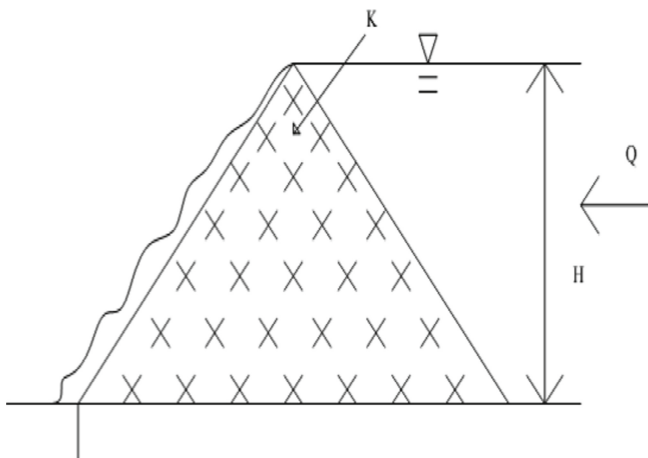


Fig. 6. Illustration of water level at the top of the dam.

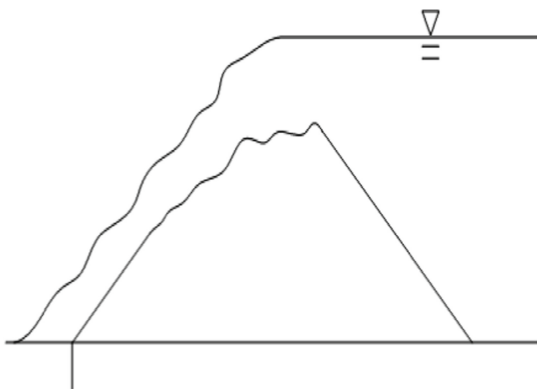


Fig. 7. Illustration of water level higher than the dam structure (Theory).

3 Results

Figures 8–10 depict various water levels in the experiment, indicating that the results are the same as the presumed theoretical conditions. The water level rose slowly to the height of the dam body, and the dam overflowed when the water level exceeded the height of the dam body. However, as shown in Fig. 9, the side slopes in the left corner indicate that some of the water had broken through the dam body when the water level had yet to exceed the height of the dam body. This may have been because of the K value of the material. The heights of the dam body and water levels were calculated according to the proportions in the photos shown in Fig. 11. This figure depicts the flow rate versus time and the height of the dam body versus time for monitoring the formation of the

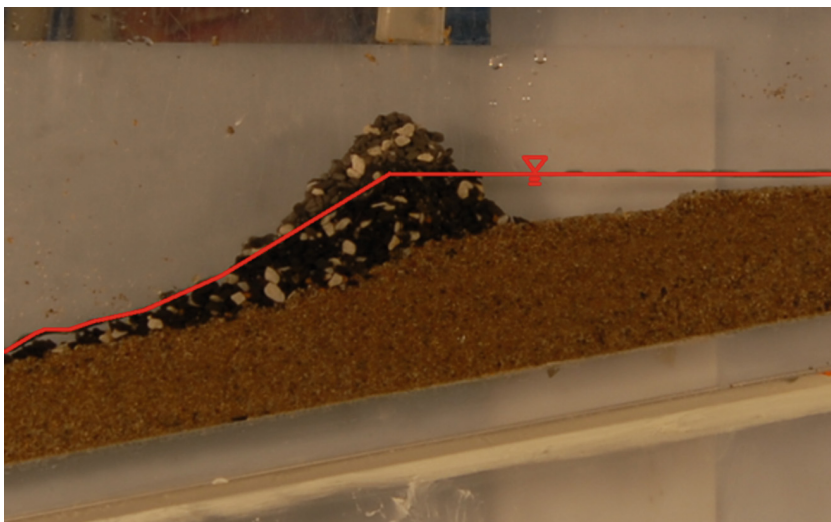


Fig. 8. Water level at 1/2 height of the Dam (Experiment).

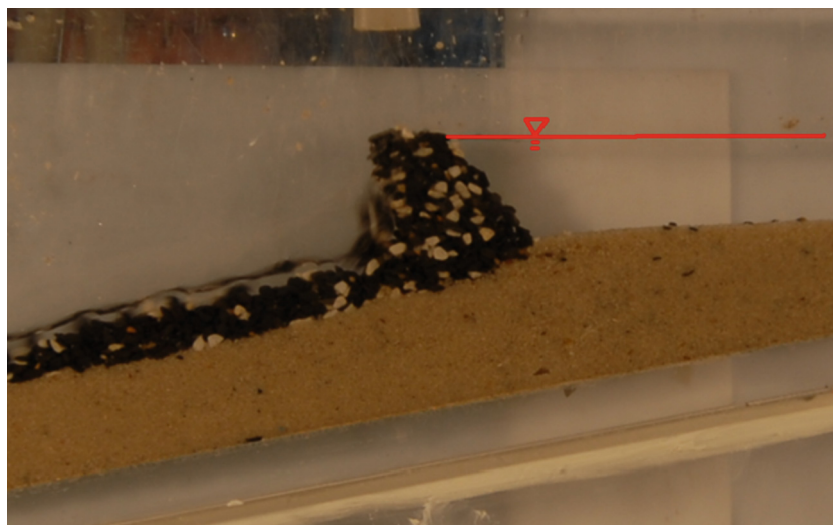


Fig. 9. Water level at the top of the dam (Experiment).

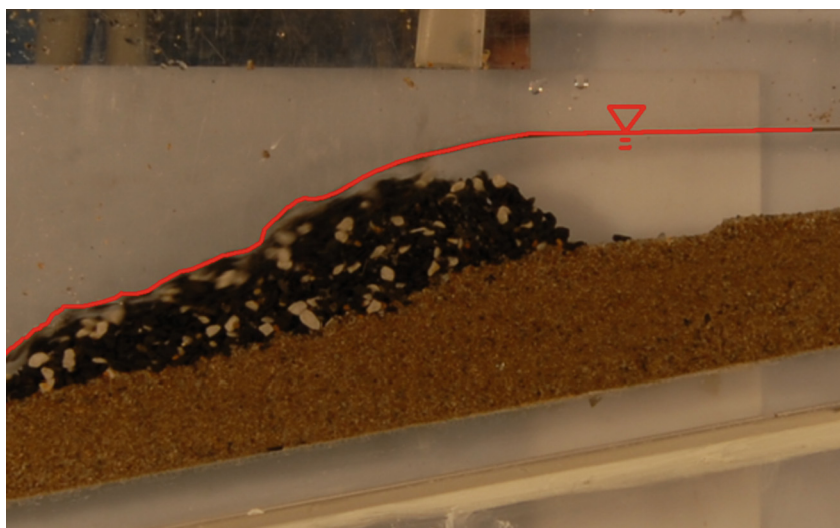


Fig. 10. Water level higher than the height of the dam.

dam body and the occurrence of the dam break. As shown in this figure, the formation of the dam body and the dam break occurred only in the first trial; the first formation of the dam body and the dam break took longer than those in subsequent trials did.

The height of the water level above the dam body was used as the basis (height of dam body/water level) for comparing the flow rate, and the data are presented in Fig. 12 (in which the red line in is mainly 1). The final value obtained is the value of the dam

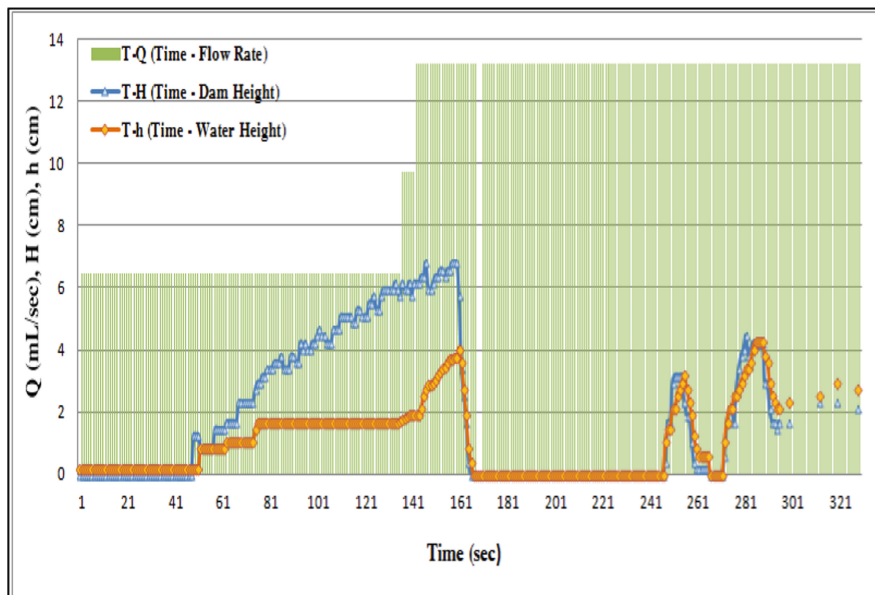


Fig. 11. Experiment simulation.

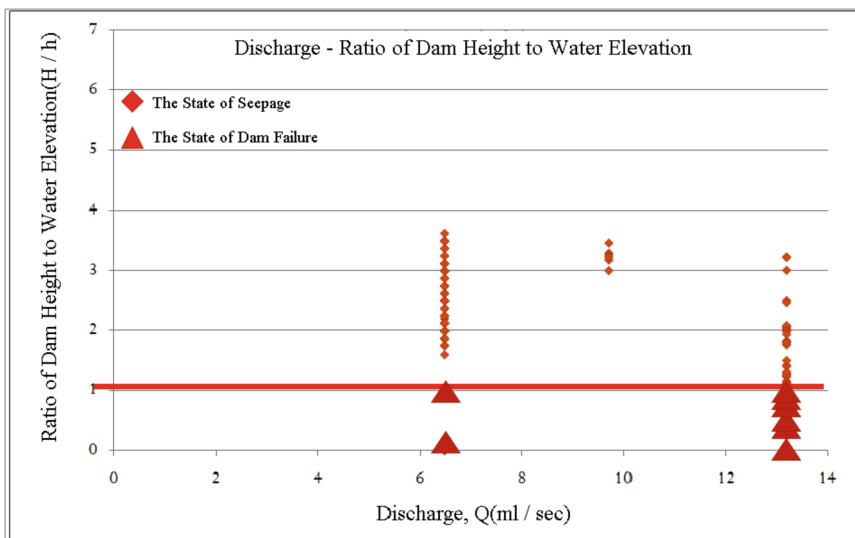


Fig. 12. Graph of Dam Height/Water Elevation vs. Discharge (ml/sec).

break caused by overflow; a value less than 1 indicates a dam break, and the dam does not break if the value is higher than 1.

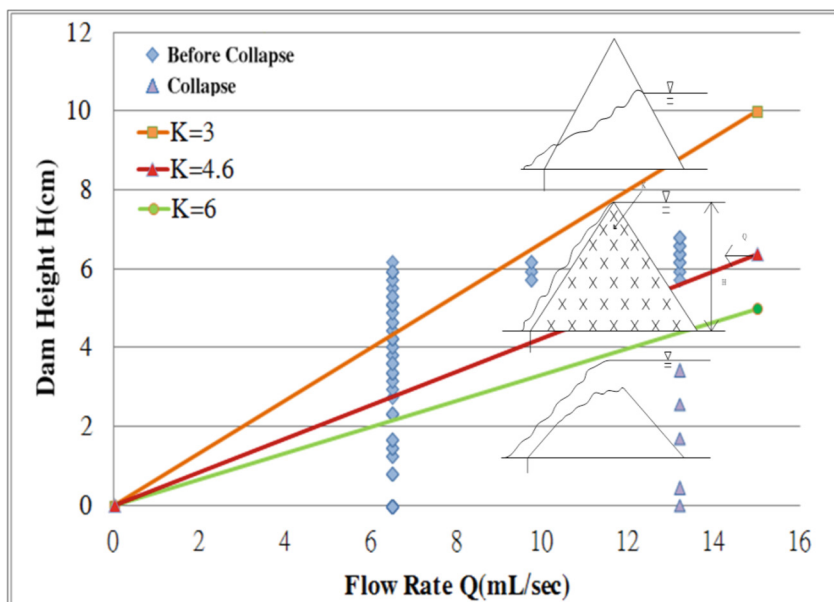


Fig. 13. Graph of Dam height (cm) vs. flow rate (mL/sec).

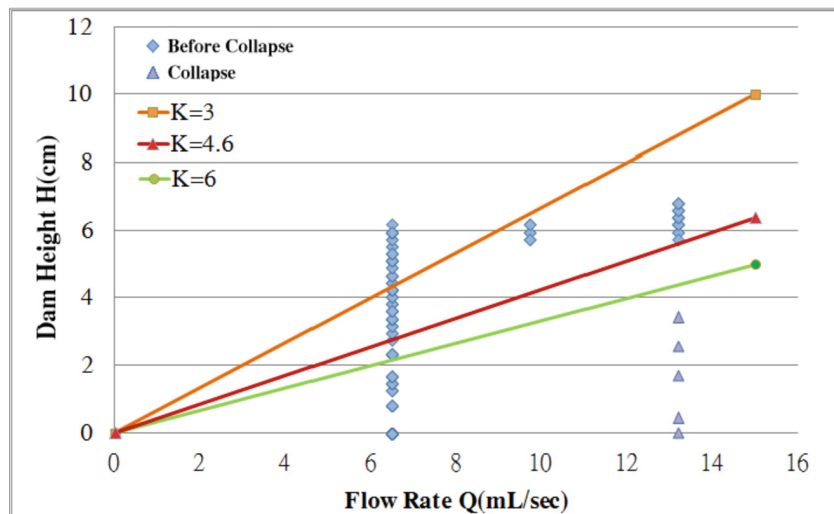


Fig. 14. Graph of K value.

The theoretical value was incorporated into the process of determining the dam break in the first trial, as shown in Fig. 13. This figure mainly indicates that when K is greater than 4.6, a dam break occurs. Moreover, $K = 4.6$ is used as a demarcation point, and this is because a dam does not break when the value is less than 4.6. The data associated with the dam break for the next two to three trials were added and plotted as shown in Fig. 14, indicating the presence of numerous values when K is greater than 4.6. This is mainly because the dam body is slowly formed after the first time the dam breaks; these values are thus confirmed to represent the dam break.

4 Summary and Conclusions

This experiment mainly involved simulating the effect of typhoons and floods on a permeable dam. After the dam of a tributary breaks, large-grained gravel carried by water is fed into the main stream, thus potentially forming a permeable dam body at the confluence. After the permeable dam breaks, large amounts of gravel flow into the main stream, causing water to flow under the gravel layer. However, we observed only a gravel layer. This phenomenon occurs in several parts of the catchment area of the Shihmen Reservoir. We sought to understand this phenomenon and process by conducting an experiment. We also conducted an indoor experiment involving theoretical examination for determining how a dam break occurs when K is higher than 4.6; $K = 4.6$ indicated the demarcation point, and a K value less than 4.6 indicated that a dam break does not occur. As shown in Fig. 14, many K values are obviously greater than 4.6 when the main dam body breaks and after the dam breaks the second and third times. This is mainly because the dam body forms slowly (when K is greater than 4.6) after the first dam break. Therefore, these values are confirmed to represent the dam break.

References

1. Dai Yong, T.: Doctoral Thesis. National Taiwan University, Taipei, Taiwan (1992)
2. Yeh, Z.X., Duan, J.-H., Lian, H.-B.: Construction and Planning Agency. Chinese Soil and Water Conservation Society, Ministry of the Interior (1998)
3. Konrad, C.P.: Simulating the recovery of suspended sediment transport and river-bed stability in response to dam removal on the Elwha River, Washington. *Ecol. Eng.* **35**(7), 1104–1115 (2009). <https://doi.org/10.1016/j.ecoleng.2009.03.018>
4. CALFED Ecosystem Restoration Program Final Technical Memorandum (2007)
5. Gibson, S.: *Sedimentology*, **56**, 3, 661–676. <https://doi.org/10.1111/j.1365-3091.2008.00991.x> (2009)
6. Lin, G. F., Lai, J. S., Tu, K. L., Chen, L.H.: Agricultural Engineering Conference Proceedings, pp. 100–1–100–6 (2005)
7. Kleinhans, M.G. *Netherlands Geograp. Stud.* **293**, 317 (2002)
8. Einstein, H.A.: *J. Hydraul. Div.* **94**(5), 1197–1206 (1968)
9. Lunt, I.A., Bridge, J.S.: *Sedimentology*, **54**, 1, 71–87 (2007). <https://doi.org/10.1111/j.1365-091.2006.00829.x>
10. Diplas, P., Parker, G.: *Dynamics of Gravel-Bed Rivers*, pp. 313–329 (1992)
11. Poff, N.L., David, D.H.: *BioScience*, **52**, 8, 659–668. [https://doi.org/10.1641/0006-3568\(2002](https://doi.org/10.1641/0006-3568(2002))

12. Hsiao, P.J., Ku, C.Y., Hsieh, P.C.: *J. Soil Water Conserv.* **39**(1), 29–47 (2007)
13. Ku, C.Y., Hsu, S.M., Chung, M.C., Fei, L.Y., Lee, J.F., Su, T.W.: *Geophys. Soc.* **65** (2008)
14. Liu, F.-C.: Master Thesis. Feng Chia University, Taichung, Taiwan, Graduate Institute of Civil and Hydraulic Engineering (2003)
15. Bear, J. Eisevier, New York, 764–766 (1972)
16. Liggett, J.A.: *J. Hydraul. Div.* **103**(4), 353–365 (1977)
17. Schaffernak, F. *Allgem. Bauzeitung*, **252** (1917)
18. Katopodes, N.D., Strelkoff, T.: *J. Hydraul. Div. ASCE* **104**(September), 1269–1288 (1978)
19. Katopodes, N.D., Strelkoff, T.: *J. Eng. Mech. Div. ASCE* **105**(2), 317–334 (1979)
20. Balloffet, A., Scheffler, M.L.: Numerical analysis of the Teton Dam failure flood. *J. Hydraul. Res.* **20**(4), 317–328 (1982). <https://doi.org/10.1080/00221688209499478>
21. Ivanov, V.V., Medenikova, E.S.: *Soviet Hydrol.* **4**, 391–400 (1970)
22. Yomota, A., Nagai, A., Maruyama, T., Tejima, S.: Transactions of the Japanese society of irrigation. *Drain. Reclam. Eng.* **55**, 38–45 (1975). (in Japanese)
23. Kadoya, M., Hayase, Y.: *Drain. Reclam. Eng.* **49**, 4, 45–56 (1981). (in Japanese)
24. Chen, R.S., Pi, L.C., Huang, Y.H.: *Hydrological Proc.* **17**, 13, 2541–2553. <https://doi.org/10.1002/hyp.1266> (2003)



Assessment of Climate Change Impacts on Streamflow - A Case Study of Naryn River Basin, Central Asia

Jiansen Wu¹, Guohe Huang^{1,2(✉)}, Jing Liu¹, Li Sun¹, and Jie Sun¹

¹ School of Environmental Science and Engineering, Xiamen University of Technology,
Xiamen 361024, China
huanggg@uregina.ca

² State Key Laboratory of Water Environment Simulation, School of Environment,
Beijing Normal University, Beijing 100875, China

Abstract. This study developed an ensemble streamflow forecast modeling system (ESFMS) for long-term streamflow assessment under climate change. ESFMS consists of multiple global climate models and Soil and Water Assessment Tool (SWAT) models. ESFMS can not only reflect the uncertainty in climate scenarios, but also capture the combination of snowmelt and rainfall-streamflow processes in a simple operation. ESFMS is applied to the Naryn River Basin (in Central Asia) to analyse streamflow changes in the 21st century. The major findings are: (i) average annual streamflow of the Naryn River Basin shows an increasing trend under all conditions in the 21st century; (ii) the maximum average growth rate is $7.2 \text{ m}^3/\text{s}$ per year in May and the minimum is $0.2 \text{ m}^3/\text{s}$ per year in July; (iii) the spring streamflow change is more sensitive to climate change.

Keywords: Climate change · Naryn River · Streamflow · SWAT

1 Introduction

Climate change is one of the most discussed global changes in the 21st century, which has a significant impact on environmental change and human activities [1]. According to the Intergovernmental Panel on Climate Change (IPCC), the global average surface temperature is likely to increase by about 2°C by the end of the 21st century compared to the baseline data from 1986 to 2005 [2, 3]. Due to this, throughout the 21st century, global temperatures are expected to continue to rise and global precipitation patterns to change [4, 5]. Therefore, hydrological cycles, climatic factors and ecology are likely to change in many parts of the world in the near future.

In recent years, in order to quantitatively study the impact of climate change on streamflow, a large number of studies have been conducted [6]. For example, Chanapathi et al. (2020) assessed the impact of climate change on the streamflow of the Krishna River through changes in hydrological processes. The results showed that under RCP 4.5, surface streamflow, water production, and streamflow may increase by 50%; under

RCP 8.5, they may increase by the end of this century [7]. López-Ballesteros et al. (2020) conducted a detailed study on the characteristics of streamflow changes in Aracthos River basin. The results indicated that precipitation and streamflow would decrease, maximum and minimum temperatures would increase in the future compared with historical periods [8]. Overall, all of these studies suggest that climate change has a significant impact on streamflow.

The Naryn River is a tributary on the right bank of the Syr Darya, with a cold and arid climate. The river originates from the Tianshan glaciers, and the water flow is formed by the combined action of snowmelt and precipitation [9]. The terrain of this area is complex and the elevation is changeable, resulting in a complex and changeable climate and hydrological system. Therefore, the aim of this study is to develop an ensemble streamflow forecast modeling system (ESFMS) to assess the response of streamflow to climate change in Naryn River Basin. ESFMS integrates Global Climate model (GCM) and Soil and Water Assessment Tool (SWAT) model into one framework. ESFMS has the advantage of predicting the streamflow in the Naryn River Basin in the 21st century. Specifically, the ESFMS is able to (i) reflect uncertainty in climate models and emission scenarios; (ii) snowmelt process is not neglected in the hydrological simulation process with simple operation; and (iii) generate long-term streamflow to achieve sustainable management of water resources. The results of this study are expected to provide managers with reliable information on water resources and allow watershed planners to develop management strategies.

2 Material and Methods

In this study, ESFMS is developed and applied to the Naryn River Basin. In ESFMS, eight climate scenarios are set to extract future climate conditions (four climate scenarios and two representative concentration paths) to reflect the uncertainty of climate change and drive the SWAT model to generate future streamflow. Finally, the future streamflow is evaluated and the characteristics of the Naryn River Basin in the 21st century are pointed out.

The SWAT model is used to simulate monthly streamflow [10, 11]. The basic driving force of the model is the water balance equation as follows:

$$SW_t = SW_0 + \sum_{i=1}^t (R_{day} - Q_{surf} - E_a - W_{seep} - Q_{gw}) \quad (1)$$

where SW_t is soil water content. SW_0 , R_{day} , Q_{surf} , E_a , W_{seep} and Q_{gw} are the initial soil water content, the amount of precipitation, surface streamflow, evaporation, percolation and groundwater outflow at the time i , respectively.

There are several metrics that can be used to check the performance of the SWAT model. In this study, Nash–Sutcliffe Efficiency (NSE), Percent Bias (PBIAS), and Coefficient of Determination (R^2) were used to evaluate model performance [12]. The NSE is a normalized statistic used to determine the relative magnitude of the residual variance compared to the variance of the measured data. The NSE ranges from $-\infty$ to 1; where the higher value indicates the good performance of the model; PBIAS measures the estimation bias of a model. Positive and negative PBIAS indicate underestimation and

overestimation, respectively. The optimal value of PBIAS is 0. The value of R^2 varies between 0 and 1, where the higher value indicates the smaller error variance [13].

$$NSE = 1 - \frac{\sum_1^n (Q_i^{obs} - Q_i^{sim})^2}{\sum_1^n (Q_i^{obs} - Q_i^{mean})^2} \quad (2)$$

$$PBIAS = \frac{\sum (Q_i^{obs} - Q_i^{sim}) * 100}{\sum Q_i^{obs}} \quad (3)$$

$$R^2 = \frac{(n \sum Q_i^{obs} Q_i^{sim} - \sum Q_i^{obs} \sum Q_i^{sim})^2}{[n \sum (Q_i^{obs})^2 - (\sum Q_i^{obs})^2][n \sum (Q_i^{sim})^2 - (\sum Q_i^{sim})^2]} \quad (4)$$

where Q_i^{obs} and Q_i^{sim} is the observed and simulated streamflow, respectively.

3 Result and Discussion

In order to accurately predict the streamflow in the Naryn River Basin under a variable environment, the parameters associated with the monthly hydrological process were calibrated during 1951–1969 and validated during 1970–1974. Result shows that the NSE values are 0.80 and 0.63, PBIAS values are −3.3 and 6.5, and the values of R^2 reach 0.80 and 0.64 during calibration and validation, respectively. The results reveal the applicability of SWAT in streamflow prediction in the Naryn River Basin.

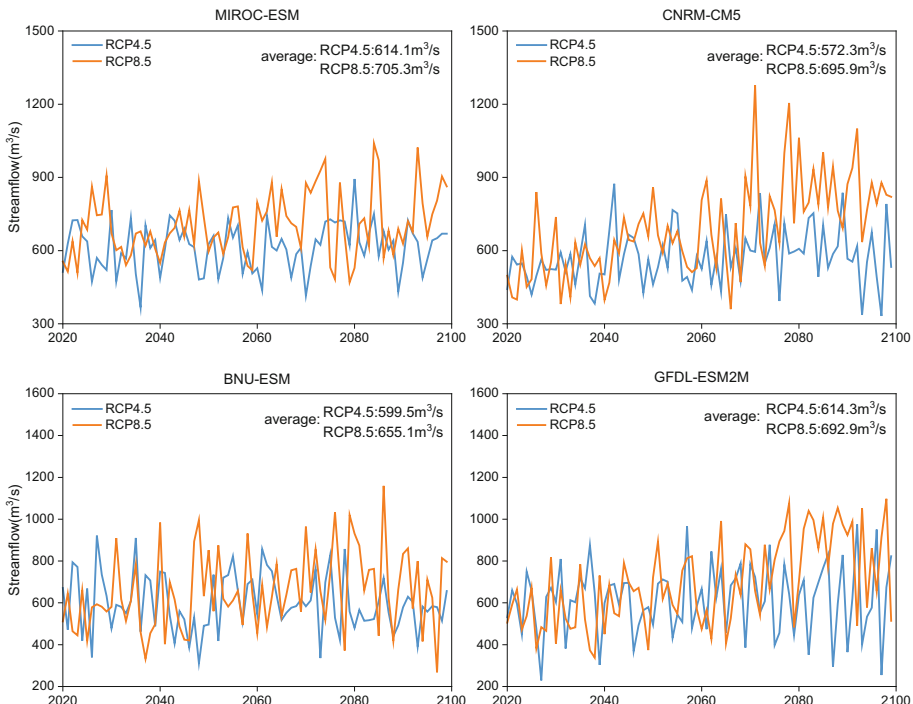


Fig. 1. Projected annual streamflow during the period 2020–2099

Figure 1 shows the projected streamflow in the Naryn River Basin from 2020 to 2099. There are some differences in eight scenarios. For example, under the MIROC-ESM model, the average streamflow of the two RCP scenarios are $614.1 \text{ m}^3/\text{s}$ (RCP4.5) and $705.3 \text{ m}^3/\text{s}$ (RCP8.5) over the period 2020–2099 respectively. Under the CNRM-CM5 model, the average annual streamflow of the two RCP scenarios are $572.3 \text{ m}^3/\text{s}$ (RCP4.5) and $695.9 \text{ m}^3/\text{s}$ (RCP8.5), respectively. Under the BNU-ESM model, the average annual streamflow of the two RCP scenarios are $599.5 \text{ m}^3/\text{s}$ (RCP4.5) and $655.1 \text{ m}^3/\text{s}$ (RCP8.5), respectively. Under the GFDL-ESM2M model, the average annual streamflow of the two RCP scenarios are $614.3 \text{ m}^3/\text{s}$ (RCP4.5) and $692.9 \text{ m}^3/\text{s}$ (RCP8.5), respectively. In general, the streamflow of RCP4.5 is less than that of RCP8.5. The streamflow of MIROC-ESM model is higher than that of other models, which is consistent with the change trend of temperature and precipitation. By comparing various scenarios, the possible streamflow range of Naryn River Basin in the future can be obtained, which avoids the error caused by single scenario prediction.

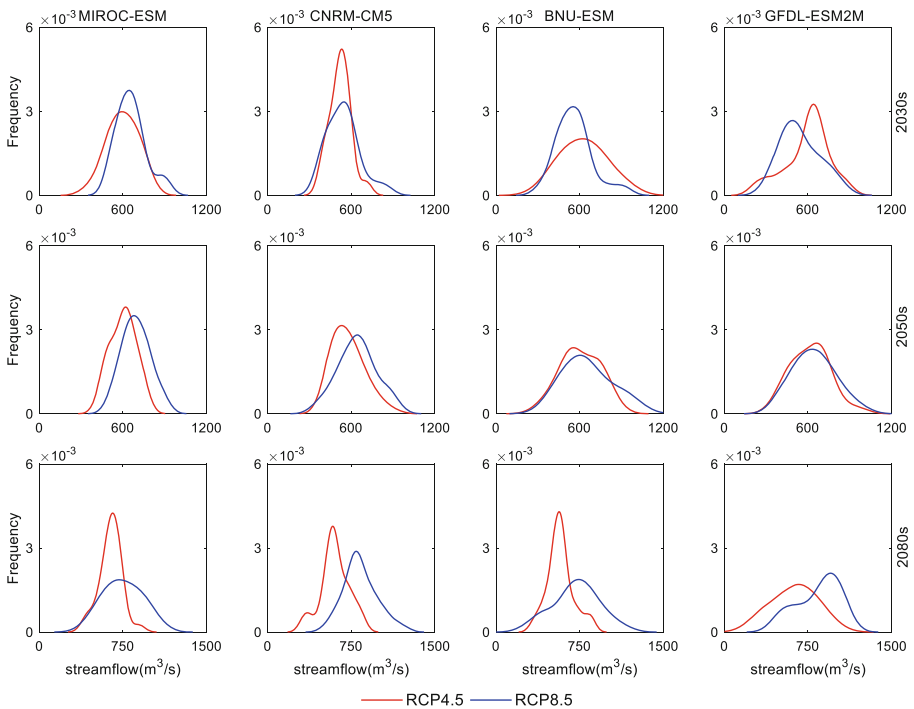


Fig. 2. Probability distributions of annual streamflow

Figure 2 shows the distribution of annual streamflow in the 2030s, 2050s and 2080s. The results manifest that the Naryn River Basin had the smallest streamflow differences in the 2030s, followed by the 2050s and 2080s. For instance, the average streamflow under CNRM-CM5 is about $530 \text{ m}^3/\text{s}$ in the 2030s, while in the 2080s, the average streamflow fluctuated between 602.9 and $853.3 \text{ m}^3/\text{s}$. This result is similar to the deviation between

precipitation and temperature. These results imply that there are uncertainties under different climate scenarios, and that they expand over time.

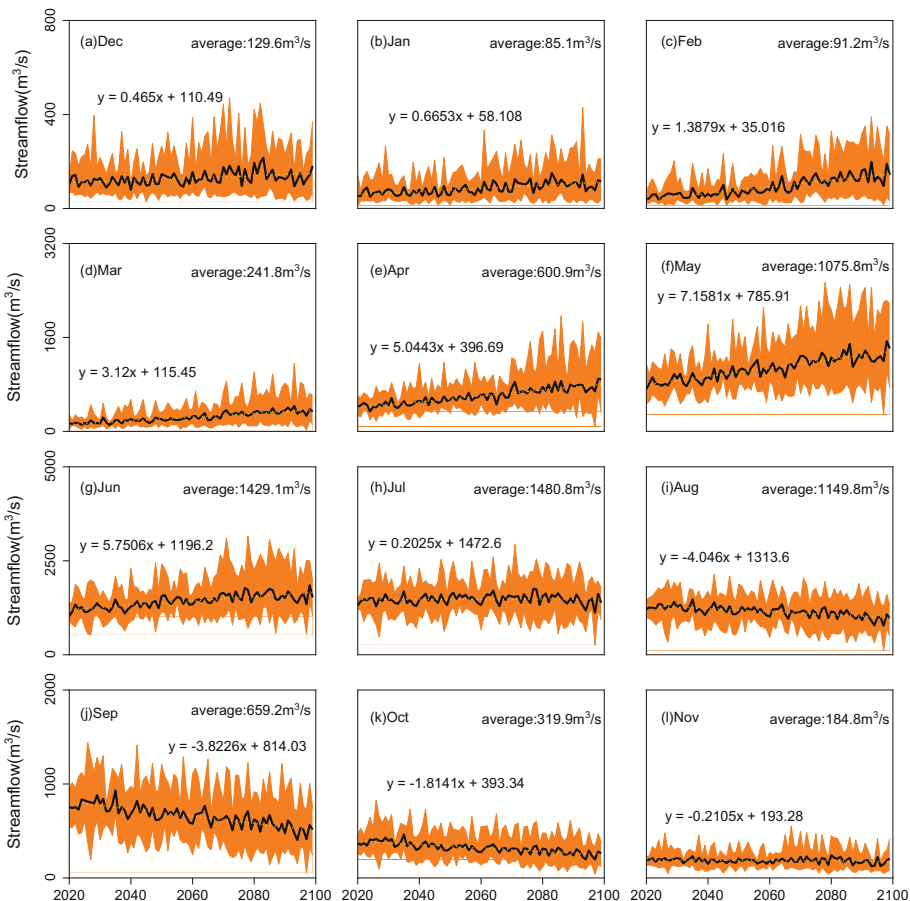


Fig. 3. Monthly streamflow during the period 2020–2099

Figure 3 depicts the change of streamflow in different months. The average annual monthly streamflow was the lowest in January ($85.1 \text{ m}^3/\text{s}$) and the highest in July ($1480.8 \text{ m}^3/\text{s}$). In addition, the total streamflow in winter, spring and summer showed an increasing trend. The largest increase is $7.2 \text{ m}^3/\text{s}$ in May and the smallest increase is $0.2 \text{ m}^3/\text{s}$ in July. On the whole, the streamflow in winter and spring showed a high increasing trend, while the streamflow in autumn shows a decreasing trend, indicating that the annual streamflow increases mainly came from winter and spring. The variation of streamflow in October and November is small. This not only indicates the accuracy of climate prediction of autumn streamflow, but also indicates that the response of autumn streamflow to climate change is relatively stable. However, the results suggest that the spring show significant differences between the different scenarios. For example, in May,

the annual mean of the minimum forecast streamflow for all scenarios is $723.1 \text{ m}^3/\text{s}$, while the annual mean of the maximum forecast streamflow is $1536.8 \text{ m}^3/\text{s}$, a difference of 113%. It is possible that due to the complexity of streamflow formation, streamflow generation in spring is more sensitive to climate change. Snowmelt streamflow is more complex than precipitation streamflow because of the comprehensive influence of snow depth and temperature. Therefore, there are great uncertainties in the interpretation of snowmelt streamflow under different climate scenarios.

4 Conclusions

In this study, ESFMS has been developed to assess the streamflow of the Naryn River Basin. ESFMS consists of a variety of GCMs and SWAT models. ESFMS not only reflects the uncertainty of climate change, but also reflects a series of impacts of climate change on streamflow. The integrated model can effectively simulate the streamflow process through snow melt and precipitation with simple operation.

Some major findings can be summarized as follows: (i) the streamflow would increase in the future, ranging from $572.3 \text{ m}^3/\text{s}$ to $705.3 \text{ m}^3/\text{s}$; (ii) the maximum average growth rate in spring is $7.2 \text{ m}^3/\text{s}$, and the minimum average growth rate in July is $0.2 \text{ m}^3/\text{s}$; (iii) the annual streamflow increment mainly comes from spring; (iv) the autumn streamflow is relatively stable in response to climate change, while the spring streamflow is more sensitive to climate change. Based on the above results, the precipitation, temperature and streamflow of the Naryn River Basin from 2020 to 2099 are determined, which is beneficial to local water resources management and provides a basis for decision makers. Nevertheless, there are still some limitations to this study. For example, land-use is also an important factor affecting streamflow, and this paper only considers the impact of climate change on streamflow. That may not be enough to provide a more accurate forecast. Therefore, the impacts of climate change and land-use on streamflow should be combined in future studies.

Acknowledgements. This research was supported by the Strategic Priority Research Program of Chinese Academy of Sciences (XDA20060302) and the National Key Research & Development Project of China (2016YFC0502803).

References

1. Sun, J., Li, Y.P., Zhuang, X.W., Jin, S.W., Huang, G.H., Feng, R.F.: Identifying water resources management strategies in adaptation to climate change under uncertainty. *Mitig. Adapt. Strat. Glob. Change* **23**(4), 553–578 (2017). <https://doi.org/10.1007/s11027-017-9749-9>
2. Zhao, Q.D., et al.: Projecting climate change impacts on hydrological processes on the Tibetan Plateau with model calibration against the glacier inventory data and observed streamflow. *J. Hydrol.* **573**, 60–81 (2019)
3. Khan, G., Chen, X., Bao, A., Wang, Y., Meng, F.H.: Hydrological modeling of the Upper Indus Basin: a case study from a high-altitude glacierized Catchment Hunza. *Water* **9**(1), 0017 (2017)

4. Azhoni, A., Holman, I., Jude, S.: Contextual and interdependent causes of climate change adaptation barriers: insights from water management institutions in Himachal Pradesh, India. *Sci. Total Environ.* **576**, 817–828 (2017)
5. Dittes, B., Kaiser, M., Špačková, O., Rieger, W., Disse, M., Straub, D.: Risk-based flood protection planning under climate change and modeling uncertainty: a pre-alpine case study. *Nat. Hazards Earth Syst. Sci.* **18**(5), 1327–1347 (2018)
6. Bhatta, B., Shrestha, S., Shrestha, P.K., Talchhabadel, R.: Evaluation and application of a SWAT model to assess the climate change impact on the hydrology of the Himalayan River. *CATENA* **181**, P104082 (2019)
7. Tirupathi, C., Shashidhar, T.: Investigating the impact of climate and land-use land cover changes on hydrological predictions over the Krishna River basin under present and future scenarios. *Sci. Total Environ.* **721**(10), 137736 (2020)
8. López-Ballesteros, A., Senent-Aparicio, J., Martínez, C., Pérez-Sánchez, J.: Assessment of future hydrologic alteration due to climate change in the Aracthos River basin (NW Greece). *Sci. Total Environ.* **733**, 139299 (2020)
9. Gan, R., Luo, Y., Zuo, Q., Sun, L.: Effects of projected climate change on the glacier and runoff generation in the Naryn River Basin, Central Asia. *J. Hydrol.* **523**(523), 240–251 (2015)
10. Arnold, J.G., Fohrer, N.: SWAT2000: current capabilities and research opportunities in applied watershed modelling. *Hydrol. Process.* **19**(3), 563–572 (2005)
11. Ficklin, D.L., Stewart, I.T., Maurer, E.P.: Effects of projected climate change on the hydrology in the Mono Lake Basin, California. *Clim. Change* **116**(1), 111–131 (2013)
12. Luo, Y., Arnoldb, J., Liu, S.Y., Wang, X.Y., Chen, X.: Inclusion of glacier processes for distributed hydrological modeling at basin scale with application to a watershed in Tianshan Mountains, Northwest China. *J. Hydrol.* **477**, 72–85 (2013)
13. Neitsch, S.L., Arnold, J.G., Kiniry, J.R., Williams, J.R.: Soil water assessment tool theoretical document, version 2005. Grassland, Soil and Water Research Laboratory, Agricultural Research Service, 808 East Blackland Road, Temple, Texas, 76502 (2005)



Joint-Risk Evaluation of Extreme Precipitation Using Copulas

L. Sun¹, J. Sun^{2(✉)}, and Y. P. Li³

¹ School of Environmental Science and Engineering, Xiamen University of Technology, Xiamen 361024, China

² Nanjing Institute of Environmental Science, Ministry of Ecology and Environment of the People's Republic of China, Nanjing 210042, China
sunj220@163.com

³ Environment and Energy Systems Engineering Research Center, School of Environment, Beijing Normal University, Beijing 100875, China

Abstract. Effective identification of extreme precipitation characteristics can help urban storm management. In this study, maximum consecutive 5-day precipitation (RX5D), annual count of days when precipitation is higher than 30 mm (R30), and annual total extreme precipitation (R95p) are selected for reflecting extreme precipitation characterise. Copula method is developed for investigating the dependence relationships between these indices. Take Xiamen Island as a case study, where is a coastal city with intense precipitation in rainy season. Results show that R95p will significantly increase with an average rate of 4.3 mm/year, making 91.5% of contribution to the total precipitation increment. In the 10-year return period level, the R95p is larger than 785 mm accompanied with RX5D larger than 311 mm and R30 larger than 15.6 days. Such results can help managers decide the flood control infrastructure design parameters.

Keywords: Copula · Extreme precipitation · Joint risk

1 Introduction

Changes in extreme precipitation could bring direct and indirect negative impacts on human health and socioeconomic development [1, 2]. Especially, in coastal city of Southern China (e.g., Xiamen, Shenzhen, and Guangzhou), extreme precipitation often occurs accompanied with intense precipitation amount and frequency, leading to urban storm and other secondary disasters. For effectively management urban storm and mitigation extreme precipitation risk, it is very valuable to address the rules of extreme precipitation [3]. Previously, some methods (e.g., Mann-Kendall trend test and thresholds of absolute and percentile) were developed for quantifying the trends of extreme precipitation characteristics [4–6]. These approaches can capture the trends of single extreme precipitation index; however, they are subjective and cannot quantitatively the correlated features of different extreme precipitation indices. Therefore, it is necessary to develop robust method to explore the relationship between two indices, and evaluate their individual and joint risks. Copula, as a powerful statistical analysis method, has been widely

used to assess the joint probabilistic behaviours of hydrometeorological features [3, 7]. Besides, copula methods can accurately assess the severity of the extreme precipitation event under a large joint recurrence period, which is beneficial for designing urban storm management infrastructures.

Xiamen, as a coastal city, is located in Southeast China. Xiamen has a monsoonal humid subtropical climate with annual rainfall is 1,350 mm. Due to climate change, disastrous weather, such as rainstorm, typhoon and high temperature, occurs occasionally [8]. With the implementation of “sponge city” in Xiamen, stormwater infrastructure (i.e., low impact development facilities) are widely developed, which has a target to capture rate of about 80% of annual precipitation [9]. It is necessary to explore the changes of local precipitation, especially the extreme values. Such assessment is helpful for provide support for stormwater infrastructure design. Therefore, the objective of this paper is to analyze the changes of extreme precipitation and associated interactions in Xiamen island. The changing trend of extreme precipitation indices and joint return periods are expected to support local sponge city construction.

2 Methodology

2.1 Indicator Selection and Calculation

Considering the fact that Xiamen is a coastal city with intense precipitation in rainy season, three indicators that can reflect the heavy rainfall are selected. They are maximum consecutive 5-day precipitation (RX5D, mm), annual count of days when precipitation us higher than 30 mm (R30, days) and annual total extreme precipitation (rainfall amount is higher than >95th percentile, R95p, mm). In addition, annual total precipitation (PRCP-TOT, mm) is also chosen for exploring the changing trends of local precipitation in the past 60 years, which can reflect the degree of climate humidity. In this study, daily precipitation data of Xiamen station from 1960–2019 are calculated and their temporal distribution of extreme precipitation indices are analyzed with RClimDex model [10].

2.2 Bivariate Copula Functions

Copula functions are considered to build time-interdependence relationships between different precipitation indicators [11]. According to the theory of copula functions, the joint probability distributions of two correlated random variables can be expressed as:

$$F(x, y) = C(F_X(x), F_Y(y)) \quad (1)$$

where $u = F_X(x)$ and $v = F_Y(y)$ are continuous marginal cumulative distributions functions (CDF) of random variables X and Y. x and y are the values of random variables X and Y. $C(u, v)$ is the copula function that can be written as [12]:

$$C(u, v) = F(F_X^{-1}(u), F_Y^{-1}(v)) \quad (2)$$

The conditional cumulative distribution of X ($X \leq x$) under given variable Y can be derived as

$$F_{X \leq x|Y=y}(x, y) = \frac{\partial C(u, v)}{\partial v} \quad (3)$$

According to the fitted optimal copula, the conditional probability density function (PDF) of X ($X \leq x$) under $Y = y$ can express as:

$$f_{X|Y}(x|y) = c(f_Y(y), f_X(x)) \cdot f_X(x) \quad (4)$$

where $c()$ represents the PDF of the copula function with marginal probability density distributions $f_X(x)$ and $f_Y(y)$, respectively. There are many copula families can be applied in practical bivariate analysis. In this study, six copulas (e.g., Gaussian, Clayton, Frank, Gumbel, Liner-spearman and Tawn) are adopted due to their capabilities of capturing various kinds of dependence structures [13]. Parameters of root mean square error (RMSE), determinant coefficient (R^2) and Akaike information criterion (AIC) are used for testing and selecting the best fitted copula functions for modeling the dependence structure of extreme precipitation characteristics [7].

2.3 Return Period

Return period (RP) of extreme precipitation event is a basic criterion for design of urban storm-runoff infrastructure, and provides a simple means of storm risk analysis. Once the marginal distributions are fitted for the extreme precipitation indicators, the risk of extreme precipitation indices can be quantitatively assessed based on the univariate RP. The RP of a single extreme precipitation index is described as the time between two consecutive events [3]:

$$T_1 = \frac{1}{1 - F_X(x)}, \quad T_2 = \frac{1}{F_X(x)} \quad (5)$$

T_1 (T_2) represents the RP of precipitation indicator with value greater (less) than or equal to a certain value of x . In bivariate extreme precipitation analysis, the joint return periods when both X and Y exceed the specific values (i.e., $X > x$ and $Y > y$) can be calculated as [14]:

$$T\{X > x, Y > y\} = \frac{1}{P(X > x, Y > y)} = \frac{1}{1 - u - v + C(u, v)} \quad (6)$$

3 Result and Discussion

Figure 1 shows the variation trends of extreme precipitation during 1960–2019 of Xiamen island. Increasing trends are found among the four indices. In detail, the total precipitation will significantly ($p < 0.05$) increase with an average rate of 4.7 mm/year; R95p will significantly increase with an average rate of 4.3 mm/year; RX5D will increase with an average rate of 0.9 mm/year; and R30 will significantly increase with a rate of 0.05 day/year. Such results show that Xiamen is facing with intensifying extreme precipitation events. Results also show that the amount of extreme heavy precipitation (R95p) makes a great contribution to the total precipitation increment (accounting about 91.5%), revealing that rainstorms would become frequent and intense.

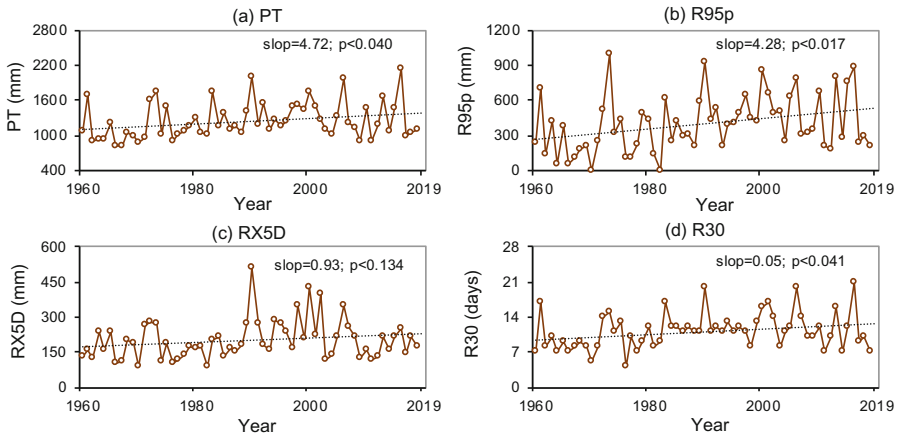


Fig. 1. Trends of extreme indices during 1960–2019

Figure 2 presents the cumulative probability distributions and return period curves of three extreme precipitation indices. In this study, the marginal distributions for three extreme precipitation indices (i.e. R95p, RX5D and R30) are modelled based on eight parametric probabilistic distributions (i.e. Gaussian, log-Normal, Gamma, Generalized Extreme value, Gumbel, Pearson type III, Weibull, and Generalized Pareto distribution). Results show that the best distributions for R95p, RX5D and R30 are Generalized Pareto, Gaussian and Gamma, respectively. According to the Eq. (5), the relationships between return period and extreme values are modelled in Fig. 2b. Results indicate that when the

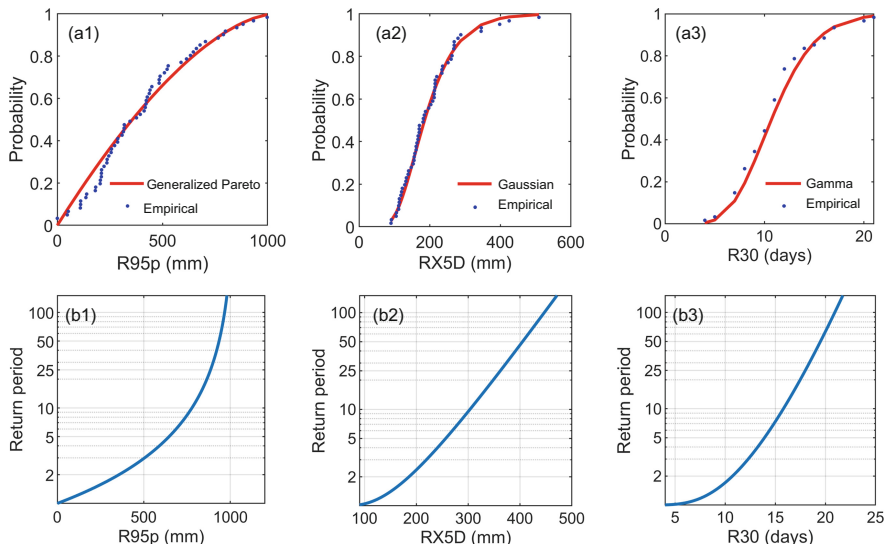


Fig. 2. (a) Cumulative Probability distributions and (b) return period curves of three extreme precipitation indices

period is about 10 years, the values of R95p, RX5D and R30 are 785 mm, 311 mm, and 15.6 days, respectively. In the past 60 years, about 6–8 years have exceed these values. About 50% of years are within the values of 2-year return period.

Table 1. Joint distribution simulation performances under different copulas

Copula	R95p-RX5D			R30-R95p			R30-RX5D		
	RMSE	NSE	AIC	RMSE	NSE	AIC	RMSE	NSE	AIC
Gaussian	0.132	0.998	-321.6	0.089	0.998	-383.5	0.096	0.998	-372.4
Clayton	0.111	0.988	-348.9	0.238	0.988	-227.0	0.167	0.993	-283.7
Frank	0.157	0.998	-292.9	0.103	0.997	-360.7	0.115	0.997	-343.6
Gumbel	0.183	0.998	-268.9	0.094	0.998	-375.8	0.124	0.996	-330.5
Liner-spearman	0.157	0.996	-293.3	0.138	0.996	-313.5	0.135	0.995	-317.6
Tawn	0.162	0.999	-288.1	0.080	0.997	-401.5	0.098	0.998	-368.2

The dependence relationships of extreme precipitation indices are modelled through six copula functions (as seen in Table 1). According to simulation results (i.e., RMSE, NSE and AIC), the best copula functions that can effectively model the dependences of R95p-RX5D, R30-R95p and R30-RX5D are Clayton, Tawn and Gaussian, respectively. Then, the joint cumulative probability distributions of these indices are presented in Fig. 3a, which reflects the probability of $X > x$ and $Y > y$. For example, the cumulative probability of $R95p > 355$ mm and $RX5D > 177$ mm is 0.5; the cumulative probability of $R95p > 471$ mm and $R30 > 12.7$ mm is 0.3. Such probability can help quantify the flood risk of Xiamen island. The joint return period of two combined indices (labelled as $T_{\{X, Y\}}$) is calculated according to Eq. (6), which reflects the joint risk of simultaneous occurrence of different precipitation extremes. For instance, $T_{\{R95p, RX5D\}}$ indicates return period pf a strong precipitation event with the precipitation amount and precipitation duration exceed their specific thresholds. As shown in Fig. 3b, each index gradually tends to be less likely to occur along the direction of increasing joint return period, meaning that the return period of single variable in this direction also gradually increases. Take the 10-year joint return period as an example, the values of R95p and RX5D in the combined event $\{R95p, RX5D\}$ are larger than 785 mm and 311 mm. Such results can help managers decide design return period during flood risk mitigation management.

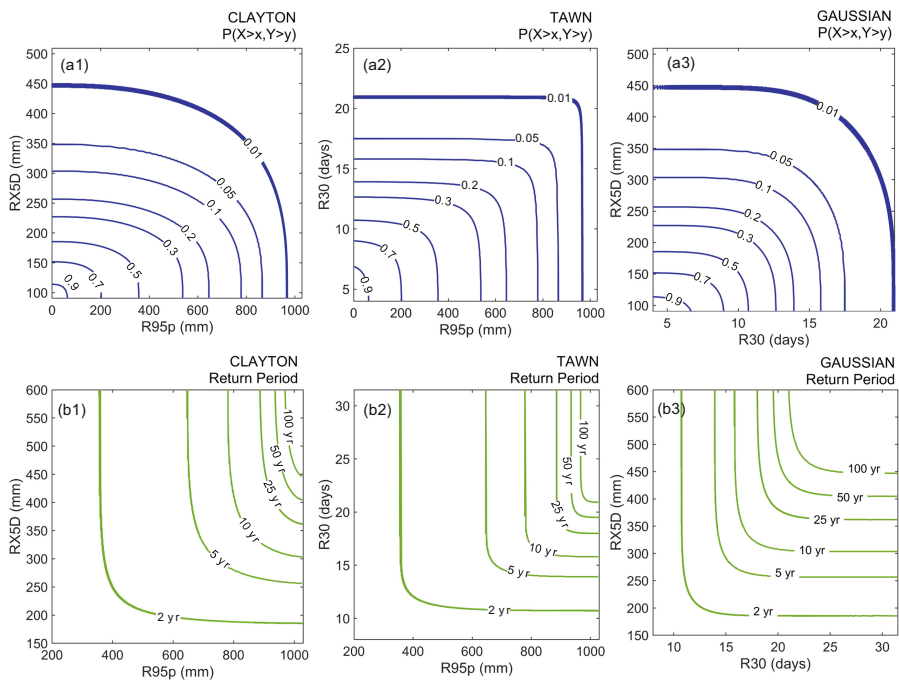


Fig. 3. (a) Joint cumulative probability distributions and (b) Joint return period curves of combined indices

4 Conclusions

In this study, copula method is developed for identifying the characterise of extreme precipitation and associated dependence relationships. The method is applied to Xiamen Island, where is a coastal city with intense precipitation in rainy season. According to the past 60-year daily precipitation from 1960 to 2019, the trends and probability characteristics of the extreme precipitation indices (i.e., R95p, RX5D, and R30) are analyzed. Then, copula functions of different combinations of precipitation indexes are established for quantifying the joint risk of extreme precipitation indices. Results show that Xiamen is facing with intensifying extreme precipitation events; the amount of extreme heavy precipitation (R95p) will significantly increase with an average rate of 4.3 mm/year, making about 91.5% of contribution to the total precipitation increment. According to the simulation performances of (RMSE, R^2 and AIC), the copula functions that most fitted for R95p-RX5D, R95p-R30, and R30-RX5D are Clayton, Tawn and Gaussian, respectively. The joint return period of two combined indices can reflect the joint risk of simultaneous occurrence of different precipitation extremes. Accordingly, the results of 10-year return period level indicate that the R95p is larger than 785 mm accompanied with RX5D larger than 311 mm and R30 larger than 15.6 days. Such results can help managers decide the flood control infrastructure design parameters.

Acknowledgments. This research is supported by Young and Middle-aged Teachers Education Research Project of Fujian Province (JAT190650).

References

1. Tramblay, Y., Somot, S.: Future evolution of extreme precipitation in the Mediterranean. *Clim. Change* **151**(2), 289–302 (2018)
2. Kim, I.-W., Oh, J., Woo, S., Kripalani, R.H.: Evaluation of precipitation extremes over the Asian domain: observation and modelling studies. *Clim. Dyn.* **52**(3–4), 1317–1342 (2018)
3. Sun, C.X., Huang, G.H., Fan, Y.: Multi-indicator evaluation for extreme precipitation events in the past 60 years over the Loess plateau. *Water* **12**, 193 (2020)
4. Santos, M., Fragoso, M.: Precipitation variability in Northern Portugal: data homogeneity assessment and trends in extreme precipitation indices. *Atmos. Res.* **131**, 34–45 (2013)
5. Zilli, M.T., Carvalho, L.M.V., Liebmann, B., Dias, M.A.S.: A comprehensive analysis of trends in extreme precipitation over southeastern coast of Brazil. *Int. J. Climatol.* **37**(5), 2269–2279 (2017)
6. Shawul, A.A., Chakma, S.: Trend of extreme precipitation indices and analysis of long-term climate variability in the Upper Awash basin, Ethiopia. *Theoret. Appl. Climatol.* **140**, 635–652 (2020)
7. Liu, Y.R., Li, Y.P., Ma, Y., Jia, Q.M., Su, Y.Y.: Development of a Bayesian-copula-based frequency analysis method for hydrological risk assessment - The Naryn River in Central Asia. *J. Hydrol.* **58**, 124349 (2020)
8. Lin, T., Cao, X., Huang, N., Xu, L.L., Li, X.H., Zha, Y., Lin, J.Y.: Social cognition of climate change in coastal community: a case study in Xiamen City, China. *Ocean Coast. Manage.* **207**, 104429 (2021)
9. Randall, M., Sun, F.B., Zhang, Y.Y., Jensen, M.B.: Evaluating sponge city volume capture ratio at the catchment scale using SWMM. *J. Environ. Manage.* **246**(15), 745–757 (2019)
10. Sein, K.K., Chidthaisong, A., Oo, K.L.: Observed trends and changes in temperature and precipitation extreme indices over Myanmar. *Atmosphere* **9**(12), 477 (2018)
11. Sadegh, M., Ragno, E., AghaKouchak, A.: Multivariate Copula Analysis Toolbox (MvCAT): describing dependence and underlying uncertainty using a Bayesian framework. *Water Resour. Res.* **53**, 5166–5183 (2017)
12. Hochrainer-Stigler, S., Balkovič, J., Silm, K., Timonina-Farkas, A.: Large scale extreme risk assessment using Copulas: an application to drought events under climate change for Austria. *Comput. Manage. Sci.* **16**(4), 651–669 (2019)
13. Jhong, B.C., Tung, C.P.: Evaluating future joint probability of precipitation extremes with a Copula-based assessing approach in climate change. *Water Resour. Manage.* **32**, 4253–4274 (2018)
14. Assani, A., Guerfi, N.: Analysis of the joint link between extreme temperatures, precipitation and climate indices in winter in the three hydroclimate regions of Southern Quebec. *Atmosphere* **8**(4), 75 (2017)



Optimal Allocation of Flood Control Capacity of Multiple Reservoir System

Hongya Qiu^{1,2}, Jianzhong Zhou^{1,2(✉)}, Lu Chen^{1,2(✉)}, and Yuxin Zhu^{1,2}

¹ School of Civil and Hydraulic Engineering, Huazhong University of Science and Technology,
Wuhan 430074, China
chen_lu@hust.edu.cn

² Hubei Key Laboratory of Digital Valley Science and Technology, Wuhan 430074, China

Abstract. Reasonable allocation of flood control capacity is associated with flood control safety, which is very important. A model for the optimal operation of multiple reservoir system considering the reserve demand of flood control capacity is proposed in this paper. The model takes into account the complex equality and inequality constraints during optimal operation process. The dynamic programming-progressive optimality algorithm (DP-POA) is adopted to solve the proposed optimal operation model. The multiple hydropower reservoirs in the lower reaches of Jinsha River in the upper Yangtze River in China is selected as a case study. The results show that DP-POA can fully take advantage of the flood control capacity such that the reserve demand of flood control storage is met in certain periods. In addition, the multiple hydropower reservoirs cooperates with each other to maximize the hydropower generation under the condition of reserve flood control capacity. The calculated total reserve flood control storage exceeds the preset values $35 \times 10^8 \text{ m}^3$, and the maximum hydropower generation of multiple reservoir system is $507.27 \times 10^8 \text{ kWh}$. Thus, this paper provides a novel optimization strategy for the optimal allocation of multiple hydropower reservoirs.

Keywords: Multiple reservoir system · Flood control capacity · Optimal allocation · Hydropower generation · Optimization strategy

1 Introduction

Flood is the most common natural disaster in China, and its impact is one of the most significant disasters in the world [1]. In order to reduce flood disaster loss, various countries have creatively adopted some flood control measures, mainly including engineering measures and non-engineering measures [2]. In the past decades, many flood control projects have been built to improve flood control standards and reduce the chance of suffering from flood disasters. However, flood is still one of the major threats to human nature today [3]. At the same time, with the continuous development of economy and increasing social wealth, the economic loss from flood disaster will be greater and greater. To solve this problem, the reasonable regulation policy of flood control capacity obtained by the optimal operation of multiple reservoir system to achieve flood control safety is of great significance.

In recent years, scholars at home and abroad have done a lot of in-depth research on optimal operation of reservoir for flood control and obtained some important research results. Multi-objective hierarchy optimization operation model was proposed for optimal operation of complex multiple reservoir system [4]. The research findings obtained indicate that the designed model can reduce flood disaster loss in the case of ensuring safe discharge capacity in river channels. The multi-purpose reservoirs with navigation, hydropower, water supply, flood control and other functions were taken as research object to study the flood control policies [5]. The results obtained show that the proposed method can fully take advantage of flood control storage of multiple reservoir system to reduce flood peak occurred at downstream flood control points. Two improved algorithms were designed and applied to the Danjiangkou Reservoir in China [6]. The results demonstrate that the proposed method is suitable to different flood scenarios and can obtain reasonable optimal operation policies.

However, these research findings were mainly concentrated in the utilization of flood control capacity to make the maximum flood regulation level minimum or the maximum discharge minimum, ignoring the specified reserve demand of flood control capacity over the operation process. It is well known that major floods always last for a long time and present multi-peak characteristics, and the reservoir usually needs to reserve a certain amount of storage to tackle large floods that may occur at any time in the future. To deal with the subsequent flood peak or intercept the subsequent flood volume, certain flood control capacity should be reserved to guarantee downstream flood control safety. Literature review indicates that there are no studies considering reserve demand of flood control capacity in certain periods during optimal flood control operation.

To refill this gap, this paper innovatively integrates the reserve demand of flood control capacity to the optimal operation process, and the model is solved by dynamic programming-progressive optimality algorithm (DP-POA). Finally, the jointly operation policy of flood control considering reserving demand of flood control capacity in certain periods is obtained and discussed.

2 Method

2.1 Optimization Model of Multiple Reservoir System

The flood control system in a large river basin often consists of more than one reservoirs, forming a multiple reservoir system. In this study, for the hydropower reservoirs designed primarily to focus on hydropower generation while considering flood control, the objective function is the maximum hydropower generation, while the reserve demand of flood control capacity in certain periods is transformed into constraints.

Objective Function. In order to give full play to the potential of flood resources and exploit flood resources in flood season, maximizing the hydropower generation is the objective function, as shown below:

$$\begin{cases} E = \max \sum_{i=1}^N \sum_{t=1}^T (P_{i,t} \Delta t - Violation_t) \\ P_{i,t} = k_i H_{i,t} Q_{i,t} \end{cases} \quad (1)$$

where E denotes total hydropower generation produced during operation periods; $P_{i,t}$, $k_{i,t}$, $H_{i,t}$ and $Q_{i,t}$ denote the power output, power production coefficient, water head and turbine discharge of reservoir i at period t , respectively. Δt denotes the length of operation period. It is noteworthy that the penalty method is used to punish the period that does not meet the reserve requirements, and $Violation_t$ denotes the violation value of reserve flood control capacity of multiple reservoir system at period t .

Constraints. Optimal operation of reservoirs has a series of equality and inequality constraints. It has the characteristics of nonlinear, discreteness, dynamic and so on. The equality and inequality constraints are summarized below:

(1) Water balance equations

$$\begin{cases} V_{i,t+1} = V_{i,t} + (I_{i,t} - Q_{i,t}^{total}) \\ I_{i,t} = q_{i,t} + \sum_{j=1}^{N_i} O_{j,t} \\ O_{i,t} = Q_{i,t}^s + Q_{i,t} \end{cases} \quad (2)$$

where $V_{i,t}$, $I_{i,t}$, $Q_{i,t}^{total}$, $q_{i,t}$, $Q_{i,t}^s$ denote the storage volume, inflow, outflow, local inflow, water spillage of reservoir i at period t , respectively; N_i denotes the number of upstream reservoirs with direct connection to the reservoir i .

(2) Water head equations

$$H_{i,t} = \frac{1}{2}(Z_{i,t} + Z_{i,t} - 1) - Z_{i,t}^d \quad (3)$$

where $Z_{i,t}$ and $Z_{i,t}^d$ denote the forebay water level and downstream water level of reservoir i at period t , respectively.

(3) Forebay water level limits

$$Z_{i,t}^{\min} \leq Z_{i,t} \leq Z_{i,t}^{\max} \quad (4)$$

where $Z_{i,t}^{\min}$ and $Z_{i,t}^{\max}$ denote the minimum and maximum forebay water levels of reservoir i at period t , respectively.

(4) Forebay water level fluctuation limits

$$|Z_{i,t} - Z_{i,t-1}| \leq \Delta Z_i^{\max} \quad (5)$$

where ΔZ_i^{\max} denotes the acceptable maximum fluctuation of forebay water level of reservoir i .

(5) Turbine discharge limits

$$Q_{i,t}^{\min} \leq Q_{i,t} \leq \min(Q_{i,t}^{\max}, Q_{i,t}^c) \quad (6)$$

where $Q_{i,t}^{\min}$, $Q_{i,t}^{\max}$ and $Q_{i,t}^c$ denote the minimum and maximum turbine discharges as well as reservoir discharge capacity of reservoir i at period t , respectively.

(6) Total discharge limits

$$Q_{i,t}^{\text{total,min}} \leq Q_{i,t}^{\text{total}} \leq Q_{i,t}^{\text{total,max}} \quad (7)$$

where $Q_{i,t}^{\text{total,min}}$ and $Q_{i,t}^{\text{total,max}}$ denote the minimum and maximum total discharges of reservoir i at period t , respectively.

(7) Power output limits

$$P_{i,t}^{\min} \leq P_{i,t} \leq \min(P_{i,t}^{\max}, P_{i,t}^e) \quad (8)$$

where $P_{i,t}^{\min}$, $P_{i,t}^{\max}$ and $P_{i,t}^e$ denote the minimum and maximum power outputs as well as expected power outputs of reservoir i at period t , respectively.

(8) Total power output limits

$$P_t^{\text{total,min}} \leq \sum_{i=1}^N P_{i,t} \leq P_t^{\text{total,max}} \quad (9)$$

where $P_t^{\text{total,min}}$ and $P_t^{\text{total,max}}$ denote the minimum and maximum total power outputs of multiple hydropower reservoirs at period t .

(9) Initial and final forebay water level limits

$$\begin{cases} Z_{i,0} = Z_i^{\text{initial}} \\ Z_{i,T} = Z_i^{\text{target}} \end{cases} \quad (10)$$

where Z_i^{initial} and Z_i^{target} denote the preset initial and target forebay water levels of reservoir i at period 0 and T , respectively.

(10) Nonlinear characteristic curves limits

$$\begin{cases} V_{i,t} = f_{i,1}(Z_{i,t}) \\ Q_{i,t}^c = f_{i,2}(Z_{i,t-1}) \\ Z_{i,t}^d = f_{i,3}(Q_{i,t}^{\text{total}}) \\ P_{i,t}^e = f_{i,4}(H_{i,t}, Q_{i,t}) \end{cases} \quad (11)$$

where $f_{i,1}(\cdot)$, $f_{i,2}(\cdot)$, $f_{i,3}(\cdot)$ and $f_{i,4}(\cdot)$ denote the nonlinear stage-storage curve, stage-discharge capacity curve, stage-downstream water level curve and stage-discharge-head-output curve of reservoir i , respectively.

(11) Reserve flood control capacity limits

$$\sum_{i=1}^N V_{i,t}^{\text{reserve}} \geq V_t^{\text{target}} \quad (12)$$

where $V_{i,t}^{\text{reserve}}$ denotes the reserve flood control capacity of reservoir i at period t ; V_t^{total} denotes target reserve flood storage of multiple hydropower reservoirs.

2.2 Optimization Methods

Optimal operation of reservoirs is a typical dynamic and nonlinear optimization problem with multiple constraints. In this study, the dynamic programming-progressive optimality algorithm (DP-POA) is adopted to solve the optimal operation model to achieve optimal allocation of flood control capacity for multiple reservoir system. The dynamic programming (DP) method [7] is commonly used in optimal operation of reservoirs, while facing the problem of ‘curse of dimensionality’, limiting its optimization ability for multiple reservoir system. To tackle this difficulties, the multistage optimization model is divided into multiple two-stage optimization sub models by the POA to alleviate the curse of dimensionality.

However, the optimization results obtained by POA are sensitive to the initial operation line, affecting the convergence ability of the overall optimal solution [8]. Therefore, the DP-POA is often applied to overcome the drawback. This paper adopts DP-POA to solve the above established optimization model of multiple reservoir system, and the detail implementation steps can be found in the original paper.

3 Study Area and Data

Jinsha River originates from Tuotuo River. It locates at the upper reaches of the Yangtze River. The catchment area of Jinsha River is about 5.02 hundred thousand km², accounting for about 26% of the whole Yangtze River Basin. Its average annual flow is 4750 m³/s. Jinsha River has a drop of 3300 m, which is rich in hydropower resources. Especially, the Wudongde Reservoir (WDD), Baihetan Reservoir (BHT), Xiluodu Reservoir (XLD), and Xiangjiaba Reservoir (XJB) are four cascade reservoirs located at the lower reaches of Jinsha River. They are all hydropower reservoirs whose main functions are for hydropower generation. Meanwhile, they also have flood control task in flood season, that is, to cooperate with Three Gorge Reservoir (TGR) for the flood control safety of downstream Jingjiang section and Chenglingji section.

The actual inflow sequence from July 1 to September 30 in 2019 is used as the input data of the established optimization model of multiple reservoir system. The reserve flood capacity of WDD, XLD, and XJB from July 11 to August 31 is set to 35×10^8 m³. The installed capacity of WDD, BHT, XLD, and XJB are 10.2 million kW, 16 million kW, 13.86 million kW, and 7.76 million kW, respectively. The initial water levels of WDD, BHT, XLD, and XJB cascade reservoirs are set to 952 m, 775 m, 560 m, and 370 m. And the end water levels of WDD, BHT, XLD, and XJB are set to 975 m, 800 m, 600 m, and 380 m. The daily rises of water level of four cascade reservoirs are set to 2, 2, 3, and 4 m. And the daily drops of water level of four cascade reservoirs are set to 1, 0, 3, and 4 m. The minimum outflows of WDD, BHT, XLD, and XJB are 1160, 1260, 1500, and 1700 m³/s. The maximum outflows of WDD, BHT, XLD, and XJB are set to 15000, 15000, 28000, and 28000 m³/s.

4 Results and Discussion

The DP-POA is applied to solve the above established optimal operation model. Figure 1 shows water level process with corresponding fluctuations, respectively, indicating that

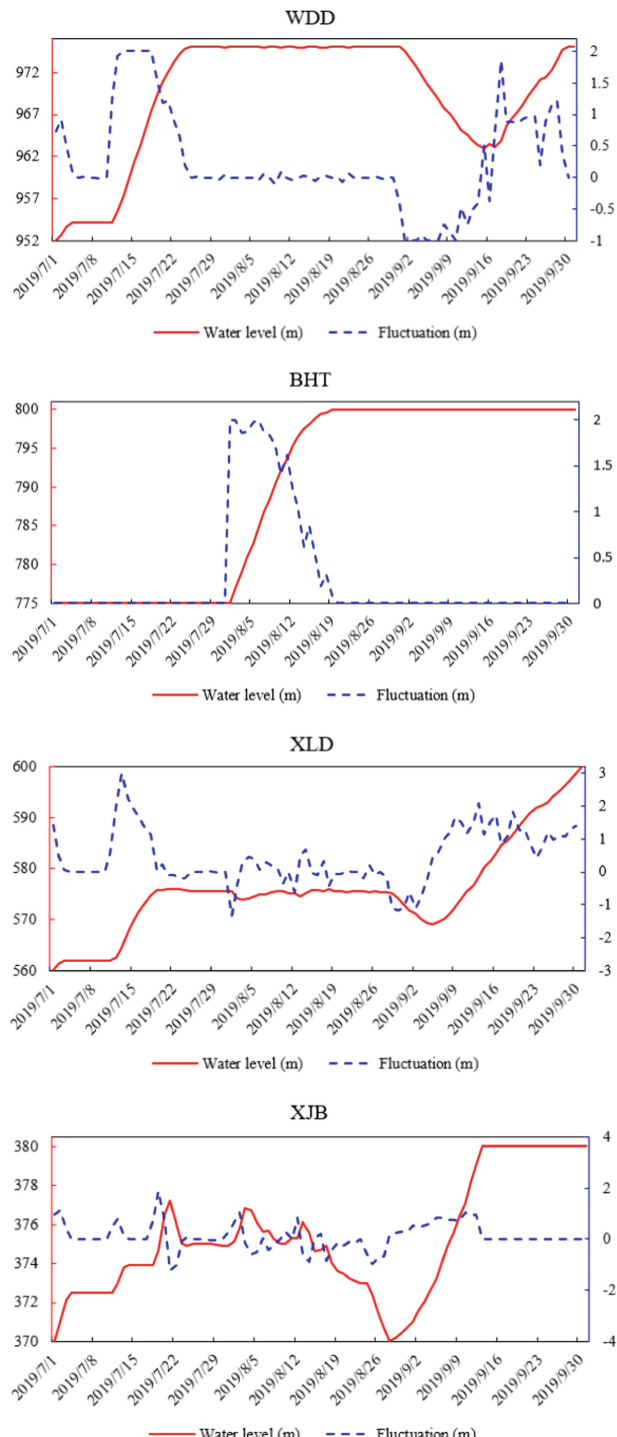


Fig. 1. Water level processes of multiple reservoirs with fluctuations period by period.

the forebay water levels of WDD, BHT, XLD, and XJB during each period all meet the forebay water level limits and corresponding fluctuation limits. Table 1 shows the minimum and maximum water levels as well as the corresponding fluctuations of multiple reservoirs, indicating that the water level processes are in the boundaries of their corresponding constraints. Figure 2 gives the flow process of multiple reservoirs period by period, indicating that each reservoir dynamically adjusts the storage and release of flood according to the corresponding inflow to meet the reserve demand of flood control capacity. Also, it can be seen from Table 2 that the outflows of all reservoirs are in the boundaries of constraints. These results demonstrate the usefulness of the DP-POA hybrid algorithms.

Further, the reserve flood control capacity of multiple reservoir system during optimization operation process are shown in Fig. 3 and are compared to the preset reserve flood control capacity values. Figure 3 shows that the total reserve flood control capacity gradually decreased from July 7 to July 20, however, it still meets the minimum requirement of more than 3.5 billion m³ reserve flood control capacity. Then it remains at 3.5 billion m³ until August 19. Subsequently, it slightly increases to the end of operation periods. The reason may be that multiple reservoir system empties the flood control capacity as far as possible to in advance to prepare for the coming large flood, resulting in the total reserve flood control capacity is greater than preset 3.5 billion m³. Then, the water level of WDD rises about from July 11; the water level of BHT rises about from August 1; the water level of XLD rises about from July 12, and the water level of XJB rises about from July 15. Then they operate at high water level to increase the hydropower generation under the premise of ensuring the flood control safety. As a result, Table 3 shows that the total hydropower generation of multiple reservoir system is 507.27×10^8 kWh.

In summary, the DP-POA hybrid algorithm is an effective and efficient algorithm to solve the optimization model of multiple reservoir system. Meanwhile, the optimal allocation of flood control storage of multiple hydropower reservoirs can meet the reserve demand for flood control capacity. As a result, the hydropower generation ability of multiple reservoir system during flood season are fully utilized.

Table 1. Statistical results of water level process.

Reservoirs	Z_{min} (m)	Z_{max} (m)	ΔZ_{min} (m)	ΔZ_{max} (m)
WDD	952	975	-1	2
BHT	775	800	0	2
XLD	560	598.61	-1.33	3
XJB	370	380	-1.21	1.88

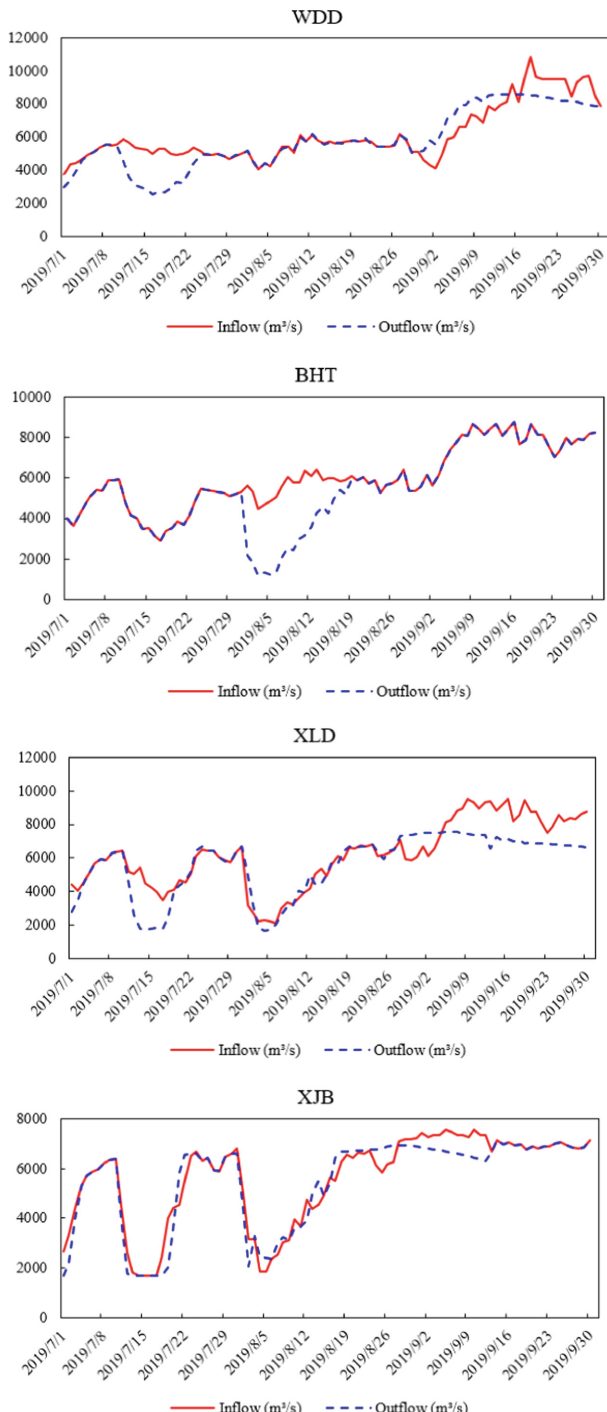
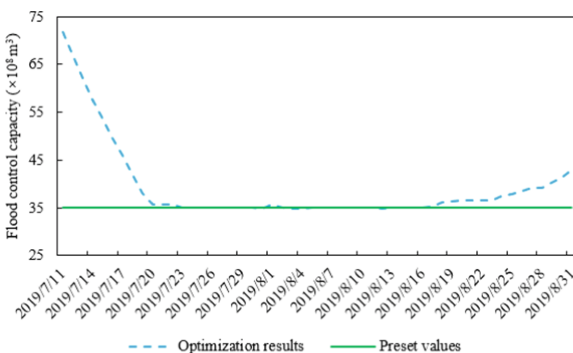


Fig. 2. Flow processes of multiple reservoirs period by period.

Table 2. Statistical results of outflow.

Reservoirs	Q_{min} (m ³ /s)	Q_{max} (m ³ /s)
WDD	2520	8590
BHT	1170	8770
XLD	1660	7560
XJB	1700	7130

**Fig. 3.** Comparison results of optimized reserve flood control capacity and the preset values.**Table 3.** Hydropower generations of multiple hydropower reservoirs.

Reservoirs	WDD	BHT	XLD	XJB	Total
Hydropower generation ($\times 10^8 \text{ kWh}$)	162.6	22.08	213.84	108.75	507.27

Acknowledgments. This study was supported by Natural Science Foundation of China (No. 52039004); National Natural Science Funds for Excellent Young Scholar (No. 51922047); Natural Science Foundation of China (No. U1865202); Natural Science Foundation of Hubei Province (No. 2020CFA101); Water conservancy science and technology innovation project of Guangdong province (No. 2020-23).

References

1. Rabiul, I., Roslina, K., Aznor, A.S., Jan, J.S., Rahim, A.A.: A review on mechanism of flood disaster management in Asia. Int. Rev. Manage. Market. **6**(1), 29–52 (2006)
2. Chan, N.W., Ghani, A.A., Samat, N., Hasan, N.N.N., Tan, M.L.: Integrating structural and non-structural flood management measures for greater effectiveness in flood loss reduction in the Kelantan river basin, Malaysia. In: Nazri, F.M. (ed.) AICCE 2019. LNCE, vol. 53, pp. 1151–1162. Springer, Cham (2020). https://doi.org/10.1007/978-3-030-32816-0_87

3. Qiu, H.Y., Chen, L., Zhou, J.Z., He, Z.Z., Zhang, J.H.: Risk analysis of water supply-hydropower generation-environment nexus in the cascade reservoir operation. *J. Cleaner Prod.* **283**, 124239 (2021)
4. Jia, B.Y., Zhong, P.A., Chen, J., Wu, Y.N.: Coordinated optimal operation model of complex flood control system. *Adv. Water Sci.* **26**(4), 560–571 (2015)
5. Zhu, D., Mei, Y., Xu, X., Liu, Z., Wu, Z., Cai, H.: Optimal operation of a parallel multireservoir system for flood control using a stagewise compensation method. *Water Resour. Manage.* **35**(6), 1689–1710 (2021)
6. Zhao, T., Zhao, J., Xiaohui Lei, X., Wang, B.W.: Improved dynamic programming for reservoir flood control operation. *Water Resour. Manage.* **31**(7), 2047–2063 (2017)
7. Yakowitz, S.: Dynamic programming applications in water resources. *Water Resour. Res.* **18**(4), 673–696 (1982)
8. Zhou, C., et al.: Optimal operation of cascade reservoirs for flood control of multiple areas downstream: a case study in the upper Yangtze river basin. *Water* **10**(9), 1250 (2018)



Experimental Study for Optimizing of Low Impact Development Facilities in Taiwan

Fu-Ming Chang^(✉)

Da-Yeh University, No.168, University Rd., Dacun, Changhua 515006, Taiwan
Changfm@mail.dyu.edu.tw

Abstract. With the development of urbanization, continued urbanization and development result in an increase of impervious areas and surface runoff. One of the biggest problems with surface runoff is that rainwater cannot seep into the soil, which means that the rainwater infiltration rate is too low during typhoons or extreme rainfall. The practice of low-impact development (LID) is considered a promising strategy for controlling urban rainwater runoff and urban ecosystems. However, this requires a lot of laboratory work to test the characteristics of LID and propose appropriate management to optimize LID. In this research, we propose an indoor experiment method, which optimizes the size of different types of LIDs by conducting intensive indoor experiments in a tree box experiment project. Optimize the infiltration rate of LID facility units through indoor experiments to reduce surface runoff. Therefore, the main goal of optimization is to increase the infiltration rate, which is an index to quantify the reduction of surface runoff. For the tree box system in the LID facility unit, the best soil ratio is soil plus sand, which significantly reduces surface runoff. We hope that the newly proposed method can inspire the establishment of LID strategies to reduce surface runoff.

Keywords: Low Impact Development (LID) · Surface runoff · Climate change

1 Introduction

With the development of urbanization, the increase in population and building density, and the living environment composed of impervious surfaces have reduced the coverage and infiltration area of plants, and the land lacks infiltration interception functions [1–3]. A large amount of impervious material prevents rainwater infiltration, which not only leads to an increase in surface runoff in the city, but also changes the time of rainwater concentration, flood peak time and the shape of the water level. The area of the floodplain that could be used for flood storage has been reduced due to land development, resulting in a decline in flood control capacity. If the drainage system is not substantially improved, the urban flooding problem will become more serious when extreme events under climate change occur.

The cities in Taiwan are highly developed and built-up areas. The uneven distribution of water resources in Taiwan on the spatial and temporal scales is due to the effects of climate change and changes in rainfall patterns. Whether it is the continuous intensity of short-term and long-term rainfall or the total cumulative rainfall of typhoons, the frequency of heavy rainfall and typhoons has increased in the past 10 years. Heavy rainfall and typhoons have caused serious urban flooding in low-lying areas.

Due to the development of urbanization, Taiwan's impervious area has gradually increased. It will lead to infiltration and reduced groundwater supply capacity, thereby indirectly reducing river flow and groundwater quality [4–6]. Urbanization is the main factor that changes the surface runoff in cities. The peak flow increases, the flow in the rivers increases, and the base flow decreases [7, 8]. The development of watersheds will also affect the frequency and intensity of flood events, especially in metropolitan watersheds [9–11]. As the impervious area increases, the amount of infiltration on the surface decreases, and the impervious surface of Manning's roughness decreases. On the other hand, it will shorten the time, speed up the flow rate of water on the surface, and increase the peak discharge [11, 12]. Du et al. (2015) [13] summarized four factors that promote the peak discharge of urbanization effects. First, the impervious area will reduce evaporation. Second, impervious surfaces reduce infiltration after rainfall and increase surface runoff. Third, due to the impervious surface, drainage system and surface roughness reduction, rainwater concentration time and stagnation time will be reduced. Finally, the combined effect can increase flood risk.

Current flood control methods can be divided into two categories: engineering methods and non-engineering methods [14]. Traditional engineering methods mainly include the construction of dikes and flood walls, spillway, reservoirs and pumping stations. Others adopt management methods and measures to reduce flood losses (such as strengthening the management of floodplains, planning protection areas and flood detention areas, etc.), but in urban areas under development, there are limited water conservancy sites that can be used for planning the above use. Making it difficult to implement flood control measures. In today's social development, non-engineering methods are more suitable for development behavior, and low-impact development (LID) is a means of using distributed concepts and land management strategies to deal with storm runoff. These technologies include: permeable pavements, bioretention, grass swales, green roofs, tree boxes and rain barrels [15–18]. Low-impact development has become another method used in urban areas to control rainfall runoff systems, prevent water pollution, provide environmental friendliness, and develop ecosystems [8, 17, 19, 20].

Compared with traditional impervious asphalt, permeable paving can reduce surface runoff, flood peaks, and delay high-permeability peak flows [12, 21–23]. Permeable pavement is mainly used for temporary storage of surface runoff, and the surface runoff slowly enters groundwater resources through permeation. The installation of permeable pavement can reduce the average runoff by 50%–93% [24]. Hunt (2002) showed that 75% of the water can flow through the porous media under the permeable pavement, and the remaining 25% can be infiltrated through the permeable parking lot in North Carolina. Collins et al. (2008) proposed that permeable concrete paving and concrete grids can maintain rainfall infiltration of up to 6 mm without any surface runoff. Permeable pavement can not only reduce runoff, but also eliminate runoff, even in the case of heavy

rainfall [21, 22]. Fassman and Blackbourn (2010) [25] conducted a study on permeable pavement to prove that the technology can realize the development of hydrology. Two parking lots with porous pavement reduced runoff by 93% [26].

The approach of Low Impact Development is beneficial to the river basin; however, a study of the overall planning and design of Low Impact Development is necessary [1, 27–29]. This study conducted experiments to evaluate three return periods for three different permeable surfaces. Measure penetration, peak discharge, and concentration time to check the ability of these penetration surfaces. This research uses the Tree Box Filter in the Low Impact Development facility unit for laboratory experiments. Through laboratory experiments, we have obtained the infiltration behavior of street trees on the sidewalk through extreme rainfall and reduce the changes in surface runoff. The Tree Box Filter can adjust the response and strain of the environment under climate change.

2 Materials and Methods

The experiment in this study evaluated the effectiveness of the infiltration rate of the tree box filtration facility. Its main purpose is to obtain LID reference infiltration and runoff results for future planning.

2.1 Experiment Condition

According to the experience of the United States [30–33] a certain proportion of LID design area must be able to reduce runoff. Based on the effective impermeability index, we calculated that the appropriate ratio of LID to impermeable area is about 1/3–1/4. In the study, the experiment was carried out in a test box with a length of 120 cm and a width of 120 cm. Converted by 1:4 surface area, the test box can be regarded as a catchment area 120 cm long and 240 cm wide, with a slope of 1%, $n = 0.02$, and Horner design rainfall model to simulate the storm water level, and the recurrence period It is 5 years, 25 years and 50 years. Figure 1, Fig. 2, and Fig. 3 show the one-hour design hydrological process lines for the 5-year, 25-year, and 50-year return periods in the test flask.

2.2 Experiment Setting

In this study, the experiment performed in an acrylic box container (120 cm * 120 cm * 100 cm), with two different Tree Box Filter design, and the frequency of the inflow conditions of 5, 25, 50 years (experimental details showed in Table 1). The elevation of experimental unit is shown in Fig. 4. In this unit, the layers from bottom to top are: Gravel Grading, PVC (drainage cell), Non-Woven, Mix Layer (improved mixing layer), Tree.

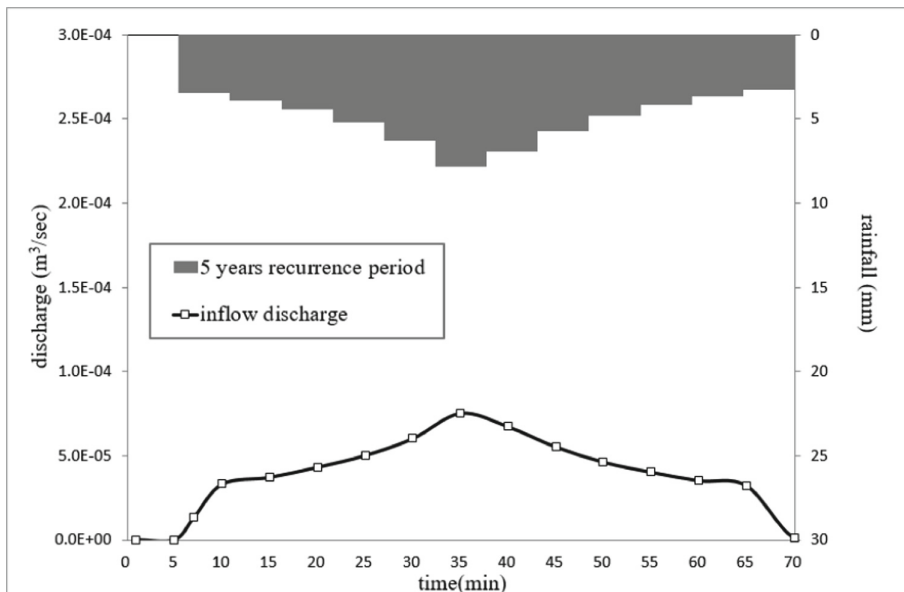


Fig. 1. The rainstorm hydrograph with the recurrence period of 5 years

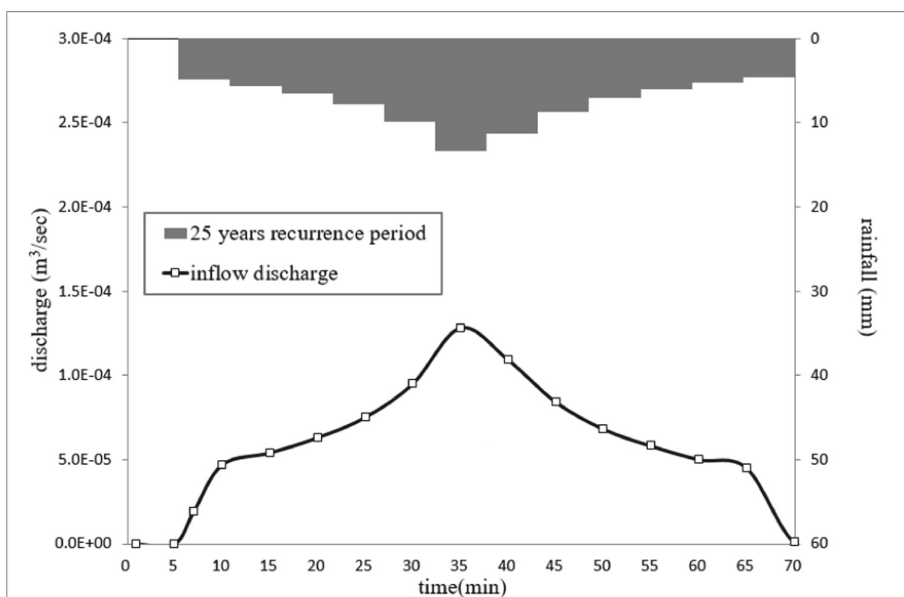


Fig. 2. The rainstorm hydrograph with the recurrence period of 25 years

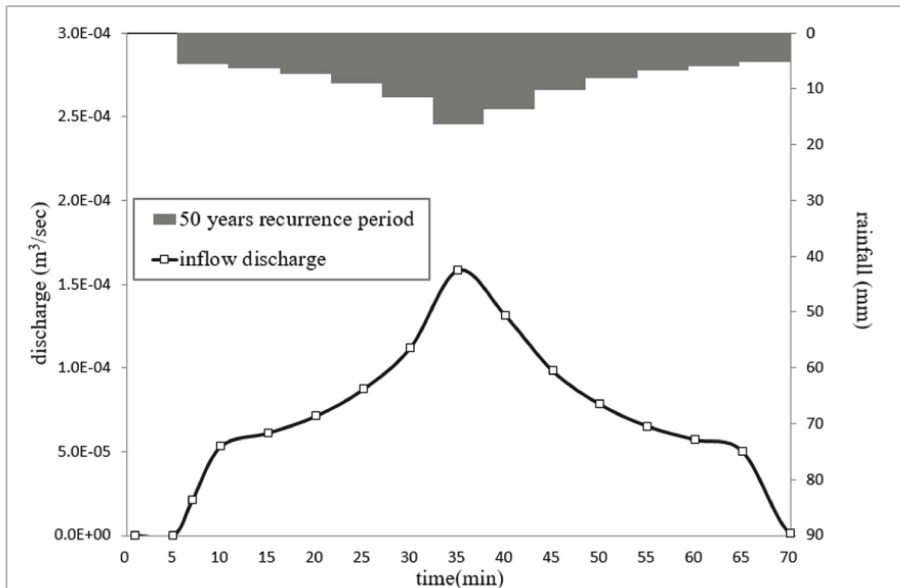


Fig. 3. The rainstorm hydrograph with the recurrence period of 50 years

Table 1. Experiment details.

Number	Design	Inflow condition	Remark
P1	Section 1	5-years rainfall flood	Bischofia javanica Blume
P2		25-years rainfall flood	
P3		50-years rainfall flood	
P4	Section 2	5-years rainfall flood	Millettia pinnata
P5		25-years rainfall flood	
P6		50-years rainfall flood	

2.3 Setting of Units and Experimental Procedure

In the test box of this research, in the acrylic box container (120 cm * 120 cm * 100 cm), spread 40 cm gravel gradation under the drainage trough, and place PVC (drainage cell) in the gravel gradation, and put it on the top Lay the Non-Woven, spread a 45 cm Mix Layer on it, and then plant the tree on the Mix Layer. The whole unit is shown in Fig. 4. According to the design in Fig. 4, pave the graded gravel (coarse aggregate) on the graded base, set up the capillary drainage groove at the rectangular opening of the 2 mm × 20 cm PVC pipe, and use the capillary drainage to guide the water to the PVC pipe grid to maintain Conduct water evenly, and use a grader to ensure that the floor is level. The whole unit is shown in Fig. 5, Fig. 6, Fig. 7, Fig. 8, Fig. 9 and Fig. 10. The overall experimental setup is shown in Fig. 11.

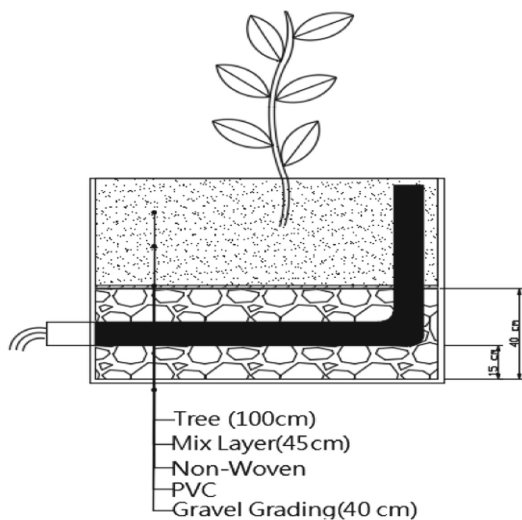


Fig. 4. The elevation of experimental unit.

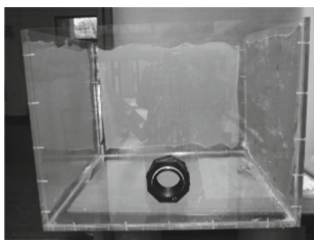


Fig. 5. Acrylic box container.



Fig. 6. Gravel grading



Fig. 7. Non-Woven Layer



Fig. 8. Mix Layer



Fig. 9. Bischofia javanica



Fig. 10. Millettia pinnata

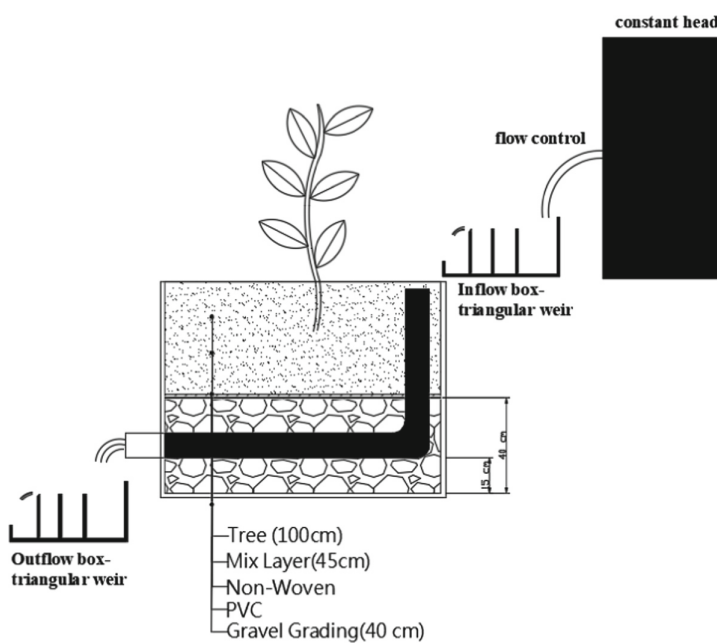


Fig. 11. Experimental setup

2.4 Experimental Procedure

In the experiment process, mainly in the experimental layout diagram (Fig. 11), the pipeline is connected to the constant head box to dynamically flow into the triangular weir, the pipeline is used to control the water volume, the reading device enters the water tank (triangular weir) to control the flow, and the side orifice is read. The whole process of the outlet trough (triangular weir) to obtain the flow rate and observe the changes in the water level of the side orifice during the experiment. The total time of the experiment for controlling the water inlet conditions is 80 min. After 80 min, the water inlet is stopped. After the experiment, the water in the water tank is drained from the side pipe. The total time is 100 min.

3 Results and Discussions

The comparison between the inflow and outflow shows that the Tree Box Filter reduces the peak emissions of all simulation scenarios and hinders the peak time. The experimental results of *Bischofia javanica Blume* are shown in Fig. 12, Fig. 13 and Fig. 14, and the experimental results of *Millettia pinnata* are shown in Fig. 15, Fig. 16 and Fig. 17.

The water retention of Tree Box Filter is shown in Table 2. This shows that the material is important for this function. It has adsorption effect on *Bischofia javanica Blume* and *Millettia pinnata*, the water retention can reach 50–70% under the peak of 5 years, and the water retention capacity of peak is about 30–50% in 25 and 50 years.

From the Tree Box Filter in this study, the results in the figure show that when the inflow flow enters the Tree Box Filter, the adsorption of the soil medium can greatly reduce the rainfall caused by the flood, and it can be effectively accumulated in the Tree Box Filter. Inside, reduce the occurrence of surface runoff.

Table 2. The water retention of Tree Box Filter

Type	<i>Bischofia javanica Blume</i>			<i>Millettia pinnata</i>		
Number	T1	T2	T3	T4	T5	T6
Flow condition	5 years	25 years	50 years	5 years	25 years	50 years
Water retention (%)	66.33	48.81	40.15	54.2	42.32	37.53

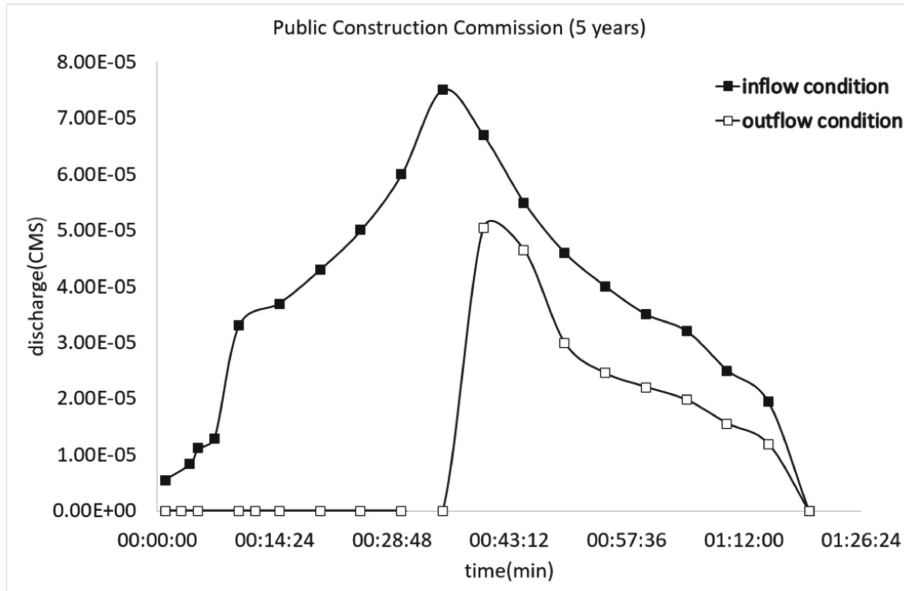


Fig. 12. Bisxhofia Javanica Blume experiment results for 5-year return period

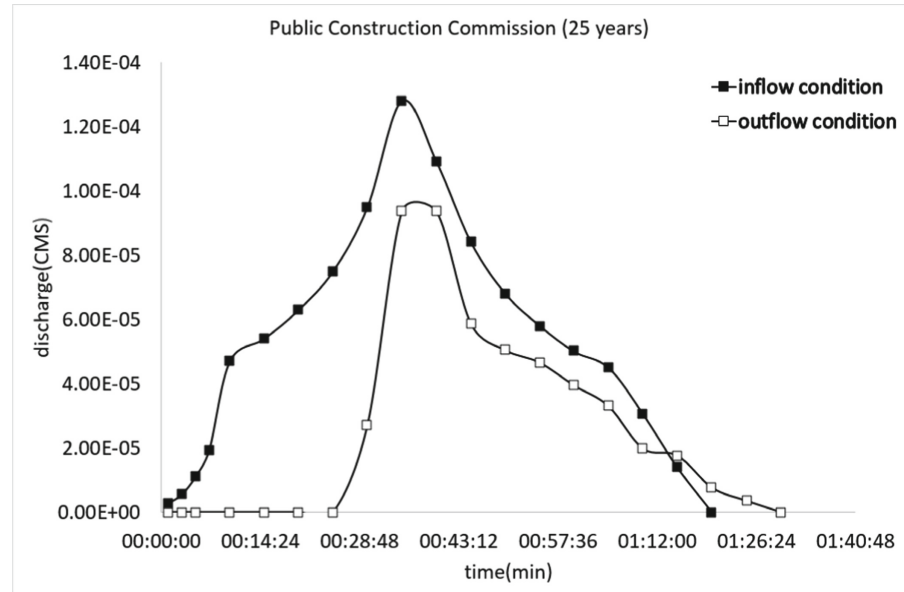


Fig. 13. Bisxhofia Javanica Blume experiment results for 25-year return period

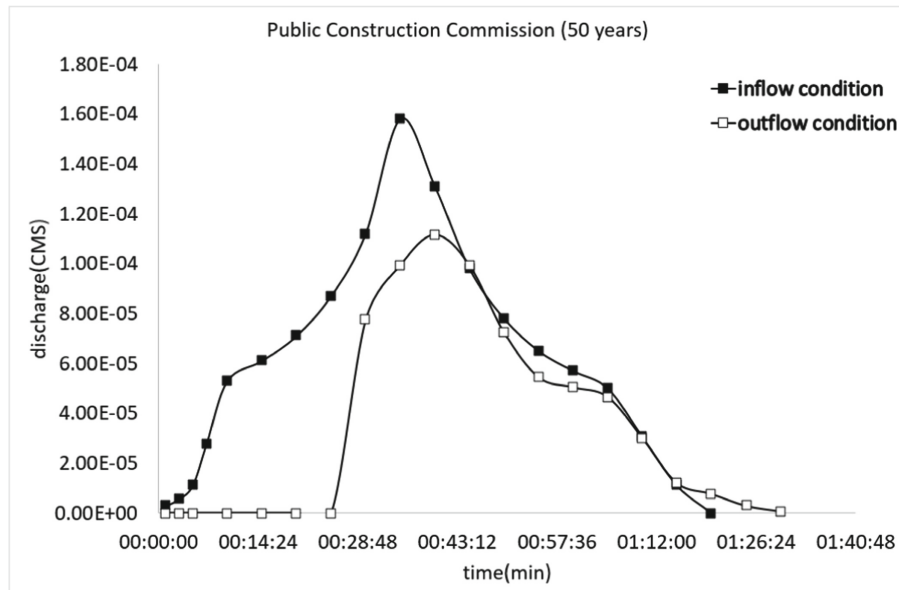


Fig. 14. Bisxhofia Javanica Blume experiment results for 50-year return period

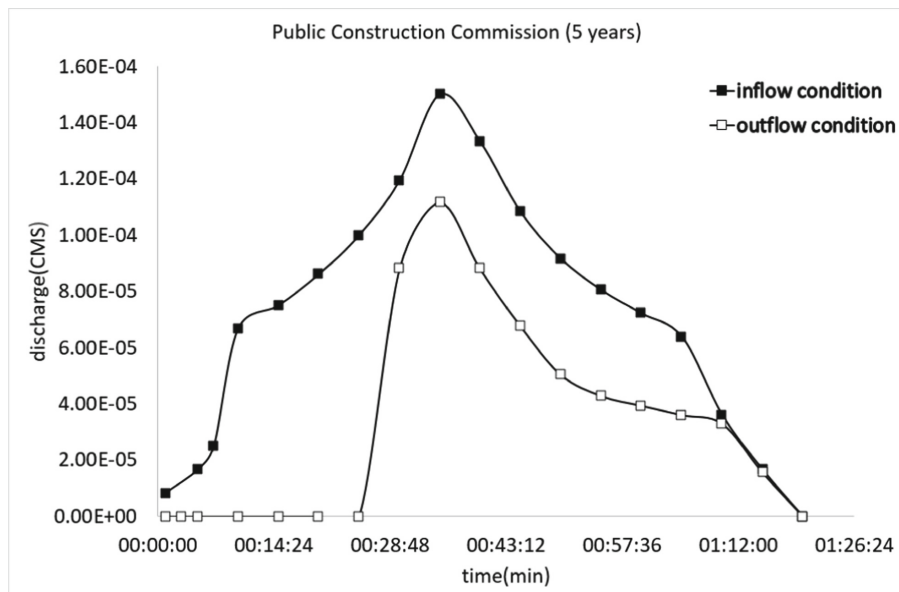


Fig. 15. Millettia Pinnata experiment results for 5-year return period

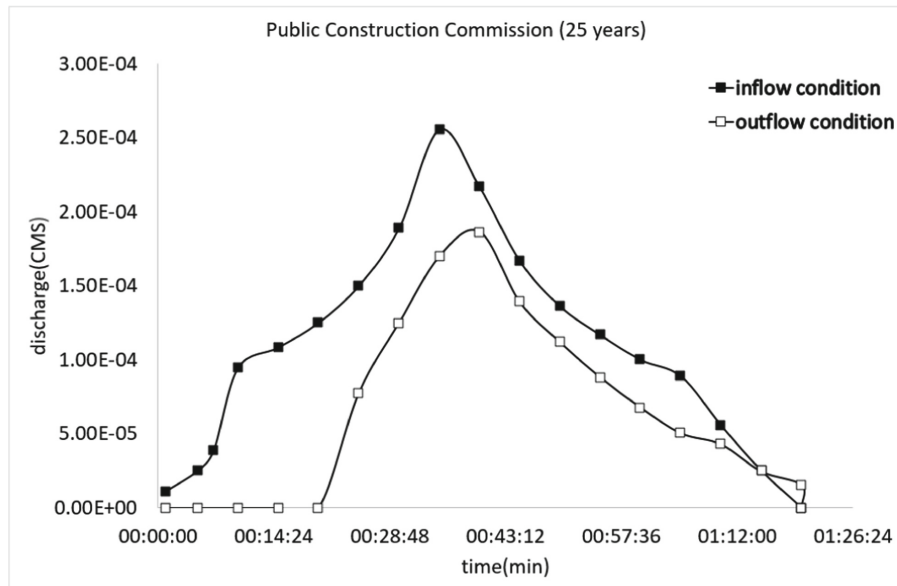


Fig. 16. Millettia Pinnata experiment results for 25-year return period

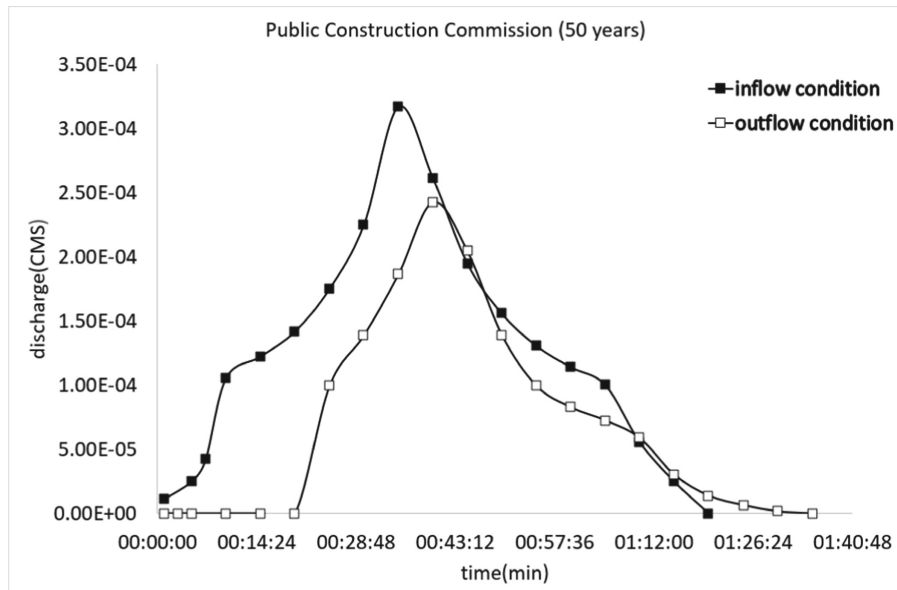


Fig. 17. Millettia Pinnata experiment results for 50-year return period

4 Conclusion

The experiment shown that Tree Box Filter can effectively increase water retention in response to climate change. Bisixhofia javanica Blume has a water retention capacity of 40%–70%, and Millettia Pinnata has a water retention capacity of 35%–55%. Its 5-year water retention performance (66.33% and 54.2%, respectively) is the best among the three rainfall conditions (5 years, 25 years, and 50 years).

The reason why the water retention performance of the 5-year flood front flow is better than the 50-year peak flow is that the water flows into the Tree Box Filter container at a slower rate, and the adsorption of the soil itself, the water is stored in the Tree Box Filter container. For 50 In the annual rainfall flood, the water flow quickly flows to the drainage hole, which reduces the water retention performance. In Taiwan, heavy rains have occurred frequently in recent years. The use of a properly proportioned Tree Box Filter can delay the arrival of flood peaks, slow down runoff, and protect trees from being uprooted when floods or typhoons come.

References

1. Bedan, E.S., Clausen, J.C.: Stormwater runoff quality and quantity from traditional and low impact development watersheds. *JAWRA J. Am. Water Resour. Assoc.* **45**(4), 998–1008 (2009)
2. LeFevre, N.-J., Watkins, D.W., Gierke, J.S., Brophy-Price, J.: Hydrologic performance monitoring of an underdrained low-impact development storm-water management system. *J. Irrig. Drain. Eng.* **136**(5), 333–339 (2010)
3. Peng, J., Ouyang, J., Yu, L., Wu, X.: The model and simulation of low impact development of the sponge airport. *China Water Supply* **20**(2), 383–394 (2020)
4. Harbor, J.M.: A practical method for estimating the impact of land-use change on surface runoff, groundwater recharge and wetland hydrology. *J. Am. Plan. Assoc.* **60**(1), 95–108 (1994)
5. Moscrip, A.L., Montgomery, D.R.: Urbanization, flood frequency, and Salmon abundance in Puget lowland streams. *J. Am. Water Resour. Assoc.* **33**(6), 1289–1297 (1997)
6. Poudel, U., Ahmad, S., Stephen, H.: Watershed Management 2020, pp. 219–232. American Society of Civil Engineers, Reston, VA (2020)
7. Imanov, F., Aliyeva, I.: Underground flow study of Great Caucasian rivers within Azerbaijan. *Acta Scientiarum Polonorum Formatio Circumiectus* **19**(1), 61–72 (2020)
8. Randhir, T.O., Raposa, S.: Urbanization and watershed sustainability: collaborative simulation modeling of future development states. *J. Hydrol.* **519**, 1526–1536 (2014)
9. Adnan, M.S.G., et al.: The use of watershed geomorphic data in flash flood susceptibility zoning: a case study of the Karnaphuli and Sangu river basins of Bangladesh. *Nat. Hazards* **99**(1), 425–448 (2019)
10. Kefi, M., Mishra, B.K., Kumar, P., Masago, Y., Fukushi, K.: Assessment of tangible direct flood damage using a spatial analysis approach under the effects of climate change: case study in an urban watershed in Hanoi, Vietnam. *ISPRS Int. J. Geo-Inf.* **7**(1), 29 (2018)
11. Wang, M., Zhang, D., Cheng, Y., Tan, S.K.: Assessing performance of porous pavements and bioretention cells for stormwater management in response to probable climatic changes. *J. Environ. Manage.* **243**, 157–167 (2019)
12. Hunt, B., Stevens, S., Mayes, D.: Proceedings of the 9th International Conference on Urban Drainage, Global Solutions for Urban Drainage, ASCE, Portland, Ore (2002)

13. Du, S., Shi, P., Van Rompaey, A., Wen, J.: Quantifying the impact of impervious surface location on flood peak discharge in urban areas. *Nat. Hazards* **76**(3), 1457–1471 (2015)
14. Den, S., Selaman, O.S., Mah, D.Y.: Society awareness and acceptance on the concepts of water sensitive urban drainage design (WSUD) in Sarawak. *J. Civ. Eng. Sci. Technol.* **5**(2), 16–21 (2014)
15. ASCE (American Society of Civil Engineers) Design and Construction of Urban Stormwater Management Systems. ASCE Manuals and Reports of Engineering Practice No. 77 (1992)
16. Coffman, L.S., Cheng, M., Weinstein, N., Clar, M.: 25th Annual Conference on Water Resources Planning and Management, ASCE, Reston, VA, 1–8 (1998)
17. Elliott, A.H., Trowsdale, S.A.: A review of models of low impact urban stormwater drainage. *Environ. Modell. Softw.* **22**(3), 394–405 (2007)
18. USEPA (U.S. Environmental Protection Agency) Low Impact Development (LID) A Literature Review EPA-841-B-00-005. (2000)
19. Ahiablame, L.M., Engel, B.A., Chaubey, I.: Effectiveness of low impact development practices: literature review and suggestions for future research. *Water Air Soil Pollut.* **223**(7), 4253–4273 (2012)
20. Kayhanian, M., Fruchtman, B.D., Gulliver, J.S., Montanaro, C., Ranieri, E., Wuertz, S.: Review of highway runoff characteristics: comparative analysis and universal implications. *Water Res.* **46**(20), 6609–6624 (2012)
21. Bean, E.Z., Hunt, W.F., Bidelspach, D.A.: Field survey of permeable pavement surface infiltration rates. *J. Irrig. Drainage Eng.* **133**(3), 247–255 (2007)
22. Brattebo, B.O., Booth, D.B.: Long-term stormwater quantity and quality performance of permeable pavement systems. *Water Res.* **37**(18), 4369–4376 (2003)
23. Pratt, C.J., Mantle, J.D.G., Schofield, P.A.: Urban stormwater reduction and quality improvement through the use of permeable pavements. *Water Sci. Technol.* **21**(8–9), 769–778 (1989)
24. USEPA (US Environmental Protection Agency). Washington, D.C.: Office of Water. EPA 832-F-99-023 (1999)
25. Fassman, E.A., Blackbourn, S.: Urban runoff mitigation by a permeable pavement system over impermeable soils. *J. Hydrol. Eng.* **15**, 475–485 (2010)
26. Dreelin, E.A., Fowler, L., Carroll, C.R.: A test of porous pavement effectiveness on clay soils during natural storm events. *Water Res.* **40**(4), 799–805 (2006)
27. Selbig, W.R., Bannerman, R.T.: U.S. Geological Survey Scientific Investigations Report, 2008-5008, p. 57 (2008)
28. Wang, X., Shuster, W., Pal, C., Buchberger, S., Bonta, J., Avadhanula, K.: Low impact development design—integrating suitability analysis and site planning for reduction of post-development stormwater quantity. *Sustainability* **2**(8), 2467–2482 (2010)
29. Zimmerman, M.J., Barbaro, J.R., Sorenson, J.R., Waldron, M.C.: U.S. Geological Survey Scientific Investigations Report, 2010-5007, p. 113 (2010)
30. Blackler, G.E., Guo, J.C.Y.: Paved area reduction factors under temporally varied rainfall and infiltration. *J. Irrig. Drain. Eng.* **139**(2), 173–179 (2013)
31. Earles, T., Guo, J.C.Y., MacKenzie, K., Clary, J., Tillack, S.: Water quality to flood control. *Low Impact Dev.* **2010**, 362–371 (2010). [https://doi.org/10.1061/41099\(367\)32](https://doi.org/10.1061/41099(367)32)
32. Guo, J.C.: Volume-based imperviousness for storm water designs. *J. Irrig. Drain. Eng.* **134**(2), 193–196 (2008)
33. Guo, J.C.Y., Blackler, G.E., Andrew Earles, T., MacKenzie, K.: Incentive index developed to evaluate storm-water low-impact designs. *J. Environ. Eng.* **136**(12), 1341–1346 (2010)

Green Building Technology and Urban Planning



Design of Green Infrastructure for the Revaluation of the Ventanilla-Peru Wetlands and the Protection of the Environment

Doris Esenarro^{1,2(✉)}, Joseline Quijano¹, Ciro Rodriguez¹, Jennifer Arteaga³,
and Karina Hinojosa¹

¹ Universidad Nacional Federico Villarreal - UNFV, Lima, Perú
doris.esenarro@erp.edu.pe, {2016232001, crodriguez,
khinojosa}@unfv.edu.pe

² Ricardo Palma University URP, Lima, Peru

³ Universidad de Ciencias Aplicadas - UPC, Lima, Perú
U20151C024@upc.edu.pe

Abstract. The purpose of this research is the design of a green infrastructure that allows a regional conservation area to revalue the Ventanilla wetlands to promote ecotourism through spaces for the conservation of natural resources, turning it into a tourist attraction. The proposal considers design and construction criteria with adequate technology, biodegradable, and sustainable materials where environmental impact is minimized in this context. The collection of information through field visits and the use of different software for the topographic survey. Results show that the infrastructure design proposed was validated by a survey of potential users of the place, with 75% of the interviewees agreeing with the design proposal that allows interaction and harmony with nature, giving it a landscape value, generating local, national, and international visitors. The value is in the ecosystem services that the landscape provides to the city due to the design and construction criteria with adequate technology, biodegradable, and sustainable materials minimizing the environmental impact and promoting the cultural exchange, preservation, and ecological awareness wetland.

Keywords: Green infrastructure · Revaluation · Ecotourism · Ventanilla wetlands · Landscape value

1 Introduction

The design of a green infrastructure complies with the strengthening of ecosystems [1], helps to restore the integrity of the landscape and face climate change [2]; it is considered ecological principles, which consists of minimizing the number of resources consumed in the construction process and contribute to a social and environmental environment [3]. The proposed Green Infrastructure works as an interconnected network of spaces where the values of natural ecosystems are preserved, offering benefits to the population [4], which provides a strategic approach to the conservation of nature necessary for the environmental, social, and economic sustainability of a territory [5, 6]. Design planning

consists of conserving, enhancing, or restoring nature to minimize vulnerability and identify ways to maximize opportunities [7].

On the Peruvian coast, specifically in Lima's department, a group of wetlands forms the "Biological Corridor of the Central Coast of Peru." Wetlands provide multiple ecosystem goods and services to nearby human populations, such as the provision of fiber and a landscape suitable for tourism activities [8].

The Regional Conservation Area (RCA) Ventanilla Wetlands stands out for its great importance due to its location, and at the same time, it faces the degradation process. In the 1980s, this area had 1,500 ha, of which only 275.45 ha remain [9]. It is a conservation area under the protection of the regional government of Callao, has an ecosystem that includes lagoons, habitat in avifauna with more than 121 different families of resident and migratory birds and other types of wildlife, it is possible to find more than 20 kinds of plant communities, being the most predominant known as the reed plant, cattail, and reed. However, these ecosystems are fragile and threatened with a high risk of deterioration.

Despite the great potential of this resource, it has no tourist significance. There are half a dozen urbanizations and more than 300 human settlements, of which 220 are recognized so far; this process is related to the fact that Ventanilla is the eighth metropolitan district that attracts the highest intra-metropolitan migration and with the rest of the country, with a net migration rate of 14.96. The AA surrounds the wetlands. HH and vehicular roads, which contaminate the swamp due to their proximity to it.

Environmental contamination in this ecosystem is constant due to industrial companies, transportation, and human activity since there is a lack of ecological awareness and education, which has led to the degradation of the area, as well as the overexploitation of its resources, mainly due to bird hunting, fishing, cattail extraction, and the use of pasture for livestock and water extraction [10].

Competent authorities are absent in its management and conservation by the regional conservation area; this shows their lack of coordination and strategies about the tourist service, thus losing the potential of its natural resources and ecotourism as an ecological system in the district of Ventanilla in the Callao region.

Ventanilla's wetlands are in the process of recovery, although with many limitations, one of the leading causes being that both public and private institutions violate norms and transgress legal provisions [11]. Currently, the resource lacks adequate tourist infrastructure for tours, which means that tourists do not receive pleasant visits. Therefore, this research aims to propose a green infrastructure design that allows the revaluation of the wetlands of Ventanilla; it is intended to increase the new tourists through ecotourism and has a green infrastructure that does not transgress biodiversity to promote education and environmental awareness involving the surrounding population, organizations, and tourists [1].

2 Materials and Method

The methodology used in the present investigation was exploratory and applicative, which was validated by the bibliographic review, the collection of information through field visits, and different software for the topographic survey. As an application, an infrastructure design is proposed, which was validated by a survey of potential users of the place [12].

2.1 Study Area

The Ventanilla Wetlands RCA is located in the lower and central-western part of the Chillón River Basin, Department of Lima, Constitutional Province of Callao, District of Ventanilla. It has an area of 275.45 ha, according to D.S. No. 074-2006-AG of December 20, 2006, which established its creation [13]. This habitat maintains its functioning by hosting more than 50 bird species and 35 plant species. It is composed of gramadales, reed beds, coastal lagoons, and water bodies habitats for a great diversity of organisms because of its position concerning other wetlands [14] (Fig. 1).

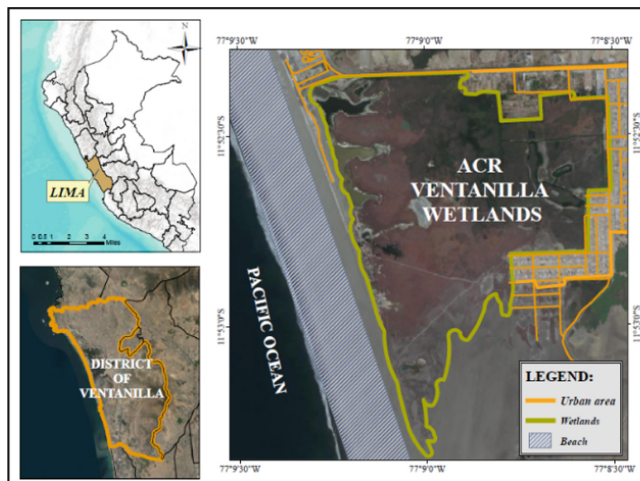


Fig. 1. Geographical location and delimitation of the study area “Wetlands of Ventanilla Conservation Area”.

2.2 Climate

The Ventanilla wetlands are located on the Peruvian desert coast and have a microclimate determined by the fact that it is a closed micro-watershed [15] (Fig. 2).

(a) The average annual temperature is 19.75 °C, with maximum temperatures in February (27 °C) and minimum temperatures in September (14.8 °C), (b) The relative humidity is 80% (in November) and 85% (in September), with an annual average of 83%, and with more significant variations during the day in the summer season (c) Rainfall indicates that the area corresponds to the minor rainy sector of the Chillón River basin, with an average of 15.6 mm, with maximums of 2.8 mm and minimums of 0.2 mm per year, making it an arid climate zone, (d) Winds are weak (13.6 km/h).

2.3 Vegetation

The flora is distributed according to different physical and chemical conditions such as water levels, characteristics, and soil type [16] (Fig. 3).

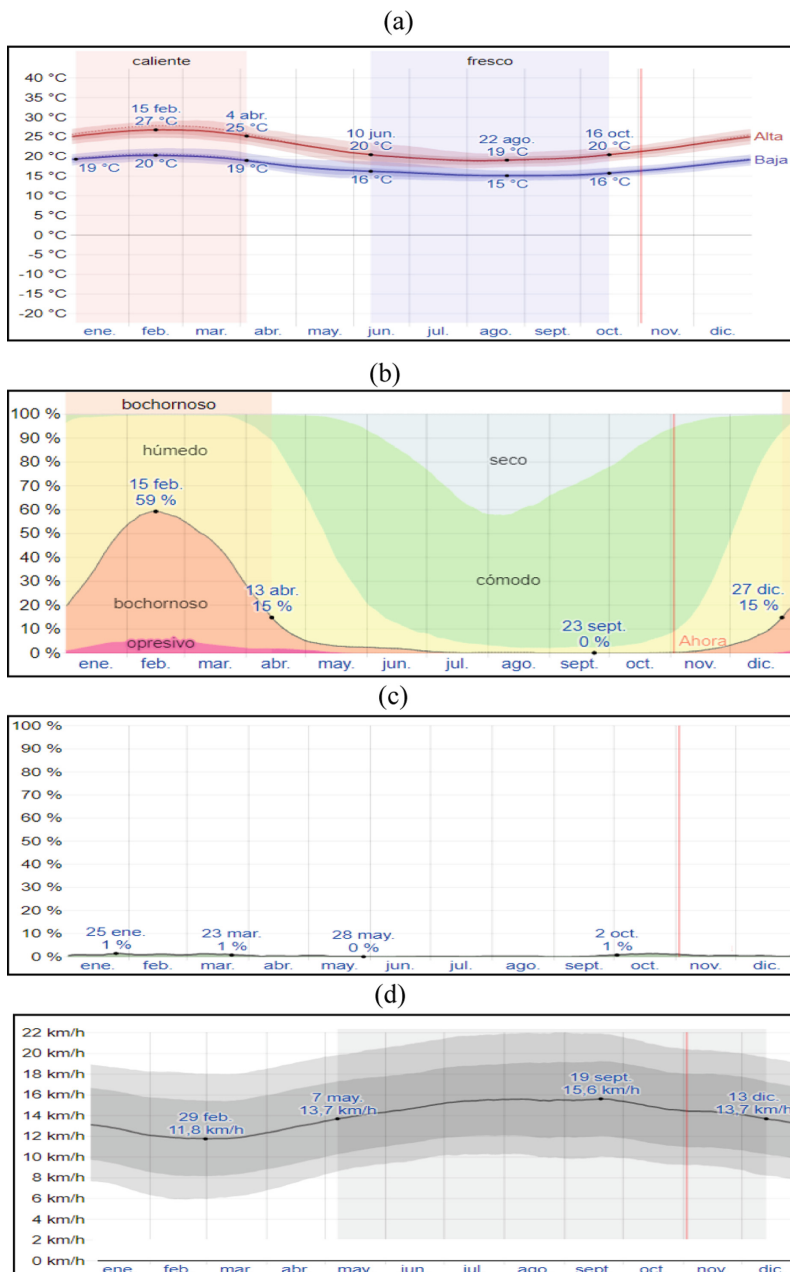


Fig. 2. Atmospheric conditions were typical of the Ventanilla wetland.

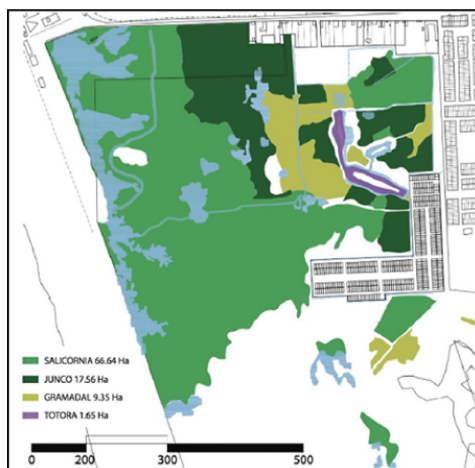


Fig. 3. Principal vegetation in the Ventanilla Wetlands Conservation Area.

2.4 Soil Science

Studies have identified two types of soils: Eutric Fluvisol (irrigated) and desert Litosol-type soils. The analysis determines that they have a sandy and sandy loam texture, with a pH range between 7.8 and 8.38, alkaline soils with accumulations of salts, with a low

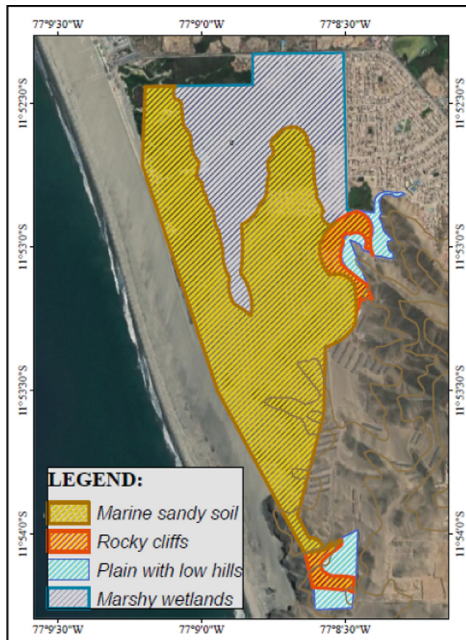


Fig. 4. Soil types in the Wetlands of Ventanilla Conservation Area.

content of organic matter between 0.4 and 1.07% with limitations for agricultural use [17]. It presents a type of marshy soil with the particularity of being fine sand since it is located next to the Beaches area of the Costa Azul Complex. In the wetlands in the re-run of the trails, seepage is observed, the humidity is due to the soil's porosity (Fig. 4).

2.5 Materials

For the informal survey of the determined area, ARGIS 10.4 and Google Earth Pro software was used, a survey was conducted, and AutoCAD 2017 and Sketchup 2020 programs were needed to design the presentation of the proposal.

2.6 Criteria of the Sustainable Architectural Approach

The sustainable construction of the proposal is based on conceiving the design, management, and execution of the project through the rational, appropriate use of the natural and cultural resources of the wetland, seeking the minimization of the environmental impacts of the construction, as well as contributing to the improvement and recovery of the environment multiply, both in the social, economic and ecological aspects [18] (Fig. 5).

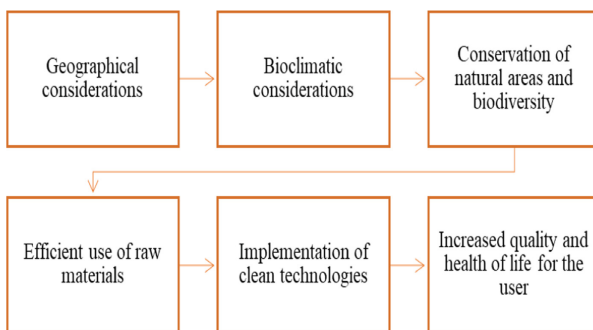


Fig. 5. Sustainable construction criteria of the proposal.

2.7 Sustainable Building Materials

Materials are sustainable by fulfilling technical functions, ensuring safety, consuming fewer non-renewable resources, and producing less environmental impact. To minimize the environmental impact made by using building materials, it is essential to select them properly to reduce energy consumption in the building and install them, generate less waste when manufactured and put on-site, and reduce the direct and indirect pollution they make [19] (Fig. 6).



Fig. 6. Primarily sustainable materials for the construction of the proposal.

2.8 Project Users

The project has two types of users: the person in charge of the conservation, administration, and care of the regional conservation area wetlands de Ventanilla and, on the other hand, the visitors who will be able to visit the swamp and make use of the different spaces and activities proposed by the project.

School and university students, teachers, institutions, national and international tourists come for observation, interpretation, flora and fauna research, and recreation and leisure activities.

2.9 Technology Applied to the Project: Green Roofs

Green roofs were implemented because they are capable of retaining an average value of 69% of the water precipitated in a rainfall event under normal conditions; this volume of water is mainly absorbed by the vegetation and released back into the atmosphere by evaporation; the remaining water is stored in the substrate. An extensive roof type was chosen, which requires little irrigation and is generally installed in inaccessible places, the plants have a substrate depth of less than or equal to 10 cm, the approximate weight of the system ranges between 60 and 140 kg/m², and this type of green roof is the most suitable for use in existing buildings since minimal reinforcements are needed in the structure to support the additional weight [20] (Fig. 7).

2.10 The Tourist Carrying Capacity of the Project

The project is located in a fragile natural environment to estimate the maximum number of visitors who can visit the site without hurting it. The maximum number of visitors that can access the project during one day was determined. The following formula for physical carrying capacity was applied:

Where it was determined that S is the space the length of the interpretive trail of the project, Sp is the space needed by the visitor for their displacement, Hv is the amount of time that the project will be open to the public, and Tv is the time required to visit the site, calculating the maximum carrying capacity of the research in the Ventanilla Wetlands would be 3840 people per day [21].

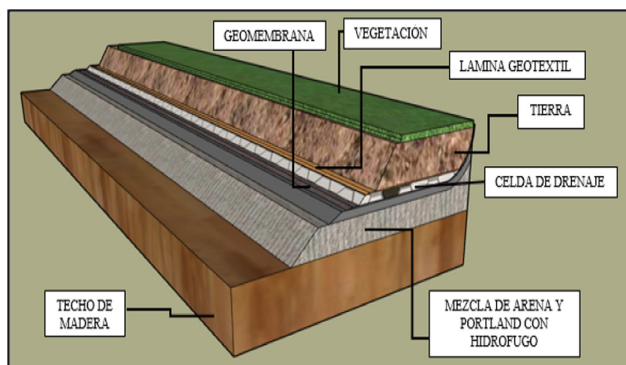


Fig. 7. Consideration for the multilayer system of green roof fabrication.

3 Results

3.1 Survey Results Conducted

The surveys carried out to users, both tourists and locals, were carried out with 16 Likert-type questions, with four alternatives, with a sample of 480 respondents, as the results are presented in the attached graph below. Therefore, the results of the surveys can be shown, in which 75 was obtained, which are in substantial agreement (Fig. 8).

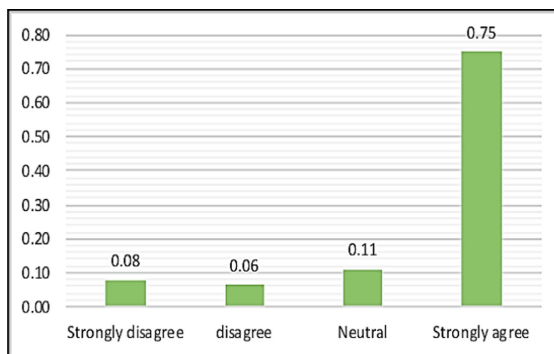


Fig. 8. Results of the surveys carried out.

3.2 Proposal

The project has areas aimed at promoting the revaluation of the Ventanilla wetlands through environmental education. In addition, there will be spaces for talks and artistic workshops to create learning and interpretation playful for children, families, and the community.

The discussions and workshops will include dynamic courses to learn by doing and become aware of the importance of wetlands. A conservation area with a research laboratory was considered necessary because university students, young people visit the swamp, and adults and conservation are promoted, so a site is viewed for studying animal and plant species in the wetland [22].



Fig. 9. Current tourist equipment of the ACR wetlands de Ventanilla

Figure 9 These areas are oriented to promote awareness and revaluation of the wetlands. You can see the connection between the areas that will allow the interaction and integration of visitors with the swamp (Fig. 10).



Fig. 10. Satellite view and organization of the proposed areas of the “Wetlands of Ventanilla Conservation Area” project.

Table 1 shows nine areas that were considered and their respective location in the Ventanilla wetlands regional conservation area (Fig. 11).

Table 1. Coordinates by areas.

Areas	UTM coordinates	
	X	Y
a- Bicycle parking	266681.15 m E	8686435.74 m S
b- Main hall	266682.61 m E	8686401.75 m S
c- Administration	266672.24 m E	8686365.54 m S
d- Conservation	266678.00 m E	8686308.29 m S
e- Intermediate rest space	266440.83 m E	8686167.73 m S
f- Awareness	266443.27 m E	8686326.14 m S
g- Viewpoint	266364.63 m E	8686307.32 m S
h- Interpretation	266391.45 m E	8686156.43 m S
i- Research	266538.47 m E	8686099.31 m S



(a)

Fig. 11. Project proposal to the Ventanilla Wetland. (a) Bicycle parking,

Figure 12, we can see a conservation area that will allow studying flora and fauna of the wetland; the interpretation area has space for children and adults where workshops and art exhibitions are held, the intermediate space was considered a rest area and allowed the connection to the different regions, the viewpoint enables to appreciate the landscape and bird watching, The research area is a space that will allow learning where you can find information about the place for educational purposes and the awareness area is a space for exhibitions and meetings based on inductive themes in the recovery and importance of the wetland, these areas will allow the local population and the rest of the city will benefit from its significant educational, cultural and social impact.

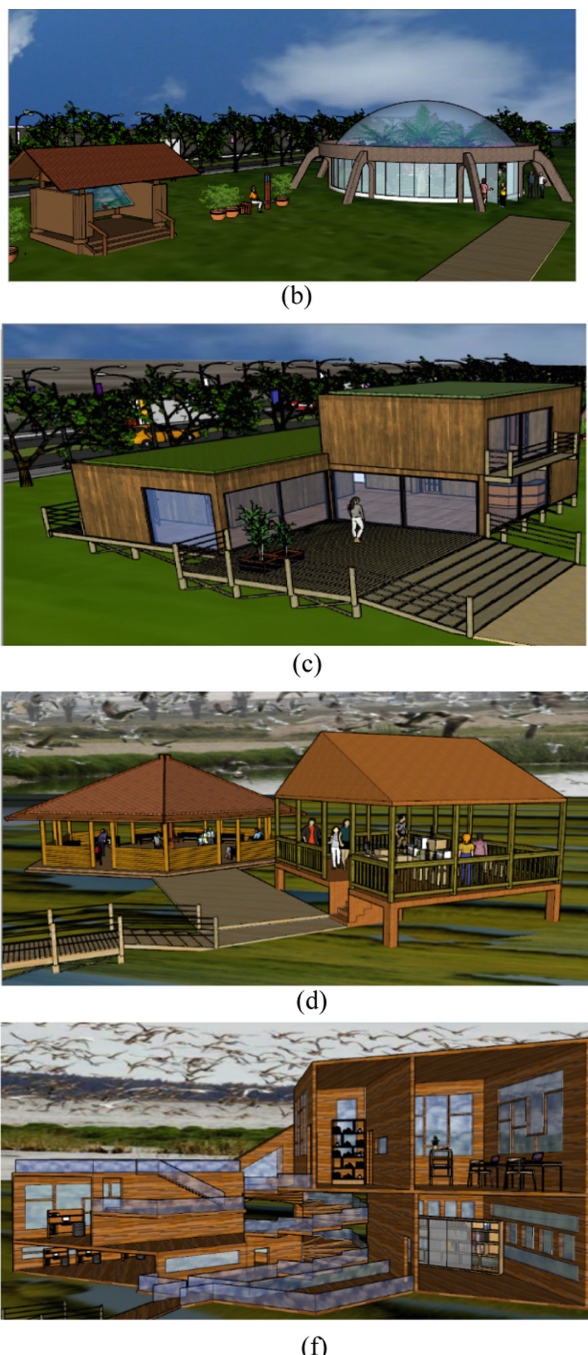


Fig. 12. Areas of the Ventanilla Wetland project proposal, (b) (g) Viewpoint, (c) Interpretation area, (d) Research area (f).

4 Discussion

Through the generation of environmental awareness, ecological infrastructure projects have made an essential contribution to the recovery and preservation of the place, integrating the urban with the natural, turning natural spaces into places for recreation and leisure without affecting their nature.

The Minghu Wetland Park project by Turenscape architects is located in Liupanshui, Guizhou, China. It was developed within a wetland that presented pollution problems, so they opted for an ecological infrastructure through regenerative design techniques where pedestrian and bicycle paths were incorporated on the green spaces along the watercourses, forming a circuit around and between the terraces of the wetlands. The objective of this project was to provide ecosystem services, stormwater management, water purification, and habitat recovery, as well as the creation of a public space resulting in an environmental interpretation system where visitors understand the natural and cultural significance of the place [23]. On the other hand, the Salburúa Nature Interpretation Center project was developed by Qve architects, located in Vitoria, Alava, Spain. It stands out for promoting the knowledge of wetlands and showing their natural values. The importance of biodiversity and the natural heritage of Vitoria-Gasteiz generating an integration, it is a space open to the public with resources and services of exhibition space, classrooms, observatory where it hosts leisure and entertainment activities, interpretation, dissemination and communication, study and research on biodiversity. Simultaneously, the Suncheon International Wetlands Center project created by Gansam Architects has designed a visitor center to accommodate the 2.8 million annual visitors to the Suncheon wetlands in Korea. The design foresees a green roof and a wooden facade to integrate the structure into the environment while using passive strategies to minimize the amount of light entering the building in the summer and increase the lighting in winter [24]. This project succeeded in allowing visitors to walk from end to end, always enjoying Suncheon Bay, connecting visitors with nature and teaching them what wetland ecosystems represent, and encouraging wetland preservation.

For the realization of this project of green infrastructure for the revaluation of the wetlands of Ventanilla, it was determined through the survey that most people consider that the wetlands are a tourist and ecological attraction which requires an adequate green infrastructure that allows the preservation of biodiversity and the creation of trails where the landscape is observed, this would favor the increase of the influx of visitors [25]. For this reason, the project has the necessary infrastructure for the development of environmental research that will allow for the adequate study of the wetland's natural resources.

The project stands out to integrate visitors with the natural environment; it has spaces that fulfill conservation and environmental research and programs with activities that promote biodiversity and environmental awareness in which visitors can participate.

5 Conclusions

The project proposes a green infrastructure design that allows the revaluation of the Ventanilla wetlands and reduces the environmental impact by disseminating their ecological

importance and economic and tourism potential. This project enables the conservation of flora and fauna of the wetlands through preservation programs and environmental awareness, which helps scientific research be carried out, allowing environmental education for the area and visitors' inhabitants.

The project provides an ecotourism potential and an adequate service to satisfy visitors' needs and allow social integration to connect the urban and the environment. Furthermore, the activities in the project proposed that its inhabitants also become part of the natural area and recognize it as such, promoting its conservation so that the inhabitants and visitors of the wetlands can appreciate the landscape without negatively impacting it, turning the space into a recreational and tourist attraction.

References

1. Wang, J., Liu, J., Wang, H., Mei, C.: Approaches to multi-objective optimization and assessment of green infrastructure and their multi-functional effectiveness: a review. *Water* **12**, 2714 (2020)
2. Ekka, A., Pande, S., Jiang, Y., der Zaag, P.: Anthropogenic modifications and river ecosystem services: a landscape perspective. *Water* **12**, 2706 (2020)
3. Quintero, L., Quintero, J.: Infraestructuras verdes vivas: características tipológicas, beneficios e implementación. *Cuadernos de Vivienda y Urbanismo*. **12**, 1–20 (2019)
4. Cole, L., McPhearson, T., Polacow, C.: Green infrastructure. Cornell University, pp. 261–270 (2017)
5. Amado, M., Rodrigues, E., Poggi, F., Pinheiro, M.D., Amado, A.R., José, H.: Using different levels of information in planning green infrastructure in Luanda, Angola. *Sustainability* **12**, 3162 (2020)
6. Vásquez, A.: Infraestructura verde, servicios ecosistémicos y sus aportes para enfrentar el cambio climático en ciudades: el caso del corredor ribereño del río Mapocho en Santiago de Chile. *Revista de Geografía Norte Grande* **63**, 63–86 (2016)
7. Qi, Y., et al.: Addressing challenges of urban water management in Chinese sponge cities via nature-based solutions. *Water* **12**, 2788 (2020)
8. Leon, B., Cano, A., Young, K.: Current use of flora and vegetation in the wetlands of the central coast of Peru. *Biol. Conserv.* **1998**, 191–104 (2019)
9. Villagra Dill'erva, M.: Center for Environmental Research and Education in the Ventanilla - Callao Wetlands. Peruvian University of Applied Sciences (UPC), Lima (2017)
10. CEGMA: Memories of actions carried out in the Ventanilla Wetlands, Lime (2003)
11. Aranibar, E.L.S.S., Esenarro, D., Ascama, L., Rodriguez, C.: Design of green infrastructure for sustainable urban transportation in Lomas Del Paraíso in Villa María Del Triunfo. *J. Green Eng.* **10**(11), 11180–11192 (2020)
12. Li, X., et al.: Valuation of wetland ecosystem services in national nature reserves in China's coastal zones. *Sustainability* **12**, 3131 (2020)
13. Esenarro, D., Rodriguez C., Huachaca, K., Cachay, B., Aylas, C.: Classification and characterization of the sustainable wetland Bello Horizonte, pp. 13453–13458. *Test Engineering & Management* (2020). ISSN 0193-4120
14. Ramos, L., Esenarro, D., Rodriguez, C., Lagos, J.: Recovery of public spaces for the conservation of green areas in Tablada Lurin. *IOP Conf. Ser. Mater. Sci. Eng.* **910**, 012020 (2020). <https://doi.org/10.1088/1757-899X/910/1/01>
15. Corner, J.: The Landscape Urbanism Reader, pp. 23–33. *Terra Fluxus* (2006)
16. Aponte, H., Cano, A.: Comparative floristic study of six wetlands of the central coast of Peru: update and new challenges for their conservation. *Lat. Am. Conserv. Mag.* **3**, 15–27 (2013)

17. Alvarez, C., Iannaccone, J.: New bird records in the Ventanilla wetlands, Callao, Peru. *Biologist* **6**, 68–71 (2008)
18. Cornejo, C.: Sustainability, architecture and evaluation. *Bull. UCAL Creativity Res. Cent.* **1**, 10–16 (2016)
19. Acosta, D.: Sustainable architecture and construction: concepts, problems and strategies. *Dearquitectura*, 15–23 (2009)
20. Esenarro, D., Escate, I., Anco, L., Tassara, C., Rodriguez, C.: Proposal for an ecological research center for the recovery and revaluation of biodiversity in the town of Quichas-Lima, Peru. *Int. J. Environ. Sci. Dev.* **11**(4), 212–216 (2020). ISSN 2010-0264. <https://doi.org/10.18178/ijesd.2020.11.4.1253>
21. Morales, J.A., Cristancho, M.A., Baquero-Rodríguez, G.A.: Trends in the design, construction, and operation of green roofs to improve the rainwater quality. State of the art. *Water Eng.* **21**, 179–196 (2017)
22. Kongjian, Y.: Slow down: Minghu wetland park in Liupanshui. *Landscape Archit. Front.* **2**, 130–137 (2014)
23. Mondragón, D.Y.M., Garcia, C.R.S.: Fortalecimiento del desarrollo turístico sostenible en los humedales de Ventanilla, departamento de Lima, Perú. *INNOVA Res. J.* **4**(3.1), 126–134 (2019)
24. Ventosilla, V.V., Esenarro, D., Maldonado, C., Rodriguez, C., Miranda, A.C.: Green infrastructure design for connectivity in the Villa wetlands wildlife refuge. *J. Green Eng.* **10**(12), 12753–12765 (2020)
25. Gill, S., Handley, J., Ennos, A., Pauleit, S.: Adapting cities to climate change: the role of green infrastructure. *Built Environ.* **33**, 115–133 (2007)



Effect of the Window Design Features on Natural Ventilation

Inoka Manthilake, Anusha Wijewardane^(✉), and Rumesh Rangana

Department of Mechanical Engineering, University of Moratuwa, Moratuwa, Sri Lanka
anusha@uom.lk

Abstract. Air vents and windows significantly affect the temperature, humidity, air distribution and air quality of domestic buildings. It is notable that, in most of the modern residential building designs in Sri Lanka, the air vents are not available while, air vents were a popular feature in traditional buildings. This paper investigates the effect of air vents on the distribution of indoor temperature and air velocity of a domestic unit. This was carried out by simulations of a living room for four different window and air vent arrangements. The window comprises of two features: one which is closable and typically covers 80% of the area, while the other is a lattice which is always open. The latter is located on top of the former. The air vent is located at a distance above the window. The four designs which were compared are: 1. without air vents, (a) closed and (b) open window and 2. with air vents, (a) closed and (b) open window. The simulations revealed that introducing the air vents increases vorticity of indoor air while, creating a better temperature distribution. This serves as a factor to increase indoor thermal comfort. Further simulations were carried out to find the optimum shape of the air vent and number of air vents. Through which, a relationship is to be formulated between the window design parameters towards establishing thermal comfort in domestic buildings in tropics.

Keywords: Air vents · Natural ventilation · Traditional buildings · Window design

1 Introduction

Natural ventilation is an important strategy for the passive cooling of buildings, as it improves the healthy indoor conditions and provides thermal comfort for the users, through indoor air renewal. This avoids the need of active ventilation, with 10% higher energy cost and air conditioning systems, with 40% higher energy cost [1] compared to naturally ventilated buildings and reduces the maintenance cost too [2]. This paper presents an analysis of a traditional method used in ancient buildings to achieve passive cooling by natural ventilation. The type of buildings concerned here are around hundred years old. In these buildings a window, a lattice and a set of air vents are installed to achieve ventilation.

As a tropical country, Sri Lanka experiences a warm and humid climate with mean annual temperature 26.5 °C–28.5 °C [3] and Relative Humidity (RH) variation 75%–83% [3]. Since it is a small island in Indian Ocean it experiences a coastal climate throughout the year. Therefore, theoretically the temperature needs to be reduced by less than five degrees to bring the condition of air to a comfortable level. For example, tree shades cut down the radiative temperature by almost 7 °C [4]. If the outdoor air is sufficiently clean, and the means of manipulating the condition of outdoor air such as shading is used, creating a comfortable indoor environment by natural ventilation methods can be very effective to do away with active cooling and associated costs.

Passive cooling by natural ventilation depends on external factors like outdoor temperature, wind force, wind direction, topography of the building context and internal factors like building's shape, orientation, window type, size, its position and air vents. Ventilated indoor environment conditions can be improved by varying these internal factors. For example, the natural ventilation performance of a room is better when the opening groups are in opposite directions to each other [5] and the dispersion of contaminant concentrations due to natural ventilation is affected by the type of air inlet [6].

The natural ventilation conditions can be investigated using various computational tools such as Computational Fluid Dynamics (CFD) in Ansys Fluent [7, 8]. These programs consist of models based on principles of energy conservation, mass conservation and momentum conservation in the space and time domain and can be used to calculate velocities, temperatures, pressures, vorticities and other fluid characteristics.

In the traditional buildings, a window, a lattice and a set of air vents are installed to achieve ventilation for a room. The information and reasoning behind the relative sizing and the placement of these features are not widely documented in literature. Therefore, the aim of this paper is to analyse the influence of different sizes and shapes of the air vents on natural ventilation. The objectives are to explore the available literature, designing, to develop computational models for CFD simulation, to analyse the simulated results and making recommendations for field studies in future.

2 Methodology

A virtual model building was designed for testing the effect of air vents and other window features in buildings. For a set of selected cases, the airflow was simulated using Computational Fluid Dynamics software, Analysis Fluent. The resulted flow patterns were analysed with regards to internal distribution of air flow velocities and air temperature.

3 Design of the Model Room

Referring to the typical room sizes of traditional buildings, a model room was designed for simulations. It is of size 4 m × 4 m × 5 m (13.12 ft × 13.12 ft × 16.40 ft) (W × H × L) and consists of a set of four windows of size 0.5 m × 1.5 m (1.64 ft × 4.92 ft) (W × H) on an external wall (Fig. 1). The orientation of the wall was selected as east as it was the most affected side from solar heat gains based on Cooling Load Temperature Difference (CLTD) calculations. Noon was selected as the design time of the day since

that is when the heat gains are maximum. The windows can be opened and closed. A lattice frame is placed on top of the window and the air vents are placed at a distance away above the lattice frame. Both of these are always open. Five types of frequently used shapes of air vents were considered in this study as shown in Fig. 1. An open door is placed on one side of the opposite wall to the windows as it is the typical location of the door.

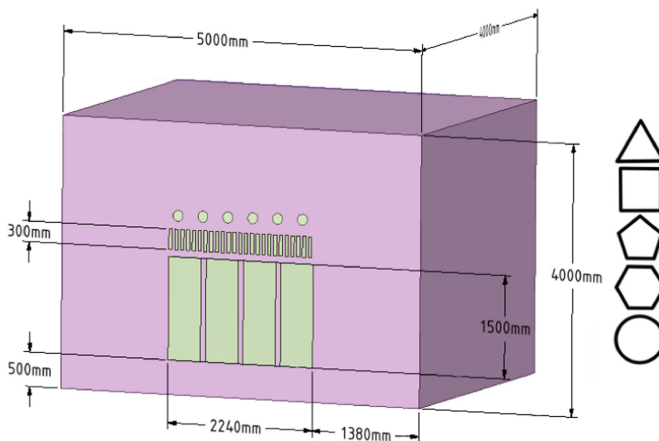


Fig. 1. Traditional window and air vent arrangement on the left side, and the shapes of air vents used in traditional buildings on the right side.

The building model was created in three-dimensional (3D) geometry since two-dimensional (2D) models does not give realistic air flow simulations, as separation of air flow around sharp edges are not considered in them [9, 10]. A 2D model will provide realistic solutions only if the applied boundary conditions and the model are symmetrical to any plane [11]. Hence, the most appropriate choice for this study is 3D modelling. However, the main disadvantage in 3D modelling is that it will take more time to converge to a solution. The external atmospheric zone size is selected as $25\text{ m} \times 25\text{ m} \times 20\text{ m}$ ($82.02\text{ ft} \times 82.02\text{ ft} \times 65.62\text{ ft}$) ($\text{W} \times \text{L} \times \text{H}$) after performing many simulations. The test room under investigation is located centrally in the external atmospheric zone as shown in Fig. 2.

The assumptions involved with the analysis are; only the wall with windows is an external wall while all others are internal, there are no objects in front of the external wall, only wind induced air flow is considered, constant air properties are assumed with reference to atmospheric temperature, wind direction is perpendicular to the window and air vent opening, wind velocity is constant and fluctuation is negligible. Continuity Equation, Momentum Equations and Energy Balance Equation were solved simultaneously during the simulations.

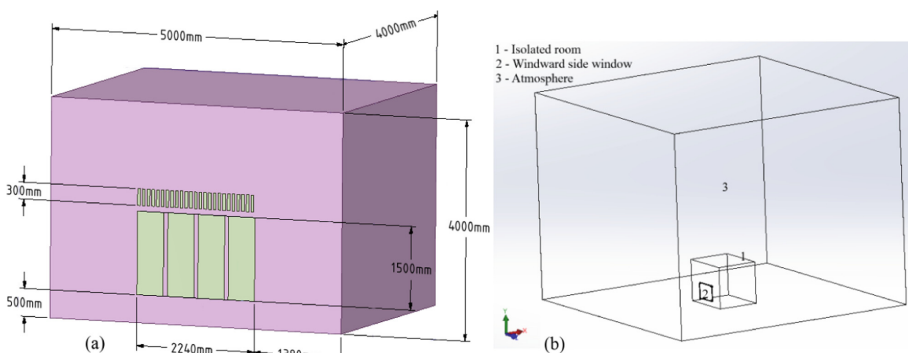


Fig. 2. (a) Test case room model and (b) computational domain for test case room with external atmosphere.

4 Design of Simulations

A series of simulations were designed as mentioned below to compare the effect of various window and air vent features on ventilation in terms of the indoor temperature distribution and air velocity.

1. Effect of different features of the window
2. Effect of shape of the air vents
3. Effect of number of air vents
4. Effect of having air vents on opposite wall.

A nine-point grid shown as in Fig. 3 was chosen to compare the temperature and air velocity distribution in the zone. The grid points 5 and 7 are on the windowed wall and points 6, 2, 4 and 8 are on the opposite side to windows. Grid point 4 is at the door and grid point 9 is in the middle of the room.

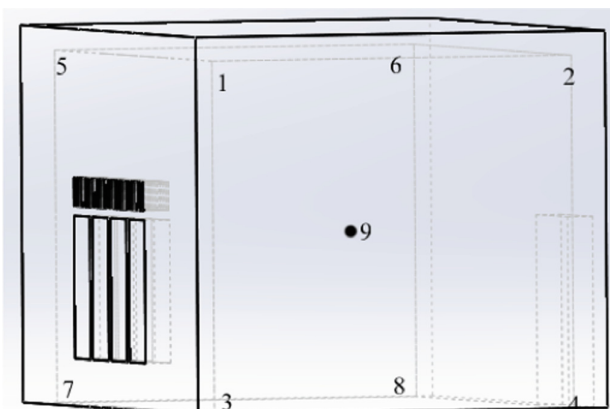


Fig. 3. Test Layout of the grid for obtaining values of performance indices.

A series of simulations were performed with combinations described in the next section.

5 Results and Discussion

5.1 Fonts Effect of Air Vents on Indoor Air Flow Characteristics

Four combinations are compared as shown in the Fig. 4. Firstly, no air vents and with windows (a) closed and (b) open and Secondly, with air vents and windows (a) closed and (b) open. Figure 5(a) shows the air temperature of considered grid points for each case simulated and the Fig. 5(b) presents the air velocity of the grid points.

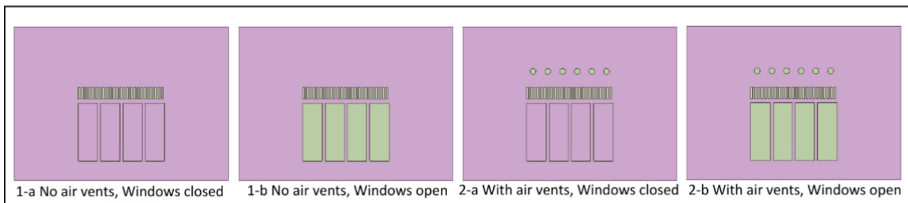


Fig. 4. Combinations of window features.

Temperature Variation. The door-side grid points show a lower value with lowest at the door compared to the other side of the room. For the cases 1a and 2a with closed windows, the temperature variation shows similar patterns and with the introduction of air vents the indoor temperature reduces in the case 2a by 0.2–0.3 K (0.36–0.54 °F).

With opened windows, the cases 1b and 2b show similar patterns with 0.8–1.5 K (1.44–2.7 °F) reduction in indoor temperature. With air vents, the overall temperature appears to fall even more by 0.1–0.3 K (0.18–0.54 °F). Comparing the temperature variation at the middle of the room, as a more general point, with closed windows, the air vents cause a temperature reduction of 0.11 K (0.198 °F), while that with open windows is 1.45 K (2.61 °F).

Air Velocity Variation. For Case 1a with only lattice openings, the air velocity is low. With introduction of air vents (2a) and opening windows (1b and 2b) the indoor velocity increases. In the same order, the air velocity variation in the middle of the room is 0.034 ms^{-1} (0.112 fts^{-1}), 0.057 ms^{-1} (0.187 fts^{-1}) and 0.069 ms^{-1} (0.226 fts^{-1}) respectively. According to the equivalent wind chill temperature equation [12] this increase in air velocity causes a reduction of 0.19 K (0.342 °F), 1.76 K (3.168 °F) and 2.17 K (3.906 °F) air temperature as sensed by the skin.

Among the analysed cases, case 2b has the minimum temperature and maximum velocity values which shows the effect of air vents on indoor temperature distribution and air flow. Performance of the indoor natural ventilation is also significantly influenced by the size and location of the openings [2] and wind generated pressure fields around the openings effects the indoor air distribution. This study shows that the increase in number of openings up along the wall cause a larger indoor air intake and it alters internal airflow trajectory thus the temperature distribution.

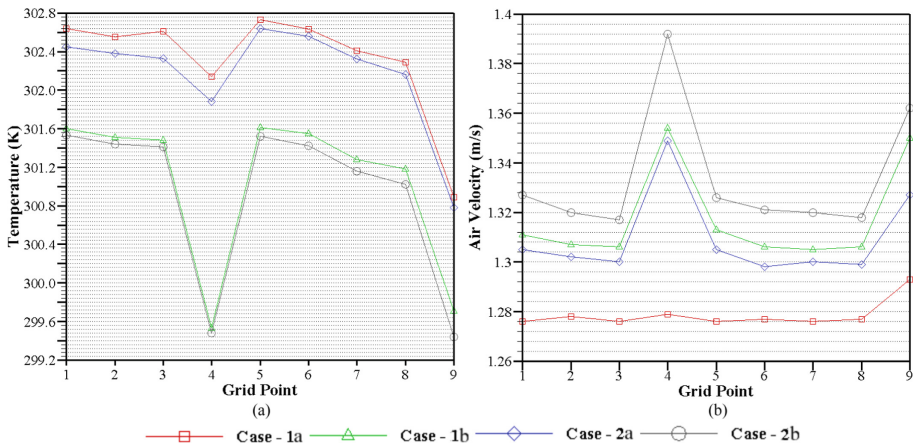


Fig. 5. Effect of air vents on indoor air flow characteristics: distribution of indoor air (a) temperature and (b) velocity.

5.2 Effect of Air Vents Shape on Indoor Air Flow Characteristics

Triangular, square, pentagonal, hexagonal and circular shapes were considered for simulations (see Fig. 1). The change of shape from triangular, square, pentagon, hexagon and circular shows an effect in reducing the temperature and increasing the velocity at grid points (Fig. 6) respectively. Changing the shape of the air vents from triangular to circular shape have caused a reduction in temperature by 0.24 K (0.432 °F) at the middle of the room (Fig. 6(a)) and an increase of air velocity by 0.012 ms⁻¹ (0.039 fts⁻¹) (Fig. 6(b)). Larger angles cause smaller load losses at the inlet, resulting in higher rates of indoor air renewal and improved thermal comfort. Which may be the reason for circular shape being the one most frequently appearing in the older traditional buildings.

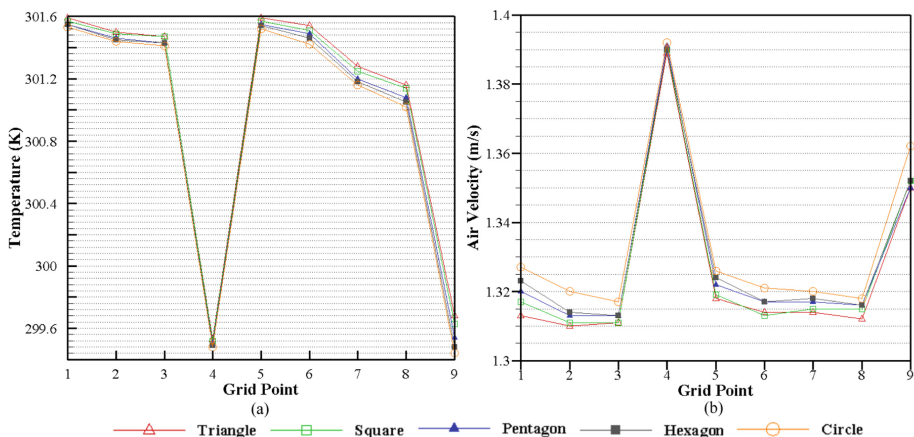


Fig. 6. Effect of air vents shape on indoor air flow characteristics: distribution of indoor air (a) temperature and (b) velocity.

5.3 Effect of Number of Air Vents on Indoor Air Flow Characteristics

Increasing the number of air vents (1, 3, 6 and 12) shows a considerable increase of air velocity (Fig. 7(b)) and flow circulation within the indoor space as expected. Increasing the number of air vents from one vent to twelve vents have caused a reduction in temperature by 0.24 K (0.432 °F) at the middle of the room (Fig. 7(a)) and an increase of air velocity by 0.005 ms^{-1} (0.016 fts^{-1}). Which causes the temperature to reduce by 0.416° as felt by the skin.

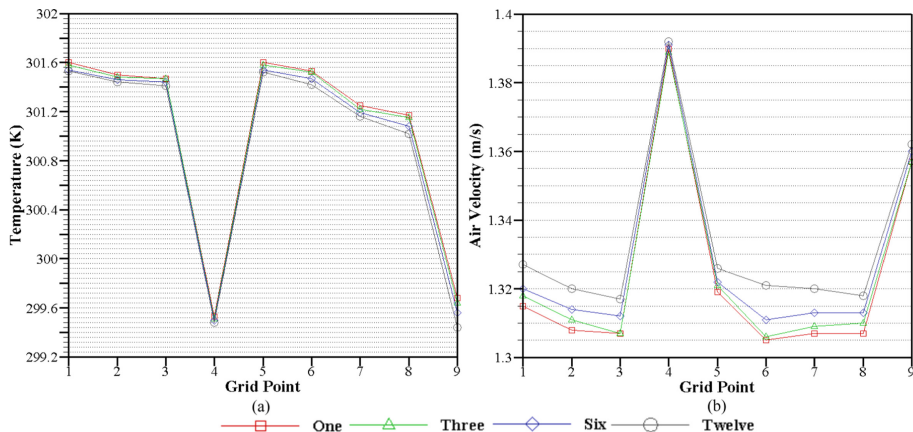


Fig. 7. Effect of number of air vents on indoor air flow characteristics: distribution of indoor air (a) temperature and (b) velocity.

5.4 Effect of Air Vents on Opposite Walls of the Room on Indoor Air Flow Characteristics

Compared to the design with twelve circular air vents only on window wall, when twelve air vents were introduced to the opposite wall the air temperature at the middle of the room is reduced by 0.18 K (0.324 °F) (Fig. 8(a)), and the air velocity is increased by 0.016 ms^{-1} (0.052 fts^{-1}) (Fig. 8(b)). Which is as felt by the skin is estimated to be a reduction of 0.276° .

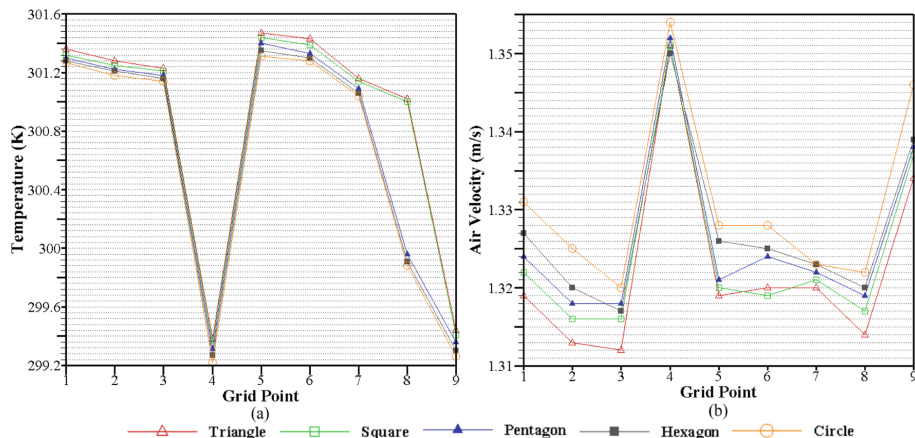


Fig. 8. Effect of air vents on opposite walls of the room on indoor air flow characteristics: distribution of indoor air (a) temperature and (b) velocity.

6 Conclusions

The results of the initial study showed that the indoor temperature is lowered by 0.34 to 0.39% when the windows are open and the existence of air vents bring it further down by 0.02 to 0.1%. Introducing air vents on the opposite wall reduces this further by 0.06%. This verifies that introducing the air vents makes a positive influence in natural ventilation. It was observed that the airflow in the internal environment is affected by the shape of the air vent and at the middle of the room, circular shape caused reduction of the temperature by 0.07% and increase of air velocity by 0.9% compared to the triangular shape.

Higher ventilation rates are achieved when the number of air vents increased, as it increases the area of air intake. Simulation results show that increment of number of vents from one to twelve reduces the indoor temperature by 0.02 to 0.08% and increases the indoor air velocity by 0.5 to 1.2%. Perceived temperature has reduced by 0.1 to 0.4% due to this increment in air velocity. Simulation results further reveal that increasing the number of vents promotes temperature uniformity throughout the room thus creating a lower temperature gradient across the room; however, this needs to be further investigated with smaller grid sizes.

Introducing air vents on opposite walls gave the best performance out of all the combinations, due to more openings cause more swirling and the area increment for indoor air renewal. Here, the indoor temperature is lowered by 0.5 to 1% and air velocity is increased by 3.5 to 6% which caused a reduction of perceived temperature by 2.3 to 5% compared to the design with no air vents and closed windows.

References

1. Aderhold, J., et al.: InN thin films grown by metalorganic molecular beam epitaxy on sapphire substrates. *J. Cryst. Growth* **222**(4), 701–705 (2001)

2. Allocca, C., Chen, Q., Glicksman, L.: Design analysis of single-sided natural ventilation. *Energy Build.* **35**(8), 785–795 (2003)
3. Sacht, H., Lukiantchuki, M.: Windows size and the performance of natural ventilation. *Procedia Eng.* **196**, 972–979 (2017)
4. Climate of Sri Lanka (2020). Meteo.gov.lk
5. Arsmson, D., Stringer, P., Ennos, A.: The effect of tree shade and grass on surface and globe temperatures in an urban area. *Urban Forest. Urban Greening* **11**(3), 245–255 (2012)
6. Gao, C., Lee, W.: Evaluating the influence of openings configuration on natural ventilation performance of residential units in Hong Kong. *Build. Environ.* **46**(4), 961–969 (2011)
7. Lee, E., Khan, J., Feigley, C., Ahmed, M., Hussey, J.: An investigation of air inlet types in mixing ventilation. *Build. Environ.* **42**(3), 1089–1098 (2007)
8. Asfour, O., Gadi, M.: Using CFD to investigate ventilation characteristics of vaults as wind-inducing devices in buildings. *Appl. Energy* **85**(12), 1126–1140 (2008)
9. King, M., et al.: Modelling urban airflow and natural ventilation using a GPU-based lattice-Boltzmann method. *Build. Environ.* **125**, 273–284 (2017)
10. Visagavel, K., Srinivasan, P.: Analysis of single side ventilated and cross ventilated rooms by varying the width of the window opening using CFD. *Sol. Energy* **83**(1), 2–5 (2009)
11. Evola, G., Popov, V.: Computational analysis of wind driven natural ventilation in buildings. *Energy Build.* **38**(5), 491–501 (2006)
12. Prakash, D., Ravikumar, P.: Analysis of thermal comfort and indoor air flow characteristics for a residential building room under generalized window opening position at the adjacent walls. *Int. J. Sustain. Built Environ.* **4**(1), 42–57 (2015)
13. ASHRAE Handbook - Fundamentals. American Society of Heating, Refrigerating and Air-Conditioning Engineers, Atlanta (1993)



How to Make Green Building Certification & Rating Systems More Pandemic-Sustainable?

A. Tleuken¹, G. Tokazhanov¹, M. Guney^{1,2}, A. Turkyilmaz^{1,3}, and F. Karaca^{1,2}(✉)

¹ Department of Civil and Environmental Engineering, School of Engineering and Digital Sciences, Nazarbayev University, 53 Kabanbay Batyr Ave., Nur-Sultan 010000, Kazakhstan
{aidana.tleuken, galym.tokazhanov, mert.guney, ali.turkyilmaz, ferhat.karaca}@nu.edu.kz

² The Environment and Resource Efficiency Cluster (EREC), Nazarbayev University, Nur-Sultan 010000, Kazakhstan

³ Master of Engineering Management Program, Nazarbayev University, Nur-Sultan 010000, Kazakhstan

Abstract. The present study demonstrates a gap analysis (in response to the COVID-19 pandemic) of the best known widely used green building certification and rating systems (GBC&RSs): LEED, WELL, BREEAM, CASBEE. These systems have been analyzed for their missing responses according to a list of selected pandemic-sustainable indicators. The gap levels for each system have been calculated and then compared to each other. Among four GBC&RSs, BREEAM exhibited the smallest gap score, whereas LEED and WELL held the largest gap scores. Following these results, we suggest courses of action for each system to remove the gaps that will result in achieving a better response under pandemic conditions.

Keywords: Residential buildings · BREEAM · CASBEE · COVID-19 · LEED · Sustainability · SARS-CoV-2 · WELL

1 Introduction

The construction industry is globally recognized as one of the greatest polluters of the environment [1]. Therefore, the necessity of developing and executing environmentally sound and sustainable decisions is very high. Large chapters and institutions constantly develop their perspectives towards better buildings for tomorrow which will consume less energy, produce less waste, and minimally pollute the air [2]. This urge to action also impacts the development of international building codes which help assess the buildings and certify their level of ‘greeness’, thus promoting sustainability principles [3]. Therefore, comprehensive green building certification and rating systems (GBC&RS) are rising in popularity in the construction industry, making it more common for new buildings to be assessed and classified as ‘green’ buildings. Examples of such rating systems include LEED, WELL, Green Star, BREEAM, and Green Globes [2].

In December 2019, a new virus outbreak had happened in Wuhan, China [4]. It led to profound changes in lifestyles around the globe by forcing people to remain at their homes for long periods, with some changes becoming permanent. As a result, residences are becoming more important as not only homes but also as offices and study places. Therefore, it is imperative to closely consider the role of residential buildings as a tool to develop sustainability including the periods of pandemics and post-pandemics. Considering that scientists consistently predict the rise of zoonotic diseases in the future, the importance of residential sustainability may also rise [5, 6]. Different countries follow varying building codes along with their specific systems of sustainability assessments and green building certifications. In the present study, we aim to cover global GBC&RSs by choosing systems from different parts of the world that possess a good level of impact on the international scientific and industrial development, namely LEED (from the USA), WELL (USA), BREEAM (UK), and CASBEE (Japan) [7].

Previous research on the readiness levels of different GBC&RS has developed a list of pandemic-sustainable indicators in three categories: health & safety, environmental resources consumption, and comfort [8]. Each of these categories consists of specific indicators that would potentially provide sustainability for residential houses during pandemics. No single study defines one complete system to measure the building readiness responding to the pandemic – such a system is yet to be developed with all the necessary indicators of pandemic sustainability – however, different GBC&RSs may perform better in specific categories. For instance, BREEAM and CASBEE seem more balanced in terms of pandemic response, and they have some indicators from each of the listed categories, albeit some indicators also lacking. On the contrary, WELL, as a tool directed towards improving the wellbeing of residents, responds better to the indicators of comfort category. Finally, LEED, oriented on better energy performance, provides the best response in terms of environmental efficiency.

The present study aims to investigate internationally recognized GBC&RS by analyzing the criteria they need to implement to offer solutions for residential buildings that will make them less vulnerable to pandemics. It aims to provide a significant improvement for the certification systems by ensuring additional pandemic-sustainable criteria to offer better health & safety, comfort, and environmentally-friendly functions and services.

2 Methods

The pandemic-sustainable indicators which can help residential buildings and their residents better endure pandemics and used in the present study are based on earlier research [8] where they have been developed after a thorough literature review and round-table expert discussions (Table 1). A detailed discussion on how each indicator is essential to pandemics situations can be found in our previous study [8]. The sustainability concept is mainly represented through environmental and social pillars. Such systems as LEED, BREEAM, CASBEE, and WELL are internationally recognized both in industry and in research [7]. LEED is the most popular rating system designed in the US and targeting different building types [9]. Although the main focus of LEED is energy efficiency, it also emphasizes water preservation, waste management, and the wellbeing of the residents. BREEAM is an ecological evaluation system of the buildings designed in the

UK, touching all three sustainability pillars – environmental, social, and economic [10, 11]. CASBEE is a building evaluation method focusing on environmental characteristics and has been recently developed in Japan [12]. Finally, WELL is a US scorecard building standard that puts occupants' health and wellbeing as a design priority [13, 14], and differentiates itself from other GBC&RS as they mostly focus on environmental efficiency.

In the present study, a gap analysis technique is employed to assess the sustainability of the defined building certification systems to pandemics. Gap analysis is a tool to compare the actual conduct with the anticipated performance [15]. Thus, the relevant strategies and actions can be determined for further improvement based on the analyzed gaps in the performance of the assessment system. In contrast to other tools and methods (e.g., risk assessment), gap analysis is mainly beneficial due to its focus on the current state (e.g., rather than analyzing future states). We claim that a pandemic-sustainable GBC&RS's desired state is to adapt all the indicators listed in Table 1. Thus, the ideal future state is fully addressing all these criteria. Thereby, first, the selected systems are analyzed for any missing indicators in each category and subcategory – determining the current state. Then, the gap levels are calculated for the categories of pandemic-sustainable indicators – the portions of those missing indicators. After that, the total gap levels are calculated for each of GBC&RSs by:

$$\text{total gap level} = \frac{(\text{health\&safety gap level} + \text{env. resources gap level} + \text{comfort gap level})}{3} \quad (1)$$

After calculating the gap levels, a gap analysis has been performed followed by the development of suggestions for improvement.

Table 1. List of pandemic-sustainable indicators used in the present study

Category	Subcategory	Indicators
Health & safety	Prevention of Virus Propagation (PVP)	PVP1. Use of smart/innovative air quality control technologies PVP2. Use of touchless technologies PVP3. Self-cleaning spaces PVP4. Proper selection of indoor materials PVP5. Natural light PVP6. Adjustability of indoor temperature and humidity
	Mental Health (MH)	MH1. Availability of greenery and gardens MH2. Availability of outdoor spaces in the building

(continued)

Table 1. (*continued*)

Category	Subcategory	Indicators
		MH3. Access to common building spaces with sufficient safety and social distance MH4. Household-level activity/sport spaces
	Air Quality (AQ)	AQ1. Efficiency of air filtration systems against pathogen propagation AQ2. Monitor and control indoor air pollution AQ3. Control the airflows in micro spaces AQ4. Level of natural ventilation
	Water Quality and Availability (WQ)	WQ1. Safety measures of drinking water and/or tap water from contamination WQ2. Maintenance and/or decontamination of the building water system for infection
	Wastewater Management (WWM)	WWM1. Specific measures to limit virus propagation at household level WWM2. Availability of separate toilets for infected WWM3. Separation of greywater
Environmental resources	Energy Use (EU)	EU1. Access to backup energy sources EU2. Promotion of sustainable and alternative energy sources EU3. Use of energy-efficient appliances
	Waste Management (WM)	WM1. Proper segregation of medical waste WM2. Disinfection of household waste WM3. Management of an increased amount of waste
	Water Consumption (WC)	WC1. Access to alternative water sources WC2. Use of water-efficient appliances and fixtures

(continued)

Table 1. (continued)

Category	Subcategory	Indicators
Comfort	Personal Comfort (PC)	PC1. Specific emphasis on household-level ICT infrastructure access
		PC2. Levels of indoor space adjustability
		PC3. Personal space
		PC4. Design level adjustments on noise insulation and acoustics
	Local Services (LS)	LS1. Availability of self-dependent services in the residential complexes
	LS2. Urban/community farming	

3 Results and Discussion

3.1 LEED

3.1.1 Gap Level

Starting from the Health & Safety category, it is seen that in the subcategory of “Preventing virus propagation,” LEED does not respond to such indicators as PVP2 and PVP5. In “Water quality and availability,” – WQ1 indicator is also not included. Furthermore, the entirety of “Waste management” and “Mental health” subcategories are not considered. Thus, the gap level for the subcategory is calculated as 53%. Although LEED is positioned as an environmentally efficient and energy-focused system, it does not address some of the Environmental Resources category indicators. From the “Energy use” subcategory, EU1; and from “Waste management” – WM1, WM2, and WM3 are missing. Thus, the gap level for this subcategory is 50%. The whole Comfort category is not addressed in the LEED rating system – both Personal comfort and Local services subcategories. Thus, the gap level for the subcategory is 100%. To conclude, the total gap level is 68%.

3.1.2 Suggested Actions

To close the identified gap, the following actions are suggested: First, to prevent further virus propagation, it is needed to add the criteria regarding using touchless technologies to avoid touching the surfaces in the building and set some criteria for the minimal amount of natural light incoming inside the residence as it helps prevent the activity of bacteria. For better mental health state of the occupants, the system needs to promote making available (1) either greenery or gardens, (2) outdoor spaces in the building (e.g., balconies), (3) access to common building spaces while providing sufficient safety and social distance, and (4) household-level activity/sports spaces. For better water quality, it is required to control the safety measures of drinking water and/or tap water from contamination. As a measure of wastewater management to prevent bacterial and viral

propagation, it is advised to develop specific measures to limit virus propagation at the household level, such as a good level of sealing of pipes, sinks, and air conditioning. If it is accessible, separate toilets for infected people and setting greywater separation technologies to impede the virus transport are suggested to be installed. In terms of environmental resources, first, the installation of additional backup energy sources can be advised to be added, as lockdowns could bring increased energy demands. As residential waste generation has notably increased during lockdowns, the following criteria could improve its management: proper segregation of medical waste, disinfection of household waste, and management of the increased amount of waste. Last but not least, the comfort category is vital for the residents' wellbeing. First, as criteria of personal comfort, specific emphasis should be put on household-level ICT infrastructure access so that residents could use online medical services, study, and work remotely. Making indoor spaces adjustable, ensuring personal space, and regulating noise insulation and acoustics would improve occupants' personal comfort. In addition, it is needed to make available self-dependent services (pharmacies and stores) and urban/community farming in the residential complexes to avoid potential shortages of necessary goods.

3.2 BREEAM

3.2.1 Gap Level

Health & Safety category is well covered in BREEAM along with some indicators missing in: "Prevention of virus propagation" – PVP2 and PVP3, Mental health – MH2, Air quality – AQ1, and Wastewater management – WWM1, WWM2, WWM3. Thus, the gap level for the subcategory is 37%. The Environmental Resources category does not respond to subcategories of water management (WM1, WM2, WM3 indicators) and waste consumption (WC2). Thus, the gap level for the subcategory is 50%. The Comfort category lacks a couple of indicators of personal comfort – PC1 and PC2. Thus, the gap level for the subcategory is 33%. To conclude, the total gap level is 40%.

3.2.2 Suggested Actions

The gap could be closed with the following indicators being addressed in the system: First, acquiring touchless technologies and establishing self-cleaning spaces would prevent virus propagation. For a better state of residents' mental health, it is required to have a safe and sound connection of the outdoor spaces inside the building (e.g., balconies). The efficiency of air filtration systems against pathogen propagation should be established to provide decent air quality to the occupants. Several wastewater management strategies and measures limiting virus propagation are advised to be included in BREEAM, such as availability of separate toilets for infected, and separation of greywater. In contrast, effective waste management requires proper segregation of medical waste, disinfection of household waste, and management of the increased amount of waste. Use of water-efficient appliances and fixtures are required for cases of increased water consumption during lockdowns. For personal comfort, ensure a good level of ICT access and adjustable indoor space.

3.3 CASBEE

3.3.1 Gap Level

Health & Safety category has several gaps in terms of CASBEE's response, namely, in the following subcategories: Prevention of virus propagation (PVP1, PVP2, and PVP3 indicators), Mental health (MH2 and MH4), Air quality (AQ1 and AQ3), Water quality (WQ1, WQ2), and Wastewater management (WWM1, WWM2, and WWM3). Thus, the gap level for the subcategory is 63%. In the Environmental Resources category, energy use indicator EU1 and all three indicators of "Water management" are missing. Thus, the gap level for the subcategory is 50%. The Comfort category is partially addressed by CASBEE, with some missing indicators in personal comfort – PC3 – and Local services – LS1, LS2. Thus, the gap level for the subcategory is 50%. To conclude, the total gap level is 54%.

3.3.2 Suggested Actions

As further action, the following changes are advised: To impede viral spread, demand use of smart/innovative air quality control technologies (as they can indicate when the pathogens' amount is greater than allowed), touchless technologies, and self-cleaning spaces. Ensuring the occupants' better mental health states can be achieved by setting requirements of availability of outdoor spaces in the building and household-level activity/sports spaces. Air and water quality can be achieved through the addition of the following criteria into the standard: efficiency of air filtration systems against pathogen propagation, control the airflows in micro spaces, safety measures of drinking water and/or tap water from contamination, and maintenance and/or decontamination of the building water system for infection. To limit the spread of pathogens through wastewater, specific measures to limit virus propagation at the household level, creating separate toilets for infected and separating greywater criteria would be effective. Waste management could be especially problematic during lockdowns; therefore, proper segregation of medical waste, disinfection of household waste, and pre-developed management strategies of an increased waste amount would make these periods smoother. Although CASBEE ensures residents' comfort well, additional beneficial criteria could be providing personal space for the residents and demanding self-dependent services in the residential complexes with urban/community farming development.

3.4 WELL

3.4.1 Gap Level

In Health & safety category, WELL does not respond to preventing virus propagation (PVP2), mental health (MH2 and MH3), and wastewater management (WWM1, WWM2, WWM3). Thus, the gap level for the subcategory is 32%. Talking about the Environmental Resources category, all the subcategories are facing missed responses from the standard. Thus, the gap level for the subcategory is 100%. In the Comfort category, some of the indicators of personal comfort (PC1, PC2, PC3) and local services (LS1) are not being addressed. Thus, the gap level for the subcategory is 67%. To conclude, the total gap state level is 67%.

3.4.2 Suggested Actions

For Health and safety category, we suggest establishing the use of touchless technologies, making available outdoor spaces inside the buildings and also common spaces accessible (with sufficient safety and social distance). To make wastewater management effective, proper sealing of pipes and separation of greywater are advised to be arranged to limit virus propagation at the household level. In addition, the development of separate toilets for the infected is suggested. To improve energy use, it is needed to develop access to backup energy sources, ensure the promotion of sustainable/alternative energy sources, and establish the use of energy-efficient appliances. Waste management strategies could become more effective during pandemics with the following strategies included: proper segregation of medical waste, disinfection of household waste, and management of the increased amount of waste. In turn, water consumption could be improved with the establishment of access to alternative water sources and the use of water-efficient appliances. Comfort issues could be overcome if the following criteria are specified in the standard: decent ICT infrastructure, adjustable indoor space to perform different functions, and available personal space. Whilst, requiring self-dependent services in the residential complexes would help not to run out of necessary medicines and food during lockdowns.

For the summary of the gap values and further courses of action, see Table 2.

Table 2. Summary of gap analysis for investigated green building certification & rating systems (GBC&RS)

Tool	Category	Current gap score (%)		Suggested actions to close the gap in terms of pandemic-sustainable indicators
LEED	Health & safety	53	68	<u>Prevention of virus propagation:</u> Use of touchless technologies; Natural light <u>Mental health:</u> Availability of greenery and gardens; Availability of outdoor spaces in the building; Access to common building spaces with sufficient safety and social distance; Household-level activity/sport spaces <u>Water quality:</u> Safety measures of drinking water and/or tap water from contamination <u>Wastewater management:</u> Specific measures to limit virus propagation at household level; Availability of separate toilets for infected; Separation of greywater
	Environmental resources	50		<u>Energy use:</u> Access to backup energy sources <u>Waste management:</u> Proper segregation of medical waste; Disinfection of household waste; Management of an increased amount of waste

(continued)

Table 2. (continued)

Tool	Category	Current gap score (%)	Suggested actions to close the gap in terms of pandemic-sustainable indicators
	Comfort	100	<p>Personal comfort: Specific emphasis on household-level ICT infrastructure access; Levels of indoor space adjustability; Personal space; Design level adjustments on noise insulation and acoustics</p> <p><u>Local services:</u> Availability of self-dependent services in the residential complexes; Urban/community farming</p>
BREEAM	Health & safety	37	<p><u>Prevention of virus propagation:</u> Use of touchless technologies; Self-cleaning spaces</p> <p><u>Mental health:</u> Availability of outdoor spaces in the building</p> <p><u>Air quality:</u> Efficiency of air filtration systems against pathogen propagation</p> <p><u>Wastewater management:</u> Specific measures to limit virus propagation at household level; Availability of separate toilets for infected; Separation of greywater</p>
	Environmental resources	50	<p><u>Waste management:</u> Proper segregation of medical waste; Disinfection of household waste; Management of an increased amount of waste</p> <p><u>Water consumption:</u> Use of water-efficient appliances and fixtures</p>
	Comfort	33	<p><u>Personal comfort:</u> Specific emphasis on household-level ICT infrastructure access; Levels of indoor space adjustability</p>
CASBEE	Health & safety	63	<p><u>Prevention of virus propagation:</u> Use of smart/innovative air quality control technologies; Use of touchless technologies; Self-cleaning spaces</p> <p><u>Mental health:</u> Availability of outdoor spaces in the building; Household-level activity/sport spaces</p> <p><u>Air quality:</u> Efficiency of air filtration systems against pathogen propagation; Control the airflows in micro spaces</p> <p><u>Water quality:</u> Safety measures of drinking water and/or tap water from contamination; Maintenance and/or decontamination of the building water system for infection</p> <p><u>Wastewater management:</u> Specific measures to limit virus propagation at household level; Availability of separate toilets for infected; Separation of greywater</p>

(continued)

Table 2. (continued)

Tool	Category	Current gap score (%)	Suggested actions to close the gap in terms of pandemic-sustainable indicators
	Environmental resources	50	<u>Energy use:</u> Access to backup energy sources <u>Waste management:</u> Proper segregation of medical waste; Disinfection of household waste; Management of an increased amount of waste
	Comfort	50	<u>Personal comfort:</u> Personal space <u>Local services:</u> Availability of self-dependent services in the residential complexes; Urban/community farming
WELL	Health & safety	32	<u>Prevention of virus propagation:</u> Use of touchless technologies <u>Mental health:</u> Availability of outdoor spaces in the building; Access to common building spaces with sufficient safety and social distance <u>Wastewater management:</u> Specific measures to limit virus propagation at household level; Availability of separate toilets for infected; Separation of greywater
	Environmental resources	100	<u>Energy use:</u> Access to backup energy sources; Promotion of sustainable and alternative energy sources; Use of energy-efficient appliances <u>Waste management:</u> Proper segregation of medical waste; Disinfection of household waste; Management of an increased amount of waste <u>Water consumption:</u> Access to alternative water sources; Use of water-efficient appliances and fixtures
	Comfort	67	<u>Personal comfort:</u> Specific emphasis on household-level ICT infrastructure access; Levels of indoor space adjustability; Personal space <u>Local services:</u> Availability of self-dependent services in the residential complexes

Overall, comparing the gap levels by categories (Fig. 1), we see that the gap for Health & Safety is the smallest for WELL and BREEAM and largest for CASBEE. The Environmental Resources category is equally half-covered by LEED, CASBEE, and BREEAM, while WELL has the absolute gap level for that – 100%. LEED has the largest gap state level over the category of Comfort, whereas it is currently best covered by BREEAM, which has a minimal gap level for the same category. Overall, the total values of current gap states have the largest numbers for LEED and WELL whereas BREEAM has the least gap level (Fig. 2).

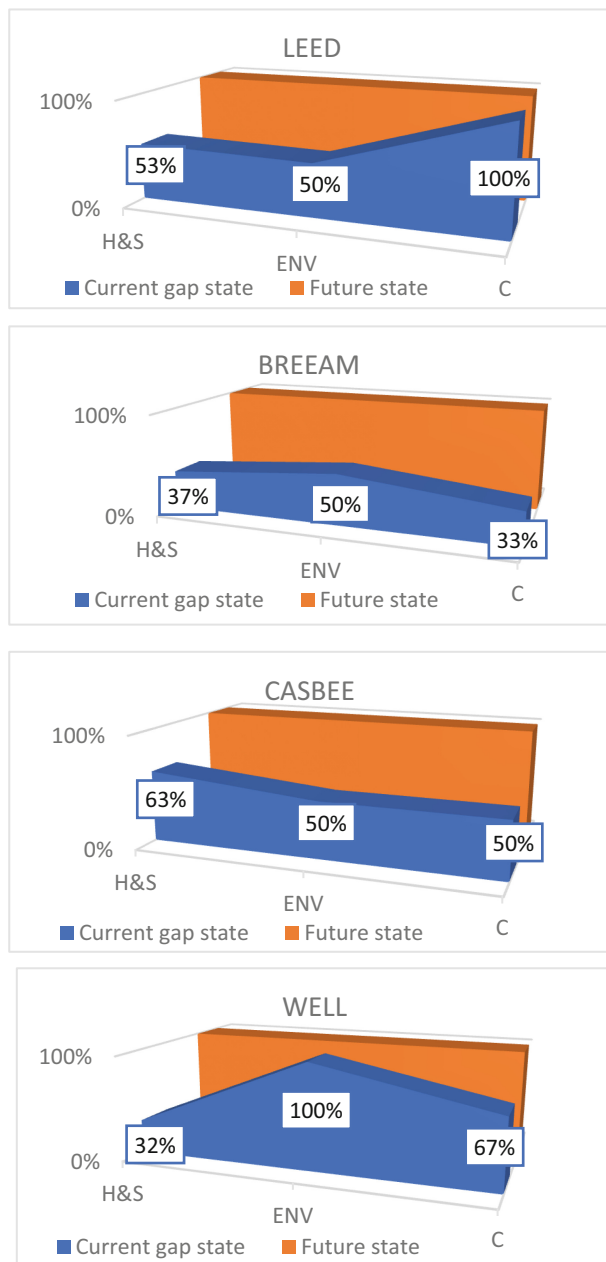


Fig. 1. Current gap states of GBC&RS (by category).

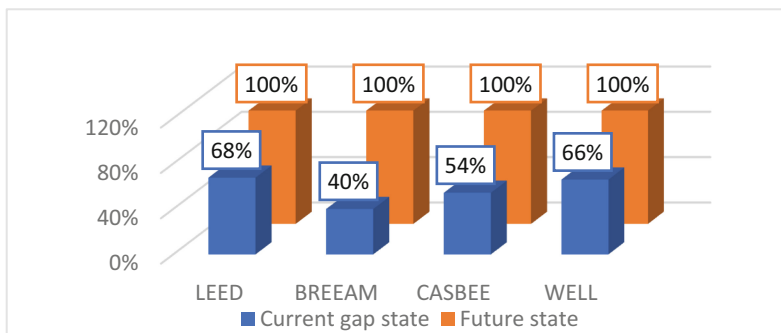


Fig. 2. Current gap states of GBC&RS (total score).

4 Conclusion

The present work assesses the need for existing global green building certification & rating systems (GBC&RS) to implement indicators that would make them more sustainable to pandemics and, as a result, would improve residential buildings' pandemic requirements. The COVID-19 pandemic has taught us a lesson: our homes are the best multi-functional shelters, where we could live, work, study, and have leisure. Therefore, the present study aims to add value to the residential buildings' development by suggesting a set of indicators on green building concepts. Overall, a gap analysis has been performed, clearly identifying the particular missing responses from four major GBC&RS: BREEAM, LEED, WELL, and CASBEE. It was found that the BREEAM system has the minimum gap state, whereas the maximum one was noted in LEED. The main limitations of the present study include consideration of a limited number of certification and rating systems and a focus on environmental and social sustainability pillars only. Future work can be directed towards both improvements of existing and development of new building codes and certifications that would extensively consider pandemic issues.

Acknowledgments. The authors acknowledge the financial support from Nazarbayev University's Faculty Development Competitive Research Grant Program (FDCRGP, Funder Project Reference: 280720FD1904).

References

1. Akhanova, G., Nadeem, A., Kim, J.R., Azhar, S.: A framework of building sustainability assessment system for the commercial buildings in Kazakhstan. *Sustainability* **11**, 1–24 (2019). <https://doi.org/10.3390/su11174754>
2. World Green Building Council Rating tools. <https://www.worldgbc.org/rating-tools>
3. Diaz-Sarachaga, J.M., Jato-Espino, D., Alsulami, B., Castro-Fresno, D.: Evaluation of existing sustainable infrastructure rating systems for their application in developing countries. *Ecol. Indic.* **71**, 491–502 (2016). <https://doi.org/10.1016/j.ecolind.2016.07.033>

4. WHO Timeline - COVID-19. <https://www.who.int/news/item/27-04-2020-who-timeline---covid-19>. Accessed 1 Jan 2021
5. Hui, D.S., et al.: The continuing 2019-nCoV epidemic threat of novel coronaviruses to global health — the latest 2019 novel coronavirus outbreak in Wuhan, China. *Int. J. Infect. Dis.* **91**, 264–266 (2020). <https://doi.org/10.1016/j.ijid.2020.01.009>
6. Morris, A. Coronavirus outbreak is part of worldwide increase in disease spread. <https://www.azcentral.com/story/news/local/arizona-health/2020/03/30/coronavirus-covid-19-outbreak-part-worldwide-increase-disease-spread/5048560002/>. Accessed 1 May 2021
7. Bernardi, E., Carlucci, S., Cornaro, C., Bohne, R.A.: An analysis of the most adopted rating systems for assessing the environmental impact of buildings. *Sustainability* **9**, 1–27 (2017). <https://doi.org/10.3390/su9071226>
8. Tleuken, A., Tokazhanov, G., Guney, M., Turkyilmaz, A., Karaca, F.: Readiness assessment of green building certification systems for residential buildings during pandemics. *Sustainability* **13**, 1–31 (2021). <https://doi.org/10.3390/su13020460>
9. Awadh, O.: Sustainability and green building rating systems: LEED, BREEAM, GSAS and Estidama critical analysis. *J. Build. Eng.* **11**, 25–29 (2017). <https://doi.org/10.1016/j.jobe.2017.03.010>
10. BREEAM BREEAM Communities. Technical Manual SD202 - 0.1:2012, p. 175 (2012)
11. Mahmoud, S., Zayed, T., Fahmy, M.: Development of sustainability assessment tool for existing buildings. *Sustain. Cities Soc.* **44**, 99–119 (2019). <https://doi.org/10.1016/j.scs.2018.09.024>
12. IBEC CASBEE for New Construction Tool-1 (2004)
13. IWBI The WELL Building Standard (2016)
14. US Green Building Council What is WELL? <https://www.usgbc.org/articles/what-well>
15. Smartsheet Guide to Gap Analysis with Examples. <https://www.smartsheet.com/gap-analysis-method-examples>



Assessing Risk Factors in the Implementation of Green Building Projects: Empirical Research from Vietnam

Hung D. Nguyen¹(✉), Quang N. H. Do², and Laura Macchion¹

¹ Department of Management and Engineering, University of Padova, Stradella S. Nicola, 3, 36100 Vicenza, Italy

duyhung.nguyen@studenti.unipd.it

² GREENVIET Green Building Consultancy Company, Ho Chi Minh City, Vietnam

Abstract. In line with the sustainable trend in the construction industry worldwide, there have been a number of studies that examined risks in Green Building (GB) projects recently. This study aimed to assess risk factors that GB projects often face through a questionnaire survey with 69 GB practitioners in Vietnam. Notably, this study evaluated GB risk factors according to three features: likelihood occurrence, the magnitude of impact, and risk controllability. The results indicated the top five crucial risks are “Owners lacks determination”; “Lack of experience of designers about GB”; “Project managers lack experience in GB projects”; “Underestimation of initial investment cost”; and “Project managers lack design management experience”. This paper could be a helpful reference for the construction industry by providing a profoundly assessing GB projects’ risks. Additionally, this study contributes empirical research of risk assessment in GB projects in Vietnam. Therefore, this study may contribute to the development of sustainable trends in the construction industry worldwide.

Keywords: Green building · Risk assessment · Developing countries

1 Introduction

Construction industries and their activities have contributed significantly to environmental pollutants in the world [1]. To handle this problem, Green Buildings (GBs) has been considered a helpful solution to decrease the influence on the environment by construction communities [2, 3]. According to previous studies, GBs are different from traditional buildings by emphasizing environmental and social features [3]. Recently, there has been noteworthy development of GBs worldwide. Notably, GBs have also received attention in emerging economies [4]. According to the previous research, several developing countries had a significant GB development recently, and this was anticipated to grow quicker in the near future [5].

However, many hindrances can restrain the development of GBs [6]. Recently, risks in GB projects is a substantial barrier and got more attention from researchers and construction practitioners [3]. Indeed, previous research claimed that “No construction

project is risk-free” [7]. Every construction project usually faces various problems related to different aspects, such as cost, schedule, and human resources. Interestingly, according to previous studies, GB risks were higher than risks in conventional risks [8, 9]. Thereby, risks should be managed efficiently for achieving project targets [10, 11]. This finding indicated that managing risks is crucial for success in any GB project. Indeed, managing risks in GB projects is more challenging compared to traditional projects due to the purpose of achieving sustainability which differs from the typical target such as quality, schedule, and cost [12]. GB projects tend to adopt the latest construction technologies and green materials to achieve sustainability, which could lead to uncertainties in financial, technical, quality, safety, and environmental [9].

Recently, a number of studies attempted to examine the GB risk topic. Nevertheless, such studies were mainly implemented in some countries, including Singapore, China, The United States, and Australia. As far as we know, a lack of studies was conducted in developing countries. Thus, this indicated the necessity to investigate risks in GB projects in less explored countries. Moreover, the previous studies mainly assess GB risks based on the traditional approach: evaluate risk based on two features, including occurrence and magnitude of impact. In this research, we examined the risk controllability of GB risk factors, which was recommended by previous research in the risk literature [13]. Such research could provide more helpful information about GB risks to practitioners. Indeed, some risks may be more controllable than others in nature.

In summary, this study assesses risk factors profoundly in GB projects in Vietnam according to three features: likelihood occurrence, the magnitude of impact, and risk controllability. This research thus contributes to the body of knowledge in this field by providing a new viewpoint of GB risk in a developing country.

2 Develop a List of GB Risk Factors

Recently, a number of researchers endeavored to investigate risk in GB projects in several countries.

In Singapore, Hwang et al. [8] examined risks in GB projects. This research revealed a list of critical risks in GB projects, such as “Complex procedure to obtain approval,” “Overlooked high initial cost,” and “Lack of availability of green material and equipment.” Likewise, another research in Singapore investigated risk factors in commercial GB projects [9]. This study also revealed the list of critical risk factors such as “Inflation,” “Damages caused by human error,” and “Shortage of green materials.” Notably, both these studies attempted to compare GB risks with risks in traditional projects. The outcomes demonstrated that risks in GB projects are more critical compared to risks in conventional projects. This is understandable since GBs adopt novel technologies and green material to achieve sustainability; thereby, GB projects have to confront more uncertainties than traditional projects.

Another study examined risks linked to GB projects in China [14]. The result indicated the two most crucial risks were “Lack of experienced managers in the operation phase” and “The satisfaction of public with GB projects is meager”. Similarly, in China, Qin et al. [15] evaluated risk factors in GB projects and ranked the critical degree of risks based on their occurrence likelihood and impact. Interestingly, the outcome exposed the

diversity in risk evaluation between various parties in GB projects. This could help stakeholders in the risk management process by allocating risk based on their specific risks.

In Kuwait, Ismael et al. [16] tried to explore risks associated with GB projects. This research proved that the most severe risks were the inexperience of both designers and contractors with GBs. Notably, another research assessed risks in GB projects based on a questionnaire in 56 different countries from all the continents [17]. The outcome revealed the high consensus in risk assessment between various roles.

Based on the result of a comprehensive literature review, this study created a list of GB risks. This list was then reviewed and complemented by a group of GB experts. Furthermore, in our previous research, we attempted to reduce the number of risk factors using data reduction techniques. Finally, the 30 most crucial risk factor was identified. Describe of these risks and their corresponding sources were presented in Table 1.

Table 1. List of risk factors in GB projects.

Code	Risk factors	Sources
RF1	Lack of GB experienced contractors	[3, 8, 12, 15–20]
RF2	Lack of GB experienced professionals	[3, 8, 9, 12, 15, 16, 20]
RF3	Project managers lacks experience	[15, 17, 20]
RF4	Unfamiliarity with green materials	[8]
RF5	Difficulty in the selection of GB contractors	[3, 16, 19, 20]
RF6	Improper quality control process	[3, 9, 20, 21]
RF7	Detail design are unclear or possible errors	[8, 9, 12, 20]
RF8	The performance of GB projects is not reached	[3, 15]
RF9	Lack of adequate GB maintenance	[3, 15]
RF10	Lack of experienced managers in the operation phase	[3]
RF11	Evaluation results do not reach the target	[3, 15, 16, 18–20]
RF12	The lack of cooperation in the GB trial operation stage	[15]
RF13	Difficulties in operating green solutions	[16]
RF14	Late involvement of GB consultants	[22]
RF15	Inefficient communication and coordination	[3, 8, 12, 18]
RF16	Project managers lack design management experience	[15, 17, 19, 20]
RF17	Lack of experience of designers	[3, 15–20, 23]
RF18	The owner lacks determination	[22]
RF19	Long payback period	[16, 18, 24]

(continued)

Table 1. (*continued*)

Code	Risk factors	Sources
RF20	High costs of sustainable materials and equipment	[9, 15, 16, 20, 25]
RF21	Lack of accurate estimation	[3, 15, 21, 23, 26]
RF22	Underestimation of initial investment cost	[3, 8, 16]
RF23	Increasing inflation rate	[3, 8, 9, 12, 15, 17, 18, 20, 21]
RF24	Complex planning approval and permit procedures	[3, 12, 27]
RF25	Change in regulations/policies	[3, 9, 16, 17, 19, 20, 25]
RF26	Unclear contract conditions for dispute resolution	[8, 12, 17, 21, 25]
RF27	Delay in decision-making	[22]
RF28	Green material quality problems	[12, 16–18]
RF29	Lack of availability of green materials	[3, 8, 9, 12, 15–18, 20, 21, 26]
RF30	No general standards for green materials	[22]

3 Research Methodology

This research conducted a questionnaire survey to assess risk factors in GB projects. In this survey, the participants were asked to (1) assess risk factors based on three features: impact level, likelihood, and controllability; (2) provide their background information such as company scale, experience, and GB knowledge. The survey questionnaires were sent to 260 GB practitioners (by email or hand-delivery). The respondents were identified based on the construction companies that experienced GB projects in Vietnam. As a result, we received 76 answers with a response rate was 29% (i.e., 44 hard copies and 32 online forms). In which, seven answers were omitted because of unfinished answers or participants' experience is less than three years. Finally, 69 responses were used to calculate the evaluation of GB risk factors.

This study aimed to assess 30 risk factors according to three features (i.e., magnitude of impact, likelihood occurrence, and risk controllability). The significance of risk factors would then be calculated based on the impact level, likelihood occurrence, and controllability. The scale of features was presented in Table 2.

Based on the input from the survey, this study determined the LO, MI, and RC of risks. Among these, LO and MI were calculated using Eqs. 1–2, respectively [8].

$$LO^i = \frac{1}{n} \sum_{j=1}^n LO_j^i \quad (1)$$

$$MI^i = \frac{1}{n} \sum_{j=1}^n MI_j^i \quad (2)$$

Table 2. The scales for risk assessment

Scales	The magnitude of Impact (MI)	Likelihood of Occurrence (LO)	Risk controllability (RC)
1	Very insignificant	Very unlikely	Extremely easy to control
2	Insignificant	Unlikely	Easy to control
3	Fairly significant	Fairly likely	Medium to control
4	Significant	Likely	Difficult to control
5	Very significant	Very likely	Greatly difficult to control

While RC was calculated using Eqs. 3 [13].

$$RC^i = \frac{1}{n} \sum_{j=1}^n RC_j^i \quad (3)$$

Where n denotes the number of responses, LO is the likelihood occurrence, MI is the magnitude of impact, and RC is the risk controllability.

After that, the risk assessment (RA) was calculated based on the traditional approach (Eq. 4). This method has been commonly used in risk literature [8, 28].

$$RA = \sqrt{LO \times MI} \quad (4)$$

Notably, this research also considered the risk controllability of risk as recommended by Dikmen et al. [13]. To assess risk more comprehensively, this research recommended calculating the risk significance (RS) by the following equation:

$$RS = \sqrt[3]{LO \times MI \times RC} \quad (5)$$

4 Result and Discussion

4.1 Demographics of Survey Participants

Table 3 presents the characteristics of the survey participants. In general, this survey covered various types of construction companies. Table 3 shows that 91.3% of the respondents worked at international or national companies. Additionally, 62.32% of the participants have rich experience in the construction industry (≥ 10 years). The large scale of companies and rich understanding of the respondents indicated the reliability of collected data.

In this research, the respondents were classified into three groups: owner, designer, and contractor. According to Table 3, most of them (68.12%) worked for owner agencies; 11 participants (15.94%) were designers, and seven respondents (10.14%) were contractors. Regarding the GB knowledge and involvement, most of the participants (94.2%) were ‘familiar’ or ‘expert’ with GB projects, and 92.75% of the participants participated

Table 3. Characteristics of respondents

Characteristics		Frequency	Percent (%)
Company scales	International	38	55.07
	National	25	36.23
	Multi-cities/provinces	3	4.35
	Within a province/city	3	4.35
Project role	Owners	47	68.12
	Designers	11	15.94
	Contractors	7	10.14
	Others	4	5.80
Year of experience	3–5 years	26	37.68
	6–10 years	10	14.49
	11–15 years	15	21.74
	More than 15 years	18	26.09
GB knowledge	Expert	25	36.23
	Familiar	40	57.97
	Somewhat familiar	4	5.80
GB involvement	Often	35	50.72
	Occasionally	29	42.03
	Rarely	5	7.25
GB types	Commercial	25	36.23
	Education	3	4.35
	Industry	30	43.48
	Residential	11	15.94
	(n = 69)		

in GB projects more than ‘rarely’. These findings indicated that the respondents have sufficient abilities to assess GB risks.

In terms of GB type, most respondents participated and were familiar with commercial (25) and industry (30) GB projects in Vietnam. The number of respondents experienced with residential GBs was 11, and only three respondents answered that they usually joined in education GB projects.

4.2 The Assessment Results of GB Risk Factors

Firstly, Cronbach’s alpha was determined to test the consistency and reliability of the collected data. According to previous studies, the values of alpha should be at least 0.7 [29]. In this research, the alpha for LO, MI, and RC was calculated separately and have

the values of 0.935, 0.914, and 0.923, respectively. This indicated that the collected data is appropriate for further analysis. Based on the inputs from the questionnaire survey, this study calculated the parameters for every risk factor, including likelihood occurrence, magnitude impact, risk controllability, risk assessment, and risk significance. Table 4 presents the mean values and the corresponding ranking for the 30 risk factors according to each parameter.

Table 4. The assessment results of GB risk factors

Code	LO		MI		RC		RA		RS	
	Mean	Rank								
RF1	3.35	12	3.54	21	3.19	15	3.44	16	3.35	17
RF2	3.28	16	3.81	3	3.28	13	3.53	9	3.45	11
RF3	3.54	4	3.8	4	3.32	11	3.66	2	3.55	3
RF4	3.46	6	3.46	23	3.13	21	3.46	15	3.35	18
RF5	3.03	25	3.17	30	2.99	28	3.1	29	3.06	29
RF6	3.13	23	3.33	27	3.04	25	3.23	24	3.17	25
RF7	3.14	21	3.65	8	3.17	18	3.39	19	3.32	19
RF8	3.12	24	3.39	24	3.19	16	3.25	22	3.23	23
RF9	3.38	9	3.65	9	3.14	20	3.51	11	3.38	15
RF10	3.36	10	3.58	19	3.2	14	3.47	14	3.38	16
RF11	2.96	27	3.48	22	3.04	26	3.21	25	3.15	26
RF12	3.14	22	3.65	10	3.1	23	3.39	20	3.29	21
RF13	2.96	28	3.36	26	2.97	30	3.15	28	3.09	28
RF14	3.26	18	3.61	15	3.36	6	3.43	18	3.41	14
RF15	3.29	15	3.8	5	3.32	11	3.53	9	3.46	8
RF16	3.59	2	3.65	11	3.36	7	3.62	3	3.53	5
RF17	3.61	1	3.8	6	3.32	11	3.7	1	3.57	2
RF18	3.35	12	3.83	1	3.65	1	3.58	6	3.60	1
RF19	3.59	3	3.65	12	3.13	22	3.62	4	3.45	11
RF20	3.49	5	3.61	16	3.17	18	3.55	7	3.42	13
RF21	3.16	20	3.61	17	3.09	24	3.38	21	3.28	22
RF22	3.41	8	3.83	2	3.39	5	3.61	5	3.54	4
RF23	3.35	12	3.65	13	3.55	4	3.5	13	3.51	6
RF24	3.28	17	3.61	18	3.61	2	3.44	17	3.49	7
RF25	2.86	29	3.57	20	3.59	3	3.19	26	3.32	20
RF26	2.83	30	3.26	29	3.01	27	3.04	30	3.03	30

(continued)

Table 4. (*continued*)

Code	LO		MI		RC		RA		RS	
	Mean	Rank								
RF27	3.33	14	3.7	7	3.33	8	3.51	12	3.45	11
RF28	2.97	26	3.38	25	2.99	29	3.17	27	3.11	27
RF29	3.43	7	3.62	14	3.33	9	3.53	9	3.46	9
RF30	3.19	19	3.32	28	3.17	18	3.25	23	3.23	24

Overview of Risk Assessment Results. As illustrated in Table 4, all the risk factors have RS greater than 3.00, which signifies that risks in GB projects are relatively high.

Regarding LO values, 26 risk factors were evaluated higher than 3.00, which implies these risks were moderately likely to happen in GB projects. In which, the top five risk factors in likelihood occurrence were RF17 (“Lack of experience of designers”), RF16 (“Project managers lack design management experience”), RF19 (“Long payback period”), RF3 (“Project managers lacks experience”), RF20 (“High costs of sustainable materials and equipment”).

In terms of MI values, all 30 risk factors had evaluations higher than 3.00 that indicated the significant effect of these risk factors on GB projects. The top five impact risk factors were RF18 (“The Owner lacks determination”), RF22 (“Underestimation of initial investment cost”), RF2 (“Lack of GB experienced professionals”), RF3 (“Project managers lacks experience”), and RF15 (“Inefficient communication and coordination”).

Regarding RC values, 27 risk factors were assessed above 3.00, signifying that these risks are not easy to control in GB projects. The top five most challenging control risk factors were RF18 (“The Owner lacks determination”), RF24 (“Complex planning approval and permit procedures”), RF25 (“Change in regulations/policies”), RF23 (“Increasing inflation rate”), and RF22 (“Underestimation of initial investment cost”).

Most Critical Risk Factors. In this step, we will discuss the top five critical risk factors based on the RS values:

The risk factor RF18, “Owners lacks determination,” is the most critical risk with a mean value of RS was 3.60. This factor reflected the essential role of owners in the implementation of GB projects in Vietnam. This risk also revealed a problem in Vietnam: owners tend to give up as they face significant difficulties in GB projects. Notably, this factor has the highest MI and RC, which makes this risk factor more critical. At the same time, the likelihood of occurrence of this risk is not too high (LO ranked 12th). Thus, if only using the traditional method, this risk factor just ranked sixth, making practitioners underestimate this risk factor. To mitigate this risk, provide the necessary knowledge to owners may be helpful and may improve the implementation process of GB projects.

The risk RF17, “Lack of experience of designers,” occupied the second position with an RS value was 3.57. This factor revealed a significant problem in Vietnam: designers frequently do not have enough experience with GB projects. This is the most common problem in Vietnam, which is demonstrated by the highest LO values. Moreover, such

issues can affect GB projects dramatically, with MI rated sixth. Fortunately, it seems we still can control this risk factor which reflects by its RC ranked 11th. Indeed, we can mitigate this significantly by training the designers.

The third position is the risk RF3 (“Project managers lack experience”), with an RS value was 3.55. This risk reflects the incapacity of the project managers in GB projects. Indeed, GB projects are complex construction projects. Thus, to manage GB projects efficiently, project managers need knowledge and experience about GB. The results of LO and MI indicated that this factor is a common problem and has a high impact in Vietnam. Fortunately, like RF17, we can mitigate this risk by providing suitable training programs to construction practitioners.

The risk RF22, “Underestimation of initial investment cost,” was in the fourth position (RS value was 3.54). This is the problem that also had a high evaluation in previous studies [8, 16]. This reflects an issue that practitioners frequently neglect some critical costs at the beginning of GB projects (e.g., green material cost and GB consultant cost). Notably, this risk factor has a very high impact, with the MI value ranked second. Indeed, this problem could lead to cost overrun in the implementation of GB projects. Also, the likelihood of occurrence is in the top ten common risks.

Finally, the fifth position belonged to the risk RF16 (Project managers lack design management experience) with an RS value was 3.53. This factor reflects another problem related to the human resources risks in the design phase of GB projects. This reflects the critical role of project managers in the design phase of GB projects. Notably, this risk factor is the second most common risk in Vietnam (LO ranked second) while its impact level ranked 11th. Thus, if we only calculate the traditional method, this risk is ranked third (RA ranked third). However, its RC ranked seventh due to high controllability.

5 Conclusion

To reduce the negative impacts of the construction industry on the environment, develop GBs is a potential solution. However, construction practitioners usually confront many risk factors in the implementation process of GB projects. Therefore, we need to provide more knowledge about risks in GB projects for construction practitioners to manage risks better. However, GB currently lacks research in this direction, especially in developing countries. Thus, this research aimed to deeply assess GB projects in Vietnam by evaluating three features: likelihood occurrence, the magnitude of impact, and controllability.

This research revealed detailed assessments of GB risk according to likelihood occurrence, the magnitude of impact, controllability, risk assessment, and risk significance. The result also exposed the ranking of risk factors according to each parameter. The top five risk factors are: “The Owner lacks determination”; “Lack of experience of designers about GB”; “Project managers lack experience in GB projects”; “Underestimation of initial investment cost”; and “Project managers lack design management experience.” These detailed assessment results could be a helpful reference for practitioners in the risk management process. Indeed, the results may help practitioners understand GB risks thoroughly and find a proper risk management strategy in GB projects.

Although a number of previous studies have investigated GB risks, not much research has explored risks in GB projects in developing countries. To the best of our knowledge,

very little research assessed GB risk in developing countries, especially no study considers the risk controllability in the GB risk assessment process. To fill the gaps, this study provided an in-depth assessment of GB risks in Vietnam. Even though this study focuses on the Vietnamese context, the methodology and findings could be helpful to other developing countries.

Acknowledgments. The research is funded by the Fondazione Cassa di Risparmio di Padova e Rovigo.

References

1. Kientzel, J., Kok, G.: Environmental assessment methodologies for commercial buildings: an elicitation study of U.S. building professionals' beliefs on leadership in energy and environmental design (LEED). *Sustainability* **3**, 2392–2412 (2011). <https://doi.org/10.3390/su3122392>
2. Retzlaff, R.: Developing policies for green buildings: what can the United States learn from the Netherlands? *Sustain. Sci. Pract. Policy* **6**, 28–38 (2010). <https://doi.org/10.1080/15487733.2010.11908040>
3. Nguyen, H.D., Macchion, L.: Risk management in green building: a review of the current state of research and future directions. *Environ Dev Sustain* (2022). <https://doi.org/10.1007/s10668-022-02168-y>
4. Hassan, M.E., Kandil, A., Senouci, A., Al-Derham, H.: Organizational behavior attributes and sustainable construction adoption: an econometric analysis using data from Qatar. *J. Constr. Eng. Manag.* **142**, 05016016 (2016). [https://doi.org/10.1061/\(ASCE\)CO.1943-7862.0001196](https://doi.org/10.1061/(ASCE)CO.1943-7862.0001196)
5. Dodge-Data, Analytics: World Green Building Trends 2018: Smart Market Report. U.S. Green Building Council (2018)
6. Gan, X., Zuo, J., Ye, K., et al.: Why sustainable construction? Why not? An owner's perspective. *Habitat Int.* **47**, 61–68 (2015). <https://doi.org/10.1016/j.habitatint.2015.01.005>
7. Latham, M.: Constructing the team: final report of the government/industry review of procurement and contractual arrangements in the UK construction industry (1994)
8. Hwang, B.-G., Shan, M., Phua, H., Chi, S.: An exploratory analysis of risks in green residential building construction projects: the case of Singapore. *Sustainability* **9**, 1116 (2017). <https://doi.org/10.3390/su9071116>
9. Hwang, B., Shan, M., Supa'at, N.N.B.: Green commercial building projects in Singapore: critical risk factors and mitigation measures. *Sustain. Soc.* **30**, 237–247 (2017). <https://doi.org/10.1016/j.scs.2017.01.020>
10. Chapman, C., Ward, S.: Why risk efficiency is a key aspect of best practice projects. *Int. J. Proj. Manag.* **22**, 619–632 (2004). <https://doi.org/10.1016/j.ijproman.2004.05.001>
11. Du, L., Tang, W., Liu, C., et al.: Enhancing engineer–procure–construct project performance by partnering in international markets: perspective from Chinese construction companies. *Int. J. Proj. Manag.* **34**, 30–43 (2016). <https://doi.org/10.1016/j.ijproman.2015.09.003>
12. Zhao, X., Hwang, B.-G.G., Gao, Y.: A fuzzy synthetic evaluation approach for risk assessment: a case of Singapore's green projects. *J. Clean. Prod.* **115**, 203–213 (2016). <https://doi.org/10.1016/j.jclepro.2015.11.042>
13. Dikmen, I., Budayan, C., Talat Birgonul, M., Hayat, E.: Effects of risk attitude and controllability assumption on risk ratings: observational study on international construction project risk assessment. *J. Manag. Eng.* **34**, 1–12 (2018). [https://doi.org/10.1061/\(ASCE\)ME.1943-5479.0000643](https://doi.org/10.1061/(ASCE)ME.1943-5479.0000643)

14. Tao, X., Xiang-Yuan, S.: Identification of risk in green building projects based on the perspective of sustainability. In: IOP Conference Series: Materials Science and Engineering, p. 32053 (2018)
15. Qin, X., Mo, Y., Jing, L.: Risk perceptions of the life-cycle of green buildings in China. *J. Clean. Prod.* **126**, 148–158 (2016). <https://doi.org/10.1016/j.jclepro.2016.03.103>
16. Ismael, D., Shealy, T.: Sustainable construction risk perceptions in the Kuwaiti construction industry. *Sustainability* **10**, 1854 (2018). <https://doi.org/10.3390/su10061854>
17. Rafindadi, A.D., Mikić, M., Kovačić, I., Cekić, Z.: Global perception of sustainable construction project risks. *Procedia Soc. Behav. Sci.* **119**, 456–465 (2014). <https://doi.org/10.1016/j.sbspro.2014.03.051>
18. Ranawaka, I., Mallawaarachchi, H.: A risk-responsive framework for green retrofit projects in Sri Lanka. *Built Environ. Proj. Asset. Manag.* **8**, 477–490 (2018). <https://doi.org/10.1108/BEPAM-10-2017-0088>
19. Yang, R.J., Zou, P.X.W.W., Wang, J.: Modelling stakeholder-associated risk networks in green building projects. *Int. J. Proj. Manag.* **34**, 66–81 (2016). <https://doi.org/10.1016/j.ijproman.2015.09.010>
20. El-Sayegh, S.M., Manjikian, S., Ibrahim, A., et al.: Risk identification and assessment in sustainable construction projects in the UAE. *Int. J. Constr. Manag.* **21**, 327–336 (2021). <https://doi.org/10.1080/15623599.2018.1536963>
21. Guan, L., Abbasi, A., Ryan, M.J.: Analyzing green building project risk interdependencies using interpretive structural modeling. *J. Clean. Prod.* **256**, 120372 (2020). <https://doi.org/10.1016/j.jclepro.2020.120372>
22. Nguyen, H.D., Do, Q.N.H., Macchion, L.: Influence of practitioners' characteristics on risk assessment in Green Building projects in emerging economies: a case of Vietnam. *Eng. Constr. Architect. Manage.* (2021, ahead-of-print). <https://doi.org/10.1108/ECAM-05-2021-0436>
23. Krechowicz, M.: Effective risk management in innovative projects: a case study of the construction of energy-efficient, sustainable building of the laboratory of intelligent building in Cracow. In: IOP Conference Series: Materials Science and Engineering, p. 62006. IOP Publishing, Bristol, UK (2017)
24. Chan, A.P.C.C., Darko, A., Ameyaw, E.E., Owusu-Manu, D.-G.G.: Barriers affecting the adoption of green building technologies. *J. Manag. Eng.* **33**, 4016057 (2017). [https://doi.org/10.1061/\(ASCE\)ME.1943-5479.0000507](https://doi.org/10.1061/(ASCE)ME.1943-5479.0000507)
25. Zhao, X., Hwang, B.-G., See, Y.L.: Green retrofit projects: risk assessment and mitigation. In: Thirty-First Annual Conference 7–9 September 2015, p. 125 (2015)
26. Hwang, B.-G., Zhao, X., See, Y.L., Zhong, Y.: Addressing risks in green retrofit projects: the case of Singapore. *Proj. Manag. J.* **46**, 76–89 (2015). <https://doi.org/10.1002/pmj.21512>
27. Polat, G., Turkoglu, H., Gurgun, A.P.: Identification of material-related risks in green buildings. *Procedia Eng.* **196**, 956–963 (2017). <https://doi.org/10.1016/j.proeng.2017.08.036>
28. Taroun, A.: Towards a better modelling and assessment of construction risk: insights from a literature review. *Int. J. Proj. Manag.* **32**, 101–115 (2014). <https://doi.org/10.1016/j.ijproman.2013.03.004>
29. Nunnally, J.C.: *Psychometric Theory* 3E. Tata McGraw-Hill Education, New York (1994)



Environmental Affordances: A Practical Approach for Designing Child-Friendly Streets in High-Density Community

Qianxi Zhang^{1,2} , Wu Deng¹ (✉) , Yat Ming Loo¹ , Siyu Ma^{1,3} , Yuanli Ma¹ , and Weixuan Chen¹

¹ Department of Architecture and Engineering, University of Nottingham Ningbo China,
199 Taikang East Road, Ningbo 315100, China

wu.deng@nottingham.edu.cn

² School of Design, NingboTech University, No. 1 South Qianhu Road, Ningbo 315100, China

³ School of Architecture and Transportation Engineering, Ningbo University of Technology,
No. 201 Fenghua Road, Ningbo 315211, China

Abstract. Advocating for child-responsive urban settings can bring five benefits for sustainable development and designing child-friendly street environment in neighbourhood level plays an important role in children's healthy growth. However, a series of problems and dangerous conditions are exacerbated by currently vehicle-oriented street design, especially in the high-density residential area. This research examines using the approach of environmental affordance to assess the street spatial resources and promote the child-friendly street design. The study conducted in the Mingdong community, Ningbo city, China. It's a typical high-density community and one main street inside for children travelling from home to school was selected as the research sample. To collect the data, researcher used the methods of observation, documentation and interview with children to identify the actualized affordance. Descriptive and correlation analysis were applied in the street redesign strategies. In the end of study, new physical elements were added on the potential affordance based on the framework of safe environment, size and layout of the street, place to pause and stay, place to play and learn, green space and the quality of equipment and materials. It leads to better design solutions for child-friendly street spaces in high-density community.

Keywords: Child-friendly street design · Environmental affordance approach · High-density community · Practice in Mingdong community

1 Background

1.1 Child Friendliness as a Driven for Urban Sustainability

Children are the future of society. Their healthy growth is the basic foundation for the sustainable development of countries. So as to meet the challenge of realizing children's justices in an gradually urbanized world, United Nations Children's Fund (UNICEF)

launched the Child Friendly Cities Initiative (CFCI) in 1996, which proposed a roadmap to create securer, more fair, rightful, inclusive and child-friendly cities and communities around the world [1] (see Fig. 1). Practically, advocating for child-responsive urban settings can also bring five benefits for the sustainable development, including: (1) health, (2) safety, (3) citizenship, (4) environment, (5) prosperity (see Fig. 2).

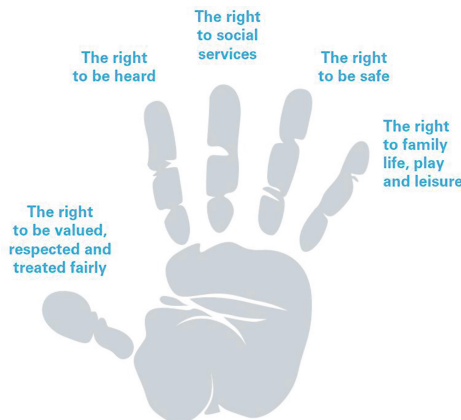


Fig. 1. Five goal identified in the CFCI framework for action

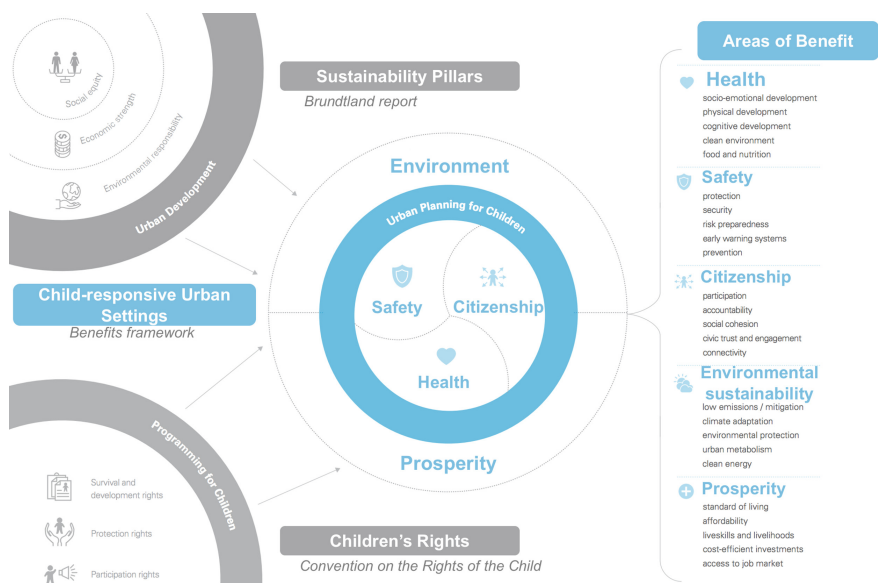


Fig. 2. Child-friendliness and five types of values

1.2 Importance of Child-Friendly Streets in Neighborhood Scale for Children's Growth

The street is the most natural and high-quality place where children's play activity occurs [2]. And due to the limited range of children's activities, the streets near the home are children's "first playground" where are importantly informal spaces for children's outdoor play activities [3]. Constructing an organic connection between children and their living neighborhoods through community streets and making streets a place for children to play spontaneously and touch nature is of great significance to children's social and intellectual development.

1.3 Street Design Challenges

Whereas, challenges like road traffic collisions, psychological health problems, insufficiency physical activity and environmental air pollution are all exacerbated by currently vehicle-oriented street design [4]. Streets with risks and unfriendly settings make children in unsafe environments and decrease opportunities for children's daily social learning and outdoor activities. These challenges affect all children, especially for children from lower-income, high density areas [5].

Therefore, how to transform the vehicle-oriented streets to child-friendly streets in high-density community by design intervention is the key research question in this research.

2 Environmental Affordance Concept and Implications for Design Practice

Environmental affordance is a medium concept proposed by psychologist James Gibson in 1977 to express the interaction between the physical environment and its users. It means the functional potential of environmental settings which convey meanings and benefits in how they encourage human usage [6]. For example, a park bench has the affordance of sitting for adults, on the other hand, it may also have the affordance of climbing and jumping for children. Harry Heft further developed the affordance theory based on Gibson's view. He accounted that the occurrence of environmental behavior can be defined as the "actualization" of the corresponding affordance, and according to whether the environmental behavior occurs or not, affordance could be further divided as "potential affordances" and "actualized affordances" [7]. The higher the ratio of affordance is realized, the better the utilization efficiency of the environment.

Therefore, environmental affordance provides a theoretical perspective to connect form-giving and need-supporting. It's also a conceptual structure and a common language linking the multi-stakeholders like designers and users. The approach based on environmental affordance presents the advantages as follows: (1) it's embedded in the particular user perception supported by design characters; (2) considers the key interrelationships between spatial features; (3) it intentionally links the detailed requirements of the spatial users; (4) it supplies a pathway to assess the possibility of the space meeting the expected behavioral outcomes [8].

Accordingly, it could be a practical approach when designers need to evaluate or design child-friendly spaces.

3 Children's Needs for Street Environmental Affordances

Designing child-friendly street must consider children's needs, also the older adults looking after children. Children on different ages have different spatial needs, but the design should also be universal for all ages, especially in the high-density communities with less space. Based on previous research, some criteria of street environmental affordance (see Fig. 3) are needed to meet children's needs and assess the street quality, including:

(1) Safe environment. Children's mental and physical development are less developed than adults and they are more lack of ability to defend the dangerous settings in the outdoor environment. To ensure children's health and growth, the street design should avoid less traffic violence, unfriendly play facilities, excessive noise and air pollution.

(2) Size and layout of the street. Children's activities on streets also need enough space with suitable size and layout, to promote gathering play, social communication, cycling and running. Children's unstructured play also demands more space and safe distances for motoring or jumping on limited lane, meanwhile wider pavements permit more freedom to play and develop independence.

(3) Place to pause and stay. Compared to adults, children regularly walk slower and exhaust more easily. They need places along the street to rest, eat and reorganize. Places to pause and stay supply children with proper space to rest while using streets near home. These spaces can invite social interactions to use streets for longer time.

(4) Place to play and learn. Play is particularly important to children's physical and cognitive development, during which could enhance creativity and socializing skills. Streets bring chances of outdoor play and learning into children's daily lives. Unstructured play comes from interactions with daily environments. It develops children's imagination, and cognitive ability by allowing them to make decisions and take the lead.

(5) Green space. Plants has obvious benefits for a street. They can provide oxygen, provide comfortable shade and beautify the streets. Green space also demands the diversity and volume of plants. The organization of green plants, especially trees, must be effective. It needs rational arrangement to visually and psychologically split the street from other space.

(6) Quality of equipment and materials. Sufficient equipment and detail materials promote the street spatial quality and friendliness. The effective elements of street design contain pavements, furniture, illumination, signs, shelters and waterscape. The dissimilarity, location and quantity of all these settings and resources can appeal children to do outdoor activities on streets rather than indoor house.

Based on this framework of children's needs for street environmental affordances, designer could assess the existing street settings and add children's proposed requirements into the corresponding types. Meanwhile, it's also a referable design principle for child-friendly street spatial intervention.



Fig. 3. Children's needs for street environment

4 Case Study

4.1 The Site Location and the Street Sample

This study was conducted in Mingdong community occupying 19.56 ha land, which was built in year 1996 with around 5500 residents living in it. It's a typical high-density community located in the center of Ningbo city, China. Due to the lack of public activity space planning during the construction in the early 21st century, there is no big park or playground inside the community. The activities of residents are mainly scattered on sidewalks, street corners and pocket gardens. Most public space are occupied by vehicles and parking, which caused road traffic crashes, ambient air pollution and lack of physical activity. And children in this community didn't have enough child-responsive space and facilities to play (see Fig. 4).



Fig. 4. Insufficient public space and children's activities with dangers on street

One street between the community and the adjacent school was selected as the research sample, which is a main pathway for children travel from home to school. The length of this street is 78 m and the width of it is partly 3.5 m and partly 5.3 m. One side of this street is a long wall and another side is surrounded by parking spaces which caused some traffic dangers. Besides, due to dull pavement, long-term occupancy by

parking, and lack of facilities, this street has become a road with few people walking, and it urgently need regeneration and redesign (see Fig. 5).



Fig. 5. Sample street location and street photos

4.2 Data Collection

To collect data, several methods like observation and interview the children were used as follow: The purpose of observation was to collect the existing street environmental affordance by making documentation on photo and map.

The research collected data about the children's preferences by interview with using case photos (see Fig. 6). 12 children were asked their opinions about the quality of street and what type of games they usually play (see Fig. 7).

Meanwhile, researcher used some tools to guide children to propose their design ideas of the sample street, such as case pictures of the streets that they would choose according to their preferences. Finally, researcher used participant-generated mapping to better understand children's preferences, for example, children hoped the street could be like a park and there would be trees, playable facilities in the street (see Fig. 8).



Fig. 6. Various streets used photos to understand children's preferences



Fig. 7. Interview with children to get their augments about the quality of sample street

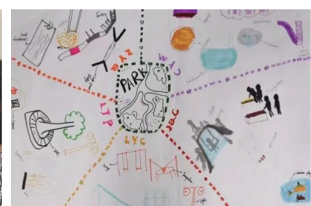


Fig. 8. Participant-generated design mapping

4.3 Data Analysis

The study used qualitative and quantitative methods to analyze the data. The procedure was divided into two sessions: one was assessment of street environmental affordance quality based on observation; another one were the positive and negative opinions from interview with children, as well as their preferences and needs for the sample street.

Assessment of Street Environmental Affordance Quality. After site survey and observation, qualitatively descriptive analysis was made to describe quality of street's physical settings. The street environmental affordance categories were: safe environment, size and layout of streets, place to pause and stay, place to play and learn, green space, quality of equipment and materials. Quantitative analysis was to evaluate each categories of the street affordances. Likert scale with three parts was used to score the existing street environmental affordance, such as: excellent (score 3), sufficient (score 2), and poor (score 1).The following Table 1 shows the assessment result of the environmental affordances quality. Accordingly, a radar chart of assessment result was obtained (see Fig. 9).

Table 1. Assessment of street environmental affordances quality

No.	Street affordance categories	Actualized affordances elements	Quality score		
			Excellent	Sufficient	Poor
1.	Safe environment	Crowd vehicle occupancy No lighting at night Not easy for parents to watch	○	○	●
2.	Size and layout of the street	Enough for pedestrian to walk Clear boundaries Balance between street width and building height	○	●	○
3.	Place to pause and stay	No benches to sit No shelter supplying shade	○	○	●
4.	Place to play and learn	No play facilities No knowledge walls No space for learning	○	○	●
5.	Green space	A line of trees along the sidewalk No floral plants	○	●	○
6.	The quality of equipment and materials	Few equipment Slippery pavement	○	○	●

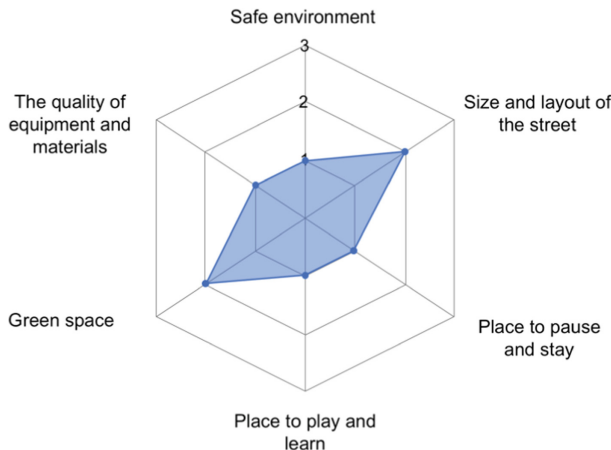


Fig. 9. Radar chart of the assessment of street quality

Judgements and Preferences from Children. Qualitatively descriptive analysis was conducted to describe children's positive and negative judgements on the quality of the sample street. Another qualitative description was concluded to define children's needs for the street, as well as their redesign proposals. Table 2 shows the detailed positive & negative judgements, as well as the needs and preferences from children, as the Table 2 shows.

Table 2. Judgements and preferences from children

No.	Conditions	Aspects		Children's needs and preferences
		Positive	Negative	
1.	Safe environment		Too much cars Not safe Vehicles affect and endangered activities	Reduce vehicles and car parking
2.	Size and layout of the street		Not big enough for various activities	More space to do various activities
3.	Place to pause and stay		No benches to sit	More various street seats to rest More shelters
4.	Place to play and learn		No play facilities	More play facilities More learning medium

(continued)

Table 2. (*continued*)

No.	Conditions	Aspects		Children's needs and preferences
		Positive	Negative	
5.	Green space	Side trees for shade	Less variety of vegetation which made streets more beautiful and comfortable	More green More colorful flowers
6.	The quality of equipment and materials		No street lamp	More lighting Safer materials Colorful materials

4.4 Design Strategies

Based on the affordance-based analysis framework, researcher combined the environmental affordance demand, the realization of the affordance of this street, judgements and preferences about the streets from children. Then researcher proposed a series of child-friendly design strategies, as the Table 3 shows. In practice, these strategies were developed to detailed design (see Fig. 10), and the streets environments was transformed to be more friendly for children compared to the state before redesign. (see Fig. 11).

Table 3. Strategies to design child-friendly street

No.	Street affordance categories	Design strategies
1.	Safe environment	Remove existing parking spots along the sidewalk Add a multifunctional safety fence at the edge of the road Add street lamps for night light
2.	Size and layout of the street	Eliminate useless facilities on the street to make more space
3.	Place to pause and stay	Add a rest belt with a seat Partially set ceiling and seat
4.	Place to play and learn	Add interactive game devices on the existing vertical walls Paint the playful graphics on ground to promotes physical activity Add graphic design with knowledge and information on different interfaces Add game facilities such as seesaws in larger spaces

(continued)

Table 3. (continued)

No.	Street affordance categories	Design strategies
5.	Green space	Add the mini sharing garden by potted plants
6.	The quality of equipment and materials	Reduce objects with hidden safety hazards in the street Change the brick paving to a colorful plastic floor

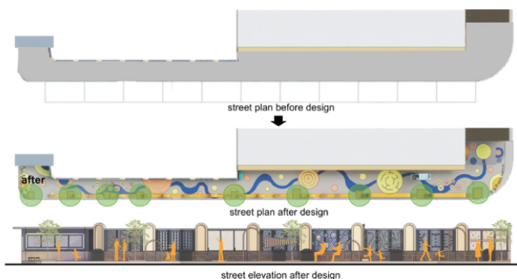


Fig. 10. Street plan to compare the street before and after design



Fig. 11. Four perspectives to compare the street before and after design

5 Conclusions and Future Work

This article offers a practical approach of affordance-based analysis framework for child-friendly street design, and suggests a certain methods to transform the data and findings into design strategies, which involved children's participation in the co-design process, including the survey process. Few research have linked the environmental affordance approach to child-responsive design. This research contributed our understanding of environmental affordances with the potential to lead to better design solutions for child-friendly street spaces in those old high-density communities.

The disadvantage of this research is that the analysis of the street sample is relatively simple. It's lack of quantitatively scientific analysis of environmental affordances, also lack of the evaluation of the design results, which needs to be further deepened in the future research.

Acknowledgments. I sincerely appreciate everyone who supported my research. I would like to express my gratitude to all of the children in Mingdong community for their great experience which were shared to me. The research is supported by the Zhejiang Provincial Philosophy and Social Science Foundation of China under grant 22NDQN291YB.

References

1. Askew, J.: Shaping Urbanization for Children: A Handbook on Child-Responsive Urban Planning: By Jens Aerts, New York, United Nations Children's Fund (UNICEF) (2018)
2. Qianxi, Z., Shanshan, W., Xinkai, W.: Multi-dimensional construction of children's outdoor play space as an old community renewal catalyst. *Archit. Cult.* **11**, 146–149 (2019)
3. Yao, S., Huajie, Y., Miaoqian, Z., Menghan, L.: Construction strategy of street environment in child-friendly community. *Archit. J. S(2)*, 58–163 (2020)
4. Karsten, L., Van Vliet, W.: Children in the city: reclaiming the street. *Child. Youth Environ.* **16**(1), 151–167 (2006)
5. Peyton, A.: Designing streets for kids. In: Sustainable Urban Environments: Research, Design and Planning for the Next 50 Years (2019)
6. Gibson, J.: The Ecological Approach to Visual Perception: Classic Edition. Psychology Press (2014)
7. Heft, H.: Affordances and the body: an intentional analysis of Gibson's ecological approach to visual perception. *J. Theory Soc. Behav.* **19**(1), 1–30 (1989)
8. Bardenhagen, E., Rodiek, S.: Affordance-based evaluations that focus on supporting the needs of users. *HERD Health Environ. Res. Des. J.* **9**(2), 147–155 (2016)
9. Ekawati, S.A.: Children-friendly streets as urban playgrounds. *Procedia Soc. Behav. Sci.* **179**, 94–108 (2015)
10. Jacobs, A.B.: Great streets. *ACCESS Mag.* **1**(3), 23–27 (1993)



Study on the Ecological Regeneration Strategy of Urban Industrial Sites—Taking Diamond Bay in Dalian as an Example

Jun Wang, XiaoYu Qiu, and Su Xu^(✉)

East China University of Science and Technology, No. 130, MeiLong Road, Shanghai, China
xusutju@126.com

Abstract. Guided by the concept of urban renewal, this article summarizes the development and current situation of the renewal and transformation of industrial sites at home and abroad. It also proposes strategies for improving the public space landscape of industrial sites from the perspective of the characteristics of site and public demands. Taking the Diamond Bay Coastal Park in Dalian as an example, the article gives suggestions for improvement from four aspects, its integrality of spatial layout, the protection and inheritance of industrial heritage, the artistic treatment of the site, and the restoration of the ecological base, to finally get the direction of shaping the open space of urban industrial sites. This study offers a new perspective on the shaping of the open spaces of urban industrial sites in the context of inner urban regeneration as an alternative to urban sprawl, with the research objective of achieving both environmental and social sustainability.

Keywords: Industrial sites · Urban public space · Landscape shaping · Urban renewal

1 Introduction

In recent years, industrialization and urbanization in China have been developing rapidly. In this process, with the continuous adjustment of urban industrial structure and spatial structure, a large number of industrial heritage sites have been left in the urban central area. Nowadays, the renewal of industrial heritage in China is still in the exploration stage, and how to make the renewal of industrial sites promote the joint development of economy, society and ecological environment is becoming more and more the focus of attention.

Recently, in October 2020, China's national conference included 'urban regeneration' in its national plan for the first time, and made it clear that the implementation of urban regeneration actions should promote the quality and structural optimisation of urban space, and that it should accelerate the upgrading of the functions of old factories and other urban stock areas. As an industrial site, the subject of this study fits perfectly into the national development plan.

For the renewal of industrial sites in urban regeneration, the “memory of place” of industrial history should be continued based on the needs of economic, social and cultural benefits and ecological and environmental benefits [1], while taking into account its “vitality benefits” as a special public space in the city. This article examines the regeneration of typical industrial sites at home and abroad and proposes a strategy for shaping the open space vitality of urban industrial sites, especially coastal industrial sites, based on the regeneration strategies of typical industrial sites at home and abroad, combined with the exploration and practice in Dalian, to provide support for the development of urban regeneration.

2 Review of Studies on Industrial Site Renewal

The first symposium on urban renewal was held in the Netherlands, which defined urban renewal as the process of continuously repairing and renewing the spatial environment and building facilities in built-up areas after they have been damaged or even lost due to natural or man-made influences, so as to eventually restore their functional benefits. The concept of Brownfield was first proposed by the U.S. Congress in 1980 with the presence or potential of certain pollutants in the area as the main criterion for classifying Brownfield sites, which covers the industrial sites [2]. In 2001, Harvard University held another conference on “Treatment of Brownfield and Wastewater and Design Renovation”, which complemented the forms and means of renovating industrial sites and explored ways to rejuvenate them. In the 21st century when the “industrial landscape” attracted much attention, the President of the International Institute for the Conservation of Industrial Heritage (TICCIH) proposed a holistic landscape strategy, i.e., a shift in the scope of conservation and renewal from individual remains to groups of sites and the industrial landscape as a whole [3].

Scholars have the following views on the specific regeneration strategies for public open space in urban industrial sites. Yan Bo et al., taking the renovation of Jiangnan Shipyard as an example, attempted to explore the road of regeneration suitable for waterfront industrial sites from the perspectives of inheriting urban culture, utilizing the original landscape, renovating the remaining buildings and restoring the waterfront ecology [4]. Liu Lingwen et al. also gave their own insights on the heritage of the ship industry. They studied a large number of cases of ship industry transformation at home and abroad by analogy and summarized them, and analyzed the individual form of the ship industry compared with other industrial sites, and proposed specific development strategies: clearing project positioning, recreating cultural landscape, transforming industrial heritage and organizing spatial forms [5]. Another example is Pu Peiyong’s view that old urban industrial sites witnessed the industrial civilization in the third-tier cities. He also emphasized the importance of industrial heritage, namely, the historiographic value of “local knowledge”, the emotional value of “mass memory”, and the aesthetic value of “cultural identity”. Based on these three values, he also proposed the targeted reshaping strategies [6]. While, Hu Liu et al. gave renewal strategies for industrial sites in mining areas from an ecological landscape perspective: classifying the sites according to the contamination and establishing a restoration model for them; constructing

an ecological landscape succession in the temporal dimension; proposing a landscape development model of reuse of geomorphology and in situ ecological restoration, and providing corresponding recreation types for different restoration stages [7].

In the practice of urban industrial heritage regeneration, there are many excellent cases at home and abroad. This paper focuses on four excellent transformation cases, namely North Star Park in Germany, Darling Harbour Waterfront Industrial Site in Sydney, Hudson Riverwalk Park in New York and Yangpu Riverfront Public Space in Shanghai, and compares their regeneration strategies for industrial sites with those of the sites under study in an attempt to derive the feasibility of regeneration strategies for this site (Table 1).

Table 1. A table summarising the best international examples of industrial site regeneration.

Industrial Site Project Name	German North Star Park	Sydney Darling Harbour Waterfront Industrial Site	New York Hudson Riverwalk Park	Shanghai Yangpu Riverfront Public Space
Size	160 ha	20 ha	223 ha	5.5 km
Industrial site renewal strategy	1. The use of existing buildings is adapted and the structures are used only as signage 2. The use of industrial waste to create a new high point for public viewing and to guide recreational activities	1. The preservation of the port buildings, the continuation of the historical and cultural aspects of the waterfront industrial area, and the maintenance of the water transport model, while integrating the waterfront transport function, combined with new land transport facilities	1. Dozens of disused piers overlooking the water have been transformed into functional areas for urban recreation, including sports fields, leisure facilities and parking buildings	1. Architectural infrastructure. Using trestle and foundation design to provide a two-way roaming experience 2. exploring new contemporary material technologies, ‘new to history’ 3. Combine industrial heritage with civic open space, so that structures are not just monoliths to be entered or viewed, but facilities to be used for rest and relaxation

(continued)

Table 1. (*continued*)

Industrial Site Project Name	German North Star Park	Sydney Darling Harbour Waterfront Industrial Site	New York Hudson Riverwalk Park	Shanghai Yangpu Riverfront Public Space
Other renewal strategies	1. The existing topography is adapted to the site, with pedestrian bridges linking traffic and balancing height differences 2. The waterfront is linked to the park by an artistic topography, an amphitheatre and a cycle path 3. The site is used as part of a cycling greenway and the width of the path is set more in line with cycling	1. Increased public space and enhanced waterfront accessibility. The driveway through the site is elevated and does not interfere with public movement. Increase the number of public buildings and integrate them with the civic square. Increase leisure and entertainment facilities and hold cultural events 2. Enrich the waterfront leisure offerings and create a large leisure area, including entertainment, dining and shopping	1. “Bottom-up” public participation, mobilising citizen input and civic organisations in the design process 2. The introduction of the concept of ‘neighbourhood revitalisation’, moving away from mass demolition and towards the revitalisation of neighbourhoods 3. Famous for its recreational and fitness activities, with continuous cycle paths along the shoreline, linking the various marina parks as a whole	1. A civic fitness trail along the riverfront, infused with all-age fitness facilities, to build a city-wide civic activity space
Summary	The site is designed to suit the site’s elevation, respecting the current state of the site and incorporating topographical design and public activities	The design is fully integrated into the life of the public by introducing a wide range of businesses to ‘interpret’ the site	Bringing about urban vitality and achieving small-scale, phased, incremental regeneration. Emphasis on a continuous process of regeneration	The flexible use of industrial heritage buildings and structures, the focus on creating a public development space for citizens, the injection of art and science, so that the Yangpu Riverfront becomes a public artwork

3 Study on Area Overview

3.1 Site History

Dalian is one of the most important industrial bases in China, with a history of 100 years of development. Dahua Group, originally Dalian Chemical Plant, was built in 1933 and was the largest and earliest built chemical raw material and chemical fertilizer production in China. In 2002, Dahua realized the plant site and planned to implement a relocation

and renovation program. In 2008, the area of the old plant was partially demolished. In 2014, Diamond Bay Coastal Park was officially opened.

3.2 Site Features

The Diamond Bay area in Dalian faces challenges such as industrial decline, resource waste, and environmental pollution, but it also enjoys the characteristics of a unique geographical location, rich historical and cultural heritage, and open space plasticity [8].

Firstly, it enjoys superior geographical location and transportation conditions, occupying an important spatial position in the city. The Diamond Bay is the only bay in the center of Dalian. And the Diamond Bay Coastal Park, the subject of this study, is located in the northwest of the bay in a coastal location, north of Wanjing Street and south of the residential area of Ocean Diamond Bay. There are 4 bus lines surrounding it and the subway Line 5 under construction. The section of the Line 5, from Suoyuwan Nan Station to Dalian Railway Station, is the construction site of the widely expected submarine tunnel in Dalian, which will lead to Qingniwa Bridge, the center of Dalian city. It takes over the flow of people from the north and saves a lot of time for the traveling public. The subject of the study is located less than 300 m from the Soyuwan Nan Station. Its important transportation status will bring a huge opportunity for the future planning and development of the site.

Secondly, it is a crucial occasion for the transmission of history and humanity. Dalian Chemical Plant, built in 1933, was the largest and earliest built chemical raw material and chemical fertilizer production site in China. With the continuous improvement of manufacturing capacity, the chemical factory plant expanded its production and coverage, and accumulated over the years to form a unique industrial fabric. Since the chemical plant prepared for the relocation and renovation project, it has kicked off the transformation of the Dahua Plant. Dalian Chemical Plant embraces a rich historical and humanistic connotation, and the industrial remains here are numerous and large in scale. It is for this reason that after the renovation, Dahua will become an important site for the display of industrial history and culture to showcase the style of Dalian industrial area.

Thirdly, there are abundant industrial relics available, and the spatial variety is diverse and complicated. In the eastern part of the site, there are still industrial remains of chemical plants that have not yet been dismantled which could reflect the current era, and the old factory texture, plants, equipment, components, and sites, etc. (see Fig. 1). All of them have important historical and cultural values and are precious industrial heritage in China. The independent space shaped by it and the special urban texture provide an excellent base for the current design of public space renewal. However, the subject of the study is a completed park, where the number of industrial relics left currently is scarce, and the industrial heritage landscape is largely destroyed. So, most of the buildings in the park are common ornaments with “marine theme” (see Fig. 2), with a tendency of “a thousand parks with a same look”. In order to restore the original industrial site landscape, some of the remains in the eastern part of the site can be relocated.



Fig. 1. Industrial heritages in and around the site

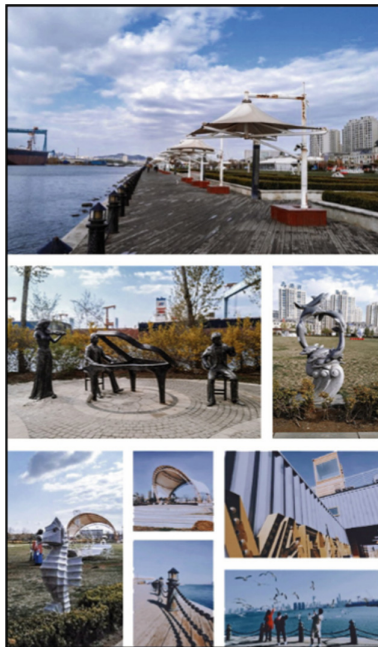


Fig. 2. Distribution of current facilities on the site

3.3 Current Problems

There are four main problems with the current construction of Diamond Bay Coastal Park. First, from a macro point of view, Diamond Bay Park is located on the south side of Sino-Ocean Land and Qingxiu Blue Bay residential area, and currently, it is visited by mostly residents of the surrounding area, which is relatively not open enough. Besides, it is relatively isolated as no continuous greenway has been formed in the plan, and there is no green space around to connect with it, which is still unattractive after the traffic becoming convenient. Secondly, since the real estate developer did not follow the principle of protecting industrial sites, the site was greatly demolished and new facilities were built, which results that there are few industrial remains in the site, and the completed park space has no connection with the historical heritage, and the industrial site has been destroyed. Thirdly, the recreational facilities are only the stacking of restaurants and playground facilities, lacking the elements and vitality of the important civic activity space in the city, which makes it become a one-size-fits-all urban park. Finally, the ecological substrate of the site is broken due to the pollution of the chemical plant. Although it is located in the coastal area, waterlogging still occurs in the rainy days. What's worse, there are no ecological facilities in the park at this stage to attempt to address the problems.

4 Public Space Improvement Strategies to the Diamond Bay Coastal Park

4.1 Making the Planning Lead the Overall Spatial Pattern

A landscape, which aims to change the old into the new and co-exist the old with the new, would be formed by incorporating new design elements on the basis of maintaining the human history and spatial pattern of the original space. It makes the planning lead the overall layout, important sites, industrial heritage elements and the surrounding environment. This mode of transformation of industrial sites is organic and sustainable, which can protect the valuable remains of industrial sites more comprehensively.

The current nature of the Diamond Bay Coastal Park site is mainly residential. And the site has a unique structural fabric due to its past industrial production process, which is obviously different from the surrounding urban fabrics. It is recommended that the park be renovated in a way that re-integrates the original characteristics and qualities of the industrial site into the public's urban life. The central idea of "returning the factory to the people" should be implemented into the design concept of "creating an ecological and living coastal city public space with industrial heritage as the main line". By realizing the "reuse" of industrial heritage, the "restoration" of industrial brownfield, and the "new integration" of urban life, the rich history and culture of Dalian Chemical Plant and industrial heritage will be re-presented to the public. It will create a public open space with regional characteristics by breaking the fragmentation situation of the industrial land to the central area of the city, and improving the public functions of the city. In the long term, there is a long coastline to the east of the site and factories that have not yet been moved, and these giant factories in the center of the city will eventually move out of the center of the city as the city grows, leaving a large area of industrial sites and the coastal coastline with huge development potential. In the future, a coastal greenway can be planned to create the continuity of the waterfront area, build a citizen's coastal fitness trail, inject all-age fitness activity facilities, and build a activity site for the whole citizens.

4.2 Preservation and Inheritance of Industrial Heritage

The protection and inheritance of industrial heritage refers to the protection and inheritance of symbolic elements, industrial structures, production equipment and other representative elements with obvious "industrial civilization" characteristics within the site, or the protection and inheritance of a characteristic space or space with obvious industrial characteristics as the iconic dominant element of the public space of industrial sites, so as to shape an overall landscape environment with historical connotation, cultural heritage and ecological benefits.

The industrial heritage that can be excavated within the current site of Diamond Bay Coastal Park is minimal. In order to create a community memory of industrial sites, part of the industrial heritage on the east side that has not yet been demolished should be salvaged and partially transferred to the Coastal Park site, so that the valuable history is integrated in the open space of the city. The Civic Industrial Coastal Park, which integrates sightseeing and browsing, exhibition services, and convention and entertainment,

is designed with environmental and ecological concepts to provide open space for the area for holding performances and community events and gathering. These actions not only preserve the heritage while providing a space for cultural leisure for the citizens, but also enhance the cultural influence of Dalian city and increase the tourism resources of the city.

In addition, the transformation of the industrial buildings can also bring out their maximum heritage significance and make them integrate with the landscape design. There is a unique location advantage between the site and the Dalian Shipyard on the south side, so, the design can introduce the history of the shipbuilding industry, which could make the site of the study reflect the industrial style of the shipyard well. Then, Diamond Bay Coastal Park can be transformed into a ship science museum using the eastern workshop building to display various ship products in the course of Dalian's history. Ship structures and sculptures can also be set in the site of the study, forming a movable outdoor exhibition and changing the outdoor exhibits at different times so as to attract more citizens to watch the exhibitions.

4.3 Artistic Treatment and Re-creation of the Site

We summarize the constituent elements of industrial sites, and deconstruct them in groups according to their scale and individual characteristics, in order to extract the most unique local industrial elements, and redesign them through modern landscape planning and design creative concepts and artistic techniques. This fully demonstrates the artistic quality and cultural heritage of industrial characteristics, so that whenever people enter this public space, they can feel the unique atmosphere and historical culture of the original industrial site. At the same time, it can also reflect the modernization and innovation of open public space.

The public space design of Diamond Bay Coastal Park aims not only to transform the industrial site into a pleasant urban open public space, but also to build new industrial aesthetic values. For example, the structural prototype of the steel corridor is derived from the site's crane tower with its aerial gallery and pipes. We reintegrated and transformed them into functional facilities such as seating, climbing ropes and awnings, using slender steel structural columns and linearly arranged steel cables to make the steel corridor transparent and clear, and created a kind of floating posture that is detached from the site. Inspired by the state of pipes in old factories, the railings and lampposts can see the use of components in the Yangpu River and Xuhui Riverside in Shanghai. Through the combination of single construction "water pipes", a series of railings and lampposts with different linear shapes and arrangements are formed. These vignette elements float above the existing environment while still maintaining a connection to the existing environment.

4.4 Restoration of Ecological Substrates

The vegetation that grows on industrial sites and the ecosystem that gradually forms after the end of the economic operation of industrial production is a reflection of nature's ecological self-cycle. We should follow the attitude of "design combined with nature" in the design of industrial site landscape reconstruction, and give full respect, affirmation

and protection to these wild native vegetation, animals and ecological chain. Because this kind of ecosystem that survives in the extreme harsh environment is of great ecological value.

The substrate site is hard and overgrown, and the green space is cluttered with dead grass, but it reveals a tenacity that provides the possibility of brownfield ecosystem restoration. Design concepts such as low impact development and sponge city can be applied to maintain the original geomorphic state and create a depressed wetland that can collect rainwater. The bottom of the pond is not closed for waterproof treatment, so that the collected rainwater can naturally infiltrate into the soil, replenishing ground-water while solving the problem of low terrain and high drainage pressure, and also optimizing the hydrological system within the site. It also serves to retain precipitation and save rainwater for discharge into the municipal pipe network during heavy rains. In addition, by setting up pumping facilities and irrigation systems, the water collected in the wetland can also be widely applied to the entire landscape site for watering. In the low-lying wetland, native aquatic plants and water-resistant trees could be planted to form a distinctive landscape style. The design of the rain garden is combined with a characteristic steel structure corridor bridge to link the paths in all directions. At the same time, it is also supposed to combine with elements such as a platform, a pavilion and a display wall to form a multifunctional landscape artifact suspended above the wetland.

5 Conclusion

This article firstly compares the research overview of industrial sites at home and abroad to understand the development trend, initially exploring the renewal and improvement strategies of industrial sites. On the theoretical basis, it proposes a strategy for the renewal and improvement of the industrial sites in Dalian Diamond Bay Coastal Park, and gives the following four suggestions. First, from the macroscopic point of view, making the plan lead the overall pattern, and opening up the urban coastal site to create the continuity of the waterfront area. Second, protecting and inheriting the industrial remains in and around the site to continue the historical heritage. Third, artistically processing and re-creating the site to show the unique industrial aesthetics. Finally, restoring the ecological substrate to revive the healthy urban space.

How to deal with the protection and reuse of industrial sites in the process of urban industrial restructuring is an important issue in the road of urban renewal. The opening up of industrial sites and the reshaping of public space provide favorable technical support for the inheritance and renewal of industrial sites. These two aspects promote and support each other. The reshaping of the public space landscape releases space and vitality for the renewal of industrial sites, and provides more opportunities for the industrial heritage continuation. Under this background, the urban renewal of industrial sites can take into account both future and historical needs, and achieve the sustainable development of both environment and society.

Acknowledgements. This research is supported by China National Social Science Fund, No. 19BJY063, The IV Peak Plateau Discipline of Shanghai Design, Key Courses in Shanghai.

References

1. Shan, X.: Research on the reuse of the remains of old urban industrial areas under the urban renewal—taking the Xinyi area in Harbin as an example. In: Proceedings of the 2016 China Urban Planning Annual Conference, pp. 703–711. Town Planning Institute of China (2016)
2. Neil, K., Shen, W.: Post-industrial landscapes - contemporary issues and strategies related to industrial sites-site transformation and landscape regeneration. *Urban Environ. Des.* **05**, 10–15 (2007)
3. Shan, J.: Focus on new cultural heritage: conservation of industrial heritage. *Beijing Plann. Rev.* **02**, 11–14 (2007)
4. Yan, B., Deng, S., Gu, H.: Reflections on the renewal of urban waterfront industrial sites under the expo in 2010. *Gardens China* **25**(08), 47–52 (2009)
5. Liu, L., Li, X.: Research on the protection of shipbuilding industrial heritage and the construction of creative industry cluster. *Shanghai Urban Plann. Rev.* **05**, 89–94 (2012)
6. Pu, P.: Remodeling heritage values in the transformation of old industrial areas in third-line construction cities: an example of the transformation of Xicaoping industrial site area in Panzhihua. *Mod. Urban Res.* **02**, 94–100 (2017)
7. Hu, L., Lin, J.: Exploration of ecological landscape restoration strategies in tin mining areas-taking Gejiu city as an example. *Gardens China* **32**(02), 52–57 (2016)
8. Wang, H.: Protection and utilization of industrial heritage in urban centers. Dalian University of Technology (2018)

Resource Management, Green Behavior and Sustainable Development



Scenario Analysis of Annual Heating Energy Demand in North China from 2020 to 2050

Haizhu Zhou, Xionglei Cheng, Yitong Li, Lining Zhou, and Xiaoping Li^(✉)

China Academy of Building Research, Beijing 100013, China
lixpcab@163.com

Abstract. Heating energy consumption in north China accounts for about 20% of the total building energy consumption. In this paper, a multiple regression model based on principal component analysis is established to study the primary energy consumption of central heating in north China (PECCH). Specifically, considering the limited amount of historical data, cross validation is used to determine the optimal value of the hyperparameter for PCA. Then a multiple regression model (Mr-PCA) is established, with the principal component as the independent variable and the PECCH as the dependent variable. It has been verified that the optimal number of principal components is 3 for the Mr-PCA, with a mean absolute percentage error (MAPE) of 2.3%. The results of scenario analysis show that by 2050, in the case of basic scenario, medium control scenario and enhanced control scenario, the PECCH will be 270 million tec, 210 million tec and 170 million tec respectively. The implementation of enhanced control measures is conducive to the realization of China's future goal of carbon neutral.

Keywords: Heating · North China · Scenario analysis

1 Introduction

The building energy consumption of operation accounts for 22% of the total energy consumption in China [1], with an obvious trend of long-term growth. It is an important field for achieving the goal of the carbon peak and carbon neutral. For all kinds of building energy consumption, the primary energy consumption of central heating in North China (PECCH) accounts for about 20%. The proportion and total amount of the PECCH are related to the control targets of total building energy consumption and energy intensity in China. How to predict PECCH by scientific methods has become an urgent problem.

Some scholars have proposed prediction models for the PECCH. Yang Xiu [2] created the CBEM (China Building Energy Model) model based on the characteristics of building energy consumption. And the overall energy consumption of Chinese buildings is calculated from the bottom up. Peng Chen [3] develops the Technology and Behavior Model (TBM), and analyzes the impact of the building area growth on energy in northern cities and towns, then the total energy consumption control target of heating in China is put forward. However, the two models both take the energy consumption intensity as the input parameter in the heating energy consumption prediction, and the analysis

of factors such as energy-saving policies, standards and technologies is not comprehensive enough. Some data driven methods are used to predict energy consumption, such as linear regression, artificial neural networks, and support vector machines. Most of the data driven methods focus on the energy consumption of individual buildings and have limited application scope, but the data analysis methods in it have certain reference significance for the study of the PECCH.

The purpose of this paper is to provide an improved multivariate analysis model for the prediction of the PECCH, and analyze the PECCH of different development scenarios from 2030 to 2050, so as to provide reasonable information for the realization of energy conservation and carbon neutral goals in China.

2 Methods and Data

2.1 Model Overview

For the energy consumption of central heating in northern China, there may be no obvious independence among many influencing factors, and it is necessary to solve the problem of collinearity in regression analysis. In addition, the historical data that can be obtained does not exceed 15 years, which limits the generalization ability of the model. To solve the above problems, principal component analysis (PCA) method is applied to eliminate the interference of multiple impact indicators. Then, according to the results of multiple linear regression, the hyperparameter of the model is optimized. In this process, cross validation (CV) is applied to make full use of the limited training data. The model framework is shown in Fig. 1.

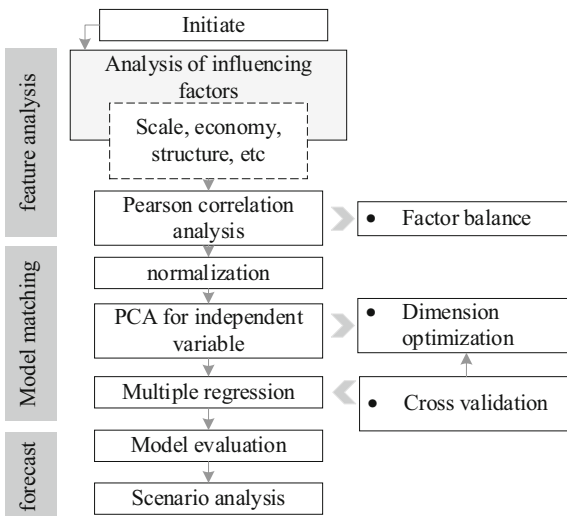


Fig. 1. Framework of the PECCH prediction model.

2.2 Mathematical Model

PCA Model. PCA is an effective method for data compression and information extraction [4]. It is a statistical analysis technique to reduce the dimensionality of input data and reveal the linear correlation between variables. In order to keep the data consistent before PCA analysis, we need to standardize the data and get the data set Z.

Assuming that $\lambda_1 \geq \lambda_2 \geq \dots \geq \lambda_f \geq 0$ is the eigenvalue of the covariance matrix V of Z. $L = [L_1, L_2, \dots, L_f]$, in which $L_i = [\gamma_{1i}, \gamma_{2i}, \dots, \gamma_{fi}]$. T is the unit orthogonal eigenvector of V corresponding to λ_i , then the i-th principal component Y_i of sample data Z can be expressed as:

$$Y_i = Z^T L_i = \gamma_{1i} z_1 + \gamma_{2i} z_2 + \dots + \gamma_{fi} z_f \quad (1)$$

Cross-Validation and Multiple Regression. For the above f principal components, a multiple linear regression model is established and solved by the least square method. In order to make effective use of training data, k-fold cross validation is performed on principal component data. Suppose there is a data set D_n , n is the sample size, A_1, A_2, \dots, A_k is a subset of D_n , and for any subset A_j , there is a relation $M(A_j) \approx n/K$, in which M is the number of samples in the subset, and the final generalization error estimate is shown in Eq. 2.

$$R_{CV} = \frac{1}{K} \sum_{j=1}^K \left[\frac{1}{M(A_j)} \sum_{i \in A_j} L(s(D_n^{(-A_j)})) ; \xi_j \right] \quad (2)$$

Where L is the loss function, $D_n^{(-A_j)}$ is the remaining sample after removing the subset A_j , and s is the training model.

This paper selects $K = 5$ for cross-validation analysis. That is, in the data from 2006 to 2018, the data from 2006 to 2015 is used as the training data for applying cross-validation, and the data from 2016 to 2018 is used as the data for model evaluation. For the evaluation of the model effect, The mean absolute percentage error (MAPE) is used, as shown in Eq. 3, where n is the total amount of predicted data, Y_i is the actual value, and y'_i is the predicted value.

$$\text{MAPE} = \sum_{i=1}^N \left| \frac{y_i - y'_i}{y_i} \right| \times \frac{100}{n} \quad (3)$$

Analysis of Influencing Factors and Data Selection. In previous studies, Peng Chen and Jiang Yi [3] analyzed the main factors affecting heating energy consumption. Referring to the research results, a series of possible influencing factors from the aspects of heat source, heat supply network and terminal node is analyzed, such as energy conversion efficiency, transportation process, economy and promotion of energy saving standards.

For heat sources, coal-fired cogeneration and coal-fired boilers is largely used in China, supplemented by a small number of gas-fired boilers and renewable energy at current stage. The near future will be a critical period for the adjustment of heat source structure, with the cogeneration and industrial waste heat be developed. In addition to

the heat source structure, the key to the energy consumption of the pump is the length of the heat supply network. The heating demand is mainly determined by the heating area and the temperature difference between indoor and outdoor, based on which the central heating area and the heating area of residential buildings is selected as the influencing factors.

Building energy demand is greatly affected by climate change [4, 5], and the heating degree days (HDD) reflects the heating demand during the heating season. Energy-saving standards have a significant impact on the heat demand of buildings [6]. In this paper, the implementation time of the standard reflects its impact on the macro heating energy consumption. Economy and energy influence each other [7], and GDP is an important manifestation of changes in economic conditions. In addition, in China, the government invests a lot of money every year to upgrade the central heating infrastructure. In this process, PECCCH will inevitably change.

In summary, 13 influencing factors of PECCCH are preliminarily determined, including climate conditions, heat source structure, central heating area, energy-saving standard, economic conditions, reform activities, etc. Data sources are website of National Bureau of statistics, *statistical yearbook of China's urban and rural construction, annual development report of China's heating industry*, etc. The data of each factor over the years are shown in Table 1, and the Pearson correlation coefficient between the corresponding indicators is shown in Fig. 2, which reflects the linear correlation between variables [8]. It can be seen that there is a strong collinearity among the 13 independent variables, which requires the analysis model to have excellent adaptability to the collinearity factors.

Table 1. Data of each factor over the years

Item years	Unit	2006	2008	2010	2012	2014	2016	2018
HDD ^a /A	°C·d	2812	2844	2942	3115	2772	2739	2841
Energy consumption of coal fired boiler ^b /B	Ten thousand tce	638	718	718	744	691	638	531
Proportion of gas fired boilers ^b /C	%	0.40	0.60	1.00	1.90	3.84	6.06	10.00
Proportion of hot spot cogeneration ^b /D	%	32.35	34.80	37.31	39.60	42.40	44.42	48.00
Proportion of industrial waste heat ^b /E	%	0.3	0.7	1.3	1.7	2.2	3.0	2.6
Length of central heating pipe ^c /F	10000 km	7.99	10.46	12.41	14.74	17.47	20.14	37.11

(continued)

Table 1. (continued)

Item years	Unit	2006	2008	2010	2012	2014	2016	2018
Central heating area ^{c/G}	100 million m ²	82	90	98	106	126	136	147
Heating area of residential buildings ^{c/H}	100 million m ²	18.7	24.4	30.7	37.6	45.0	55.2	64
Implementation of three step energy saving standard for residential buildings/I	0/1	0	0	1	1	1	1	1
Implementation of four step energy saving standard for residential buildings/J	0/1	0	0	0	0	1	1	1
Three step implementation of energy saving standards for public buildings/K	0/1	0	0	0	0	0	1	1
GDP ^{c/L}	Trillion RMB	21.9	31.9	41.2	53.9	64.4	74.6	91.9
Fixed assets investment in central heating construction ^{c/M}	100 million RMB	223.6	269.7	433.2	630.3	575.45	481.87	420.04
PECCH/N	100 million tce	1.57	1.65	1.73	1.82	1.87	1.98	2.08

^a According to the meteorological parameters of each region; ^b Report on China's future energy situation and low carbon development of buildings, report on 2020 national heating academic annual meeting (Tsinghua University building energy conservation research center); ^c Statistical yearbook of urban and rural construction in China

Future Scenario Setting. According to different processes such as the development of total heating area and the change of heat source structure, Prediction of PECCH is in three scenarios, namely, basic scenario, medium control scenario and enhanced control scenario. Refer to relevant research results [9, 10], the following hypotheses are made.

Basic scenario is that China will continue to follow the current development model, and the heating energy consumption per capita will gradually approach that of developed countries, and the GDP will reach 351 trillion yuan in 2050; The central heating area will be 26.3 billion m² in 2030 and 28.1 billion m² in 2050; the proportion of coal-fired boilers will be reduced by 33% in 2030 and 47% in 2050; The energy consumption of cogeneration will peak in 2030, increasing 14% compared with the current, and

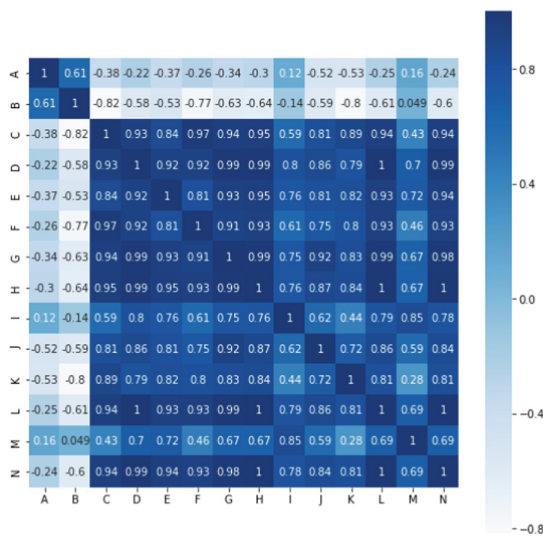


Fig. 2. Pearson correlation coefficient of each factor.

its proportion will rise to 51% in 2050. Industrial waste heat will achieve a certain development, accounting for 6% in 2030 and 8% in 2050. Medium control scenario is the energy consumption of central heating in the north by taking into account the resource situation in China and by means of technological progress, controlling the total heating area, improving the utilization rate of primary energy and reducing the use of coal-fired boilers. In this scenario, the proportion of coal-fired boilers in China will decrease by 52% in 2030 and 66% in 2050, while the proportion of coal-fired cogeneration will increase by 20% in 2030 and 24% in 2050. The utilization of industrial waste heat is developing faster, accounting for 8% by 2030. As the population is no longer increasing, and more flexible heating methods such as renewable energy were widely developed, the area of central heating reached 23.9 billion m² in 2030 and then slowed down to 25.3 billion m² in 2050.

The Enhanced control scenario is to consider that China's heating carbon emissions will reach the peak in 2030 and achieve carbon neutralization by 2060, significant progress has been made in energy-saving technology of central heating, the control of total central heating area has been enhanced, and the industrial waste heat and cogeneration with higher efficiency have been fully utilized. In this scenario, the central heating area in northern China will be 21.7 billion m² in 2030, Compared with the current, the proportion of coal-fired boilers is reduced by 71%, the proportion of coal-fired cogeneration is increased by 25%, and the utilization of industrial waste heat is increased by 3.5 times; in 2050, the proportion of coal-fired boilers is reduced by 92%, the proportion of cogeneration is increased to 62%, the proportion of industrial waste heat is increased to 11.7%, and the central heating area is controlled within 22.6 billion m².

3 Model Verification Results

Figures 3 and 4 show the prediction results of Mr-PCA applying different principal components. It can be seen from Fig. 3 that when 2, 3 and 4 principal components are used for modeling, the data of training set all have good fitting performance. However, for the validation data set from 2016 to 2018, when the principal component is 3, there is a better prediction effect, and the MAPE value on the validation set is only 2.3%, which is supported by the further analysis in Fig. 4.

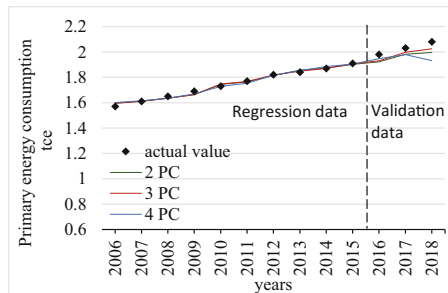


Fig. 3. Prediction effect of Mr-PCA model under different principal components.

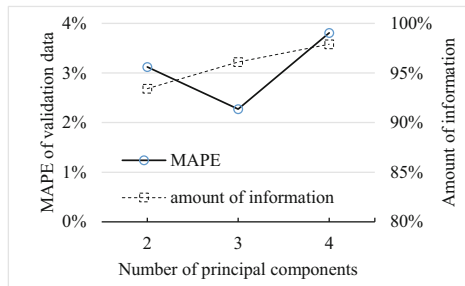


Fig. 4. Analysis of data information quantity and model accuracy under different principal components.

4 Scenario Analysis

In the basic scenario, due to the growth of China's GDP and the increase of heating area, the PECCH will maintain rapid growth in the next 10 years. Although some progress has been made in the utilization of industrial waste heat, the structure of heat source with coal-fired boiler as the major role has not been effectively optimized, and the energy utilization still has a low efficiency, resulting in that the PECCH will reach 250 million tce in 2030. Subsequently, the growth rate of heating area slowed down, and the PECCH entered a stable development period, but there are still urban expansion and people's

expansion of heating consumption demand, the PECCCH will rise slowly, reaching 270 million tce in 2050, and the energy consumption intensity of heating is 9.5 kgce/m^2 .

In the medium control scenario, the use of coal-fired boiler is compressed, and the heat source structure is effectively adjusted, which has a certain inhibitory effect on the increase of the PECCCH. Although the growth of building area has been controlled, the PECCCH will increase in the near future and reach the peak of 230 million tce in 2030 due to the growth inertia brought by economic development. After that, with the saturation of heating demand and the progress of technology, the utilization of industrial waste heat has developed rapidly, replacing a large number of primary energy boilers. The PECCCH will drop to 210 million tce in 2050. Correspondingly, the energy consumption intensity of heating will reach 9.7 kgce/m^2 in 2030 and 8.3 kgce/m^2 in 2050.

In the strengthened control scenario, the coverage area of central heating should be strictly controlled from now on, which plays a decisive role in restraining the rapid increase of the PECCCH. The PECCCH will reach a peak of 210 million tce in 2030 after a period of inertia growth. Subsequently, the multiple growth of industrial waste heat utilization offsets a large amount of primary energy consumption. The rapid reduction of coal-fired boilers and the increase of the proportion of cogeneration will greatly improve the heat source efficiency. The primary energy consumption of central heating can be reduced to 170 million tce in 2050. Correspondingly, the energy consumption intensity will drop to 7.5 kgce/m^2 . The future development trend of The PECCCH under the three scenarios is shown in Fig. 5.

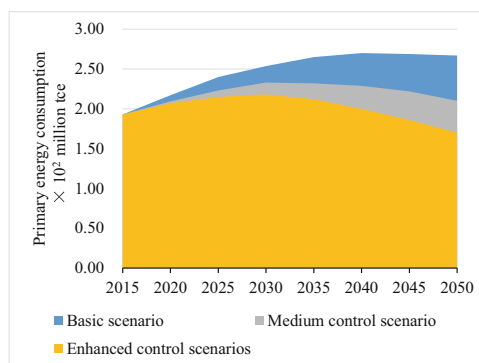


Fig. 5. Future development trend of The PECCCH under the three scenarios.

5 Conclusion

For the 13 influencing factors of The PECCCH, when three principal components are used for regression modeling, the prediction error is the lowest, and the MAPE value is only 2.3%. In the case of basic scenario, medium control scenario and strengthened control scenario, the expected PECCCH values of 2030 are 250 million tce, 230 million tce and 210 million tce respectively. In this period, through the use of certain control

means, the PECCCH can basically reach the peak. For the above three scenarios, The PECCCH in 2050 is 270 million tce, 210 million tce and 170 million tce respectively, and the corresponding energy consumption intensity is 9.5 kgce/m², 8.3 kgce/m² and 7.5 kgce/m² respectively. Through the optimization of heat source structure and heating scale, China's heating energy consumption and intensity can be both reduced in 2050, thus contributing to the realization of China's carbon neutral goal.

References

1. Tsinghua University Building Energy Conservation Research Center: 2020 annual report on China building energy efficiency, pp. 8–9. China Architecture Publishing, Beijing (2020)
2. Xiu ,Y.: Study of China's building energy efficiency based on energy data. Tsinghua University, Beijing (2009)
3. Jiang, Y., Peng, C., Da, Y.: Technology roadmap of building energy conservation in China. *Constr. Sci. Technol.* **17**, 12–19 (2012)
4. Azevedo, J.A., Chapman, L., Muller, C.L.: Critique and suggested modifications of the degree days methodology to enable long-term electricity consumption assessments: a case study in Birmingham, UK. *Meteorol. Appl.* **22**(4), 789–796 (2015)
5. You, Q., Fraedrich, K., Sielmann, F., et al.: Present and projected degree days in China from observation, reanalysis and simulations. *Clim. Dyn.* **43**(5–6), 1449–1462 (2014)
6. Yingpeng, D., Shuangping, C., Xiaohui, L.: Comparison of energy saving effects of Chongqing residential buildings under different energy saving standards. *Shangxi Archit.* **43**(26), 175–176 (2017)
7. Zhao, T., Yin, Y., Li, X.: Study on the correlation of energy and economic growth. *J. Xidian Univ. (Soc. Sci. Ed.)* **19**(001), 33–39 (2009)
8. Marcellán, F., Marriaga, M., Pérez, T.E., Piñar, M.A.: Matrix Pearson equations satisfied by Koornwinder weights in two variables. *Acta Appl. Math.* **153**(1), 81–100 (2017). <https://doi.org/10.1007/s10440-017-0121-6>
9. Yi, J.: China's future energy scenario and low carbon building development path [EB/OL]. <https://www.doc88.com/p-39039774632790.html>. Accessed 13 May 2020
10. Yi, J.: Report on the development of China's heating industry in 2020 [EB/OL]. https://mp.weixin.qq.com/s/KEBTkCRjG_SU7rVyHkqK2w. Accessed 31 Aug 2020



An Integrated Bi-level Optimization Model for Planning Water-Food-Energy Nexus System Under Uncertainty

Y. Ma¹ , Y. P. Li^{1,2} (✉), and G. H. Huang^{1,2}

¹ State Key Joint Laboratory of Environmental Simulation and Pollution Control,
School of Environment, Beijing Normal University, Beijing 100875, China
scut_my@163.com

² Institute for Energy, Environment and Sustainable Communities, University of Regina,
Regina, SK S4S 7H9, Canada

Abstract. In this study, a fuzzy bi-level programming (FBP) method is developed for planning water-food-energy (WFE) nexus system. FBP can tackle fuzzy uncertainty expressed as flexible variable and balance the conflict existed in different decision levels. Then, an FBP-WFE model is formulated for Amu Darya River Basin (ARB), in which two-level stakeholders are involved. The upper-level decision maker aims to maximize system benefit, and the lower-level decision maker aims to maximize food production. Three countries, fourteen states, fifteen water users and six planning periods (2021–2050) are also involved in the developed model. Major findings are (i) agricultural sector is the largest water user in ARB (accounting for 78.2%), implying that improving irrigation efficiency and reducing agricultural water allocation are crucial for alleviating water scarcity problem; (ii) there is competition for water resources between electricity generation and food production, with the increasing electricity demand level, the food production would decrease by 2.6%. The obtained results can provide policy supports for decision makers to alleviate water shortage, ensure food security and energy supply security.

Keywords: Bi-level programming · Water-food-energy nexus · Optimization · Uncertainty

1 Introduction

1.1 A Subsection Sample

Water, food and energy are closely interrelated, forming a water-food-energy (WFE) nexus system. The processes of pumping, distributing and treating water need energy. The energy generation, cooling and fuel mining also require water [1]. In addition, agricultural cultivation and food production need to consume a large amount of water and energy. Therefore, it is crucial for decision makers to plan the WFE nexus system synergistically to realize sustainable development. However, the planning process of

WFE nexus system often involves different stakeholders with conflicting objectives. Conventional optimization methods have limitation in solving hierarchical decision-making problems.

Bi-level programming (BP), which involves two-level objectives, has advantages in tackling hierarchical decision-making problem. For example, Cai et al. (2018) [2] applied BP method to explore optimal land use schemes for agricultural nonpoint source pollution management, where the gaming relationship between different managers was considered. Fernandez et al. (2021) [3] applied BP to manage community energy system for optimal energy sharing and trading, in which the conflict between total revenue and storage facility's revenue was resolved. However, affected by subjective policies and underdeveloped market, some parameters in WFE nexus system may characterized by fuzzy uncertainty. Thus, the flexible fuzzy programming (FFP) can be introduced into BP to tackle uncertain input parameters.

Therefore, this study aims to develop a fuzzy bi-level programming (FBP) method to plan WFE nexus system, and a real case of Amu Darya River Basin (ARB) is applied to show the effectiveness of the developed model. The innovation and contribution include: (i) an FBP method is developed to solve hierarchical decision-making problem and tackle fuzzy uncertainty in WFE nexus system; (2) an FBP-WFE model is formulated for ARB, and various electricity demand levels are designed to explore the relationship among water, food and energy; (iii) a set of management schemes can be obtained for decision makers in ARB to provide numerical policy support for sustainable development.

2 Methodology

Bi-level programming (BP) is developed according to Stackelberg games and has advantage in solving decentralized planning problem with two-level executors in hierarchical structure. However, affected by subjective judgments of policy makers, some real-world planning problems are plagued with fuzzy uncertainty [4]. Flexible fuzzy programming (FFP), which can tackle fuzzy uncertainty through fuzzy ranking methods, can be introduced BP to solve above-mentioned problem [5]. Thus, a fuzzy bi-level programming (FBP) method can be developed as:

$$\underset{x}{\text{Max}} f_U(x, y) = ax + by \quad (1)$$

where y solves:

$$\underset{y}{\text{Max}} f_L(x, y) = cx + dy \quad (2)$$

subject to:

$$\varphi x + \beta y \tilde{\leq} h \quad (3)$$

$$x, y \geq 0 \quad (4)$$

where $x \in R^{n1}$ is decision variable controlled by upper-level decision maker and $y \in R^{n2}$ is controlled by lower-level decision maker, $a, c \in R^{n1}$, $b, d \in R^{n2}$, φ is an $m \times n_1$ matrix, β is an $m \times n_2$ matrix, $h \in R^m$. According to the fuzzy set theory, a fuzzy number $\tilde{\xi}$ can be introduced to tackle constraint (1c), in which $\tilde{\xi}$ is shown as three prominent points $\tilde{\xi} = [\xi_{(1)}, \xi_{(2)}, \xi_{(3)}]$. Then, ϑ_{ξ} (i.e. $\vartheta_{\xi} = \xi_{(3)} - \xi_{(2)}$) and ϑ'_{ξ} (i.e. $\vartheta'_{\xi} = \xi_{(2)} - \xi_{(1)}$) can be introduced to tackle the lateral margins of $\tilde{\xi}$. Then, FBP can be formulated as:

$$\underset{x}{\text{Max}} f_U(x, y) = ax + by \quad (5)$$

where y solves:

$$\underset{y}{\text{Max}} f_L(x, y) = cx + dy \quad (6)$$

subject to:

$$\varphi x + \beta y \leq h + \left[\xi_{(2)} + \frac{\vartheta_{\xi} - \vartheta'_{\xi}}{3} \right] (1-\alpha) \quad (7)$$

$$x, y \geq 0 \quad (8)$$

$$0 \leq \varphi \leq 1 \quad (9)$$

3 Case Study

3.1 Statement of Problem

The Amu Darya River is the largest river in Central Asia and one of the two major water sources of the Aral Sea. It has a total length of 2,540 km and an average annual flow of 65 km³ [6]. Before the disintegration of the Soviet Union, the Amu Darya River Basin (ARB) was the main cotton production base. The rapid agricultural expansion and low agricultural irrigation efficiency (mainly flood irrigation) caused a lot of water resources to be wasted, leading to water shortage, ecological degradation and food crisis. Besides, the upstream country has vigorously developed the hydropower industry, and the interception of water resources by reservoirs has caused serious water shortage in the lower Amu Darya area. Therefore, the water, food and energy are closely linked to form a water-food-energy (WFE) nexus system. In order to realize the sustainable development of the ARB, it is crucial to make comprehensive management of the WFE nexus system.

3.2 Modeling Formulation

In order to alleviate water scarcity problem, and ensure food security and energy supply security, an FBP-based WFE management (FBP-WFE) model is formulated for ARB. The developed model involves two-level decision makers, where the upper-level decision maker aims to maximize system benefit, and the lower-level decision maker aims to maximize the amount of food production. Three countries, fourteen states, fifteen water users and six planning periods (2021–2050, 5 years in a period) are involved in the developed model. For exploring the impact of electricity demand on WFE nexus system, three electricity demand levels (low, medium and high) are designed. Besides, as shown in Table 1, six α levels are considered to tackle the fuzzy uncertainty during the modelling formulation. The FBP-WFE model is:

Upper-level:

$$\begin{aligned}
 \text{Max } f_U = & \sum_i^I \sum_j^J \sum_t^T BW_{ijt} \times AW_{ijt} - \sum_i^I \sum_j^J \sum_t^T CE_{it} \times (PSE_{ijt} + TSE_{ijt} + UEE_{ijt}) \times AW_{ijt} / \gamma_{ijt} \\
 & - \sum_i^I \sum_{j=1}^{10} \sum_t^T QF_{ijt} \times PF_{ijt} \times AW_{ijt} / WPC_{ijt} - \sum_i^I \sum_{j=1}^{10} \sum_t^T FC_{ijt} \times AW_{ijt} / WPC_{ijt} \\
 & + \sum_i^I \sum_t^T BEW_{it} \times EW_{it} \times PTH_{it} \times \varphi_{THit} \times (1 - \eta_t) \\
 & + \sum_i^I \sum_t^T BEW_{it} \times EW_{it} \times PHY_{it} \times \varphi_{HYit} \times (1 - \eta_t) \\
 & - \sum_i^I \sum_t^T CE_{it} \times (PUE_{it} + TSEE_{it} + UEE_{it}) \times EW_{it} / \gamma_{it} \\
 & + \sum_t^T \left[\left(TAA_t - \sum_i^I \sum_j^J AW_{ijt} / \gamma_{ijt} - \sum_i^I EW_{it} / \gamma_{it} - WAL_t \right) \times \alpha + \beta \right]
 \end{aligned} \tag{10}$$

Lower-level:

$$\text{Max } f_{L1} = \sum_i^I \sum_j^J \sum_{t=4,5,8}^T YA_{ijt} \times AW_{ijt} / WPC_{ijt} \tag{11}$$

Key constraints:

(1) Water demand constraint.

$$AW_{ijt} \geq TW_{ijt}, \quad \forall i, j, t \quad (12)$$

(2) Water availability constraint.

$$\sum_i^I \sum_j^J AW_{ijt} / \gamma_{ijt} + \sum_i^I EW_{it} / \gamma \gamma_{it} + WAL_t \leq TAA_t, \quad \forall t \quad (13)$$

(3) Total electricity demand constraint.

$$\begin{aligned} & \sum_i^I EW_{it} \times PTH_{it} \times \varphi_{THit} \times (1 - \eta_t) \\ & + \sum_i^I EW_{it} \times PHY_{it} \times \varphi_{HYit} \times (1 - \eta_t) + IOE_t \geq ELD_t, \quad \forall t \end{aligned} \quad (14)$$

(4) The constraints of electricity demand for different countries.

$$\begin{aligned} & \sum_{i=1}^3 EW_{it} \times PTH_{it} \times \varphi_{THit} \times (1 - \eta_t) \\ & + \sum_{i=1}^3 EW_{it} \times PHY_{it} \times \varphi_{HYit} \times (1 - \eta_t) - TAOE_t \geq TAED_t, \quad \forall t \end{aligned} \quad (15)$$

$$\begin{aligned} & \sum_{i=4}^{10} EW_{it} \times PTH_{it} \times \varphi_{THit} \times (1 - \eta_t) \\ & + \sum_{i=4}^{10} EW_{it} \times PHY_{it} \times \varphi_{HYit} \times (1 - \eta_t) - UZOE_t \geq UZED_t, \quad \forall t \end{aligned} \quad (16)$$

$$\begin{aligned} & \sum_{i=11}^{14} EW_{it} \times PTH_{it} \times \varphi_{THit} \times (1 - \eta_t) \\ & + \sum_{i=11}^{14} EW_{it} \times PHY_{it} \times \varphi_{HYit} \times (1 - \eta_t) - TUOE_t \geq TUED_t, \quad \forall t \end{aligned} \quad (17)$$

(5) Cultivated area constraint.

$$ARE_t^{\min} \leq \sum_i^I \sum_{j=1}^{10} AW_{ijt} / WPC_{ijt} \leq ARE_t^{\max}, \quad \forall t \quad (18)$$

(6) The constraint of electricity consumed for water allocation.

$$\begin{aligned} & \sum_i^I \sum_j^J (PSE_{ijt} + TSE_{ijt} + UE_{ijt}) \times AW_{ijt} / \gamma_{ijt} \\ & + \sum_i^I (PUE_{it} + TSEE_{it} + UEE_{it}) \times EW_{it} / \gamma_{it} \leq ALE_t + \left[\xi_{(2)} + \frac{\vartheta_\xi - \vartheta'_\xi}{3} \right] (1 - \alpha), \forall t \end{aligned} \quad (19)$$

Table 1. The design of electricity demand and α level.

	t = 1	t = 2	t = 3	t = 4	t = 5	t = 6
<i>Electricity demand level (10^9 kWh)</i>						
L	321.65	337.98	357.81	379.99	404.73	432.34
M	337.74	354.88	375.70	398.99	424.97	453.96
H	353.82	371.78	393.59	417.99	445.20	475.58
<i>α level (Electricity consumed for water allocation, 10^9 kWh)</i>						
$\alpha = 0$	69.38	72.91	77.18	81.97	87.30	93.26
$\alpha = 0.2$	69.27	72.79	77.06	81.84	87.17	93.11
$\alpha = 0.4$	69.16	72.67	76.94	81.71	87.03	92.97
$\alpha = 0.6$	69.05	72.56	76.81	81.58	86.89	92.82
$\alpha = 0.8$	68.94	72.44	76.69	81.45	86.75	92.67
$\alpha = 1$	68.83	72.33	76.57	81.32	86.61	92.52

4 Result and Discussion

Figure 1(a) presents the amount of water allocation for different water users under different scenarios, indicating that total amount of water allocation in the Amu Darya River Basin (ARB) would be 1071.5 km^3 to 1073.0 km^3 over the planning horizon. With the increasing α level, the total amount of water allocation would decrease nearly 1.2%, which owing to the declined constraint-violation degree. Higher α level means that less electricity can be consumed for pumping, transporting and distributing water, thus less water resources can be distributed to water users. Meanwhile, the system reliability would be increase with the high α level. Figure 1 (b) shows the proportion of water allocation. In terms of time scale, the proportion of agricultural water allocation would decrease by 12.7% to 13.3% over the planning horizon, while the proportion of water allocation for industry, electricity generation and ecological sector would increase by 4.9% to 5.0%, 1.9% to 2.3% and 3.5%, respectively. Besides, For the ARB, the agriculture would still be the main user of water resources over the planning horizon, accounting for nearly 78.2%, of which animal husbandry accounts for 31.2%. Therefore, improving the efficiency of agricultural irrigation and reducing the amount of water allocated to the agricultural sector are crucial to alleviate the water shortage problem in ARB.

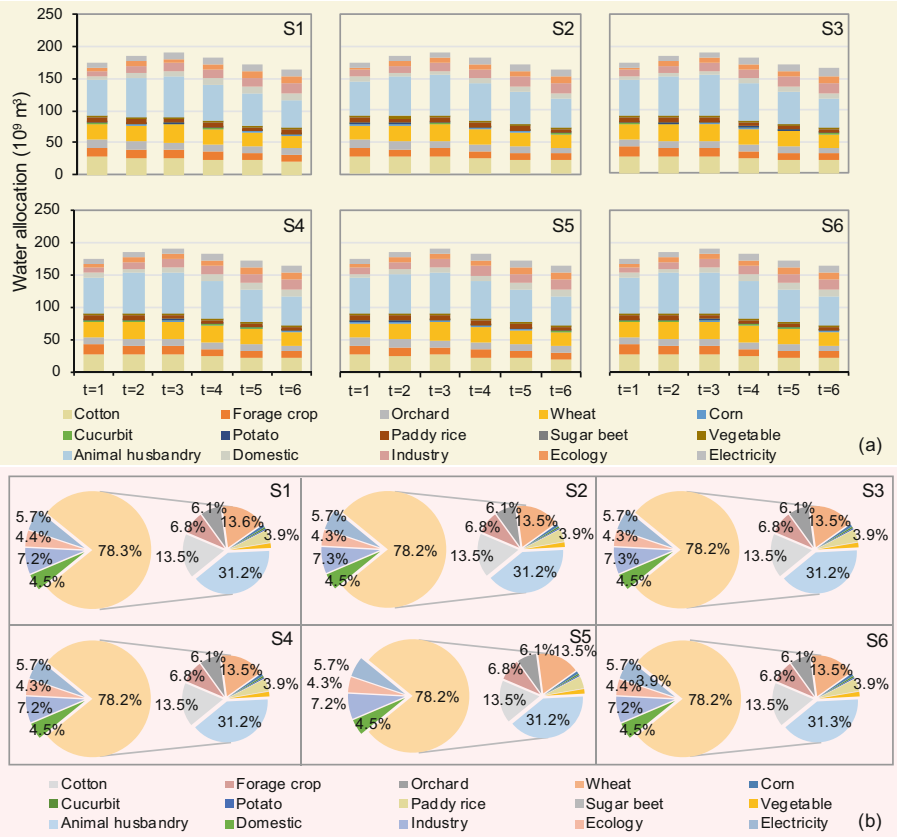


Fig. 1. Water allocation schemes for S1 to S6.

Figure 2 shows the result of food production under different scenarios which obtained from conventional single-level model and bi-level (FBP-WFE) model. The obtained result indicates that in order to ensure food security in ARB, the amount of food production should be 133.2×10^9 kg to 134.5×10^9 kg over the planning horizon. In particular, wheat is the most important food crop for ARB, accounting for nearly 73.8%. When α level increases from 0 to 1, the food production would decrease by 2.2% to 7.9%. Correspondingly, the constraint-violation degree would be decline with the rising α level. Besides, with the increasing electricity demand level (i.e., from L to H), the amount of food production under various scenarios would decrease by 2.6% averagely, which indicates that electricity generation would squeeze the water resources allocated for food production. Therefore, while developing the economy, policy makers should give priority to ensuring water for food production. The result also shows that compared with conventional single-level model, the food production obtained from FBP-WFE model would increase by 20.1% to 21.3%. This is because FBP-WFE model has two-level objectives which aim to maximize system benefit and food production simultaneously, while conventional single-level model only focuses on system benefit. Therefore, the

FBP-WFE model has more superiority than conventional single-level model, and can provide comprehensive policy support about alleviating water shortage and ensuring food security for ARB.

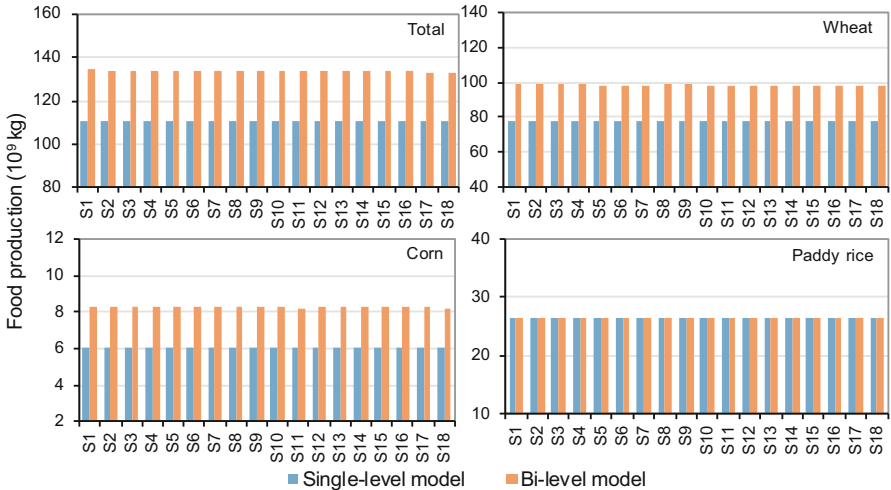


Fig. 2. Food production under different scenarios

Figure 3 presents the solution of electricity generation for Tajikistan, Uzbekistan and Turkmenistan over the planning horizon. With the rising α level (i.e., from 0 to 1), the total amount of electricity generation would increase by 1.1% to 1.8%. This is because with the increasing α level, the water allocated to other users would be decrease, thus more water can be saved for electricity generation. For different countries, Turkmenistan is the largest electricity producer in the ARB (i.e., accounting for 45.8%), followed by Tajikistan (i.e., accounting for 27.3%) and Uzbekistan (i.e., accounting for 26.9%). As a country located on the upper reach of the Amu Darya River, Tajikistan's electricity production is mainly based on hydropower, which accounts for nearly 95.0%. The electricity generation in Uzbekistan and Turkmenistan mainly rely on thermal power, in which the thermal power account for 81.9% and 85.8%, respectively. Therefore, reducing the proportion of hydropower generation in Tajikistan can alleviate the contradiction in water resources competition among multiple countries in the ARB.

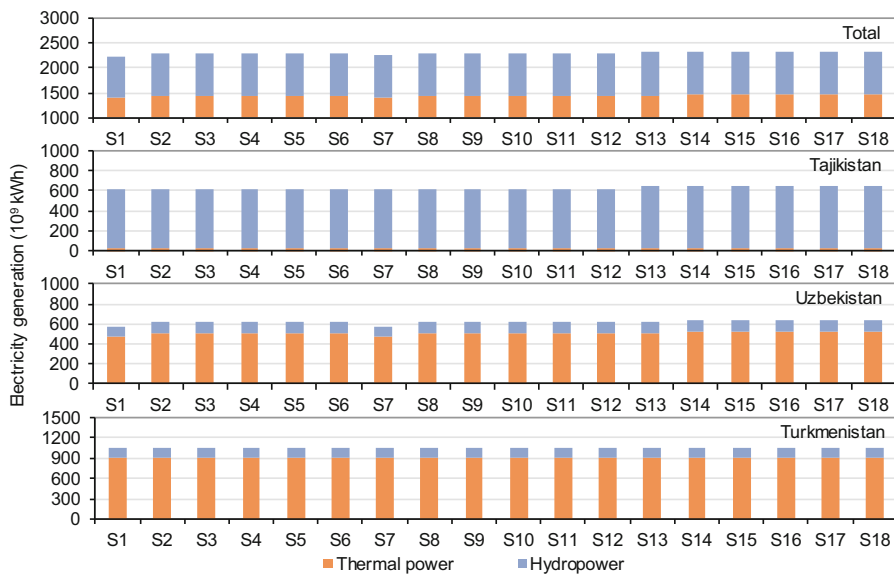


Fig. 3. Electricity generation for Tajikistan, Uzbekistan and Turkmenistan

5 Conclusions

In this study, a fuzzy bi-level programming (FBP) method has been developed for planning water-food-energy (WFE) nexus system, where the problems of hierarchical decision making and fuzzy uncertainty could be tackled simultaneously. Then, an FBP-WFE model has been formulated for Amu Darya River Basin (ARB), where the upper-level model aims to maximize system benefit and the lower-level model aims to maximize food production. Three countries, fourteen states, fifteen water users and six planning periods has been involved in the FBP-WFE model. Some major findings are (i) agricultural sector would be the largest water consumer in ARB (accounting for 78.2% of total water allocation), thus improving irrigation efficiency and reducing agricultural water allocation are crucial for alleviating water scarcity problem; (ii) decision makers should consider the impact of uncertainty during the management of WFE nexus system, with the increasing α level (from 0 to 1), the total amount of water allocation would decrease nearly 1.2%, the food production would decrease by 2.2% to 7.9%; (iii) with the increasing electricity demand level (from L to H), the food production would decrease by 2.6% averagely, which indicates that electricity generation would squeeze the water resources allocated for food production, thus managers should focus on food security alongside economic development. The obtained results can provide various management schemes for decision makers to achieve sustainable development.

Acknowledgments. This research was supported by the Strategic Priority Research Program of Chinese Academy of Sciences (XDA20060302) and the National Key Research and Development Program of China (2016YFC0502803).

Appendix A. Nomenclatures for parameters and variables

i	Different states in Amu Darya River Basin, with $i = 1$ for Gorno-Badakhshan, $i = 2$ for Khatlon, $i = 3$ for RRT, $i = 4$ for Surkhnadarya, $i = 5$ for Kashkadarya, $i = 6$ for Samarkand, $i = 7$ for Navoi, $i = 8$ for Bukhara, $i = 9$ for Khorezm, $i = 10$ for Karakalpakstan, $i = 11$ for Mary, $i = 12$ for Ahal, $i = 13$ for Lelap, $i = 14$ for Dashaguz
j	Water users, with $j = 1$ for cotton, $j = 2$ for forage crop, $j = 3$ for orchard, $j = 4$ for wheat, $j = 5$ for corn, $j = 6$ for cucurbit, $j = 7$ for potato, $j = 8$ for rice, $j = 9$ for sugar beet, $j = 10$ for vegetable, $j = 11$ for animal husbandry, $j = 12$ for domestic, $j = 13$ for industry, $j = 14$ for ecology
t	Planning periods (2021–2050), $t = 1, 2, \dots, 6$
BW_{ijt}	Net benefit for water user j in state i under planning period t (US\$/m ³)
AW_{ijt}	Water allocation for user j in state i under planning period t (m ³)
CE_{it}	Unit cost for water transport for state i under planning period t (US\$/m ³)
PSE_{ijt}	Electricity consumed for pumping water (KWh/m ³)
TSE_{ijt}	Electricity consumed for transporting water (KWh/m ³)
UE_{ijt}	Electricity consumed for distributing water (KWh/m ³)
γ_{ijt}	Water allocation efficiency
QF_{ijt}	The amount of fertilizer consumed by user j in state i under planning period t (kg/ha)
PF_{ijt}	Unit cost for fertilizer for user j in state i under planning period t (US\$/kg)
WPC_{ijt}	Water requirement per unit planting area (m ³ /ha)
FC_{ijt}	Fixed cost for agricultural planting for user j in state i under planning period t (US\$/ha)
BEW_{ijt}	Net benefit per unit of electricity generation (US\$/KWh)
EW_{it}	Water allocated for electricity generation (m ³)
PTH_{it}	Water allocation ratio for thermal power generation (%)
φ_{THit}	Coefficient of water consumption in thermal power generation (KWh/m ³)
η_t	Electricity transmission loss ratio (%)
PTH_{it}	Water allocation ratio for thermal power generation (%)
φ_{HYit}	Coefficient of water consumption in hydropower generation (KWh/m ³)
PHY_{it}	Water allocation ratio for hydropower generation (%)
TAA_t	The total volume of water resources in period t (m ³)
WAL_t	Water loss in channel of Amu Darya river in period t (m ³)
YA_{ijt}	Crop output per area for user j in state i under planning period t (kg/ha)
TW_{ijt}	Water demand for user j in state i under planning period t (m ³)
IOE_t	The amount of imported electricity (KWh)

(continued)

(continued)

ELD_t	The total amount of electricity demand (KWh)
$TAED_t$	The amount of electricity demand for Tajikistan (KWh)
$UZED_t$	The amount of electricity demand for Uzbekistan (KWh)
$TUED_t$	The amount of electricity demand for Turkmenistan (KWh)
ARE_t^{\min}	The minimum area of cultivated land (ha)
ARE_t^{\max}	The maximum area of cultivated land (ha)
ALE_t	The amount of electricity consumed during water allocation (KWh)

References

1. Lv, J., Li, Y.P., Shan, B.G., Jin, S.W., Suo, C.: Planning energy-water nexus system under multiple uncertainties – a case study of Hebei province. *Appl. Energy* **29**, 389–403 (2018)
2. Cai, Y., Rong, Q., Yang, Z., Yue, W., Tan, Q.: An export coefficient based inexact fuzzy bi-level multi-objective programming model for the management of agricultural nonpoint source pollution under uncertainty. *J. Hydrol.* **557**, 713–725 (2018)
3. Fernandez, E., Hossain, M.J., Mahmud, K., Nizami, M., Kashif, M.: A bi-level optimization-based community energy management system for optimal energy sharing and trading among peers. *J. Clean. Prod.* **279**, 123254 (2021)
4. Suo, C., Li, Y.P., Sun, J., Yin, S.: An air quality index-based multistage type-2-fuzzy interval-stochastic programming model for energy and environmental systems management under multiple uncertainties. *Environ. Res.* **167**, 98–114 (2018)
5. Sun, J., Li, Y.P., Suo, C., Liu, Y.R.: Impacts of irrigation efficiency on agricultural water-land nexus system management under multiple uncertainties—a case study in Amu Darya River basin, Central Asia. *Agricul. Water Manag.* **216**, 76–88 (2019)
6. Jalilov, S.M., Keskinen, M., Varis, O., Amer, S., Ward, F.A.: Managing the water–energy–food nexus: Gains and losses from new water development in Amu Darya River Basin. *J. Hydrol.* **539**, 648–661 (2016)



Recovery of Eco-friendly Spaces for Ecotourism and the Integration of Visitors in Morro de Calzada – Peru

Doris Esenarro^{1,2,3,4(✉)}, Judith Ocmin¹, Elizabeth Segovia^{1,3}, Carla Tassara¹, and Violeta Vega^{1,3}

¹ Federico Villarreal National University UNFV, Lima, Peru

doris.esenarro@urp.edu.pe

² Ricardo Palma University URP, Lima, Peru

³ Specialized Institute for Ecosystems and Natural Resources Research (INERN), UNFV, Lima, Peru

⁴ Graduate School, EUPG, UNFV, Lima, Peru

Abstract. This research work aims to recover eco-friendly spaces for ecotourism. The integration of visitors to Morro de Calzada-Peru, the lack of infrastructure is one of the main obstacles that slow the growth of the tourism sector, limiting the development and enhancement of hundreds of attractions that could attract visitor flows and generate income that would contribute to local development. As is the case of Morro de Calzada, it currently does not have an infrastructure that provides comfort to visitors searching for nature. The same would allow the integration and pleasant experience.

Regarding the methodology used, a case study approach was adopted; the characteristics of the place were identified, the attributes that influence as; tourist infrastructure, climatic factors, floristic composition, among other components of the geographical area. Fundamental data that were considered for the execution of the 3D modeled design. Likewise, it was supported by an online survey, which was directed to residents and visitors. In conclusion, a design proposal is proposed as a development model that seeks to integrate conservation and care of the environment by applying clean technologies.

Keywords: Comfort · Ecotourism infrastructure · Interpretive trail · Solar panels · Sustainable constructions

1 Introduction

In the San Martin Region of the Moyobamba province is “El Mirador Morro de Calzada” an essential attraction of the region; it has calcareous formations, a cloudy, humid climate, with temperate temperatures in the day and cold at night, it has its ecosystem varied in flora and fauna [1]. The same characteristics have led it to today as a tourist destination for nature, adventure sports, relaxation, and research. Tourism has become an industry of great interest worldwide, so the infrastructure of a goal is essential to provide

quality services, therefore, develop a unique tourist experience [2]. However, the lack of infrastructure hinders the development of the goal, as is the case in this research [3].

The proposal for the sector lies in quality and environmentally sustainable tourism [4].

The model will be developed based on principles and considerations of sustainable construction that allow harmony with the environment and conservation with them [5].

It will be necessary to know the characteristics of the place, temperature, vegetation, humidity, soil, and movements; optimal air conditions in the infrastructure.

The development of an ecotourism infrastructure design aims to improve ecotourism services [5] on the road that leads to Morro de Calzada. This provides a quality service to visitors who search for natural spaces but to move; they also require comfort. This represents a psychophysiological state that involves all our senses, hence the need to study the effect of environmental, thermal, acoustic, visual stimuli on our psyche or body.

This research proposes developing a “Ecotourism infrastructure design for the comfort of visitors to Morro de Calzada”. The characteristics of the place, the elements offered by the natural attraction that generates satisfaction, and the attributes that influence it, such as the tourist infrastructure of this geographical area, were identified. [6] To meet this objective, this article is structured; after this introduction, in a literature review section, the research methodology is described, and the research findings are shown. The article ends with the discussion, conclusions, and references used in it.

2 Method

2.1 Compilation

Ecotourism or nature tourism represents a valuable line of the modern economy [7]; human beings seek more interaction with nature every day. As a result, it is positioning itself as an alternative for employment and income for local communities and acting as an activity that allows for valuable resources and awareness of the environment for both visitors and residents.

Table 1. Ecotourism activities.

Interpretive hiking	Observation of natural attractions
Photo safari	Ecosystem observation
Environmental education	Geology observation
Bird watching	Observation of fossils
Environmental Observation	Nature observation
Flora and fauna rescue	Research projects
Ecotourism	Connection and interaction with nature

In Table 1 shows the activities carried out in ecotourism are visualized.

Selection of Building Materials. Natural materials are less energy-intensive and less polluting, thus helping to reduce pollution. As local materials have a low energy cost level and less pollution, it contributes to the local economy [8]. However, durable materials can save energy costs in maintenance and the production and installation of spare parts.

Table 2. Table captions should be placed above the tables.

Priority	Source
Primary	Materials found in nature, such as stones, earth, flora
Secondary	Materials are made from recycled products such as plastics, aluminum, wood
Tertiary	Human-made materials (artificial, synthetic, non-renewable)

Table 2 shows the eco-friendly materials to be used in the proposal.

Bikeway. The importance of bicycles has become an alternative for managing sustainable mobility **and** maintaining social distancing due to COVID - 19.

Interpretive Trail. The **interpretive** trails are defined as organized infrastructures found in the natural, rural, or urban environment to facilitate and favor the visitor's realization and recreation with the natural environment or protected area where the trail is located.

Solar Panels. Energy generation systems that use sunlight and renewable energy are the ecological energies whose demand grows more [7]. Solar panels are manufactured today in the format of independent, large and small modules, which facilitates their applicability and locates them either in open or closed fields, depending on the characteristics [9]. Electric power generation (Fig. 1).



Fig. 1. Electric power generation. The solar panels will be incorporated for the proposals and take advantage of the solar radiation of the place.

2.2 Sample

The population is made up of both residents of the Calzada district and national visitors searching for attractions in the San Martín region. The sample allowed to apply the survey and determine both residents and visitors to the Calzada district. We are obtaining a selection of 355 from a universe of 4,609 inhabitants and a universe of 3,931 visitors, a sample of 350. [10].

Study of the geographical location and survey taken. The research area is located in the district of Calzada; it is one of the six districts of the province of Moyobamba, belonging to the region of San Martín. It has an area of 116.00 km², located 12.5 km. from the city of Moyobamba (east) and 12.5 km from Rioja (west) on the left side of the marginal jungle road, at km 493 and 494 (entry point) in the Alto Mayo valley (Fig. 2).

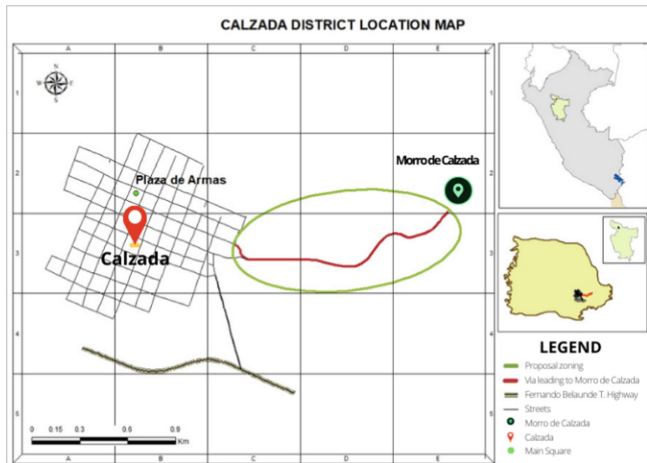


Fig. 2. Calzada district location map. Shows the access from the city of Moyobamba by overland paved road (Fernando Belaunde Terry Road), passing through the Main Square of the Calzada district to access the Morro access road de Calzada.

2.3 Research Design

Type of Investigation.

Non-experimental design – Crossed. Because the variables are not manipulated, the data were collected over time, considering the study area's social, environmental, and tourist information.

Level of Investigation.

Descriptive. Consider all aspects of the study area environment.

2.4 Materials

The following are the materials used for this investigation:

Cartographic Information. For the cartographic information, digital materials were used for the location, delimitation, and field information.

Softwares.

AutoCAD: It is a way to develop ideas in 3D; it allows you to translate design research into your workflows before you design. It is an essential tool in Architecture, Engineering, and Construction, to achieve a reality in which each addition we make to the environment we have built works in harmony with the natural environment in which it is inserted.

ArcGis: Software was used for georeferenced the research site and 3D.

Google Earth Pro: It was used to make a morphological survey of the research site.

3 Research Stages

3.1 Preliminary Stage

It consists of the bibliographic review of the information collected according to research similar to the subject. In this phase, the study is carried out to have a better panorama in the field stage.

The data collection techniques were:

- Bibliographic review and records of the study area.
- Study and reading of documents, reports, books, and theses related to research.
- Elaboration of thematic maps.

3.2 Field Stage

The information collection was carried out through notes in a field notebook, taking photographs, state of the floristic composition, the shape of the area, information panels, the importance of the commitment, and the needs of the surrounding population site.

3.3 Cabinet Stage

With the information collected in the field, an ecotourism infrastructure was proposed that allows harmonization with the environment, use of local materials, generation of comfortable spaces.

Taking as a starting point:

- The population needs to be appreciated in the application of the surveys.
- Selection of materials according to the prioritization criteria.
- Use of software for 3D modeling.

4 Current Diagnosis

The Morro de Calzada ecosystem is part of the mountain range known as the eastern mountain range. It has a natural elevation that exceeds 1400 m above sea level. It has a variable floral composition and structure. The material that composes the soil is mainly calcareous [10].

4.1 Vegetable Cover

The presence of the flora is developed by the climate of very dense humid forests, where there is always the presence of fogs. Consequently, the vegetation varies in arboreal and epiphytic species, especially Araceae orchids, bromeliads or achupallas, ferns, mosses, and lichens [2]. As shown in Fig. 3, the vegetation varies in arboreal and epiphytic, and lichens.

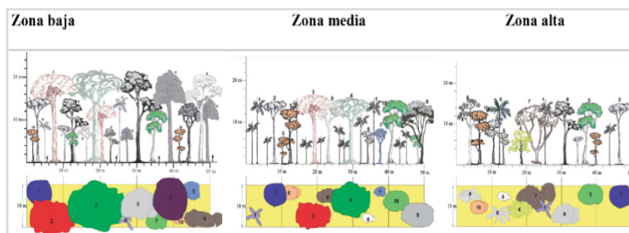


Fig. 3. Structural profiles by zones.

4.2 Physical Factors

Geology. The geological **unit** of the area is the geological formation, a Neogene system corresponding to the Cenozoic era.

Soil. The area is suitable for cultivating low agrological quality with soil limitations, corresponding to Type C soil.

Geomorphology. Andean Cordillera (Great morphostructural unit), Mountains and denudation structural hills (Morphostructural Subunit), and colluvial alluvial foothills (Geomorphological unit).

Hydrology. Rainfall **occurs** in all months of the year, reaching 1200 and 1700 and a pronounced reduction from May to August and maximum between October and March.

Climatology. It is characterized by the influence of the life zone, pre-montane tropical humid forest. The **months** with the highest temperatures are: September and October (29.4 °C); the lowest temperature occurs in July (17.2 °C); and it rains with greater intensity in March (158.21 mm/month). Mostly cloudy sky in the afternoon. Hot weather in the day. It is a relaxing time in the morning and evening. It rains on some afternoons. Moderate incidence of direct solar radiation. As shown in Fig. 4.

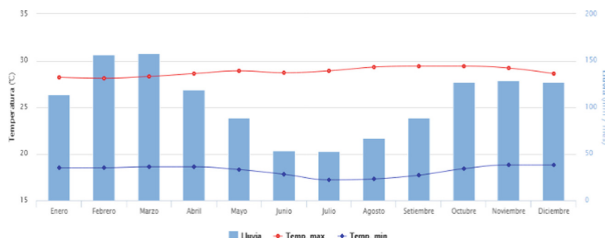


Fig. 4. Average temperature.

Building Material:

The Calzada District is an area that does not have a well-differentiated urban area; it shows the characteristics of the houses in general.

- Bricks or cement blocks: represents 34.16%.
- Quinchas: represents 39.04%.
- Wood represents 12.05%.

Data were obtained from the population and housing census of the Calzada district.

5 Proposal

5.1 Purpose

The purpose is to contribute to the generation of scientific studies to provide solutions integrated with nature. Allows the care and conservation of the environment with the ecotourism infrastructure and improves the quality of service for visitors and economic development for the local population.

Promotes ecotourism activity to achieve the commitment of both residents and visitors [11] (Fig. 5).

5.2 Infrastructure Description

It is characterized by a path with an irregular curvilinear shape that leads to the Morro de Calzada Viewpoint. Given the current situation according to the selection criteria for an ecotourism infrastructure, specifically for the road, we would use recycled materials converted into pavers and compacted that resist the heavy transit.

To generate traffic comfort and harmonize with the landscape, the infrastructure would be made of primary materials, opting for the most appropriate "Guayaquil cane," since in the area that is in the greater quantity that resource, both for the beginning, end, and course of the route along the path. In addition, native species belong to the town of Calzada to alter the ecosystem and value the existing species [12].

Given the lack of interpretive trails, the implementation of these is proposed, which will allow us to know the existing species, the characteristics of the area, and the culture.

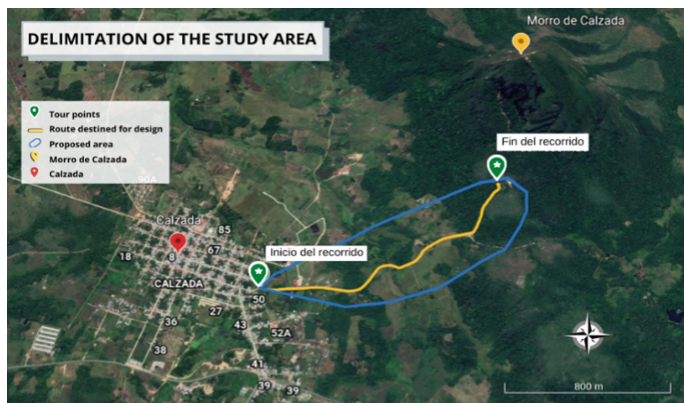


Fig. 5. Location of the ecotourism infrastructure project and its accessibility.



Fig. 6. Current state of the road to Morro de Calzada.

Currently, the access road to Morro de Calzada presents a deficiency of tourist infrastructure, as shown in Fig. 6. It lacks an interpretive path; it has a minimal shadow projected from some trees found along the way. Furthermore, it does not have places for breaks, such as benches for rest, and a place to recharge the devices' batteries to carry out activities such as flora photography (Figs. 7 and 8).

5.3 Function

Visitor service stands for the purchase of handicrafts, bicycle rental, and tasting typical food. The service posts are Guayaquil cane, a roof of braided palm trees, and rainwater collection for the corresponding user. The capture of solar energy through solar panels to take advantage of the electric fluid [12, 13].



Fig. 7. Front view of the ecotourism infrastructure proposal. It shows the facade of the proposal with the materials according to the place.



Fig. 8. Craft stall and bicycle rental, energy generation through solar panels. It can be seen that bicycles have a place for charging energy, which is recharged by solar panels.

5.4 Sustainable Finishes

- Informative panels based on wood and Guayaquil.
- Guayaquil-based bows for the model.
- Cobblestone floor made from recycled materials.
- Guayaquil-based benches and tables.
- Acoustic, thermal, and visual comfort is due to endemic vegetation.

Figure 9 shows the information panels in which it allows users to know all the existing infrastructure.



Fig. 9. Information panels.

5.5 Advantage

Construction with bamboo is the ideal material for sustainability and is available in the area, which generates a lower investment cost; a rapidly developing plant is suitable for construction given its flexibility and ease of molding as in the arch in the path. In addition, it is resistant to seismic activity, generates comfortable spaces, and provides a healthy environment [14].

The social integration spaces are adapted to the user's needs in continuous interaction with the design model; the materials used, the spatial proportions, and the shapes and colors play a significant role in harmonizing the place. And the comfort that it generates makes social integration fluid [15].



Fig. 10. Installation of solar panels for charging points on the road.

Figure 10 can see the clean technologies such as solar panels applied in the proposal, taking advantage of the climatological characteristics.

In Fig. 11, we can see the incorporation of bicycle parking to encourage cycling, minimize vehicles' use, and avoid noise pollution.

In Fig. 12, we can see the incorporation of social areas that allow visitors to integrate and enjoy nature.



Fig. 11. Bicycle parking spots.



Fig. 12. Social integration spaces.

6 Conclusions

The Calzada district has great potential to position itself as an ecotourism destination. Local resources make the ecotourism infrastructure viable, allowing social integration and visual, acoustic, and thermal comfort. The main objective of this research is to develop an ecotourism infrastructure design for the development of ecotourism and how it allows the care of the environment. In this way, it was carried out with the appropriate characteristics such as care with the color of the panels, materials to be used, and infrastructure according to the standards reviewed in the various documents [16].

6.1 Specific Conclusions

- 1) The structural profiles by zones allow knowing the type of vegetation to use to generate shade. Consequently, thermal comfort on the journey is achieved.
- 2) The ecotourism infrastructure proposal is determined by selecting construction materials and strategic criteria that allow the project to be sustainable and economically viable. The proposed infrastructure preserves and protects environmental wealth, values local cultural manifestations, and creates awareness for the benefit of the

- environment by respecting the principles of social, cultural, biological, commercial, and economic sustainability.
- 3) This research will contribute to developing the local economy and the cultural identity and care of natural resources to not extract excessively and contribute to ecotourism activity [17].

References

1. Mego Aguilar, M., Malca Torres, M.Y.: Structure and Floristic Composition of the Morro de Calzada Ecosystem, and its Ecotourism Value, Moyobamba, 2016. Faculty of Ecology, National University of San Martín. Thesis (2017). <http://hdl.handle.net/11458/2708>
2. Esenarro, D., Escate, I., Anco, L., Tassara, C., Rodriguez, C.: Proposal for an ecological research center for the recovery and revaluation of biodiversity in the town of Quichas-Lima, Peru. *Int. J. Environ. Sci. Dev.* **11**(4), 212–216 (2020). 10.18178, ISSN 2010-0264
3. Esenarro, D., Rodriguez, C., Arteaga, J., Garcia, G., Flores, F.: Sustainable use of natural resources to improve the quality of life in the Alto Palcazu population center, Iscozazin-Peru. *Int. J. Environ. Sci. Devel.* **12**(5), 146–150 (2021). <https://doi.org/10.18178/ijesd.2021.12.5.1332>
4. Cornejo, C.: Sustainability, architecture and evaluation. *Bull. UCAL Creat. Res. Center.* **1**, 10–16 (2016)
5. Millán-Rojas, E.E., Sánchez-Castillo, V., Gómez-Cano, C.A.: Ecoturismo implementado en el mundo globalizado como alternativa de desarrollo económico y social. *Clio América* **14**(27), 380–389 (2020). <https://doi.org/10.21676/23897848.3433>
6. Drabczyk, K., Bogdanowicz, K.A., Iwan, A.: Engineering concept of energy storage systems based on new type of silicon photovoltaic module and lithium ion batteries. *Energies* **13**(14), 3701 (2020). <https://doi.org/10.3390/en13143701>
7. Pons-Valladares, O., Nikolic, J.: Sustainable design, construction, refurbishment and restoration of architecture: a review. *Sustainability* **12**(22), 9741 (2020). <https://doi.org/10.3390/su12229741>
8. Chácon, L.: Bicycles: a mobility alternative to maintaining social distancing. SPDA Environmental News. <https://www.actualidadambiental.pe/bicicletas-una-alternativa-de-movilidad-para-mantener-el-distanciamiento-social/> (2020)
9. Rodriguez, C., Esenarro, D., Alburquerque, C., Vega, M., Ramirez, V.: Theme park of renewable energies for mitigation of CO₂ in the urban area of the district of Chorrillos, Peru. *IOP Conf. Ser. Mater. Sci. Eng.* **910**(1), 012021 (2020). <https://doi.org/10.1088/1757-899X/910/1/012021>
10. Mondragón, D.Y.M., Garcia, C.R.S.: Fortalecimiento del desarrollo turístico sostenible en los humedales de Ventanilla, departamento de Lima, Perú. *INNOVA Res. J.* **4**(3.1), 126–134 (2019). <https://doi.org/10.33890/innova.v4.n3.1.2019.1082>
11. Amado, M., Rodrigues, E., Poggi, F., Pinheiro, M.D., Amado, A.R., José, H.: Using different levels of information in planning green infrastructure in Luanda Angola. *Sustainability* **12**, 3162 (2020)
12. Jo, S.-H., Woo, J., Byun, G.-S., Jeong, J.-H., Jeong, H.: Study on the integral compensator using supercapacitor for energy harvesting in low-power sections of solar energy. *Energies* **14**(8), 2262 (2021). <https://doi.org/10.3390/en14082262>
13. Ramos, L., Esenarro, D., Rodriguez, C., Lagos, J.: Recovery of public spaces for the conservation of green areas in Tablada Lurin. *IOP Conf. Ser. Mater. Sci. Eng.* **910**, 012020 (2020). <https://doi.org/10.1088/1757-899X/910/1/012020>

14. Song, Y., Peng, W.: Earth observation for sustainable infrastructure: a review. *Remote Sens.* **13**(8), 1528 (2021). <https://doi.org/10.3390/rs13081528>
15. Vukmirovic, M., Gavrilovic, S., Stojanovic, D.: The improvement of the comfort of public spaces as a local initiative in coping with climate change. *Sustainability* **11**(23), 6546 (2019). <https://doi.org/10.3390/su11236546>
16. Vega, V., Esenarro, D., Maldonado, C., Rodriguez, C., Córdova, A. : Green infrastructure design for connectivity in the villa wetlands wildlife refuge. *J. Green Eng. (JGE)* **10**(12) (2020)
17. Wang, J., Liu, J., Wang, H., Mei, C.: Approaches to multi-objective optimization and assessment of green infrastructure and their multi-functional effectiveness: a review. *Water* **12**, 2714 (2020)
18. Leon, B., Cano, A., Young, K.: Current use of flora and vegetation in the wetlands of the central coast of peru. *Biol. Conserv.* **199**, 104–191 (2019)



Planning Water-Food-Energy Nexus System Towards Sustainable Development Under Uncertainty

Y. F. Zhang¹, Y. P. Li^{1,2(✉)}, and G. H. Huang²

¹ State Key Joint Laboratory of Environmental Simulation and Pollution Control,
School of Environment, Beijing Normal University, Beijing 100875, China
yongping.li@iseis.org

² Institute for Energy, Environment and Sustainable Communities, University of Regina,
Regina, SK S4S 7H9, Canada

Abstract. In this study, a copula-based stochastic fractional programming (CSFP) method is developed for planning water-food-energy nexus (WFEN) system. CSFP method can deal with bi-objective optimization problems and address correlated uncertainties within nexus system. Then, a CSFP-WFEN model is proposed and applied to an arid region, where 16 scenarios with different joint probabilities associated with various water availabilities, land resources and available electricity are analysed. Major findings are: (i) water allocation for Uzbekistan should be primarily constrained for alleviating water shortage risk over time; (ii) scheme of agricultural production should consider ramping up cash crop and shrinking livestock farming for adapting limited resources and enhancing the marginal benefit; (iii) from 2021 to 2035, hydropower generation would increase by 10.3% and thermal power would decrease by 3.5%, which implies that electricity generation patterns should change towards renewable energy in the future; (iv) correlated uncertainties (corresponding to the joint probability risk) have a significant influence on marginal benefit and water allocation patterns, decision makers should adjust strategies towards sustainable development according to risk attitude and local resources conditions under uncertainty.

Keywords: Fractional programming · Copula · Water-food-energy nexus

1 Introduction

Water, food and energy resources are the essential necessities for human survival and social development, and they are inextricably linked. Water is indispensable for sustaining stabilized energy generation, normal crops growth, food production and, in turn, the whole process of water allocation, such as water conveyance and infield irrigation, needs to consume electricity [1, 2]. Increasing population and expanding agriculture have substantially exacerbated conflicts between water, food and energy resources, especially in developing countries that already experience water scarcity. Therefore, it is imperative to conduct integrated management from the water-food-energy nexus (WFEN) perspective.

In reality, WFEN system is plagued with a variety of uncertainties. For instance, water availability affected by random events often possesses highly stochastic uncertainty, entailing random features in land and electricity resources [3, 4]. These uncertainties and their complex interactions may result in needless errors and exacerbate the conflict of resources allocation among different users. Stochastic programming (SP) method has been extensively adopted for addressing complex uncertainties within nexus system. However, SP method is incapable of handling intricate and complex interactions among multiple random parameters [5–7]. Copula, as a tool for constructing multivariate joint distribution without restriction of distribution type, can describe complex interrelationships between variables and reflect joint violation risk in nexus system [8]. Moreover, in arid regions, high marginal benefit tends to be preferred to managers for achieving regional sustainability. Linear fractional programming (LFP) method can be introduced to solve marginal effectiveness problems for balancing contradictory targets of economic benefits maximization and resources conservation [9, 10].

This study aims to develop a copula-based stochastic fractional programming (CSFP) method to plan WFEN system under uncertainty. Combining the superiority of CSP and LFP into one framework, CSFP has novelties and advantages in: (i) dealing with stochastic uncertainties presented as different probability distributions and unknown correlations; (ii) reflecting marginal effectiveness about minimum water use and maximum system benefit; (iii) analysing the compromise between system violation risk and marginal benefit. Multiple scenarios associated with different groups of water availabilities, arable land and electricity resources are examined. Results will help decision makers: (i) analyse interactions between water, land and energy resources and disclose their joint risk on WFEN system in association with different scenarios; (ii) achieve trade-offs among system violation risk, economic benefit and resources conservation; (iii) identify joint planning strategies of WFEN system in a sustainable way.

2 Methodology

Through introducing CSP method into the LFP framework, a copula-based stochastic fractional programming can be developed as:

$$\text{Max} f = \left(\sum_{j=1}^n c_j x_j + \alpha \right) / \left(\sum_{j=1}^n d_j x_j + \beta \right) \quad (1a)$$

subject to:

$$\sum_{j=1}^n a_{ij} x_j \leq b_i(\omega)^{(p_i)}, \quad i = 1, 2, \dots, m \quad (1b)$$

$$C(F(b_1(t)), \dots, F(b_i(t)), \dots, F(b_m(t))) \geq 1 - p \quad (1c)$$

$$x_j \geq 0, \quad j = 1, 2, \dots, n \quad (1d)$$

According to Charnes and Cooper (1962) [11], assuming the objective is continuously differentiable and the sign of denominator is constant on the feasible region, model (1) can be transformed from a fractional one to a linear version as:

$$\text{Max } g = \sum_{j=1}^n c_j x_j^* + \alpha \cdot r \quad (2a)$$

subject to:

$$\sum_{j=1}^n a_{ij} x_j^* \leq b_i(\omega)^{(p_i)}, \quad i = 1, 2, \dots, m \quad (2b)$$

$$C(F(b_1(t)), \dots, F(b_i(t)), \dots, F(b_m(t))) \geq 1 - p \quad (2c)$$

$$\sum_{j=1}^n d_j x_j^* + \beta \cdot r = 1 \quad (2d)$$

$$x_j^* = x_j \cdot r, \quad j = 1, 2, \dots, n \quad (2e)$$

where $F(b_i(t)) = 1 - p_i$ denotes the cumulative distribution of random variable $b_i(t)$. Equation (2b) is a set of individual probabilistic constraints. The individual probabilities of constraints can be determined by solving Eq. (2c) in the following way: if there are m random variables, the violation probabilities of the former $(m - 1)$ constraints (i.e., $p_i, i = 1, \dots, m - 1$) are predefined and the last probability is obtained through solving the equation $C(F(b_1(t)), \dots, F(b_i(t)), \dots, F(b_m(t))) \geq 1 - p$. Because the copula function is a non-decreasing monotonous function, a single value for $F(b_m(t))$ can be obtained. Moreover, since the values of $p_i, i = 1, \dots, m - 1$ are predefined, a series of combinations of individual probabilities can be obtained for one overall constraint violation probability [i.e., p in Eq. (2c)]. Therefore, the stochastic constraint in Eq. (1c) can be transformed into a set of linear constraints in Eqs. (2b) with the constraint in Eq. (2c) being solved. In other words, the joint probabilistic constraints associated with copula relationship can be transformed into linear ones by letting the random variable take a set of individual probabilistic constraints with the corresponding individual probabilities determined by copula. Based on the branch-and-bound algorithm, optimal solution of CSFP can be obtained through the transform of $x_j^* = x_j \cdot r (j = 1, 2, \dots, n)$.

3 Case Study

3.1 Study Area

Syr Darya is one of the main rivers across agricultural regions in four Central Asian countries with average annual surface water resources of 37.20 km^3 . The scarce precipitation and arid climate have caused increasing risks and competitions for agricultural production, energy generation, as well as sustainable development in downstream regions [12]. Almost 90% of water withdrawal is delivered to agriculture resulting from expansive

planting of water-intensive crops, such as rice and cotton. Meanwhile, the majority of energy demand (accounting for 80%) could be met by hydropower generation given the total existing feasible hydropower potential. Massive water withdrawal for economic activities has left little amount of water for ecosystem in the basin, threatening key ecological functions supplied by grasslands, woodlands, water bodies and wetlands [13]. A great challenge has emerged in dealing with complex nexus of water, food and energy in an effective and sustainable way amid future uncertain supplies.

3.2 CSFP-WFEN Modeling Formulation

A CSFP-WFEN model can be developed for planning WFEN system considering four countries and twelve states in the Syr Darya River basin. The objective aims at achieving maximizing marginal benefit (i.e. system benefits per unit of the allocated water) under the given joint probability level over three planning periods (2020–2035). The system benefit includes net income from water allocation to agriculture (including crop planting and livestock farming), electricity, domestic, industrial, municipal and ecological sectors. In detail, the CSFP-WFEN model can be formulated as:

$$\begin{aligned}
 Max f = & \left\{ \begin{array}{l} \sum_{i=1}^I \sum_{j=1}^{14} \sum_{t=1}^T BW_{ijt} \times SW_{ijt} / (1 + LF_{ijt}) - \sum_{i=1}^I \sum_{j=1}^{10} \sum_{t=1}^T CE_{it} \times ESW_{ijt} \times SW_{ijt} / \gamma_{ijt} \\ - \sum_{i=1}^I \sum_{j=1}^{10} \sum_{t=1}^T (QF_{ijt} \times PF_{ijt} + FC_{ijt}) \times SW_{ijt} / (1 + LF_{ijt}) / WPC_{ijt} \\ + \sum_{i=1}^I \sum_{t=1}^T BW_{i17t} \times SW_{i17t} / GWD_{it} - \sum_{i=1}^I \sum_{t=1}^T CE_{it} \times ESW_{i17t} \times SW_{i17t} / \gamma_{i17t} \\ + \sum_{t=1}^T BP_t \times \left[\sum_{n=1}^N HWS_{nt} \times \varphi_{nt} + \sum_{m=1}^M FWS_{mt} \times \eta_{mt} \right] \\ - \sum_{t=1}^T \sum_{m=1}^M CE_{mt} \times FWS_{mt} \times \eta_{mt} / \gamma_{mt} - \sum_{t=1}^T \sum_{m=1}^M FWS_{mt} \times \eta_{mt} \times PFC_{mt} \\ + \sum_{t=1}^T (EB_{wshe}{}d_t + EB_{recr}{}t + EB_{health}{}t + EB_{agr}{}t + EB_{trans}{}t + EB_{fish}{}t) \end{array} \right\} \\
 & / \left(\sum_{t=1}^T \sum_{i=1}^I \sum_{j=1}^J SW_{ijt} + \sum_{t=1}^T \sum_{n=1}^N HWS_{nt} + \sum_{t=1}^T \sum_{m=1}^M FWS_{mt} \right) \quad (3)
 \end{aligned}$$

Subject to:

(1) Constraints for system risk of water, land and hydropower availabilities:

$$C(1 - p_{S1}, 1 - p_{S2}, 1 - p_{S3}) = 1 - ps \quad (4)$$

$$\Pr \left\{ \sum_{i=1}^I \sum_{j=1}^J AW_{ijt} / \gamma_{ijt} + \sum_{n=1}^N HWA_{nt} + \sum_{m=1}^M FWA_{mt} / \gamma_{mt} \leq TAA_t \right\} \geq 1 - p_{S1} \quad (5)$$

$$\Pr \left\{ \sum_{n=3}^7 HWS_{nt} \times \varphi_{nt} \leq MSHP_t \right\} \geq 1 - p_{S2}, \forall t \quad (6)$$

$$\Pr \left\{ \sum_{i=1}^I \sum_j^{10} SW_{ijt} / (1 + LF_{ijt}) / WPC_{ijt} \leq AS_t^{\max} \right\} \geq 1 - p_{S3}, \forall t \quad (7)$$

(2) Constraints for electricity demands:

$$ED_t \leq IE_t + \sum_m^M FWS_{mt} \times \eta_{mt} + \sum_n^N HWS_{nt} \times \varphi_{nt}, \forall t \quad (8)$$

Constraints for food security:

$$\sum_i^I \sum_j^J YA_{ijt} \times SW_{ijt} / (1 + LF_{ijt}) / WPC_{ijt} \geq \sum_i^J FD_{it} \times PO_{it} \quad \forall t \quad (9)$$

Constraints for ecological water requirement:

$$TSA_t - \sum_i^I \sum_j^J SW_{ijt} / \gamma_{ijt} - \sum_m^M FWS_{mt} / \gamma \gamma_{mt} \geq WSL_t \quad \forall t \quad (10)$$

Constraints for salinity control:

$$\sum_{j=1}^{10} LF_{ijt} \times SW_{ijt} / (1 + LF_{ijt}) \leq TLW_{it} \quad (11)$$

Constraints for grassland coverage:

$$\sum_i^I SW_{i16t} / GWD_{it} \geq TDS_t, \forall t \quad (12)$$

In this study, 16 representative scenarios with four joint constraint-violation levels (i.e. $p = 0.01, 0.10, 0.15$ and 0.20) and corresponding individual constraint-violation levels (p, p_1, p_2, p_3) were examined. The detailed descriptions for these scenarios were illustrated in Table 1, where p denoted the joint constraint-violation level; p_1, p_2 and p_3 denoted the individual constraint-violation levels corresponding to the water availability, arable area and energy resources, respectively. The values of joint cumulative distribution and marginal cumulative distributions are obtained through using Clayton-Frank Copula under different scenarios. The fitting simulated random values would be used as the inputs of CSFP-WFEN to achieve the desired planning results.

Table 1. Scenarios design

Scenario	(p, p_1, p_2, p_3)	Water availability (10^9 m^3)	Arable land (10^6 ha)	Electricity (10^9 kWh)
S1	(0.010,0.002,0.002,0.006)	210.583	15.594	616.413
S2	(0.010,0.002,0.004,0.004)	210.583	15.829	610.998
S3	(0.010,0.004,0.002,0.004)	221.456	15.594	610.998
S4	(0.010,0.004,0.004,0.002)	221.456	15.829	602.425
S5	(0.100,0.004,0.004,0.078)	258.549	16.631	647.707
S6	(0.100,0.004,0.030,0.061)	258.549	16.766	643.519
S7	(0.100,0.030,0.040,0.061)	264.806	16.631	643.519
S8	(0.100,0.030,0.030,0.043)	264.806	16.766	638.525
S9	(0.150,0.004,0.004,0.120)	269.896	16.876	653.478
S10	(0.150,0.004,0.050,0.089)	269.896	16.970	650.479
S11	(0.150,0.050,0.004,0.089)	274.228	16.876	650.479
S12	(0.150,0.050,0.050,0.057)	274.228	16.970	647.174
S13	(0.200,0.004,0.004,0.161)	281.427	17.126	653.994
S14	(0.200,0.004,0.080,0.111)	281.427	17.254	648.219
S15	(0.200,0.080,0.004,0.111)	287.368	17.126	648.219
S16	(0.200,0.080,0.080,0.057)	287.368	17.254	641.051

4 Case Study

Figure 1 represented the results of marginal benefit and water-use pattern under 16 scenarios with multiple joint and individual probability levels. The lowest marginal benefit would be $1.43 \text{ \$/m}^3$ under S1 ($p = 0.01$); the highest one would be $1.47 \text{ \$/m}^3$ under S16 ($p = 0.20$). The amount of water use will range from $0.55 \times 10^{12} \text{ m}^3$ ($p = 0.01$, S1) to $0.652 \times 10^{12} \text{ m}^3$ ($p = 0.20$, S15). The marginal benefits would increase with joint constraint-violation levels. This is mainly because that more risk of violation is allowed as p increases, leading to a decreased strictness for satisfactory level of system constraints and hence an expanded decision space for optimal marginal benefit. Higher joint or individual p level can render higher marginal effectiveness, corresponding to higher risk of constraint-violation and advantageous condition of WFEN system. As shown in Fig. 1, Namangan in Uzbekistan accounts for the greatest water amount in all states, which would remarkably decrease from period 1 to 3 (e.g. by an average of 75.4%). This is because Uzbekistan has the largest land resources and population throughout the basin, corresponding to the highest water requirement. For achieving the maximum marginal benefit, more water should be saved from region with the largest water consumption amid exacerbating contradiction between resource supply and demand over time.

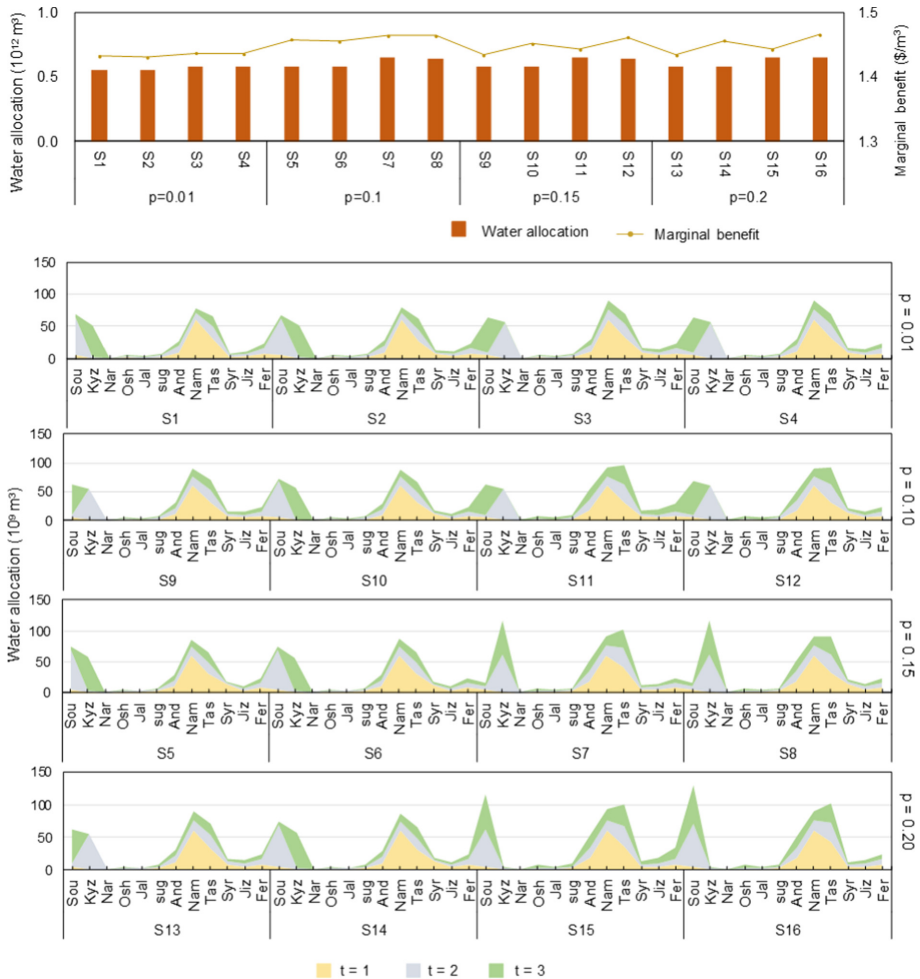


Fig. 1. Marginal benefits and water use under 16 scenarios (water users presented in the horizontal axis from right to left are: South Kazakhstan, Kyzylorda, Narin, Osh, Jalalabad, Sugd, Andizhan, Namangan, Tashikent, Syrdarya, Jizzah, Ferghana).

Figure 2 shows the water use patterns among different users. Agriculture accounts for the largest water amount across all scenarios and periods, indicating that agriculture keeps the major water user across the Syr Darya River basin. From $p = 0.01$ to $p = 0.20$, proportion of water resources allocated to agriculture would increase with rising joint probability (from 52.4% in S1 to 63.2% in S16). More specifically, the share of stock-farming water use would decrease and cash crop planting would be expanded as p diminishing. This is because stock farming possesses the character of high feeding cost and water demand, leading to more water allocated to cash crop planting for avoiding mass waste under the condition of water deficit. Under low risk of water scarcity,

managers should place emphasis on expanding agriculture production, especially crop plantation.

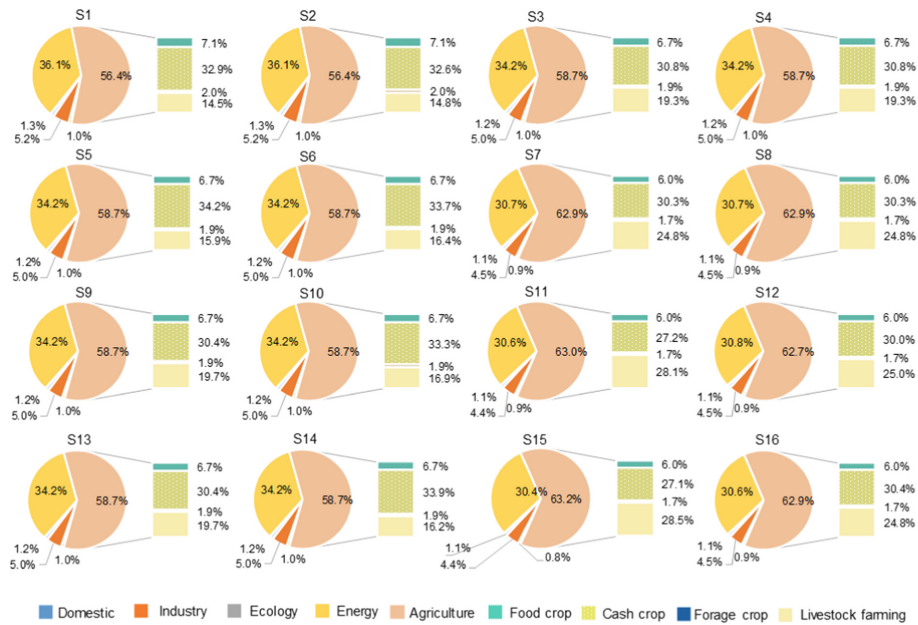


Fig. 2. Water use among different sectors under 16 scenarios.

Figure 3 indicates electric generation and water use over three periods. Generally, the electric generation would ascend throughout the planning horizon amid soaring energy demand and increasing generation capacity, ranging from 245.6×10^{12} kWh ($t = 1$) to 255.9×10^{12} kWh ($t = 3$). Water allocation to electric generation would ascend by 0.6% over time. In four countries, Uzbekistan accounts for the highest electric generation amount but shows a decrease tendency over time. For example, power generation of Uzbekistan would decline by 0.5% and those of Kazakhstan, Kyrgyzstan and Tajikistan would increase by 83.2%, 7.3% and 14.7%, respectively. This may attribute to the high electricity demand of Uzbekistan and high potential of electricity generation in Kazakhstan. The planning of power generation in the basin would change towards a sustainable aspect in the future. From 2021 to 2035, hydropower generation would increase by 10.3% and thermal power would decrease by 3.5%. Policy-makers should adjust energy-generation schemes towards renewable energy based on increased demands and changed resources conditions, such as developing hydropower generation.

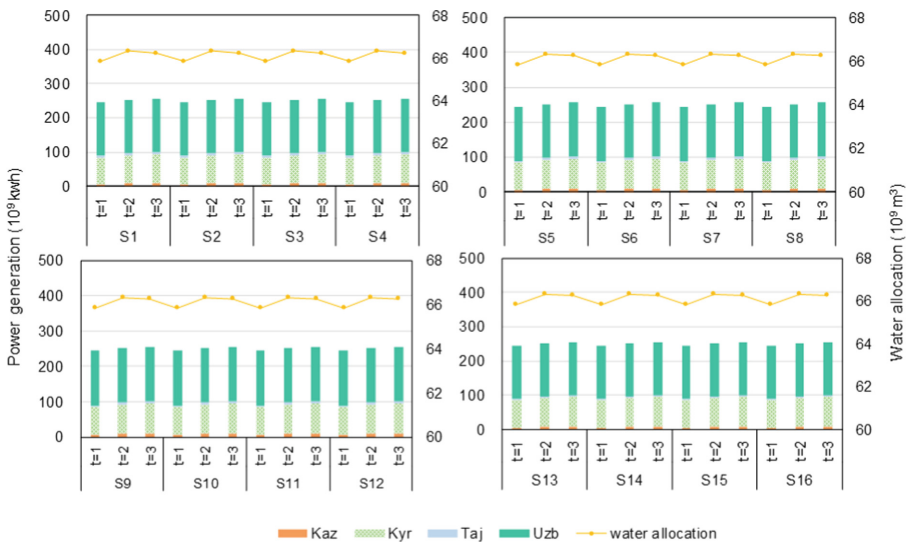


Fig. 3. Power generation and water use under different periods.

5 Conclusions

In this study, a CSFP method has been developed through combining of CSP and FP techniques. CSFP has advantages in handling ratio optimization problems and reflecting system joint risk. The proposed method has employed to the WFEN system of the Syr Darya River basin. Sixteen scenarios about probability levels of water, land and hydropower resources are considered. Major findings are: (i) marginal effectiveness would increase from $1.43 \text{ \$/m}^3$ to $1.47 \text{ \$/m}^3$ along with joint probability risk of WFEN system; (ii) water allocation for Uzbekistan should be primarily constrained for alleviating water shortage risk over time; (iii) scheme of agricultural production should consider ramping up cash crop and shrinking livestock farming for adapting limited resources; (iv) from 2021 to 2035, hydropower generation would increase by 10.3% and thermal power would decrease by 3.5%, which implies that electricity generation patterns should change towards renewable energy in the future. These findings can provide optimal decision alternatives for WFEN management under the conflicts among economic production, electricity demand as well as water resources conservation.

Acknowledgments. This research was supported by the Strategic Priority Research Program of Chinese Academy of Sciences (XDA20060302) and the National Key Research and Development Program of China (2016YFC0502803). The authors are grateful to the editors and the anonymous reviewers for their insightful comments and suggestions.

Appendix A

Nomenclature for variables and parameters.

f	marginal benefit over planning horizon (US\$/m ³)
i	states in Syr Darya River basin
j	water users
t	planning periods
m	thermal power plants
n	hydropower stations
SW_{ijt}	water withdrawn for user i in state j under period t (m ³)
HWS_{nt}	water withdrawn for hydropower station n in period t (m ³)
FWS_{mt}	water withdrawn for thermal power plant m in period t (m ³)
BW_{ijt}	benefit for water user i in state j under period t (US\$/kWh)
BP_t	benefit of generating energy in period t (US\$/kWh)
φ_{it}	coefficient of energy output per unit water in period t (kWh/m ³)
η_{it}	coefficient of energy output per unit water in period t (kWh/m ³)
TSA_t	upstream water amount of Syr Darya River basin in period t (m ³)
WSL_t	inflow water to the Aral Sea from Syr Darya River basin in period t (m ³)
ESW_{ijt}	electricity utilization amount per unit water under period t (kWh/m ³)
γ_{ijt}	efficiency of water allocation for user i in state j under period t
LF_{ijt}	leaching fraction for crop i in state j under period t
QF_{ijt}	quantity of fertilizer applied to crop i in state j under period t (kg/ha)
PF_{ijt}	unit cost of fertilizer of crop i in state j under period t (US\$/kg)
QS_{ijt}	quantity of seed of crop i in state j under period t (kg/ha)
PS_{ijt}	cost of seed of crop i in state j under period t (US\$/kg)
WPC_{ijt}	water requirement for crop i in state j under period t (m ³ /ha)
EB_t	ecological benefit value in period t (US\$)
TW_{ijt}	minimum water requirement of user i in state j under period t (m ³)
WSL_t	minimum environmental flow of Syr Darya river (m ³)
$MSHP_t$	maximum energy availability from hydropower stations under period t (kWh)
IE_t	import electricity in different countries under period t (kWh)
ED_t	minimum electricity demand in different countries under period t (kWh)
YA_{ijt}	yield per unit area of crop i in state j under period t (kg/ha)
FD_{it}	food demand in state i under period t (kg per capita)
PO_{it}	population in state i under period t (people)
AS_t	maximum arable area in Syr Darya River basin under period t (ha)
GWD_{it}	water demand per area of grassland in state i under period t (m ³ /ha)
TLW_{it}	permissible leaching water amount of state i under period t (m ³)
TDS_{it}	minimum grassland coverage of Syr Darya River basin in period t (ha)

References

1. Ngancha, P.B., Kusakana, K., Markus, E.D.: Energy savings configuration for a water-pumping system. *Int. J. Smart Grid Clean Energy* **4**(9), 805–812 (2020)
2. Jaipraditham, C.: Investment cost analysis for electricity generation with renewable energy and measurement of water pressure from weir to water conservation of small hydropower project. *Int. J. Smart Grid Clean Energy* **1**(6), 67–75 (2017)
3. Sun, J., Li, Y.P., Suo, C., Liu, Y.R.: Impacts of irrigation efficiency on agricultural water-land nexus system management under multiple uncertainties—a case study in Amu Darya River basin, Central Asia. *Agric. Water Manag.* **216**, 76–88 (2019)
4. Vergara-Araya, M., Lehn, H., Poganić, W.: Integrated water, waste and energy management systems – a case study from Curauma, Chile. *Resources, Conservation Recycling* **156**, 104725 (2020)
5. Hua, W.Q., Li, D., Sun, H.J., Matthews, P., Meng, F.L.: Stochastic environmental and economic dispatch of power systems with virtual power plant in energy and reserve markets. *Int. J. Smart Grid Clean Energy* **4**(7), 231–239 (2018)
6. Woo, P.S., Kimb, B.H.: Risk analysis of power information control system based on smart grid security standardization. *Int. J. Smart Grid Clean Energy* **2**(8), 140–148 (2019)
7. Hussien, W.A., Memon, F.A., Savic, D.A.: A risk-based assessment of the household water-energy-food nexus under the impact of seasonal variability. *J. Clean. Prod.* **171**, 1275–1289 (2018)
8. Yu, L., et al.: A copula-based fuzzy interval-random programming approach for planning water-energy nexus system under uncertainty. *Energy* **196**, 117063 (2020)
9. Zappone, A., Jorswieck, E.A.: Energy-efficient resource allocation in future wireless networks by sequential fractional programming. *Digital Signal Process* **60**, 324–337 (2017)
10. Zhang, Y.F., Li, Y.P., Sun, J., Huang, G.H.: Optimizing water resources allocation and soil salinity control for supporting agricultural and environmental sustainable development in Central Asia. *Sci. Total Environ.* **704**, 135281 (2020)
11. Charnes, A., Cooper, W.W.: An explicit general solution in linear fractional programming. *Naval Research Logistics Quarterly* **20**(3), 449–467 (1973)
12. CAWATER-info (2015). <http://www.cawater-info.net/indexe.htm>
13. FAO (Food and Agriculture Organization of the United Nations): Regional overview of food insecurity and nutrition in Europe and Central Asia 2018, Budapest (2018)



Assessing Consumers' Intentions Towards Green Alternatives of Disposable Packaging: A Case Study in Beijing and Shanghai

Kaiyan Yang¹ and Sujitra Vassanadumrongdee^{2(✉)}

¹ EDS Program, Chulalongkorn University, Bangkok 10330, Thailand

² Environment Research Institute, Chulalongkorn University, Bangkok 10330, Thailand
sujitra20@gmail.com

Abstract. China's plastic pollution has gotten worse, especially during the COVID pandemic when the city's lockdowns boosted the food takeout business. Although the government has made efforts in curbing the use of conventional single-use plastic packaging, the problem is still looming up in the critical time of building ecological civilization. The key to resolve the overwhelming usage of disposable plastic packaging lies in reduction, along with using green alternatives: biodegradable packaging and returnable containers. The study investigated consumers' willingness to adopt new alternatives by applying the extended classical behavioral theory: the theory of planned behavior (TPB). The measurement scale, developed upon previous literature, gains validated reliability and validity after running confirmatory factory analysis (CFA) in SmartPLS. The study distributed 536 questionnaires online, targeting consumers from Beijing and Shanghai. 430 valid samples were collected and analyzed, with results showing that consumers' perceived behavior control has strong and positive effect on their willingness to pay more to using biodegradable packaging and willingness to participate in the returnable container programs. The environmental attitude, social norms and past green behavior show less direct relationships with people's adopting intentions. Their effects on the intentions are mediated by perceived behavior control disproportionately.

Keywords: Plastic pollution · Online food delivery · Behavioral intention

1 Introduction

Nowadays plastic is dispensable for people's ordinary living. With lightweight, water-resistant and portable properties, the low-cost material is widely used in packaging. For many reasons, the recycling of plastic waste is rather low. Data shows that the global production of plastics in 2018 reached 454 million metric tons, with an expected growth rate of 3.2% from 2020 to 2027. A latest research estimated that 11% of plastic waste generated globally, about 19–23 million metric tons, went into aquatic ecosystems in 2016 [1] and caused severe environmental pollution. China is regarded as the world's greatest plastic user, but is failing to manage its plastic waste in a sustainable manner. It is

estimated that most of the plastic waste is generated by packaging industry, with foods and beverage sector claiming the biggest share [2]. China's two online food delivery companies, Meituan and Ele.me, account for the biggest share of the market. The total amount of packaging waste from online food take-out business witnessed a skyrocket increase from 0.2 million metric tonnes in 2015 to 1.5 million metric tons in 2017, 75% of which is plastic containers [3]. Beijing and Shanghai are among the top 5 regarding online food demand. Worse still, COVID-19 facilitates the habit cultivation of ordering online due to city lockdowns.

Existing researches validated that reducing the total usage of single-use plastics is the key to address this plastic crisis [4]. The alternatives were developed in other countries to curb the usage of plastic packaging for online food delivery. In New York City, a third-party delivery service provider, DeliverZero, offers reusable containers for participating restaurants. Those containers will be returned and reused for other deliveries. Biodegradable packaging has been promoted as another green alternative. At macro-level, in order to curtail the use of disposable plastics, China has "New Normal" policy, comprised of "New plastic ban" and "waste sorting" campaigns, in major cities such as Beijing and Shanghai. In such context, studying the influential factors of individual consumption behavior towards traditional disposable plastic packaging and its green alternative becomes meaningful. The study thus proposes one research question: What factors influence consumers' adopting intention towards green alternatives of disposable packaging on food take-out against COVID-19 and "New Normal" policy paradigm?

2 Literature Review and Hypotheses Development

Consumption behaviors, derived human behaviors, gain a lot of attention in many fields as its correspondent theories can be applied to multiple disciplines such as business economics, social science, computer science and so on [5]. The most used behavioral theories in studying pro-environmental or sustainable behaviors are Theory of Reasoned Action (TRA), Theory of Planned Behavior (TPB), Theory of Interpersonal Behavior (TIB), Nudge Theory (NT), Value-Belief-Norm Theory (VBN) and other cognitive and learning theories [6–9].

However, none of these theories are perfect. TRA was criticized for unable to predict behaviors because of insufficient constructs. It argues that behavioral intention is decided by two constructs, respectively attitude and subjective norms [10]. For this concern, TRA was extended into TPB by adding one more construct, perceived behavior control [11]. Numerous studies have validated the superiority of TPB over TRA [12–14]. Even so, there are still loopholes in this theory which are detected by some studies. For this reason, researchers started to incorporate new constructs into TPB to better predict behaviors. Some researchers combine TPB with other theories such as VBN, TIB, TRA and so on [15]. It is investigated that the most commonly used new constructs in this regard are situational, cultural factors and habits or past experience [16, 17]. Existing literature proves that by introducing new factors into TPB, the prediction of intentions and behaviors becomes more accurate [18].

2.1 The Extended Theory of Planned Behavior

Situational factors and past behaviors are the most widely-incorporated new constructs of TPB. Regulations, policies, media, facilities, weather, occasions, the surroundings, cultures, and product price and properties mentioned above are situational factors [19]. Some studies cluster it under social norms [20]. This research is conducted against "New Normal" policies in China. Against this backdrop, policies and regulations are situational factors that can be clustered under SN, which will exert effects on people's routine intention and behaviors [21]. Past experience or behaviors are also being proven to be an influential factor of behavioral intention [22]. A study found that the past recycling behavior of college students has a significant impact on their future intention or attitude towards recycling [23].

2.2 Hypotheses Development

Most biodegradable plastics can only be degraded under certain industrial conditions, which means they need to be sorted and put separately. Returnable containers can be shared and reused for many times, which requires consumers to return the containers through collecting facilities. Biodegradable plastics are more expensive compared to conventional plastics and returnable container services. While returnable container programs are more inconvenient in terms of post-consumption disposal. Therefore, the adopting intention in this study is replaced by the willingness to pay more (WTM) for biodegradable plastic packaging and the willingness to participate (WTP) in returnable container programs.

In TPB, attitude is defined as the positive or negative evaluation of performing a specific behavior from individuals' viewpoints [11]. Many studies have proven that pro-environmental attitudes can positively influence people's pro-environmental intentions or behaviors [17, 24]. A study found that Hong Kong college students' recycling behavioral intention is positively related to their environmental attitude [25]. In environmental studies, it is estimated that PBC serves as the mediator between attitudes and intentions in regard of responsible behavior towards marine protection [26].

Social norms can be defined as the pressure from the society which pushes individuals to conduct certain behaviors [12]. It is proven that social norms is an influential factor of people's green behavioral intention [27]. As mentioned above, situational factors are counted as a part of social norms in some studies [20]. Policies, as a situational factor, play an important role in predicting people's behavioral intention, which can drive people to change their behavioral intentions [28]. Perceived behavior control can mediate the effect of social norms on managers' intention to take environmental measures [29].

Perceived behavioral control (PBC) refers to the ease or difficulty of an individual to perform a particular behavior [11]. It is dependent on control beliefs and perceived power. The former can be regarded as the driver or barrier that individuals perceive will influence they perform certain behaviors [11, 12]. While the later one is the evaluation of individuals towards the above behavior driving or impeding factors [12]. Empirical evidence proves that PBC can directly influences both on behavioral intention and actual behaviors [14].

Studies have validated that people who take a small step doing something are prone to doing more difficult things in this regard [30, 31]. For example, those who do a small thing in protecting the environment may move forward by adopting more complicated pro-environment behaviors [32]. In this sense, it is important for decision-makers to assist people in making small changes in their behavioral patterns so that leapfrog achievements can be realized one day. It is found that past behavior (experience) can be mediated by perceived behavior control in terms on online purchasing intentions [33].

Based the above argument, the research adopts extended TPB, comprised of attitude, social norms, perceived behavior control, past green behavior and intention, as the underlying theory. In this regard, the study proposes several hypotheses below. Figure 1 is the conceptual framework of the research, which reflects the relations between different constructs.

Hypothesis 1a (H1a) Environmental attitude and awareness positively affect people's WTM for biodegradable packaging and WTP in returnable container program.

Hypothesis 1b (H1b) Environmental attitude and awareness is mediated by perceived behavior control when influencing WTP and WTP.

Hypothesis 2a (H2a) Social norms positively influence people's WTM for biodegradable packaging and WTP in returnable container program.

Hypothesis 2b (H2b) Social norms is mediated by perceived behavior control when influencing WTP and WTP.

Hypothesis 3 (H3) Perceived behavior control positively affects people's WTM for biodegradable packaging and WTP in returnable container program.

Hypothesis 4a (H4a) Past green behaviors positively influence people's WTM for biodegradable packaging and WTP in returnable container program.

Hypothesis 4b (H4b) Past green behaviors is mediated by perceived behavior control when influencing WTP and WTP.

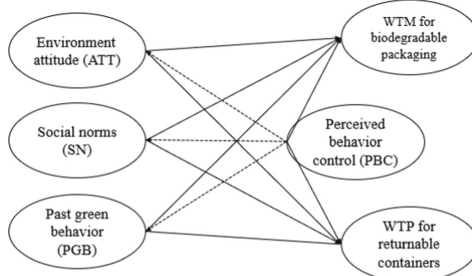


Fig. 1. Conceptual framework.

3 Methodology

3.1 Measurement Scale

The measurement scales are adapted from previous literature, which is comprised of the measurements of biodegradable packaging and returnable containers. As shown in

Table 1, items with “a” and “b” are respectively established to measure the psychological constructs of choosing biodegradable packaging and returnable containers. Items without “a” or “b” are set to measure the constructs of two alternatives. 5 point-Likert scale is used to measure the items, ranging from “strongly disagree”, “disagree”, “neither agree nor disagree”, “agree” to “strongly agree”.

3.2 Data Collection

The research selected Beijing and Shanghai as the study areas since they have all officially implemented mandatory “waste sorting” regulations citywide respectively in 2019 and 2020. Anonymous questionnaires were distributed through both online platforms including a data collection website, credamo.com, and social media platform, WeChat, where respondents were paid for filling questionnaires. The questionnaire is comprised two scales which respectively estimate the psychological constructs of “biodegradable packaging” and “returnable containers”.

Table 1. Measurement scale

Latent variables	Items	Measurement scale	Source
Attitude and awareness	ATT1	It is very pressing to address “white pollution” problem	[34]
	ATT2	“White pollution” is majorly caused by the overuse of disposable plastics in food take-out	[35]
	ATT3	I am aware that disposable plastics take 100–450 years to degrade in the natural environment	[36]
Social norms	SN1	The waste sorting regulation encourages me to use the alternatives to replace conventional disposable packaging for food take-out	[36]
	SN2	The new plastic ban policy encourages me to use the alternatives to replace conventional disposable packaging for food take-out	
	SN3a/b	The media’s publicity makes me think about using biodegradable plastic packaging/returnable containers in the future	[37]
	SN4a/b	If my family or friends use biodegradable packaging/returnable containers for food take-out, I will try them	[38]

(continued)

Table 1. (continued)

Latent variables	Items	Measurement scale	Source
Perceived behavior control	PBC1a/b	Considering the disposal way, I am confident that if I want to, I can use and dispose biodegradable packaging in an appropriate way/rent and return returnable containers for food take-out	[12]
	PBC2a/b	It is easy for me to use and dispose biodegradable packaging/rent and return returnable containers	[34]
	PBC3a/b	I can pay a premium for biodegradable packaging/deposit enough money to rent containers	
	PBC4a/b	I am confident that I have enough time and resources to use and dispose biodegradable packaging/participate in the returnable container program	
Past green behaviors	PGB1	I sort food waste from packaging waste, whenever possible	[37]
	PGB2	I reuse non-contaminated plastic bags from food take-out packaging, whenever possible	
	PGB3	I recycle food take-out packaging whenever possible	
WTP for biodegradable packaging	WTM1	It is acceptable for me to pay more for biodegradable packaging for food take-out in the future	[39, 40]
	WTM2	The probability that I will pay more for biodegradable packaging for food take-out is very high	[34]
	WTM3	I am willing to consider spending more for biodegradable packaging	[41]
WTP for Returnable containers	WTP1	It is acceptable for me to pay a deposit for renting returnable containers for food take-out in the future	[39, 40]
	WTP2	I am willing to use returnable containers for food take-out in the future	[36]
	WTP3	The probability that I will participate in a returnable container program for food take-out is very high	[34]

4 Data Analysis

4.1 Descriptive Analysis

536 questionnaires were distributed in February 2021, which ends up with 430 valid samples for further analysis. More female (71.5%) was engaging in this survey. Half of the respondents come from Beijing and Shanghai respectively, mainly clustering in the age groups of 18–30 (69.2%). Most of them (90%) have accepted high education (bachelor or above) and work in private companies (25.7%) or still pursue their education (36.9%). The proportions of different monthly income groups, ranging from below 5,000RMB to above 20,000RMB, are around 10–25%.

Table 2. Socio-demographic characteristics of respondents (N = 430).

Variable	Item	Frequency	Percentage
Gender	Male	124	28.50%
	Female	306	71.50%
Location	Beijing	215	50.00%
	Shanghai	215	50%
Age group	below 18	4	1%
	18–30	297	69.20%
	31–45	121	28%
	46–65	8	1.80%
	above 65	0	0%
Education	Primary school and below	0	0%
	middle schools	14	3.27%
	professional schools	41	9.58%
	Bachelor or equivalent	248	57.71%
	Master and the above	127	29.44%
Occupation/company	Students	158	36.90%
	Civil servant	7	1.60%
	SOEs	67	15.70%
	Private company	111	25.70%
	Foreign company	26	6.10%
	Public organizations	43	10%
	Freelancers	11	2.34%
	Non-workers (retired or unemployed)	7	1.63%
Monthly income	below 5000RMB	55	12.85%
	5000–8000RMB	85	19.63%
	8000–12000RMB	106	25.75%

(continued)

Table 2. (*continued*)

Variable	Item	Frequency	Percentage
	12000-15000RMB	68	24.53%
	15000-20000RMB	48	11.21%
	above 20000RMB	68	15.89%

The questionnaire also investigates to what extent that the respondents are willing to pay more for biodegradable packaging and participate in returnable containers programs. Around 40% and 50% of the respondents are only willing to walk for less than 100 m and 100–500 m to return the containers. Less than 15% of the consumers would like to walk more than 500 m to return the containers. Approaching 75% of the respondents are willing to pay less than 30RMB of deposit, the rest would like to pay more than 30RMB of deposit. The willingness to pay more for the fee of using biodegradable packaging shows the same trend. As the fee increases, the respondents show lower willingness to pay.

4.2 Measurement Model

The study used Partial Least Squares Structural Equation Modelling (PLS-SEM), which can address a broad range of problems with less restrictive assumptions. The reliability and validity of the measurement model are tested using SmartPLS (v.3.2.9). Composite reliability (CR) shows higher superiority when it comes to assessing scale reliability [42]. If CR value is more than 0.7, it can be concluded that the internal consistency of the scale is reliable. As shown in Table 2, CR of the latent variables of both alternatives are higher than 0.7, showing adequate reliability. The AVE needs to be >0.5 to ensure sufficient convergent validity [43]. All the constructs' measurements of biodegradable packaging have sufficient convergent validity as shown below. Most constructs of returnable containers are more than 0.5, meaning that the convergent validity is adequate in general. The discriminant validity is assessed based on Fornell-Larcker criterion, which requires that the square root of AVE is bigger than inter-correlations. Based on SmartPLS's result, all the constructs' scales of two models have adequate discriminant validity.

4.3 Structural Model

4.3.1 Model Fit

Fit indices of the estimated model are comprised of SRMR, d_ULS, d_G. The criterion of SRMR, d_ULS and d_G are respectively < 0.08 , 0.95 and 0.95. The indices of both models, shown in Table 3, which are SRMR = 0.081 (≈ 0.08), d_ULS = 0.784 (<0.95), d_G = 0.25 (<0.95) for biodegradable packaging, and SRMR = 0.066 (<0.08), d_ULS = 0.585 (<0.95), d_G = 0.212 (<0.95) for returnable container. It's indicating reliable and adequate fit.

Table 3. Confirmatory factor analysis

Criterion	Biodegradable packaging			Returnable container	
	Estimated model		Result	Estimated model	Result
Internal consistency reliability [43, 44]					
Composite reliability > 0.7	ATT	0.777	adequate	0.723	adequate
	PBC	0.879		0.889	
	PGB	0.795		0.794	
	SN	0.755		0.83	
	WTM	0.922		0.947	
Convergent validity [43, 44]					
AVE > 0.5	ATT	0.538	adequate	0.487	adequate
	PBC	0.708		0.671	
	PGB	0.565		0.569	
	SN	0.507		0.623	
	WTM	0.798		0.857	
Discriminant validity [43]					
Fornell-Larcker criterion	Inter-correlations < the square root of AVE		adequate	Inter-correlations < the square root of AVE	adequate

4.3.2 Hypotheses Testing

A structural model was built via the bootstrapping procedure in SmartPLS, with a sub-sample size of 5,000. The endogenous variables' R² values of estimated model of biodegradable packaging can explain 20.4% and 21.1% of PBC and WTM, and that of the estimated model of returnable containers can explain 16.8% and 55.5% of PBC and WTP. According to previous study [42], R² reflects the model's predictive power. The predictive power of estimated constructs is acceptable.

For biodegradable packaging: Hypothesis 1a (path coefficient = 0.08, p-value = 0.199 > 0.1) and H2a (PC = 0.19, p-value = 0.19 > 0.1) are not supported. It suggests that environmental attitude and social norms have no direct positive effect on consumers' willingness to pay more for biodegradable packaging. H3 (PC = 0.455, p-value < 0.01) and H4a (PC = -0.014, p-value < 0.01) are supported, proving that perceived behavior control (PBC) and past green behavior (PGB) have positive influences on consumers' willingness to pay more (WTM). H1b (PC = 0.115, p-value < 0.05), 2b (PC = 0.19, p-value < 0.01) and 4b (PC = 0.310, p-value < 0.01) concern about the mediation effects between two constructs, which are all supported. It means that PBC can mediate the effect between ATT, SN, PGB and WTM. As H1a and H2a are not supported, which suggest that there exists a complete mediation effect of PBC on the path of ATT, SN and WTM.

For returnable containers: H1a ($PC = 0.017$, $p\text{-value} = 0.670 > 0.1$) and H4a ($PC = 0.016$, $p\text{-value} = 0.695 > 0.1$) are not supported. It suggests that environmental attitude and past green behavior have no direct positive effect on consumers' willingness to participate in returnable container's programs. H3 ($PC = 0.666$, $p\text{-value} < 0.01$) and H2a ($PC = 0.016$, $p\text{-value} < 0.01$) are supported, proving that perceived behavior control (PBC) and social norms (SN) have positive influences on consumers' willingness to participate (WTP). Hypothesis 1b ($PC = 0.098$, $p\text{-value} < 0.05$), 2b ($PC = 0.340$, $p\text{-value} < 0.01$) and 4b ($PC = 0.091$, $p\text{-value} < 0.1$) reflect the mediation effects between two constructs, which are all supported. It means that PBC can mediate the effect between ATT, SN, PGB and WTP. As in this model, H1a and H4a are not supported, which suggests that there exists a complete mediation effect of PBC on the path of ATT, PGB and WTP (Figs. 2 and 3, Table 4).

Table 4. Hypotheses test

Hypotheses	Path	Biodegradable packaging		
		Returnable containers		
		Path coefficient	p	Test result
hypothesis 1a	ATT-WTM/WTP	0.08	0.119	not supported
		0.017	0.67	not supported
hypothesis 1b	ATT-PBC	0.115	0.021	supported
		0.098	0.034	supported
hypothesis 2a	SN-WTM/WTP	-0.065	0.247	not supported
		0.151	0	supported
hypothesis 2b	SN-PBC	0.19	0	supported
		0.34	0	supported
hypothesis 3	PBC-WTM/WTP	0.455	0	supported
		0.666	0	supported
hypothesis 4a	PGB-WTM/WTP	-0.014	0	not supported
		0.016	0.695	not supported
hypothesis 4b	PGB-PBC	0.32	0	supported
		0.091	0.075	supported

$p < 0.01^{***}$; $p < 0.05^{**}$; $p < 0.1^*$.

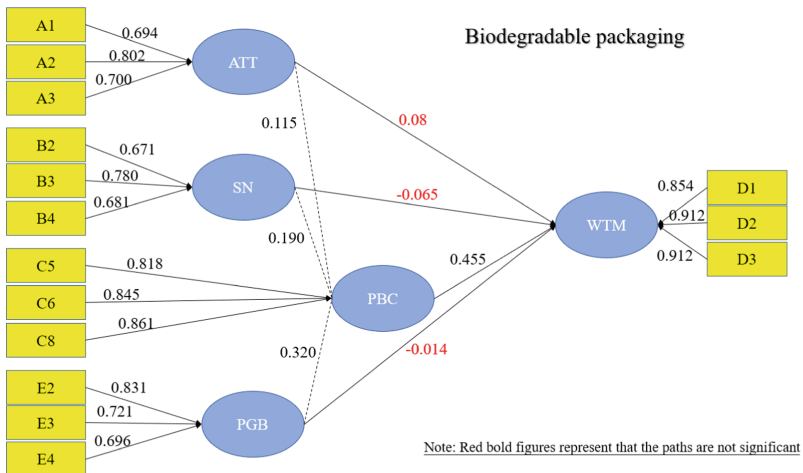


Fig. 2. Path analysis result of biodegradable packaging.

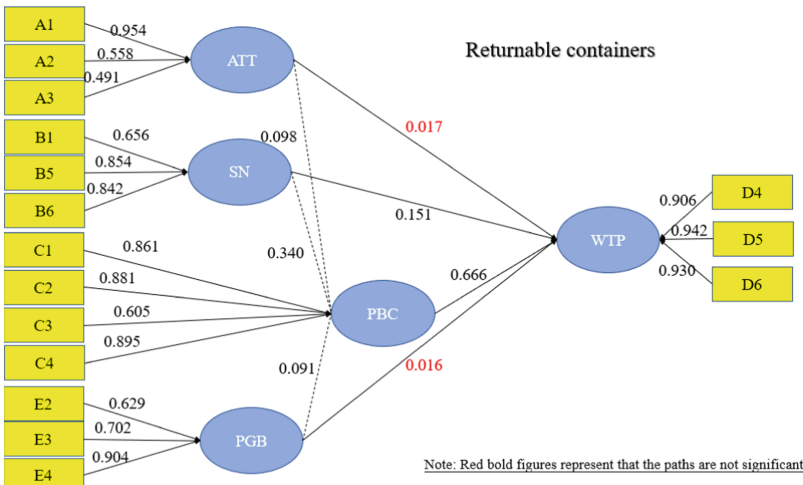


Fig. 3. Path analysis result of returnable containers.

5 Discussion

5.1 General Discussion

The study seeks to examine consumers' intention of replacing conventional plastic packaging with green alternatives. Applying the theory of planned behavior (TPB), the study examines the relationships between the environmental attitude (ATT), social norms (SN), perceived behavior control (PBC), past green behavior (PGB) and willingness to pay more (WTM) or willingness to participate (WTP). The result shows that ATT, SN and

PGB cannot directly affect consumers' adopting intentions towards biodegradable packaging and returnable containers. However, PBC can serve as the mediator between ATT, SN, PGB and WTM or WTP, which is consistent with previous research findings [26, 29, 33]. It is probably because that people are not familiar with new alternatives due to its limit of use. In this case, even though they are concerning about the environmental problems caused by single-use plastics and are positively influenced by their social networks when it comes to adopting new alternatives, they show hesitation for the lack of knowledge and experience of using biodegradable packaging and returnable containers (PBC). Nevertheless, in the case of biodegradable packaging, PBC and PGB show direct positive effects on consumers' WTM for new packaging choice. In regard of returnable containers, SN and PBC can directly and positively influence consumers' WTP in a returnable program.

5.2 Policy Implications

The findings generate some policy implications which provide suggestions for developing green alternatives to phase out conventional disposable packaging. To promote the use of green alternatives, the government should make efforts in improving consumers' perceived behavior control (PBC). The result demonstrates that PBC can not only exert direct effects on consumers' intentions of adopting alternatives (WTM and WTP) but also mediate the relationships between their environmental attitude (ATT), social norms (SN) and the adopting intentions (WTM and WTP). Regarding PBC, consumers' major concern lies in the accessibility, difficulty, time and resources of renting returnable containers and disposing biodegradable packaging [45–47]. The government should support the expansion of returnable containers programs by providing more policy or monetary incentives, in order to cut down the time, money and other resources that consumers spend on renting and using the containers [22]. Apart from it, cheaper and more durable biodegradable packaging should be provided to consumers to replace conventional ones. Placing more garbage bins to recycle used biodegradable packaging waste is also important [36].

5.3 Limitations

The study also has some limitations in regard to validating the explanation of complete mediation effect of PBC on ATT, SN, PGB and WTM/WTP. In the future research, it should be put into consideration. What's more, the research is conducted under a specific cultural and policy context, it is doubted that the result of the research can be directly applied to other cultures.

6 Conclusion

The research is conducted under the context of COVID-19 and China's "New Plastic Ban" policy, when people's online food ordering habit has been changed due to city lockdowns and the roll-out of new policy to restrict the use of disposable plastics in pilot cities (mainly Beijing and Shanghai). First, it fills the gap of TPB in the reality by

extending it with new constructs. Besides, although there exists studies proving that perceived behavior control can generating mediation effect between attitude, social norms and intentions [33, 48], to the best of my knowledge, there is no single study proves that the complete mediation of PBC existing between attitude, social norms and intentions. The study deducts that when people are not familiar with the new choices, they tend to consider more regarding the availability and accessibility (perceived behavior control) of adopting them. As a result, PBC shows strong relationship with their intentions and can even mediate the relationships of other constructs with intentions.

Acknowledgement. This research was funded by the Ratchadapisek Sompoch Endowment Fund (2020) under Microplastic and Plastic Pollution Cluster, Chulalongkorn University.

References

1. A. Single-, A. Resolutions, and M. Litter **1518**, 1515 (2020)
2. Plastic Pollution - Our World in Data. <https://ourworldindata.org/plastic-pollution> Accessed 05 July 2021
3. Song, G., Zhang, H., Duan, H., Xu, M.: Resour. Conserv. Recycl. **130**, 226 (2018)
4. Miller, R.: Plastic shopping bags: An analysis of policy instruments for plastic bag reduction. MS thesis (2012)
5. Kwon, H.R., Silva, E.A.: Mapping the landscape of behavioral theories: systematic literature review. J. Plan. Literat. **35**(2), 161–179 (2020). <https://doi.org/10.1177/088542219881135>
6. Hassan, L.M., Shiu, E., Shaw, D.: J. Bus. Ethics **136**, 219 (2016)
7. Ceglia, D., de Oliveira Lima, S.H., Leocádio, Á. L.: Sustain. Dev. **23**, 414 (2015)
8. Janmaimool, P.: Int. J. Sociol. Soc. Policy **37**, 788 (2017)
9. Pronello, C. (2018)
10. Nasri, W., Charfeddine, L.: J. High Technol. Manag. Res. **23**, 1 (2012)
11. Icek, A.: Organ. Behav. Hum. Decis. Process. **50**, 179 (1991)
12. Yadav, R., Pathak, G.S.: Ecol. Econ. **134**, 114 (2017)
13. Hanss, D., Böhm, G., Doran, R., Homburg, A.: Sustain. Dev. **24**, 357 (2016)
14. Hunt, H.R., Gross, A.M.: Behav. Modif. **33**, 795 (2009)
15. Si, H., Shi, J.-G., Tang, D., Wen, S., Miao, W., Duan, K.: Application of the theory of planned behavior in environmental science: a comprehensive bibliometric analysis. Int. J. Environ. Res. Public Health **16**(15), 2788 (2019). <https://doi.org/10.3390/ijerph16152788>
16. Liu, Y., Bai, Y.: Resour. Conserv. Recycl. **87**, 145 (2014)
17. Ertz, M., Karakas, F., Sarigöllü, E.: J. Bus. Res. **69**, 3971 (2016)
18. Kumar, A.: Resour. Conserv. Recycl. **141**, 378 (2019)
19. Hong, Z., Park, I.K.: Sustain. **10**, 1 (2018)
20. Yue, T., Long, R., Chen, H.: Energy Policy **62**, 665 (2013)
21. Wang, Z., Guo, D., Wang, X.: J. Clean. Prod. **137**, 850 (2016)
22. Nguyen, H.T.T., Hung, R.J., Lee, C.H., Nguyen, H.T.T.: Sustain. **11**, 1 (2018)
23. Ahmad, M.S., Bazmi, A.A., Bhutto, A.W., Shahzadi, K., Bukhari, N.: Appl. Res. Qual. Life **11**, 253 (2016)
24. Yu, T.Y., Yu, T.K.: Int. J. Environ. Res. Public Health **14** (2017)
25. Wan, C., Cheung, R., Shen, G.Q.: Facilities **30**, 630 (2012)
26. Lin, Y.-C., Liu, G.-Y., Chang, C.-Y., Lin, C.-F., Huang, C.-Y., Chen, L.-W., Yeh, T.-K.: Perceived behavioral control as a mediator between attitudes and intentions toward marine responsible environmental behavior. Water **13**(5), 580 (2021). <https://doi.org/10.3390/w13050580>

27. Farrow, K., Grolleau, G., Ibanez, L.: *Ecol. Econ.* **140**, 1 (2017)
28. Werfel, S.H.: *Nat. Clim. Chang.* **7**, 512 (2017)
29. Sánchez-Medina, A.J., Romero-Quintero, L., Sosa-Cabrera, S.: *PLoS ONE* **9**, 1 (2014)
30. Suher, J., Hoyer, W.D.: *J. Mark. Res.* **57**, 548 (2020)
31. Fanghella, V., d'Adda, G., Tavoni, M.: *Front. Psychol.* **10**, 1 (2019)
32. Arias, C., Trujillo, C.A.: Perceived consumer effectiveness as a trigger of behavioral spillover effects: a path towards recycling. *Sustainability* **12**(11), 4348 (2020). <https://doi.org/10.3390/su12114348>
33. Giantari, I.G., Zain, D., Rahayu, M., Solimun: *Int. J. Bus. Manag. Invent.* **2**, 30 (2013)
34. Mamun, A.A., Fazal, S., Ahmad, G., Yaacob, M., Mohamad, M.R.: Willingness to pay for environmentally friendly products among low-income households along coastal peninsular Malaysia. *Sustainability* **10**(5), 1316 (2018). <https://doi.org/10.3390/su10051316>
35. Martinho, G., Pires, A., Portela, G., Fonseca, M.: Factors affecting consumers' choices concerning sustainable packaging during product purchase and recycling. *Resour. Conserv. Recycl.* **103**, 58–68 (2015). <https://doi.org/10.1016/j.resconrec.2015.07.012>
36. Cudjoe, D., Yuan, Q., Han, M.S.: An assessment of the influence of awareness of benefits and perceived difficulties on waste sorting intention in Beijing. *J. Clean. Product.* **272**, 123084 (2020). <https://doi.org/10.1016/j.jclepro.2020.123084>
37. Trivedi, R.H., Patel, J.D., Acharya, N.: *J. Clean. Prod.* **196**, 11 (2018)
38. Chen, C.-C., Chen, C.-W., Tung, Y.-C.: Exploring the consumer behavior of intention to purchase green products in belt and road countries: an empirical analysis. *Sustainability* **10**(3), 854 (2018)
39. Prakash, G., Pathak, P.: *J. Clean. Prod.* **141**, 385 (2017)
40. Wei, S., Ang, T., Jancenelle, V.E.: *J. Retail. Consum. Serv.* **45**, 230 (2018)
41. Zhang, L., Fan, Y., Zhang, W., Zhang, S.: *Sustain.* **11**, 1 (2019)
42. Hair, J.F., Risher, J.J., Sarstedt, M., Ringle, C.M.: *Eur. Bus. Rev.* **31**, 2 (2019)
43. Fornell, C., Larcker, D.F.: *J. Mark. Res.* **18**, 39 (1981)
44. Henseler, J., Hubona, G., Ray, P.A.: *Ind. Manag. Data Syst.* **116**, 2 (2016)
45. Ertz, M., Huang, R., Jo, M.S., Karakas, F., Sarigöllü, E.: *J. Environ. Manage.* **193**, 334 (2017)
46. Khan, F., Ahmed, W., Najmi, A.: *Resour. Conserv. Recycl.* **142**, 49 (2019)
47. Liao, C., Zhao, D., Zhang, S.: *41*, 186 (2018)
48. Liu, H., Kennedy, M., Liu, H., Hong, F., Ha, T., Ning, Z.: *Sex. Health* **10**, 487 (2013)

Environmental Biology and Biodiversity Conservation



Comparative Evaluation of APTI of Plant Species at Two Different Sites Near CCI-Rajban Cement Factory, Sirmaur

M. Amin Mir¹ , Kim Andrews¹, and Bilal Ahmad Mir²

¹ Department of Mathematics and Natural Sciences, Prince Mohammad Bin Fahd University, Al Khobar, Kingdom of Saudi Arabia
mmir@pmu.edu.sa

² Department of Environmental Sciences, Alpine Group of Institutions Dehradun, Dehradun, Uttarakhand, India

Abstract. The study in reference was carried out to measure the Air pollution Tolerance Index of plant species close to cement factory CCI Rajban in reference to the controlled site situated at 20 kms away from the cement plant. The APTI is useful to implement the tolerance index levels of plant species for air contamination. The pollution tolerant species can act as impurity sinks so could help to supervise and abate the ill effects of air pollution. Plants having high value for air pollution are stipulate to improve the greenery and thus aids in long term execution of air pollution in a specified affected area. The work in reference estimates the APTI of various plant species viz, Teak, Sal, Mango, Mallotus and Gauva plant species have been found less tolerable and more sensitive (<1 to 16). Peepal plant species are Intermediate tolerant and sensitive (16–29). The genus Eucalyptus plant are found out to be tolerant for the air pollution (30–100).

Keywords: Teak · Sal · Mango · Mallotus · APTI · Pollution · NO₂ · SO₂

1 Introduction

The main pollution creating substances released in air include dust, CO₂, NO, NO₂, and SO₂, smog etc. Also polychlorinated compounds like, CFC's, benzo-furans, organic carbon containing substances, metals, non-metals, HCl, HF are released also in the atmosphere. As cement industries are adding more CO₂ to the atmosphere as per the results and are under continuous observation. As per the results the industrial sector adds nearly 5–7% of the total CO₂ and is of concern for being anthropogenic in nature leading to global warming. Also the cement industries add million tons of kiln dust every year to the atmosphere and have direct effect on the respiratory systems of the living being. In addition to the generation of CO₂ the cement manufacturing process produces millions of tons of the waste product cement kiln dust each year contributing to respiratory and pollution health risks. So efforts are being made to reduce the addition of these anthropogenic substances to the atmosphere by cement industries and many methods

have been developed to measure the impact of these pollutants to the vegetation. One among them is the estimation of ascorbic content which directly provides information about the pollution index of the area.

Vitamin C (L-Ascorbic acid) a - water soluble vitamin having strong reducing and oxidizing property and is a well-known coenzyme for hydroxylation reaction. Being a strong reducing agent it does play a crucial role in fixing CO₂ during photosynthesis. Ascorbic acid is a strong reducer and plays an important role in photosynthetic carbon fixation, and its concentration is directly proportional to the CO₂ fixation. Plants are more vulnerable to pollution by air as compared to animals, so set off most felicitous firm related to bio-monitoring of the environment. Tiwari S, Bansal S (1993) [1] calculated APTI of 25 plant species and every plant have different behaviour towards the pollution tolerance index. Studies carried out by J. Pandey and M. Agarwal (1994) [2] have reported reduction in the height of plants, basal diameter, canopy area, biomass, chlorophyll, ascorbic acid and nitrogen concentration in the leaves of plants associated with pollution. Study by Chander Sekaran et al., (1998) [3] have related the air quality of Tamil Nadu cement plant. The concentration of SPM, SO₂ and NO_x have been found to be under control because of strict actions against the industries. The study by Mohanty S. K (1999) [4] recognized many effective pollution minimizing measures for the better quality of air district Koraput. The effect of dust particles on plants includes the blockage and damage of stomata leading to minimizing of photosynthesis and respiration was studied by Iqbal and Shafif (2001) [5]. In 2010 Pradhan, A. [6] investigated concentrations of SO₂ (320, 667 and 1334 gm⁻³) and many potential measures have been taken into consideration to purify the varieties of *Raphanus sativus* and *Brassica rapa*. The effect of soil pH have direct impact on plant-soil chemical interactions, especially the availability of micronutrients and toxic chemicals were studied by Atwell et al. (2013) [7]. A. S. Shannigrahi, T. Fukushima, R.C. Sharma (2004) [8], studied the flora which disinfects the atmosphere naturally by sucking the ill gases and some particulate materials via leaves. The depletion in the concentration of chlorophyll leading to decline in the production under polluted environment and some-how showing some tolerance against to pollution by plants are said to be tolerant was studied by Singh and Verma (2007) [9]. A study by Sumitra Giri et al., (2013) [10] studied the chlorophyll content of the leaves of many plant species i.e. *Azadirachta indica*, *Nerium oleander*, *Mangifera indica* and - *Dalbergia sissoo* in relation to air pollution generated by the industries and automobiles. A. Balasubramanian, C. N. Hari Prasath, K. Gobalakrishnan and S. Radhakrishnan (2018) [11], as per their study analysis of APTI in the Coimbatore Urban City come to the conclusion that on overall, *Thespesia populnea* and *Pongamia pinnata* are tolerable against pollution and could help in controlling the air pollution in many cities.

2 Materials and Methods

2.1 Description of Study Area

The industrial hub of Himachal Pradesh is Paonta Sahib, located in the Sirmaur district towards south, on NH-7. Main industries are Cement industry (CCI, Rajban is one of the biggest Cement Production Plant), Power Generation (Hydro Power Plant in Himachal

and Uttarakhand), Pharmaceutical industry (Mankind Pharma, Sun Pharmaceuticals), textiles and many chemical industries. It has Asia's biggest limestone market (in village Barwas of about 32 kms of mining area.)

2.2 Geographical Conditions of Paonta Sahib

It is located on southernmost portion of the Himachal Pradesh, Sirmaur district and lies at 30.438°N and 77.624°E at an elevation of 389 m i.e. 1,276 feet. Paonta Sahib is situated on the banks of Yamuna River, which is also a connecting line between Uttarakhand and Himachal Pradesh. The nearby cities to it are Nahan of Himachal Pradesh, from Haryana side is Yamunanagar, Uttar Pradesh side is Saharanpur and Dehradun from Uttarakhand.

2.3 Meteorological Conditions of Paonta Sahib

Paonta Sahib have sub-tropical monsoon climate with a characterized seasonal rhythm, as summers are hot, winters are slight cold, and the average temperature ranges from (0 °C to 40 °C).

2.4 Land Utilization Pattern

The pattern have been divided into five different areas with their area utilized. They are-

Area under forest - 48704 ha

Irrigated area - 14,964 ha

Unirrigated area - 32,073 ha

Cultural waste (including gauchar and groves) - 72,568 ha

Area not available for cultivation - 54,719 ha.

2.5 Vegetation of Paonta Sahib

The lowest point of the Southern boundary of the district is 427 m above sea level and highest range of Chur Dhar which is at an altitude of 3658 m in the north. The forest is grown between these two extremes as the elevation itself. It ranges between scrub, sal and bamboo forests to the fur and alpine forest to the higher elevations. The main forest type are deodar, chir pine, oak, fir, spruce, kale, pine and bamboo. Due to wide variation in the altitude a large variety of fauna is available in the forests. The main crops cultivated in this district are wheat, maize, paddy, oil seed, pulses, potato, sugarcane, ginger, vegetables (peas, tomato, capsicum, cabbage, cauliflower), spices (pepper and coriander). Fruits of different varieties are grown depending upon terrain, climatic conditions and soil. Important fruits grown are apple, plum, mandarins, apricot, pear, dry fruits (almond and walnut), citrus fruits (sweet orange, kagzi lime, kinnow) and subtropical fruits (mango, guava, litchi, papaya).

2.6 Study Sites

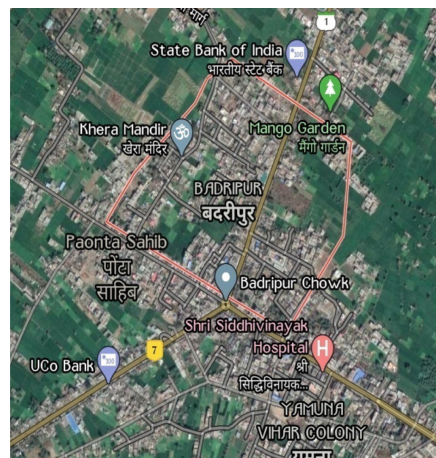
The following sites were selected for the study.

SITE 1: Rajban is a very small town near Paonta Sahib in Sirmaur district. It is located on 30.5188°N, 77.6593°E coordinates. One of the oldest cement factory (CCI) is located in this state.

SITE 2: Badripur with coordinates 30.450001 latitude and 77.620003 longitudes which is 20 kms away from the factory).



CCI, Rajban



Badripur Village

2.7 Sample Collected

The sample of leaves from the plants were selected randomly in the area of reference in winter season during early morning and at height of 2 to 2.5 m. Three replicates of each plant were used. Fully matured leaves of plants were stored in polythene bags and then were analysed in laboratory for biochemical testing. Aqueous extracts were prepared with standard procedures.

2.8 Measurement of Dust Deposited on Leaves

The individual leaf area will be calculated by sketching the out border of leaves on graph paper. The deposited amount of dust on the leaves was calculated by the given equation:-

$$W = W_2 - W_1 / A$$

Where, W = Dust Amount (mg/cm^2), W_2 = Weight of dust with leaf, W_1 = Weight of leaf without dust, A = Leaf total Area in cm^2 .

2.9 Biochemical Analysis

The sample of leaves have been analysed to calculate total chlorophyll, ascorbic acid content, pH of leaves and relative water content by the methods of Maclachlam & Zalik (1963) [12], Bajaj and Kaur (1981) [13]. The APTI was computed as per the methods of Singh and Rao (1983) [14] by considering the following equation:-

$$\text{APTI} = \frac{(AT + P) + R}{10}$$

Where A = Ascorbic acid Content (mg/g FW), T = Total chlorophyll content (mg/g FW), P = pH of Leaf extract and R = the relative content of water (%) leaves. As per APTI values the plants having 1–11 APTI value are sensitive, 12–16 are intermediate and ≥ 17 are tolerant.

2.10 Relative Leaf Water Content (RWC)

Relative water mentions a very important factor, the water balance of a plant, which shows the amount of water as absolute, needed by the plants to maintain the full saturation. The RWC, stated by M. A. Matin 1989, [15] expresses in percentage the water content at full turgor for a given tissue at a particular time:

For relative leaf water content was determined and calculated with the formula:-

$$RWC = \frac{W - DW \times 100}{TW - DW}$$

Where, FW = Fresh weight content, DW = dry weight content, TW = turgid weight.

The mentioned procedure of Savage MJ et al. (1983) with few modifications was applied [16]:

For Fresh weight- few leaves were collected, which were immediately wrapped to overcome evaporation loss were stored at dark place. The leaves were weighted to have full tissue FW. The leaves then were dipped in a de-ionized water and were kept overnight and the samples were kept away from physiological activity by means of physical inhibition growth and respiration (kept in a refrigerator at darkness).

To determine turgid weight, the leaves were then dried, reweighted and kept in a dryer at 6 °C for about 24 h. For Dry weight- reweight and calculated RWC. The pieces of the tissues were used to analyse a variety of physiological processes in plants, even it should be kept in consideration the possible heterogeneity of the leaf and canopy to get a good study about the RWC and other physiological parameters.

2.11 Total Chlorophyll Content (TCH)

Total Chlorophyll determination of the plant samples was done by the spectrophotometric method (Arnon, 1949) [17].

About 1 g of leaf materials was chopped, crushed and then extracted using 20 ml of 80% acetone, left for 15 min and then the material at 5000 rpm was centrifuged for about 5 min. The supernatant of the centrifuged sample was taken and its absorbance was measured at 645 nm and 663 nm. The Chlorophyll level varies with the pollution stress at the study site. The chlorophyll content was determined by the below given equation in mg/g fresh weight.

Formula

$$\text{Chlorophyll a} = 12.7(\text{OD at } 663 \text{ nm}) - 2.69(\text{OD at } 645 \text{ nm}) \times V/(100 \times W)$$

$$\text{Chlorophyll b} = 22.9(\text{OD at } 645 \text{ nm}) - 4.68(\text{OD at } 6663 \text{ nm}) \times V/(100 \times W)$$

$$\text{Chlorophyll (a + b)} = 20.2(\text{OD at } 645\text{nm}) + 8.02(\text{OD at } 663 \text{ nm}) \times V/(100 \times W)$$

Where, W = fresh weight of sample (g), V = volume of the sample (ml) OD = optical density/(a = absorbance).

2.12 Leaf Extract pH

The pH of the leaf extract was obtained by homogenizing 1 g of leaf sample, which was after grinding was dissolved in water and then allowing the mixture to stabilize for 15 min. The pH of high value indicates that the plants are tolerant towards polluted environment and the lower level indicates that the species are sensitive.

2.13 Ascorbic Acid Content

The ascorbic acid content was determined by spectrophotometric method (Barker J et al. 1952) [18] in which 1 g of chopped leaf material was taken and the added 4 ml of oxalic acid - EDTA extract solution, followed by addition of 1 ml of orthophosphoric acid and 1ml 5% tetraoxosulphate (VI) acid, which was then followed by addition of 2 ml of ammonium molybdate and 3 ml of H₂O. The whole mixture was filtered and the filtrate was taken for absorbance measurement at 760 nm.

2.14 Plants Selected for Study

For evaluation of APTI seven different plant species were selected. They are Teak (*Tectona grandis*), Sal (*Shorea robusta*), Eucalyptus (*Eucalyptus grandis*), Mango (*Mangifera indica*), Kumkum (*Mallotus philippensis*), Gauva (*Psidium guajava*), Pepal (*Ficus religiosa*).

3 Results and Discussion

The substantial comparative studies has been focused on the measurement and monitoring of APTI of plants growing close to the side of cement plant CCI Rajban and for controlled site (Badripur) the residential area of about 20 kms away from the factory has been taken into the considerations. The APTI is a useful implementation, to way in the tolerance levels of plant species towards air contamination. The tolerant species are used as impurity sink and helps to supervise and abate the adverse influence of air pollution. Plants with high value for APTI are stipulate for green belt improvement and aids in long term management of air pollutant in specified affected area (Tables 1, 2, 3 and Figs. 1, 2, 3).

Table 1. The table showing the RWC (%), pH, Total chlorophyll content, Ascorbic acid, APTI of various plant species in the month of May–June (Not March-April)

Name of plant species	RWC (%)	pH	Total chlorophyll content (mg/g)	Ascorbic acid (mg/g)	APTI of Jan–Feb
Teak (Polluted)	90.69	6.2	2.24	6.19	14.41
(Controlled)	78.58	5.2	2.26	5.00	11.62
SAL (Polluted)	72.24	4.3	7.32	5.12	13.63
(Controlled)	63.32	6.3	3.49	2.37	7.93
Eucalyptus (Polluted)	72.53	6.7	3.43	0.09	17.38
(Controlled)	71.3	10.4	0.34	3.44	16.85
Mango (Polluted)	82.43	6.6	3.43	6.59	14.85
(Controlled)	69.69	4.2	3.59	6.00	11.64
Mallotus (Polluted)	81.13	5.5	1.46	1.16	8.91
(Controlled)	85.80	6.1	1.64	1.69	9.8
Guava (Polluted)	81.8	6.6	0.167	3.35	10.55
(Controlled)	79.1	6.7	0.216	3.00	9.98
Peepal (Polluted)	37.40	5.3	4.4	0.51	18.5
(Controlled)	67.0	5.6	0.564	1.54	8.11

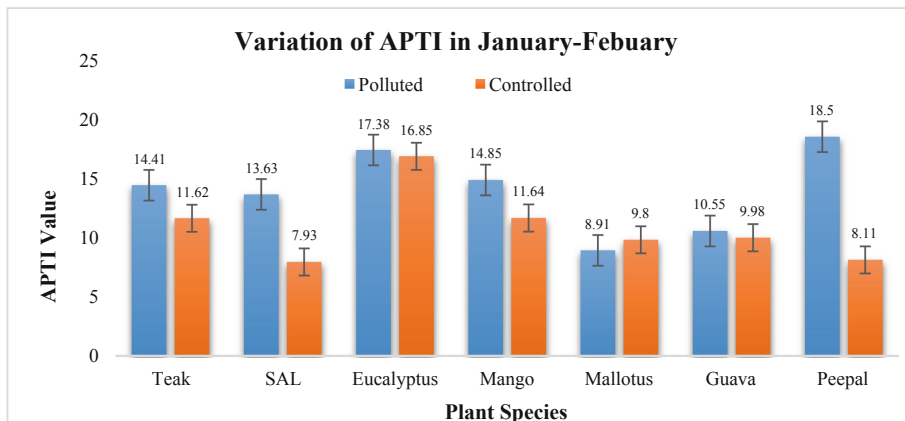


Fig. 1. The variation of APTI values by various plant species, controlled and polluted

Table 2. The table showing the RWC (%), pH, Total chlorophyll content, Ascorbic acid, APTI of various plant species in the month of March–April

Name of the plant species	RWC (%)	pH	Total chlorophyll content (mg/g)	Ascorbic acid (mg/g)	APTI of Mar–April
Teak (Controlled)	71.78	3.63	37.3	2.3	13.5
(Polluted)	54.79	5.45	23.5	1.8	13.1
SAL (Controlled)	64.25	6.31	2.3	1.4	7.6
(Polluted)	51.33	4.9	2.2	0.5	12.3
Eucalyptus (Controlled)	81.62	4.63	4.4	3.4	16.2
(Polluted)	42.29	6.1	1.4	0.5	22.2
Mango (Controlled)	88.72	5.8	5.8	2.1	19.3
(Polluted)	81.83	5.5	2.4	1.7	13.3
Mallotus (Controlled)	77.32	4.1	4.2	0.6	8.3
(Polluted)	78.45	5.8	6.2	0.05	8.4
Guava (Controlled)	52.22	6.3	0.3	7.3	9.8
(Polluted)	60.5 1	6.3	0.1	8.4	11.3
Peepal (Controlled)	63.32	5.2	4.5	7.9	12.3
(Polluted)	37.40	5.3	2.3	.51	18.5

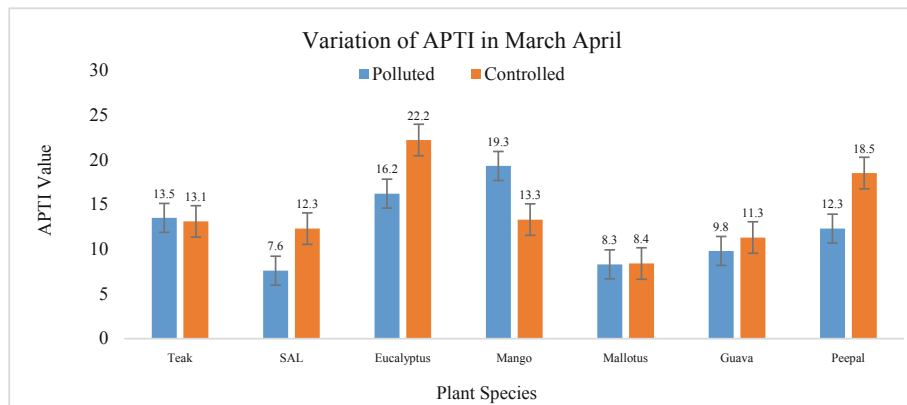


Fig. 2. The variation of APTI values by various plant species, controlled and polluted.

Table 3. The table showing the RWC (%), pH, Total chlorophyll content, Ascorbic acid, APTI of various plant species in the month of March–April

Name of plant species	RWC (%)	pH	Total chlorophyll content (mg/g)	Ascorbic acid (mg/g)	APTI of May–June
Teak (Polluted)	71.9	4.6	24.7	2.2	13.5
(Controlled)	68.8	4.6	32.1	2.1	14.6
SAL (Polluted)	87.3	6.3	5.1	2.0	11.2
(Controlled)	64.6	6.4	3.2	1.5	7.9
Eucalyptus (Polluted)	55.5	6.7	4.2	0.4	24
(Controlled)	94.9	8.1	4.1	23.1	37.4
Mango (Polluted)	68.2	5.6	0.4	1.1	7.5
(Controlled)	77.7	5.4	3.2	4.1	11.2
Mallotus (Polluted)	94.5	4.2	0.3	0.2	9.5
(Controlled)	89.1	4.7	3.7	0.4	9.2
Guava (Polluted)	76.6	6.7	0.4	3.9	10.7
(Controlled)	81.4	6.8	0.8	1.9	9.6
Peepal (Polluted)	67.4	5.3	4.5	0.5	16.4
(Controlled)	73.8	6.9	2.1	4.6	11.5

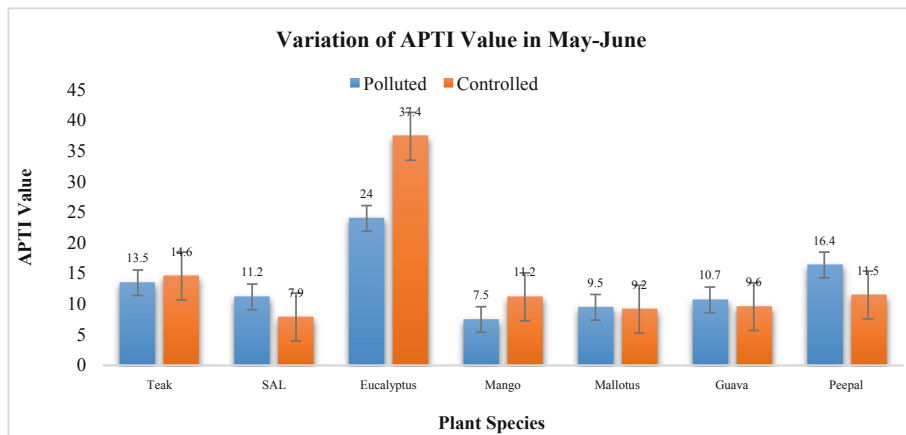


Fig. 3. The variation of APTI values by various plant species, controlled and polluted.

APTI index is used by Scientists to specify the plants against air pollution. The study relates the air pollution tolerance index (APTI) of seven plant species which showed marginal differences in relation to the biochemical parameters taken under study, like Ascorbic acid content, pH of leaf extracts, Total chlorophyll content and Relative Water Content (RWC). Among tree species selected, accounted highest APTI of industrial zone and residential zone. Teak (*Tectona grandis*) Plant Species-The APTI mean value which was observed maximum at controlled site (13.7) and minimum was at polluted site (13.2). According to the APTI value, the tolerant range was 11.62 to 14.65, so the teak species are observed to be sensitive to air pollution. Sal (*Shorea robusta*) Plant Species – The observed mean APTI value was observed maximum at polluted site (12.41) and minimum was at controlled site (7.83). With the APTI value, the tolerant range was 7.66 to 13.63, so the sal plant species are found to be sensitive to air pollution. Eucalyptus (*Eucalyptus grandis*) Plant Species – The APTI mean value were maximum at controlled site (23.53) and minimum was (21.26) at polluted site. With the calculated APTI value, the tolerant range was 16.28 to 37.48, so the eucalyptus plant species are considered tolerable to air contamination. Mango (*Mangifera indica*) Plant Species – The maximum APTI mean value at controlled site observed was (14.06) and minimum was at polluted site (11.89). For the given APTI value, the tolerant range was 7.51 to 19.31, the mango plant species were less tolerable and more sensitive for the air pollution. Kumkum (*Mallotus philippensis*) Plant Species – The APTI mean value at controlled site (9.15) was maximum and at polluted site was 8.97. The APTI value for Mallotus plant species the tolerant range was 8.39 to 9.58, the plant species were found to be sensitive for the contamination in air. Gauva (*Psidium guajava*) Plant Species-Maximum APTI mean value was 10.79 at polluted site and minimum APTI mean value was 9.81 at controlled site. The values for APTIs for guava plant species, the tolerant range was 9.60 to 11.37, they were less tolerable and more sensitive for the pollutants in air. Peepal (*Ficus religiosa*) Plant Species – 17.8 was maximum mean APTI value at polluted site and 10.69 was minimum mean APTI value at controlled site. The tolerant

range 8.11 to 18.5, which represents that the plant species are intermediate of tolerance and sensitivity.

4 Conclusion

The substantial studies was focused on the measurement and monitoring of Air pollution Tolerance Index of plant species growing close to the side of cement plant CCI Rajban and in the controlled site which is being 20 kms away from the cement plant. The APTI are useful implement to way in the tolerance levels of plant species towards air contamination. The tolerant species can be used as impurity sink and helps to supervise and abate the adverse influence of air pollution. Plants with high value for APTI are stipulate for green belt improvement and aids in long term management of air pollutant in specified affected area. As we took different plant species for estimating the air pollution tolerance we came to know that - Teak, Sal, Mango, Mallotus and Gauva plant species are less tolerable and more sensitive (<1 to 16). Peepal plant species are Intermediate of tolerance and sensitivity (16–29). Eucalyptus plant species are found out to be tolerant for the air pollution (30–100).

References

1. Tiwari, S., Bansal, S., Rai, S.: Expected performance indices of some planted trees of Bhopal. Indian J. Environ. Health **35**, 282–286 (1993)
2. Pandey, J., Agrawal, M.: Evaluation of air pollution phytotoxicity in a seasonally dry tropical urban environment using three woody perennials. New Phytol. **126**(1), 53–61 (1994)
3. Chandrasekharan, G.E., Ravichandran, C., Mohan, C.A.: A short report on ambient air quality in the vicinity of a cement plant at Dalmiapuram. Indian J. Environ. Protect. **181**, 7–9 (1998)
4. Mohanty, S.K., Singh, U., Balasubramanian, V., Jha, K.P.: Nitrogen deep-placement technologies for productivity, profitability and environmental quality of rainfed lowland rice systems. Nutr. Cycl. Agroecosyst. **53**, 43–57 (1999)
5. Iqbal, M.Z., Shafiq, M., Syed, K.A.: Toxic effects of lead and cadmium individually and in combination on germination and growth of Leucaena leucocephala (Lam.de wit). Pakistan J. Botany **33**, 551–557 (2001)
6. Pradhan, A., Plummer, J.A., Nelson, M.N., Cowling, W.A., Yan, G.: Successful induction of trigenomic hexaploid Brassica from a triploid hybrid of *B. napus* L. and *B. nigra* (L.) Koch. Euphytica **176**, 87–98 (2010)
7. Atwell, S., et al.: Genome-wide association study of 107 phenotypes in *Arabidopsis thaliana* inbred lines. Nature **465**, 627–631 (2010)
8. Shannigrahi, A.S., Fukushima, T., Sharma, R.C.: Anticipated air pollution of some plant species considered for green belt development in and industrial/urban area in India: an overview. Int. J. Environ. Stud. **61**(2), 125–137 (2004)
9. Singh, S.N., Verma, A.: Phytoremediation of air pollutants, a review. In: Singh, S.N., Tripathi, R.D. (eds.) Environmental Bioremediation Technology, pp. 293–314. Springer, Cham (2007). https://doi.org/10.1007/978-3-540-34793-4_13
10. Giri, S., Shrivastava, D., Deshmukh, K., Dubey, P.: Effect of air pollution on chlorophyll content of leaves. Curr. Agric. Res. J. **1**(2), 93–98 (2013)
11. Balasubramanian, A., Hari Prasath, C.N., Gobalakrishnan, K., Radhakrishnan, S.: Air pollution tolerance index (APTI) assessment in tree species of coimbatore urban city, Tamil Nadu, India. Int. J. Environ. Climate Change **4**, 27–38 (2018)

12. Maclachlan, S., Zalik, S.: Plastid structure, chlorophyll concentration, and free amino acid composition of a chlorophyll mutant barley. *Can. J. Bot.* **41**, 7 (1963)
13. Bajaj and Kaur: Spectrophotometric determination of L-ascorbic acid in vegetables and fruits. *Analyst* **106**(1258), 117–120 (1981)
14. Singh, S.K., Rao, D.N.: Evaluation of the plants for their tolerance to air pollution. In: Proceedings of Symposium on Air Pollution Control Held at IIT Delhi, pp. 218–224 (1983)
15. Matin, M.A., Brown, J.H., Ferguson, H.: Leaf water potential, relative water content, and diffusive resistance as screening techniques for drought resistance in barley. *Agron. J.* **81**(1), 100–105 (1989)
16. Savage, M.J., Wiebe, H.H., Cass, A.: In situ field measurements of leaf water potential using thermocouple psychrometers. *Plant Physiol.* **73**, 609–613 (1983)
17. Arnon, D.I.: Copper enzymes in isolated chloroplasts polyphenoloxidase in Beta vulgaris< / REFATL. *Plant Physiol.* **24**(1), 1–15 (1949)
18. Barker, J., Mapson, L.W.: The ascorbic acid content of potato tubers. III, The influence of storage in nitrogen, air and pure oxygen. *New Phytol.* **51**, 90–115 (1952)



Elemental Status of European Mole (*T. europaea*) in the Conditions of the Plast Region of the Chelyabinsk Oblast in Russian

Margarita Samburova¹ , Vladimir Safonov² , Tatyana Bratashova² ,
and Emil Salimzade²

¹ BIOS LLC, Moscow, Russia

² Astrakhan State University, Astrakhan, Russia

safonovbio@gmail.com

Abstract. The changes in the conditions of natural objects are studied for the expansion of the possibilities of biogeochemical indication and ecological-geochemical evaluation of the environment. In the present article, the authors presented the study results on the elemental status of the indicator species European mole (*T. europaea*). The studied specimens inhabited a technogenic formation (tailing dump of the gold-arsenic deposit) and reference areas (>15 km from the tailing dump). It was established that moles from the tailing dump had lower content of calcium in kidneys (by 1.4 times) and higher content of phosphorus in the liver (by 1.3 times) and fur (1.8 times), and magnesium in muscles (by 1.4 times). The levels of copper and zinc were elevated in all the organs and fur (by 1.4–2.1 and 1.2–1.5 times, respectively). In moles that inhabited the reference areas, a deficiency of selenium was observed (its levels in fur and tissues were 1.7–8.9 times lower than in moles from the tailing dump). It could be associated with a low concentration of selenium in the soil. Animals from the tailing dump had high levels of accumulated toxins, especially mercury, which levels were higher by 98.9 times in the liver, 115.3 times in kidneys, and 70.8 times in muscles than in the respective organs of the moles from the reference areas. Thus, the unfavorable influence of the tailing dump on the conditions of mole habitat and the general ecological situation does not affect the metabolism of macroelements as much as the accumulation of non-essential elements from the group of heavy metals.

Keywords: Biochemistry · Heavy metals · Mineral elements · European mole

1 Introduction

Modern human activity in the biosphere significantly affects the health of biogeocenoses and redistribution of chemical elements and their compounds. In the polluted environment, fast changes occur in the living conditions. The specified processes are the subjects of the studies on ecological geochemistry and toxicology [1].

Certain mineral elements are essential for living organisms for the synthesis of biological molecules that are parts of complex organic structures involved in physiological

processes. However, the content of heavy metals and other toxicants is limited in the living organisms in the norm or they are not essential at all. They pollute the environment during ore-mining, technogenic processes of industrial plants, functioning of energetic complexes, and application of fertilizers and pesticides. Chemical elements get into an organism via different pathways and circulate with blood to internal organs wherein they interfere with metabolic processes. Toxic elements substitute essential microelements in the structure of biomolecules. Because of the insufficiency of the mechanisms of elimination of these metabolites, they get accumulated in tissues and organs [2, 3].

Traditionally used soil, water, and air tests are not always sufficient for the evaluation of the potential toxicity of the compounds that get into the environment. Biological processes and systems involved in the ecological monitoring are studied for the evaluation of time and space-related factors on the health, effects of anthropogenic processes, natural disasters, and intentional anthropogenic intervention in the ecosystems, including the measures on their recreation, remediation, and reintroduction. An increase in the number of studies is observed that allow for the development of methods of maintenance of ecological systems resistance, which is understood as the possibility to resist perturbations and return to the initial state after the end of the stress actor impact. The objects of such studies should reflect the occurring changes associated with the impact of the changed factor. In turn, it is necessary to have tools and inventories for the measurement, analysis, and interpretation of these changes [4, 5]. The involvement of the associated taxons of plants and animals in the biogeochemical indication reflects the degree of a transition of mineral elements along the trophic chains. The comparison of the levels of elements in the soil and living objects describes the degree of their bioavailability, which allows for the evaluation of the risks for the ecology of biogeocenoses and human health.

Perspective objects of the studies are insectivorous animals that are considered to be more precise bioindicators in the evaluation of the ecological situation, unlike other small mammals. Moles primarily eat earthworms that are also very sensitive to environmental pollution. The advantages of a mole over other insectivorous animals include a long life circle and the possibility of precise estimation of the animal's age. Dependence between the age and levels of heavy metals was established in the internal organs. Thus, such observations provide data on the long-term impact of environmental pollution [6, 7]. The accumulation of heavy metals in the kidney and liver in the representatives of *Talpa* specimens is more expressed than in other small mammals, like rabbits [8, 9]. The studies on the accumulation of toxic elements in the feeding chain "soil – earthworm – mole" attract the interest of researchers as well as the evaluation of the content of heavy metals in the system "host/parasite", wherein the tissues of a parasite have manifold higher accumulation of toxicants than in the liver and kidneys of the host. This approach provides ecological monitoring in the cases of a long-term direct or indirect effect of low levels of anthropogenic pollutants that reduce the suitability of above-the-ground ecosystems for living organisms [8, 10].

The elemental composition of the soil, water, and air that changed under the influence of technogenic activities affect higher trophic levels. The changes that occur in the structure and composition of the soil, landscape, and waters are evaluated in several studies conducted in the Plast Region of the Chelyabinsk Oblast (Russia). In the specified region, long-term active mining of gold deposits is ongoing, which resulted in the

formation of a tailing dump consisting of processed ore [11]. During the biogeochemical evaluation of the local ecology, the authors focused on the study of the elemental composition in the insectivorous animals-indicators (*Talpa europaea*) associated with the studied soils.

2 Materials and Methods

The study of macro and microelemental composition of fur and tissues of small mammals is a part of a major study on the influence of technogenic formations on the ecology of biogeocenoses of the Plast Region. The authors caught adult specimens of European moles (*T. europaea*) using tunnel mole traps on the territory of the tailing dump of the Novotroitsk gold-arsenic deposit ($N = 4$) and reference areas (>15 km from the tailing dump) nearby river Kabanka and Village Demarino ($N = 5$). The probes of fur and tissues were taken according to the principles of humanity to experimental animals of the European Directive (86/609/EEC) and Helsinki declaration.

The samples of fur, liver, kidney, and muscle tissues were prepared for the analysis according to the "Method of identification of chemical elements in biological media and preparations and inductively coupled plasma atomic emission spectrometry and inductively coupled plasma mass spectrometry. MUK 4.1.1483-03". The evaluation of the total content of chemical elements was performed in 3 parallel weighted samples using a mass-spectrometer Nexion 300D (Perkin Elmer, USA). The list of the tested elements included calcium (Ca), phosphorus (P), magnesium (Mg), microelements iron (Fe), copper (Cu), zinc (Zn), selenium (Se), iodine (I), heavy metals cadmium (Cd), mercury (Hg), and lead (Pb). The obtained data were processed by the methods of mathematical analysis and software program Statistica 13.5 (Statsoft Inc.). The results were expressed as mathematical expectation \pm standard error. The significance of differences between the parameters was identified with the Student's t-test. The correlations between the element levels were calculated by Pierson's correlation coefficient.

3 Results

In comparison with the soil of the reference areas located further than 15 km from the tailing dump, the surface soil layer of the tailing dump was looser, had poorer plantstand, and contained more sand and clay.

The balance of calcium in adult animals was maintained due to the absorption of compounds taken up with nutrients via the gastro-digestive tract and the elimination with kidneys. It varies depending on the resorption intensity and formation of bone tissues [12]. Animals that inhabit the surface of the tailing dump had decreased levels of Ca in the tissues of the liver and kidneys, and the levels of the microelement in kidneys were decreased by 1.4 times (Table 1). The analysis of animal muscular tissue and fur did not reveal significant differences. However, in one of the animals caught in the tailing dump, the content of Ca in muscles was very high (1328 mg/kg). The explanation of the causes of a high concentration of Ca in this single case is associated with difficulties because hypercalcemia is characterized by numerous factors.

Table 1. The content of macroelements in the samples of fur and tissues of European mole (*T. europaea*).

Sample		Ca	P	Mg
Liver	Tailing dump	168.75 ± 9.33	5042.75 ± 163.33*	260.25 ± 12.55
	Reference areas	250.6 ± 106.36	3919.8 ± 155.96	242.2 ± 15.93
Kidneys	Tailing dump	168 ± 13.36*	4269 ± 234.34	276.5 ± 23.89
	Reference areas	236.2 ± 23.29	3449.2 ± 267.12	219.2 ± 10.73
Muscles	Tailing dump	502.25 ± 276.28	2863.25 ± 279.98	326.75 ± 22.64*
	Reference areas	177.4 ± 18.94	2423.8 ± 288.95	239 ± 19.81
Fur	Tailing dump	3873.75 ± 261.45	786.25 ± 138.34*	1234 ± 96.52
	Reference areas	3332 ± 175.37	429 ± 40.33	1009 ± 89.79

* Differences are significant at $P < 0.05$

The samples obtained from the moles that inhabited the tailing dump tended to have high levels of phosphorus. The levels of phosphorus were 1.3 times higher in the liver, 1.2 times higher in the kidneys, 1.2 times higher in muscles, and 1.8 times higher in fur. The most often cause of hyperphosphatemia in mammals is a dysbalance in the Ca:P ratio with a decrease in the level of Ca and kidney failure.

Magnesium plays a central role in phosphate metabolism. In moles that inhabit the techosol of the tailing dump, the levels of Mg are elevated: in the liver – by 1.1 times, in the kidneys – by 1.3 times, in muscles – by 1.4 times, and in the fur – by 1.2 times. The study of quantitative interactions between Mg and other elements demonstrated its negative correlation with the level of Fe in the samples of animals that lived in the reference areas ($r = -0.58$ ($P < 0.01$)).

The microelement status of moles that inhabit the Novotroitsk tailing dump is characterized by peculiarities in the levels of some elements. Primarily, the levels of those elements were elevated in comparison with moles that lived on the reference territories (Table 2).

The levels of Fe did not differ significantly from the studied animals and positively correlated with the levels of Cu in soft tissues in animals from the tailing dump $r = +0.74$ ($P < 0.01$) and reference areas – $r = +0.67$. Besides, there were no significant differences revealed in the tissues and fur in animals that inhabited the areas of the Plast Region. The studied tissues do not deposit iodine and the metabolism is very quick. It is considered that the period of half-life of iodine is not more than 9 days. There is a moderate correlation between the level of iodine in mole tissues and zinc – $r = +0.49$ and selenium – $r = +0.38$ ($P < 0.05$).

Selenium plays a key role in the system of antioxidant protection. Still, it can cause poisoning in humans and animals in high concentrations. The normal levels of selenium in organs and tissues of terrestrial animals are 0.3–1.7 mg/kg. Higher levels of selenium ($P < 0.01$) involved in the detoxication of organs indicate the protective function of the element against heavy metals [13]. In the studied animals from the Novotroitsk tailing dump, the levels of selenium in different tissues were 1.7–8.9 times higher than

Table 2. The content of microelements in the samples of fur and tissues of European mole (*T. europaea*).

Sample		Fe	Cu	Zn	I	Se
Liver	Tailing dump	187 ± 21.78	6.46 ± 0.53*	28.45 ± 1.04*	0.20 ± 0.01	0.98 ± 0.06*
	Reference areas	136.78 ± 19.31	4.6 ± 0.5	24.17 ± 1.17	0.31 ± 0.11	0.11 ± 0.03
Kidneys	Tailing dump	97.35 ± 10.59	5.86 ± 0.57*	27.87 ± 1.88	0.16 ± 0.05	1.15 ± 0.13*
	Reference areas	190 ± 51.15	4.17 ± 0.11	25.74 ± 2.00	0.15 ± 0.04	0.68 ± 0.06
Muscles	Tailing dump	70.4 ± 13.13	3.03 ± 0.25	29.07 ± 2.81*	0.97 ± 0.83	0.24 ± 0.01*
	Reference areas	70.12 ± 16.38	2.67 ± 0.35	19.91 ± 0.83	0.08 ± 0.02	0.04 ± 0.01
Fur	Tailing dump	791 ± 137.17	12.72 ± 2.27*	174.5 ± 10.31*	1.54 ± 0.13	0.81 ± 0.12*
	Reference areas	509.6 ± 64.48	6.16 ± 0.43	136.6 ± 4.6	1.69 ± 0.42	0.11 ± 0.01

* Differences are significant at $P < 0.05$

in animals that lived on the reference areas. Since the level of selenium in moles from the tailing dump was moderate (0.24 ± 0.01 – 1.15 ± 0.13 mg/kg), it can be suggested that moles from the reference areas have a selenium deficiency.

Earlier studies [7] showed that the levels of heavy metals, like Zn and Cu, in moles were higher in kidneys than in the liver. In the present study, there were no differences in the accumulation of the above-mentioned elements in these organs. A significant increase in the levels of Cu in moles from the tailing dump was observed in the liver by 1.4 times, kidneys – by 1.4 times, fur – by 2.1 times, Zn in the liver – by 1.2 times, muscles – by 1.5 times, and fur – by 1.3 times. There were no correlations revealed between two microelements in animals.

Table 3 contains the results of the tests of samples taken from European moles for heavy metals that exert the most negative effect on living organisms and lack effective systems of their homeostasis.

The emission of toxic elements presented in Table 3 is associated with open and underground ore mining in the Chelyabinsk Oblast. Presently, there is no evidence of the essential role of cadmium, mercury, and lead. Thus, cadmium does not exert a biological role in the development and functioning of plants and animals. Still, being an active toxicant, it provides the pathogenesis of numerous diseases. Among small mammals, insectivorous animals are one of the best indicators of cadmium because animals that they consume accumulate more cadmium than above-ground plants that are consumed by grass-eating animals [14, 15]. The present study showed that an increase in the levels of cadmium in the liver of the European mole by 1.8 times and in kidneys by 2.5 times. Still, it was within the normal range. There was a tendency to the accumulation of

Table 3. The content of the most toxic elements in the group of heavy metals in the samples of fur and tissues of European mole (*T. europaea*).

Sample		Cd	Hg	Pb
Liver	Tailing dump	0.048 ± 0.019	0.178 ± 0.014*	0.226 ± 0.018*
	Reference areas	0.026 ± 0.015	0.0018 ± 0	0.039 ± 0.006
Kidneys	Tailing dump	0.087 ± 0.034	0.291 ± 0.0232*	0.152 ± 0.027*
	Reference areas	0.035 ± 0.007	0.0019 ± 0.0001	0.05 ± 0.006
Muscles	Tailing dump	0.004 ± 0.002	0.1275 ± 0.0115*	0.165 ± 0.052*
	Reference areas	0.006 ± 0	0.0018 ± 0	0.09 ± 0.044
Fur	Tailing dump	0.131 ± 0.033*	0.368 ± 0.086*	4.255 ± 0.828*
	Reference areas	0.04 ± 0.005	0.011 ± 0.002	1.024 ± 0.32

* Differences are significant at $P < 0.05$

cadmium by the liver, which agreed with the published data on terrestrial mammals. A statistically significant difference in the level of cadmium was revealed in fur samples. The fur of moles that inhabited the tailing dump contained 3.3 times more cadmium.

It is difficult to say if European moles from the tailing dump can be negatively affected by cadmium. However, there was a statistically significant difference in the level of mercury and lead in the liver, kidneys, muscles, and fur of these animals. The levels of mercury in the taxons of biogeocenoses should be strictly controlled, especially, its organic methylated forms that can easily go through biological membranes [16]. The total content of mercury in the liver was higher than in moles from the reference areas by 98.9 times in the liver, by 115.3 times in kidneys, by 70.8 times in muscles, and by 33.5 times in fur. The highest levels of mercury were revealed in the kidneys. Environmental pollution with mercury is a side effect of refractory gold ore processing. There are data on the capability of selenium to reduce the toxic effect of mercury. In the present study, a strong positive correlation was revealed between the levels of selenium in the liver $r = +0.85$ and kidneys $r = +0.90$ ($P < 0.01$) of moles in the Plast Region, which can be caused by the redistribution of this microelement in the organs with the highest concentration of toxicants.

The establishment of a tailing dump for the ore processing and enriching industry resulted in the contamination of the environment with lead, which was proved by a significant increase in the levels of lead by 5.8 times in the liver, 3.0 times in the kidneys, 1.8 times in muscles, and 4.2 times in the fur of moles that inhabited the tailing dump. The accumulation of lead in the liver is typical when it is ingested via the intestinal wall.

4 Conclusions

The analysis of the macroelement composition of fur and tissues of European mole (*T. europaea*) did not reveal major differences between the parameters of animals that inhabited the tailing dump and the reference areas. Still, there were significantly lower

levels of calcium in the kidneys, higher levels of phosphorus in the liver and fur, and magnesium in muscles of moles from the tailing dump.

The microelement content demonstrated more expressed changes in the moles that inhabited the polluted area. The levels of copper and zinc were elevated by 1.4–2.1 and 1.2–1.5 times, respectively. At the same time, moles that lived in the reference areas had a deficiency of selenium, which could be associated with low levels of the element in the soil. Probably, selenium is involved in mechanisms that protect mole tissues from the influence of heavy metals. A strong positive correlation was established between selenium and mercury in kidneys and liver of moles that lived in the tailing dump.

The studied heavy metals tended to accumulate in the organs involved in the detoxication (kidneys and liver), while in muscles, their content was lower. It was shown that toxicants accumulated in moles, especially, mercury, which levels in the liver in animals from the tailing dump was higher by 98.9 times, in kidneys – by 115.3 times, and muscles – by 70.8 times than in the respective organs of moles from the reference areas.

Thus, in the case of the unfavorable effect of technogenic formation on the mole habitat and ecological situation, the lowest changes were observed in the macroelement metabolism and the most significant changes were revealed in the accumulation of nonessential heavy metals.

References

1. Gadzala-Kopciuch, R., Berecka, B., Bartoszewicz, J., Buszewski, B.: Some considerations about bioindicators in environmental monitoring. *Pol. J. Environ. Stud.* **13**(5), 453–462 (2004)
2. Korobova, E.M.: Combined assessment of the ecological and geochemical state of anthropogenically impacted areas. *Geochem. Int.* **55**(10), 861–871 (2017). <https://doi.org/10.1134/S0016702917100068>
3. Safonov, V.A.: Assessment of heavy metals in milk produced by black-and-white Holstein cows from Moscow. *Curr. Res. Nutr. Food Sci.* **8**(2), 410–415 (2020)
4. Burger, J.: Bioindicators: types, development, and use in ecological assessment and research. *Environ. Bioindic.* **1**(1), 22–39 (2007)
5. Moiseenko, T.I.: Evolution of ecosystems under an anthropogenic load: from disorganization to self-organization. *Geochem. Int.* **58**(10), 1083–1091 (2020)
6. Komarnicki, G.J.K.: Tissue, sex and age specific accumulation of heavy metals (Zn, Cu, Pb, Cd) by populations of the mole (*Talpa europaea L.*) in a central urban area. *Chemosphere* **41**, 1593–1602 (2000)
7. Pankakoski, E., Hyvärinen, H., Jalkanen, M., Koivisto, I.: *Environ. Accumulation of heavy metals in the mole in Finland. Environ. Pollut.* **80**(1), 9–16 (1993)
8. Adalid, R., Torres, J., Miñarro, M., Miquel, J., Fuentes, M.V., Eira, C.: Mercury, lead and cadmium concentrations in *Talpa occidentalis* and in their digeneans of the genus *Ityogonimus*. *Acta Parasitol.* **64**(3), 464–470 (2019)
9. Mukhacheva, S.V.: Peculiarities of accumulation of heavy metals in organism of small mammals from sympatric populations affected by chemical environmental pollution. In: Proceedings of 1st Ural International Ecological Congress “Environmental Safety of Mining Regions” 2007, pp. 22–27. Ekaterinburg (2007)

10. Nesterkova, D.V., Vorobeichik, E.L., Reznichenko, I.S.: The effect of heavy metals on the soil-earthworm-European mole food chain under the conditions of environmental pollution caused by the emissions of a copper smelting plant. *Contemp. Probl. Ecol.* **7**(5), 587–596 (2014). <https://doi.org/10.1134/S1995425514050096>
11. Rylnikova, M.V., Radchenko, D.N., Tsupkina, M.V., Safonov, V.A.: The study of ecological influence of the Novotroitsk tailing dump on plant coverage and living organisms. The issues of the Tula State Agrarian University. *Earth Sci.* **1**, 108–120 (2020)
12. Rosol, T.J., Capen, C.: Pathophysiology of calcium, phosphorus, and magnesium metabolism in animals. *Vet. Clin. North Am. Small Anim. Pract.* **26**(5), 1155–1184 (1995)
13. Chaplygin, W.A., Zaitsev, V.F., Golubkina, N.A., Ershova, T.S., Hursanov, A.S.: Bioaccumulation of mercury and selenium in the body of the Russian (*Acipenser gueldenstaedtii*) and the Persian (*Acipenser persicus*) sturgeons. *Vestnik of Astrakhan State Technical University. Ser. Fishing Ind.* **3**, 122–126 (2017)
14. Veltman, K., Huijbregts, M.A., Hamers, T., Wijnhoven, S., Hendriks, A.J.: Cadmium accumulation in herbivorous and carnivorous small mammals: meta-analysis of field data and validation of the bioaccumulation model optimal modeling for ecotoxicological applications. *Environ. Toxicol. Chem.* **26**(7), 1488–1496 (2007)
15. Massányi, P., Tataruch, F., Slameka, J., Toman, R., Jurík, R.: Accumulation of lead, cadmium, and mercury in liver and kidney of the brown hare (*Lepus europaeus*) in relation to the season, age, and sex in the West Slovakian Lowland. *Environ. Sci. Health A* **38**(7), 1299–1309 (2003)
16. Safonov, V.A., Danilova, V.N., Ermakov, V.V., Vorobyov, V.I.: Mercury and methylmercury in surface waters of arid and humid regions, and the role of humic acids in mercury migration. *Period. Tche Quim* **16**(31), 892–902 (2019)



Effects of Crude Oil and Chemically Dispersed Crude Oil on the Antioxidant Response and Apoptosis in the Respiratory Tree of Sea Cucumber (*Apostichopus japonicus*)

Xishan Li^{1,2} , Deqi Xiong², Nan Li¹, Yuhang Zou^{1,2}, Wei Yang¹, Zhonglei Ju^{1,2}, and Guoxiang Liao^{2,3}

¹ College of Environmental Science and Engineering, Dalian Maritime University, Dalian 116026, Liaoning, China

² National Marine Environmental Monitoring Center, Dalian 116023, Liaoning, China
liaogx2008@126.com

³ State Environmental Protection Key Laboratory of Coastal Ecosystem, Dalian 116023, Liaoning, China

Abstract. This study aimed to compare the effects of crude oil and chemically dispersed crude oil on the antioxidant response and cell apoptosis in the respiratory tree of sea cucumber (*Apostichopus japonicus*). Results showed that compared to the water-accommodated fractions (WAF) of Oman crude oil, chemically enhanced WAF (CEWAF, Oman crude oil dispersed by Guangming-2 chemical dispersant) exposure caused a more significant reduction in the glutathione S-transferase (GST) activity and a more significant increase in the caspase-3 activity. Both WAF and CEWAF exposure had no overt impact on the peroxidase (POD) activity. Besides, Guangming-2 alone exposure caused no remarkable changes in the activities of GST, POD, and caspase-3. This study revealed that the addition of chemical dispersant to disperse crude oil could aggravate the negative effect of crude oil on antioxidant defense enzyme activities (especially GST) and cause severer cell apoptosis in sea cucumber.

Keywords: Oil pollution · Dispersant · Sea cucumber · Oxidative stress

1 Introduction

As one of the most numerous mariculture species in China, sea cucumbers (*Apostichopus japonicus*, *A. japonicus*) are cultured around the coastal provinces of the Yellow Sea and Bohai Sea, such as Liaoning, Shandong, and Hebei [1, 2]. However, in recent years, several large-scale oil spill accidents have happened around the Yellow Sea and Bohai Sea, leading to serious economic losses in the mariculture industry, especially the *A. japonicus* culture [3]. For instance, in July 2010, two crude oil pipelines in Xingang Port of Dalian (China) ruptured and exploded, which resulted in over 1500 t of crude oil spilled into the Yellow Sea and severely affected mariculture industry near Dalian,

especially offshore shellfish and sea cucumber farms [3]. From June to July 2011, a series of oil spills (named the 2011 Bohai bay oil spill) happened at the Penglai 19-3 oil field. Spilled oil polluted over 840 km² of sea area in the Bohai Bay and led to over CNY 12.56 billion economic losses [4]. To quickly clean up oil slicks and reduce the impact on coastal human activities, spraying chemical dispersant has been regarded as one of the most effective emergency responses to oil spill accidents [5, 6]. For example, during the 2010 *Deepwater Horizon* oil spill, approximately 1.8 million gallons of chemical dispersant were sprayed [7]. Over 200 t of chemical dispersant were used during the 2010 Xingang Port oil spill [6]. The main components of chemical dispersants used commonly, like Corexit® EC9500/9527 (used in the 2010 *Deepwater Horizon* oil spill) or Guangming-2 (GM-2, permitted by the China Maritime Safety Administration), are a mixture of surfactants, solvents, and other additives that could make the oil slicks more soluble in the water column[8]. To date, many studies have found that the addition of chemical dispersants could enhance the toxic effects of oil pollution on various aquatic organisms, including fishes, shellfishes, and sea urchins, etc. [3, 5, 6, 9, 10]. Considering that, the use of chemical dispersants as an emergency response during oil spill accidents is still disputed. Additionally, as an important local economic species in the Yellow Sea and Bohai Sea, the effects of oil pollution and chemical dispersant exposure on sea cucumber are still limited. Thus, in the present study, *A. japonicus* was acutely exposed to the water-accommodated fractions (WAF) and chemically enhanced WAF (CEWAF, dispersed by GM-2) of Oman crude oil for 24 h. The study was aimed to compare the effects of crude oil WAF and CEWAF on the antioxidant defense capacity and cell apoptosis in respiratory tree of *A. japonicus* through determined the glutathione S-transferase (GST) activity, peroxidase (POD) activity and caspase-3 activity.

2 Materials and Methods

2.1 Preparation of Exposure Solutions

Oman crude oil and GM-2 chemical dispersant were supplied by Dalian Petro Co., Ltd., and Qingdao Guangming Environmental Technology Co., Ltd., respectively. The preparation procedures of WAF (Oman crude oil only), CEWAF (Oman crude oil dispersed by GM-2 chemical dispersant), and DISP (GM-2 chemical dispersant only) solutions were conducted using the pre-filtered natural seawater (salinity: 32.0 ± 1.0 psu) at an oil loading rate of 5 g·L⁻¹ or at a dispersant-to-oil ratio of 1:5 (*m/m*), based on the standard methods as described previously [3, 6, 11].

2.2 *A. Japonicus* Acute Toxicity Tests

A. japonicus were purchased from the Pikou Sea Cucumber Aquaculture Zoning of Dalian (China) and acclimatized for 7 d with temperature 16.0 ± 0.5 °C, pH 7.9 ± 0.2, salinity 32.0 ± 1.0 psu, and dissolved oxygen 7.1 ± 0.3 mg·L⁻¹. After the acclimation period, *A. japonicus* were exposed to WAF, CEWAF, and GM-2 alone (DISP) for 24 h. A control group was set with *A. japonicus* exposed to pre-filtered natural seawater only. At the end of the exposure period, the respiratory trees of *A. japonicus* were dissected and frozen immediately using liquid nitrogen for subsequent biochemical analysis.

2.3 Total Protein (TP) Content

Total protein (TP) content of *A. japonicus* respiratory tree was measured using the Bradford method [12] with the Total Protein Assay Kit (Bradford Method) (Nanjing Jiancheng Bioengineering Institute, China). Briefly, the tissues were homogenized in pre-cold 100 mM potassium phosphate (PBS) buffer (pH 7.4) at a ratio of 1:9 (*m/v*). 50 μ L of the homogenate and 3 mL of Coomassie reagent were mixed well and incubated for 10 min. Then, the optical density (OD) value at 595 nm of the mixture was measured using an Epoch 2 microplate ultraviolet-visible (UV-Vis) spectrophotometer (BioTek, USA). The TP content of each sample was expressed as mg per mL ($\text{mg}\cdot\text{L}^{-1}$).

2.4 Glutathione S-Transferase (GST) Activity

GST activity of *A. japonicus* respiratory tree was measured using the 1-chloro-2, 4-dinitrobenzene (CDNB) method [13] with the Glutathione S-transferase Assay Kit (Nanjing Jiancheng Bioengineering Institute, China). Briefly, 0.1 mL of tissue homogenate and 0.3 mL of matrix solution were mixed well and incubated at 37 °C for 10 min. Then, 1 mL of GST Assay Buffer and 1 mL of ethanol were added to the incubate solution. After being mixed well, the mixture was centrifuged for 10 min at 3,500 rpm, and then the supernate was collected. 2 mL of supernate, 2 mL of GST Assay Buffer, and 0.5 mL of GST Substrate (CDNB) Solution were mixed well and incubated at room temperature (ca. 25 °C) for 15 min. Then, the OD value at 412 nm of the final incubate was measured using the Epoch 2 spectrophotometer. The GST activity was normalized to the TP concentration for each sample and expressed in units per mg protein ($\text{U}\cdot\text{mgprot}^{-1}$).

2.5 Peroxidase (POD) Activity

POD activity of *A. japonicus* respiratory tree was measured using the *o*-dianisidine method [14] with the Peroxidase Assay Kit (Nanjing Jiancheng Bioengineering Institute, China). Briefly, 0.1 mL of tissue homogenate and 3.9 mL of glucose oxidase reagent mixture (consisted of glucose oxidase, horse-radish peroxidase, and 1% *o*-dianisidine) were mixed well and incubated at 37 °C for 30 min. Then, the OD value at 420 nm of the reaction mixture was measured using the Epoch 2 spectrophotometer. The POD activity of each sample was normalized to the TP concentration and expressed in units per mg protein ($\text{U}\cdot\text{mgprot}^{-1}$).

2.6 Caspase-3 Activity

Caspase-3 activity of *A. japonicus* respiratory tree was assessed using the Ac-DEVD-pNA method [15] with the Caspase-3 Activity Assay Kit (Nanjing Jiancheng Bioengineering Institute, China). Briefly, 50 μ L of tissue homogenate, 5 μ L of 4 mM Ac-DEVD-pNA substrate, and 50 μ L of Reaction Buffer were mixed well and incubated at 37 °C for 12 h. Then, the OD value at 400 nm of the reaction mixture was measured using the Epoch 2 spectrophotometer. The relative caspase-3 activity of each sample was expressed as $\text{OD}_{(\text{sample})}/\text{OD}_{(\text{negative control})}$.

2.7 Statistical Analysis

Data were presented as the mean \pm standard deviation. Statistical differences between different treatment groups were assessed through one-way analysis of variance (one-way ANOVA) using GraphPad Prism Ver 9.0 (GraphPad Software, USA).

3 Results and Discussion

3.1 GST Activity

The GST activity in the respiratory tree of *A. japonicus* following different exposure is shown in Fig. 1. Results showed that compared to the Control ($73.83 \pm 4.83 \text{ U}\cdot\text{mgprot}^{-1}$), no significant impact on the GST activity was observed following DISP exposure ($69.79 \pm 4.17 \text{ U}\cdot\text{mgprot}^{-1}; p = 0.73 > 0.05$). The GST activity values in the WAF and CEWAF treatment groups were $48.66 \pm 7.21 \text{ U}\cdot\text{mgprot}^{-1}$ and $17.68 \pm 1.01 \text{ U}\cdot\text{mgprot}^{-1}$, respectively, manifesting that compared to the Control, both WAF and CEWAF exposure could cause a remarkable reduction in the GST activity ($p = 0.0074$ and $0.0001 < 0.01$, respectively). Besides, the results also showed that the GST activity in the CEWAF treatment group was significantly lower than in the WAF or DISP treatment groups ($p = 0.0018$ and $0.0003 < 0.01$, respectively).

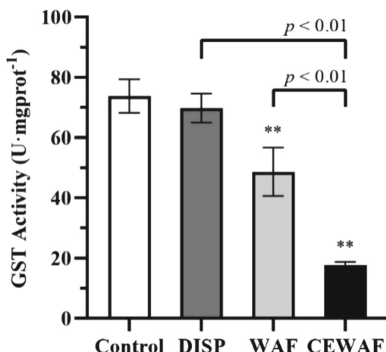


Fig. 1. GST activity in the respiratory trees of *A. japonicus* following exposure to WAF (light-grey filled) and CEWAF (black filled) of Oman crude oil, and GM-2 chemical dispersant only (dark-grey filled). The Control was the *A. japonicus* exposed to pre-filtered natural seawater only (white filled). Asterisks (**) denotes the significant differences between the treatments and the Control ($p < 0.01$). Dark traits denote the significant differences among the treatments.

As is well-known, GSTs (EC 2.5.1.18) refer to a family of intracellular antioxidant enzymes that participate in phase II detoxification processes through catalyzing the conjugation of glutathione (GSH) with some endogenous toxic metabolites and exogenous contaminants (like oil-derived hydrocarbons), to decrease the reactivity of these compounds with cellular macromolecules [16–18]. The detoxification ability of GSTs plays a vital role in cellular protection under oxidative stresses [18]. Our results manifested that both WAF and CEWAF exposure could inhibit the GST activity in the respiratory

tree of *A. japonicus*, thereby affecting the amount of GSH conjugating with oil-derived hydrocarbons and then might reducing the antioxidant capacity. The use of GM-2 chemical dispersant for dispersing the Oman crude oil (CEWAF) could cause more significant inhibition of GST activity than Oman crude oil alone (WAF) exposure did. Besides, our results also confirmed the previous studies that high polluted marine environment could cause a significant impact on the GSTs activity of marine organisms, revealing that GST activity could be regarded to be an exposure biomarker of marine environmental contamination [19].

3.2 POD Activity

The POD activity in the respiratory tree of *A. japonicus* following different exposure is shown in Fig. 2. Results showed that the POD activity in the Control, DISP, WAF, and CEWAF treatment groups were $6.07 \pm 0.30 \text{ U}\cdot\text{mgprot}^{-1}$, $6.15 \pm 1.11 \text{ U}\cdot\text{mgprot}^{-1}$, $7.26 \pm 0.28 \text{ U}\cdot\text{mgprot}^{-1}$, and $6.61 \pm 1.10 \text{ U}\cdot\text{mgprot}^{-1}$, respectively. Through one-way ANOVA, no statistical differences were observed between different treatment groups and the Control ($p = 0.97$, 0.49, and 0.91 > 0.05 for DISP, WAF, and CEWAF exposure, respectively). Meanwhile, there were also no statistical differences between CEWAF exposure and WAF or DISP exposure ($p = 0.55$ and 0.85 > 0.05, respectively).

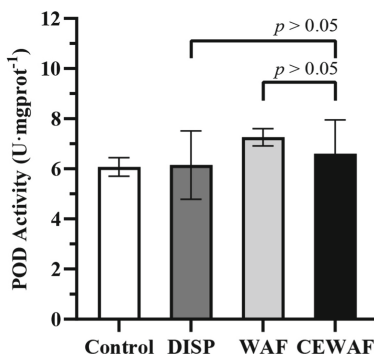


Fig. 2. POD activity in the respiratory trees of *A. japonicus* following exposure to WAF (light-grey filled) and CEWAF (black filled) of Oman crude oil, and GM-2 chemical dispersant only (dark-grey filled).

As one of the main antioxidant enzymes, mainly POD could convert hydrogen peroxide (H_2O_2) into water and oxygen, to reduce the negative effects of reactive oxygen species (ROS) in the cell [20]. Induction of POD activity could be regarded as an antioxidant defensive mechanism against the oxidative stress in the tissues of aquatic organisms following exposure to environmental contaminants. Sabir et al. [21] reported an increase in POD activity in the different organs of ray-finned fish *Cirrhina mrigala* exposed to heavy metal. On the contrary, Bagnyukova et al. [22] observed a lower peroxidase activity in the goldfish *Carassius auratus* exposed to waterborne iron due to the inactivation of peroxidase enzymes induced by oxidative stress. Differently, our results showed that

no pronounced changes in the POD activity were observed in the respiratory trees of *A. japonicus* under Oman crude oil WAF and CEWAF exposure. We implied that oil acute exposure might not cause an overt increase in the level of H₂O₂ (as a particular substrate for the oxidation of POD) and thereby induce no significant changes in the POD activity.

3.3 Caspase-3 Activity

To assess the induction of cell apoptosis in the respiratory tree of *A. japonicus* following different exposure, the relative changes in the caspase-3 activity were detected and are shown in Fig. 3. Results showed that the relative caspase-3 activities in *A. japonicus* following exposure to DISP, WAF, and CEWAF solutions were 7.16 ± 0.29 , 8.28 ± 0.31 , and 9.36 ± 0.29 (fold). Compared to the Control (7.28 ± 0.34), WAF and CEWAF exposure could cause a significant increase in the relative caspase-3 activities ($p = 0.0071$ and $0.0015 < 0.01$, respectively), while no overt impact was observed in *A. japonicus* following DISP exposure ($p = 0.87 > 0.05$). Besides, the results also manifested that CEWAF exposure caused a more remarkable increase in the relative caspase-3 activity than DISP or WAF exposure did ($p = 0.0004$ and $0.0052 < 0.01$, respectively).

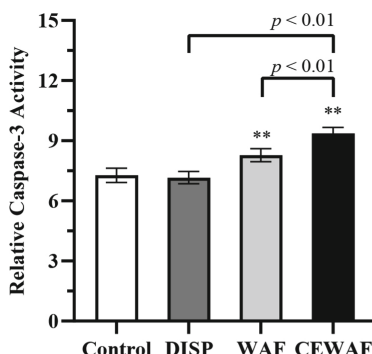


Fig. 3. Relative caspase-3 activity in the respiratory trees of *A. japonicus* following exposure to WAF (light-grey filled) and CEWAF (black filled) of Oman crude oil, and GM-2 chemical dispersant only (dark-grey filled). Asterisks (**) denotes the significant differences between the treatments and the Control ($p < 0.01$).

Caspase-3 is one of the key executioners or final effectors for cellular apoptosis to occur [23, 24]. Increased caspase-3 activity observed in the present study indicated that oil acute exposure could induce an elevated level of cellular apoptosis in the respiratory tree of *A. japonicus*. Under normal conditions, cellular apoptosis is a physiological programmed process *in vivo* to eliminate redundant, unwanted, or damaged cells from the body [24–26], which is widely regarded as a part of the cell developmental pathway for most multicellular organisms [27]. It has been corroborated that cellular apoptosis is one of the crucial survival mechanisms for most marine organisms undergoing stressful environmental conditions [28, 29]. Our previous work also reported that high temperature and oil pollution co-exposure could cause an elevated level of cellular apoptosis in the body wall of *A. japonicus*. The results of the present study clearly indicated that crude

oil exposure caused a significant increase of the apoptosis level in the respiratory tree of *A. japonicus*, and crude oil dispersed by GM-2 chemical dispersant exposure induced a higher apoptosis level than crude oil alone exposure did, which might further lead to a severer negative effect on *A. japonicus*.

During the biotransformation processes in marine organisms, oil-derived hydrocarbons could stimulate ROS production. Our previous work has also confirmed that both WAF and CEWAF exposure could induce a significant increase in the ROS level in the respiratory tree of *A. japonicus* [3]. For scavenge the overproduced ROS, the antioxidant enzymatic system is regarded as the primary defense line to maintain the redox homeostasis within certain limits [3, 30, 31]. Our previous work found that crude oil exposure caused a subtle increase in the total antioxidant capacity (T-AOC), while the present study manifested that crude oil exposure caused no overt impact on the POD activity and a remarkable reduction in the GST activity, which are two of the main antioxidant enzymes. Besides, compared to the Control, chemically dispersed crude oil exposure caused a 3.57-fold lower of T-AOC and a 4.18-fold lower of GST activity. T-AOC is an integrated parameter to assess the cumulative action of the antioxidant enzymatic activities, like GST and POD [32]. The inconsistency of the changes in GST, POD, and T-AOC indicated that, except for GST, there were other antioxidant enzymatic activities, such as superoxide dismutase (SOD), catalase (CAT), and glutathione peroxidase (GPx), that crude oil exposure might induce to eliminated the overproduced ROS. Nevertheless, all the results still manifested that chemically dispersed crude oil exposure could cause a more insufficient antioxidant level and thereby lead to severer oxidative damage and cellular apoptosis in *A. japonicus* than crude oil alone exposure did, which was mainly attributed to the addition of chemical dispersant solubilizing higher levels of oil-derived hydrocarbons into the water column.

4 Conclusions

The present study revealed that the addition of chemical dispersant to disperse crude oil could aggravate the negative effects of crude oil on antioxidant defense enzyme activities (especially GST) and cause severer cell apoptosis in sea cucumber. Hence, during oil spill accidents, the application of chemical dispersants in the emergency responses planning and decision making needs more comprehensive consideration of ecological effects, especially for the mariculture industry.

Acknowledgments. The authors are grateful for the financial supports from the National Key Research and Development Program of China (grant number 2018YFD0900606) and the National Natural Science Foundation of China (grant numbers 42076215 and 42076167).

References

1. Fisheries and Fisheries Administration Bureau of the Ministry of Agriculture: China Fishery Statistical Yearbook 2018, p. 181. China Argriculture Press, Beijing (2018)

2. Hamel, J.F., Mercier, A.: Population status, fisheries and trade of sea cucumbers in temperate areas of the Northern Hemisphere. In: Sea cucumbers: a global review of fisheries and trade, FAO Fisheries and Aquaculture Technical Paper, Rome, Italy, pp. 257–292 (2008)
3. Li, X., et al.: Antioxidant response and oxidative stress in the respiratory tree of sea cucumber (*Apostichopus japonicus*) following exposure to crude oil and chemical dispersant. *J. Mar. Sci. Eng.* **8**, 547 (2020)
4. Pan, G., Qiu, S., Liu, X., Hu, X.: Estimating the economic damages from the Penglai 19-3 oil spill to the Yantai fisheries in the Bohai Sea of northeast China. *Mar. Policy* **62**, 18–24 (2015)
5. Li, X., Ding, G., Xiong, Y., Ma, X., Fan, Y., Xiong, D.: Toxicity of water-accommodated fractions (WAF), chemically enhanced WAF (CEWAF) of Oman crude oil and dispersant to early-life stages of zebrafish (*Danio rerio*). *Bull. Environ. Contam. Toxicol.* **101**, 314–319 (2018)
6. Li, X., Xiong, D., Ju, Z., Xiong, Y., Ding, G., Liao, G.: Phenotypic and transcriptomic consequences in zebrafish early-life stages following exposure to crude oil and chemical dispersant at sublethal concentrations. *Sci. Total Environ.* **763**, 143053 (2021)
7. Greer, J.B., Pasparakis, C., Stieglitz, J.D., Benetti, D., Grosell, M., Schlenk, D.: Effects of Corexit 9500A and Corexit-crude oil mixtures on transcriptomic pathways and developmental toxicity in early life stage mahi-mahi (*Coryphaena hippurus*). *Aquat. Toxicol.* **212**, 233–240 (2019)
8. National Academies of Sciences Engineering and Medicine: The Use of Dispersants in Marine Oil Spill Response, p. 410. The National Academies Press, Washington, DC, USA (2019)
9. Duan, M., Yang, B., Ding, G., Xiong, D.: Effects on mutation of *Cylla* and *SP-Runt* gene in sea urchins of dispersed oil. *Mar. Environ. Sci.* **34**, 468–472,480 (2015)
10. Prince, R.C.: Oil spill dispersants: boon or bane? *Environ. Sci. Technol.* **49**, 6376–6384 (2015)
11. Singer, M.M., et al.: Standardization of the preparation and quantitation of water-accommodated fractions of petroleum for toxicity testing. *Mar. Pollut. Bull.* **40**, 1007–1016 (2000)
12. Bradford, M.M.: A rapid and sensitive method for the quantitation of microgram quantities of protein utilizing the principle of protein-dye binding. *Anal. Biochem.* **72**, 248–254 (1976)
13. Vontas, J.G., Enayati, A.A., Small, G.J., Hemingway, J.: A simple biochemical assay for glutathione S-transferase activity and its possible field application for screening glutathione S-transferase-based insecticide resistance. *Pestic. Biochem. Physiol.* **68**, 184–192 (2000)
14. Chiba, T.: Spectroscopy | Visible spectroscopy and colorimetry. In: Caballero, B. (ed.) Encyclopedia of Food Sciences and Nutrition (Second Edition), pp. 5454–5459. Academic Press, Oxford (2003)
15. Marissen, W.E., Guo, Y., Thomas, A.A.M., Matts, R.L., Lloyd, R.E.: Identification of caspase 3-mediated cleavage and functional alteration of eukaryotic initiation factor 2 α in apoptosis. *J. Biol. Chem.* **275**, 9314–9323 (2000)
16. Nimmo, I.A.: The glutathione S-transferases of fish. *Fish Physiol. Biochem.* **3**, 163–172 (1987)
17. Tarazi, S., et al.: Enhanced soluble expression of glutathione S-transferase Mu from *Rutilus kutum* by co-expression with Hsp70 and introducing a novel inhibitor for its activity. *Process Biochem.* **111**, 261–266 (2021)
18. Yin, Z.: Glutathione S-Transferase. In: Schwab, M. (ed.) Encyclopedia of Cancer, pp. 1926–1928. Springer, Heidelberg (2017). https://doi.org/10.1007/3-540-30683-8_665
19. Rudneva, I., Kuzminova, N., Skuratovskaya, E.: Glutathione-S-transferase activity in tissues of black sea fish species. *Asian J. Exp. Biol. Sci.* **1**, 141–150 (2010)
20. Pereira, L.F., Goodwin, P.H., Erickson, L.: Peroxidase activity during susceptible and resistant interactions between cassava (*Manihot esculenta*) and *Xanthomonas axonopodis* pv. *manihotis* and *Xanthomonas cassavae*. *J. Phytopathol.* **148**, 575–577 (2000)

21. Sabir, K., Javed, M., Latif, F., Ayub, M.: Effect of various levels of iron on peroxidase activity in the fish, *Cirrhina mrigala*. In: Proceedings of 6th International Fisheries Symposium & Expo-2017 “Innovative and Sustainable Aquaculture for Blue Revolution”, Lahore, Pakistan, pp. 13–18 (2018)
22. Bagnyukova, T.V., Chahrak, O.I., Lushchak, V.I.: Coordinated response of goldfish antioxidant defenses to environmental stress. *Aquat. Toxicol.* **78**, 325–331 (2006)
23. Jia, R., et al.: Effects of nitrite exposure on haematological parameters, oxidative stress and apoptosis in juvenile turbot (*Scophthalmus maximus*). *Aquat. Toxicol.* **169**, 1–9 (2015)
24. Hengartner, M.O.: The biochemistry of apoptosis. *Nature* **407**, 770–776 (2000)
25. Ahamed, M., Akhtar, M.J., Alhadlaq, H.A.: Co-exposure to SiO₂ nanoparticles and arsenic induced augmentation of oxidative stress and mitochondria-dependent apoptosis in human cells. *Int. J. Environ. Res. Public Health* **16**, 3199 (2019)
26. Li, X., et al.: Combined effects of elevated temperature and crude oil pollution on oxidative stress and apoptosis in sea cucumber (*Apostichopus japonicus*, Selenka). *Int. J. Environ. Res. Public Health* **18**, 801 (2021)
27. Johnstone, J., Nash, S., Hernandez, E., Rahman, M.S.: Effects of elevated temperature on gonadal functions, cellular apoptosis, and oxidative stress in Atlantic sea urchin *Arbacia punctulata*. *Mar. Environ. Res.* **149**, 40–49 (2019)
28. Rahman, M.S., Rahman, M.S.: Effects of elevated temperature on prooxidant-antioxidant homeostasis and redox status in the American oyster: Signaling pathways of cellular apoptosis during heat stress. *Environ. Res.* **196**, 110428 (2021)
29. Barbosa, D.B., de Abreu Mello, A., Allodi, S., de Barros, C.M.: Acute exposure to water-soluble fractions of marine diesel oil: evaluation of apoptosis and oxidative stress in an ascidian. *Chemosphere* **211**, 308–315 (2018)
30. Cui, Y., et al.: Effects of aerial exposure on oxidative stress, antioxidant and non-specific immune responses of juvenile sea cucumber *Apostichopus japonicus* under low temperature. *Fish Shellfish Immunol.* **101**, 58–65 (2020)
31. Rampon, C., Volovitch, M., Joliot, A., Vriz, S.: Hydrogen peroxide and redox regulation of developments. *Antioxidants* **7**, 159 (2018)
32. Ghiselli, A., Serafini, M., Natella, F., Scaccini, C.: Total antioxidant capacity as a tool to assess redox status: critical view and experimental data. *Free Radical Biol. Med.* **29**, 1106–1114 (2000)



Environmental Impact of Fluorine Pollution in Tursunzade Manufactured Biogeochemical Province (Tajikistan)

Vladimir Safonov¹ (✉) , Vadim Ermakov¹ , and Margarita Samburova²

¹ Laboratory of Environment Biogeochemistry, Vernadsky Institute of Geochemistry and Analytical Chemistry, Moscow, Russia

safonovbio@gmail.com

² BIOS LLC, Moscow, Russia

Abstract. Fluorine environmental emissions are often associated with the activities of metallurgical industries. It is common knowledge that fluoride excess negatively affects the state of vegetation, health of animals and human who often suffer from pathologies that are named with the general term “fluorosis”. Soil, water, leaves and fruits of agricultural crops were sampled in the area of aluminum production (Tursunzade, Tajikistan) and the content of fluoride in them was determined as well. Also, the clinical condition of local cattle was evaluated. The X-ray examination was performed for animals of 1–12 months and adult cows. The phosphorus content in the surface water bodies was found to be 1.1–31.5 mg/l, in soils – from 220 to 1000 mg/kg, depending on the distance from the aluminum plant. As for the fruit samples, phosphorus was detected in the amount of 8–122 mg/kg of, as for the cultivated plants leaves – 70–180 mg/kg. The highest concentration of fluoride was determined in the mowing of herbage plants (growing in the southwest direction from the plant, at a distance of 2–3 km from it) – 610 mg/kg. The development of fluorosis was diagnosed in cattle, young animals aged 2.5–3 years also suffered from the wear and blackening of the teeth enamel. At the same time animals of different ages demonstrated the tail vertebrae softening and anomalies of bone development. This study revealed the presence of total pollution of all the environmental objects and the need for measures in order to correct the fluoride content in biogeocenoses.

Keywords: Fluorine · Fluorosis · Biogeochemical Provinces · Soil · Plants · Cattle

1 Introduction

Fluorine (F) is a typical nonmetal of the periodic system 17th (VIIA) group. Its electron configuration of the valence shell is $1s22s22p5$, its atomic mass is 18.9984. Currently, the fluorine “plastic” role is beyond doubt, one of its most well-known characteristics is the ability to seal tooth enamel. Nevertheless, the fluorine biochemistry remains a subject of different modern studies. The element (in the form of fluoride-ions) effect

on the biochemical processes depends on the dose. The fluoride-ion can replace the hydroxyl-ion both in bone apatite and in non-mineralized tissues, possibly embedded in the active enzyme center. While participating in carbohydrate metabolism, fluoride increases the level of the blood glucose level, which also leads to an increase in the lactic acid and inorganic phosphorus level in it. Fluorides enhance the activity of adenylate-cyclase, but inhibit the fatty acids oxidation, tissue respiration and bone phosphatase activity. The excessive intake of fluorides in animals and humans negatively affects the development of the central nervous system, thyroid function. All in all, it leads to the increased generation of free radicals [1, 2]. The negative effect on the thyroid gland and the goiter development while the fluoride excess may be explained by the iodine and fluorine antagonism. The interactions between the exchange of calcium, iron, copper and fluorine are widely known. The parallels between the metabolism of fluorine and calcium not only in animals, but also in the plants are of particular importance.

The main natural source of fluorine is volcanic activity, acidic fumes containing HF are released during eruptions. The volume of fluorine intake from atmospheric precipitation, aerosols, surface and drinking water is largely dependent on the current volcanic activity. The main technogenic sources of fluorine emission into the environment are represented by enterprises aimed on the extraction and processing of phosphorites, apatites and fluorite, metallurgical production of aluminum and other metals that require the cryolite and fluorite use. In addition to such fluorine sources, it is necessary to mark that emissions from fuel combustion, cement production, production and use of fertilizers, fluorinated pesticides, medicines, plastics, and refrigerants become fluorine sources as well [3, 4]. Gaseous fluorine is used as an oxidizer in liquid rocket fuel, for the production of uranium fluorides and the separation of its isotopes.

In the most cases, the average content of fluoride in uncontaminated soils is close to 300 mg/kg, the average data for various types of soils is 85–560 mg/kg. In areas located near the industrial complexes, the content of this element reaches 1000 mg/kg [5]. A lower content is typical for a number of sandy loam and meadow-alluvial soils. The dependence of the content of water-soluble fluorine forms on its total content in the soil and its intake into plants is positive, but rather complex, as it largely depends on the pH level of the medium [6, 7]. Nevertheless, the biogenic migration of fluorine, despite its high chemical activity, is small and significantly lower than the one of other halogens. This element has a low coefficient of biophilicity, which is 0.007 units and characterizes the ratio of the average amount of the element in living matter to its average content in the lithosphere, and is poorly accumulated by plants from soils. The coefficient of biological absorption does not exceed 0.1. As for most herbage plants, the level of fluorine is typical, equal to 1–10 mg/kg of dry weight, rarely – 20–30 mg/kg. However, in technogenic biogeochemical provinces, plants can accumulate up to 200–2000 mg/kg of fluorine in the dry mass as a result of atmospheric pollution [8].

In order to monitor the aerotechnogenic fluorine environmental pollution, a number of methods using herbage plants have been developed. The latter are able to accumulate fluorine compounds from the atmospheric air (in the absence of an obvious need for fluorine for the vital plants' activity) more efficiently than other pollutants, which is due to the high reactivity of these compounds. The basis of environmental monitoring methods is the ability of plants to accumulate fluoride compounds at different levels

of trace elements in the environment (air, water, soil). Visual assessment of the plant complex draws attention to signs of damage: chlorosis and necrosis of leaves, changes in the content of pigments: chlorophyll and carotenoids [9, 10].

In the areas of active volcanism, some arid regions, zones of phosphorites and apatites extraction and processing, the endemic and man-made fluorosis of farm animals and the population is often found. Animals suffer from a pathological condition of varying severity with a predominant teeth and skeleton lesion. The term fluorosis includes a wide range of clinical manifestations of fluoride toxicity. Their high concentrations disrupt the metabolism of calcium, the rate of bone accretion and resorption increases, the total turnover of calcium in the body accelerates. An excess of fluorides affects the collagen synthesis in the bones. The consumption of large fluorides amounts (5–40 mg/day) with drinking water causes serious forms of skeletal deformities: kyphosis, spine immobility, joint deformities. During the experiment, it was found that adult pregnant and lactating mice and their offspring demonstrated liver and kidney damage and other abnormalities while the level of sodium fluoride was 500 mg/kg in drinking water. The animals showed signs of oxidative stress: decreased activity of superoxide dismutase and glutathione peroxidase in red blood cells and increased expression of stress proteins [11]. Therefore, chronic fluoride intoxication can activate the mitochondrial pathways of neuronal apoptosis through the activation of procaspase-8 and caspase-3, which ultimately initiates the neuron degradation [12, 13]. The maximum permissible level of fluoride in farm animal feed is considered to be 20–50 mg/kg of dry matter. The exact level depends on the type of animal and the type of feeding. As for people, the maximum permissible intake level of an element from food is 35–40 mg/kg of dry matter [14]. The consequence of the fluorosis is the problem of the cattle housing and reproduction.

The modern technogenic supply of the element to the biogeocenoses is associated with the objects of aluminum production associated with the fluorine use. This article summarizes the results of work which included the study of technogenic fluorine environmental pollution in the Tursunzade biogeochemical province on the territory of Tajikistan, formed due to the operation of an aluminum plant which was built near Tursunzad in 1975. The environmental monitoring data that existed before the start of this study are insufficient for a complete ecological and geochemical assessment of the fluorine accumulation and impact in the biosphere objects.

2 Materials and Methods

A number of the authors' studies were aimed at the large-scale biogeochemical testing of the Central Asian biosphere region, known for contrasts in geological, geochemical and technogenic relations. Special attention was paid to the potential formation sources of biogeochemical provinces and endemias. Such sources included geochemical barriers and ore bodies, large industrial objects, inland bodies, massifs with intensive evaporation of moisture.

For this study, samples of water, soil, fruit trees (fruits and leaves), cereal cultivars were taken in a zone of 1–20 km from the aluminum plant (State Unitary Enterprise "Tajik Aluminum Company" (TALCO)), Tursunzade, Tajikistan (Fig. 1). The clinical condition of the local cattle kept in small farms was also evaluated in calves aged 1, 3,

9 and 12 months and adult cows, which underwent the X-ray examination of the caudal spine. The regular environmental monitoring data of the Tursunzadevsky district were also used in this study.



Fig. 1. The aluminum plant location near the Tursunzade city.

The authors performed quantitative determination of fluorine in soil samples and biomaterials by the alkaline hydrolysis of the material, the introduction of an orthophosphoric acid excess, followed by the initial potential measurement of the solution and the potential measurement after the fluorine addition at pH = 1.0. The measurement was carried out by a potentiometer with fluoride-selective electrodes. The MS Excel software was used during the results processing.

3 Results

In comparison with the soil of the reference areas located further than 15 km from the tailing dump, the surface soil layer of the tailing dump was looser, had poorer plant stand, and contained more sand and clay.

Regular pollution monitoring performed in the territories adjacent to the aluminum production allowed to establish that the greatest air pollution with hydrogen fluoride was considered to be the Sariasiysky district characteristic, which territory is located at

a distance of 11.5 km from the plant. The maximum concentrations of the compound were, therefore, 0.048 mg/m³. While analyzing water samples from Tursunzade water supply sources, it was figured out that the fluorine content was 0.3–0.5 mg/l. At the same time, it was determined that the element content is 31.5 mg/l at a distance of 1 km from the plant, 13 mg/l – at a distance of 3 km from the plant, 1.1 – 4.7 mg/l – in a zone of 3–30 km from the plant (samples taken from open reservoirs).

The Tursunzade district soil is also polluted by fluorine emissions. The fluoride concentration near the emission sources is 400–1000 mg/kg, up to 500 mg/kg at a distance of 5–6 km and 220–340 mg/kg at a distance of 24–26 km. As for soil samples from more remote areas (the distance from the plant is more than 26 km), the concentration of fluorine is at the level of 280–380 mg/kg. The content of water-soluble fluorine forms in samples obtained at a distance of 5–6 km from the plant exceeds the maximum permissible concentrations by 1.8–2.5 times.

It is worth noting the fluorine ability to lead to significant changes in soil processes. The element increases the solubility of organic matter, which causes its intensive loss in irrigated areas-dehumification. At the same time, the redox potential and biological activity of the soil cover decreases and the quantitative and qualitative composition of soil microorganisms changes. In the areas affected by plant emissions, the growth of cultivated plants was slowed down in comparison with more distant ones (>25 km). The tomatoes, bell peppers, onions, potatoes blossoms fell off and there were changes in the leaves' color and shape typical of chlorosis. As a result, the crop yield was reduced. A high fluorine content was also detected in the samples of these plants fruits, it was 50–60 mg/kg. The most pronounced changes due to a fluoride excess were noted in pomegranate: leaf necrosis occurred during the early spring period; more stable specimens retained leaves but the yield and quality of fruits were significantly reduced. Fruit trees (figs, apricots, persimmons, cherry plums) and grapes examined in the zone of 5–20 km from the aluminum plant had shrinking leaves, some of the fruits fell before ripening.

Fruit crops were sampled from farms located at different distances from the plant. The concentration of fluorine in mountain cherry plum (the zone of 13–23 km) was at the level of 63 mg/kg, in pomegranate – 12 mg/kg, in apples – 61 mg/kg and in grapes it was 52 mg/kg. Then the 35–40 km zone located on the territory of Uzbekistan (Southern station and Denau district) was taken for the experiment; therefore, the fluorine content in mountain cherry plum was 47 mg/kg, in grapes – 21–37 mg/kg, in apricots – 122 mg/kg. At a distance of more than 70 km in the Altynsay district (Surkhandarya region, Uzbekistan), the following levels of fluoride were detected: alycha – 25 mg/kg, grapes (farm 1) – 10 mg/kg, grapes (farm 2) – 8–12 mg/kg. As for the leaves of cultivated plants (peach, pomegranate, walnut and grape) located at a distance of 10 km from the plant, it was noted that they contained 70–180 mg/kg of fluoride at its permissible concentration of no more than 10 mg/kg. The leaves of these plants also contained a reduced amount of chlorophyll. Plants in other zones (in comparison with similar ones) were considered to be more depressed, which indicates a negative impact of anthropogenic load.

The toxic effects of aluminum plant emissions are expressed, among other things, in the reduction of the species diversity of herbage and flowering plants. It was revealed that on the basis of environmental monitoring data, 114 species of wild plants of the

Tursunzadevsky district disappeared from biocenoses, and about 70 species turned out to be resistant to pollution. The chemical compounds formed by fluorine affect the plants' growth, development and yield, also influencing the respiration intensity, the photosynthesis process, the activity of a number of key enzymes and the state of various metabolic processes, in particular, mineral metabolism.

During the study of samples of wheat and other cereals collected in May-June, it was revealed that the highest concentrations of fluorine were determined in samples obtained in the south-west direction from the source of emissions (zone of 1–20 km from the plant), – the concentration of fluorine was 98–360 mg/kg. The total aluminum content was also measured in herbage plants, it was the highest one at a distance of 2–3 km from the plant – up to 610 mg/kg. Probably, the emissions are transformed during air migration and aluminum compounds fall into the soil and surface water before fluorine compounds.

Due to the fluoride environmental excess, there are violations in the cattle population. The fluorine content in compound feeds produced in a number of farms of the region exceeds the permissible level by 6 times. Such fluorine compounds block the processes of carbohydrate metabolism in cattle, the glucose and lactic acid level in the blood significantly increases, the glycogen level in the liver decreases, respiration is being inhibited, therefore, fatty acid oxidation, phosphatase activity in bone tissue are developed. There is a violation of the optimal Ca:P ratio in bone tissues, calcification suppression of cartilage tissue, so that rickets develops during the latest periods [12]. The most dangerous is the fluorine presence on the surface of food plants and its accumulation in the green mass due to fluorine-containing dust of gaseous fluorine compounds. A high fluoride content, even if it does not harm plants (for example, species resistant to it), causes great damage while feeding such plants to animals, especially ruminants.

A severe form of chronic intoxication of the animal's body with fluoride, called fluorosis, was observed during the study in farms adjacent to the Tursunzade plant. Fluorosis provokes pathological changes in the animals physiology, disrupts the iodine and calcium exchange. As for sick animals, they suffer from the teeth blackening, appearance of yellow and brown mottling on the enamel; the surface of their teeth wears out quickly, with a severe course, the worn teeth become shaky, break down and fall out. The tubular bones of some animals are deformed, local cattle also demonstrate signs of damage to the legs joints in the form of edema, a spine deflection, difficulty in movement and feeding. The examination of the animals proved that signs of tooth wear are observed in young individuals at the age of 2.5–3 years. Against the background of rapid tooth abrasion, the animals did not consume coarse feed well, which was the reason for low fatness. The productivity of sick animals was about 2 thousand kg of milk per year. The mentioned characteristic signs, such as black-brown enamel pigmentation, shaky teeth and bleeding gums, were observed in 72% of the examined animals. There were also manifestations of a pathological condition in the form of anomalies of the facial skull part, last tail vertebrae softening, severe exhaustion of individual individuals. The data showed that the fluoride content in the animals exceeds the established norms. The X-ray examination of the posterior spine part in calves of different ages and adult cows allowed the authors of this article to establish the presence of deformities from 1 to 9 tail vertebrae and signs of impaired mineral metabolism in the stagnant tissue and osteodystrophy signs. Violation

of vertebral mineralization in animals at the stage of early ontogenesis occurs due to the mineral metabolism violation in mothers and, probably, the fluoride intake with milk [15].

The toxic effect of fluorine compounds on the tissues of the endocrine glands, in particular the thyroid gland, determines the iodine-deficient state of the body, increases the intensity of lipid peroxidation processes against the background of insufficient activity of the antioxidant defense system. Changes in the balance of lipid peroxidation and the antioxidant defense system cause the destruction of membrane cell structures and (in combination with other etiological factors) contribute to the development of a wide range of pathologies.

Despite the zoning of territories based on the presence of endemias, which include fluorosis, measures for prevention and treatment still are not being sufficiently developed [16]. The problem of human and animal fluorosis is particularly acute in areas with developed industry associated with the aluminum production, apatites and phosphorites processing. In these territories, the morbidity increase in population and reproductive problems of cattle and small cattle, a decrease in their productivity are recorded as well. It is necessary to improve the methods of cleaning the emissions of aluminum production, but even when such production is closed in a polluted area, a fluoride excess in soils and plants may be observed for a long time [17].

The fight against the fluorosis content should include environmental monitoring of areas enriched with fluoride, preference in the use of feed and food products produced in areas with normal levels of trace elements, the use of medicines that reduce the fluoride absorption in animals and humans, and the purification of drinking water. Agriculture in polluted areas should give preference to pigs and chickens breeding since such animals are less susceptible to fluorosis. It is possible to increase the resistance of plants and reduce the fluoride intake into them by optimizing the macronutrients N, P, K, Ca and Mg levels. Phytoremediation with the planting of fluorine-accumulator-cultures is possible in territories similar to the Tursunzade biogeochemical province [10, 18].

Further work aimed at the biogeochemistry of fluorine studying should solve the following tasks: the contribution assessment of volatile fluorine compounds to global and local biogeochemical cycles; the regulation of biogeochemical processes in order to optimize the fluorine intake in plants and food; the study of metabolic processes involving fluorine in animals and humans, the improvement of measures for the fluorosis prevention [14]. It is also necessary to continue working on biogeochemical mapping of countries and regions by the fluorine and other mineral elements levels [19].

4 Conclusions

The mentioned above works carried out in the Tursunzade biogeochemical province were organized in order to determine the fluorine level in the agrobiocenoses taxons. They established the presence of total pollution of all the environmental objects. The complex of studies made it possible to determine the impact of aluminum plant emissions on the biodiversity of the vegetation cover, the metabolism and development of plants, the metabolism and the state of animal health. Pathological disorders of mineral metabolism, expressed in discoloration and premature destruction of teeth, joints swelling, softening

of the terminal vertebrae of the tail were detected in the most of the cattle. The harvest of fruit crops obtained in farms located near the aluminum plant is unsuitable for food consumption due to the high fluoride content in it. The green mass of herbage plants also contains high concentrations of fluoride and is undesirable for feeding animals.

Thus, the ecological state of the surveyed area requires the introduction of technologies that reduce toxic emissions of aluminum production, and the implementation of measures that correct the level of fluoride in the environment.

Acknowledgements. This work was supported by the RFBS Grant No. 19-05-00054.

References

1. Blaylock, R.L.: Excitotoxicity: a possible central mechanism in fluoride neurotoxicity. *Fluoride* **37**(4), 301–314 (2004)
2. Dec, K., et al.: The influence of fluorine on the disturbances of homeostasis in the central nervous system. *Biol. Trace Elem. Res.* **177**(2), 224–234 (2007)
3. Wang, M., Yang, J.-Y., He, W.-Y., Li, J.-X., Zhu, Y.-Y., Yang, X.: Vertical distribution of fluorine in farmland soil profiles around phosphorous chemical industry factories. *Environ. Sci. Pollut. Res.* **26**(1), 855–866 (2018). <https://doi.org/10.1007/s11356-018-3647>
4. Moiseenko, T.I., Gashkina, N.A., Dinu, M.I.: Enrichment of surface water by elements: effects of air pollution, acidification and eutrophication. *Environ. Processes. Int. J.* **3**(1), 39–58 (2016)
5. Ermakov, V.V., Krechetova, E.V., Dikareva, A.V., Dutov, V.M.: Natural-man-made and technogenic biogeochemical provinces enriched by fluorine. *Men und spurenelemente* **18**, 712–716 (1998)
6. Chen, D., Zhou, Yu., Cui, S.-F., Yang, J.: Effects of fluorine on the growth of Chinese cabbage (*Brassica campestris* L.) and oilseed rape (*Brassica napus* L.) at seedling stage Archives of Agronomy and Soil Science (Preprint <https://doi.org/10.1080/03650340.2021.1937605>) (2021)
7. Shi, M., et al.: Characteristics and effects of fluorine release from shallow high-fluoride soils. *Environ. Earth Sci.* **78**(20), 1 (2019). <https://doi.org/10.1007/s12665-019-8618-0>
8. Ermakov, V.F.: Elements and their Compounds in the Environment. vol. 3, (ed E Merian, M Anke, M Ihnat and M Stoeppler), pp. 1415–1421. WILEY-VCH VerlagGmbH and Co. KGaA, Weinheim (2004)
9. Rylnikova, M.V., Radchenko, D.N., Tsupkina, M.V., Safonov, V.A.: The study of ecological influence of the Novotroitsk tailing dump. The issues of the Tula State Agrarian University. *Earth Sci.* **1**, 108–20 (2020)
10. Bech, J., Korobova, E., Abreu, M., Bini, C., Chon, H.T., Pérez-Sirvent, C.: Soil pollution and reclamation. *J. Geochem. Explor.* **147**, 77 (2014)
11. Bouaziz, H., Croute, F., Boudawara, T., Soleilhavoup, J.P., Zeghal, N.: Oxidative stress induced by fluoride in adult mice and their suckling pups. *Exp. Toxicol. Pathol.* **58**(5), 339–349 (2007)
12. Amit, R.G., Sahadeb, D., Devendra, S.: Ameliorative effect of *Tamarindus indica* L. on biochemical parameters of serum and urine in cattle from fluoride endemic area. *Veterinarski arhiv* **5**(83), 487–96 (2013)
13. Xu, B., Xu, Z., Xia, T.: Effects of the Fas/Fas-L pathway on fluoride-induced apoptosis in SH-SY5Y cells. *Environ. Toxicol.* **26**(1), 86–92 (2011)

14. Bombik, E., Bombik, A., Rymuza, K.: The influence of environmental pollution with fluorine compounds on the level of fluoride in soil, feed and eggs of laying hens in Central Pomerania. Poland. Environ. Monit. Assess. **192**, 178 (2020)
15. Chernitskiy, A.E., Skogoreva, T.S., Safonov, V.A.: Study of interrelations of the bioelement status of mother and fetus at cattle. J. Mech. Continua Math. Sci. S **10**, 154–170 (2020)
16. Ermakov, V., et al.: Relationship of the mobile forms of calcium and strontium in soils with their accumulation in meadow plants in the area of Kashin-Beck endemia. Environ. Geochem. Health **42**(1), 159–171 (2020)
17. He, L., et al.: Fluorine enrichment of vegetables and soil around an abandoned aluminium plant and its risk to human health. Environ. Geochem. Health **43**(3), 1137–1154 (2020). <https://doi.org/10.1007/s10653-020-00568-5>
18. Weerasooriyagedara, M., et al.: Phytoremediation of fluoride from the environmental matrices: a review on its application strategies. Groundw. Sustain. Dev. **10**, 100349 (2020)
19. Safonov, V.A., Ermakov, V.V., Degtyarev, A.P. and Dogadkin, N.N.: Prospects of biogeochemical method implementation in identifying rhenium anomalies. IOP Conf. Ser. Earth Environ. Sci. **421**(6), 062035 (2020)



Analysis on Bird Communities Response to Different Urban Land-Cover and Land-Use Types in Greater Manchester

Yihao Liu^(✉)

School of Environment, Education and Development, University of Manchester, Manchester M13 9PL, UK
yihao.liu@postgrad.manchester.ac.uk

Abstract. Nowadays the process of global urbanization is unstoppable, leading to a serious threat to local biodiversity. Urbanization may result in biodiversity decline or even species extinction, while sometimes help maintain species abundance in some developed countries. Different land-cover and land-use types affect species diversity in different aspects and directions, so it's important to understand the pattern of species distribution across different characteristics of urban landscape, which helps city-designers and decision-makers to mitigate detrimental influences of urbanization on local biodiversity by rational urban planning and effective conservation protection. This study uses bird, which are highly sensitive to environmental changes, as the ecological indicators.

This paper studies the differences of species richness, abundance and community composition from five urban land-cover and seven land-use types, and analyses patterns of bird distribution in different land use purposes on the same land cover landscape. This study used bird species richness, Shannon and Simpson diversity index across Greater Manchester to evaluate bird diversity. This study also used Generalized Linear Model to model the relationship between bird species richness and land-cover or land-use density, and used Redundancy Analysis (RDA) to interpret the response of bird communities to land-cover and land-use density. Green spaces (especially for public parks land use) and water bodies have relatively higher bird species richness. Built areas have the lowest species richness, especially the institutional land use (including religious grounds, school grounds, and institutional grounds). Considering different land-use purposes, public parks and recreation have the highest bird diversity in green spaces land-cover, followed by amenity land and domestic gardens. In built-up areas, species diversity in institutional land use is higher than previously developed land use. Clear understanding the relationships between land-cover and land-use types and bird species diversity and communities composition will help better policy making for potential future land-cover and land-use planning.

Keywords: Spatial ecology · Avian · Greater Manchester · Species richness · Land cover · Land use

1 Introduction

Nowadays because of the widespread of COVID-19 pandemic, people gradually realize the importance of ecosystems to human beings' health, which motivate them to protect and maintain the nature environment [1]. Intergovernmental science-policy Platform for Biodiversity and Ecosystem Services (IPBES) reports that the spread of infectious diseases will be caused by less abundant biodiversity and dysfunctional ecosystems [1, 2]. Therefore, protecting and restoring biodiversity and nature can be beneficial for people's physical and mental health, and further help human beings to better face future challenges.

Global urbanization is a great threat to ecosystems and biodiversity, because of the fragmented natural habitats caused by rapidly changing urban land use purpose, leading to the decline or extinction of ecological communities [3]. Green spaces are the most important and principle land-cover types as habitats for species in cities, because of their dense tree cover providing essential food and living resources [4]. Birds are sensitive to habitat, human-caused changes or environmental contaminants, have relatively lower monitoring costs, are wide-spread across various habitats, and have been well-developed [5], so they are viewed as a useful tool for environmental monitoring.

Greater Manchester is under an intense urbanization caused by development pressures, but it's impressively biodiverse. However, few urban ecological studies especially land-cover and land-use studies have been carried out in this region.

This paper will detect the changes of bird species diversity and community composition in Greater Manchester across different land-cover types, and analyse different relationships between land-cover types for different land use and bird species. Clear understanding of these relationships will help better policy making for potential future land-cover and land-use planning.

2 Methodology

2.1 Research Area

Greater Manchester, located on the North West England, $53^{\circ}30'N$, $2^{\circ}19'W$, consists of more than 50% high-density urban areas (dominated by built up areas), transitional areas, and peri-urban areas (Fig. 1). Although natural habitats have been fragmented by intense urbanization, numerous small fragmented areas of different habitats can help support small populations of a wide variety of species. There are some protected species detected in Greater Manchester, including little ringed plovers, barn owls, badgers, kingfishers, peregrine falcons, water voles, great crested newts, and even some European Protected Species [6].

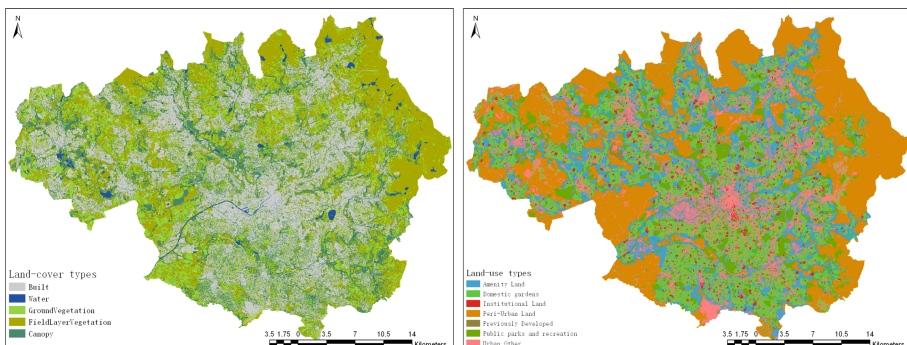


Fig. 1. Land-cover and land-use types in Greater Manchester [7].

2.2 Research Design

Greater Manchester was digitally overlaid by 1×1 km grids by ArcGIS Pro [8], and their locations were represented by the centroid coordinate of grids. Occurrence records data of bird species were from National Biodiversity Network, focusing on records detected after 2015, and were sampled in different grids based on their locations. Species records data occurring at less than 20 grids were removed from the analysis because of the distortion multivariate patterns from rare species [9]. 230 bird species found in study area were classified into five dietary guild according to the species-level dataset built by Wilman et al.: plant and seed eaters, fruit and nectar eaters, invertebrate eaters, vertebrate and fish and carrion eaters, and omnivore [10].

To identify land-cover and land-use types composition inside each grids, the focal density with a Gaussian filter of land-cover and land-use were calculated within a 500-m buffer and 100-m sigma, which means cells inside sigma were given more weight.

2.3 Statistical Analyses

In order to analyse bird species richness and diversity, the study summarized species detections records, species richness index, Shannon diversity index, and Simpson diversity index across different land-cover and land-use types. Then the analysis used general linear model (GLM) of the Poisson family [11], which is suitable for count data, to model the relationship between bird species richness and land-cover or land-use density inside each grids.

This study also used Redundancy Analysis method (RDA), which can interpret the response of bird communities to land-cover and land-use density and explore their relationships [12]. Before computing RDA of bird communities, bird abundance data were pre-transformed using Hellinger transformation method to avoid Euclidean distance, and plotted into biplots based on bird species scores and grid scores. Finally, this study compared bird communities composition inside different land-cover and land-use types to investigate bird communities structures.

3 Results

3.1 Species Richness and Diversity

As Table 1 shows, three green spaces layer have relatively higher species richness and diversity indexes, followed by water layer. Built areas have the lowest diversity index. Considering different land-use purposes, public parks and recreation have the highest bird diversity in green spaces land-cover, followed by amenity land and domestic gardens. In built-up areas, species diversity in institutional land use is higher than previously developed land use.

Table 1. Bird richness and diversity index within different land-cover and land-use types

Land-cover type	Total species richness	Total number of detections	Shannon diversity	Simpson diversity
Field layer vegetation	191	37,703	70.65	51.38
Water	150	14,844	66.87	49.99
Canopy	171	44,252	61.31	45.92
Ground vegetation	172	19,692	60.40	42.47
Built	167	42,243	54.63	39.99
Land-use type				
Peri-urban	192	47,700	74.37	55.02
Public parks and recreation	171	26,715	70.84	54.26
Amenity land	166	32,643	62.69	48.09
Urban other	158	25,041	53.48	38.56
Institutional land	96	2,313	50.63	37.85
Domestic gardens	155	34,304	46.03	33.34
Previously developed land	15	18	14.29	13.50
Total	230	168,735		

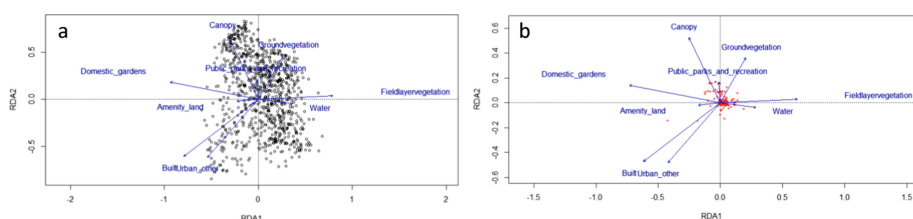
GLM analysis (Table 2) shows an encouraging positive relationship between water-body and bird species richness, an unexpected negative (although weak) relationship between ground and field vegetation with species richness, and an significant negative relationship between built areas and richness. Among land-use types, public parks and recreation have a weak positive relationship with bird richness, others have a negative influence. The negative correlation between domestic parks, amenity land and Institutional land with bird richness are much weaker than the negative correlation between previously developed land and other urban land use with bird richness. There is no linear relationship between canopy and peri-urban land with bird richness.

Table 2. Summary of GLM

	Estimated coefficients	Standard errors	z-value	p-value
Intercept	3.324	0.014	227.112	<0.001
Water	1.412	0.086	16.327	<0.001
Field layer vegetation	-0.095	0.059	-1.620	0.105
Ground vegetation	-0.409	0.077	-5.335	<0.001
Built	-0.804	0.061	-13.218	<0.001
Canopy	NA	NA	NA	NA
Public parks and recreation	0.122	0.033	3.670	<0.001
Domestic gardens	-0.220	0.035	-6.368	<0.001
Amenity land	-0.314	0.033	-9.388	<0.001
Institutional land	-0.366	0.108	-3.375	<0.001
Urban other	-0.731	0.041	-17.826	<0.001
Previously developed land	-0.740	0.187	-3.947	<0.001
Peri-urban	NA	NA	NA	NA

3.2 Bird Community Composition

Figure 2 plots the explanatory variable which pass the permutation test at 95% confidence level [12]. According to the length of arrows, canopy, domestic gardens, field layer vegetation, and built areas have the most significant influence on bird distribution. Less sites are distributed in the third quadrant, which are related to built and urban other areas. Several bird species are distributed far away from others, especially in the third quadrant (*Columba livia* and *Apus apus*) correlating to some human-related land-use types, while most of others are clustered together in the right part with short projection, showing that they are related to either green spaces and water land cover or intermediate ecological conditions.

**Fig. 2.** RDA in different land-covers and seven land-use types (a) site scores, (b) species scores.

All dietary guilds can be found in Greater Manchester, though fruit and nectar dietary only includes one bird species: *Psittacula krameri*. Omnivore eaters have the highest proportion in the study area, Omnivores account for the largest proportion in all land-cover

and land-use types, followed by invertebrate eater, plant and seed eaters, vertebrates, fish and carrion eaters, in turn.

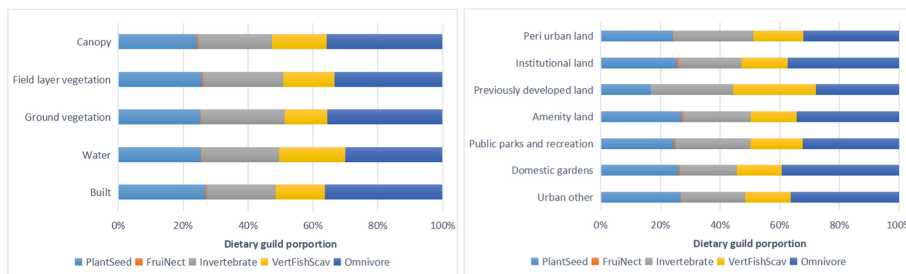


Fig. 3. Composition of birds dietary guilds in Greater Manchester.

4 Discussion

4.1 Species Richness and Diversity

In Greater Manchester, urban regions play an essential role in protecting and restoring bird diversity, since they sustain higher bird species richness and more bird individuals (total bird detections within city areas occupy more than 70% through comparing peri-urban with other regions). There are even some globally vulnerable species inside Red List [13] (e.g., *Anser cygnoides*), and European Protected Species [6] (e.g., *Falco peregrinus*, *Charadrius dubius*) recorded inside cities. Some bird species (e.g., *Xema Sabini*, *Calidris pugnax*, etc.) are only distributed within city regions, which strongly demonstrates that urban landscape is a suitable habitat for both high-density bird species and conservation species [14].

Species richness in green spaces are relatively higher, which has been proved by many other studies. Field layer vegetation has higher diversity index and less negative impact on species richness than ground vegetation, partly because the area of ground vegetation is smaller and more dispersed, leading to less abundance of bird species [15]. Some researches prove that establishing corridors between small green spaces can accelerate birds' movement and regularly interaction with connecting green spaces, therefore facilitating the growth number of bird species and individuals [16]. Considering different land-use purposes in green spaces, species diversity in public parks and recreation is much higher than others, and they have a positive influence in richness. The most important reason is that vegetation in public parks are much more complex and heterogeneous in structure, which can provide diverse habitats and dietary for multiple bird species [17]. Amenity land and domestic gardens are designed and maintained for safety, visual, or environmental purposes with less structural changes are more homogeneity, so they are less suitable for different species survival [18]. Therefore, city designers should consider the vegetation structure, including diverse trees species, woods, forbs and shrubs, while make the future land-use plan.

Waterbodies have encouragingly high species diversity and significant positive relationship with bird species richness. Waterbirds get food and shelters from waterways, and nest and breed near water, although waterways within cities are under high human-related pressure [19]. This can be demonstrated by some studies, which prove that waterbird diversity are not influenced by the level of urbanization, so they can survive in not only natural habitats but also human-built areas [20]. Potential future land-use planning cannot ignore the essential role of urban water in optimizing habitats.

The lowest species richness and most negative impact occur in built up regions as expected, influenced by intense artificial pressure, barren vegetation, heavy pollution and noise, high collision risks and mortality [3]. Some researches find the highest number of species and individuals occurring in built areas, especially in residential areas [21], because of common bird feeders and enough edible garbages for food. However, this analysis is unable to show this trend because we did not classify finer land-use types. Nowadays urbanization and the displacement of natural habitats by building are unstoppable, sufficient quantity and quality of green spaces between buildings, or sufficient bird feeders in the built areas, can help to protect, sustain and restore bird abundance.

4.2 Bird Community Composition

The characteristic of urban bird communities in Greater Manchester is classical. Several dominate species (e.g., *Passer montanus*, *Columba livia*, etc.) account for more than 75% of total individuals inside cities. These abundant species, which adapt to complex urban habitats better than others, are mostly distribute near buildings and make use of human refuse [22].

Only one bird species (*Psittacula krameri*) mainly eats fruit and nectar. This is an invasive alien species, which is original from Africa and Asia. *Psittacula krameri* prefer to live in built regions, public parks, and domestic gardens, and negatively affect other cavity nesters. The European Community notes invasive species cause serious damage to both biodiversity, economy and health [23], therefore weighing the pros and cons of invasive alien species before developing suitable strategies is important to control the spread and reduce biodiversity loss.

Omnivores (e.g. *Chroicocephalus ridibundus*) and granivores (e.g. *Columba livia*) tend to distribute in highly urbanized areas, since they can benefit from anthropogenic food sources (garbage, feeders, or human-source seeds) [22, 24]. Some scientists also find that omnivores have an advantage in temperate regions, because they can live based on human-related resources in winter when there is limited natural sources comparing to tropical regions [25]. Dietary composition in Greater Manchester can show this trend, which omnivores and granivores are dominate inside cities.

Invertebrate eaters (mainly insect) and vertebrates, fish, and carrion eaters occupy the rest, and bird species based on invertebrate dietary are slightly more. More invertebrate eaters are distributed in regions where have more vegetation cover (e.g., canopy, public parks, ground vegetation or field layer vegetation), possibly because tree species in study area are suitable for arthropods and provide rich food for insectivores [26]. In addition, insectivores in abundant waterways also have higher proportion than human-related land cover, which is consistent with former studies [27]. The analysis clearly shows that the highest proportion of vertebrates, fish, and carrion eaters are located near waterways,

where have the most suitable nesting sites and corresponding food resources. Most of these waterbirds have a positive relationship with water variable according to Fig. 3. Therefore, carnivorous and insectivorous distributed in Greater Manchester will decline if the rapid urbanization influence and reduce the area of water and vegetation cover.

5 Conclusion

This paper clearly reveals the important role of cities in sustaining bird species diversity and shows the relationship between bird diversity and community composition with urban landscape. Green spaces (field layer vegetation, ground vegetation and canopy in turn) and water land cover have the highest species richness. Considering different land-use purposes, public parks and recreation have the highest bird diversity in green spaces land-cover, followed by amenity land and domestic gardens. This is determined by their vegetation structural complexity. The lowest species richness, diversity, and most negative contribution to species diversity are in built-up regions. Previously developed land use has a lower diversity and more negative influence because of the high intensity of artificial pressure, barren vegetation, heavy pollution and noise, high collision risks and mortality.

There are 230 bird species distributed in Greater Manchester, and more than 70% of them live inside cities. Several dominate species account for more than 75% of total urban individuals, which is the classical characteristics of urban bird communities. Omnivores and granivores tend to distribute in the most highly urbanized areas (e.g. built-up areas), since they can benefit from anthropogenic food sources. More insectivores are distributed in regions where have more vegetation cover (e.g., canopy, public parks, ground vegetation or field layer vegetation) or near abundant waterways. The highest proportion of vertebrates, fish, and carrion eaters are located near land-cover type.

To protect and maintain biodiversity inside cities, city designers should consider the vegetation structure, including diverse trees species, woods, forbs and shrubs, while make the future land-use plan, establishing some corridors between small green spaces can also facilitate the growth number of bird species and individuals. What's more, future land-use planning cannot ignore the essential role of urban water in optimizing habitats and supporting healthy waterbird communities. In highly urbanized areas, decision-makers can design more green spaces between buildings, or sufficient bird feeders in the built areas, to help protect and sustain bird abundance.

Acknowledgements. I would like to express my thanks to Dr. Matthew Dennis for his patient professional and logistical guidance and Dr. Gail Millin-Chalabi for her useful practical advice. I also would like to express my thanks to every professor in the University of Manchester, who gave me essential associated knowledge background and writing skills. Lastly, I want to thank my parents who supported me for further learning and my friends who encouraged and accompanied me when I was in trouble.

References

1. EC (2020): EU Biodiversity Strategy for 2030. Bringing Nature Back Into Our Lives. Brussels. <https://eur-lex.europa.eu/legal-content/EN/TXT/?qid=1590574123338&uri=CELEX:52020DC0380#footnote2>. Accessed 8 Aug 2021
2. IPBES (2019): Global Assessment Report on Biodiversity and Ecosystem Services. Available at: <https://ipbes.net/global-assessment>. Accessed 14 Aug 2021
3. Seress, G., Liker, A.: Habitat urbanization and its effects on birds. *Acta zoologica Academiae Scientiarum Hungaricae* (Budapest, Hungary : 1994) **61**(4), 373–408 (2015)
4. Kong, F., et al.: Urban green space network development for biodiversity conservation: identification based on graph theory and gravity modeling. *Landsc. Urban Plan.* **95**(1), 16–27 (2010)
5. Pertti, K.: Birds as a tool in environmental monitoring. *Ann. Zool. Fenn.* **26**(3), 153–166 (1989)
6. AGMA: An Ecological Framework for Greater Manchester (2008). <https://www.lancswt.org.uk/sites/default/files/2018-08/An%20Ecological%20Framework%20for%20Greater%20Manchester.pdf>. Accessed 13 July 2021
7. Dennis, M., et al.: Mapping urban green infrastructure: a novel landscape-based approach to incorporating land use and land cover in the mapping of human-dominated systems. *Land (Basel)* **7**(1), 17 (2018)
8. Esri: (2021) ArcGIS Pro. The world's leading GIS software. <https://www.esri.com/en-us/arcgis/products/arcgis-pro/overview>. Accessed 14 Aug 2021
9. Braak, ter.: Canonical correspondence analysis: a new eigenvector technique for multivariate direct gradient analysis. *Ecology (Durham)* **67**(5), 1167–1179 (1986)
10. Wilman, H., et al.: Elton Traits 1.0: Species-level foraging attributes of the world's birds and mammals. *Ecology (Durham)* **95**(7), 2027–2027 (2014)
11. Borcard, D., Gillet, F., Legendre, P.: Numerical Ecology with R. 2nd ed. 2018. Cham: Springer International Publishing (2018)
12. Fletcher, R., Fortin, M.J.: Spatial Ecology and Conservation Modeling: Applications with R. 1st ed. 2018. Cham: Springer International Publishing (2018)
13. An, A., et al.: Changing abundance and distribution of the wintering swan goose *Anser Cygnoides* in the middle and lower Yangtze river floodplain: an investigation combining a field survey with satellite telemetry. *Sustain. (Basel, Switzerland)* **11**(5), 1398 (2019)
14. Beninde, J., et al.: Biodiversity in cities needs space: a meta-analysis of factors determining intra-urban biodiversity variation. *Ecol. Lett.* **18**(6), 581–592 (2015)
15. Khera, N., Mehta, V., Sabata, B.: Interrelationship of birds and habitat features in urban greenspaces in Delhi India. *Urban Forestry Urban Greening* **8**(3), 187–196 (2009)
16. Sodhi, N.S., et al.: Bird use of linear areas of a tropical city: implications for park connector design and management. *Landsc. Urban Plan.* **45**(2), 123–130 (1999)
17. Silva, C.P., et al.: Bird richness and abundance in response to urban form in a Latin American city: Valdivia, Chile as a case study. *PLoS ONE* **10**(9), e0138120–e0138120 (2015)
18. Ferenc, M., Sedláček, O., Fuchs, R.: How to improve urban greenspace for woodland birds: site and local-scale determinants of bird species richness. *Urban Ecosyst.* **17**(2), 625–640 (2013). <https://doi.org/10.1007/s11252-013-0328-x>
19. Ma, Z., et al.: Managing wetland habitats for waterbirds: an international perspective. *Wetlands (Wilmington, N.C.)* **30**(1), 15–27 (2010)
20. Andrade, R., et al.: Waterbird community composition, abundance, and diversity along an urban gradient. *Landsc. Urban Plan.* **170**, 103–111 (2018)
21. Sandström, U., Angelstam, P., Mikusiński, G.: Ecological diversity of birds in relation to the structure of urban green space. *Landsc. Urban Plan.* **77**(1), 39–53 (2006)

22. Jokimäki, J., Suhonen, J.: Distribution and habitat selection of wintering birds in urban environments. *Landsc. Urban Plan.* **39**(4), 253–263 (1998)
23. Genovesi, P.: European strategy on invasive alien species. Council of Europe (2003)
24. Kark, S., et al.: Living in the city: can anyone become an ‘urban exploiter’? *J. Biogeogr.* **34**(4), 638–651 (2007)
25. Lim, H.C., Sodhi, N.S.: Responses of avian guilds to urbanisation in a tropical city. *Landsc. Urban Plan.* **66**(4), 199–215 (2004)
26. Vehviläinen, H., Koricheva, J., Ruohomäki, K.: Effects of stand tree species composition and diversity on abundance of predatory arthropods. *Oikos* **117**(6), 935–943 (2008)
27. Hayes, W.M., et al.: Bird communities across varying landcover types in a Neotropical city. *Biotropica* **52**(1), 151–164 (2020)

Author Index

A

- Adisak, Nathakaranakule, 143
Amaya, Pedro, 14
Amin Mir, M., 103, 355
Andrews, Kim, 355
Arteaga, Jennifer, 225

B

- Bratashova, Tatyana, 367

C

- Chang, Fu-Ming, 173, 210
Chen, Changping, 91
Chen, Lu, 200
Chen, Weixuan, 272
Cheng, Xionglei, 295

D

- Deng, Wu, 272
Do, Quang N. H., 261
Dondukov, Bato, 51
Dondukova, Galina, 51
Dorzhigushaeva, Oyuna, 51

E

- Ermakov, Vadim, 384
Esenarro, Doris, 14, 225, 315

F

- Fang, Wei, 155
Fang, Weiguo, 78

G

- Guney, M., 248

H

- Hadba, Lujain, 3
Han, Y. L., 125, 133
Hinojosa, Karina, 225
Hu, He, 78
Huang, G. H., 304, 328
Huang, Guohe, 186

J

- Jia, Lingyun, 110
Jiang, H., 125, 133
Jiang, Xin, 91
Jin, Guoliang, 78
Jintana, Srimuk, 143
Ju, Zhonglei, 375

K

- Karaca, F., 248
Karamanis, Dimitris, 44

L

- Li, Nan, 375
Li, Xiaoping, 295
Li, Xishan, 375
Li, Y. P., 163, 193, 304, 328
Li, Ying, 63
Li, Yitong, 295
Liao, Guoxiang, 375
Liu, Jing, 186
Liu, Yihao, 393
Loo, Yat Ming, 272
Luo, Tingyu, 78

M

- Ma, Guoye, 110
 Ma, Siyu, 272
 Ma, Yuanli, 272, 304
 Macchion, Laura, 261
 Manthilake, Inoka, 239
 Martins, Miguel, 3
 Mendonça, Paulo, 3
 Mir, Bilal Ahmad, 355
 Muñoz, Cesar, 14

N

- Nguyen, Hung D., 261

O

- Ocmin, Judith, 315

P

- Pattana, Rakkwamsuk, 143
 Pipat, Chaiwatworakul, 143

Q

- Qian, Changzhao, 91
 Qiu, Hongya, 200
 Qiu, Xiao Yu, 283
 Quijano, Joseline, 225

R

- Rangana, Rumesh, 239
 Rodriguez, Ciro, 14, 225

S

- Safonov, Vladimir, 367, 384
 Saldaña, Heiner, 14
 Salimzade, Emil, 367
 Samburova, Margarita, 367, 384
 Segovia, Elizabeth, 315
 Shi, Yishao, 29
 Silva, Lígia T., 3
 Siriluk, Chiarakorn, 143
 Sun, Jie, 186, 193
 Sun, Li, 186, 193

Surapong, Chirarattananon, 143

T

- Tassara, Carla, 315
 Tleukan, A., 248
 Tokazhanov, G., 248
 Turkyilmaz, A., 248

V

- Vassanadumrongdee, Sujitra, 339
 Vega, Violeta, 315

W

- Wang, Jun, 283
 Wang, Yurong, 155
 Wijewardane, Anusha, 239
 Wu, Jiansen, 186

X

- Xiong, Deqi, 375
 Xu, P. L., 125, 133
 Xu, Su, 283

Y

- Yang, Kaiyan, 339
 Yang, Qianqian, 29
 Yang, Wei, 375
 Yang, Xin, 155

Z

- Zhai, X. B., 163
 Zhang, J. B., 125, 133
 Zhang, Mengmeng, 63
 Zhang, Qianxi, 272
 Zhang, Y. F., 328
 Zhou, Haizhu, 295
 Zhou, Jianzhong, 155, 200
 Zhou, Lining, 295
 Zhu, M. L., 125, 133
 Zhu, Yuxin, 200
 Zou, Yuhang, 375